

**CELLULOSE AND CELLULOSE DERIVATIVES:
Physico-chemical aspects and industrial applications**

CELLULOSE AND CELLULOSE DERIVATIVES: Physico-chemical aspects and industrial applications

Editors:

JOHN F KENNEDY

Director of Birmingham Carbohydrate and Protein Technology Group,
Research Laboratory for the Chemistry of Bioactive Carbohydrates and Proteins,
School of Chemistry, The University of Birmingham, Birmingham, England
and Professor of Applied Chemistry,
The North East Wales Institute of Higher Education, Wrexham, Clwyd, Wales

GLYN O PHILLIPS

Chairman of Newtech Innovation Centre,
Chairman of Research Transfer Ltd,
(Newtech Innovation Centre),
Professorial Fellow of The North East Wales Institute of Higher Education,
Wrexham, Clwyd, Wales and Professor of Chemistry, University of Salford, England

PETER A WILLIAMS

Head of the Multidisciplinary Research and Innovation Centre and the
Centre of Expertise in Water Soluble Polymers,
The North East Wales Institute of Higher Education, Wrexham, Clwyd, Wales

Guest Editor:

LENNART PICULELL

Lektor and Associate Professor,
Department of Physical Chemistry 1,
The Chemical Center,
Lund University, Lund, Sweden

WOODHEAD PUBLISHING LIMITED

Published by Woodhead Publishing Limited, Abington Hall, Granta Park
Great Abington, Cambridge CB21 6AH, UK
www.woodheadpublishing.com

Woodhead Publishing India Private Limited, G-2, Vardaan House, 7/28 Ansari Road
Daryaganj, New Delhi 110002, India

First published 1995
Reprinted 2000, 2002, 2005, 2006, 2009
© 1995, Woodhead Publishing Limited
The authors have asserted their moral rights.

This book contains information obtained from authentic and highly regarded sources. Reprinted material is quoted with permission, and sources are indicated. Reasonable efforts have been made to publish reliable data and information, but the authors and the publishers cannot assume responsibility for the validity of all materials. Neither the authors nor the publishers, nor anyone else associated with this publication, shall be liable for any loss, damage or liability directly or indirectly caused or alleged to be caused by this book.

Neither this book nor any part may be reproduced or transmitted in any form or by any means, electronic or mechanical, including photocopying, microfilming and recording, or by any information storage or retrieval system, without permission in writing from Woodhead Publishing Limited.

The consent of Woodhead Publishing Limited does not extend to copying for general distribution, for promotion, for creating new works, or for resale. Specific permission must be obtained in writing from Woodhead Publishing Limited for such copying.

Trademark notice: Product or corporate names may be trademarks or registered trademarks, and are used only for identification and explanation, without intent to infringe.

British Library Cataloguing in Publication Data
A catalogue record for this book is available from the British Library.

ISBN 978-1-85573-212-4

Printed by Berforts South East Limited, UK



CELLUCON CONFERENCES AND THE CELLUCON TRUST

Cellucon Conferences as an organisation was initiated in 1982, and Cellucon '84, which was the original conference, set out to establish the strength of British expertise in the field of cellulose and its derivatives. This laid the foundation for subsequent conferences in Wales (1986), Japan (1988), Wales (1989), Czechoslovakia (1990), USA (1991), Wales (1992), Sweden (1993) and Wales (1994). They have had truly international audiences drawn from the major industries involved in the production and use of cellulose pulp and derivatives of cellulose, plus representatives of academic institutions and government research centres. This diverse audience has allowed the cross-fertilization of many ideas which has done much to give the cellulose field the higher profile that it rightly deserves.

Cellucon Conferences are organised by the Cellucon Trust, an official UK charitable trust with worldwide objectives in education in wood and cellulose. The Cellucon Trust is continuing to extend the knowledge of all aspects of cellulose worldwide. At least one book has been published from each Cellucon Conference as the proceedings thereof. This volume arises from the 1993 conference held in Lund, Sweden and the conferences in Wales 1994, Russia, Finland, etc, will generate further useful books in the area.

THE CELLUCON TRUST TRUSTEES AND DIRECTORS

Prof G O Phillips (Chairman)	Newtech Innovation Centre, UK
Prof J F Kennedy (Deputy Chairman and Treasurer)	The North East Wales Institute, UK and The University of Birmingham, UK
Dr P A Williams (Secretary)	The North East Wales Institute, UK
Mr T Greenway	Akzo Nobel Surface Chemistry Ltd, UK
Mr W B Painting	Hoechst (UK) Ltd, UK
Dr C A White	Fisons Scientific, UK

CELLUCON CONFERENCES ORGANISING COMMITTEE

Prof G O Phillips (Chairman)	Newtech Innovation Centre, UK
Prof J F Kennedy (Deputy Chairman and Treasurer)	The North East Wales Institute, UK and The University of Birmingham, UK
Dr P A Williams (Secretariat)	The North East Wales Institute, UK
Mr H Hughes (Secretariat)	The North East Wales Institute, UK
Mr P Bale	Hercules Ltd, UK
Prof W B Banks	University College of North Wales, UK
Prof C Bucke	The University of Westminster, UK
Dr H L Chum	American Chemical Society (Cellulose, Paper and Textile Division), USA
Dr A Fowler	Courtaulds Ltd, UK
Dr K Geddes	Crown Berger Europe Ltd, UK
Mr T Greenway	Akzo Nobel Surface Chemistry Ltd, UK
Prof J Guthrie	University of Leeds, UK
Dr H Hatakeyama	National Institute of Materials and Chemical Research, Japan
Dr M B Huglin	University of Salford, UK
Dr P Levison	Whatman International Ltd, UK
Dr J Meadows	The North East Wales Institute, UK
Mr W B Painting	Hoechst (UK) Ltd, UK
Mr A Poyner	Aqualon (UK) Ltd, UK
Mr R Price	Shotton Paper Co Ltd, UK
Prof J Roberts	Institute of Science and Technology, University of Manchester, UK
Dr J F Webber	The Forestry Authority, UK
Dr C A White	Fisons Scientific, UK

Cellucon Conferences are sponsored by:

The Biochemical Society, UK – Chembiotech Ltd, UK – Hoechst (UK) Ltd, UK – The North East Wales Institute of Higher Education, UK – The University of Birmingham, UK – The University of Lund, Sweden – Welsh Development Agency – Whatman Speciality Products Division, UK.

Cellucon Conferences are supported by:

The American Chemical Society (Cellulose, Paper and Textile Division), USA – Aqualon (UK) Ltd, UK – Akzo Nobel Surface Chemistry Ltd, UK – Courtaulds Chemicals and Plastics, UK – Crown Berger Europe Ltd, UK – DOW Chemicals, UK – The Forestry Commission, UK – The Southern Regional Research Center, USA – Shotton Paper Company Ltd, UK – Syracuse Cellulose Conferences, USA.

ACKNOWLEDGEMENTS

This book arises from the International Conference on Cellulose and Cellulose Derivatives: Physico-Chemical Aspects and Industrial Applications – Cellucon '93 – which was held at The Chemical Center, The University of Lund, Lund, Sweden. This meeting owed its success to the invaluable work of the Organizing Committee.

MEMBERS OF THE ORGANISING COMMITTEE – CELLUCON '93

Björn Lindman (Chairman)	The University of Lund, Sweden
Lennart Piculell (Chairman)	The University of Lund, Sweden
Lars Andersson	Akzo Nobel Surface Chemistry AB, Stenungsund, Sweden
Anders Carlsson	Karlshamns Lipidteknik AB, Stockholm, Sweden
Lennart Dahlgren	Akzo Nobel Surface Chemistry AB, Stenungsund, Sweden
Kristen Holmberg	Institute of Surface Chemistry, Stockholm, Sweden
John F Kennedy	The North East Wales Institute, Deeside and The University of Birmingham, UK
Haydn Hughes	The North East Wales Institute, Deeside, UK
Mary Malmsten	Institute of Surface Chemistry, Stockholm, Sweden
Mary Molund	The University of Lund, Sweden
Lars Ödberg	Swedish Pulp and Paper Research Institute, Stockholm, Sweden
Gerd Olofsson	The University of Lund, Sweden
W Bruce Painting	Hoechst (UK) Ltd, UK
Glyn O Phillips	Newtech Innovation Centre, Wrexham, UK
Folke Tjerneld	The University of Lund, Sweden
Peter A Williams	The North East Wales Institute, Deeside, UK

THE CELLUCON CONFERENCES

- | | |
|-------------------------------------|---|
| 1984 Cellucon '84 UK | CELLULOSE AND ITS DERIVATIVES
Chemistry, Biochemistry and Applications |
| 1986 Cellucon '86 UK | WOOD AND CELLULOSICS
Industrial Technology, Biotechnology,
Structure and Properties |
| 1987 Cellucon '88 Japan | CELLULOSICS AND WOOD
Fundamentals and Applications |
| 1989 Cellucon '89 UK | CELLULOSE: SOURCES AND
EXPLOITATION
Industrial Utilisation, Biotechnology and
Physico-Chemical Properties |
| 1990 Cellucon '90
Czechoslovakia | CELLULOSE
New Trends in the Complex Utilisation of
Lignocellulosics (Phytomass) |
| 1991 Cellucon '91 USA | CELLULOSE
A Joint Meeting of: ACS Cellulose, Paper and
Textile Division, The Cellucon Trust, and 11th
Syracuse Cellulose Conference |
| 1992 Cellucon '92 UK | SELECTIVE PURIFICATION AND
SEPARATION PROCESSES
The Role of Cellulosic Materials |
| 1993 Cellucon '93 Sweden | CELLULOSE AND CELLULOSE
DERIVATIVES
Physico-Chemical Aspects and Industrial
Applications |
| 1994 Cellucon '94 UK | CHEMISTRY AND PROCESSING OF WOOD
AND PLANT FIBROUS MATERIALS |

The proceedings of conferences prior to 1993 were published by Ellis Horwood, Simon and Schuster International Group, Market Cross House, Cooper Street, Chichester, West Sussex, PO19 1EB, England.

THE CELLUCON TRUST is a registered charity, UK Registration No: 328582 and a company limited by guarantee, UK Registration No: 2483804 with its registered offices at The School of Chemistry, The University of Birmingham, Birmingham, B15 2TT, England.

CONTENTS

Preface	xv
PART 1: BIOSYNTHESIS AND BIODEGRADATION OF CELLULOSE	1
1 Cellulose production by <i>Acetobacter xylinum</i> in the presence of cellulase	3
T Nakamura, K Tajima, M Fujiwara, M Takai and J Hayashi	
2 Synthesis and characterization of bacterial cellulose composite (BCC)	9
K Tajima, M Fujiwara, M Takai and J Hayashi	
3 Effect of the process of biosynthesis on molecular properties of bacterial cellulose	15
H Struszczyk, K Wrześniewska-Tosik, D Cienchańska and E Wesolowska	
4 Direct soluble cellulose of <i>Celsol</i> : properties and behaviour	29
H Struszczyk, D Cienchańska, D Wawro, P Nousiainen and M Matero	
5 Hydrolysis of cellulose and cellooligosaccharides catalysed by cellobiohydrolase II studied by proton NMR and HPLC	37
A Teleman, A Valkeajärvi, A Koivula, L Ruohonen and T Drakenberg	
6 Modification of pine kraft pulp using hydrolytic and oxidizing enzymes	43
M-L Niku-Paavola, M Ranua, A Suurnäkki and A Kantelinen	
PART 2: STRUCTURE AND REACTIVITY OF CELLULOSE	49
7 Packing energy calculations on the crystalline structure of cellulose I	51
A Aabloo, A D French and R-H Mikelsaar	
8 Molecular modelling of parallel and antiparallel structure of native cellulose	57
R-H Mikelsaar and A Aabloo	
9 Cellulose I crystallinity as determined with diffuse reflectance Fourier transform infrared spectrometry and wide angle X-ray scattering	63
S H D Hulleman, J M van Hazendonk and J E G van Dam	
10 Order of crystalline cellulose detected with the atomic force microscopy (AFM)	69
L Kuutti, J Pere, J Peltonen and O Teleman	

11	Structural changes of cellulose and their effects on the OH/CH₂ valency vibration range in FTIR spectra	75
	D Fengel	
12	Structural change of cellulose polymorphs by milling	85
	K Kimura, Y Shimizu and J Hayashi	
13	Structural characterisation of lignocellulosic samples using ¹³C-CP/MAS-NMR-spectroscopy and chemometrics	93
	H Lennholm and T Iversen	
14	A microcalorimetric technique for the study of water vapour sorption on cellulose materials	101
	K Bogolitsyn, N Volkova and I Wadsö	
15	A method for the determination of the surface tension of cellulosic fibres in their natural state and its relation with chemical composition	107
	J M van Hazendonk, J C van der Putten and J T F Keurentjes	
16	The influence of cellulose degradation on insulation life in power transformers	115
	A M Emsley	
17	Thermocatalytic destruction of cellulose	125
	G Dobele, T Dizhbite, G Rossinskaya and G Telysheva	
18	Solubility of cellulose and its derivatives	131
	A M Boчек, G A Petropavlovsky and A V Yakimansky	
 PART 3: DERIVATIVES OF CELLULOSE AND THEIR PROPERTIES		
		139
19	Derivatisation of cellulose in homogeneous reaction	141
	M Diamantoglou and E F Kundinger	
20	¹³C NMR spectroscopic studies on regioselective derivatization of cellulose	153
	I Nehls, B Philipp and W Wagenknecht	
21	Investigations on homogeneous synthesis of carboxy group-containing cellulose derivatives and the determination of the substituent distribution using HPLC	161
	T J Heinze, U Erler and D Klemm	
22	Preparation of new unsaturated polysaccharide derivatives and investigation of crosslinking reactions	169
	D Klemm and S Vogt	
23	Analysis of carboxymethyl cellulose heterogeneity by sedimentation transport in water cadoxen	177
	P N Lavrenko, O V Okatova, B Philipp and H Dautzenberg	
24	New metallic derivatives of cellulose. Compounds of microcrystalline cellulose and potassium	185
	N E Kotelnikova, D Fengel, V P Kotelnikov and M Stoll	
25	Structure of cellulose-polyacrylamide graft copolymers	191
	S I Klenin, E N Bykova, S F Petrova and V A Molotkov	

26	Hydrogels of carboxymethylcellulose and bischloroformate diethylene glycol	199
	R Pernikis and B Lazdina	
27	Some aspects of cellulose carbamate	207
	H Struszczyk and A Urbanowski	
28	Investigations of amidation of C-6-carboxycellulose	213
	K Rahn, T Heinze and D Klemm	
29	Effects of solvent addition to acetylation medium on cellulose triacetate prepared from low-grade dissolving pulp	219
	S Saka and T Takahashi	
30	Photofunctional cellulosic materials	227
	K Arai and S Sano	
31	Reactions of bromodeoxycellulose with various thiols in lithium bromide/<i>N, N</i>-dimethylacetamide	233
	N Aoki, K Furuhata and M Sakamoto	
32	Investigation of cellulose derivatives. Method of obtaining the whole molecular characteristics by velocity ultracentrifugation	239
	E B Tarabukina, G M Pavlov and S Ya Frenkel	
33	The degradation of cellulose nitrate in composite museum artefacts: isolation replica cellulose replacement and regular inspection in storage and on display	245
	M Robson	
34	Water sorption by sulfonic and carboxylic cellulose derivatives as a function of counterions and relative humidity	249
	J Berthold, J Desbrières, M Rinaudo and L Salmén	
PART 4: ASSOCIATION THICKENING AND GELATION OF CELLULOSICS, ETC		255
35	Comparative behaviour of cellulose derivatives and microbial polysaccharides. Relation between stiffness and rheological properties	257
	M Rinaudo	
36	Xanthan the natural water soluble cellulose derivative	265
	B E Christensen, B T Stokke and O Smidsrød	
37	Effect of temperature of high-methoxyl pectin gelation	279
	J A Lopes da Silva and M P Goncalves	
38	Phase behaviour of mixtures of associative polyelectrolyte with oppositely charged surfactant	287
	F Guillemet, L Piculell, S Nilsson and B Lindman	
39	The interaction of amphiphiles with polysaccharides	295
	K Shirahama, S Sato, L Yang and N Takisawa	
40	Interaction between nonionic polymers or surfactants and ethylhydroxyethylcellulose characterised by Fourier transform NMR self-diffusion	307
	K Zhang, B Lindman and M Jonströmer	

41	Formation of hydrogen-bonding polymer complex gels from carboxymethylcellulose and poly(methacrylic acid)	315
	M Sakamoto, H J Kim, K Mimura, Y J Lee and T Inoue	
42	Effects on phase behaviour and viscosity of hydrophobic modification of a nonionic cellulose ether. Influence of cosolutes	323
	K Thuresson, S Nilsson and B Lindman	
43	Structure and solution properties of modified hydroxyethyl cellulose	331
	U Kästner, H Hoffman, R Dönges and R Ehrler	
44	Intra- and intermolecular hydrophobic associations in aqueous solutions of amphiphilic derivatives of alginate	339
	A Siquin, P Hubert and E Dellacherie	
45	Fluorescence studies of cellulose ethers in aqueous solution and in films	345
	F M Winnik	
46	Modification of cellulose-based polyelectrolyte adlayer by surfactant. Null ellipsometry and SFA study	355
	V Shubin and P Petrov	
47	Ellipsometry studies of the interfacial behaviour of ethyl(hydroxyethyl)cellulose	363
	F Tiberg and M Malmsten	
PART 5: APPLICATIONS OF CELLULOSICS		371
48	Chiral nematic suspensions of cellulose	373
	J-F Revol, L Godbout, X-M Dong and D G Gray	
49	Novel results of structural investigations on crystalline and liquid crystalline cellulose derivatives and their potential application	381
	P Zugenmaier	
50	Flow-induced structures in isotropic and anisotropic cellulose derivative blends	393
	S G James, J Schatzle, V Tsakalos, E Peuvrel-Disdier and P Navard	
51	Shear induced texture of lyotropic hydroxypropyl cellulose in flexible polyester resin	401
	M Mucha and Z Kotarski	
52	Studies on membranes blended with cellulose cuoxam/casein	407
	L Zhang, G Yang and L Xiao	
53	On the use of clouding polymers for purifying chemical systems	417
	G Karlström, H-O Johansson and F Tjerneld	
54	Surfaces coated with ethyl(hydroxyethyl) cellulose: temperature effects on adsorption and interaction	425
	P M Claesson and M Malmsten	
55	Sodium cellulose sulphate as a component for polyelectrolyte complex formation—preparation, characterisation, testing	435
	H Dautzenberg, B Lukanoff and K Neubauer	

56	Porous cellulose matrices—a novel excipient in pharmaceutical formulation	445
	R Davidson, H Nyqvist and G Ragnarsson	
57	Cellulose ethers for cement extrusion	453
	D Schweizer and C Sorg	
58	Water-soluble polymers in tunnelling and slurry supported excavations	463
	S A Jefferis	
59	Larch wood polysaccharides as the potential raw material for improvement of cellulose materials and porous ceramic properties	471
	F Kurgan and R Belodubrovskiy	
60	Rheology of cellulose viscose	475
	B Lönnberg, S Rosenberg and K Lönnqvist	
PART 6: WOOD, PULP AND FIBRES		483
61	The effect of chlorine-free bleaching of dissolving pulp from Siberian wood species on structural changes and its properties	485
	R Belodubrovskiy, V Kosheleva, O Zarudskaia, L Zvezdina and M Lazareva	
62	Some aspects of lignin modification	491
	K Wrzesniewska-Tosik and H Struszczyk	
63	Thermodynamics of the wood matrix state	499
	K Bogolitsyn	
64	Effect of grinding on structure and reactivity of pulps	507
	H Schleicher and J Kunze	
65	Cellulose recrystallization in the alkaline pulping of wood	517
	E Evstigneyev and A Shashilov	
66	Wide-angle X-ray and solid state ¹³C-NMR studies of cellulose alkalization	523
	H P Fink, E Walenta, J Kunze and G Mann	
67	The effect of refining in the fibre structure and properties in unbleached eucalypt pulps	529
	J Gominho and H Pereira	
68	Biological delignification of Brazilian lignocellulosic residues	535
	S P D'O Barreto, A C D Coelho, J F Kennedy, J L Lima Filho, E H M Melo and M Paterson	
69	Investigations of cellulose and lignins by molecular hydrodynamic methods	541
	G Pavlov	
70	The reactivity of chlorine-free bleached dissolving pulp in respect to its chemical processing	547
	K Fischer and I Schmidt	
71	The effect of plasma-chemical treatment on the properties of cellulosic materials	555
	T Mironova and R Belodubrovskiy	

72	Spinning of fibres through the N-methylmorpholine-N-oxide process	561
	S A Mortimer and A Peguy	
	Cellucon '93 participants	569
	Index	583

PREFACE

Scandinavia, the University and city of Lund brought a very special flavour to Cellucon. The Scandinavian cellulose scientists and those of the neighbouring countries of Russia and the former Soviet Union all made a very special contribution. The result is this excellent volume, which reviews particularly the more physical aspects of cellulose chemistry.

Increasingly cellulose is providing the basic structure for a wide range of end products. The production of viscose and paper remains a major pathway for the utilisation of wood pulp. Environmental stringencies have imposed greater technical and economic burdens on the processor. This volume describes how ingeniously they are coming to terms with these new challenges. Radiation modification, for example, opens up the cellulose structure, enabling less carbon disulphide and sodium hydroxide to be needed for viscose production. The environmental load, and consequent costs are also reduced. Other grinding technologies can achieve similar results and chlorine-free bleaching overcomes another obstacle.

Chemical modification too has proceeded apace. There are consequent end uses in novel fibers, pharmaceuticals, drug delivery systems, and cross-linked hydrogels. There is a major section of this volume devoted to new cellulose derivatives, applications and gels. Biodegradable and biocompatible products too are identified.

No meeting on cellulose would be complete without a consideration of the role of cellulose as associative, thickening and gelation agents. The detailed rheological behaviour and phase separation effects needed to produce specific results have also been discussed extensively in this volume.

The study of the structural aspects of cellulose continues to be an active area of scientific research, with new spectroscopic and computer systems making a markedly significant contribution. In many ways those studying cellulose structure remain a race apart. Consequently, it is most valuable to have recorded succinctly here their latest views, so that those generalists amongst us can keep up with their developing ideas.

New solvent systems have also contributed greatly to the fabrication of new cellulosic fibers and none more than the morpholine oxides. These are also included.

It is fascinating to observe how the scope of cellulose chemistry and technology has now extended so widely, from the use of cellulose ethers for cement extrusion, tunnelling and slurry supported excavations to the biosynthesis of new celluloses. This volume, like its predecessors will keep all concerned up to date with the newer cellulosic advances.

Finally, mention must be made of the fellowship and hospitality of our Swedish hosts. We all greatly enjoyed the occasion. The Cellucon family has now grown to include almost all countries of the world. This volume testifies to the buoyancy of the subject. It has been transformed from the *Cinderella* of Chemistry in the late 1960s to now being the *Belle of the Ball!* Innovation and application are clearly demonstrated here. The Cellucon Trust is pleased to continue to promote the continuing development of the subject.

Glyn O Phillips
Chairman, Cellucon Trust

Professor Bjorn Lindman
Chairman, Cellucon '93 Organising Committee

Part 1:
Biosynthesis and biodegradation
of cellulose

1 Cellulose production by *Acetobacter xylinum* in the presence of cellulase

T Nakamura, K Tajima, M Fujiwara, M Takai and J Hayashi –
Department of Applied Chemistry, Faculty of Engineering, Hokkaido
University, Sapporo, Japan

ABSTRACT

The cellulose productivity by *Acetobacter xylinum*, cellulose producing bacteria, is enhanced by a small amount of heat-denatured cellulase. Effect of an endoglucanase, two exoglucanases and two β -D-glucosidases, purified from a commercial cellulase preparation of *Trichoderma viride* using anion exchange column Mono Q and gel filtration column Superdex 75, has been studied on cellulose production. The heat-denatured cellulase components showed a little enhancement of cellulose productivity compared with the standard culture. In the native state, the β -D-glucosidase fraction is the most effective component for cellulose production. These results suggest that enhancement of cellulose productivity by heat-denatured cellulase mainly result from β -D-glucosidase component in the commercial cellulase.

INTRODUCTION

A kind of *A.xylinum* produces pure cellulose without lignin, hemicellulose or pectic substances as compared to green plant celluloses.[1] The cellulose is called bacterial cellulose(BC) or biocellulose. Although the BC has superior mechanical properties such as Young's modulus compared with green plant celluloses, it has few commercial applications[2] due to its high price. The BC productivity is less than 15% yield based on sugars. Therefore it must be enhanced for reducing cost.

We have recently found the fact that cellulose biosynthesis by *A.xylinum* with a small amount of heat-denatured cellulase resulted in enhancement of cellulose productivity. At present the role of that enzyme in culture is not yet well understood. The cellulase, cellulose-hydrolyzing enzyme, consists of three main components: Endoglucanase(EC 3.2.1.4), exoglucanase(EC 3.2.1.91) and β -D-glucosidase(EC 3.2.1.21).[3,4] Endoglucanase and exoglucanase act synergistically to hydrolyze to cellobiose and oligosaccharides.[5] β -D-Glucosidase hydrolyzes oligosugars such as cellobiose or cellotriose to form glucose. There is limited information available on which cellulase components are effective for cellulose biosynthesis by *A.xylinum*.

The first step in a study on the enhancement effect of cellulase components for cellulose production is the isolation of substantial amounts of enzymes of a commercial cellulase preparation derived from *T.viride*. An endoglucanase, two exoglucanases and

4 Biosynthesis and biodegradation of cellulose

The first step in a study on the enhancement effect of cellulase components for cellulose production is the isolation of substantial amounts of enzymes of a commercial cellulase preparation derived from *T. viride*. An endoglucanase, two exoglucanases and two β -D-glucosidases could be detected, and purified from the enzyme preparation using anion exchange and gel filtration columns. The effectiveness of purified enzymes was evaluated by comparison of cellulose yield. In this paper, the effectiveness of the cellulase component and its mechanism have been discussed. Effect of other hydrolases in cellulose biosynthesis, interaction between the enzymes and cellulose have been also described.

MATERIALS AND METHODS

Enzymes

A commercial cellulase preparation of *T. viride* origin, Onozuka R-10, was purchased from YAKULT HONSHA Co., Ltd. Lysozyme, invertase, chitosanase and chitinase preparations were products of Wako pure chemical industries. β -D-Glucosidase commercial preparations, different origin, were products of Wako, Oriental, Toyobo and Sigma.

Cellulase assays

All activities were expressed in International Units(U) mL⁻¹.

Endoglucanase activity; Endoglucanase activity was measured in a mixture containing 2.0mL of a 1.0% carboxymethyl cellulose(Nacalai) solution in 0.05M sodium acetate buffer, pH 5.0 and 0.1mL of enzyme solution. After incubation at 40°C for 10min, the reaction was stopped by addition of dinitrosalicylic acid(DNS) reagent. The mixture was boiled at 100°C for 5min and then cooled to room temperature. Reducing sugars were measured as absorbance at 525nm on a spectrometer(JUSCO UVIDEC-320) and expressed as equivalents of glucose.

Exoglucanase activity; 0.2mL of enzyme solutions were added to 2.0mL 1.0% Avicel cellulose(Merk) suspension in 0.05M sodium acetate buffer, pH 5.0. The reaction mixture was incubated in a shaking incubator at 30°C for 2h. After centrifugation 1.0mL was taken and analyzed for reducing sugars by method of Nelson and Somogyi.[6,7]

β -D-Glucosidase activity; 4-nitrophenyl- β -D-glucopyranoside(4NPG, Sigma) was dissolved in 0.05M sodium acetate buffer, pH 5.0. To 1.0mL of the substrate solution(1mM), 0.1mL of enzyme solution was added and incubated at 40°C for 10min. The amount of released 4-nitrophenol in the reaction mixture was measured at 400nm. 4-Nitrophenol was used as a standard.

Cellulase purification

A crude cellulase was saturated with ammonium sulfate at a 90% saturation. The resulting precipitate was collected by centrifugation(10000g, 30min), dissolved in 20mM Tris HCl buffer, pH 8.0. The solution desalted with ultrafilter units(ADVANTEC UHP-43K) using the ultrafilter(ADVANTEC Q0100) and the enzyme solution was used in the following procedure.

The scheme for purification of cellulase is shown in Fig.1. Anion exchange chromatography was performed on a Mono Q HR 5/5 column(Pharmacia). The column was equilibrated with 20mM Tris-HCl buffer, pH 8.0. The enzyme solution was loaded on the column and eluted with same buffer a linear gradient from 0 to 0.6M sodium chloride, pH 8.0. Protein was detected as absorbance of 280nm with a flow cell. The eluted fractions were analyzed for endoglucanase, exoglucanase and β -D-glucosidase activities[8]. Fractions(1.0mL) were collected at a flow rate of 1.0mL/min.

Gel filtration chromatography was carried out on a Superdex 75 HR 10/30 column(Pharmacia). The enzyme sample was loaded on the column previously equilibrated with 20mM Tris-HCl, 0.1M NaCl buffer, pH 8.0 and eluted with same buffer at a flow rate of 1.0mL/min. After desalting by ultrafiltration, each purified enzyme solution was

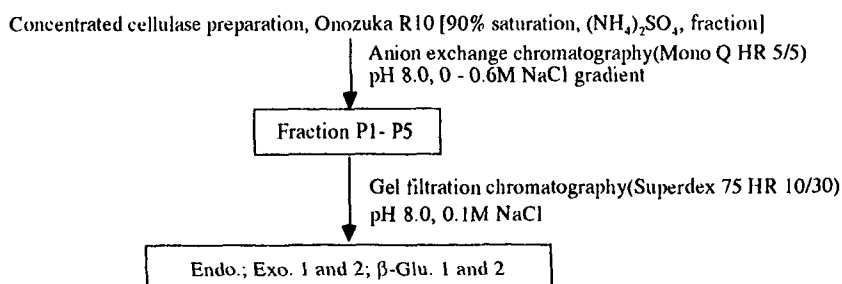


Fig.1 Purification scheme of cellulase components from cellulase preparation. lyophilized.

Cellulose biosynthesis

The bacterial strain used in this study is *Acetobacter xylinum* ATCC 10245. The organisms were cultivated under static condition at 28°C in steam sterilized(121°C, 1.2Kg/cm², 20min) Hestrin and Schramm's (HS) medium[9] or enzyme-containing(0.1% w/v) HS medium for four days. Cellulose membrane produced in 50mL erlenmeyer flasks containing 15mL of the culture was taken out by tweezers and then washed with 1% NaOH solution at room temperature for 3 days. Subsequently the membrane was washed with 1% acetic acid solution for 2 days and then thoroughly washed with distilled water. The cellulose yields were measured by weight after being air dried on glass plates.

Affinity measurements

Lysozyme, invertase, chitinase, chitosanase, β-D-glucosidase or cellulase and 5mM phosphate-citric acid buffer pH 5.0(5.0mL) were mixed with a given amount of Avicel or cellulose powder(Whatman). The enzyme concentration was approximately 2mg/ mL. Incubation took place on a shaking incubator at 50°C for 50h. The samples were centrifuged(10000g, 15min), the supernatant was analyzed as nonadsorbed protein. Protein content was measured by absorbance at 280nm. Enzyme adsorbed on cellulose was estimated by subtracting the amount of dissolved protein from the values obtained in a similar experiment without cellulose.

RESULTS

Purification of cellulase

Initially, cellulase was applied to a Mono Q anion exchange column and separated into five fractions(P1-P5) as shown in Fig.2. Peak P1 and P2 fractions contained relative higher β-D-glucosidase activity and P1 also contained higher exoglucanase activity, whereas P2 was relatively low. Peak P3 and P5 fractions showed exoglucanase activity, and contained β-D-glucosidase activity. Peak P4, containing exoglucanase activity, showed the strongest endoglucanase activity in all peaks. Each fraction(P1-P5) was collected and concentrated in 20mM/ Tris-HCl buffer, pH 8.0 by ultrafiltration for further purification with gel filtration column.

Finally, five components were obtained by this method. The enzymes of peak P1 and P2 were designated β-Glu.1 and β-Glu.2 with high activity towards 4NPG(Table 1), respectively. The enzymes purified from P3 and P5 were called Exo.1 and Exo.2 with high activity towards Avicel. The enzyme of P4 fraction was identified as endoglucanase and was the only fraction acting to CM-cellulose and named Endo. Identification of their purity and determination of MW were measured by SDS-PAGE(data not shown). MW of β-Glu.1 was 76,000 and the ratio to crude enzyme could be calculated by 0.44%. MW of other components were not determined because of contaminants.

Effects of purified cellulase components on cellulose production

Figure 3 shows the yields of cellulose produced in cultures containing the heat-denatured(121°C, 1.2Kg/cm². 20min) cellulase components showed little enhancement of cellulose productivity compared with that of standard culture medium. Especially in the culture containing β-Glu.2, the cellulose productivity was the most enhanced.

The amount of cellulose produced in cultures containing native components is shown in Fig.4. The amount of cellulose obtained from native endoglucanase- or exoglucanase-containing medium was less than that of standard medium because of the hydrolytic effect of the enzyme fraction. On the other hand, in the β-D-glucosidase-containing cultures, the cellulose productivity was considerably enhanced as compared with control. The culture medium contained native β-D-glucosidase gave cellulose about 1.2-1.3 times higher than that of control. The native β-D-glucosidase fractions are more effective for cellulose production by *A.xylinum* than the heat-denatured β-D-glucosidase in contrast to that of endoglucanase or exoglucanases.

In addition to the effectiveness of other β-D-glucosidase, commercial preparations of different origin, was examined as shown in Fig.5. Every β-D-glucosidase-containing medium in native state increased in more cellulose production than control.

Adsorption affinity and cellulose biosynthesis

After incubation of polysaccharide-hydrolyzing enzyme, cellulase, chitosanase, chitinase, invertase, lysozyme or β-D-glucosidase with a given amount of cellulose substrate, the free protein amount P(mg) was determined. The quantity of adsorbed enzyme was calculated, and relative adsorbed amount, P(%), was defined as percent of the amount

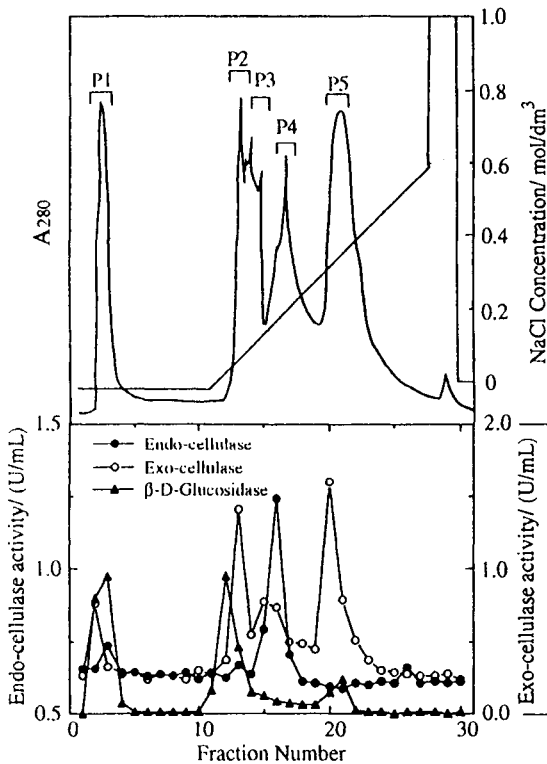


Table 1 Specific activities(U/ mg) of cellulase component.

Fraction	Substrate		
	Avicel	CMC ^{a)}	4NPG ^{b)}
β-Glu.1	1.29	7.05	0.195
β-Glu.2	1.01	5.41	0.202
Exo.1	1.74	8.89	0.192
Exo.2	3.03	8.46	0.188
Endo.	1.28	9.69	0.174

a) Carboxymethylcellulose

b) 4-Nitrophenyl-β-D-glucoside

Fig. 2 Mono Q column chromatography of cellulase, Onozuka R10. Buffer is 20mM Tris-HCl, pH8.0. The column is washed with 7mL of the same buffer and eluted with a linear gradient from 0 to 0.6M sodium chloride. Fractions(1.0mL) are collected at a flow rate of 1.0mL/min.

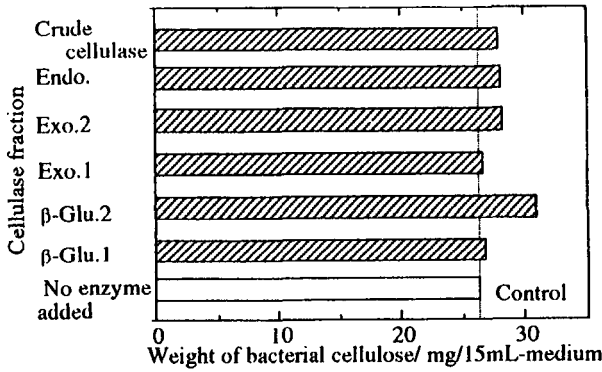


Fig.3 Weight of bacterial cellulose obtained in HS culture medium containing heat-denatured cellulase component.

Enzyme condition: Denatured at 121°C,
1.2Kg/cm², 20min
Enzyme content : 0.1% (w/v)
Incubation time : 96h
Strain : *A.xylinum* ATCC10245

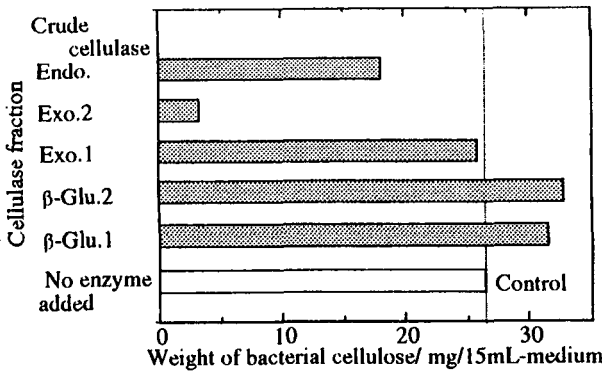


Fig.4 Weight of bacterial cellulose obtained in HS culture medium containing native cellulase component.

Enzyme content : 0.1% (w/v)
Incubation time : 96h
Strain : *A.xylinum* ATCC10245

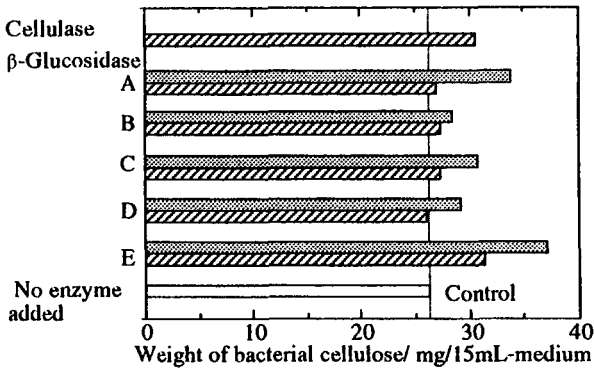


Fig.5 Weight of bacterial cellulose obtained in HS culture medium containing native or heat-denatured β-D-glucosidase.

Enzyme condition: Native state
 Denatured at 121°C,
1.2kg/cm², 20min
β-Glucosidase A : *P. lunatus* (Wako)
B : *C. saccharolyticum* (Sigma)
C : Sweet almond(Oriental)
D : Sweet almond(Toyobo)
E : Sweet almond (Sigma)
Enzyme content : 0.1% (w/v)
Incubation Time : 96h
Strain : *A.xylinum* ATCC10245

adsorbed protein divided by the amount of total protein(adsorbed and nonadsorbed protein). The adsorption data and cellulose yields are summarized in Table 2. It can be seen that the strongest interaction between the enzymes and cellulose was found for heat-denatured cellulase.

Cellulase, β-D-glucosidase and chitosanase showed a relatively large Y_r value. These data suggested that the enzymes are effective for cellulose production by *A.xylinum*, although the affinity of the enzymes to the substrate was considerably lower than those of heat-denatured cellulase.

In the native state, none of the enzymes showed high adsorption affinity to cellulose.

Table 2 Adsorption affinities and cellulose yields of enzymes.

Enzyme	Condition	P(%) ^{a)}		Cellulose yield(mg)	Relative yield ^{b)}
		Avicel	Powder		
Invertase	Native	—	—	25.1	0.98
Chitosanase		2.8	5.6	30.5	1.19
Chitinase		0.0	0.0	26.1	1.02
Lysozyme		0.0	0.0	20.5	0.80
β -Glucosidase		10.9	10.0	29.0	1.13
Cellulase		0.9	0.5	0.0	0.00
Invertase	Denatured	—	—	28.3	1.11
Chitosanase		16.1	14.8	28.3	1.12
Chitinase		18.5	27.2	25.8	1.01
Lysozyme		17.9	17.3	18.1	0.71
β -Glucosidase		12.7	8.0	28.2	1.10
Cellulase		65.4	65.9	29.0	1.13

a) Percentage of adsorbed protein/ total protein

b) Control yield is 25.6mg/ 15mL-medium

DISCUSSION

Bacterial cellulose productivity has been enhanced by the heat-denatured cellulase components as high as 1.3 times of the standard culture. The action of the components for cellulose biosynthesis will be explained in terms of adsorption affinity to the substrate, although the denatured enzymes have no activity towards cellulose.

On the other hand, native exoglucanase or endoglucanase, Exo.1, Exo.2 or Endo., acts as hydrolytic enzyme to degrade cellulose.[10] There is the fact that yields of bacterial cellulose are less than that of control in all cultures of these enzymes as shown in Fig.4. These observations suggested that the enzymes are not effective for cellulose biosynthesis.

In general native β -D-glucosidase has no activity towards crystalline cellulose and no adsorption affinity to the substrate. Thus, it seems that the β -D-glucosidase has no influence on cellulose biosynthesis. However, the β -D-glucosidase was the most effective component for cellulose production, and has no activity to crystalline cellulose(Fig.4 and Table 2). The results suggest that adsorption of enzyme to cellulose do not play an important role in cellulose production. Other β -D-glucosidases prepared from different origin are also effective for cellulose production in the native state. It may be concluded that the β -D-glucosidase has enhancing ability to synthesize cellulose and, therefore, enhancement of cellulose production by the crude cellulase is mainly caused by β -D-glucosidase component. It appears that the interaction between enzyme and bacteria affects cellulose biosynthesis by *A.xylinum*.

References

1. Deinema, M.H. and Zevenhuizen, L.(1971) *Arch.Microbiol.*, 78, 42-57.
2. Yamanaka, S., Watanabe,K., Kitamura, N., Iguchi, M., Mitsuhashi, S. and Uryu,M. (1989) *J.Mat.Sci.*, 24,3141-3145.
3. Flickinger, M.C.(1980) *Biotechnol. Bioeng.*, 22, 27-48.
4. Enari, T.M.(1983) *Micro. Enz. Biotech.*, 183-223.
5. Wood, T.M. and McCrae, S.I.(1978) *Biochem.J.*, 171, 61-72.
6. Somogyi, M.(1952) *J.Biol. Chem.*, 195, 19-23.
7. Nelson, N.(1944) *J.Biol.Chem.*, 153, 375-380.
8. Lars E.R. Berghem, L.Goran Petterson(1973) *Eur.J.Biochem*, 37, 21-30.
9. Hestrin, S. and Schramm(1954) *Biochem.J.*, 58, 345-352.
10. Shewale, J.G.(1982) *J.Biochem.*, 14, 435-443.

2 Synthesis and characterization of bacterial cellulose composite (BCC)

K Tajima, M Fujiwara, M Takai and J Hayashi – Department of Applied Chemistry, Faculty of Engineering, Hokkaido University, Japan

ABSTRACT

In general, biodegradability of a material decreases with an increase in its mechanical strength. Bacterial cellulose (BC) produced by *Acetobacter xylinum* (*A. xylinum*) is a very unique and interesting material, since it has naturally both high mechanical strength and biodegradability. We have succeeded in preparing an incorporated BC (BC composite) with water-soluble polymer, such as carboxymethyl cellulose (CMC) or methyl cellulose (MC) by adding water-soluble polymer into the standard medium of *A. xylinum*. Young's modulus of BC composites was about 1 - 3 times that of normal BC (30 - 40 GPa) and BC composites were almost degraded in soil after 28 days as well as normal BC.

This preparation method has been applied to synthesize a new type of BC having both high biodegradability and other functions.

Abbreviations; BC: Bacterial Cellulose, BCC: Bacterial Cellulose Composite, WSP: water-soluble polymer, MC: methyl cellulose, CMC: carboxymethyl cellulose, DS: degree of substitution

INTRODUCTION

Some species of the gram negative aerobe *Acetobacter xylinum* (*A. xylinum*) have the ability to synthesize cellulose as an extracellular polysaccharide. This polysaccharide is called Bacterial Cellulose (BC). It is very useful for some commercial usage because of its excellent properties such as high mechanical strength, biodegradability and so on. At present from the viewpoint of ecology, good biodegradable polymers replacing the synthetic polymers are widely sought in material industries. BC seems to be a suitable material source as such a polymer for its mechanical strength and high biodegradability. BC can be easily modified during synthesis. For example,

our laboratory has succeeded in preparing a new functional BC composite by the incubation of *A. xylinum* in the medium containing water-soluble polymer, such as CMC, MC and so on [1]. This BC membrane was incorporated with water-soluble polymer and it could function as an ultrafilter membrane. We found that BC composites made by this preparation method have larger mechanical strength. Many researchers [2-10] have used fluorescent brighteners or cellulose derivatives (carboxymethyl cellulose and so on) for clarification of cellulose assembly, and significant progress in elucidating the mechanism and control of cellulose fibrils biogenesis has been made by studying normal and altered cellulose ribbon assembly in *A. xylinum*. However, biodegradabilities and the application of these BC composites as functional materials have not been examined. In this paper, we have studied the BC composite with water-soluble polymer as a biodegradable material in detail. For this purpose, we investigated the identification of water-soluble polymer in BC composite, the content of water-soluble polymer in BC composite, the estimation of mechanical strength, and the biodegradability test.

MATERIALS AND METHODS

Two bacterial strains of *A. xylinum* NBI 1051 or ATCC 10245 were used for BC production. The molecular weight and DS of water-soluble polymers used are shown in Table 1. Dynamic Young's modulus was measured by the vibrating reed method. Biodegradability test was performed by cellulase ONOZUKA R-10 (Yakult Honsha Co., Ltd.) and in the native soil in a beaker.

Table 1 The molecular weight and DS of used water-soluble polymers.

Sample(WSP)	M.W.	DS
MC#15	15,000	1.79-1.83
MC#25	17,000	1.79-1.83
MC#100	26,000	1.79-1.83
MC#400	41,000	1.79-1.83
MC#1500	63,000	1.79-1.83
MC#4000	86,000	1.79-1.83
MC#8000	110,000	1.79-1.83
CMC(Nacalai)	13,500	0.62-0.68

RESULTS AND DISCUSSION

Yield of BC composite and content of water-soluble polymer in BC composite.

The yields of normal BC and BC composites are shown in Fig. 1. The yields of BC composites (MC) were 1.2 - 1.5 times that of normal BC. The yields of BC composites (CMC) were higher than those of BC composites (MC). They were 1.5 - 2.0 times that of normal BC.

The contents of water-soluble polymer in BC composites are shown in Fig. 2. The contents of WSP in BC composite were estimated from elementary analysis. BC composites (MC) contained 10-20 wt% MC and BC composites (CMC) contained 40-45 wt% CMC. This high content of CMC in BC composites (CMC) could be due to electrostatic interaction between cellulose and CMC. The interaction is based on electron-attractivities of carboxymethyl group of CMC. The increase weight of yields for BC composites was greater than the weight of water-soluble polymer incorporated into the BC composite. Ben-Hayyim and Ohad [2] reported that CMC induces the rate of polymerization of

glucose (30%). The hierarchical assembly process contains four steps [9]: (1) the synthesis and extrusion of tactoidal aggregates of parallel glucan chains; (2) the crystallization of adjacent glucan aggregates into 3-4 nm wide microfibrils; (3) the formation along slightly separated groups of extrusion pores of the fibrillar subunits that contain the crystallites; and (4) the fasciation of the subunits to form the composite ribbon. CMC prevents the fasciation of the larger fibrillar subunits [9]. Thus the increases of cellulose yields by the addition of MC or CMC into the medium might be performed by prevention of ribbon assembly, which is slightly rate limiting [5, 8], resulted from adsorption of MC or CMC molecules to microfibrils and bundles of microfibrils.

Mechanical strength of BC composite.

Mechanical strength was estimated by the measurement of dynamic Young's modulus. Dynamic Young's modulus was measured by vibrating reed method. The dynamic Young's modulus of BC composite is shown in Fig. 3. They were the same as or larger than those of normal BC, the maximal value was about three times that of normal BC. On BC composites (MC, 1051), the molecular weight of water-soluble polymer incorporated into BC composite did not affect Young's modulus. In contrast, on BC composites (MC, 10245), a different result was obtained depending on their molecular weights. Young's modulus of BC composites incorporated with MC #1500, #4000 and #8000 were twice that of normal BC. On the other hand, Young's modulus of BC composites incorporated with #15, #25, #100 and #400 were almost similar to that of normal BC. The reason for these results, however, has not been clarified.

Young's modulus of BC is greatly changed according to the methods of drying. For example, heat dried BC have high Young's modulus compared with that of air dried or lyophilized BC. This results from the increase in hydrogen bonding by heating. Thus, it could be thought that the increase of Young's modulus for BC composites originates from the increase of hydrogen bonding among microfibrils or ribbons based on the incorporation of water-soluble polymer. This could be supported by the results obtained from SEM observation (Fig. 3).

Young's modulus of BC composites (CMC, 1051 or 10245) were twice that of normal BC, although the contents in BC composites were very high (40 - 45 wt%, refer to Fig. 6). The significant difference between MC and CMC is in the intense inductive effect of substituent. As mentioned above, CMC binds with cellulose by hydrogen bonding and electrostatic interactions, and these results could be due to the existence of CMC which does not contribute to the increase of hydrogen bonding among ribbons.

Biodegradability of BC composite.

The results of biodegradabilities of normal BC and BC composite (1051) and (10245) are shown in Fig. 4. Both normal BC and BC composite (CMC) were completely degraded by the hydrolysis action of cellulase. On the other hand, BC composites (MC) were partially degraded (20 - 30 wt% in weight) by cellulase. SEM photographs of the surface of BC composites (MC) before degradation and after degradation (at 50 °C, 120 strokes/min, for 48 hr) are shown in Fig. 5. Many pores were observed on the surface of normal BC. However, they were not observed on the surface of BC composites (MC) and BC composites (CMC). Normal BC and BC composites (CMC) were completely degraded by cellulase after 48 hr. On the other hand, BC composites (MC) were partly degraded by cellulase. After incubation, ribbons still remained in the degraded area. When cellulase degrades cellulose, first of all, it has to

attach to the surface of cellulose. However, the surface of cellulose in BC composite is covered with water-soluble polymer binding to cellulose by hydrogen bonding. Therefore, cellulase has to attach to cellulose covered with MC or CMC. Then it has to degrade MC or CMC first. When MC and CMC were individually degraded by cellulase, CMC was degraded but MC was not. The causes of low degradability of MC by cellulase might be attributable to the high DS. Thus, the high enzymatic degradabilities of BC composite (CMC) could be due to the heterogeneous incorporation of CMC into BC and the high degradability of CMC, which is a substrate for determination of endo-cellulase activity, by cellulase. The low enzymatic degradabilities of BC composite (MC) could be due to the highly packed structure observed by SEM and the low degradability of MC by cellulase. These results could suggest that the enzymatic degradabilities of BC will be controlled by the contents, kinds or DS of water-soluble polymer incorporated into BC.

In contrast, on the biodegradation test in soil, there was no great difference between the degradabilities of normal BC, BC composites (MC) and (CMC), and they were almost completely degraded after 4 weeks. This suggests that the soil contains many microorganisms which secrete various enzymes in addition to cellulase-like enzyme.

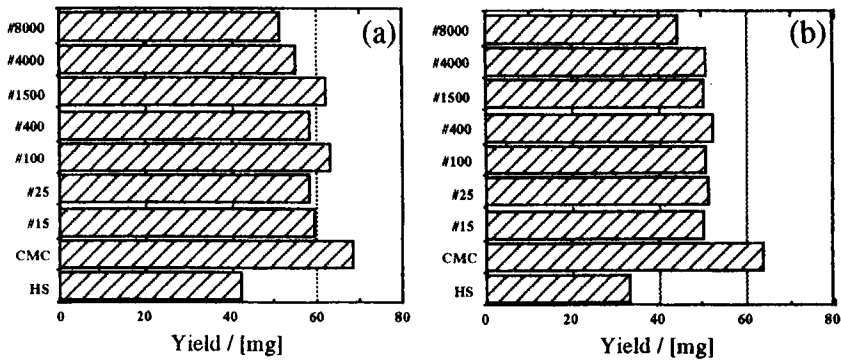


Fig.1 Yield of BC composite; (a): 1051, (b): 10245.

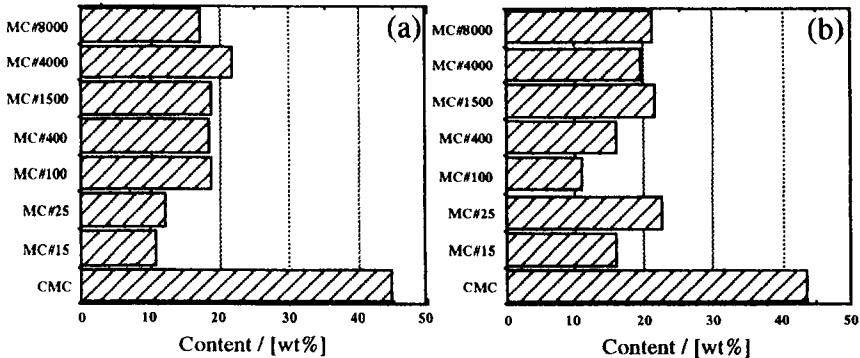


Fig.2 Content of WSP in BC composite; (a): 1051, (b): 10245.

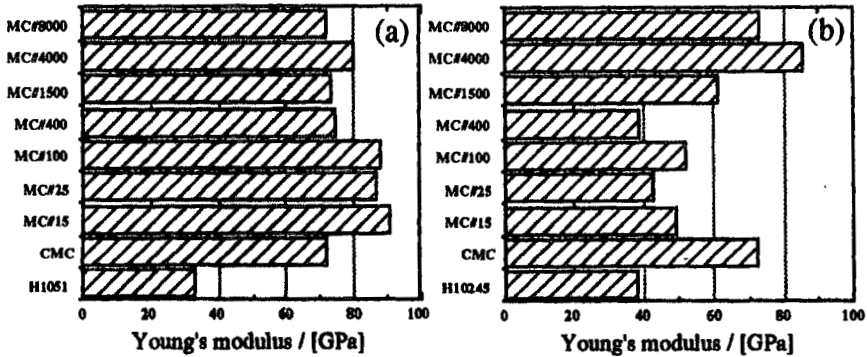


Fig.3 Young's modulus of BC composite; (a): 1051, (b): 10245.

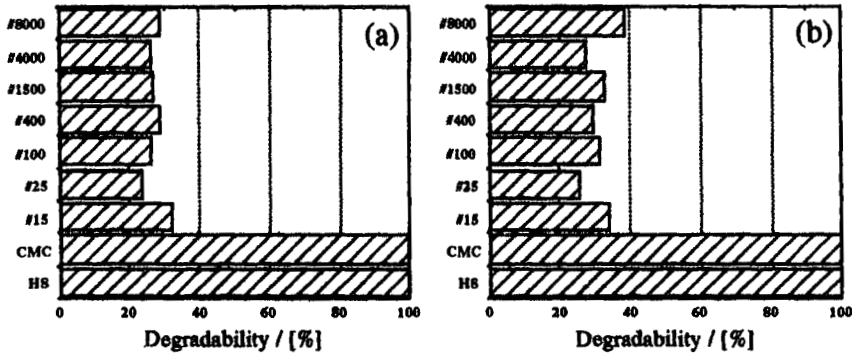


Fig.4 Biodegradability of BC composite; (a): 1051, (b): 10245.

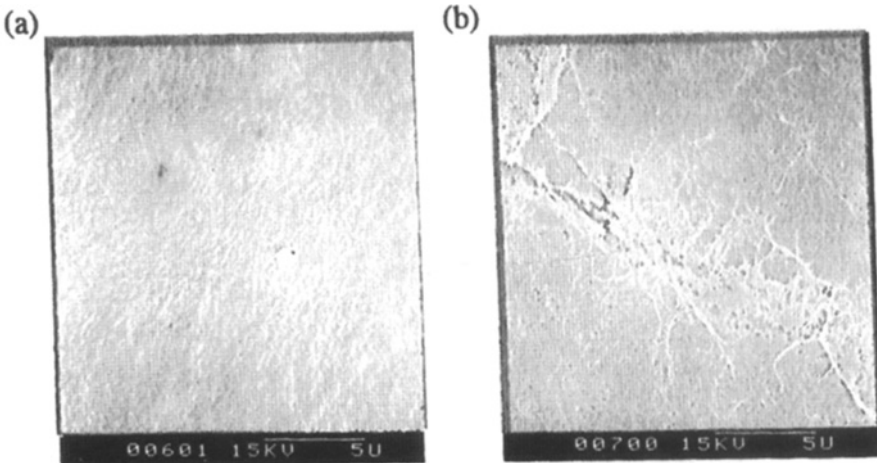


Fig.5 SEM photograph of BC composite (1051, MC#8000);(a): before degradation, (b): after degradation, x 5,000, bar is 5µm

CONCLUSIONS

We obtained the following results;

- (1) BC composite (CMC) had high mechanical strength and high biodegradability by cellulase.
- (2) BC composite (MC) had high mechanical strength and low biodegradability by cellulase.

From these results it was suggested that BC composite (CMC) can be used as a biodegradable material, and biodegradability of BC could be controlled by the incorporation of water-soluble polymer having various DS or different substituent or incorporation of two kinds of water-soluble polymers. Furthermore, this preparation method has been applied to synthesis a new type of BC having high mechanical strength, various biodegradabilities and other functions.

REFERENCES

- (1) Takai, M. *Sen-i Gakkaishi* 1991, 47, 119-129.
- (2) Ben-hayyim, G.; Ohad, I. *J. Cell. Biol.* 1965, 25, 191-207.
- (3) Benziman, M.; Haigler, C. H.; Brown, R. M., Jr.; White, A. R.; Cooper, K. M. *Proc. Natl. Acad. Sci. USA* 1980, 77, 6678-6682.
- (4) Brown, R. M., Jr.; Haigler, C. H.; Cooper, K. M. *Science* 1982, 218, 1141-1142.
- (5) Brown, R. M., Jr.; Haigler, C. H.; Suttie, J.; White, A. R.; Roberts, E.; Smith, C.; Itoh, T.; Cooper, K. M. *J. Appl. Poly. Sci.* 1983, 37, 33-78.
- (6) Haigler, C. H. *Science* 1980, 210, 903-906.
- (7) Haigler, C. H.; Benziman, M. In *Cellulose and Other Natural Polymer Systems*; R. M. Brown Jr., Ed.; Plenum Press: New York, 1982; pp 273-297.
- (8) Haigler, C. H.; White, A. R.; Brown, R. M., Jr.; Cooper, K. M. *J. Cell. Biol.* 1982, 94, 64-68.
- (9) Haigler, C. H. In *Cellulose Chemistry and its Applications*; T. P. Nevell and S. Haig Zeronian, Ed.; Ellis Horwood: New York, 1985; pp 30-83.
- (10) Haigler, C. H.; Chanzy, H. *J. Ultrastruct. Mol. Struct.* 1988, 98, 299-311.

3 Effect of the process of biosynthesis on molecular properties of bacterial cellulose

H Struszczyk, K Wrześniewska-Tosik, D Ciechańska and
E Wesołowska – Institute of Chemical Fibres, 90-570 Lodz,
C Skłodowska 19, Poland

ABSTRACT

Biosynthesis is a promising technique for the manufacture of special polymeric materials having unique properties. In this paper biosynthesis of cellulose with the use of *Acetobacter xylinum* strain in static conditions has been presented and the problem of correlation between some parameters of biosynthesis and chosen properties of cellulose, especially its molecular structure and molecular weight distribution were discussed. Some other properties of bacterial cellulose films, including biodegradability have also been presented.

INTRODUCTION

Recently biotechnological methods of polymer synthesis and transformation have widely been introduced into industry.

This tendency is supported by numerous benefits resulting from the application of biotechnology, such as mild conditions of technological processes, low energy consumption, high safety, low amount of by-products, renewable raw materials, economic aspects and others. One of the main directions of the development of biotechnology is nowadays biosynthesis of protein-type polymers, polysaccharides, cellulose included, as well as high-molecular compounds similar to synthetic polymers e.g. polyhydroxybutyrate [1-4]. Some of the above mentioned polymers - products of biosynthesis - have been characterized in view of their film and fibre-forming properties.

The highly effective strains of microorganisms used in this investigation to obtain macromolecules can be characterized by low nutrient consumption, stability of morphological and physico-chemical attributes as well as by a high rate and yield of metabolite production [4]. Some of the strains applied in the manufacture of bacterial cellulose have already been identified [1,5,6] and *Acetobacter xylinum* strain was determined as the most effective one [1,7,8]. Cellulose produced inside the bacteria cells is released from them in the form of microfibriles having shape of regular ribbons [8]. Numerous valuable properties of bacterial cellulose, such as biocompatibility, high water-sorption, film- and fibre-forming ability, some mechanical characteristics (e.g. high value of Young modulus) make it possible to consider it as a polymer for special application in technology and medicine.

Institute of Chemical Fibres, Lodz, Poland contributes to several long-term projects on special biomaterials for medicine and agriculture. Polymers obtained in

biosynthesis, including bacterial cellulose, seem to be the most suitable high molecular materials for the above mentioned applications. Specific character of biosynthesis process makes it possible to control some properties of the polymer being formed, such as e.g. their molecular structure. In the case of biomaterials their controlled properties play, a particularly significant role.

The aim of this paper is to present some recent results of the investigation into biosynthesis of cellulose with the use of *Acetobacter xylinum* Ax26 strain. The correlation between biosynthesis process parameters and the properties and behaviour of bacterial cellulose, molecular structure included, has been discussed. The results concerning the process of biodegradation were presented in view of the application of the bacterial cellulose in medicine.

EXPERIMENTAL

MATERIALS AND METHODS

Acetobacter xylinum Ax26 strain produced in the Institute of Microbiology and Fermentation, Technical University of Lodz, Poland has been used for the manufacture of bacterial cellulose. Other samples of cellulose such as softwood cellulose pulp of Fibrenier, cotton linters, regenerated cellulose from viscose fibres and microcrystalline cellulose 402 type, Microtechnic, Germany have been used to draw a comparison.

For the impregnation of the bacterial cellulose film, microcrystalline chitosan aqueous dispersion produced in the Institute of Chemical Fibres, Lodz by means of the original method [9] has been applied [10]. The dispersion of microcrystalline chitosan contained 3.17 wt.% polymer

18 Biosynthesis and biodegradation of cellulose

and had a viscometric average molecular weight of $\bar{M}_V = 4.47 \times 10^5$, deacetylation degree of 71% and water retention value of 1295%.

Bacterial cellulose was produced by a modified static method using a culture solution with pH = 6.0 containing glucose, peptone, yeast extract, disodium phosphate, citric acid and ethyl alcohol as a modifying agent. The product of biosynthesis obtained in the form of a film was washed out in sodium hydroxide solution, next in distilled water and then dried.

Basic properties of bacterial cellulose such as average molecular weight, crystallinity index and water retention value have been determined according to the previously described methods [1,11]. In order to estimate the properties of microcrystalline chitosan the methods previously described [9] have been applied.

Molecular weight distribution (MWD) of the polymers under investigation has been determined by gel permeation chromatography (GPC) using a Hewlett-Packard HP 1050 gel chromatograph with polystyrene columns from Polymer Lab. for measurements.

The biodegradation process of bacterial cellulose has been examined in a buffer solution of pH = 7.3 containing NaCl, KCl, $\text{Ca}(\text{CH}_3\text{COO})_2$, MgSO_4 and Na_2HPO_4 at $37^\circ \pm 0.1^\circ\text{C}$ in the presence of lysozyme with concentration of 100 $\mu\text{g}/\text{ml}$.

RESULTS AND DISCUSSION

The demand for special polymeric materials applicable in medicine and technology includes also products of biosynthesis of selected high molecular compounds. Unique properties of biosynthetic cellulose, i.e. its

biocompatibility, high water sorption, excellent adhesive properties and special mechanical characteristics as well as the existence of effective methods of its manufacture promote the enlargement of its application. The most important attribute of biosynthetic cellulose is the correlation between its properties and the conditions of biosynthesis. Continuous control of the biosynthesis process makes it possible to obtain products of the exactly required properties.

Many factors can affect the characteristics of bacterial cellulose. In Table 1 the effect of glucose concentration, being a carbon source, on some properties of bacterial cellulose and on the yield of biosynthesis are presented.

Table 1. Effect of glucose concentration^a in a culture solution on bacterial cellulose properties.

Glucose concentration	Yield of α -cellulose	Properties of bacterial cellulose				
		α -cellulose content	DP ^b	GPC data		
, %	, g/l			Mn $\times 10^{-4}$	Mw $\times 10^{-4}$	Pd
1.0	0.69	86	951	-	-	-
1.5	0.72	89	1124	7.2	21.9	3.1
2.0	0.61	82	1228	9.6	20.9	2.2
2.5	0.50	71	-	8.8	21.1	2.4
3.0	0.61	92	1176	7.2	23.4	3.2

Pd - polydispersity

a - biosynthesis for 120 h at temperature of 30°C.

b - by EWNN viscosimetric method.

As it can be seen from Table 1 the increase of glucose concentration in a culture solution affects both α -cellulose content in the product and its molecular weight. When the highest concentration of glucose has been applied a slight reduction of average molecular weight and a simultaneous increase of polydispersity value can be

observed. Thus, the optimum concentration of glucose in a culture solution is situated within the range of 2-3%. The search for other types of carbon sources, able to form cellulose chains in a culture solution is one of the targets of our studies. Recently we have selected ethyl alcohol as a good and effective additional low-molecular source of carbon, useful for biosynthesis of cellulose. The results of biosynthesis carried out in the presence of ethyl alcohol are presented in Tables 2-4. For comparison the results of biosynthesis of bacterial cellulose in different time obtained in the absence of ethanol are summarized in Table 5.

Table 2. Effect of biosynthesis^a time in presence of ethanol on bacterial cellulose properties.

Biosynthesis time , h	Yield of α -cellulose , g/l	Bacterial cellulose properties		
		α -cellulose content , %	CrI , %	DP* , %
48	0.35	65.7	47	-
72	0.88	81.0	52	370
96	0.77	75.6	58	760
120	1.25	77.0	52	1000
144	1.40	71.7	55	1100
168	1.40	77.5	69	1170

* - by EWNN viscosimetric method.

a - in a presence of 1 wt.% of ethanol; glucose concentration of 2% at temperature of 30°C.

As it can be seen the average molecular weight of bacterial cellulose, obtained in the culture solution without alcohol, increases gradually with the time of biosynthesis whilst polydispersity undergoes reduction (Table 5).

The introduction of an additional carbon source of ethanol

causes a significant rise of yield of biosynthesis as well as growth of crystallinity index of cellulose being formed (Tables 2 and 3). As shown in Table 4, for the longest duration of process of 168 hrs a slight decrease of average molecular weights is observed. It is probably caused by degradation activity of cellulolytic enzymes being formed in the course of the process.

Table 3. Effect of biosynthesis^a time in presence of ethanol on bacterial cellulose.

Biosynthesis time , h	Yield of α -cellulose , g/l	Bacterial cellulose properties		
		α -cellulose content , %	CrI , %	DP* , %
48	0.40	74.2	46	-
72	1.10	77.8	40	290
96	1.50	75.7	45	750
120	2.20	78.5	60	790
144	2.10	78.5	56	1340
168	2.00	74.9	73	1220

* - by EWNN viscosimetric method.

a - in a presence of 2 wt.% of ethanol; glucose concentration of 2% at temperature of 30°C.

The samples of bacterial cellulose obtained in the presence of ethanol are characterized by the multilayer structure of a formed film.

The optimization of biosynthesis conditions on a laboratory scale when *Acetobacter xylinum* Ax26 is used makes it possible to produce a cellulose film of good mechanical properties in comparison with the other cellulose films (Table 6).

Table 4. Effect of biosynthesis time in presence of 2 wt.% of ethanol on distribution of molecular weight of bacterial cellulose.

Biosynthesis time	Ethanol content	Bacterial cellulose properties		
, %	, g/l	$\overline{M}_n \times 10^{-4}$	$\overline{M}_w \times 10^{-4}$	Pd
48	2.0	-	-	-
72	2.0	-	-	-
96	2.0	8.9	15.8	1.78
120	2.0	12.9	19.6	1.52
144	2.0	14.2	20.8	1.46
168	2.0	6.3	15.7	2.46

Table 5. Effect of biosynthesis^a time on bacterial cellulose properties.

Biosynthesis time	Yield of α -cellulose	Properties of bacterial cellulose				
, %	, g/l	α -cellulose content	CrI	GPC data		
, %	, g/l	, %	, %	$\overline{M}_n \times 10^{-4}$	$\overline{M}_w \times 10^{-4}$	Pd
24	0.12	-	-	-	-	-
48	0.91	98	65	4.5	20.7	4.6
72	0.92	94	36	6.5	20.8	3.8
96	0.89	99	27	7.3	22.1	3.0
144	0.87	93	44	7.4	23.9	3.3
168	0.89	99	38	10.2	26.3	2.6
192	0.94	89	30	9.5	23.7	2.5

a - with a glucose concentration of 2 wt.% at temperature of 30°C.

Pd - polydispersity

The advantages of bacterial cellulose can be pointed out when confronting it with the other different samples of cellulose, such as a pulp, regenerated cellulose, cotton linters and microcrystalline cellulose (Tables 7 and 8).

As it can be seen from Table 7 bacterial cellulose is characterized by high water retention value, the highest among all the cellulose samples.

The α -cellulose content in bacterial cellulose is comparable with the analogous value for cotton linters.

Table 6. Some mechanical and super-molecular properties of different cellulosic films.

Type of film	Mechanical properties		Molecular properties		
	Tenacity , MPa	Elongation , %	DP [*]	CrI , %	α -cellulose content , %
Bacterial	47.4	10.5	1435	77.5	95.1
non-oriented	15.7	40.7	346	49.0	93.0
Viscose					
oriented	45.0	14.0	346	56.0	93.0

* - by EWNN viscosimetric method.

Bacterial cellulose should, first of all, be applied in medicine. Its biodegradability and sorption properties play the most important role here, e.g. for the manufacturing of wound dressings. In view of this application the samples of cellulose films from biosynthesis were the subject of biodegradation tests in a buffer solution containing lysozyme enzyme. Three kinds of materials have been tested i.e. bacterial cellulose film, the same film impregnated with microcrystalline chitosan and microcrystalline chitosan film. The results of tests have been presented in Tables 9 and 10.

It is generally known that chitosan, especially microcrystalline chitosan, is a bioactive and biodegradable polymeric material of natural origin proposed for medical application, mainly to use in the

Table 7. Some properties of different types of cellulosic materials.

Cellulosic material type	Properties of cellulose			
	α -cellulose content, %	CrI, %	WRV, %	DP*
Bacterial cellulose ^a	91.6	87	153	1450
Softwood cellulosic pulp of Fibrenier	95.1	75	53	760
Regenerated cellulose from viscose fibres	91.6	52	87	300
Cotton linters	90.9	72	37	1200
Microcrystalline cellulose of Micro-technic 402 type	88.0	69	60	530

a - obtained by biosynthesis for 120 h in presence of 2% glucose at temperature 30°C.

* - by EWNN viscosimetric method.

wound healing areas [12-14]. The bacterial cellulose matrix covered with microcrystalline chitosan is one of the new biomaterials tested now in the Institute of Chemical Fibres, Lodz, Poland.

Bacterial cellulose films subjected to the action of an enzyme undergo degradation process more slowly in comparison with a microcrystalline chitosan film (Tables 9 and 10).

The examination of a cellulose film covered with microcrystalline chitosan points out, however, that its biodegradation is slower even than the degradation of a cellulose film. This phenomenon can be explained by the protective action of microcrystalline chitosan in relation to a bacterial cellulose matrix. Such behaviour of systems

Table 8. Some molecular parameters of different types of cellulosic materials.

Type of cellulosic materials	Parameters		
	$M_n \times 10^{-4}$	$M_w \times 10^{-4}$	Pd
Bacterial cellulose	9.19	23.94	2.6
Softwood cellulose pulp of Fibrenier	4.69	11.30	2.4
Regenerated cellulose from viscose fibres	2.01	3.62	1.8
Cotton linters	10.14	22.51	2.2
Microcrystalline cellulose of Microtechnic 402 type	2.49	8.54	3.4

Table 9. Weight loss of polymeric materials during biodegradation in presence of lysozyme* .

Type of polymeric material	Weight loss of polymeric material (%), after (days)	
	3	7
Bacterial cellulosic film ^a	11.9	18.9
Bacterial cellulosic film impregnated by 1 wt.% of MCCh	4.9	6.5
Microcrystalline chitosan (MCCh) film	31.8	37.4

a - obtained for 120 h at temperature of 30°C; glucose concentration of 2%.

* - 100 µg/ml

in biodegradation conditions is very promising for practical applications.

Table 10. Some molecular parameters of different polymeric materials during biodegradation in presence of lysozyme*.

Type of polymeric material	Molecular parameters of bacterial cellulose, after (days)								
	0			3			7		
	Mn x10 ⁻⁴	Mw x10 ⁻⁴	Pd	Mn x10 ⁻⁴	Mw x10 ⁻⁴	Pd	Mn x10 ⁻⁴	Mw x10 ⁻⁴	Pd
Bacterial cellulosic film ^a	9.2	23.3	2.6	3.7	14.7	4.0	3.9	12.7	3.3
Bacterial cellulosic film impregnated by 1 wt.% of MCCh	9.2	23.3	2.6	9.9	15.7	1.6	4.7	14.8	3.0

a - obtained for 120 h at temperature of 30°C; glucose concentration of 2%.

* - 100 µg/ml

CONCLUSIONS

1. Biosynthesis of cellulose with the use of *Acetobacter xylinum* Ax26 strain carried out in the elaborated optimum conditions seems to be a promising and useful method to obtain polymers having special, valuable and programmable properties such as biodegradability, biocompatibility, high sorption and high adhesion as well as satisfactory mechanical properties of a film.
2. Parameters of biosynthesis process i.e. culture solution composition, carbon sources, duration of the process affect properties of bacterial cellulose being formed, molecular structure included.

3. Bacterial cellulose manifests considerable advantages in comparison with other kinds of cellulose due to its biodegradability in the enzymatic medium. The introduction of some additives such as microcrystalline chitosan to a bacterial cellulose film leads to obtaining valuable materials which can be applied in medicine.

REFERENCES

1. International Conference of Cellulose'91, New Orleans, USA, December 6-9th, 1991. Conference, New Orleans, USA, 1991.
2. F. Paul, S. Morin, P. Monsan, *Biotechnol. Adv.*, 4, 245 (1986).
3. S. Aiba, A. Humphrey, N.F. Millis, *Inżynieria Biochemiczna*, WNT, Warszawa, 1977.
4. Biosynteza polimerów włóknotwórczych (Biosynthesis of Fibre-Forming Polymers), monography, Institute of Chemical Fibres, Lodz, Poland, 1989.
5. J.K. Baird, P.A. Standford, I.W. Cottrell, *Biotechnology*, 1, 778 (1983).
6. I.W. Sutherland, *Biotechnology*, 3, 531 (1983).
7. K. Zaar, *J. Cell. Biol.*, 80, 773 (1979).
8. F.C. Lui, R.M. Brown, J.B. Copper, *Science*, 230, 822 (1985).
9. H. Struszczyk, *J. of Polymer Sci.*, 33, 177 (1987).
10. Finn. Pat. 77902 (1986).
11. L. Check, H. Struszczyk, *Cellulose Chemistry and Technology*, 14, 893 (1980).
12. R.A.A. Muzzarelli, *Chitin*, Pergamon Press, New York, 1978.
13. H. Struszczyk, D. Wawro and A. Niekraszewicz,

- "Biodegradation of Chitosan Fibres", Ch.J.Brine,
P.A.Sandford, J.P.Zikakis, ed. in "Advances in Chitin
and Chitosan", Elsevier App. Sci., London, New York,
1992.Proceedings of 5th International Conference on
Chitin/Chitosan, Princenton,N.J. USA, 1991.
14. H. Struszczyk, A. Niekraszewicz, Chitin Enzymology
Symposium, Senigallia, Italy, 1993.

4 Direct soluble cellulose of Celsol: properties and behaviour

H Struszczyk, D Ciechańska and D Wawro – Institute of Chemical Fibres, 90-570 Lodz, ul M C Skłodowska 19/27, Poland

P Nousiainen and M Matero – Tampere University of Technology, Fiber, Textile and Clothing Science, Tampere, Finland

ABSTRACT

Biotransformation of cellulose pulps creates a new modern cellulosic raw material suitable for direct dissolution in aqueous sodium hydroxide. A new method of cellulosic fibre and film manufacture, alternative to the viscose technology, was studied. Some properties of Celsol direct soluble cellulose, including its super-molecular parameters as well as useful behaviour such as solubility or spinnability, are presented.

INTRODUCTION

The viscose industry has been causing several environmental problems resulting from the use of carbon disulphide as a main reactant for converting the cellulose into cellulose xanthate. However, the demand for

cellulosic fibres does not seem likely to decline for the next few decades. Two main ways of new alternative methods for cellulosic fibres and films manufacture without carbon disulphide use is presently under intensive research and development to achieve:

- direct dissolution of cellulose pulp in the organic solvents, mainly in N,N'-methyldimorpholine oxide (Tencel) [1-3] or in inorganic solvents such as sodium hydroxide solution [4-5]
- cellulose derivatives soluble in aqueous sodium hydroxide solution such as cellulose carbamate [4,5-7].

Dissolving the cellulose pulp directly into an aqueous sodium hydroxide seems to be a promising perspective technique for transformation of cellulose into useful cellulosic fibres, films and other products [8]. This method should solve some problems still caused by above technologies such as organic solvent regeneration or cellulose degradation. The aim of this paper is to present some results of cellulose pulp biotransformation resulting on the modified cellulose structure and properties including its super-molecular, as well as useful, behaviour.

EXPERIMENTAL

MATERIALS AND METHODS

The several types of cellulose pulps used are presented in Table 1.

The biotransformation of cellulose pulp was achieved using selected cellulolytic enzyme type in a shaken bath, after suitable mechanical or chemical pretreatment, according to

Table 1. Some properties of cellulose pulps used.

Cellulose pulp type	Producer	Cellulose pulp properties			
		CrI	WVR, %	DP ^a	DP ^b
Fibrenier	USA	74	62	756	630
Riocell	Brasil	75	60	654	634
ITT Excell	USA	62	58	686	708
Saiccor	S.Africa	67	63	726	643
Swiecie (beech)	Poland	68	62	657	623

a - by EWNN viscosimetric method

b - by GPC method

the original technique [5].

The properties of cellulose pulp before and after biotransformation were determined as previously described [1,4,5-7]. The solubility of biotransformed cellulose was estimated according to a special test [5,8] based on a degree score of 0 to 5. The distribution of molecular weight of cellulose pulp was determined by GPC using the Hewlett-Packard apparatus HP 1050 type with a polystyrene filled column made by Polymer Lab. (UK).

RESULTS AND DISCUSSION

Development of new methods for manufacture of cellulosic fibres and films, alternatives the viscose technology, has brought solution to the field. Biotransformation of cellulose pulps creates a new cellulosic raw materials under the name of Celsol suitable for use in an environmentally safe method for manufacture of cellulosic fibres, films and other products.

Use of selected enzyme for the biotransformation process

needs a special pretreatment procedure to open the intrinsic capillary system of the cellulose material. Some results of the pretreatment process as well as biotransformation are presented in Tables 2 and 3. The cellulose pulps were subjected to the biotransformation process using the same conditions.

Table 2. Some super-molecular structure properties of biotransformed cellulose pulps.

Cellulose pulp type	Properties of cellulose pulp							
	after mechanical pretreatment				after enzymatic transformation			
	CrI %	WRV %	DP ^a	DP ^b	CrI %	WRV %	DP ^a	DP ^b
Fibrenier	79	79	632	583	68	77	485	403
Riocell	66	88	605	625	66	79	475	394
Excell	65	83	651	646	65	66	502	435
Świecie	68	108	632	540	74	94	436	347

a - by EWNN viscosimetric method

b - by GPC method

Table 3. Estimation of Celsol solution* properties.

Cellulose pulp type	Properties of Celsol solution, degree					
	with mechanical pretreatment			without mechanical pretreatment		
	solubility	spinnability	transparency	solubility	spinnability	transparency
Fibre-nier	5.0	5.0	5.0	3.5	3.5	3.5
Riocell	4.5	4.0	4.0	2.0	1.5	2.0
Excell	3.0	3.0	3.0	1.5	1.0	2.0
Świecie	3.0	4.0	3.0	2.0	1.5	2.0

* - in 9% aqueous sodium hydroxide solution

It can be concluded on a base of results summarized in Tables 2 and 3 that the pretreatment of cellulose pulps before of the biotransformation process plays an important role in manufacture of Celsol pulp. Chemical pretreatment also seems to be a suitable method for the modification of cellulose pulp intrinsic structure for promotion of the action of enzymes (Table 4). The action of enzymes during biotransformation can be observed on the basis of molecular weight distribution estimated by GPC method for selected cellulose pulps (Table 5).

Table 4. Some properties of biotransformed Saicor cellulose solution.

Pretreatment type	Cellulose solution properties, degree		
	Solubility	Spinnability	Transparency
Mechanical	4	5	4
Chemical	5	0	5

Table 5. Some super-molecular parameters of biotransformed selected cellulose pulps.

Cellulose pulp type	Treatment type	Cellulose properties		
		M_n $\cdot 10^{-4}$	M_w $\cdot 10^{-4}$	Pd
Excell	-	2.92	12.10	4.2
	mechanical	2.43	10.68	4.4
	enzymatic	2.02	8.81	4.4
	mechanical + enzymatic	1.68	6.48	3.8
Swiecie	-	3.26	10.11	3.1
	mechanical	2.33	8.75	3.6
	enzymatic	2.69	9.30	3.5
	mechanical + enzymatic	1.72	5.72	3.3

Pd - polydispersity

Assumption of mechanical pretreatment with enzymatic biotransformation caused the most significant reduction of molecular weight of cellulose pulp along with suitable activation leading to high degree of solubility, spinnability and transparency (Tables 4 and 5).

CONCLUSIONS

1. The Celsol method, using enzymatic biotransformation, has permitted cellulose pulp to be directly solubilized in aqueous sodium hydroxide. The product was suitable for production of cellulosic fibres and films.
2. The pretreatment of cellulose pulp, both mechanically and chemically, plays a very important part in the biotransformation process to manufacture Celsol pulp.
3. The alkaline solutions of Celsol pulp are characterized by great solubility, spinnability and transparency degrees suitable for manufacture of cellulosic fibres and films.

ACKNOWLEDGMENT

This paper is a part of common research realized by Institute of Chemical Fibres, Łódź, Poland with Tampere University of Technology, Tampere, Finland.

REFERENCE

1. H. Struszczyk, *Włókna Chemiczne*, 14(4), 35 (1988); 15(1), 7 (1989); 15(2), 169 (1989).
2. US Pat. 3447956 (1969).
3. H. Chanzy, M. Paillet, *Polymer*, 32, 400 (1990).

4. Cellulose'91 Conference, New Orleans, USA, 1991.
5. Polish Pat. Appl. P-289280 (1991).
6. Polish Pat. P-281342 (1989).
7. Polish Pat. P-284488 (1989).
8. Processings of Celsol Seminar, Łódź, Poland, 1992.

5 Hydrolysis of cellulose and cellooligosaccharides catalysed by cellobiohydrolase II studied by proton NMR and HPLC

A Teleman*, A Valkeajärvi**, A Koivula**, L Ruohonen** and T Drakenberg* – VTT, * Chemical Technology and ** Biotechnical Laboratory, PO Box 1401, FIN-02044 VTT, Finland

ABSTRACT

Proton NMR spectroscopy and HPLC have been used to investigate the hydrolysis of cellooligosaccharides and cellulose by cellobiohydrolase II from *Trichoderma reesei*. The cleavage pattern for the substrates cellotriose to cellohexaose has been determined. The catalytic rates were higher for the natural substrates (3.6-300 min⁻¹) than the rates earlier reported for chromophoric cellooligosaccharide derivatives (0.8-21 min⁻¹). The cellulose hydrolysis is slow compared to the hydrolysis of the soluble cellooligosaccharides. The cellotriose hydrolysis is inhibited by glucose and the inhibition is non-competitive. Cellobiohydrolase II retains maximal activity in a broad pH range, 2.5-6.5.

INTRODUCTION

The enzymatic degradation of cellulose is an important process, both ecologically and commercially. Several enzymes, such as cellobiohydrolase II (CBH II) from the filamentous fungus, *Trichoderma reesei*, participate in the hydrolysis of cellulose. As cellulose is an insoluble polymer, small soluble oligosaccharides have been used as model substrates facilitating the enzyme kinetic studies. Kinetic data as well as binding constants^{1,2} for the CBH II catalysed hydrolysis of soluble oligosaccharides have been obtained by chromophoric and fluorescence techniques. These studies were primarily conducted using 4-methylumbelliferyl β -D-glycosides derived from cellotriose, cellotetraose and cellopentaose, but the technique yielded corresponding results also

for natural substrates by means of competition experiments. In the present study the hydrolysis of cellulose and soluble cellooligosaccharides by CBH II has been studied using proton NMR spectroscopy and HPLC.

MATERIALS AND METHODS

The cellooligosaccharides and the cellulose were of commercial origin. CBH II was obtained and purified as described by Tomme et al.³. Proton NMR spectra were obtained at 599.94 MHz on a Varian UNITY 600 MHz spectrometer using 5 mm NMR tubes containing 0.7 ml solution. Typical acquisition parameters were a 9 μ s pulse (70°), a spectral width of 3000 Hz, an acquisition time of 1.3 s and a repetition time of 7.3 s. Spectra were obtained at 27°C. The HPLC equipment consisted of Waters 600 E pump, 700 WISP autoinjector and an RI detector. The column was an HC-40 cation exchange column (8x300 mm, Hamilton) with Ca²⁺ as counterion.

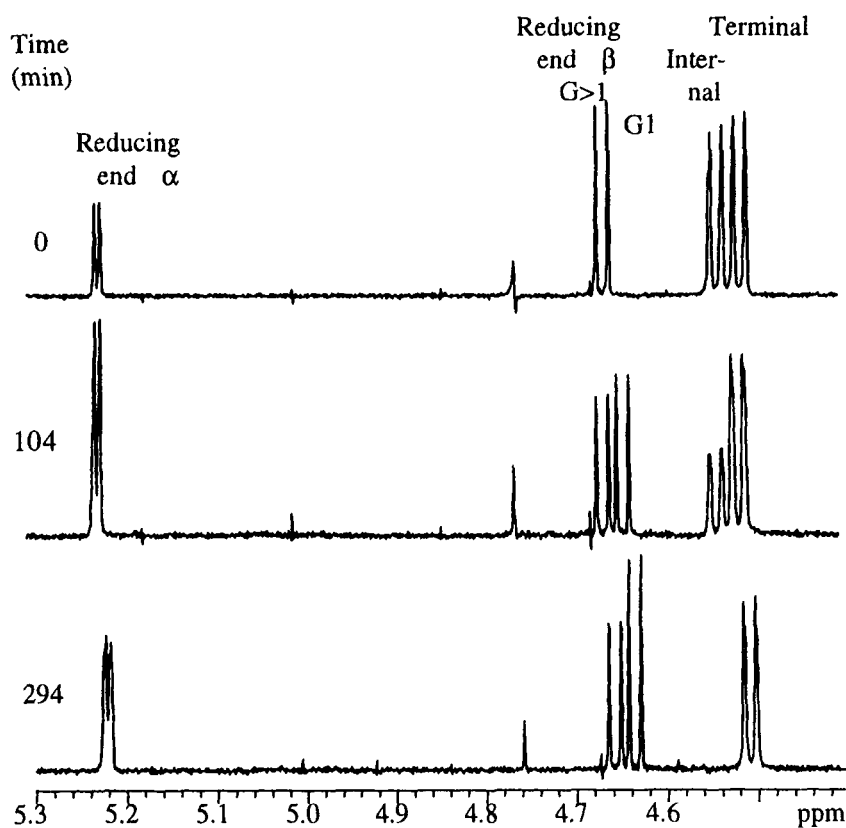


Fig. 1. The anomeric region of 600 MHz ¹H NMR spectra from enzymatic hydrolysis of cellotriose. Experimental: 5.0 mM cellotriose, 15 μ M CBH II, pD 5.0, 27°C.

RESULTS AND DISCUSSION

Resonances in the ^1H NMR spectra. For the cellooligosaccharides, the anomeric proton resonances (4.5-5.3 ppm) can be used as structural reporter signals, as they lie outside the crowded region between 3 and 4 ppm where the other proton resonances appear. The anomeric proton resonances can be divided into three types: 1) reducing end with an equilibrium distribution between α - and β -conformation, 2) internal and 3) terminal (non-reducing end). Moreover the anomeric proton resonance for β -D-glucose is well separated from the anomeric proton resonance for reducing end β of the cellooligosaccharides. Fig. 1 illustrates changes in the ^1H NMR spectrum during a hydrolysis.

Cleavage pattern. The enzyme is acting with overall inversion of configuration⁴. The cleavage pattern can thus be obtained if the hydrolysis is performed faster than the mutarotation occurs. By following the hydrolysis directly in the NMR-tube it has been possible to determine the cleavage pattern for the substrates cellotriose to cellohexaose, see Table I. For productive binding the substrate can enter the active site in either of the two possible ways, i.e. α -face up or down for the glucoside unit in the non-reducing end. The active site has in an X-ray diffraction study⁵ been shown to consist of a tunnel with at least four subsites. In order for hydrolysis to occur the glycosidic linkage between subsite B and C, where the hydrolysis occurs, has to be positioned correctly. Thus for cellooligosaccharides either a cellobiose or a cellotriose will be cleaved off from the non-reducing end.

Table I. Cleavage pattern for the CBH II hydrolysis of the substrates cellotriose to cellohexaose.

Substrate	Products	Relative amount
cellotriose	→ α -cellobiose + glucose	
cellotetraose	→ α -cellobiose + cellobiose cellotriose + glucose	49 1
cellopentaose	→ α -cellobiose + cellotriose α -cellotriose + cellobiose	50 50
cellohexaose	→ α -cellobiose + cellotetraose α -cellotriose + cellotriose	50 50

Kinetic rates. Both HPLC and NMR data show that the catalytic rates for natural substrates are much higher than for 4-methylumbelliferyl substituted substrates. The hydrolysis rate increases with the chain length from trimer to hexamer, except for the pentamer, c.f. Table II. The observation that the hydrolysis is most efficient for cellooligosaccharides with at least four glucosidic units agrees well with the three-dimensional structure of CBH II⁵.

Table II. Catalytic rates.

Substrate	k_{cat} (min^{-1})	
	HPLC	NMR
cellotriose	3.7 ± 0.6	3.6 ± 0.6
cellotetraose	220	175
cellopentaose	32	65
cellohexaose	265	300
MeUmb(Glc) ₃	$0.8 \pm 0.2^{\text{a}}$	
MeUmb(Glc) ₄	$9 \pm 2^{\text{a}}$	
MeUmb(Glc) ₅	$17 \pm 4^{\text{a}}$	
	$21 \pm 6^{\text{a}}$	

^a From van Tilbeurgh et al.¹.

Cellotriose binding constants and hydrolysis rate constants have been obtained from fitting numerical solutions using the full kinetic equations to the experimental hydrolysis curves⁶. No Michaelis-Menten approximation of initial slope was used. Our binding constant ($5.8 \cdot 10^4 \text{ M}^{-1}$) agrees with literature data, but the rate constant (3.6 min^{-1}) is five times higher than previously believed (0.8 min^{-1})^{1,2}. The cellotriose hydrolysis curve indicated product inhibition, so inhibition experiments were performed. The cellotriose degradation was followed for different sets of initial glucose and cellobiose concentrations, c.f. Fig. 2. Cellobiose has almost no effect on the cellotriose hydrolysis at the studied concentrations. However, glucose inhibits the cellotriose hydrolysis and the inhibition is non-competitive.

The hydrolysis of Avicel PH-101, microcrystalline cellulose, by CBH II is slow compared to the hydrolysis of cellotetraose, cellopentaose and cellohexaose. The initial catalytic rate is 0.5 min^{-1} , c.f. Fig. 3. The products are cellobiose (91 mol%) and glucose (9 mol%). No resonance from internal anomeric protons is detected during the hydrolysis, thereby indicating that no longer products are accumulated during the hydrolysis. The crystal breaking of the cellulose crystal seems thus to be the limiting step in the hydrolysis of cellulose by CBH II.

A study of the pH dependence of the catalytic rate shows that CBH II retains maximal activity in a broad pH range, 2.5-6.5.

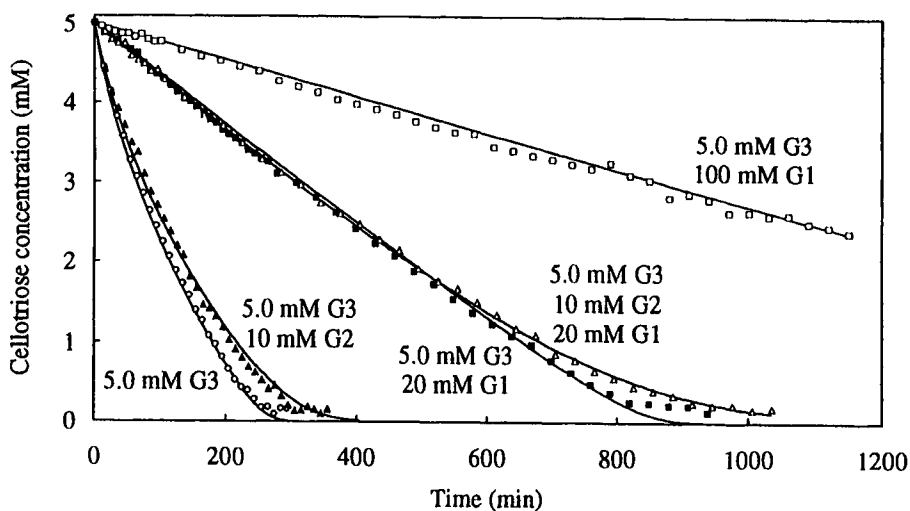


Fig. 2. Cellotriose hydrolysis. Internal anomeric proton resonance as a function of time for different combinations of initial oligosaccharide concentrations. G3 = cellotriose, G2 = cellobiose and G1 = glucose.

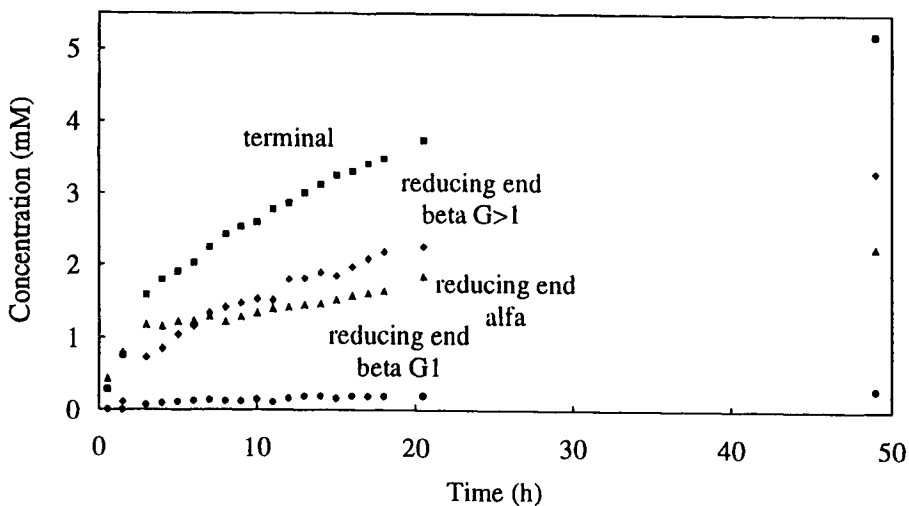


Fig. 3. Cellulose hydrolysis. Time dependent concentrations for anomeric proton resonances. Experimental: 2.0 w/V % Avicel PH-101, 20 μ M CBH II, pD 5.0, 27°C.

REFERENCES

1. H. van Tilbeurgh, G. Pettersson, R. Bhikabhai, H. De Boeck and M. Claeysens, *Eur. J. Biochem.*, 148 (1985) 329-334.
2. H. van Tilbeurgh, F. G. Loontjens, Y. Engelborgs and M. Claeysens, *Eur. J. Biochem.*, 184 (1989) 553-559.
3. P. Tomme, H. van Tilbeurgh, G. Pettersson, J. van Damme, J. Vandekerckhove, J. Knowles, T. Teeri and M. Claeysens *Eur. J. Biochem.*, 170 (1988) 575-581.
4. J. K. C. Knowles, P. Lentovaara, M. Murray and M. L. Sinnott, *J. Chem. Soc. Chem. Commun.*, (1988) 1401-1402.
5. J. Rouvinen, T. Bergfors, T. Teeri, J. K. C. Knowles and T. A. Jones, *Science*, 249, (1990) 380-386.
6. A. Teleman, A. Valkeajärvi, A. Koivula, T. Reinikainen, T. Teeri, T. Drakenberg and O. Teleman, manuscript in preparation.

6 Modification of pine kraft pulp using hydrolytic and oxidizing enzymes

M-L Niku-Paavola, M Ranua*, A Suurnäkki and A Kantelinen – VTT/Biotechnical Laboratory, PO Box 202, FIN-02151 Espoo, Finland; * The Finnish Pulp and Paper Research Institute, PO Box 70, FIN-02151 Espoo, Finland

ABSTRACT

Oxygen delignified pine kraft pulps were treated with lignin modifying enzymes: laccase (EC 1.10.3.2), Mn-dependent peroxidase (EC 1.11.1.x), lignin peroxidase (EC 1.11.1.y), and a xylanase (EC 3.2.1.8) in order to increase their bleachability. Pulps were treated either with a purified single enzyme or the enzymes were successively added in different combinations. The residual pulps were delignified with alkaline peroxide and analysed for kappa number and ISO-brightness. Xylanase treatment improved the reference brightness by 1 - 2.5 units and combination with lignin modifying enzymes improved the value by a further one unit. Lignin modifying enzymes when acting alone gave equal or even poorer pulp values than the reference.

INTRODUCTION

Hemicellulases, especially xylanases have been successfully used to increase the bleachability of kraft pulps (Viikari *et al.*, 1986). The effect of hemicellulase treatment

is indirect, based on limited hydrolysis of xylans facilitating the subsequent removal of lignin. The enzymatic modification of lignin itself would be a straightforward approach.

Lignin modifying enzymes from white-rot fungi, lignin peroxidases (LiP), Mn-dependent peroxidases (MnP) and laccase are reported to initiate a radical reaction where e.g. the $C\alpha - C\beta$ and $\beta-O-4$ ether bonds in dimeric structural units of lignin are cleaved, benzylic alcoholic and methylene groups are oxidized, aromatic rings are opened and phenols are polymerized (Schoemaker *et al.*, 1985). Thus the effect of the enzymes on the macromolecular lignin strongly depends on the lignin structure and will be primarily regulated by the rules of radical reactions. Lignin modifying enzymes have been reported to depolymerize synthetic hardwood-type DHP lignin when using veratryl alcohol as a cosubstrate, as well as lignin containing low amounts of free phenolic hydroxyl groups (Hammel & Moen, 1991) or lignin in which the hydroxyl groups have been derivatized (Tien & Kirk, 1983, Umezawa & Higuchi, 1989). In our preliminary tests, in which ground wood was treated with purified laccase and LiP, the lignin-carbohydrate ratio in the residual pulp decreased. This was calculated from the IR spectrum where also an increase in the carbonyl and carboxyl content was noticed. Solid state ^{13}C -NMR analysis of residual pulp indicated an increase in the amount of free hydroxyl and phenolic hydroxyl groups. Similar lignin modification occurs during cooking, which makes the lignin more reactive in the subsequent bleaching. Thus lignin modifying enzymes seemed to be a logical tool to improve the reactivity of chemical pulps in chlorine free bleaching sequences.

MATERIALS AND METHODS

Pulps used were commercial pine kraft pulps (kappa number 11.8 - 13.4 SCAN, ISO-brightness % 37.7 - 37.3) prepared by modified continuous cooking and delignified using oxygen.

Enzymes used were the purified xylanase pI 9 from *Trichoderma reesei* (Tenkanen *et al.*, 1992), LiP pI 3.2 purified from *Phlebia radiata* and laccase pI 4.0 and MnP pI 3.7

purified from *Trametes hirsuta*. *Trametes*-culture filtrate was produced by Genencor Int., Finland. Purification of lignin modifying enzymes was according to Niku-Paavola *et al.*, 1988.

Enzymatic treatments. The pulps were homogenized in water and the pH of the suspensions was adjusted to 5.0. The suspension was equilibrated to 50°C, a single enzyme was allowed to act for 1 h, then the second enzyme was added and allowed to act for 1 h. Enzyme doses were: xylanase 100 nkat, laccase 0.5 nkat, LiP or MnP 5 nkat/g dry pulp. In conjunction with LiP, 0.04 mg H₂O₂/g dry pulp was introduced and when MnP was added, H₂O₂ together with 0.4 mg Mn²⁺/g dry pulp were supplied. Corresponding references with a single enzyme and samples without enzymes were prepared for comparison.

Delignification. After enzyme treatment, metals were eliminated and the residual pulp was delignified by alkaline peroxide at 10 % pulp consistency for 1 - 3 h at 80°C. The amounts of chemicals used were 3 % H₂O₂, 1.5 % NaOH, 0.2 % DTPA, 0.5 % MgSO₄. In some experiments the treatment was repeated twice. Experiments where enzyme treatment was performed between the two delignification steps were also carried out. The pulp quality was analysed by kappa number (SCAN) and brightness (ISO). Samples for kappa analyses were also taken after enzyme treatment.

RESULTS AND DISCUSSION

The kappa numbers of the residual pulps after enzyme treatment showed a decrease in the series treated with xylanase and the combinations xylanase-MnP, xylanase-LiP (Fig 1). Delignification with alkaline peroxide for 1 h at 80°C decreased the kappa number most pronounced in samples treated with xylanase, with the combination xylanase-MnP or with laccase-MnP. A single lignin modifying enzyme alone did not improve the kappa number. The corresponding brightness percentages showed that xylanase treatment improved the reference value by 1 - 2.5 units except for the combination xylanase-laccase. Combination xylanase-LiP further increased the xylanase value by one unit.

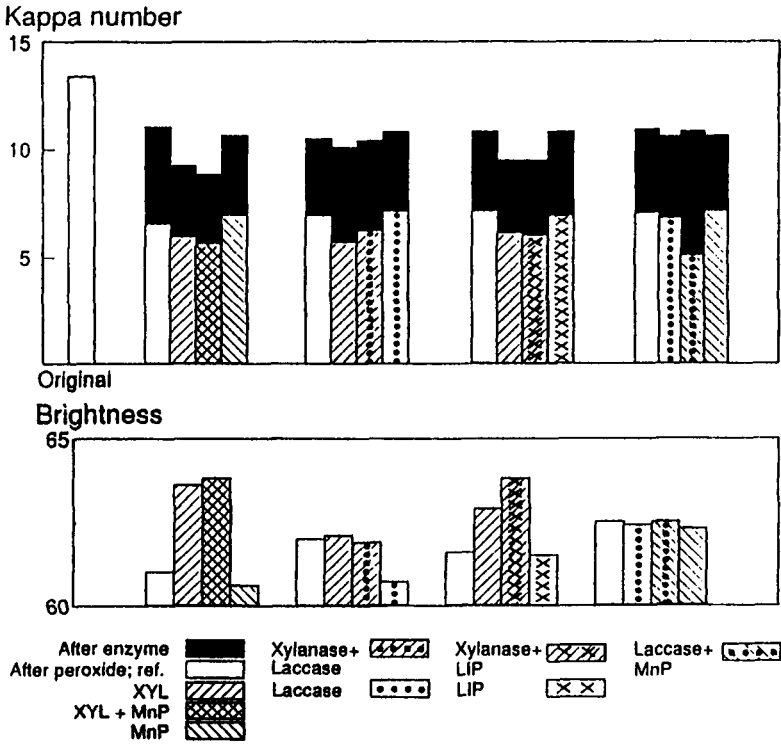


Fig 1: Pulp values after enzymatic treatment and alkaline peroxide delignification

A slight increase in brightness value was obtained also for the pulp treated with MnP alone when the alkaline peroxide step was extended to 3 h (Fig 2). All the values were better than after delignification for 1 h and were further improved by repeated peroxide or enzyme treatment. The sample treated with xylanase-MnP—xylanase reached the highest brightness value (78 %) and the lowest kappa number (4.8). The first extended alkaline peroxide step was most advantageous from the point of view of the relative differences in brightness values between the reference and enzyme-treated samples. The reference brightness 66 % was improved by 3 units due to xylanase and 5 units due to xylanase-MnP. After repeated enzyme and peroxide stages the relative differences were not improved although the final values were increased.

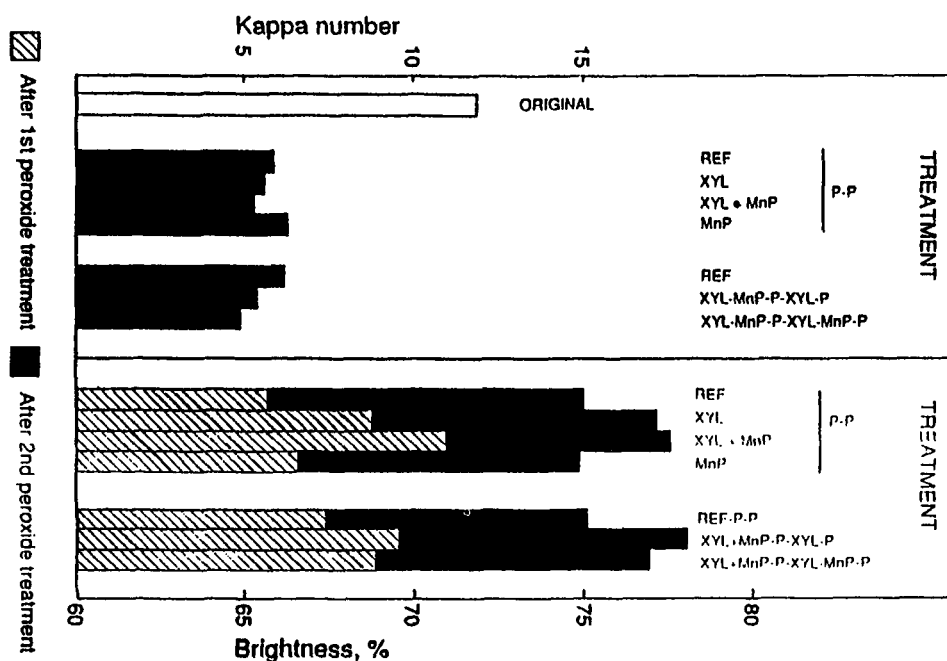


Fig 2: Pulp values after repeated, extended delignification and repeated enzymatic treatments.

The bleaching effect of xylanase has been shown to depend on the hydrolysis of reprecipitated xylan. The fibre structure is rendered more permeable for the lignin extraction in the subsequent bleaching stage. The molecular mass and amount of lignin extracted is increased by xylanase treatment (Kantelinen *et al.*, 1993).

Lignin modifying enzymes were assumed to facilitate the chlorine free delignification by increasing the reactivity of residual lignin. When oxygen delignified pulps were treated with enzymes, xylanase treatment liberated xylodextrins from the pulps and the extraction of high molecular mass lignin was noticeably improved, whereas lignin modifying enzymes did not improve these effects (Niku-Paavola *et al.*, 1993). In the present study lignin modifying enzymes increased the bleachability of lignin only when combined with xylanase. The xylanase released xylodextrins which could quench the radicals created in the lignin by lignin modifying enzymes. Lignin may then have remained in fragmented soluble form and have been more easily bleached. The

bleachability was then further enhanced by the increased permeability of pulp surfaces caused by the hydrolytic xylanase action.

ACKNOWLEDGEMENTS

Financial support was provided by The Technology Development Centre of Finland and by the Foundation for Biotechnical and Industrial Fermentation Research (A.S.).

REFERENCES

Hammel, K.E. & Moen, M.A. (1991). Depolymerization of a synthetic lignin *in vitro* by lignin peroxidase. *Enzyme Microbiol. Technol.* **13**, 15-18.

Kantelinen, A., Hortling, B., Sundquist, J., Linko, M. & Viikari, L. (1993). Proposed Mechanism of the Enzymatic Bleaching of Kraft Pulp with Xylanases. *Holzforschung*, in press.

Niku-Paavola, M.-L., Karhunen, E., Salola, P. & Raunio, V. (1988). Ligninolytic enzymes of the white-rot fungus *Phlebia radiata*. *Biochem. J.* **254**, 877-884.

Niku-Paavola, M.-L., Ranua, M., Suurnäkki, A. and Kantelinen, A. (1993). Bioresource Technology, submitted.

Schoemaker, H.E., Harvey, P.J., Bowen, R.M. & Palmer, J.M. (1985). On the mechanism of enzymatic lignin breakdown. *FEBS Lett.* **183**, 7-12.

Tenkanen, M., Puls, J. & Poutanen, K. (1992). Two major xylanases of *Trichoderma reesei*. *Enzyme Microbiol. Technol.* **14**, 566-574.

Tien, M. & Kirk, T.K. (1983). Lignin degrading enzyme from the hymenomycete *Phanerochaete chrysosporium* Burds. *Science* **221**, 661-663.

Umezawa, T. & Higuchi, T. (1989). Aromatic ring cleavage by lignin peroxidase. In: *Plant Cell Wall Polymers*, ed. N.G. Lewis & M.G. Paice. American Chemical Society, Washington, ACS Symp. Ser. No 399, pp. 503-518.

Viikari, L., Ranua, M., Kantelinen, A., Sundquist, J. and Linko, M. (1986). Bleaching with enzymes. *Proc. 3rd Int. Conf. Biotechnology in the Pulp and Paper Industry*, Stockholm, June 16-19, pp. 67-69.

Part 2:
Structure and reactivity
of cellulose

7 Packing energy calculations on the crystalline structure of cellulose I

A Aabloo¹, A D French², R-H Mikelsaar³ – ¹ Tartu University, Institute of Experimental Physics and Technology, Tähe 4 Street, EE2400 Tartu, Estonia; ² Southern Regional Research Center, USDA, 1100 Robert E Lee Blvd, PO Box 19687, New Orleans, LA 70179, USA; ³ Tartu University, Institute of General and Molecular Pathology, Veski 34 Street, EE2400 Tartu, Estonia

Abstract

The crystalline structure of native cellulose was investigated with packing energy calculations of crystals. Unit cell measurements were based on dimensions proposed by Sugiyama *et al* . The packing energy calculations of phases I α and I β of native cellulose (I) were evaluated using two different algorithms. As a first step we used the rigid ring method. The best structures found by this method were further minimized with a full optimization molecular mechanics program MM3(90). Different minimization methods gave analogous structures for best models of both phases. The best model for phase I α one-chain unit cell is in the *tg* position and is packed "up". The chains of the best model for phase I β two-chain unit cell are also in the *tg* positions and are packed "up". The structure found for the phase I β of native cellulose is completely similar with a structure proposed several years ago by Woodcock and Sarko for ramie cellulose.

Introduction

Several years ago, VanderHart and Atalla found that all crystalline native cellulose I is composed from two phases¹. Later Sugiyama *et al*², described those phases as $I\alpha$ with a triclinic one-chain unit cell and as $I\beta$ with a monoclinic two chain unit cell. They investigated *Microdictyon tenius* with electron diffraction techniques. The one-chain triclinic unit cell for the phase $I\alpha$ has parameters of $a = 0.674$ nm, $b = 0.593$ nm, $c = 1.036$ nm, $\alpha = 117^\circ$, $\beta = 113^\circ$ and $\gamma = 81^\circ$. The two-chain unit monoclinic unit cell has parameters of $a = 0.801$ nm, $b = 0.817$ nm, $c = 1.036$ nm and $\gamma = 97.3$ as published by Sugiyama *et al*². Earliest these two phases together were indexed as an eight-chain unit cell³.

Material and methods

We used two different strategies to find the most probable models using the crystal packing energy calculations. At the first step we using molecular modelling⁴ and rigid ring calculations^{5,6} to find the most probable models of both phases of native cellulose. The parallel packing of chains was presupposed. During these calculations we used P1 symmetry for the phase $I\alpha$ and P2₁ symmetry for the $I\beta$ phase. The rigid-ring method means that during the minimization process the glucose ring was kept fixed. The Arnott-Scott⁷ glucose ring was used. The torsion angles of the hydroxymethyl and hydroxyl groups and the torsion angles and the bond angles at the glycosidic linkages were allowed to vary (see Figure 1.). In the case of space group P2₁ the monomer residues were linked into the chain using a virtual bond⁸.

The best models of these calculations were further minimized with a full molecular mechanics program MM3(90)^{9,10}. During these minimizations the

dielectric constant of 4 was chosen. This value was also used for crystalline amides, polypeptides and proteins¹¹. In this method, a model of the crystal of cellulose was built of seven cellotetraose molecules placed to hexagonal close packing. All chains were arranged according to the unit cell measurements.

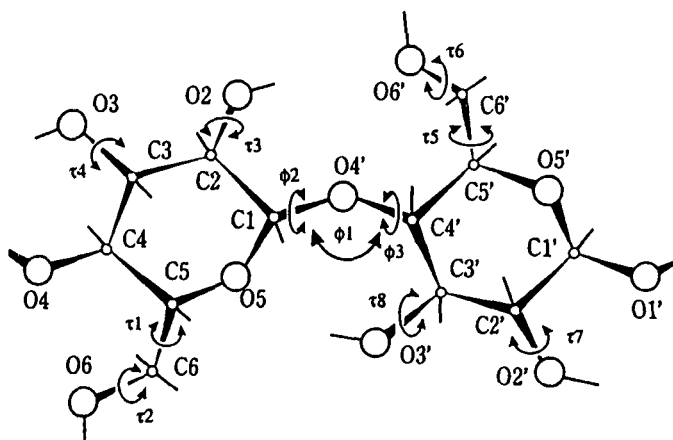


Figure 1. The unit of the cellulose chain and the variable angles by rigid-ring method.

The best model of both phases of cellulose I obtained by the rigid-ring method preserved their leader position after MM3 minimization while the conformation of these models did not change significantly. The best models of both phases are presented in Table 1.

Model	Energy kcal/mol		H-bonds in chain	H-bonds in sheet	-CH ₂ OH position
	Rigid-ring	MM3			
U α	-19.5	185	O5..HO3 O6..HO2	O3..HO6	tg
U β	-19.9	182	O5..HO3 O6..HO2	O3..HO6	tg

Table 1. The best model for the phase I α and for the phase I β of native cellulose.

As we can see in the case of the phase I the hydroxymethyl groups are in the *tg* position. The orientation of chain is "up". In the case of the phase I β the hydroxymethyl groups of both chains are also in the *tg* position and they are also packed "up". The central chain is shifted down approximately $1/4 c$ (see Figure 2.). Hydrogen bonds are completely the same for both phases. The conversion from I α phase to I β phase is possible by simple vertical shifting of sheets of chains.

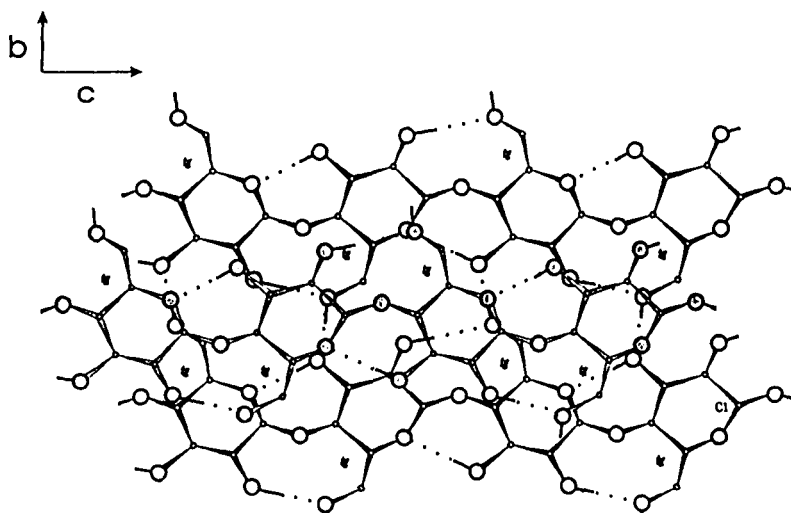


Figure 2. A projection of the cellulose chains down the *a*-axis for the phase I β .

Results and discussion

The best model of the phase I α has an energy of -19.5 kcal/mol by the rigid-ring method and 185 kcal/mol by MM3. The best model of the phase I β has energies of -19.9 kcal/mol and 182 kcal/mol, respectively. We can compare it with energies of -21.4 kcal/mol⁵ and 176 kcal/mol¹¹ calculated for cellulose II. Although the energies of both phases of native cellulose are very close, these

energies are in a good agreement with experimental data about $\alpha \rightarrow \beta \rightarrow \text{II}$ conversion. It is remarkable that the most probable model for β phase is completely analogous with a structure proposed by Woodcock and Sarko¹² for ramie cellulose. Also it is close to the structure proposed by Pertsin *et al* for ramie cellulose using similar minimization technique¹³. It means that the diffraction patterns of ramie cellulose mostly belong to the phase β . We obtained the same result for phase β without any diffraction data.

References

1. VanderHart D. L.; Atalla R. H., *Macromolecules* 1984, v. 17, p. 1465.
2. Sugiyama, J.; Vuong, R.; Chanzy, H. *Macromolecules* 1991, v. 24, p. 4168.
3. Honjo G.; Watanabe M. *Nature* 1958, v. 181, p. 326.
4. Mikelsaar, R. *Trends Biotechnol.* 1986, v. 6, p. 162.
5. Pertsin, A. J.; Nugmanov, O. K.; Marchenko, G. N.; Kitaigorodsky, A. I. *Polymer* 1984, v. 25, p. 107.
6. Mikelsaar, R.-H.; Aabloo, A. In: *Cellulosics: Chemical, Biochemical and Material Aspects*. Eds. J. F. Kennedy, G. O. Phillips, P. A. Williams. Ellis Horwood, Chichester, 1993, p. 61.
7. Arnott S.; Scott W. E. *J. Chem. Soc. Perkin II* 1972, p. 324.
8. Zugenmayer P.; Sarko A. *ACS series* 1980, v. 141, p. 226.
9. Allinger N. L.; Yuh Y. H.; Lii J.-H. *J. Amer. chem. Soc.* 1989, v. 111, p. 8551.
10. Allinger N. L.; Rahman, M.; Lii J.-H. *J. Amer. chem. Soc.* 1990, v. 112, p. 8293.
11. Stipanovic A. J.; Sarko A. *Macromolecules* 1976, v. 9, p. 851.
12. Woodcock C.; Sarko A. *Macromolecules* 1980, v. 13, p. 1183.
13. Pertsin A. J.; Nugmanov O. K.; Marchenko G. N. *Polymer* 1986, v. 27, p. 597.

8 Molecular modelling of parallel and antiparallel structure of native cellulose

R-H Mikelsaar and A Aabloo* – Tartu University, Institute of General and Molecular Pathology, 34 Veski Street, EE2400 Tartu, Estonia, * Tartu University, Institute of Experimental Physics and Technology, 4 Tähe Street, EE2400 Tartu, Estonia

Abstract

Tartu plastic space-filling atomic-molecular models were used to investigate the structure of cellulose crystalline (α and β) phases. It was elucidated that both parallel and antiparallel structures can be accommodated with unit cell geometries described by Sugiyama *et al.*¹. Packing energy calculations revealed that parallel models of α and β phases have similar energy. In contrast, in case of antiparallel structure models, β is energetically much more favourable in comparison with α phase. Our data indicate that antiparallel structure proposed for cellulose α phase is metastable and should be easily converted to β phase. So the antiparallel models are more suitable for explanations of cellulose $\alpha \rightarrow \beta \rightarrow \parallel$ interconversion.

Introduction

Recently it was elucidated that native cellulose is a mixture of two crystalline phases (α and β) the proportion of which depends on the source of cellulose^{2,3}. Horii *et al.*⁴ showed that the α phase of cellulose is metastable and, through a hydrothermal annealing treatment, can be converted readily into the thermodynamically stable β phase. Sugiyama *et al.*¹ studied cellulose from a green alga *Microdictyon* by electron diffraction and found that the major α phase has a one-chain, triclinic structure and the minor β phase is characterized by two-chain unit cell and a monoclinic structure. This study disclosed the detail molecular structure of native cellulose crystalline phases. The aim of current paper was to

use the molecular modelling method and packing energy calculations to elucidate the most favourable stereochemical structures corresponding to unit cell parameters found by Sugiyama *et al.*¹ in cellulose I α and I β crystalline phases.

Material and methods

Molecular modelling was carried out by Tartu plastic space-filling models having improved parameters and design⁵. Packing energy calculations were carried out by rigid-ring method⁶.

To present graphically the stereochemical models investigated, we drew unit cell projections on the plane crossing the c-axis at 90°. Cross-sections of up cellulose chains were given by white and down chains by grey ovals. The number of c/4 shifts of molecules in the direction of c-axis is noted by numbers inside of ovals⁷.

To make a short digital designation of the cellulose models: 1) symbols "P" and "A" were used to represent correspondingly "parallel" and "antiparallel", 2) numbers indicating c/4 shifts were applied for characterizing each chain in the unit cell, 3) underlining was used to differ up and down chains.

Results

The characteristics of the cellulose structure models investigated is presented in Table 1.

1. Molecular models fitting with cellulose I unit cell parameters

1.1. Models P1

The investigation of green alga *Microdictyon* by Sugiyama *et al.*¹ is the first work where unit cell parameters are given for pure cellulose I α phase microcrystals: $a = 0.674$ nm, $b = 0.593$ nm, $c = 1.036$ nm, $\alpha = 117^\circ$, $\beta = 113^\circ$ and $\gamma = 81^\circ$. This one-chain unit cell requires parallel packing of molecular chains. Molecular modelling by Tartu devices showed that if there are the usual intramolecular bonds O3-H...O5 and O2-H...O6 the hydroxymethyl groups should be in *tg* conformation and all parallel chains are bound by intrasheet bonds O6-H...O3. Packing energy calculations of the above-described cellulose structure imitation revealed that model P1 has potential energy -19.5 kcal/mol.

1.2. Models A1a and A1b

Two antiparallel models A1a and A1b characterized by eight-chain unit cell maybe geometrically derived from the one-chain unit cell described by Sugiyama *et al.*¹. The geometry of these two models is very similar. The only difference is that in A1a parallel chains follow each other from down right to up left dividing major angles of unit cell and in A1b from down left to up right dividing minor angles of unit cell. So A1a may be called "left" and A1b "right" type of structures. According

to molecular modelling data chains having usual intramolecular H-bonds and *tg* conformation of hydroxymethyl groups should be in models A1a and A1b bound by intrasheet bonds O6-H...O2. The potential energy values of above-described structures are rather similar: model A1a has -16.4 kcal/mol and A1b -15.5 kcal/mol.

2. Molecular models fitting with cellulose I unit cell parameters

2.1. Model P2

Sugiyama *et al.*¹ have established that I β phase of Microdictyon cellulose has two-chain monoclinic structure with unit cell parameters of $a = 0.801$ nm, $b = 0.817$ nm, $c = 1.036$ nm and $\gamma = 97.3^\circ$. The authors suppose that this structure consists of parallel molecules and the center and corner chain are staggered by $c/4$. Molecular modelling revealed that intra- and intermolecular H-bonds in model P2 are identical to those in model P1. The energy value of model P2 is close to model P1: -19.9 kcal/mol.

2.2. Model A2

Molecular modelling showed that a chain conformation and an intrasheet H-bonding network in model A2 are identical to model P2. The only difference is that sheets are parallel in model P2 and antiparallel in model A2. The potential energy of model A2 is relatively high: -15.8 kcal/mol.

2.3. Models A3a and A3b

Two antiparallel models A3a and A3b characterized by eight-chain unit cell may be geometrically derived from the two-chain unit cell described by Sugiyama *et al.*¹. These structures are similar to the "left" and "right" models A1a and A1b differing mainly by presence of intrasheet stagger of cellulose chains. The investigation by plastic models indicated that in the case where standard intramolecular H-bonds and *tg* conformation of hydroxymethyl groups are preserved the antiparallel molecular chains are bound by bonds O6-H...O3. There is considerable difference between energies of above-described two structures: the "left" type model A3a has -21.0 kcal/mol and "right" model A3b -15.1 kcal/mol.

Discussion

Our investigation revealed that both parallel and antiparallel structure models can be proposed based on cellulose I α and I β crystalline phases unit cell parameters published by Sugiyama *et al.*¹. Although they all have usual chain conformation and intramolecular H-bonding network, the potential energy values between seemingly close structures in certain cases are very different.

Sugiyama *et al.*¹ interpret their experimental data in the light of all-parallel

structure view. Following this view, the α phase structure should correspond to our model P1 and β phase to model P2.

Comparing cellulose parallel model P1 with antiparallel models A1a and A1b one can see that these models are sterically very similar. If the H-bonding network and chain polarity are not clearly established the structure characterized by eight-chain unit cell can be considered as the one-chain unit cell. We think that antiparallel model A1a having lower energy (-16.4 kcal/mol) in comparison with the model A1b (-15.5 kcal/mol) is a possible pretender for a "masked" eight-chain unit cell in the cellulose α crystal structure described by Sugiyama *et al.*¹. The antiparallel structure is not excluded also for cellulose β crystalline phase because these authors marked that the exact position of the cellulose chains in the monoclinic unit cell was even more difficult to ascertain as long as the structure refinement was not achieved. No doubt, A3a is the best antiparallel model for fitting to the unit cell structure of β crystalline phase because it has an excellent packing energy: -21.0 kcal/mol.

Table 1. Parallel and antiparallel stereochemical models for cellulose α and β crystalline phases.

Phase	Model	Unit cell designation	Intramolecular H-bonds	Intrasheet H-bonds	-CH ₂ OH group conformation	Packing energy kcal/mol
α	P1	1	O3-H...O5 O2-H...O6	O6-H...O3	tg	-19.5
β	P2	01	O3-H...O5 O2-H...O6	O6-H...O3	tg	-19.9
α	A1a	<u>00112233</u>	O3-H...O5 O2-H...O6	O6-H...O2	tg	-16.4
α	A1b	<u>00112233</u>	O3-H...O5 O2-H...O6	O6-H...O2	tg	-15.5
β	A2	<u>01</u>	O3-H...O5 O2-H...O6	O6-H...O3	tg	-15.8
β	A3a	<u>01123243</u>	O3-H...O5 O2-H...O6	O6-H...O3	tg	-21.0
β	A3b	<u>01213234</u>	O3-H...O5 O2-H...O6	O6-H...O3	tg	-15.1

If the "left" type antiparallel models A1a and A3a are thought to be the candidates for structures of cellulose α and β crystalline phases, correspondingly, it would be easy to explain the experimental data on the interconversion of these phases. Model A1a, having relatively high energy -16.4 kcal/mol, is metastable and can during annealing process easily be converted irreversibly into the model A3a, having very low energy -21.0 kcal/mol. Because the models A1a and A3a have different H-bonding networks, our conception on antiparallel cellulose structure is in accordance also with Raman-spectroscopic data⁸. The high energy barrier

between α and β crystalline phases, bound with rearrangement of hydrogen bonds, may be the reason why the proportion of these phases in different samples of native cellulose is relatively constant. The notable structural differences between models A1a and A3a allow one also to understand the differences between corresponding unit cell parameters of α and β cellulose crystalline phases.

The process of cellulose I \rightarrow II conversion can be also easily interpreted by all-antiparallel conception, because already Na-cellulose I, formed in the initial step of mercerization, has antiparallel structure^{9,10}.

References

1. Sugiyama, J.; Vuong, R.; Chanzy, H. *Macromolecules* 1991, v. 24, p. 4168.
2. Atalla, R. H.; VanderHart, D. L. *Science* 1984, v. 223, p. 283.
3. VanderHart, D. L.; Atalla, R. H. *Macromolecules* 1984, v. 17, p. 1465.
4. Horii, F.; Yamamoto, H.; Kitamaru, R.; Takahashi, M.; Higuchi, T. *Macromolecules* 1987, v. 20, p. 2946.
5. Mikelsaar, R. *Trends Biotechnol.* 1986, v. 6, p. 162.
6. Pertsin, A. J.; Nugmanov, O. K.; Marchenko, G. N.; Kitaigorodsky, A. I. *Polymer* 1984, v. 25, p. 107.
7. Mikelsaar, R.-H.; Aabloo, A. In: *Cellulosics: Chemical, Biochemical and Material Aspects*. Eds. J. F. Kennedy, G. O. Phillips, P. A. Williams. Ellis Horwood, Chichester, 1993, p. 57.
8. Atalla, R. H. In: *Cellulose Structural and Functional Aspects*. Eds. J. F. Kennedy, G. O. Phillips, P. A. Williams. Ellis Horwood, Chichester, 1989, p. 61.
9. Sarko, A.; Nishimura, H.; Okano, T. In: *Structure of Cellulose*; ACS Symposium Series 340; American Chemical Society: Washington, DC, 1987 p. 169.
10. Nishimura, H.; Okano, T.; Sarko, A. *Macromolecules* 1991, v. 24, p. 759.

9 Cellulose I crystallinity as determined with diffuse reflectance Fourier transform infrared spectrometry and wide angle X-ray scattering

S H D Hulleman, J M van Hazendonk and J E G van Dam –
ATO-DLO Agrotechnological Research Institute, PO Box 17,
NL-6700 AA Wageningen, The Netherlands

ABSTRACT

A method based on diffuse reflectance Fourier transform infrared (DRIFT) spectrometry for the quantitative determination of cellulose I crystallinity in pure cellulose samples has been developed. The ratio R between the heights of the absorbances at 1280 and 1200 cm^{-1} in the deconvoluted DRIFT spectrum was taken as a measure for crystallinity. The infrared crystallinity ratio R and the cellulose crystallinity x_c as determined with WAXS are related following the equation $x_c = 1.06 R + 0.19$. The percentage variance adjusted for is 99.7%. The equation proved to be valid for $0.26 < x_c < 0.75$. Cellulose crystallinity x_c can be predicted from DRIFT measurements with a standard error of 0.01 - 0.02 ($n = 3$). The infrared ratio R was selected to be independent of the non-cellulosic components in the fibre, which will enable the use of this method to determine the cellulose I crystallinity in plant fibres.

INTRODUCTION

Plant fibres like flax, hemp and cotton are mainly composed of cellulose (60 - 98 % (w/w)). Cellulose can be characterized by several structural parameters like crystallinity, lattice type, crystallite size and degree of polymerization. These parameters significantly contribute to the physical properties of the fibre [1,2]. Cellulose crystallinity for example influences the accessibility for chemical derivatization, swelling and water-binding properties of the fibre.

Native cellulose can be considered as a two-phase system consisting of crystalline cellulose I and amorphous cellulose. Crystalline cellulose I in plant fibres is a composite of two allomorphs of cellulose: cellulose I α and cellulose I β (respectively < 20 % and > 80 % (w/w)) [3].

Wide Angle X-ray Scattering (WAXS) is the general method for the determination of crystallinity in pure cellulose samples [4-8]. Infrared (IR) spectrometry is also considered to be a useful technique. This is a fast technique for which only small samples are needed. Several infrared bands or ratios for the determination of lattice type and for the prediction of cellulose crystallinity in pure cellulose samples have been presented in the literature [9-12]. However, the infrared ratios for the prediction of cellulose crystallinity have never been quantified.

The extraction of cellulose from plant fibres is impossible without causing any structural changes and therefore it is necessary to determine cellulose crystallinity in the intact fibre. WAXS is not suitable for the determination of crystallinity in heterogeneous materials like plant fibres due to the interference of (amorphous) non-cellulosic components. These components, such as hemicelluloses, pectin and small amounts of lignin (< 3 % (w/w)), contribute to the amorphous scattering and their presence will cause an underestimation of cellulose crystallinity. With IR spectrometry it should be possible to select a crystallinity ratio in the spectrum which is independent of the non-cellulosic components. In this study a method based on diffuse reflectance Fourier transform infrared spectrometry for the determination of cellulose I crystallinity in pure cellulose samples is presented. The DRIFT method is calibrated using crystallinity data as determined with WAXS.

EXPERIMENTAL

To obtain cellulose samples covering a broad range in crystallinity, microcrystalline cellulose (Avicel[®], Merck, Art. 2330) was ball-milled until no crystalline diffraction was observed with WAXS. Samples were taken at several milling times and crystallinity of these samples was determined with WAXS according to the method of Hermans *et al.* [6] and DRIFT spectra were recorded using particle sizes < 50 μm . The DRIFT spectra were baseline corrected at 3750 and 1900 cm^{-1} and deconvoluted (half bandwidth 20 cm^{-1} , peak width narrowing factor 1.5, Bessel apodization). The method was validated using cellulose powder (Fluka Biochemika, Art. 22183) and native cellulose (Merck, Art. 2351).

RESULTS AND DISCUSSION

WAXS diffractograms of the cellulose samples which were ball-milled for 0, 2, 10, 25, 62, 120, 173 and 500 min. were recorded. The diffractogram of 500 min. ball-milled cellulose shows no crystalline diffraction and this cellulose can be considered as amorphous. The spectra taken from non-destructively extracted non-cellulosic components show minimal absorbances at approximately 1280 and 1200 cm^{-1} . The IR spectra of cellulose samples show a decreasing absorbance at 1280 cm^{-1} with decreasing crystallinity. The band at 1200 cm^{-1} is assumed to remain constant with decreasing crystallinity. This enables the use of the ratio between these two bands as a measure for crystallinity. The ratio R of the heights of the bands at 1280 and 1200 cm^{-1} has been calculated as is shown in figure 1. In figure 2 the ratio R is plotted versus the cellulose crystallinity x_c as determined with WAXS. From this line of regression it can be deduced that the ratio R is related to cellulose crystallinity x_c following the equation:

$$x_c = 1.06 R + 0.19 \quad (1)$$

The percentage variance adjusted for is 99.7% ($n = 7$). The line of regression is valid for $0.26 < x_c < 0.75$. Crystallinity could be predicted with a standard error of 0.01 - 0.02 ($n = 3$). Equation (1) was validated using two commercial cellulose I samples. For these samples crystallinity was determined using WAXS and was calculated from equation (1) using DRIFT measurements. The values are shown in table 1.

Table 1. Cellulose I crystallinities as determined with WAXS ($x_{c,m}$) and calculated from eq. (1) using DRIFT measurements ($x_{c,p}$).

Sample	$x_{c,m}$	$x_{c,p}$
Native cellulose	0.41	0.41
Cellulose powder	0.55	0.58

It can be concluded from Table 1 that crystallinity can be predicted using DRIFT spectrometry. In future research this method will be validated using sample sizes $> 50 \mu\text{m}$, since plant fibres can not be reduced to sizes $< 50 \mu\text{m}$ without decreasing crystallinity.

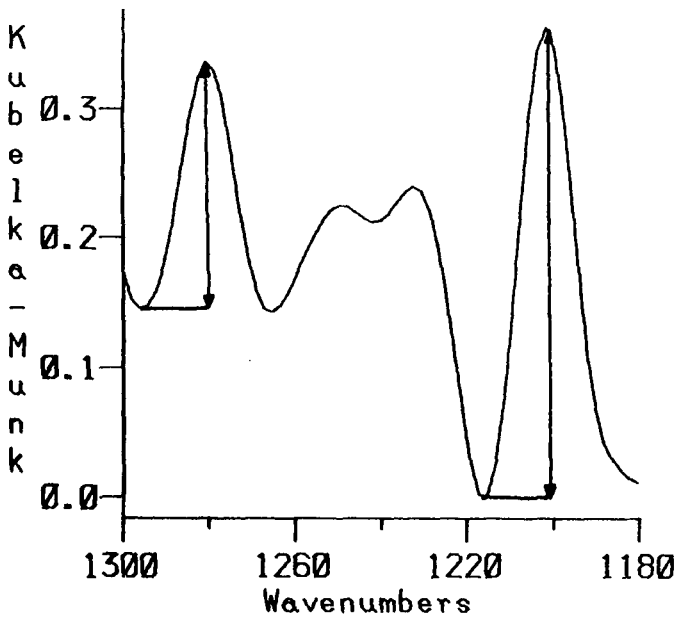


Figure 1. The calculation of the infrared ratio $R (= H_{1280}/H_{1200})$ of the heights of the bands at 1280 and 1200 cm^{-1} .

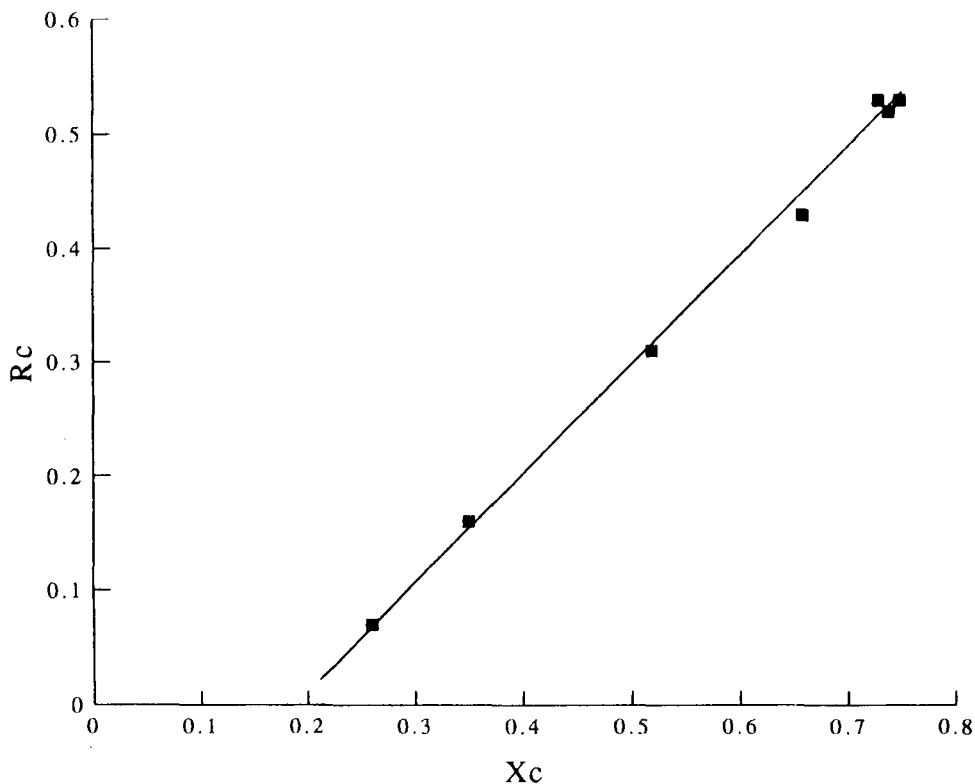


Figure 2. The infrared ratio R versus the cellulose crystallinity x_c as determined with WAXS.

CONCLUSIONS

A new method for the determination of cellulose I crystallinity in pure cellulose samples using DRIFT spectrometry has been developed. The infrared ratio R between the heights of the bands at 1280 and 1200 cm^{-1} proved to be a measure for cellulose I crystallinity. The infrared ratio R and the cellulose crystallinity x_c are related following the equation $x_c = 1.06 R + 0.19$ which is valid for $0.26 < x_c < 0.75$. The percentage variance adjusted for is 99.7%. Cellulose crystallinity can be predicted with a standard error of $0.01 - 0.02$ ($n = 3$). Since the infrared ratio R is selected to be independent from non-cellulosic fibre components, it will be possible to use this method to determine cellulose I crystallinity in plant fibres.

REFERENCES

1. N.R. Bertoniere and S.H. Zeronian, *ACS Symp. Ser.*, 340 (1987) 255-271.
2. G. Franz and W. Blaschek, *Methods in Plant Biochemistry*, 2 (1990) 291-322.
3. D.L. VanderHart and R.H. Atalla, *Macromolecules*, 20 (1987) 2117-2120.
4. H.-P. Fink, D. Fanter and B. Philipp, *Acta Polymerica*, 36 (1985) 1-8.
5. L. Segal, J.J. Creeley, A.E. Martin Jr and C.M. Conrad, *Text. Res. J.*, 29 (1959) 786-794.
6. P.H. Hermans and A. Weidinger, *J. Polym. Sci.*, 4 (1949) 135-144.
7. L.E. Alexander, *X-Ray Diffraction Methods in Polymer Science*, Wiley-Interscience, New York, 1969, p.167.
8. S. Polizzi, G. Fagherazzi, A. Benedetti, M. Battagliarin and T. Asano, *J. Appl. Cryst.*, 23 (1990) 359-365.
9. U. Richter, T. Krause and W. Schempp, *Die Angewandte Makromolekulare Chemie*, 185/186 (1991) 155-167.
10. M.L. Nelson and R.T. O'Connor, *J. Appl. Polym. Sci.*, 8 (1964) 1311-1324.
11. M.L. Nelson and R.T. O'Connor, *J. Appl. Polym. Sci.*, 8 (1964) 1325-1341.
12. F.G. Hurtubise and H. Krässig, *Anal. Chem.*, 32 (1960) 177-181.

10 Order of crystalline cellulose detected with the atomic force microscopy (AFM)

L Kuutti, J Pere, J Peltonen* and O Teleman – VTT, Biotechnology and Food Research, PO Box 1500, FIN-02044 Espoo, Finland;

* Department of Physical Chemistry, Åbo Akademi University, Porthaninkatu 3-5, FIN-20500 Turku, Finland

ABSTRACT

In this work we applied AFM for the surface study of cellulose microcrystals using highly crystalline *Valonia macrophysa* vesicles as the substrate. Vesicles were pretreated with dilute alkali and an excess of distilled water prior to imaging with AFM. An AFM image of a vesicle showed a group of closely packed microcrystals. A more detailed image of the membrane was also obtained. In the area of $14 \times 14 \text{ nm}^2$ the surface roughness was typically 1 nm. We calculated the two-dimensional fast fourier transform (FFT) of the raw data and obtained crystal parameters as well as a highly filtered inverse-transformed image. This image showed a periodicity of 1.01 nm, which may correspond to the fibre repeat unit length. Molecular modelling was used to generate a Connolly model surface of the crystalline cellulose. The data created thereby was converted to a format identical with the AFM image. The experimental images were compared with the synthetic images made by molecular modelling. Crystal surface 110 was found to fit very well to the experimental image.

INTRODUCTION

Although cellulose is the most abundant organic compound in the biosphere, its molecular structure is still relatively unknown. Atomic force microscopy (AFM) is a new powerful tool for surface imaging (Binnig *et al*, 1986). It was introduced as an application of the scanning tunneling microscope. AFM is capable of imaging soft organic surfaces with molecular resolution. The atomic force microscope is based on

scanning of the sample surface by a flexible cantilever tip. Cantilever deflection, which follows the topographical structure of the sample, is registered by an optical system comprising a diode laser as a light source and a photodetector (Fig. 1).

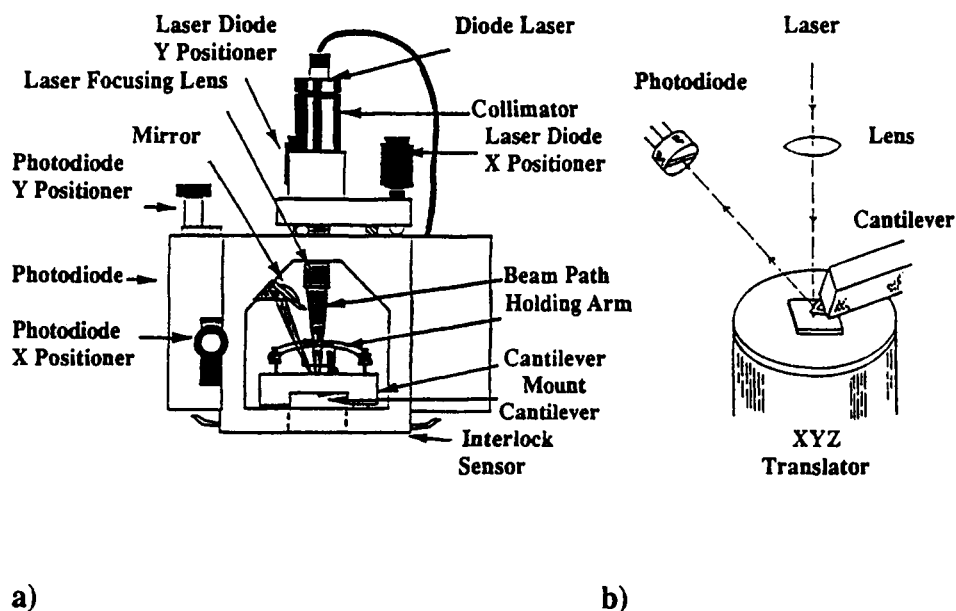


Figure 1. The Atomic Force Microscope: a) the structure of AFM head and b) the geometry of the measurement used in the AFM.

The sample is attached to an XYZ-translator which uses piezoscanners to move the sample in three dimensions. The sample is driven so close to the cantilever that they start to interact with each other. During the X-Y-scanning process, the distance between the cantilever and the sample is held constant. This can be accomplished either by adjusting the vertical position of the sample with the z-piezo (height mode, constant deflection) or by scanning over a stationary sample and detecting the variation in imaging force (force mode, deflection follows the topographical changes on the sample surface) and in both cases a 2-D topographical map can be created. The resolution of the system in Z-scale is as good as 1 Å. The maximum area that could be scanned with the used head was $15 \times 15 \mu\text{m}^2$. In this work we applied AFM for the surface study of cellulose microcrystals using highly crystalline *Valonia macrophysa* vesicles as the substrate. Molecular modelling was used to interpret the AFM images.

MATERIALS AND METHODS

Valonia macrophysa vesicles were pretreated with dilute alkali and an excess of distilled water prior to imaging by AFM. Thereafter small pieces (2 x 2 mm) of vesicles were cut and placed on the sample stubs. A Nanoscope II (Digital Instruments, Inc., Santa Barbara, USA) AFM was used to image the sample surfaces. The 100 μm cantilever tip with a spring constant of $k = 0.38 \text{ N/m}$ gave images with highest resolution. All the images (400 x 400 pixels) were measured in air. Both height and force modes were used to scan the surface of *Valonia*. The measuring unit was placed on a vibration-isolating table to eliminate external vibrational noise. In addition, high-pass filtering via both the electronics and software was used to cut off low-frequency noise.

Molecular modelling was used to generate a Connolly surface for crystalline cellulose based on the crystal structure of *Valonia ventricosa* (Gardner and Blackwell, 1974). The Connolly surface was calculated using the Discover program of BIOSYM (BIOSYM Technologies Inc., San Diego, USA). The modelled Connolly surfaces were converted to a format identical with the AFM image. The experimental images were compared with the modelled images for the three crystal planes 020, 1-10 and 110. Crystal planes 1-10 and 110 are typically the faces of cellulose microcrystals of *Valonia* (Chanzy *et al*, 1984) and crystal plane 020 is a reference face.

RESULTS AND DISCUSSION

In the AFM image of a vesicle a group of closely packed microcrystals can be seen (Fig. 2), similar to that obtained by TEM.

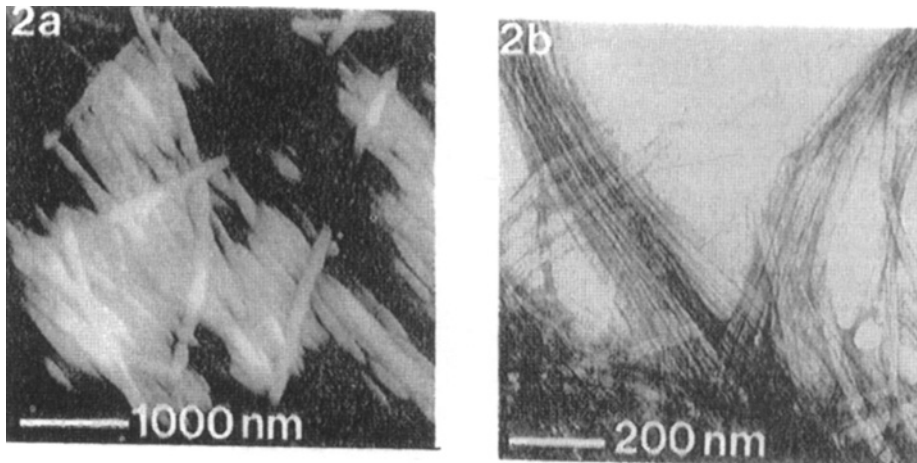


Figure 2. Macroscopic structure of a *Valonia* vesicle as revealed by a) atomic force microscopy and b) by transmission electron microscopy.

In the AFM image, the typical width of the microcrystals was 100 nm which is clearly bigger than the average diameter of 20 nm observed by TEM. This broadening of the object is due to convolution effects induced by the tip geometry (Hanley *et al*, 1992). A model illustrating the tip geometry effect has been developed (Zenhausern *et al*, 1992 and Butt *et al*, 1992), where the apparent lateral dimension of the object is given by the following expression:

$$L=4(R r)^{1/2}$$

where R is the tip radius, r is the object radius and L is the apparent lateral dimension of the object (Fig. 3).

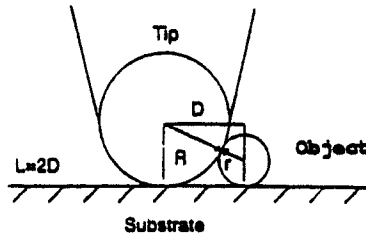


Figure 3. A model illustrating the tip-geometry effect.

With the values $R = 50$ nm (Hanley *et al*, 1992) and $L = 100$ nm, the width of one microcrystal is 25 nm. This result is comparable with the experimental data obtained by TEM, but should, however, be considered as a (rough) estimate since the shape and dimensions of the tip are only assumptions and these parameters vary from one tip to another. Furthermore, the width and the cross-sectional shape of microcrystals depend on the scanning mode used (Fig. 4). The images in fig. 4 indicate that a better dynamic response can be obtained when imaging in the force mode.

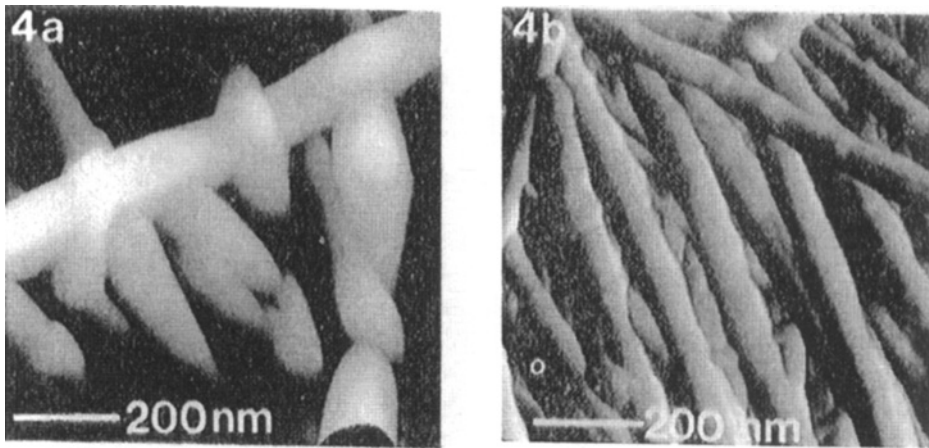


Figure 4. Effects of scanning mode on the image of *Valonia* microcrystal. Images obtained by a) the constant height mode and b) the force mode.

A more detailed image of the membrane was also obtained. Fig. 5 a shows a typical membrane surface ($14 \times 14 \text{ nm}^2$) with a surface roughness less than 1.2 nm. We calculated the two-dimensional fast fourier transform (FFT) of the raw data and obtained crystal parameters as well as a highly filtered inverse-transformed image. This image shows a periodicity of 1.01 nm, which may correspond to the fibre repeat unit length (1.038 nm, containing two glucose units, Gardner and Blackwell, 1974). The modelled Connolly surfaces were converted to the AFM image format. The experimental images were compared with the modelled images for the three crystal planes of 020, 1-10 and 110 in real space and in reciprocal space. In conclusion, the experimental image obtained most resembled the 110 crystal plane (Fig. 5 c).

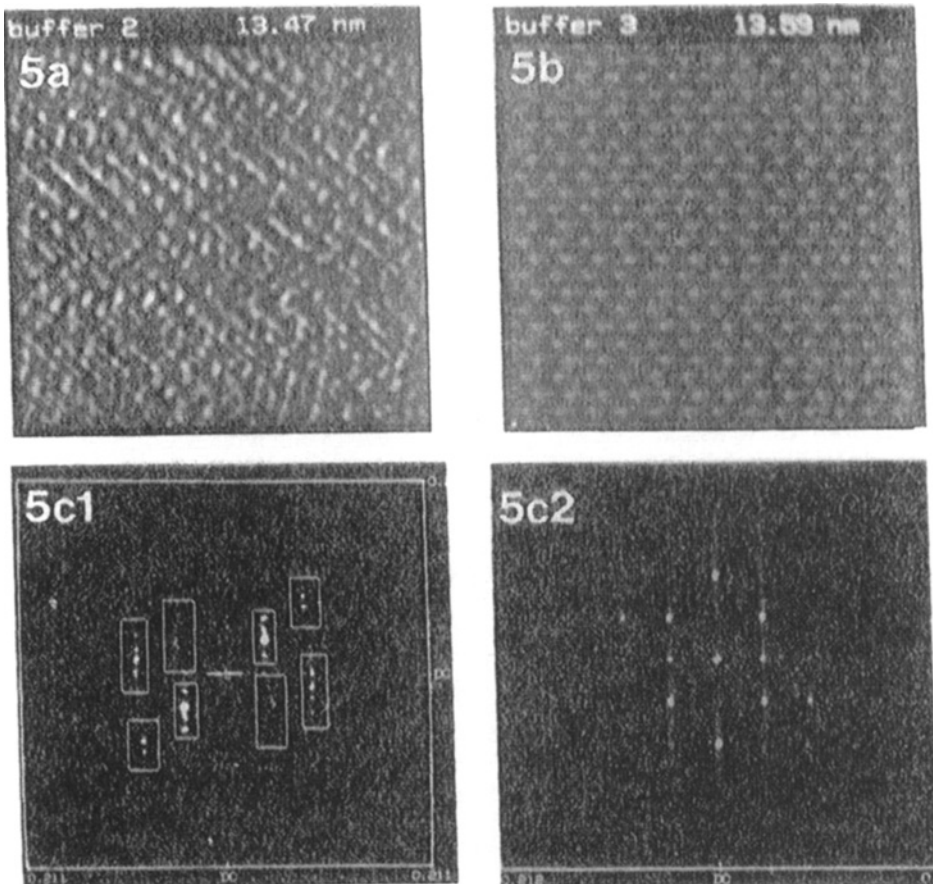


Figure 5. Molecular structure of highly crystalline *Valonia* cellulose: a) experimental image, b) synthetic image for the crystal plane 110 and c) comparisons of the two-dimensional FFT-spectra (1 experimental and 2 synthetic image).

REFERENCES

- 1) Binnig, G., Quate, C. F. and Gerber, C., *Phys. Rev. Lett.* 1986, 12, 930-933.
- 2) Gardner, K. and Blackwell, J., *Biopolymers* 1974, 13, 1975-2001.
- 3) Discover: Molecular simulation program, BIOSYM Technologies Inc., San Diego, USA
- 4) Chanzy, H., Henrissat, B. and Vuong, R., *FEBS Lett.* 1984, 172, 193-197.
- 5) Hanley, S. J., Giasson, J., Revol, J.-F. and Gray, D.G., *Polymer* 1992, 33, 4639-4642.
- 6) Zenhausern, F., Adrian, M., ten Heggler-Bordier, B., Eng, L. M. and Descouts, P., *Scanning* 1992, 14, 212-217.
- 7) Butt, H.-J., Guckenberger, R. and Rabe, J. P., *Ultramicroscopy* 1992, 46, 375-393.

11 Structural changes of cellulose and their effects on the OH/CH₂ valency vibration range in FTIR spectra

D Fengel, Institute for Wood Research, University of Munich
D-80797 Munich, Winzererstrasse 45, FR Germany

ABSTRACT

Several examples show that variations in the cellulose structure are reflected in the deconvoluted OH/CH₂ vibration range of IR spectra. Thus differences in the celluloses from higher plants and from bacteria were found, the influence of water was proved, and changes caused by thermal and mechanical treatments were traced. The deconvoluted range of 2500 to 3700 cm⁻¹ contains a great amount of information on the molecular and supramolecular structure of cellulose and its changes under chemical, thermal and mechanical influences.

INTRODUCTION

Cellulose is subject to various structural changes caused by the action of chemicals, temperature, irradiation and mechanical forces. In general, changes in compounds are easy to observe by IR spectroscopy. In particular, modern FTIR instruments excel on account of a good signal-noise ratio, a wider range of linearity and a high wavenumber accuracy. Apart from other advantages such as velocity of spectrum formation and application to very small sample quantities, the combination with an efficient computer makes various processings of the spectra such as baseline correction, normalization, subtraction, derivation etc. possible.

Spectra of cellulose obtained in an FTIR spectrometer show very clear profiles of the various bands in the fingerprint range which are qualitatively better compared to spectra from a dispersive instrument. They do not, however, provide any additional information.

Almost all reactions and transformations which take place at the cellulose molecules involve the hydroxyl groups. In a normal IR spectrum of cellulose the range of the main OH vibrations ($3000 - 4000 \text{ cm}^{-1}$) remains unresolved or only poorly resolved. For more information our studies concentrated on the OH range of the cellulose spectrum. This range was resolved by the so-called deconvolution process (Kauppinen et al. 1981). This process, as part of the spectrometer's computer program, uses a triangular apodization function. Optimum results were obtained with a K-factor of 2 and a half-width of 100 cm^{-1} (Ludwig, Fengel 1992). The deconvoluted spectra in the range of $3200 - 3700 \text{ cm}^{-1}$ for different crystalline modifications of cellulose differ not only in the band profile but also in band positions. Thus, they can be definitely distinguished independent of the degree of crystallinity (Fengel 1991; 1992).

CELLULOSE OF VARIOUS ORIGINS

Another improvement in the study of cellulose OH groups was the extension of the deconvoluted wavenumber range starting with 2500 cm^{-1} . In the range of $2800 - 2950 \text{ cm}^{-1}$ the vibrations of the CH_2 and CH_2OH groups are located (Hediger 1971; Panov, Zbankov 1988). This OH group is well defined as it belongs to the primary C(6)-atom (Fig. 1).

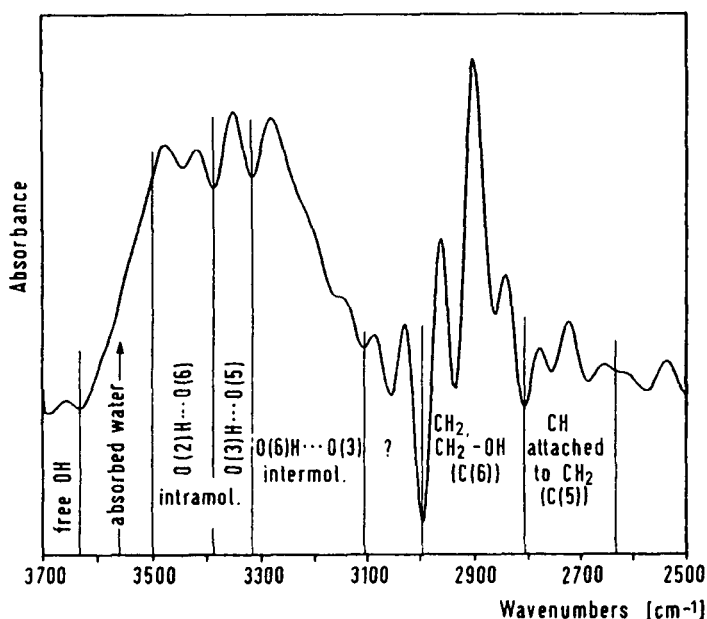


Fig. 1. Deconvoluted FTIR spectrum of cellulose ($2500 - 3700 \text{ cm}^{-1}$) with band attribution of groups and linkages

The definition of the various absorbance ranges according to groups and linkages in the cellulose molecule have been described in the literature (Liang, Marchessault 1959; Panov, Zbankov 1988; Ivanova et al. 1989). Attributions can also be found from IR studies of related compounds such as polyhydric alcohols (Hediger 1971; Bellamy 1975).

Fig. 2 shows the extended deconvoluted range from 2500 to 3700 cm^{-1} of three natural fibres. These profiles are very similar, with identical band positions. In the CH_2OH range some variations can be observed which probably indicate individual differences between the fibres. More distinctive differences can be seen with samples involving different degrees of crystallinity.

Absorbances of the bands at 3280, 3350 and 3415 cm^{-1} increase with rising crystallinity. These bands are attributed to the inter- and intra-molecular hydrogen bonds. There is a marked coincidence in the range of the CH_2OH group for the three samples. But in the range of the intermolecular H-bonds between C(6)OH and C(3)OH there are differences not only in absorbances but also in band positions when comparing bacterial cellulose and other celluloses (Fig. 3). Early in 1956, Marrinan and Mann detected a band in the IR spectra of bacterial and algal celluloses which was absent in the spectra of higher plants. This band was positioned at 3242 cm^{-1} which closely resembles that of 3236 cm^{-1} (Fig. 3).

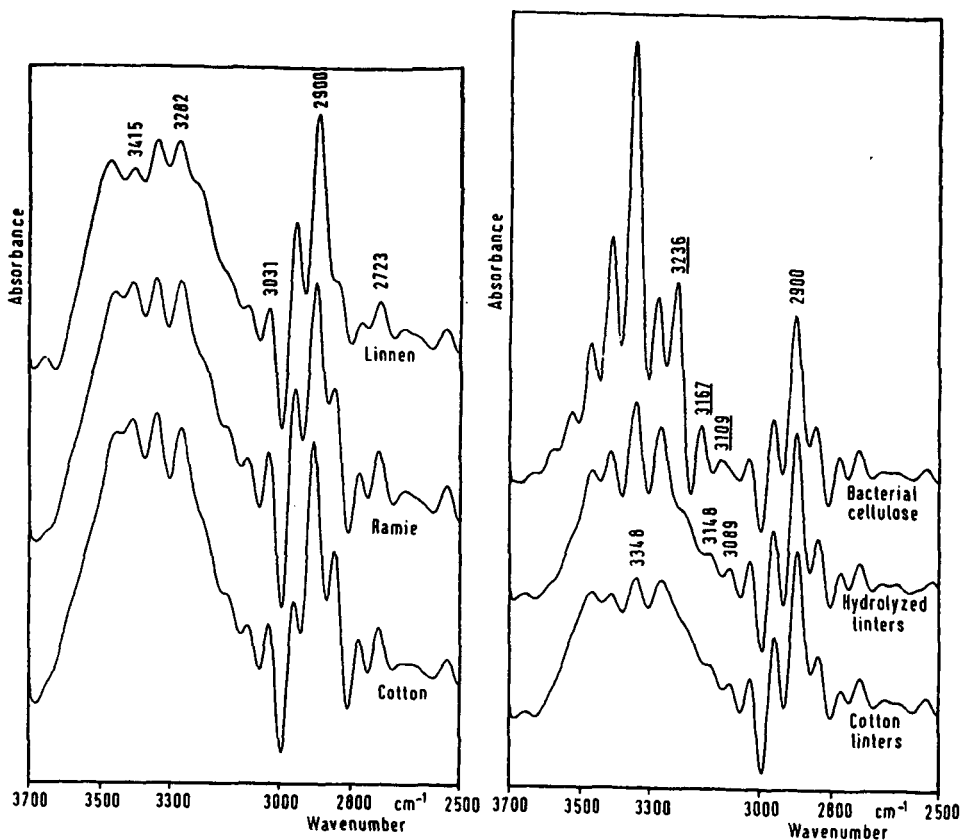


Fig. 2. left Deconvoluted FTIR spectra of three natural fibres (2500 - 3700 cm^{-1})

Fig. 3. right Deconvoluted FTIR spectra of original and hydrolyzed cotton linters and bacterial cellulose

Two types of crystalline natural cellulose I (bacterial-valonia type and cotton-ramie type) were also found by MAS¹³C NMR spectroscopy (VanderHart, Atalla 1984; Horil et al. 1987). The two types vary in the signals of C(1), C(4) and C(6). This result indicates a different chain formation which influences the glycosidic linkages as well as the intermolecular H-bonds. This effect is reflected by different band positions in the range of the O(6)H...O(3) H-bonds.

INFLUENCE OF WATER

Water may be free or H-bonded in cellulose samples and its vibrations should also appear in the wavenumber range of 3000 - 3800 cm⁻¹. In the fingerprint range there is a band at 1635 cm⁻¹ attributed to adsorbed water (Tsuboi 1957). It can be observed that this band disappears when the KBr pellets were dried at 105°C for a longer period of time (Fengel 1993). Drying also effects the profile of the deconvoluted OH range of the cellulose spectrum. In particular, the bands at 3415 and 3465 cm⁻¹ decrease and become more pronounced (Fig. 4). These bands are attributed to H-bonds in which the C(2)OH groups are involved. Thus, it can be concluded that the adsorbed water is mainly linked to this OH group.

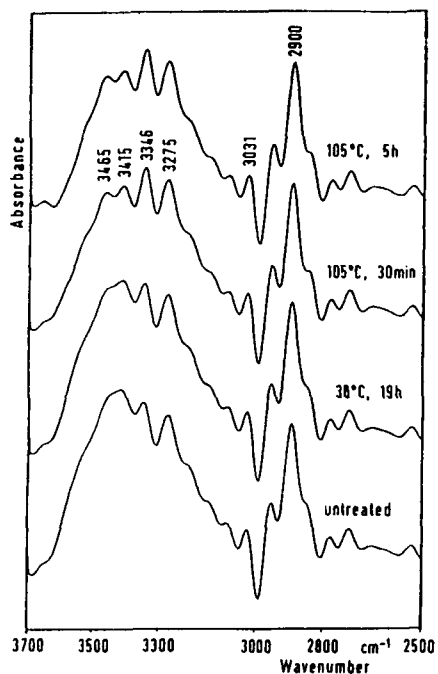


Fig. 4. left Deconvoluted FTIR spectra of cotton linters after various drying periods (2500 - 3700 cm⁻¹)

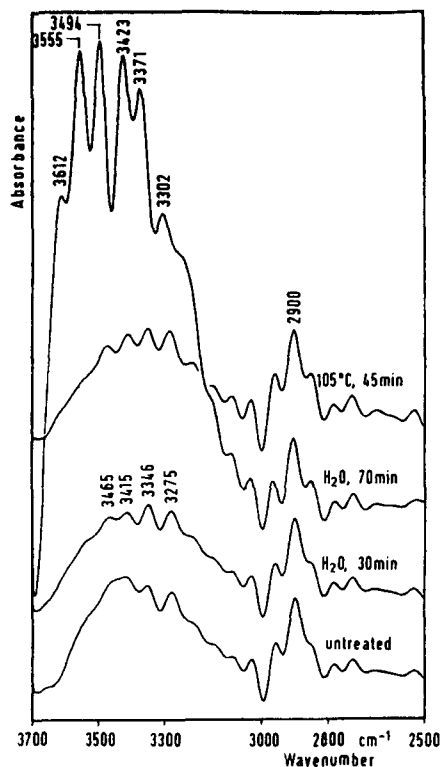


Fig. 5. right Deconvoluted FTIR spectra of cotton linters after various humidification periods (2500 - 3700 cm⁻¹)

All bands between 3200 and 3600 cm^{-1} increase when humidifying the samples by storing the KBr pellets in a humid atmosphere (Fig. 5). The uptake of a high percentage of water causes not only an increase in absorbance but also a shift in band positions. Their absorbance is reduced again by drying but the shift in bands cannot be reversed. This effect may be an indication of the interaction of cellulose with KBr under high humidity conditions. Consequently, the KBr pellets are dried for at least 1 h at 105°C before measuring is undertaken.

THERMAL TREATMENT

Another treatment which may influence the cellulose structure is high temperature heating. To study this influence cotton linters were dried in vacuum and then heated in an autoclave under nitrogen for 8 hours. The temperature varied between 100 and 220°C. Fig. 6 shows that there is no significant change in the profile up to 150°C. At 200 and 220°C a distinct change in profile appears within the range of the C(2)OH and C(3)OH groups or the respective H-bonds.

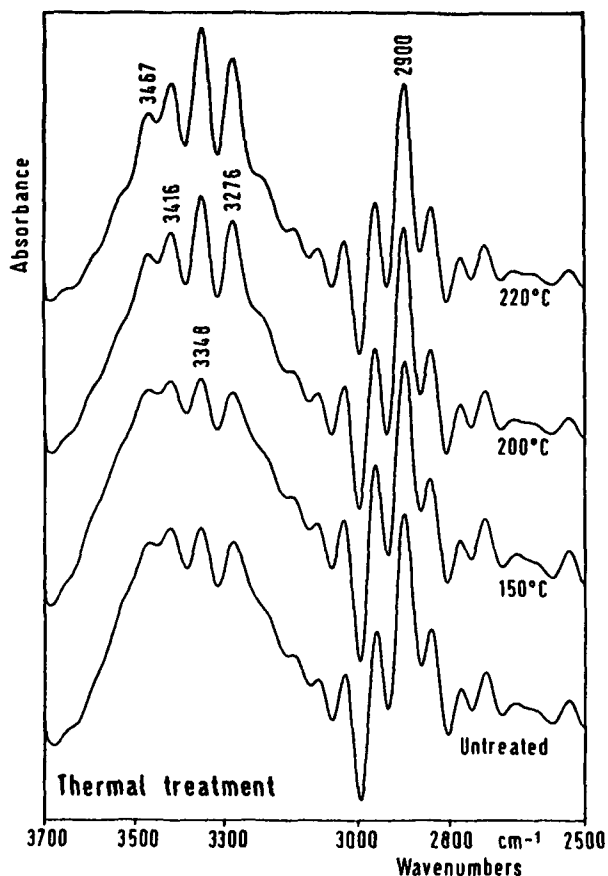


Fig. 6. Deconvoluted FTIR spectra of cotton linters after various heating periods under nitrogen (2500 - 3700 cm^{-1})

The absorbances of the various bands remain more or less stable up to 180°C (Fig. 7). At higher temperatures the bands at 2840 and 3496 cm⁻¹ decrease while the bands at 3276 and 3346 cm⁻¹ increase. When thermal treatment is carried out in the presence of water a greater increase in bands at 3276 and 3348 cm⁻¹ is observed which begins between 100 and 150°C (Fig. 8). The decrease in bands at 2843 and 3467 cm⁻¹ starts between 150 and 180°C.

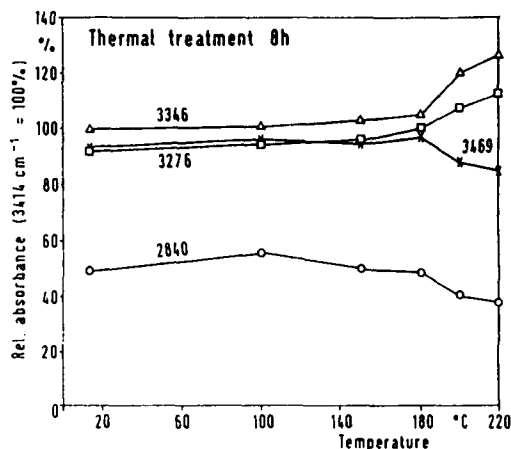


Fig. 7. Variation in the relative absorbances of some FTIR bands during heating of cotton linters under nitrogen

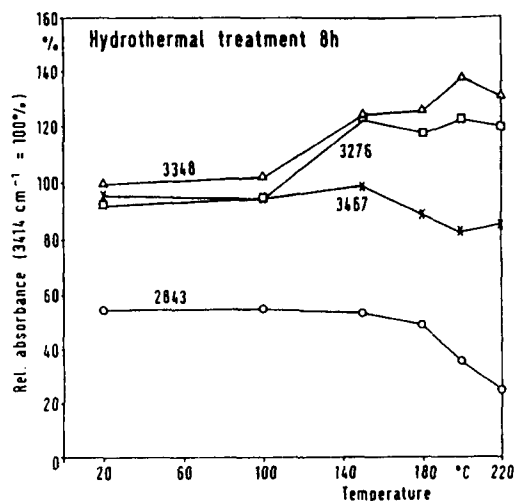


Fig. 8. Variation in the relative absorbances of some FTIR bands during heating of cotton linters with water under nitrogen

If it is assumed that the thermal treatment causes merely a hydrolytic splitting of the cellulose chains the change in absorbances must be seen as an effect of this kind of degradation. A comparison between the spectra of celluloses degraded by thermal and hydrothermal treatment at 220°C (Fig. 6) with the spectrum of cellulose degraded by acid treatment (Fig. 3) reveals identical profiles. The acceleration of hydrolysis by water is reflected by the variation

in the absorbances of certain bands. Moreover, a correlation between the band at 3276 cm^{-1} and the degree of polymerization is deducible (Fig. 9).

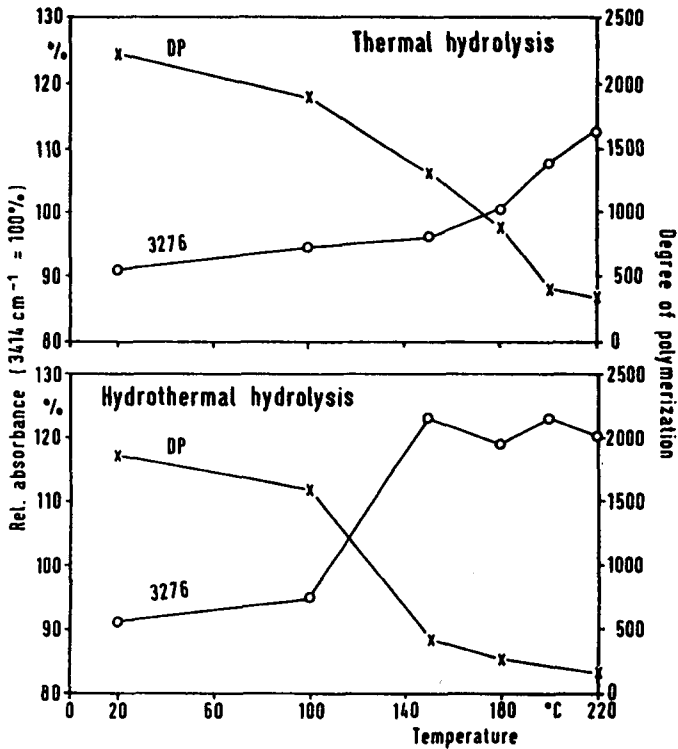


Fig. 9. Variation in the relative absorbance at 3276 cm^{-1} and the degree of polymerization (DP) during heating of cotton linters with and without water under nitrogen

BALL-MILLING AND D_2O -EXCHANGE

A further experiment whose results will be discussed here is the tracing of ball-milling of cotton linters for a period of 60 min. It is well known that ball-milling destroys the crystalline structure of cellulose and reduces its degree of polymerization. The spectra of cellulose after various periods of milling show the following two effects: One is the change in profile over approximately the whole range between 2500 and 3700 cm^{-1} , and the second is the position shift in some of the bands (Fig. 10).

The bands with greatest changes during ball-milling are characterized by a decrease, with the main drop between 0 and 20 min ball milling. Between 20 and 60 min milling there is only a slight decrease in absorbance ($2723/2708$; $3275/3283$) or no change (Figs. 12 and 13). The band at 3472 cm^{-1} is only slightly changed throughout the entire milling period. This band is another one of those unchanged in their wavenumber position.

The bands attributed to the $\text{CH}_2/\text{CH}_2\text{OH}$ are shifted between 5 and 20 min ball-milling to lower wavenumbers while the bands attributed to the intermolecular H-bonds between C(6)OH and C(3)OH are shifted to higher wavenumbers. The bands at 3345, 3414 and 3470 cm^{-1} do not change wavenumber during milling. In this range, too, only small changes in absorbances were found. This finding means that ball-milling does not effect greater changes in the conditions at the C(2)OH and C(3)OH groups, in particular concerning the O(3)H...O(5) bond of the latter. Since the early days of IR spectroscopic cellulose investigations studies of exchange with deuterium oxide were carried out (Rowen, Plyler 1950; Almin 1952; Marrinan, Mann 1956). The wavenumber range of 2400 to 2700 cm^{-1} is attributed to the OD stretching vibrations.

Air dried cotton linters were soaked in D_2O for 24 hours. After this treatment the samples were vacuum-dried for at least 24 h. Due to the additional drying of the pellets before measuring it can be assumed that all adsorbed D_2O is removed and only the exchanged OD groups are being registered.

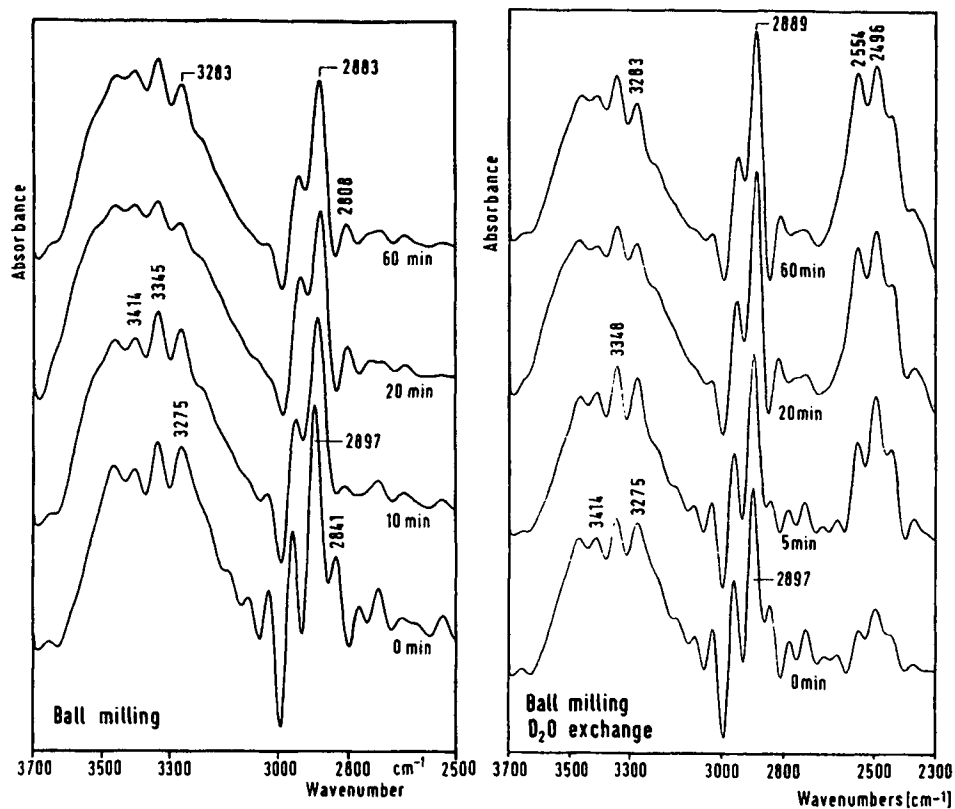
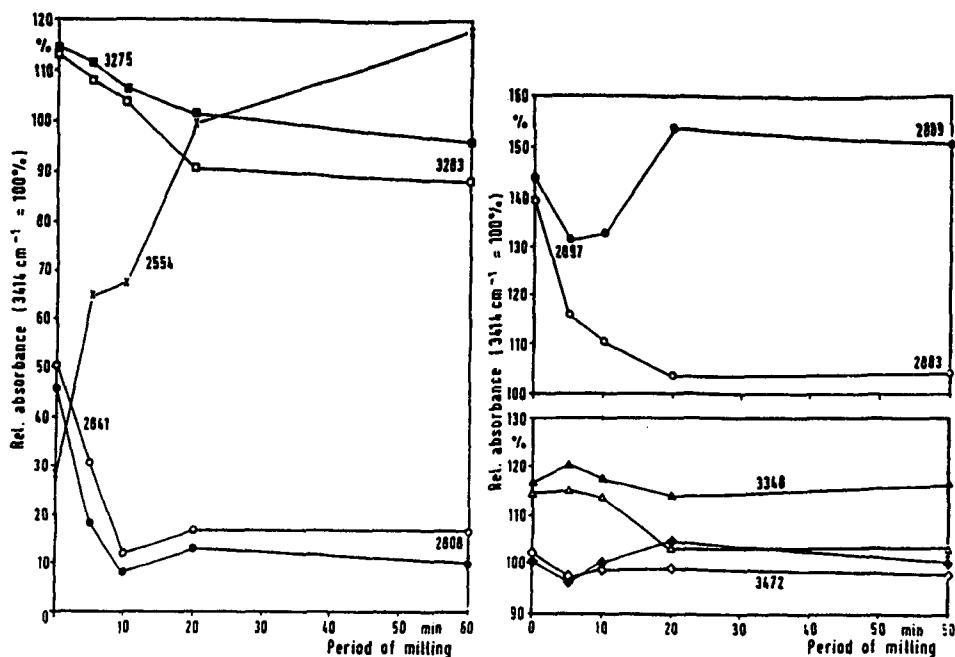


Fig. 10. left Deconvoluted FTIR spectra of cotton linters after various periods of ball-milling (2500 - 3700 cm^{-1})

Fig. 11. right Deconvoluted FTIR spectra of cotton linters after various periods of ball-milling followed by D_2O exchange (2500 - 3700 cm^{-1})

There is no visible difference in the range of 2600 to 3700 cm^{-1} between the spectra in Fig. 11 compared to those from ball-milled cellulose without D_2O exchange (Fig. 10). Three additional bands at 2450, 2496 and 2554 cm^{-1} appear which increase with increasing milling period and with reduction in crystallinity. The increase varies in the three bands; in particular the band at 2524 cm^{-1} increases faster than the other two bands. Furthermore, the absorbance at 2889 cm^{-1} increases and is much higher after 60 min milling compared to the sample without D_2O exchange.

When tracing the change in absorbances of the main bands during ball-milling a very different influence of the D_2O exchange on the course of the various curves is observed (Fig. 12). There is a very steep increase in the 2554 cm^{-1} band between 0 and 20 min milling and a more moderate increase up to 60 min milling. This band belongs to the OD vibrations. The bands at 2841 and 3275 cm^{-1} are only slightly or moderately influenced by the D_2O exchange. The same is true for the band at 3472 cm^{-1} whereas at 3348 cm^{-1} a continuous increase in the distance between the curve of non-exchanged and D_2O exchanged samples can be seen (Fig. 13). The difference between the two curves of the 2897 cm^{-1} band is very striking. During the first 5 min ball-milling a decrease is observed similar to that in the sample without D_2O exchange. Subsequently, the curve increases up to 20 min milling in contrast to the curve without D_2O exchange.



Figs. 12 and 13.

Variation in the relative absorbances of some FTIR bands during ball-milling of cotton linters without (open marks) and with (black marks) subsequent to D_2O exchange

Although the changes taking place in the IR spectra after ball-milling of the cellulose combined with D_2O exchange cannot as yet be totally explained some of them indicate variations in the molecular and supramolecular structure of cellulose.

The OH group which becomes most accessible to an OD exchange is that at the C(6) atom. Compared to the C(2)OH the C(3)OH is also relatively easily accessible to the OD exchange. C(6)OH and C(3)OH are involved in the intermolecular H-bonds. The band which is attributed to this H-bond is at 3275 cm^{-1} and also shows a difference in absorbance even though this difference between the curves with and without D_2O exchange is only moderate. This finding is probably due to the maintenance of the O(3)H...O(5) bond.

CONCLUSION

Several examples show that variations in the cellulose structure are reflected in the deconvoluted OH vibration range of IR spectra. This range contains a great amount of information on the molecular and supramolecular structure and its changes under various influences. The study of cellulose by FTIR spectroscopy will become a new dimension if interest concentrates on the vibration range of the OH groups which is effectively resolved by deconvolution.

REFERENCES

- Almin, K.E. 1950, *Svensk Papperstidn.* **55**, 767
 Bellamy, L.J. 1975, *The infrared spectra of complex molecules*. Chapman and Hall, London
 Fengel, D. 1991, The application of FTIR spectroscopy in cellulose research, Cellulose '91 Conference, Dec.2-6,1991, New Orleans, USA, Proc. in press
 Fengel, D. 1992, *Holzforschung* **46**, 283
 Fengel, D. 1993, *Holzforschung* **47**, 103
 Hedlger, H.J. 1971, *Infrarotspektroskopie. Grundlagen, Anwendungen, Interpretation*, Akad. Verlagsges., Frankfurt/M.
 Horil, F.; Hirai, A.; Kitamura, R. 1987, *Macromolecules* **20**, 2117
 Ivanova, N.V.; Korolenko, E.A.; Zbankov, R.G. 1989, *Zh.Prikl.Spektrosk.* **51**, 301
 Kauppinen, J.K.; Moffat, D.J.; Mantsch, H.H.; Cameron, D.G. 1981, *Appl. Spectrosc.* **35**, 271
 Llang, C.Y.; Marchessault, R.H. 1959, *J.Polymer Sci.* **37**, 385
 Ludwig, M.; Fengel, D. 1992, *Acta Polymer.* **43**, 261
 Marrinan, H.J.; Mann, J. 1956, *J.Polymer Sci.* **21**, 301
 Panov, V.P.; Zbankov, R.G. 1988, *Intra- and intermolecular interactions in hydrocarbons (russ.)*, Minsk
 Rowen, J.W.; Plyler, E.K. 1950, *J.Res.Natl.Bur.Std.* **44**, 313
 Tsuboi, M. 1957, *J.Polymer Sci.* **25**, 159
 VanderHart, D.L.; Atalla, R.H. 1984, *Macromolecules* **17**, 1465

12 Structural change of cellulose polymorphs by milling

K Kimura*, Y Shimizu and J Hayashi – * Tomakomai National College of Technology and Faculty of Engineering, Hokkaido University, Japan

ABSTRACT

Cellulose I, II, III₁ and III₁₁ were milled below 40 °C with a vibrating mill made of tungsten carbide after pre-cutting to under 20 mesh. All went to an amorphous state via IV. For the transformation to IV heat was not always necessary and molecular motions under the relaxed intermolecular hydrogen bonds were necessary. Mechanical energy through milling was sufficient.

III₁ was most unstable and most rapidly decrystallized, and by the hydrolysis with 2.4 M HCl at 100 °C after the milling it easily changed into the original structure, I. III₁₁ was rather stable and hardly changed into II by the hydrolysis after the milling. All amorphous samples were recrystallized into IV by the hydrolysis. Amorphous ramies milled for 80 and 100 min. were recrystallized into I and II, respectively, by immersing in water or a 1% NaOH soln. at 25 °C and air drying. During the further milling from 80 to 100 min. the irreversible change from I to II arose. But there was no violent morphological changes suggesting the change of the chain polarity systems.

INTRODUCTION

It is known that cellulose I is decrystallized by milling leading to a completely amorphous state and it is recrystallized into cellulose II. But there are few papers on milling of other cellulose polymorphs. To investigate characteristics of the polymorphs they were decrystallized by milling and recrystallized. The polymorphs in the cellulose I family change irreversibly into those in the II family. There are two hypotheses on the

cause of the irreversibility. One is the chain polarity theory by Sarko that the I and II families have parallel and antiparallel chain systems, respectively (1). Another is our chain conformation theory that the I and II families have "bent" and "bent & twisted" chain conformations, respectively (2). This study may give some information for solving the problem.

A conventional ballmilling brings much metal powder into the cellulose samples and makes the fine analysis of them difficult. To prevent this problem a mill made of tungsten carbide was used in this study. The degree of decrystallization with the mill was affected by the forms of the samples. Samples pre-cut to small size were homogeneously decrystallized, and it was revealed that all polymorphs went to an amorphous state via cellulose IV, though the milling was carried out below 40 °C. The mechanism of the transformation into IV is discussed.

EXPERIMENTAL

Raw materials : Ramie, pulp, mercerized pulp, rayon, and III₁ and III₁₁ prepared from ramie and rayon, respectively, via ammonia-cellulose (3).

Milling : The cellulose fibers were cut with the Wiley Mill and ones under 20 mesh were subjected to the milling. A vibrating sample mill made of tungsten carbide was used. The cut fibers (8 g) were put in the pot (volume of 20 ml) of the mill and milled, with cooling every 5 min. to under 40 °C. The total milling time was accounted by the sum of the milling time.

Recrystallization : The milled samples were immersed in water at 25 °C for 120 hr or in 1% NaOH aq. solution at 25 °C for 24 hr. and air dried after washing. They also were recrystallized by hydrolysis with 2.4 M HCl at 100 °C for 1 hr and air drying after washing.

RESULTS AND DISCUSSION

Fig.1 shows X-ray diffractograms of the ramie milled for various times. There was a tendency that (110) decreased most rapidly in intensity compared with (110) and (020), and (110) kept its intensity for the longest time. The results suggested that the chains in (110) molecular sheet began rotation or shifting in early in the milling but remained in the sheet until some time later. The sample milled for 45 min. shows a single peak of (110) at $2\theta=15.3^\circ$ and (020) shifted to $2\theta=22.2^\circ$. That means a change from cellulose I to IV. Ramie showed an almost complete amorphous pattern after the milling for 80 min. and the complete one after 100 min..

The milled samples were hydrolyzed with a 2.4 M HCl at 100 °C, and Fig. 2 shows their X-ray diffractograms. The sample milled for 35 min. showed a complete X-ray pattern of cellulose I by the hydrolysis. The sample transformed into IV by milling for 45 min. showed a mixture pattern of cellulose I and IV. The amorphous IV from the milling for 65 min. was recrystallized into IV. The recrystallized IV was judged as IV₁ from the main peak of OH stretching bands being at 3300 cm^{-1} in its IR spectrum. The ramie milled for 65 min. had remained in the cellulose I family. The amorphous samples milled for 80 and 100 min. showed a mixture pattern of IV and II by the hydrolysis method (f and g in Fig.2). The IV in these samples could not be judged as IV₁ or IV₁₁ from their IR spectra because they were mixtures

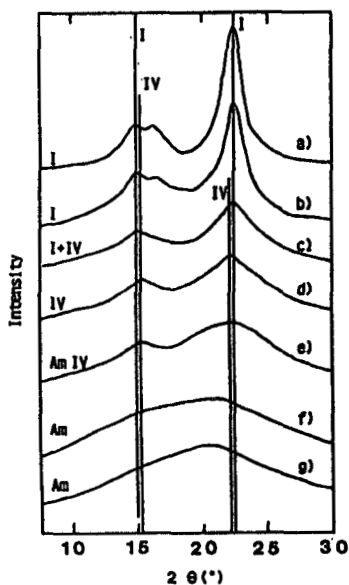


Fig.1 X-ray diffractograms of ramie milled for 0 (a)(raw m.), 20(b), 35(c), 45(d), 65(e), 80(f), and 100(g) min.

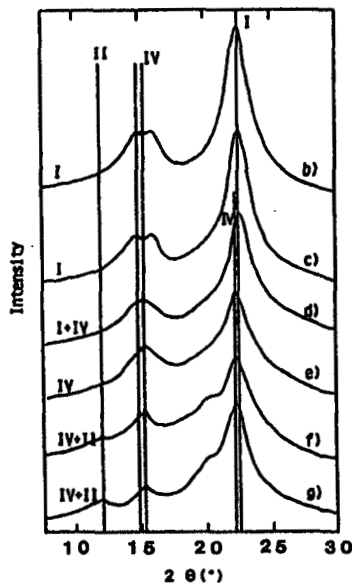


Fig.2 X-ray diffractograms of ramie recrystallized with 2.4 N HCl at 100°C after the milling for 20(b), 35(c), 45(d), 65(e), 80(f), and 100 (g) min.

with II. An amorphous cellulose has a tendency to transform easily into IV at high temperature (4). The temperature of 100 °C at which the hydrolysis was performed was not enough for the transformation into IV even for amorphous cellulose. But it was enough in the case where it was accompanied by hydrolysis. Thus, it is suggested that the IV was formed secondarily by the transformation from the high temperature.

The milled samples were recrystallized in water and a 1% NaOH solution at 25 °C. Fig.3 shows X-ray diffractograms of them. Though both samples milled for 80 and 100 min. showed similar amorphous patterns, they showed broad patterns of cellulose I and II, respectively, by recrystallization with water. By the recrystallization with 1% NaOH solution they showed clear patterns of cellulose I containing a little II and II, respectively. Accordingly, most of the ramie milled for 80 min. had remained in the cellulose I family, but it changed to the II family after the milling for 100min.. We can say that it should pass a critical point for the irreversible change from I to II during the further milling from 80 to 100 min.

Fig.4 shows SEM photographs of the ramie milled for 80 and 100 min. and of them recrystallized with a 1% NaOH solution at 25°C. There were no drastic morphological changes suggesting the change of the chain direction or mixing between microfibrils that had the parallel chain system but different chain direction (5). We have reported that for the irreversible change from I to II by mercerization, swelling was not always necessary and the change could arise during the ageing in the dry state at room temperature (6). It

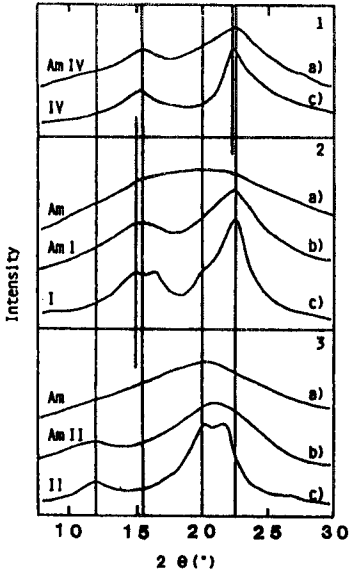


Fig. 3
X ray diffractograms of ramie milled for 45 min. (1), 80 min. (2), and 100 min. (3).
 a) : milled ramie,
 b) : a) recrystallized with water at 25°C
 c) : a) recrystallized with 1% NaOH soln. at 25°C

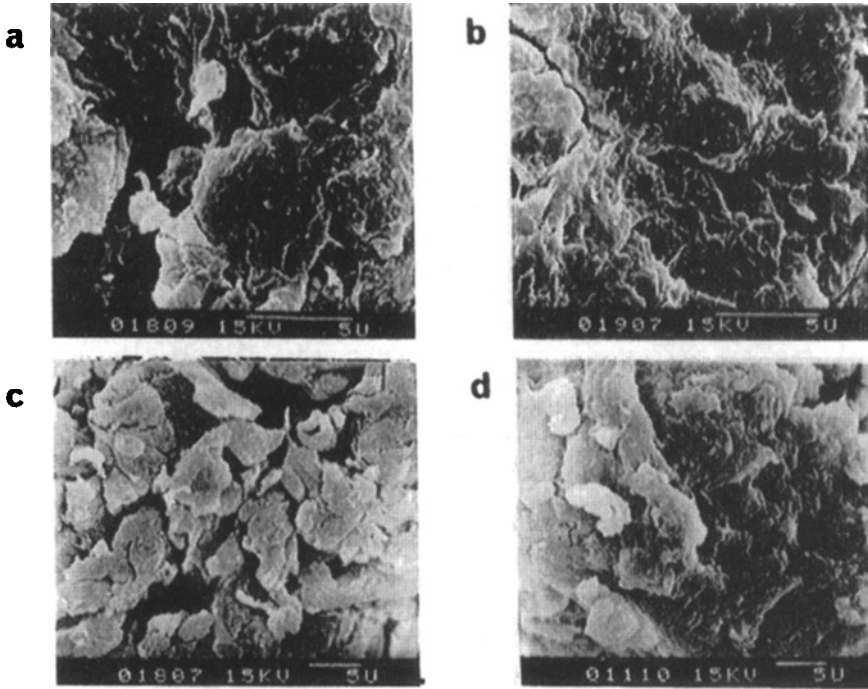


Fig. 4 SEM photographs of ramie milled for 80 (a), and 100 min. (b and c). And it of (b,c) recrystallized with a 1% NaOH aq. soln. at 25°C (d).

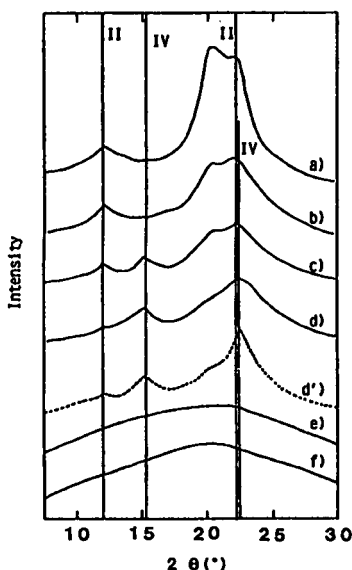


Fig.5 X-ray diffractograms of mercerized pulp milled for 0 (a)(raw m.), 15(b), 25(c), 70(d), 90(e), and 100(f) min, and of (d) recrystallized with 1% NaOH soln. at 25 °C(d').

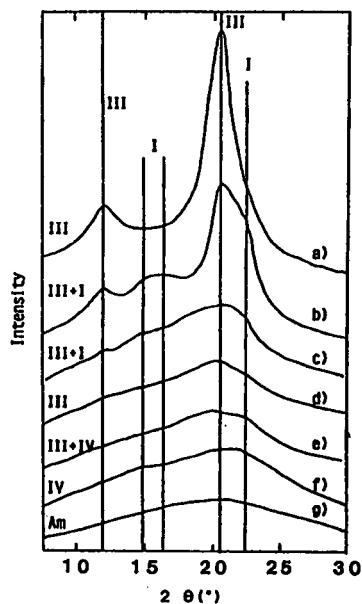


Fig.6 X-ray diffractograms of III, milled for 0 (a)(raw m.), 0(b)(cut raw m.), 2(c), 5(d), 25(e), 50(f), and 80(g) min.

is questionable that the irreversibility was based on the change of the chain polarity. It is more natural that the irreversibility was based on the change into a more stable chain conformation.

1-a and 1-c in Fig. 3 show X-ray diffractograms of the ramie milled for 45 min. before and after the recrystallization with a 1% NaOH solution at 25 °C, respectively. 1-c shows a clear pattern of IV. The IV was not one transformed secondary and should be brought from a latent structure in the milled sample. The same results were obtained for pulp, and it was believed that cellulose I went to the amorphous state via IV.

Fig. 5 shows the change of X-ray diffractogram of mercerized pulp as caused by the milling. The X-ray pattern of II on the origin changed into a mixed pattern of II and IV by the milling for 25 min. and the ratio of IV increased with increase of the milling time and that of 70 min. sample was almost IV. The IV was confirmed by the recrystallization with a 1% NaOH solution (d' in Fig. 5). The IV was judged as IV₁₁ from the main band of OH stretching at 3400 cm⁻¹ on its IR spectra. The milling over 90 min gave an almost completely amorphous pattern. Also cellulose II went to the amorphous state via IV. The amorphous samples from the II gave X-ray patterns of IV containing II effected by the hydrolysis.

Fig. 6 shows the change of X-ray diffractogram of the cellulose III₁ by the milling. The III₁ was unstable and reverted partially to cellulose I just by the cutting to under 20 mesh (b in Fig. 6). On being milled it changed rapidly to an amorphous state. The III₁ milled for only 5 min showed an almost completely amorphous pattern. The milled samples of III₁ were hydro-

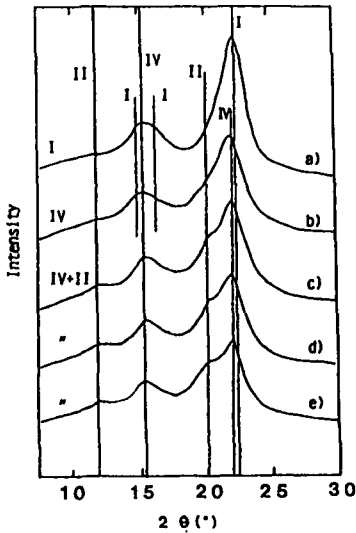


Fig. 7 X-ray diffractograms of III_1 , recrystallized with 2.4 M HCl at 100°C after the milling for 0 (a) (cut raw m.), 2 (b), 5 (c), 25 (d), and 50 (e) min..

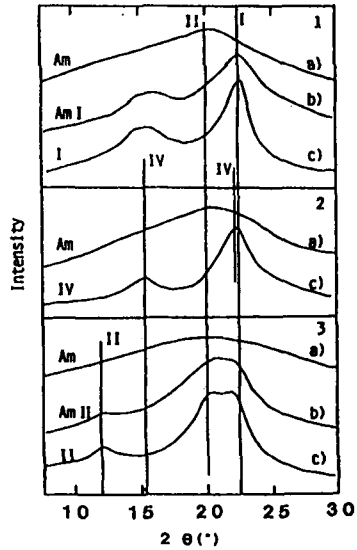


Fig. 8 X-ray diffractograms of III_1 , milled for 10 (1), 25 (2), and 80 (3) min.. (a) : milled III_1 , (b) and (c) : (a) recrystallized with water and 1% NaOH soln., respectively.

lyzed with 2.4 M HCl, Fig. 7 shows their X-ray diffractograms. The sample cut and not milled gave an X-ray pattern of I. The sample milled for 2 min. gave a mixed pattern of I and IV, and samples milled for more time gave those of IV containing II. One milled for a long time gave that of II. They were recrystallized with water and 1% NaOH solution. Fig. 8 shows part of the results. The samples milled for less than 10 min. were recrystallized into I but ones milled for 25 and 80 min. were recrystallized into the mixture of IV and II and the completely II, respectively. The conditions of the recrystallization were very mild and the crystallite forms recrystallized should reflect latent structure in the amorphous samples. So we can say that III_1 also went into an amorphous state via IV though that was not clear from the rapid change to an amorphous state.

Fig. 9 shows the change of X-ray diffractograms of the III_{11} induced by the milling. The III_{11} was more stable than III_1 and the X-ray pattern of it did not change on the cutting. On milling for less 30 min, the pattern of III_{11} was kept though it was decrystallized. The X-ray pattern of the sample milled for 40 min showed that of IV containing III_{11} . The sample milled for 70 min showed an amorphous pattern. The samples were hydrolyzed with 2.4 M HCl, their X-ray diffractograms are shown in Fig. 10.

The III_{11} just cut to under 20 mesh showed the X-ray pattern of III and the pattern was not changed by the hydrolysis. The III_{11} milled for less than 30 min. showed that of the mixed pattern of III_{11} containing II, and the proportion of II increased with increasing milling time. III_{11} was stable and only partially reverted into the original structure, II. The result was in contrast to that of III_1 , which was milled for short time and was changed

completely into its original structure, I, by the hydrolysis, even on the just cut sample. The III_{11} milled for over 40 min. showed the mixed pattern of IV and II or IV and III. Their mixed X-ray patterns are very similar to each other and are hardly distinguished. It was inferred that it was a mixture of IV and II from the results that the III_1 when milled enough changed into the mixture of IV and II by the hydrolysis.

We have reported that III_{11} hardly changed into original structure, II, and into IV_{11} by heat treatments in water, in contrast to III_1 (7). On the other hand, IV_{11} was more unstable than IV, and rather easily transformed into II by the hydrolysis (7). It was considered that the molecular chain of cellulose II type, "bent & twisted", could form stable intermolecular hydrogen bonds systems in III_{11} which was the cellulose II type unit cell and hardly formed the stable system in IV_{11} of the cellulose I type unit cell. And by the same reason III_1 was unstable and IV_1 was stable. IR spectra of the polymorphs were measured at 150 °C, and Fig.11 shows the spectra in 3μ region. OH stretching bands at $3.0-3.3\mu$ are assigned to OH of intermolecular hydrogen bonds. The bands in the III_1 were different from the others and were the most weakened by the heating. It was suggested that the bonds in III_1 were weakest and that this should easily bring the transformation to the other polymorphs. In this study the all polymorphs went to an amorphous state via IV by milling under 40 °C. It has been said that IV is formed in high temperature. but for the transformation into IV heat was not always necessary. when cellulose was regenerated from the state in which the intermolecular hydrogen bonds were relaxed by chemical reagents, IV was formed

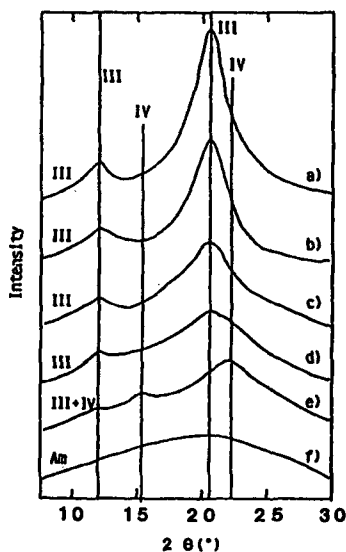


Fig.9 X-ray diffractograms of III_{11} milled for 0 (a)(raw m.), 0(b)(cut raw m.), 10(c), 30(d), 40(e), and 70(f) min..

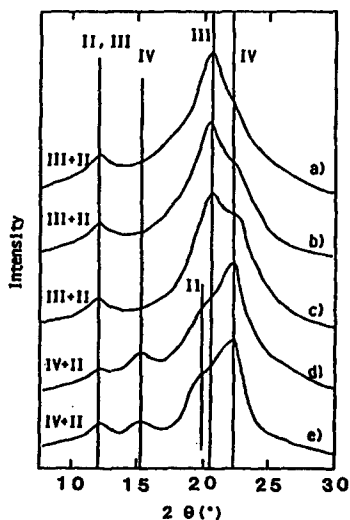


Fig.10 X-ray diffractograms of III_{11} recrystallized with 2.4 N HCl at 100°C after the milling for 0 (a)(cut raw m.), 10(b), 30(c), 40(d), and 70(e) min..

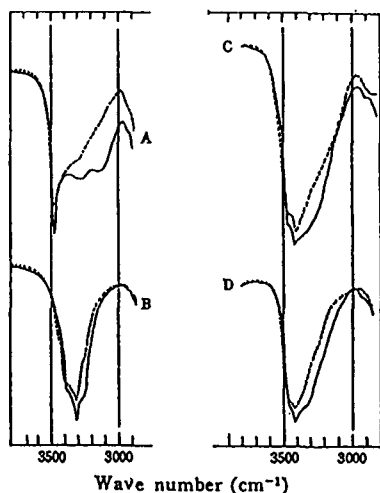


Fig.11 Infrared spectra in 3 μ region of Cell.III₁(A), Cell.I (B), Cell.II(C), and Cell III₁₁(D) measured at room temperature (—) and 150 °C (-----).

at rather lower temperature of about 80 °C. It was considered that the most important thing for the transformation to IV was relaxation of the inter-molecular hydrogen bonds. This can be achieved by many means, and the in part of mechanical energy by the milling should be one of them. In the relaxed condition the molecules should be rotating and vibrating and IV which was a more symmetrical structure should be most easily formed kinetically.

References

- (1) A.Sarko, Tappi, 61, 59 (1978); Wood and Cellulosics, edited by J.F. Kennedy, G.O.Phillips and P.A.Williams, Ellis Horwood, A.Sarko, 55, (1987)
- (2) J.Hayashi, A.Sueoka, S.Watanabe, Polym. Letters, 13, 23 (1975), The Structures of Cellulose, ACS Sympo. Series 340, Edited by R.H.Atalla, J. Hayashi, H.Kon, M.Takai, M.Hatano and T.Nozawa, 135, (1985)
- (3) J.Hayashi, T.Yamada, K.Kimura, J. Appl. Polym. Sci., Symposium, 28, 713 (1976)
- (4) A. Isogai, Y. Akishima, F. Onabe, M. Usuda, Cellulose, Edited by J.F. Kennedy, G.O. Phillips and P.A. Williams, Ellis Horwood, 105 (1989)
- (5) T. Okano, A. Sarko, J. Appl. Polym. Sci., 29, 4175 (1984); *ibid.*, 30, 325 (1985)
- (6) J. Hayashi, T. Yamada, Y. Shimizu, Cellulose and Wood, Edited by C. Schuerch, Wiley Interscience, 77 (1989)
- (7) Y. Shimizu, A. Sueoka, J. Hayashi, Abstracts of 199th ACS National Meeting, Cell Div. No. 25, Washington D.C. Aug. 23-28 (1992)

13 Structural characterisation of lignocellulosic samples using ^{13}C -CP/MAS-NMR-spectroscopy and chemometrics

H Lennholm and T Iversen – STFI, Box 5604, S-11486 Stockholm, Sweden

ABSTRACT

Four applications of how chemometric methods can be used to evaluate series of ^{13}C -CP/MAS-NMR-spectra acquired on lignocellulosic samples will here be briefly described.

1. Can the methods differentiate between the cellulose I and II polymorphs in ^{13}C -CP/MAS-NMR-spectra acquired on a series of cellulosic samples?
2. Can the methods differentiate between the cellulose I_α and I_β crystalline forms in ^{13}C -CP/MAS-NMR-spectra acquired on a series of lignocellulosic samples ?
3. Can ^{13}C -CP/MAS-NMR-spectra monitor changes in the cellulose structure in a series of bleached softwood kraft pulps pulped at various conditions ?
4. Can ^{13}C -CP/MAS-NMR-spectra monitor changes in the cellulose structure in a series of softwood kraft pulps beaten to different levels ?

INTRODUCTION

In the field of wood chemistry, ^{13}C -CP/MAS (cross polarisation magic angle spinning) NMR-spectroscopy has proven to be extremely useful. ¹ It is well known that signals from ordered and unordered regions in the cellulose polymer can be distinguished in the spectra. ^{2,3} Solid state NMR-spectra may differ in many respects from solution state NMR-spectra. For example, solid state NMR-spectra usually exhibit broader lines, due to the dipolar broadening.

The existence of non-equivalent unit cells and polymorphic crystal structures also contributes to the difference between solution and solid state NMR-spectra. The solution state ^{13}C -NMR-spectrum of a sample of dissolving pulp is shown in Fig. 1a. The solid state ^{13}C -CP/MAS-NMR-spectrum of a sample of the same dissolving pulp is shown in Fig. 1b. In addition to broadening of the peaks, spectral features that differ in many respects from those in Fig. 1a are found in Fig. 1b. The signals are split into multiplets due to the amorphous and crystalline regions in the cellulose.

This example shows that for pulp samples solid state NMR-

spectra contain considerably more information than do the solution state NMR-spectra. However, the high complexity of the solid state NMR-spectra makes them hard to evaluate visually. Chemometric methods, e.g. principal component analysis (PCA), partial least squares (PLS) and pattern recognition, are therefore advantageous.

CHEMOMETRICS

Pattern recognition by PCA can be used as a way to simplify interpretations of series of spectra. ⁵⁻⁷ PCA extracts principal components (PC:s) by calculating linear combinations of the spectral variables in all the spectra. ⁸ The extracted PC:s are independent of each other and can therefore be interpreted as arising from separate constituents in the spectra. By plotting the score values of the calculated PC:s, plots used for pattern recognition are constructed. Plotting the loading values for each PC vs. the ppm-scale also makes it possible to construct "subspectra". Such "subspectra" from statistical evaluations from series of spectra are similar to ordinary difference spectra obtained by subtraction of two spectra. The calculated "subspectra" have larger statistical reliability than the difference spectra since the latter are constructed from only two spectra.

In a PLS calculation, two matrices (e.g. physical and spectroscopic data) are related to each other. ⁹ PLS can therefore be used both to establish calibration models, and for evaluation and interpretation.

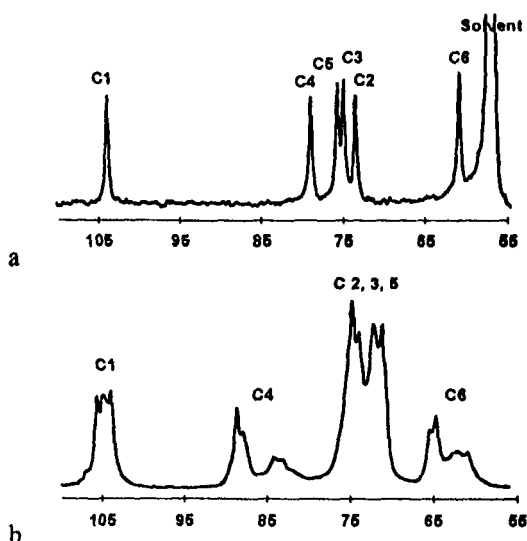


Fig. 1. a: ^{13}C -NMR-spectrum of dissolving pulp.
b: ^{13}C -CP/MAS-NMR-spectrum of the same dissolving pulp.

DIFFERENTIATION BETWEEN THE CELLULOSE I AND II POLYMORPHS

Cellulose I is the crystal form produced natively by plants and animals. When a sample of cellulose I is treated with a concentrated aqueous solution of NaOH, mercerisation occurs and the cellulose I is transformed to the cellulose II crystalline form. Cellulose II can also be obtained by regeneration, i.e. precipitation, of dissolved cellulose.

^{13}C -CP/MAS-NMR-spectra were acquired on seventeen lignocellulosic samples containing mainly cellulose I; dissolving pulp (DP), Avicel (MCC), bleached softwood

pulp (SP), cotton linters and cellulose II; mercerised cellulose (Merc.) and regenerated cellulose (Reg.). A spectrum of amorphous cellulose was also included in the matrix.

The PCA calculation extracted two significant PC:s. The PC-plot of the first two PC:s is shown in Fig. 2. The objects in the plot are the various NMR-spectra. The spectra form two groups along PC1, the cotton, DP, MCC and SP samples are found to the right, whereas the mercerised dissolving pulp and regenerated cellulose samples are found to the left.

Along PC2, the sample of amorphous cellulose is found at the bottom, whereas the most crystalline cellulose samples, cotton and regenerated cellulose, are found at the top. This can be interpreted as meaning that the PCA-model of the NMR-spectra can be used to distinguish between the cellulose I and II polymorph, and group the samples according to their relative amounts of amorphous polysaccharides. ¹⁶

DIFFERENTIATION BETWEEN THE CELLULOSE I $_{\alpha}$ AND I $_{\beta}$ CRYSTALLINE FORMS

The crystalline part of native cellulose is thought to be a mixture of two crystalline modifications, cellulose I $_{\alpha}$ and cellulose I $_{\beta}$. ^{14, 15} Cellulose I $_{\alpha}$ is thought to be the predominant form in bacterial and algal cellulose and cellulose I $_{\beta}$ the predominant form in higher plants such as cotton and ramie. The amounts of cellulose I $_{\beta}$ and cellulose I $_{\alpha}$ in cellulose samples such as *Valonia* and cotton linters can be roughly determined by spectral subtraction. ^{15, 17} The signals in the ^{13}C -CP/MAS-NMR-spectra on these substances are relatively narrow due to the relatively large lateral dimensions of the ordered, crystalline, regions in the cellulose polymer. ¹⁵

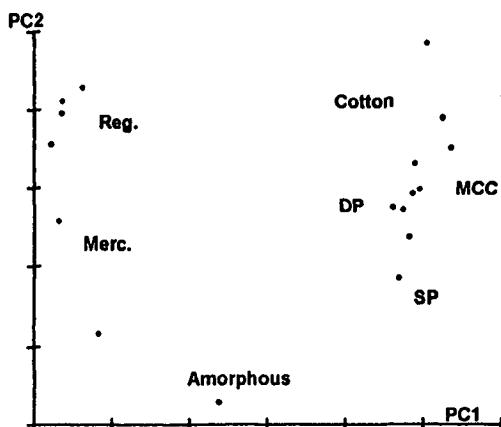


Fig. 2. PCA model calculated from the NMR-spectra of samples of cellulose I and II. Plot of PC2 vs. PC1.

At present, however, no method exists to determine the relative amounts of cellulose I_{β} and cellulose I_{α} in lignocellulosic samples with low crystallinity and high amounts of different amorphous polysaccharides and lignin.

^{13}C -CP/MAS-NMR-spectra were acquired on eleven cellulosic samples, e.g. cotton linters, cotton cambers, dissolving pulp (DP), Avicel (MCC), and cellulose from *Valonia ventricosa* and *Acetobacter xylinum*. The PCA calculation extracted two significant PC:s.

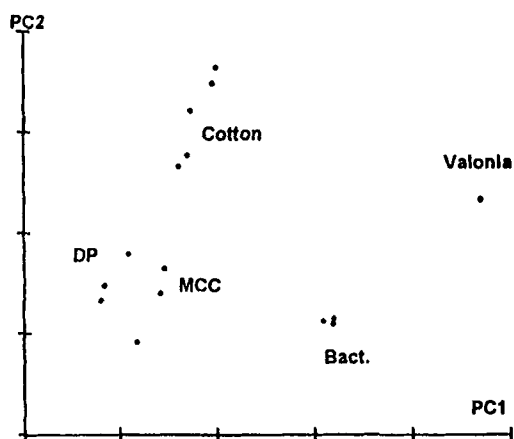


Fig. 3. PCA model calculated from the NMR-spectra of "pure" celluloses. Plot of PC2 vs. PC1.

Fig. 3 shows the PC-plot where the samples expected to contain high amounts of cellulose I_{α} (the *valonia* and bacterial cellulose samples) have high PC1 values, whereas the samples expected to contain high amounts of cellulose I_{β} (the cotton samples) have high PC2 values. Since the samples are thought to contain both cellulose I_{α} and cellulose I_{β} but in different proportions, this model appears to have extracted one PC (PC1) that exhibits variations in the relative amount of cellulose I_{α} in the samples, and one PC (PC2) that exhibits variations in the relative amount of cellulose I_{β} in the samples. To verify this interpretation, subspectra representing the spectral features contributing to each PC were constructed by plotting the loading values for the two obtained PC:s vs. the ppm scale. Variables important for the PC have high

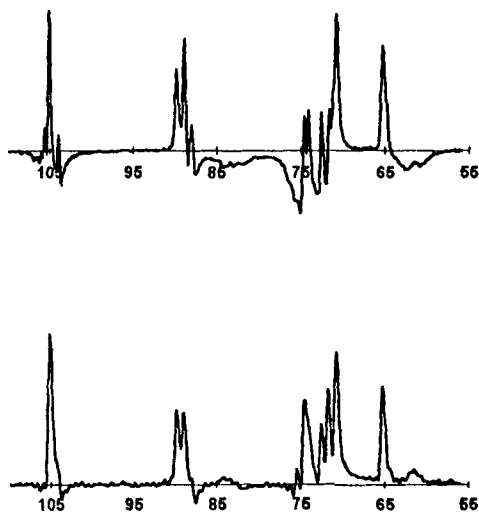


Fig. 4 a: subspectrum of PC1
b: spectrum representing cellulose I_{α}

numerical values, whereas unimportant variables have loading values close to zero in the subspectrum. The subspectrum of PC1 is shown in Fig. 4a, and exhibits large positive peaks at 105, 89-90, 71 and 65 ppm. This subspectrum thus exhibits close similarities to the difference spectrum of cellulose I_{α} , Fig. 4b. The subspectrum of PC2, shown in Fig. 4c, displays large positive peaks at 106, 104, 88-89, 75, 71, 66 and 64 ppm, and is thus similar to the difference spectrum of cellulose I_{β} , Fig. 4d. The two subspectra of Fig. 4, together with the way the cellulose samples group along the PC axes in Fig. 2, lead us to interpret PC1 as reflecting the relative amount of cellulose I_{α} in the samples, and PC2 reflecting the relative amounts of cellulose I_{β} in the samples. The PCA model obtained was then used to predict the relative amounts of cellulose I_{α} and cellulose I_{β} in some lignocellulosic samples.

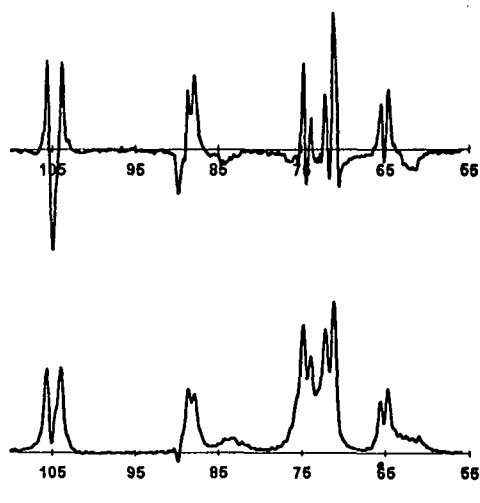


Fig. 4 c: subspectrum of PC2

d: spectrum representing cellulose I_{β}

the PC axes in Fig. 2, lead us to interpret PC1 as reflecting the relative amount of cellulose I_{α} in the samples, and PC2 reflecting the relative amounts of cellulose I_{β} in the samples. The PCA model obtained was then used to predict the relative amounts of cellulose I_{α} and cellulose I_{β} in some lignocellulosic samples.

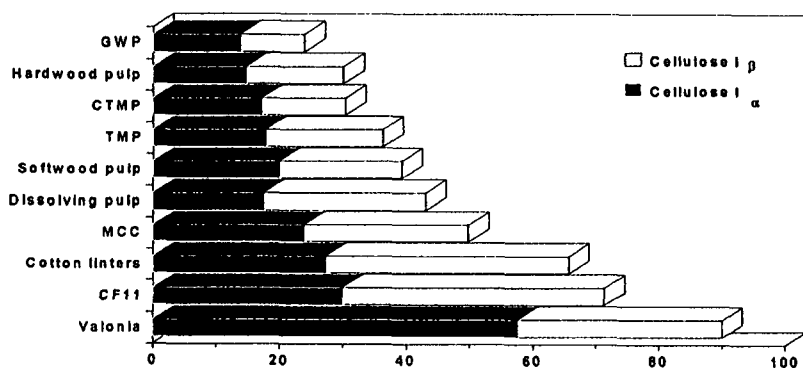


Fig. 5. Predicted relative amounts of cellulose I_{β} and cellulose I_{α} in some lignocellulosic samples.

By inserting the ^{13}C -CP/MAS-NMR-spectra on samples of amorphous cellulose, softwood pulp, hardwood pulp, thermo-mechanical pulp (TMP), chemothermomechanical pulp (CTMP) and groundwood pulp (GWP) in the PCA model, the score values for these samples were predicted.

Using the sample of amorphous cellulose, as having no cellulose I_α or I_β , and the *valonia* cellulose as having 64 % cellulose I_α and 90 % crystallinity¹⁷, the PC1 and PC2 score values for all the samples were normalised and recalculated relative to each other. The resulting values of the lignocellulosic samples are plotted in Fig. 5. The length of the bars can roughly be considered to represent the crystallinity of the samples. This shows that the PCA-model of the NMR-spectra can be used to distinguish between the cellulose I_β and I_α crystalline forms. The model could also be used to predict the relative amounts of cellulose I_β and I_α in lignocellulosic samples.¹⁸

MONITORING CHANGES IN THE ^{13}C -CP/MAS-NMR-SPECTRA IN A SERIES OF BLEACHED SOFTWOOD KRAFT PULPS PULPED AT DIFFERENT CONDITIONS

^{13}C -CP/MAS-NMR-spectroscopy has been used previously to study pulps produced in the kraft pulping process.⁷ In our experiment eight softwood kraft pulps cooked according to a factorial design in temperature, OH-charge, and HS-charge. ^{13}C -CP/MAS-NMR-spectra were acquired on the samples and a PCA model was calculated. The first extracted PC was found to be related to the change in temperature in the kraft cooks. The subspectrum of PC1 is shown in Fig. 6a. By comparison with Fig. 4b and 4d, it can be seen that the positive peaks in the subspectrum resemble the spectrum of cellulose I_β , whereas the negative peaks in the subspectrum resemble the spectrum of cellulose I_α .

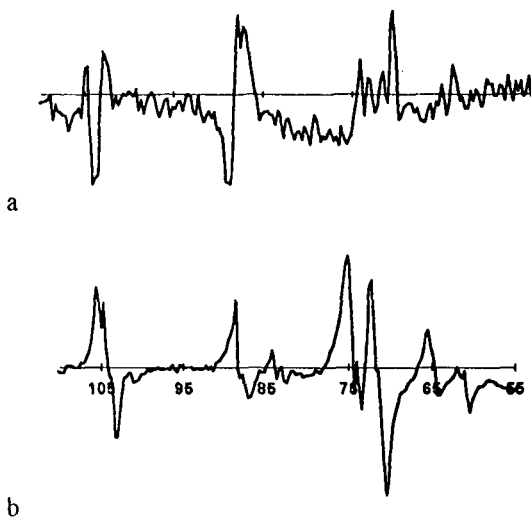


Fig. 6. a: The subspectrum from PCA on differently cooked softwood kraft pulps.

b: The subspectrum from the PLS-correlation of the softwood kraft pulps beaten to different levels.

It has been found that cellulose I_{α} can be transformed to cellulose I_{β} by steam annealing of *valonia* cellulose samples at high temperatures.¹⁹⁻²¹ The results of the PCA evaluation of the NMR-spectra therefore indicate that the cellulose I_{α} transforms to cellulose I_{β} cellulose in the softwood kraft pulps during the kraft cook.

MONITORING CHANGES IN THE ^{13}C -CP/MAS-NMR-SPECTRA IN A SERIES OF SOFTWOOD KRAFT PULPS BEATEN TO DIFFERENT LEVELS

PLS has earlier been used to study changes in pulp physical properties during the beating process.^{22, 23} VanderHart and Atalla (1987) submitted *Cladophora* cellulose to beating and recorded ^{13}C -CP/MAS-NMR-spectra on the samples. They observed a decrease in the amount of cellulose I_{α} upon beating and suggested that cellulose I_{α} was converted to cellulose I_{β} as a result of the mechanical stress.¹⁵

In our experiment, seven bleached and unbleached softwood kraft pulps were beaten to different levels. ^{13}C -CP/MAS-NMR-spectra and physical properties (tensile force, elongation, density, TEA) were measured on handsheets produced from the pulps. A PLS-analysis was carried out with the spectroscopic data as independent variables, and the physical properties as dependent variables. One PLS component that explained 82.7 % of the variance in physical properties was obtained. This PLS model could be used to predict the physical properties. The PLS-weights were also used to construct a subspectrum, shown in Fig. 6b. This subspectrum does not indicate any transformation between the cellulose crystalline forms, as in Fig. 6a, and is very hard to interpret. We just conclude that the peaks arising from the crystalline regions of the cellulose are affected.²⁴

CONCLUSIONS

Pattern recognition, PCA and PLS are valuable methods for the evaluation of ^{13}C -CP/MAS-NMR-spectra from lignocellulosic samples. The methods were found to be able to:

- ⊛ Classify lignocellulosic samples as belonging to either the cellulose I or II polymorphs by their ^{13}C -CP/MAS-NMR-spectra.
- ⊛ Determine the relative amount of cellulose I_{α} and I_{β} in lignocellulosic samples by their ^{13}C -CP/MAS-NMR-spectra.
- ⊛ Monitor the effects of pulping on softwood kraft pulps. The cellulose I_{α} in the pulps transform to cellulose I_{β} due to the higher temperature in the kraft cooks.
- ⊛ Monitor the effects of beating on softwood kraft pulps. The crystalline cellulose in the pulps are affected.

ACKNOWLEDGEMENTS

Financial support from "Carl Tryggers Stiftelse för Vetenskaplig Forskning" and the Swedish Research Council for Engineering Sciences (TFR), are gratefully acknowledged.

EXPERIMENTAL

¹³C-CP/MAS-NMR-spectra were recorded on a Bruker AMX-300 instrument operating at 75.47 MHz with a spinning rate of 5 kHz, a contact time of 0.8 ms, 37 ms acquisition time, 2.5 s between pulses, at room temperature. A total of 1000-3000 transients were accumulated for each spectrum. Spectra were referenced to external glycine, (carbonyl carbon = 176.03 ppm). The samples were moistened with water prior to recording the spectra, the resulting water content being about 50 %. ^{10, 11} The spectra were normalised by setting the area under each spectrum to unity. The intensities of 601 spectral points in the interval 110-56 ppm for each of the spectra were used in the data analysis.

The solution state ¹³C-NMR-spectrum was recorded on the sample dissolved in aqueous tetrabutylammonium hydroxide and DMSO-d₆. The signals were assigned to the carbon atoms in the anhydroglucose units using two-dimensional shift correlated spectroscopy techniques, i.e. proton-proton and proton-carbon shift correlated spectroscopy. ⁴

Amorphous cellulose was prepared from dissolving pulp by treatment with ZnCl₂. ¹² PCA and PLS calculations were performed using cross-validation ¹³. PC plots were constructed by plotting the scores of the PC:s. Subspectra were constructed by plotting the loading values for the obtained PC:s vs. the ppm scale. All computations were carried out on an IBM PS-2 microcomputer using the SIMCA 4R software package obtained from Umetri AB, Umeå, Sweden.

The difference spectra representing cellulose I_β and cellulose I_α were obtained by linear combinations of the ¹³C-CP/MAS-NMR-spectra of *Acetobacter xylinum* and Whatman CF-11 cellulose. ^{14, 15}

LITERATURE

- Hirai A, Horii, F., Kitamaru, R. (1985): *Bull. Inst. Chem. Res. Kyoto Univ.*, 63:4, 340-358.
- Atalla, R. H., Gast, J. C., Sindorf, D. W., Bartuska, V. J. and Maciel, G. E. (1980): *J. Am. Chem. Soc.*, 102, 3249.
- Maciel, G. E., Kolodziejcki, W. L., Bertran, M. S. and Dale, B. E. (1982): *Macromolecules*, 15, 686-687.
- Bax, A. and Drobny, G. (1985): *J. Magn. Reson.*, 61, 306.
- Weber, D. S. and Goux, W. J. (1992): *Carb. Res.*, 233, 65-80.
- Nordén, B. and Albano, C. (1989): *Fuel*, 68, 771-775.
- Wallbäcks, L., Edlund, U. Nordén, B (1989): *J. Wood Chem. Technol.*, 9:2, 235.
- Jolliffe, I. T. (1986): *"Principal Component Analysis"*. Springer Verlag, New York.
- Martens, H. and Naes, T. (1989): *"Multivariate Calibration"*, Wiley, New York.
- Newman, R. H. (1987): *Proceedings 4th Int. Symp. Wood. Pulp. Chem.*, Paris France, 1, 195-199.
- Horii, F, Hirai, A. Kitamaru, R. and Sakurada, I. (1985): *Cell. Chem. Technol.*, 19, 513-523.
- Patil, N. B., Dweltz, N. E. and Radhakrishnan, T. (1965): *Text. Res. J.*, 35, 517-523.
- Wold, S. (1978): *Technometrics*, 20:4, 397-405.
- VanderHart, D. L. and Atalla, R. H. (1984): *Macromolecules*, 17, 1465-1472.
- VanderHart, D. L. and Atalla, R. H. (1987): *ACS Symp. Ser. no 340*, Chap 5: 88-118.
- Lenholm, H. and Iversen, T. (1994): Submitted to *Holzforschung*.
- Yamamoto, H and Horii, F (1993): *Macromolecules*, 26, 1313-1317.
- Lenholm, H., Larsson, T. and Iversen, T. (1993): Submitted to *Carb. Res.*
- Horii, F., Yamamoto, H., Kitamaru, R., Tanahashi, M. and Higuchi, T. (1987): *Macromolecules*, 20, 2946.
- Yamamoto, H., Horii, F. and Odani, H. (1989): *Macromolecules*, 22, 4130.
- Debzi, E. M., Chanzy, H., Sugiyama, J., Tekely, P. and Exoffier, G. (1991): *Macromolecules*, 24, 6816-6822.
- Wallbäcks, L., Edlund, U. Nordén, B., Iversen, T. and Mohlin, U.-B. (1991): *Nord. Pulp and Pap. Res. J.*, 6:3, 104.
- Wallbäcks, L., Edlund, U., Nordén, B. and Iversen, T. (1991): *Nord. Pulp and Pap. Res. J.*, 6:2, 74.
- Lenholm, H., Weyer, L. and Iversen, T. (1994): Submitted to *J. Pulp Pap. Sci.*

14 A microcalorimetric technique for the study of water vapour sorption on cellulose materials

K Bogolitsyn*, N Volkova and I Wadsö – Thermochemistry, Chemical Center, Lund University, 222 10, Lund, Sweden;
* Arkhangelsk Forest Technological Institute, 16300, Arkhangelsk, Lenin emb 17, Russia

ABSTRACT

A gas flow microcalorimeter was designed for water vapour sorption/desorption measurements on solids. Three types of cellulose have been studied in sorption and desorption experiments. So far, no hysteresis effects were observed.

INTRODUCTION

Sorption and desorption of water vapour are important processes in basic and applied cellulose technology and it is of interest to characterize them by thermodynamic and kinetic parameters. At present, standard Gibbs energies (ΔG^0), enthalpies (ΔH^0) and entropies (ΔS^0) are usually derived from results of equilibrium vapour pressure measurements (sorption isotherms) conducted at different temperatures [1, 2]. However, as for many other processes, direct calorimetric measurements can be expected to give more accurate ΔH^0 -values. Further, by use of calorimetric techniques, it is usually possible to obtain reliable values for changes in heat capacities $\Delta C_p^0 = d\Delta H/dT$.

A series of microcalorimeters of the thermopile heat conduction type, equipped with different types of insertion vessels, have earlier been reported from our laboratory [3]. The present instrument is part of the same modular calorimetric system [3,4].

Design and function of the calorimetric system

Figure 1 shows schematically the different units forming the present gas sorption calorimetric system .

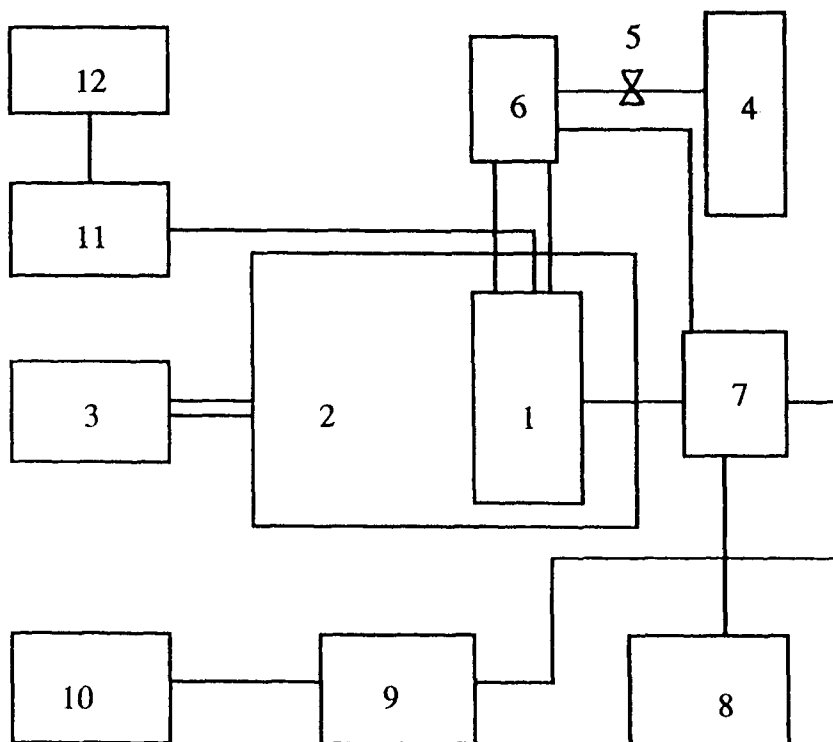


Fig.1 The gas sorption calorimetric system: 1, twin microcalorimeter; 2, thermostatted water bath; 3, temperature regulator ; 4, N₂ bottle; 5, needle valve; 6, humidity regulator ; 7, interface; 8, computer; 9, amplifier; 10, recorder; 11, peristaltic pump; 12, flowmeter.

The twin thermopile heat conduction microcalorimeter is equipped with 24 small thermocouple plates (FC 0.45-66-05 Melchor, Trenton, NJ, USA). Figure 2 shows schematically the design of the lower part of calorimetric insertion cell.

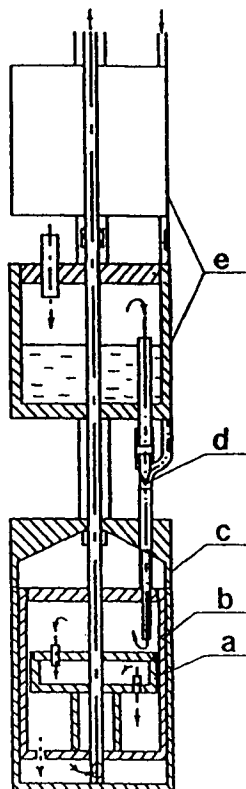


Fig.2 The calorimetric cell: a, stainless steel sample container; b, inner vessel (brass, gold plated); c, calorimetric vessel (brass, gold plated inside); d, gas mixing unit; e, vapour saturation units(brass, teflon painted inside). Arrows indicate directions of the gas flow.

During the measurements the calorimetric cell (Fig.2) is inserted into one of the calorimetric units of the twin calorimeter. The vapour saturation units (e), with cavities partially filled with water, are in thermal contact with the calorimeter heat sink. The calorimetric vessel (c), like the reference vessel, fits into aluminium cups. The thermocouple plates bridge the air gaps between these aluminium cups and the heat sink. The sample container (a) is positioned inside the inner vessel (b) of the main calorimetric vessel (c). During a measurement a flow of dry carrier gas passes through the humidity regulator (6), where it is divided into two streams. One of the streams passes through the vapour saturation units (e) and will join the flow of dry gas at the gas mixing unit (d). The ratio between the flow rates of the two streams determines the humidity of the gas passing over the sample in the sample container.

The twin calorimeter was enclosed by a steel can submerged in a thermostatted water bath (long-term thermal stability $\pm 1 \cdot 10^{-3} \text{K}$). The instrument was calibrated electrically. All experiments were conducted at 298.15K.

Before each series of experiments the sample container was charged with 20-30 mg of cellulose. The gas flow rate through the calorimeter was normally 100-200 ml/hour. The dry carrier gas (in our case N_2) was mixed with water saturated gas to form gas mixtures in the relative humidity (RH) range 0-100%. The sorption or desorption process usually required 10-15 hours to reach equilibrium.

Materials

Three different types of cellulose were employed in the experiments: Whatman cellulose powder (CF11, medium length fibers, ASH(MAX) 0.015%, Fe 5ppm, Cu 2ppm, for column chromatography); Kleenex filter paper (Kimberly-Clark, Code 7107, grinding in mill: 10 minutes); Arkhangelsk cellulose (sample prepared at the Arkhangelsk Forest Technological Institute: fir filings, 500 hours grinding in toluene, lignin extraction by dioxane, hemicellulose extraction by KOH and NaOH, cellulose content in initial filings: 47%, lignin : 24%). All samples were air dried.

Results and discussion

A typical experimental curve is shown in Figure 3.

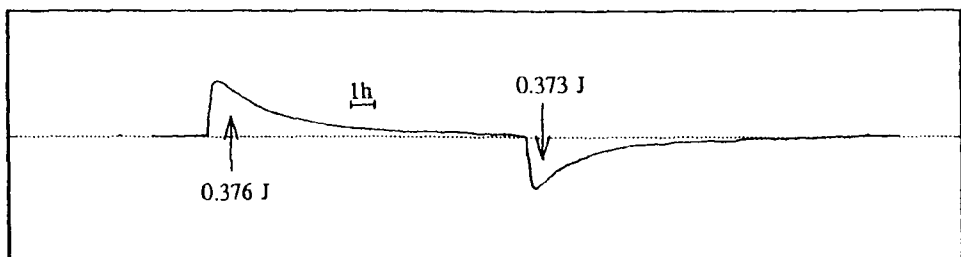


Fig.3 Typical experimental curve for sorption/desorption experiment : Filter paper- 0.020085g, sensitivity $100 \mu\text{V}$, gas flow 160 ml/h, RH 90% during sorption and RH 0% during desorption.

The results obtained with the three cellulose samples are shown in Figure 4.

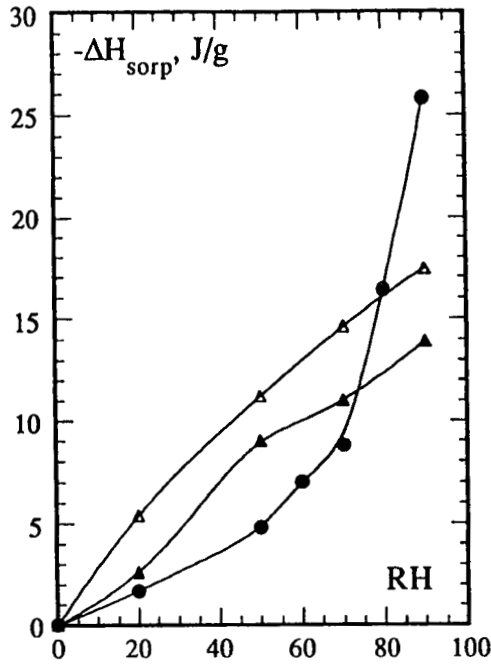


Fig.4 Integral enthalpies of water vapour sorption (J/g of cellulose) versus RH:

●, Whatman, Δ , Filter paper, \blacktriangle , Arkhangelsk cellulose.

The complete sorption isotherms were determined gravimetrically for two of the samples by equilibration over salt solutions in closed chambers (15-95% RH) [5].

Cellulose samples were dried before the measurements at 105°C until constant weight.

The adsorption isotherms are presented in Fig.5.

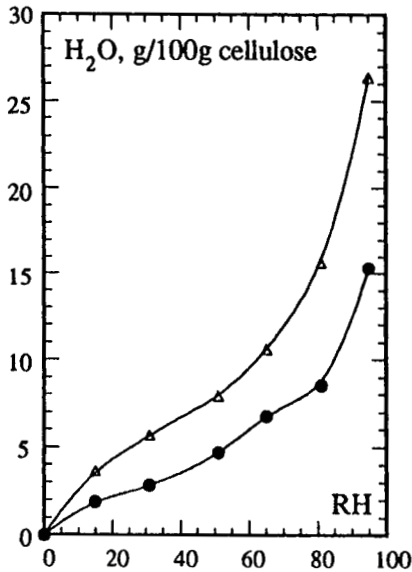


Fig.5 Equilibration adsorption isotherms: ●, Whatman, Δ , Filter paper.

The calorimetric results summarised in Fig.4 are rather similar for the Arkhangelsk sample and the Kleenex filter paper whereas the enthalpy values for the Whatman sample show a very different pattern. The sorption isotherms (Fig.5) for the two latter samples have the same appearance. The experimental results reported here are in general agreement with results reported previously (calorimetric and noncalorimetric) [6-11] for different types of cellulose. The present results will be discussed in detail later together with results from ongoing measurements.

Acknowledgement: Valuable discussions with Dr.J.Suurkuusk, ThermoMetric AB, Järfälla, Sweden, including communications from Prof.A.Bakri, Grenoble, France, concerning the design of calorimeter are gratefully acknowledged. This work has been supported by grants from the Swedish Institute and STFI (Stockholm) to K.B. and from the Royal Swedish Academy of Sciences to N.V..

References

1. C.Skaar, "*Wood-Water Relation*", Springer-Verlag, Berlin 1988.
2. R.M.Nelson Jr., *Wood and Fiber Sci.*, **1983**, 15, 8.
3. P.Bäckman, M.Bastos, L.-E. Briggner, S.Hägg, D.Hallen, P.Lönnbro, S.-O. Nilsson, G.Olofsson, A.Schön, J.Suurkuusk and I.Wadsö, *Pure Appl.Chem.*, in press.
4. J.Suurkuusk and I.Wadsö, *Chemica Scripta*, **1982**, 20, 155.
5. "*Handbook of Chemistry and Physics*", 56th edition, CRC Press, Cleveland 1975,
6. M.F.Froix and R. Nelson, *Macromolecules*, **1976**, 8, 726.
7. T.F.Child, *Polymer*, **1972**, 13, 259.
8. F.Khan and N.Pilpel, *Powder Technology*, **1987**, 50, 237.
9. R.G.Hollenbeck, G.E.Peck and D.O.Kildsig, *J.Pharmac.Sci.*, **1978**, 67,1599.
10. G.R.Sadeghnejad, P.York and N.G.Stanley-Wood in "*Pharmaceutical technology*", ed.M.H.Rubinstein, Ellis-Horwood, 1989,132.
11. I.D.Zenkoy, R.V.Zalepukhin, V.I. Slovetskii and S.P.Papkov, *Vysokomol.Soedin., Ser.A*, **1988**, 30, 1718.

15 A method for the determination of the surface tension of cellulosic fibres in their natural state and its relation with chemical composition

J M van Hazendonk*, J C van der Putten* and J T F Keurentjes** –
* ATO-DLO Agrotechnological Research Institute, PO Box 17,
NL-6700 AA Wageningen, The Netherlands; ** Akzo Research
Laboratories Arnhem, Dept CRP, Arnhem, The Netherlands

ABSTRACT

The surface tensions of several natural cellulosic fibres like flax, hemp, kenaf and cotton and a synthetic cellulosic fibre have been determined using the so-called floating test. This method determines the liquid surface tension γ_f at which fibres placed on a liquid surface remain just floating. It can be shown that γ_f is the liquid surface tension at which the contact angle $\theta \approx 0^\circ$. By measuring γ_f in both a polar and an apolar liquid system, the fibre surface tension γ_s and its dispersive and polar parts, γ_s^d and γ_s^p , respectively, can be calculated using the harmonic mean approximation. The fibre surface tensions found for untreated and extracted natural fibres are in good agreement with literature data for surface tensions of various fibre components such as cellulose, hemicellulose, lignin and waxes. Untreated natural cellulosic fibres proved to be very hydrophobic due to a waxy layer on their surface. Extraction of fatty substances significantly increases the fibre surface tension. This method can be very useful in predicting the wettability of fibres by the surrounding polymer matrix in fibre-reinforced composite materials.

INTRODUCTION

Knowledge of the surface properties of cellulosic fibres is essential to the understanding of the interaction of these fibres with a surrounding liquid. The fibre surface tension is an important property, since it highly determines the fibre wettability. In fibre-reinforced composite materials, complete wetting of the fibres by the surrounding polymer matrix is a prerequisite for good adhesion. In textile applications, wettability is important in finishing and dyeing.

Traditionally, the wettability of a solid is determined by contact angle measurements. Due to surface roughness, porosity and fibre dimensions, correct contact angle measure-

ments on fibres are hardly possible. Consequently, most contact angle measurements on cellulosic materials have been performed on regenerated films [1,2,3]. However, films of regenerated fibre components are likely to behave differently from the fibres themselves.

In a previous study [4] we developed a simplified experimental method for the determination of the surface tension of cellulosic fibres. In this floating test, fibres are placed on a liquid surface with a surface tension γ_L . The liquid surface tension γ_F , at which the transition between floating and sinking occurs corresponds to the liquid surface tension at which $\theta \approx 0^\circ$. When γ_F is measured in both a polar and an apolar liquid system, the fibre surface tension γ_S and its dispersive (γ_S^d) and polar part (γ_S^p) can be calculated. Advantages of this method are that it avoids contact angle measurements and that it is operational despite surface roughness and porosity. The variation coefficient of the γ_F measurements appears to be 1-3%.

The aim of this study is to determine the surface tension of several natural and synthetic cellulose fibres using the floating test and to relate this surface tension to the fibre chemical composition.

THEORY

Surface tension determination using contact angle measurements

Wetting of a solid fibre by a liquid is determined by the surface and interfacial tensions of the solid and the liquid according to Young:

$$\gamma_S = \gamma_{SL} + \gamma_L \cos \theta \quad (1)$$

where γ_S is the surface tension of the solid, γ_L the surface tension of the liquid, γ_{SL} the interfacial tension between the solid and the liquid and θ the equilibrium contact angle. According to Fowkes [5] a surface tension is made up of contributions from the dispersive and polar forces at the surface:

$$\gamma = \gamma^d + \gamma^p \quad (2)$$

where γ is the surface tension, γ^d and γ^p the dispersive and the polar component of the surface tension, respectively. For hydrophilic surfaces the interfacial tension between a solid and a liquid can be written as the harmonic mean of the polar and dispersive contributions [6]:

$$\gamma_{SL} = \gamma_S + \gamma_L - \frac{4\gamma_S^d \gamma_L^d}{\gamma_S^d + \gamma_L^d} - \frac{4\gamma_S^p \gamma_L^p}{\gamma_S^p + \gamma_L^p} \quad (3)$$

Combining equations (1) and (3) results in:

$$\gamma_L (1 + \cos \theta) = \frac{4\gamma_S^d \gamma_L^d}{\gamma_S^d + \gamma_L^d} + \frac{4\gamma_S^p \gamma_L^p}{\gamma_S^p + \gamma_L^p} \quad (4)$$

Equation (4) can be solved by measuring the contact angle θ on a solid with two different liquids of known but different polarity. A pair of simultaneous equations can be set up and equation (4) can be solved to obtain γ_S^d and γ_S^p and thus γ_S . Using a completely apolar

liquid ($\gamma_L^p = 0$, $\gamma_L = \gamma_L^d$), the polar term in equation (4) drops out and only one unknown, γ_s^d , is left. The second mixture has to contain a polar part to be able to calculate γ_s^p .

Floating test

When a fibre is placed on a liquid surface with high surface tension γ_L , it will remain floating. Upon a decrease in liquid surface tension it will be better wetted gradually. At complete wetting the fibre will sink, provided that the fibre density is higher than the liquid density. The transition between floating and sinking is expressed by γ_F , the surface tension of the liquid at which the fibre just floats (figure 1).

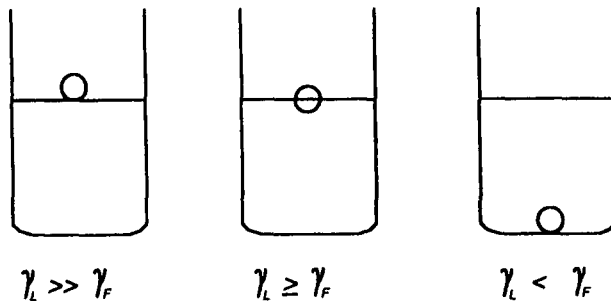


Figure 1. Three situations of a fibre brought onto a liquid surface.

Considering a cylindrical natural cellulosic fibre, the fibre density and dimensions are such that the downward gravitational force is very small as compared to the upward interfacial force [4]. Consequently, the transition between floating and sinking takes place at $\theta = 0^\circ$ [4]. Since $\theta = 0^\circ$ at γ_F , equation (4) gives:

$$\gamma_F = \gamma_L = \frac{2\gamma_s^d \gamma_L^d}{\gamma_s^d + \gamma_L^d} + \frac{2\gamma_s^p \gamma_L^p}{\gamma_s^p + \gamma_L^p} \quad (5)$$

which can be solved by measuring γ_F with two different liquids of known but different polarity.

EXPERIMENTAL

Methods

Floating test

Approximately 20 ml of a liquid with surface tension γ_L were poured into a clean 50 ml beaker. Prior to the floating test the surface tension of the liquid was measured. Twenty pieces of fibre were carefully placed on top of the liquid surface and the number of fibres that did not remain floating within 20 s was determined. Afterwards, the surface tension of each liquid was measured again in order to check whether release of surface active material from the fibres had occurred. In order to vary γ_L , mixtures were used. As a polar system water-methanol mixtures were used, giving a range in γ_L from 23 to 72 mN/m. 1-Methylnaphthalene-octane mixtures were used as completely apolar liquids, giving a range in γ_L from 22 to 38 mN/m. For both polar and apolar liquids γ_L is varied with intervals of

about 1 mN/m. The surface tension γ_f at which 50% of the fibres remain floating was determined. All experiments were carried out at 20°C and all reagents were analytical grade, purchased from Merck (Germany). Demineralized water was used throughout. The liquid surface tension was measured by the Wilhelmy plate method.

Chemical composition of fibres

The neutral sugars from the fibres were quantified by gas-liquid chromatography as their alditol acetates after pre-hydrolysis (72% sulfuric acid, 1h, 30°C) and hydrolysis (1M sulfuric acid, 3h, 100°C). 1-Methylimidazole was used as an acetylation catalyst and inositol as internal standard [7]. GLC was performed on a CP-Sil 88 capillary column (25 m x 0.25 mm i.d.). Lignin was determined as the sum of Klason and acid soluble lignin. Klason lignin was determined gravimetrically as the residue after sulfuric acid hydrolysis [8]. Acid soluble lignin was determined by UV spectroscopy at 205 nm [9]. Uronic acids were determined colorimetrically by the 4-hydroxydiphenyl assay [10].

Materials

For surface tension determinations flax, hemp, kenaf, cotton and synthetic cellulose II fibres were used. Flax, hemp and kenaf fibres were warm-water retted prior to use. Retting is the process in which bast fibres are freed from the plant by decomposition of pectins and other binding materials by micro-organisms. After retting the fibres are mechanically separated from the rest of the plant by the so-called scutching process [11]. Unretted hemp fibres, which were mechanically separated from the plant, were also used. Unretted and retted hemp fibres are named hemp 1 and hemp 2, respectively.

To study the influence of chemical fibre composition on the fibre surface tension, fats and waxes, pectins, and hemicelluloses were successively extracted from flax fibres. Fats and waxes were extracted with ethanol 96% v/v under reflux in a Soxhlet apparatus for 6h. Pectins were extracted with ammonium oxalate 1.0% w/v (pH 5.5, 80°C, 2*2h) and hemicelluloses with NaOH 6% w/v (100°C, 2h). Unextracted fibres are named R0, defatted fibres R1, fibres after extraction with ammonium oxalate R2 and those after alkaline treatment R3. Further, flax fibres coated with carboxymethylcellulose (CMC) and flax fibres coated with stearylamine (SA) were used. As to hemp, kenaf and cotton, only untreated (R0) and defatted fibres (R1) were studied. As a synthetic fibre Cordenka (Akzo) was used, which is a highly crystalline regenerated cellulose II fibre. Before use, the Cordenka fibres are treated with 96% ethanol in order to obtain a clean cellulose surface.

RESULTS

In table 1 the results of the γ_f measurements on different fibres are summarized. γ_f has been determined with both water-methanol and 1-methylnaphthalene-octane mixtures (γ_f w/m and γ_f n/o, respectively). The dispersive part of the water-methanol surface tension has been calculated according to Janczuk et al. [12]. γ_s^d , γ_s^p and γ_s are calculated according to equation (5) using the harmonic mean approximation (table 1). The surface tensions for the untreated fibres R0, the defatted fibres R1 and the flax fibres are graphically shown in figures 2, 3 and 4 respectively.

The chemical composition of the fibres used is summarized in table 2. The glucose content of the fibres can be considered to be an approximation of the cellulose content, whereas the amount of non-glucose sugars is an approximation of the hemicellulose content [13]. The sum of the estimated amounts of sugar, lignin and uronic acid never reaches 100% due to the presence of small amounts of other materials like minerals,

proteins and fatty substances and due to incomplete hydrolysis of cellulose [14]. Cotton

Table 1. The measured γ_f values and the calculated γ_s^d , γ_s^p and γ_s values.

fibre	γ_f w/m (mN/m)	γ_f n/o (mN/m)	γ_s^d (mN/m)	γ_s^p (mN/m)	γ_s (mN/m)
flax R0	26.2	31.3	31.3	2.9	34.2
flax R1	31.7	37.6	37.6	5.5	43.1
flax R2	36.4	45.3	45.3	7.6	52.9
flax R3	48.5	50 ¹	50	16.1	66.1
flax CMC	36.4	42.3	42.3	8.1	50.4
flax SA	26.5	31.1	31.1	3.1	34.2
hemp1 R0	25.6	30.5	30.5	2.6	33.1
hemp1 R1	30.6	39	39	4.5	43.5
hemp2 R0	25.1	32.5	32.5	1.9	34.4
hemp2 R1	38.6	39	39	10.5	49.5
kenaf R0	25.3	28.9	28.9	2.8	31.7
kenaf R1	32.0	38.2	38.2	5.6	43.8
cotton R0	24.5	29.0	29.0	2.2	31.2
cotton R1	47.4	50 ¹	50	15.2	65.2
Cordenka	47.8	50 ¹	50	15.6	65.6

w/m = water-methanol, n/o = 1-methylnaphthalene-octane, ¹ estimation.

and flax R3 fibres contain approximately 95% cellulose [11]. Due to poor accessibility of this highly crystalline cellulose I material, the glucose yield is only 80%. Cordenka (\approx 100% cellulose) yields more glucose after hydrolysis, probably due to a difference in accessibility and crystallite size between cellulose II and cellulose I. Table 2 shows that the uronic acid content, and thus the pectin content, is significantly reduced by the extraction with ammonium oxalate (going from R1 to R2). By the alkaline treatment (going from R2 to R3) mainly hemicelluloses and lignins are extracted.

Table 2. Chemical composition of fibres used.

Fibre	glucose	non glucose	lignin	uronic acids
flax R0/R1	68	8	3	3
flax R2	67	8	3	0.8
flax R3	80	3	0.6	0.6
hemp 1 R0/R1	67	8	4	4
hemp 2 R0/R1	67	8	4	1.5
kenaf R0/R1	48	16	14	6
cotton R0/R1	80	2	<1	1
Cordenka	92	0	0	0

DISCUSSION

Literature data for surface tensions of various cell wall components are given in table 3. Figure 2 shows that all untreated (R0) natural cellulosic fibres are very hydrophobic. This is due to a waxy deposit on the surface of natural fibres [11]. The dispersive part of their surface tension ($\gamma_s^d = 29.0 - 32.5$ mN/m) is comparable to that of waxes [15]. In contrast

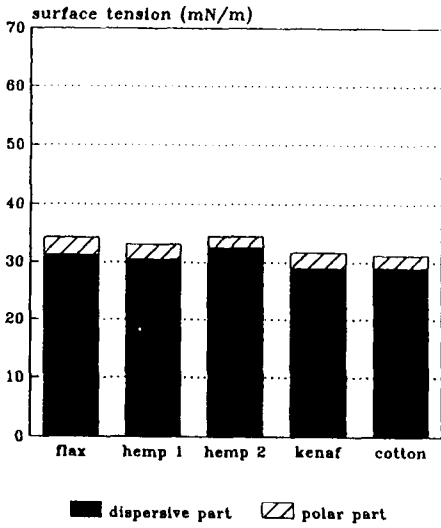


Figure 2. The surface tension γ_s and its dispersive (γ_s^d) and polar part (γ_s^p) for untreated (R0) natural fibres.

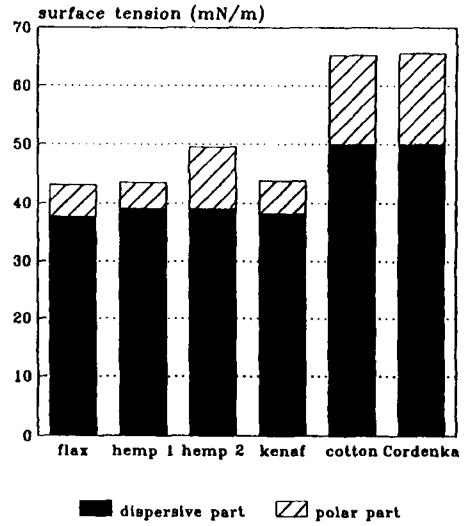


Figure 3. γ_s , γ_s^d and γ_s^p for defatted (R1) fibres.

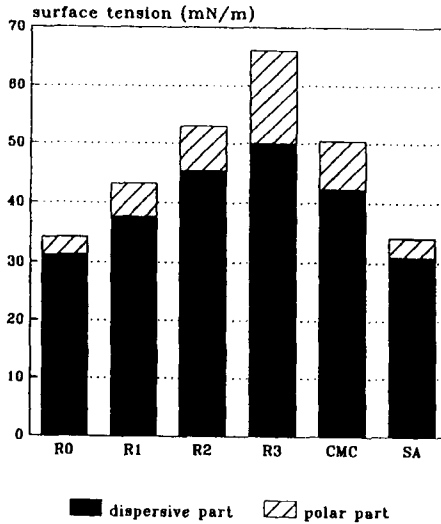


Figure 4. γ_s , γ_s^d and γ_s^p for extracted and chemically modified flax fibres.

to waxes, the R0 fibres have a small polar part in their surface tension, probably due to the presence of more polar fatty substances like triglycerides and phospholipids on the fibre surface. Other investigations [1,16] confirm the hydrophobic surface character of raw cotton fibres.

Table 3. Literature data for γ_s^d , γ_s^p and γ_s of various cell wall components.

material	γ_s^d (mN/m)	γ_s^p (mN/m)	γ_s (mN/m)	ref.
waxes	26.5 ¹	$\approx 0^1$	26.5 ¹	[15]
lignin	40 ⁴			[17]
	43.5 ²	9.0 ²	52.5 ²	[17]
hemicelluloses	35.3-39.5 ¹			[2]
cellulose	42.2 ²	26.5 ²	68.7 ²	[17]
cellulose	39-45 ⁴			[2]
cellulose (highly oriented)	51 ⁴			[2]
cellulose	19.9 ²	39.6 ²	59.5 ²	[3]
	29.4 ³	25.0 ³	54.4 ³	[3]
			66.5	[3]

¹ calculated from contact angle data (literature) using the geometric mean approximation

² geometric mean approximation

³ harmonic mean approximation

⁴ Fowkes' plot

Ethanol extraction removes the fatty substances from the fibre surface and significantly increases the surface tension of the natural fibres (figure 3). The flax, hemp and kenaf R1 fibres will then have a surface consisting of pectin, lignin and some hemicelluloses [11]. Cotton fibres mainly ($\geq 95\%$) consist of highly crystalline cellulose, which will be exposed to the fibre surface after extraction of the waxy deposit. The surface tension of the flax, unretted hemp and kenaf R1 fibres attain a value of approximately 43 mN/m, whereas that of the retted hemp fibres is slightly higher ($\gamma_s = 49.5$ mN/m). This is probably caused by the higher uronic acid and thus higher pectin content of the former fibres (table 2). From the fact that flax R1 fibres possess a lower surface tension than flax R2 fibres (figure 4; R2 fibres are depectinized) it can be concluded that pectins have a lower surface tension than hemicelluloses. This is possibly due to a higher degree of orientation of hemicelluloses as compared to pectins. It has been demonstrated by several investigators that a higher degree of orientation yields a higher surface tension [1,2].

Defatted cotton fibres, flax R3 fibres and Cordenka fibres all possess a high surface tension. For these fibres we find a γ_s^d of approximately 50 mN/m. This value is an estimation since exact determination of γ_s^d of these fibres is impossible due to the fact that the value falls out of the range of surface tensions of 1-methylnaphtalene-octane mixtures. The calculated values for γ_s are between 65.2 and 66.1 mN/m. Literature data of γ_s for cellulose are between 54.4 and 68.7 mN/m [3,17], which agree very well with our results. Most literature values of γ_s^d of cellulose are lower than the 50 mN/m we found. However, Luner and Sandell [2] found for highly oriented cellulose a γ_s^d of 51 mN/m, which is close to our results. Flax, cotton and Cordenka cellulose all are highly crystalline [18] and are thus expected to have a high γ_s^d . These results clearly stress the importance of methods that can be applied directly to fibrous materials. Measurements on films of regenerated material do not provide meaningful information on material in its natural crystalline state. When fibres are applied in their natural state (e.g. in composite materials), it is

mandatory to have information corresponding to this state.

Figure 4 summarizes the surface tensions of the flax fibres used. Successive extractions of fats, pectins and hemicelluloses each time increase the fibre surface tension. The surface tension of the untreated fibres R0 is comparable to that of waxes, that of the R1 and R2 fibres falls within the range of those for hemicelluloses and lignin and the resulting R3 fibres possess a surface tension similar to that of highly crystalline cellulose. Coating of flax fibres with CMC results in an increased surface tension, probably due to the introduction of carboxylic groups on the fibre surface. A subsequent treatment with strearylamine reduces the surface tension to that of the untreated fibres R0. The resulting SA fibres will be coated with long alifatic chains which gives them a fatty character.

CONCLUSIONS

The fibre surface tensions determined by the newly developed floating test are in good agreement with literature data for surface tensions of the various fibre components. Untreated natural cellulosic fibres possess a low surface tension due to a waxy deposit on their surface. Upon extraction of fatty substances the surface tension significantly increases. The surface tension attained depends on the chemical composition of the surface layer and varies from approximately 43 mN/m for fibres containing a considerable amount of pectin on their surface to 66 mN/m for fibres consisting of high crystalline cellulose. The effect of extractions and chemical modifications on the fibre surface tension can clearly be determined by this method. Since measurements on fibres in their natural natural state are possible, this method offers some clear advantages as compared to most existing methods.

REFERENCES

1. B.R. Ray, J.R. Anderson and J.J. Scholz, *J. Phys. Chem.*, 62 (1958) 1220.
2. P. Luner and M. Sandell, *J. Polymer Sci. C*, 28 (1969) 115.
3. A.F. Toussaint and P. Luner, in C. Schuerch (Ed.), *Cellulose and Wood Chemistry and Technology*, John Wiley & Sons, New York, 1989, p. 1515-1530.
4. J.M. van Hazendonk, J.C. van der Putten, J.T.F. Keurentjes and A. Prins, *Colloids Surf. A: Physicochem. Eng. Aspects*, 81 (1993) 251.
5. F.M. Fowkes, *Ind. Eng. Chem.*, 56 (1964) 40.
6. S. Wu, *J. Polymer Sci. C*, 34 (1971) 19.
7. A. Blakeney, H.P. Harris, R.J. Henry and B.A. Stone, *Carbohydr. Res.*, 113 (1983) 291.
8. O. Theander and E.A. Westerlund, *J. Agric. Food Chem.*, 34 (1986) 330.
9. A.G. Schönig and G. Johansson, *Svensk Papperstidn.*, 68 (1965) 607.
10. A.E.R. Ahmed and J.M. Labavitch, *J. Food Biochem.*, 1 (1977) 361.
11. M. Lewin and E.M. Pierce (Eds), *Handbook of Fiber Science and Technology, Volume IV: Fiber Chemistry*, Marcel Dekker, New York, 1985.
12. B. Janczuk, T. Bialopiotrowicz and W. Wojcik, *Colloids Surf.*, 36 (1989) 391.
13. D. Fengel and G. Wegener, *Wood: Chemistry, Ultrastructure, Reactions*, Walter de Gruyter, Berlin, 1984, p. 39-49.
14. K.A. Garleb, L.D. Bourquin and G.C. Fahey, *J. Agric. Food Chem.*, 37 (1989) 1287.
15. F.E. Bartell and H.H. Zuidema, *J. Am. Chem. Soc.*, 58 (1936) 1449.
16. R.A. Young, in R.A. Young and R.M. Rowell (Eds), *Cellulose: Structure, Modification and Hydrolysis*, John Wiley & Sons, New York, 1986, p. 115-118.
17. S.B. Lee and P. Luner, *Tappi*, 55 (1972) 116.
18. E. Treiber, in J. Brantup and E.H. Immergut (Eds), *Polymer Handbook 2nd ed.*, John Wiley & Sons, New York, 1976, p. V90-V92.

16 The influence of cellulose degradation on insulation life in power transformers

A M Emsley – Chemistry Dept, University of Surrey, Guildford, Surrey GU2 5XH, UK

ABSTRACT

Cellulose based paper, manufactured by the Kraft process and impregnated with insulating oil, is widely used to insulate the windings of power transformers. Thermal ageing reduces the degree of polymerisation of the cellulose. At a DP of ~ 250 , the strength is reduced to 20% of its initial value and below 250 paper has no strength at all, leaving it susceptible to mechanical damage, which can lead to electrical breakdown and ultimately to failure of the transformer.

A simple statistical relationship, originally developed by Ekamstam in the 1930's, can be applied to the kinetics of degradation and used as the basis for a model to estimate insulation life. The cumulative concentrations of cellulose degradation products in the oil can be used to indicate the current condition of the transformer insulation.

INTRODUCTION

The power transformer is the link between a power station and the outside world. It steps up the voltage from its generation level of 25 kV to the grid level of 415 kV in the UK. A typical 650 MVA unit costs £2M and takes 18 months to build. It contains some 12 tonnes of paper insulation wrapped around the windings some 30 to 120 μm thick and 45 tonnes of insulating oil, which also serves to cool the windings. The paper is manufactured to high standards of purity by the Kraft process and a typical composition is given in Box 1.

Advantages of using paper are:

- it is cheap compared to synthetic polymers and
- it has excellent dielectric properties when impregnated with insulating oil. (The resistivity of the impregnated paper is greater than that of either of the components individually.)

The disadvantages are:

- it deteriorates with age and becomes brittle, which makes it susceptible to defibrillation and tearing
- in fully sealed transformers, the paper becomes saturated (up to 8% by weight) with water formed during thermal degradation, which increases its conductivity.
- in free breathing transformers, the rate of ageing can be accelerated by the ingress of oxygen, which has a maximum solubility in oil of some 30,000 ppm

1 Characteristics of Kraft Insulating Paper

Cellulose constitutes 85-90% of Kraft paper, 4 - 7% is lignin (a polyaromatic hydrocarbon) and the balance is pentosans (lignocelluloses).

The initial degree of polymerisation (DP) is 1200 to 1400, but this drops to ~900 as a result of drying to a moisture level of <0.1%.

Failure of the transformer can occur when:

- paper fibres, or torn pieces, enter and block the oil stream, reducing cooling
- wet, conducting fibres bridge conductor gaps and generate a short.
- water is released from the insulation when the temperature rises, for instance during overload conditions, causing the formation of conducting gas bubbles and leading generally to thermal instability.

Many of the transformers operating today were installed in the 1960's and 1970's, with a life expectation of 25 - 40 years. In a review of transformer experience in the U.K. prior to privatisation, it was found that 50% of power transformers will have reached their intended life by the year 2000 (1). A similar picture is found in most of the developed countries.

The modern transformer operator needs methods of

- a) assessing the current condition of his units
- b) monitoring them for signs of failure and
- c) predicting their future life expectancy.

Current research is aimed at providing these tools. Many factors influence the life expectancy of a transformer, including electrical loading, mechanical movement of windings during temperature cycles, changes in compliance in the windings - leading to distortion and the build up of moisture and oxygen, which accelerates ageing. The ultimate life of the transformer is determined by the life of its insulation, unless other factors cause it to fail early. In order to predict life expectancy, a kinetic model of degradation is required under conditions relevant to transformers. To provide methods of monitoring degradation, a knowledge of the mechanisms of degradation, the distribution of degradation products and the rate at which they form is required. This paper discusses the development of such models in terms of our current knowledge of cellulose degradation kinetics and mechanisms.

THE PREDICTION OF INSULATION LIFE EXPECTANCY

A Historical Perspective of degradation of cellulose in oil

In the first reported studies of degradation of paper in oil, paper, 50 μ m thick, was degraded at temperatures in the range 90 °C to 140 °C and changes in degree of polymerisation (DP) measured as a function of time (2). The data were originally analyzed in a half life, kinetic model. They were subsequently re-analyzed by Fallou (3), who showed that they could be represented by a plot of the number of bonds broken per thousand against time. However, the resultant graph displayed a discontinuity, requiring two straight lines, which she attributed to a change in mechanism.

Further systematic studies of the change in DP of paper degraded in oil and the effects of water and oxygen have been published since. Schroff and Stannett (4) plotted log DP against time and obtained lines, which became linear after an initial period of curvature, but did not extrapolate through the origin.

Other workers have presented kinetics based on DP measurements and some have shown an apparent change in the activation energy above about 130 °C and postulated a change in mechanism (5, 6,7,8, 9,10,11). These and other results will be discussed again later.

Statistical Modelling of Random Degradation Kinetics

In the mid 1930's Kuhn and co-workers (12) investigated the degradation of cellulose from a theoretical statistical viewpoint. Their work was later developed into a kinetic model for the degradation of linear polymers by Ekamstam (13). The model has been widely applied to the degradation of cellulose under conditions of acid and alkaline hydrolysis and, in some cases to thermal degradation. It has not generally been tested for the degradation of cellulose under oil.

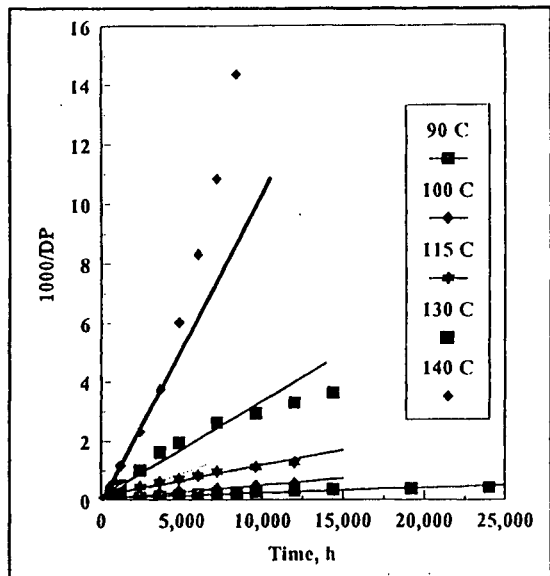


Figure 1 Application of the Ekamstam Equation to the Degradation of Cellulose in Oil (replotted from Fabre and Pichon (2))

The derivation of the equation is based on the assumption that the rate of degradation is first order rate with respect to the number of inter monomer linkages. That is, that the rate of degradation at any time is directly proportional to the number of unbroken bonds available at that time.

The derivation of the rate equation can be found in most polymer textbooks and is briefly summarised in the Appendix. The final format is:

$$\frac{1}{DP_t} - \frac{1}{DP_0} = kt$$

The Ekamstam equation is strictly applicable only in the following circumstances:

- the polymer chain is linear and of high molecular weight
- the polymer is monodisperse and the products of scission are themselves long chain molecules
- there is a low degree of chain end-chopping
- there is no loss of monomer units during scission.

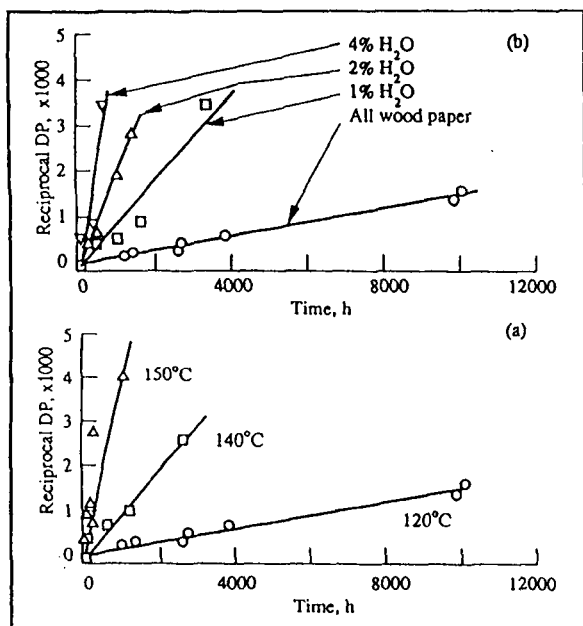


Figure 2 The influence of (a) Temperature and (b) Water on the Degradation of Paper in Oil (replotted from Schroff and Stannett (4))

2b shows the effects of increasing the moisture in the paper from <0.5% to 4%.

Other available data, for degradation under oil, when replotted in the same form, show good agreement with the Ekamstam equation (14). There is a clear tendency to increasing rates of reaction in some data at 140 °C and above, which may be indicative of autocatalysis of the reaction by water formed during the degradation process. Other data show the deviation

The Application of the First Order Model to Degradation in Oil

The original data of Fabre and Pichon have been replotted in *Figure 1* according to the Ekamstam equation. The results are substantially straight lines, which pass through the origin. Closer inspection reveals a tendency to lower rates of reaction at longer times at temperatures < ~130 °C and to higher rates of reaction at temperatures above about 130 °C.

The data of Schroff and Stannett have also been replotted in *Figures 2a and 2b*. Again good straight lines are obtained passing through the origin. Figure 2a shows the effects of temperature on the degradation rate and Figure

to lower rates of reaction previously noted in the data of Fabre and Pichon at temperatures $< 120^\circ\text{C}$.

These observed deviations may be explained by inhomogeneity of degradation of the paper, e.g. rapid degradation of the amorphous regions, or of the larger molecules, followed by a reduction in rate as the relative degree of crystallinity increases.

A Unified Model for the Kinetics of Degradation

It can be shown that the Ekamstam equation can be applied to cellulose degradation kinetics reported in the literature under a wide variety of conditions, including degradation in air, oxygen, vacuum and acid and alkaline solution. The rate constants thus obtained are plotted against temperature in *Figure 3* in the familiar Arrhenius format.

The data can be divided into five sets

2 Pre-exponential Factors from Analysis of Covariance of Degradation Rates

Data set	Pre-exponential $\times 10^7$		
		95% confidence limits $\times 10^7$	
1	3.65	0.79	16.8
2	10.7	2.41	47.1
3	35.0	8.41	146
4	77.8	18.3	330
5	347	76.6	1570

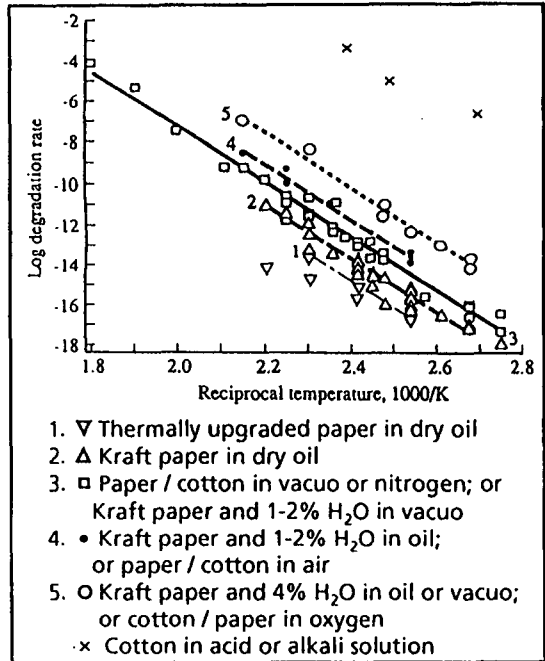


Figure 3 Analysis of Covariance of Rate Constants of Degradation of Cellulose from Random Chain Scission Kinetics

according to increasing "susceptibility to degradation" of the cellulose or "potential for oxidation" of the environment. A 6th set has been obtained for degradation in acid and alkali, by extrapolation from rates measured at very much lower temperatures. These are not included in subsequent analyses, because of the large uncertainty in their values.

Thermally upgrading of paper reduces its susceptibility to degradation. Water in oil, or the use of air or oxygen increase the potential for degradation. An analysis of covariance on the reaction conditions yields an activation energy of 111 kJ/mole, with 95% confidence limits on the mean of 106 and 116 kJ/mole. The pre-exponential factors and their 95% confidence limits, tabulated in Box 2, increase as the potential for oxidation of the reaction medium increases.

It seems likely that apparent changes in activation energy, measured during degradation in oil by some workers (5 - 11) and referred to previously, arise as a result of a change in the pre-exponential factor, rather than a change in mechanism. Build up of moisture in the paper, which can occur as the products of degradation accumulate, could, for instance, account for an increase in the pre-exponential factor. In other laboratory experiments under gas or a vacuum, the water would be continuously removed. The solubility in oil is several orders of magnitude less than that in paper, so the removal process is inefficient.

Although the data for acid and alkali degradation are not included in the analysis, they clearly would fit the calculated activation energy, with a yet larger pre-exponential.

Insulation Life Prediction

Degradation rate constants can be obtained under operational conditions by extrapolation to normal transformer temperatures. If values for the starting DP and final DP of the paper, when the insulation is liable to fail, are assumed, then an estimate of total life expectancy can be obtained. The limiting

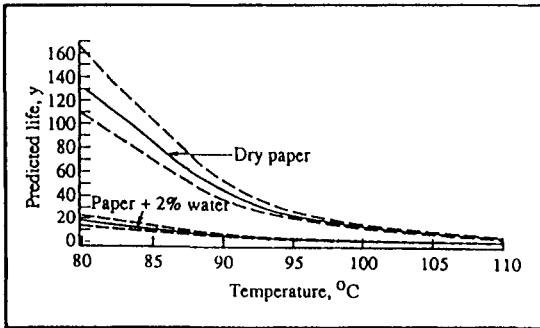


Figure 4 Insulation Life Prediction from Cellulose Degradation Kinetics

minimum value of DP is a matter of some debate, but Schroff and Stannett (4) have shown that the tensile strength of paper rapidly falls to zero at a DP below about 200 to 250. At this point therefore the paper becomes susceptible to damage, as a result for instance of movement of the windings during a temperature excursion.

Taking the case of an initial DP value of 1000 and a final value of 200 respectively, the life equation can be formulated as:

$$life = \frac{0.004}{A} e^{\frac{136000}{T}} \text{ hours}$$

Plots of insulation life against temperature are shown in *Figure 4* for standard, Kraft insulating paper in insulating oil, which is maintained dry throughout the life of the transformer and for paper containing a constant 2% by weight of moisture. In both cases, the temperature range is 80 to 110 °C, which represents the upper limits of operation of a typical transformer. The dashed lines are the errors one standard deviation from the mean.

Best estimates of insulation life, calculated this way, vary by less than a factor of 2, for any closely defined condition. However, other uncertainties in the calculation, such as the assumptions made with regard to the initial and final DP values, increase errors in the predicted life. When all factors, including water and oxygen levels, are taken into account, the total variation over all environmental conditions is a factor of 200, which highlights the need for improved ageing models to be developed.

MONITORING TRANSFORMER CONDITION

Insulation condition monitoring generally relies on chemical analysis of the oil, because the inner regions of any transformer are difficult, if not impossible, to access. By far the most popular and successful method of condition monitoring has been analysis for dissolved gases such as hydrogen, methane, ethane, ethyne, carbon monoxide. That is to say small molecular products of degradation. This technique, however, suffers from the problem that the source of the gases is not uniquely identifiable, since they could also arise from the degradation of the oil. In recent years a complementary approach has begun to emerge. The oil is analyzed for products which are specific to the degradation of paper, such as 2-furaldehyde, methyl furfural and acetyl furan. These and other similar compounds have been identified in cellulose degradation

experiments under nitrogen and *in vacuo* (15-22) and have also been shown to be products of thermal degradation of the monomer unit, glucose (23-25).

Polar products such as these can be separated from the oil and analyzed by high performance reverse phase liquid chromatography (HPLC). The method involves separating the products from the oil matrix, by adsorption on to a polar pre-column, extracting with acetonitrile/ water, and injecting on to a C_{18} column, using acetonitrile/ water as the mobile phase. The eluents all absorb in the UV and can be analyzed by using a fixed or variable wavelength UV detector. (26).

2-Furfuraldehyde Formation Kinetics

Laboratory experiments have been carried out to measure the formation of 2-furaldehyde and other products in a model transformer (1). Best estimates of initial rates of formation of 2-furaldehyde are plotted in Figure 6 and a line with the same slope as the lines in Figure 4 has been drawn through them. The close fit of the activation energy for cellulose

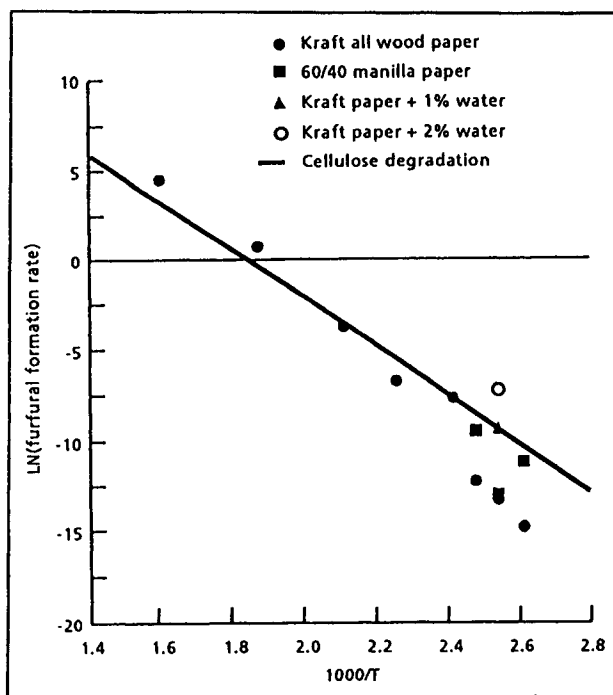


Figure 5 Comparison of Initial Rates of Formation of 2-Furaldehyde with the Activation Energy of Cellulose Degradation

degradation, calculated from changes in DP, with rates of formation of 2-furaldehyde seems to promise the possibility of a mechanistic relationship.

Current research is aimed at establishing this relationship from improved kinetic measurements and a better understanding of the mechanisms of degradation.

Systematic Studies of Operating Transformers

Model laboratory experiments have been supplemented by a systematic study of a number of transformers over a period of 5 years. The work was carried out by the CEBG prior to privatisation. Three specific paper degradation products were analysed for, as well as 3 products of degradation of phenol formaldehyde resins, which are also used to insulate transformers.

Figure 6a shows the trends in a typical transformer. Levels of the paper degradation products are < 1 mg/l rising only slowly (0.1 to 0.3 mg/l/y). Other paper degradation products such as 5-methyl-2-furfural and 2-acetyl furan are normally observed at levels < 0.2 mg/l.

Higher levels of furfural (typically 2 to 5 mg/l and rising more rapidly) were found at high paper temperatures in transformers operating towards the top end of their permissible temperature range.

In comparison, *Figure 6b* shows the effects of a temperature excursion, arising, in this instance, as a result of failure of the cooling circuit. The decrease in concentration after the fault was corrected also demonstrates the existence of a removal mechanism (decomposition, evaporation or adsorption in a cooler part of the circuit), which will need to be accommodated in future kinetic modelling.

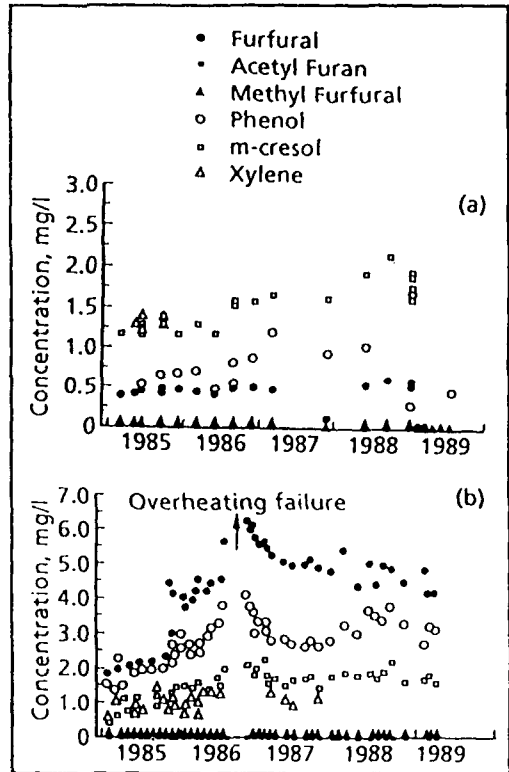


Figure 6 Cumulative Degradation Product Concentrations from Paper in Operating Transformers

CONCLUSIONS

1. Degradation of cellulose determines the ultimate life of transformer insulation, although other factors may cause it to fail prematurely.
2. The Ekamstam equation for the degradation of linear polymers by random chain scission can be applied to the degradation of cellulose over a wide range of conditions, including degradation in insulating oils.

3. A common activation applies independent of conditions.
4. The rate of degradation increases with increasing "potential for oxidation" of the conditions, as a result of an increase in the pre-exponential factor of the reaction.
5. By assuming a limiting minimum DP of 200, below which the paper strength decreases to zero, estimates of insulation life can be made under idealised, constant operational condition.
6. Furan based products, which are specific to the degradation of paper in the transformer, can be detected in the oil and can, potentially, be used as indicators of the transformer condition.
7. The temperature of the initial rates of formation of 2-furaldehyde is very similar to that for the decrease in DP of cellulose during degradation. Current research is aimed at establishing the relationship of these two factors, in order to devise a model of insulation ageing, which will provide the operator with a detailed picture of the condition of the insulation in his transformer.

ACKNOWLEDGEMENTS

This paper is published by permission of National Power PLC and the National Grid Company PLC, who also support the author in his current studies into insulation degradation in transformers.

REFERENCES

1. Emsley A.M. and Stevens G.C. (1), to be published (in IEE journal)
2. Fabre J. and Pichon A., *CIGRE Conf. Paper* 137, 1960
3. Fallou B., *Rev. Gen. Elec.*, 1970, 79, 645
4. Schroff D.H. and Stannett A.W., *IEE Proc. C., G.B.*, 1985, 132, 6, 312-9
5. Miyoshi A., *IEEE Trans. Elec. Insul.*, 1975, E1-10, 1, 13
6. Moser H.P. and Dahinden V., 1988, Transformerboard 2, Pub. H. Weidmann AG
7. Tamura, Anetai, Iskii and Kawawmura, *IEEJ*, 1981, 101-A, 30-36
8. Zhilyaev T.B., Linova L.S., Granovskaya, V.N. and Golovan, N.I.,
9. Hino T. and Suganuma T., *Shinku Kagaku*, 1967, 15, 2, 49-55
10. Hino T. and Suganuma T., *IEEE Trans. Elec. Insul.*, 1972, 7, 3, 122-6
11. Yoshida H., Ishioka Y., Suzuki T., Yanari T. and Teranishi T., *IEEE Trans Elec. Insul.*, 1987, E1-22, 6, 795
12. Kuhn W., *Ber.*, 1930, 63, p1503
13. Ekamstam A., *Ber.*, 1936, 69, p553
14. Emsley A.M. and Stevens G.C. (2), to be published (in Polymer)
15. Madorsky S.L., Hart V.E. and Strauss S., *J. Res. Nbs.*, 1956, 56, 343
16. Murphy E.J., 1962, *J. Polym. Sci.*, 1962, 58, 649-665
17. Schwenker R.F. and Beck L.R., *J. Polym. Sci., C*, 1963, 2, 331-340
18. Glassner S. and Pierce A. R., *Anal. Chem.*, 1965, 37, 525
19. MacKay G.D.M., *Can. Dept. of Forestry 42-pub.*, 1967, No 1201
20. Kilzer F.J., *High polymers*, 1971, 5, Pt 5, P1015. Ed Bikales and Segal
21. Shafizadeh F., *Cellulose chemistry and its applications.*, 1985, 266, Ed Nevell, Pub Ellis Horwood
22. Pavlath A.E. and Gregorski K.S., *Conf. Res. Thermochem. Biomass. Convers.*, 1988, p155-163

23. Houminer Y. and Patai S., *Israel J. Chem.*, 1969, 7, 4, 513
 24. Shafizadeh F. and Lai Y.Z., *J. Org. Chem.*, 1972, 37, 2, 278
 25. Shafizadeh F., Philpot C.W. and Ostonjic N., *Carbohydr. Res.*, 16, 279-287
 26. Unsworth J. and Mitchell F., *IEEE Trans., Elec. Insul.*, 1990, 25, 4, 737

APPENDIX 1. DERIVATION OF THE EKAMSTAM EQUATION

If the initial number of molecules of polymer is initially l_0 , then

$$\begin{aligned} l_0 &= N_0 - M_0 = N_0 \left(1 - \frac{M_0}{N_0}\right) \\ &= N_0 \left(1 - \frac{1}{DP_0}\right) \end{aligned}$$

where

DP_0 = initial degree of polymerisation

M_0 = the initial total number of monomer units and

N_0 = the initial total number of bonds

Similarly, the number of unbroken bonds remaining at time t is:

$$l_t = N_0 \left(1 - \frac{1}{DP_t}\right)$$

If the rate of bond scission is proportional to the number of unbroken bonds remaining.

$$-\frac{dl}{dt} = k \cdot l_t$$

so

$$l_t = l_0 e^{-kt}$$

$$\log l_t - \log l_0 = -kt$$

substituting for l_t and l_0

$$\log \left(1 - \frac{1}{DP_t}\right) - \log \left(1 - \frac{1}{DP_0}\right) = -kt$$

If DP_t and DP_0 are large this simplifies to:

$$\frac{1}{DP_t} - \frac{1}{DP_0} = kt$$

17 Thermocatalytic destruction of cellulose

G Dobele, T Dizhbite, G Rossinskaya, G Telysheva – State Institute of Wood Chemistry, 27 Dzerbenes str, LV 1006 Riga, Latvia

ABSTRACT

With the aim of elucidating the mechanism of action of different dehydration catalysts during cellulose thermal destruction, the structure and properties of solid, liquid and gaseous products of cellulose pyrolysis were investigated using pyrolytic gas-liquid chromatography, ESR and X-ray photoelectronic spectroscopy, as well as thermal analysis methods. It was established, that the development of cellulose dehydration on low-temperature stages in the presence of additives make it possible to predict the behavior of materials in the high-temperature region.

Results of this work are used to obtain cellulose-based carbon materials and for the development of practical techniques of wood fire protection.

INTRODUCTION

We have established earlier that the properties of cellulose carbonization products obtained in the

temperature range up to 500°C, are determined by the intensity of intra- and intermolecular dehydration reactions. This work set out to investigate the mechanism of cellulose and wood materials thermal destruction after introduction of dehydration catalysts providing system thermostability in the high-temperature region (phosphoric and boric acids, ammonium chloride).

METHODS OF INVESTIGATION

The object of the investigation - sulphate cellulose (crystallinity index 0.65). Phosphoric and boric acids and ammonium chloride (5% on DM) were introduced by cellulose impregnation with water solutions (modulus 1:5).

Dynamics of water evolving was determined by stepwise pyrolytic gas chromatography (SPGC). Solids after cellulose thermal treatment were analyzed on the unchanged glucopyranose units content performed by solids hydrolysis and the consequent measurement of glucose yield by GLC method.

ESR and X-ray photoelectronic spectroscopies were also used for the investigation of solids structure.

RESULTS AND DISCUSSION

Investigated additives catalyze dehydration of cellulose during its thermal treatment. Reactions with water evolving are taking place in the lower temperature region, water yield increase as the result of the catalysts addition into cellulose (Table 1, Fig.1). However, the mechanisms of their action are different.

As for the phosphoric acid action mechanism, it is known that aside from hydrolytic action this substance takes active part in low-temperature dehydration reactions, forming esters. We have estimated the temperature regions of phosphorus bonds existence: 20-150°C - hydrogen bonds; 180-350°C - esters; 250-450°C - polyphosphoric and higher than 450°C - phosphorus-carbon bonds.

Table 1

Water yield at cellulose heating up to 400°C

Additive	Water yield, % on DM
None	15.1
Phosphoric acid	27.2
Boric acid	19.9
Ammonium chloride	20.4

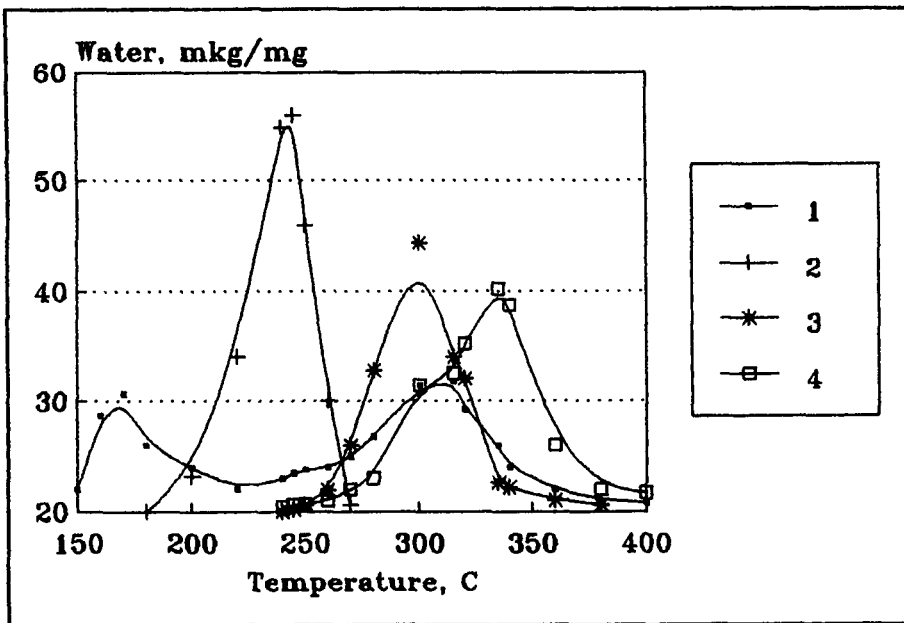


Fig.1. Water yield during cellulose pyrolysis. Additives: 1 - NH_4Cl ; 2 - H_3PO_4 ; 3 - H_3BO_3 . 4 - initial cellulose.

Boric acid action is expressed in catalysis of intermolecular dehydration mostly in the low-temperature region. Cellulose dehydration under ammonium chloride action proceeds by two stages (Fig. 1). Most probably, in the first stage ammonium chloride interacts as a Lewis acid with OH-groups of the pyranose ring. As a result, water is

eliminated and double bonds form. In the second stage the relationship between dehydration reaction and Schiff base formation may be supposed.

As well as the other dehydrating additives, phosphoric and boric acids and ammonium chloride suppress levoglucosan formation and increase the yield of dehydrated 1,6-anhydride - levoglucosenone (Table 2). However, differences in the mechanisms of the additives action on cellulose dehydration lead to differences in anhydride formation.

Table 2
1,6-anhydrides formation during cellulose
treatment at 350°C

Additive	Yield, % from a.d.s	
	Levoglucosan	Levoglucosenone
None	10.1	0.6
Phosphorus acid	0.6	16.8
Boric acid	-	5.8
Ammonium chloride	-	4.7

Maximum levoglucosenone yield was noted after adding phosphoric acid. Obviously, it is provided by protonation of glycosidic bonds and low-temperature reactions of intramolecular dehydration through the formation and decomposition of cellulose esters. Contrary to phosphoric acid, boric acid is not able to form carbonium centers at C6 of the pyranose ring with the following linking of anhydro bonds. That is the reason that levoglucosenone formation in this case is not so intensive. In the case of ammonium chloride, high yield of levoglucosenone is prevented by low-temperature dehydration leading to double bond formation. It is also possible that OH-groups at C6 are also taking part in these reactions.

The rate of involvement of cellulose glucopyranose units in dehydration and fragmentation reactions is testified by the glucose yield during the hydrolysis of solids after cellulose stepwise thermal treatment (Fig. 2). The addition

of phosphoric acid leads to the total development of these reactions at 275°C, compared with 370°C for the initial cellulose.

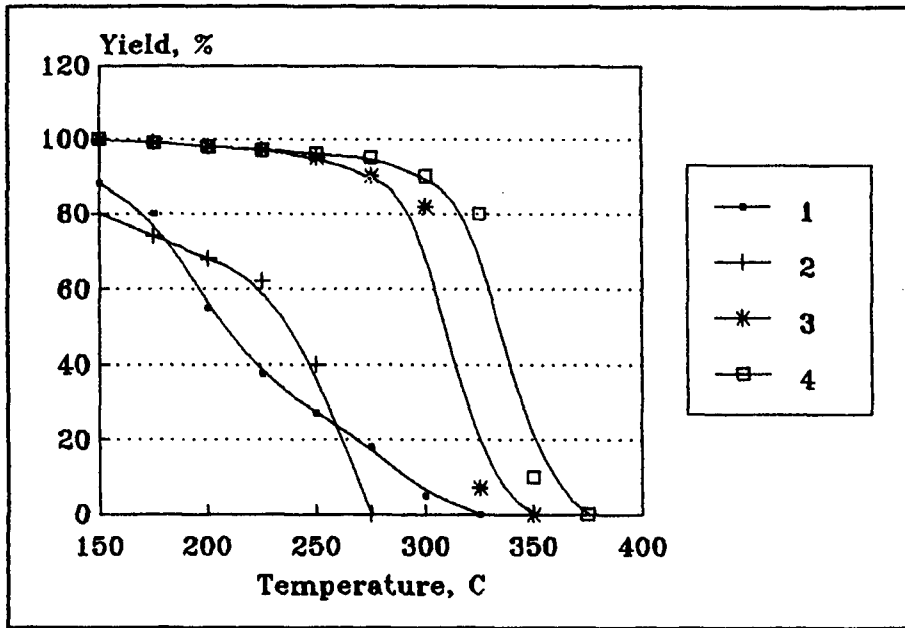


Fig.2. Glucose yield after hydrolysis of cellulose pyrolysis solids. Legend the same as in Fig.1.

ESR spectra of cellulose thermal treatment solids are caused by the presence of stable paramagnetic centers (PMC) of polyconjugated systems (PCS), which are typical for pyropolymers. Degree of PCS development may be approximately estimated by the quantity of stable PMC and the dimension of non-paired electrons delocalization area.

The most low-temperature increase in stable PMC quantity was observed after ammonium chloride introduction into cellulose (Fig. 3). After phosphoric acid introduction the intensity of PMC formation before 400°C is significantly higher than for initial cellulose. The presence of boric acid in cellulose materials leads to a decrease of the PMC quantity in comparison with the initial cellulose within all investigated temperature ranges.

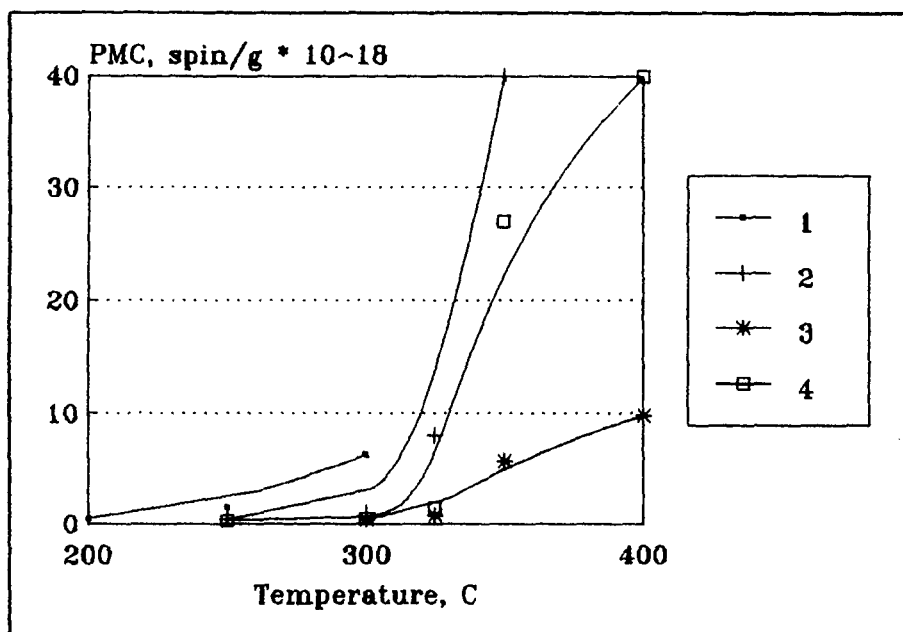


Fig.3. Stable PMC concentration in solids after cellulose pyrolysis. Legend the same as in Fig.1.

It may be explained by the inhibition of free radical reactions and the suppression of water elimination reactions. That is why the rebuilding of the structure of cellulose thermal treatment products into polyconjugated systems goes more slowly.

SUMMARY

The mechanism of action of three types of dehydrating additives, changing the direction of cellulose thermal destruction is investigated. It is established that phosphoric acid in the low-temperature step interacts with cellulose, many times forming esters; ammonium chloride, acting as a Lewis acid, catalyzes elimination reactions; boric acid action leads to the formation of quasiaromatic structures in the high-temperature stages of the process.

18 Solubility of cellulose and its derivatives

A M Bocek, G A Petropavlovsky and A V Yakimansky – Institute of Macromolecular Compounds of Russian Academy of Sciences, Bolshoi pr 31, St Petersburg, 199004 Russia

One of the main problems in the field of chemistry and technology of cellulose is the search for new solvents. During the last decades many non-aqueous solvents of cellulose have been found experimentally. For some cellulose solvents (e.g., for N-oxides of tertiary amines) several criteria have been suggested which may be used to distinguish amine oxides dissolving cellulose from non-dissolving ones [1,2]. Unfortunately, using known criteria, it is impossible to explain why some amine oxides do not dissolve cellulose.

It is known that the process of polymer dissolution should be accompanied by a decrease in the free energy of polymer-solvent systems: $\Delta F = \Delta H - T\Delta S$, where ΔF , ΔH , and ΔS are changes in the free energy, enthalpy, and entropy, respectively. It seems to be useful to analyze the roles of the enthalpic and entropic contributions in the proces-

ses of swelling and dissolution of cellulose in different solvents. One of the earliest criteria used to predict polymer solubility in any solvent is Hildebrandt's solubility parameter (δ), which is connected with the value of the density of cohesion energy.

Data about the δ value for cellulose are controversial. Based on the data on cellulose swelling, the value of $\delta = 28.6 \text{ (J/cm}^3\text{)}^{1/2}$ has been obtained [3]. From the cohesion energy of cellulose in the crystalline region ($E = 296 \text{ kJ/mole}$) the value of $\delta = 53.4 \text{ (J/cm}^3\text{)}^{1/2}$ has been found [4].

As the process of cellulose dissolution is usually connected with H-bond formation between the cellulose hydroxyl groups and solvent molecules, one of the most important criteria of dissolving ability of any solvent is the value of the interaction energy of this solvent with cellulose which should be higher than the energy of intermolecular H-bonds in cellulose itself. If the interaction energies of solvent molecules with each other and with polymer chains have close values, the possibility of polymer dissolution should depend on the entropic factor.

The present paper is devoted to the study of energetic factors in the processes of cellulose dissolution, namely, to the determination, both experimentally and theoretically, of the minimum energy of H-bond between cellulose and a solvent molecule which is sufficient for cellulose dissolution, and also the factors, affecting the interaction between solvent molecules and cellulose hydroxyl groups.

The δ value for cellulose and dispersion (δ_d), dipole-

dipole (δ_p), and H-bond (δ_h) contributions [5] to it have been determined. These characteristics have been calculated using the extrapolation of δ values for cellulose acetates with different degrees of substitution (DS) to DS = 0 (Fig.1) [6]. This procedure has led to $\delta = 56.2$

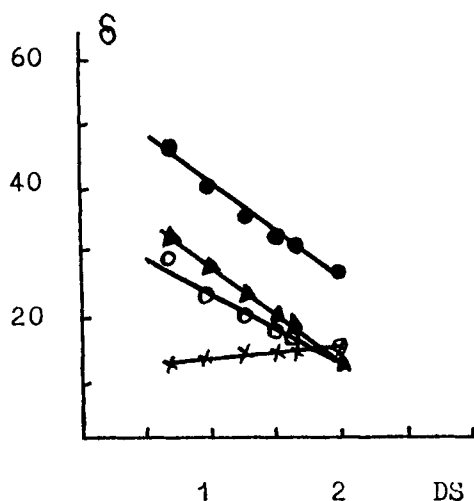


Fig.1. Values of δ (●), δ_d (x), δ_p (o), δ_h (▲) for cellulose acetates vs their DS.

[$\delta_d=11.7$, $\delta_p=35.9$, $\delta_h=42.2$ (J/cm^3) $^{1/2}$]. Using the expression $\delta_h = (\sum E_h / V_m)^{1/2}$ it has been found that the energy of one H-bond in cellulose $E_h = 25.2$ kJ/mole. It should be noted that the obtained E_h value is significantly higher than the known values of inter- and intramolecular H-bonds in cellulose [7].

Using the semiempirical MNDO method [8], quantum chemical calculations of electron structure parameters of different amine oxides and their interaction energies with

water molecule (simulating hydroxylic group of cellulose) have been carried out [9]. Cohesion energies of amine oxides in the form of dimers, E_{coh} , have been calculated according to the scheme, proposed in [10] (Figs.2,3):

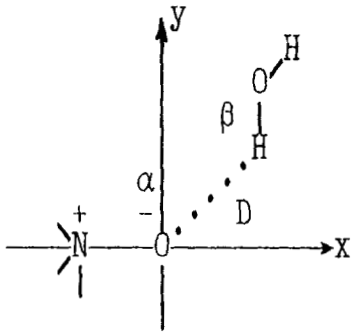


Fig.2. Geometry of H-bonded complex.

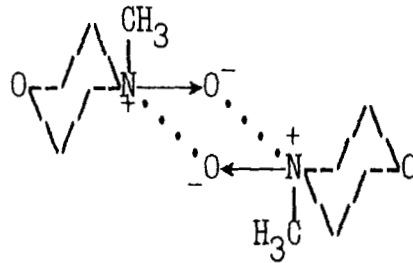


Fig.3. Dimer model of heterocyclic amine oxide [10].

As seen from Table 1, there is a correlation between the dipole moments of heterocyclic amine oxides and their dissolving ability. It has been suggested [1] that an amine oxide should have $\mu \geq 4.5$ D in order to be a cellulose solvent. However, for aliphatic tertiary amine oxides such a correlation is absent. The results of our quantum chemical calculations show [9] that for all amine oxides studied, capable of dissolving cellulose, the energy E_h of their H-bond with OH-group is higher than 25.0 kJ/mole, i.e. the value of one H-bond in cellulose itself found from the δ_h value [6].

It is known that the processes of the interaction of amine oxides with cellulose are exothermic. However, the polymer dissolution occurs only on heating the solvent-polymer system. The data presented in Table 1 permit us to explain this fact. Only for MMNO the E_h and E_{coh} values

Table 1. Parameters characterizing dissolving ability of different amine oxides with respect to cellulose.

Amine oxide	Dissolving ability	Dipole moment μ , D [9]	E_h , kJ/mole [9]	E_{coh} , kJ/mole
Trimethylamine N-oxide (TMANO)	not diss.	5.14	28.9	43.9
Triethylamine N-oxide (TEANO)	diss.	4.52	25.9	40.5
Methylmorpholine N-oxide (MMNO)	diss.	4.25	25.5	26.4
Ethylmorpholine N-oxide (EMNO)	not diss.	4.12	23.9	26.4
Morpholine N-oxide (MNO)	not diss.	4.05	18.4	-

are close to each other. In the case of TMANO and TEANO the E_{coh} value is noticeably higher than the E_h value. Therefore, on heating, first of all, the destruction of amine oxide structure occurs (entropic factor) leading to a decrease in the E_{coh} value of the solvent, and then the cellulose dissolution processes develop. It is possible to change amine oxide structure and to decrease their E_{coh} value adding a definite amount of water to them. As a result, a substantial decrease in the melting temperature is

observed for MMNO, while TEANO in the monohydrate form is liquid at room temperature. This conclusion is confirmed by the fact that with a decrease in water content in TEANO below 4 mass.% system completely loses its ability to dissolve cellulose [11]. Only temperature increase is insufficient in order to decrease the E_{coh} values of aliphatic amine oxides, TMANO and TEANO, down to the values close to E_{h} or lower. Therefore, for these two amine oxides the content of water in them is of great importance. It should be noted that TMANO on heating and adding water to it does not dissolve cellulose. It is probable, that in the regions of temperatures and water concentrations in TMANO studied it is impossible to decrease the E_{coh} value down to the value of H-bond TMANO-cellulose.

Based on the experimental data presented and results of theoretical calculations it is possible to conclude that cellulose may be dissolved by amine oxides with $E_{\text{h}} \geq 25.0$ kJ/mole. Moreover, the conditions of the dissolution process should provide the value of cohesion energy of solvent molecules $E_{\text{h}} \leq 25.0$ kJ/mole.

References

1. R.N.Armstrong, J.K.Varga, C.C.McCorsley // TAPPI Conference Papers, 5-th Intern. Dissolving Pulp. Wien, 1980, p.100-104.
2. L.K.Golova, V.G.Kulichihin, S.P.Papkov // Vysokomol. Soed., 1986, 28(A), 1795-1809.
3. E.F.Thode, R.G.Guide // TAPPI J., 1959, 42, 35.
4. W.Berger, M.Keck in "Cellulose Sources and Exploitation", Eds. J.F.Kennedy, G.O.Phillips, and P.A.Williams,

Ellis Horwood, Chichester, 1990, pp.69-78.

5. C.M.Hansen, K.Skaarup // J. Paint Technol., 1967, 39, 511.
6. A.M.Boчек, G.A.Petropavlovsky, "Cellulose solubility parameter", Cellulose Chemistry and Technology, 1993, 27, №6.
7. R.G.Zhbankov, P.V.Kozlov, "Fizika Cellulozy i ee Proizvodnyh", Nauka i Technika, Minsk, 1983, p.213.
8. M.J.S.Dewar, W.Thiel // J. Amer. Chem. Soc., 1977, 99, 4899.
9. A.V.Yakimansky, A.M.Boчек, V.A.Zubkov, G.A.Petropavlovsky // Zhurn. Prikl. Khim., 1991, 64, 622.
10. E.Maia, A.Peguy, S.Perez // Acta Crystallographica, 1981, 37, 1858.
11. V.G.Kulichihin, L.K.Golova, N.P.Kruchinin, V.V.Romanov, and Yu.Ya.Belousov in Preprints IV Internat. Symposium on Man-Made Fibers, Kalinin, 1986, v.2, pp.200-205.

Part 3:
**Derivatives of cellulose and
their properties**

19 Derivatisation of cellulose in homogeneous reaction

M Diamantoglou and E F Kundinger – Akzo Faser AG, D-63784 Obernburg, Germany

Abstract

The suitability of the DMAc/LiCl and NMP/LiCl solvent system has been investigated for derivatising cellulose homogeneously to esters, carbamates, ethers and deoxycellulose compounds. High molecular weight cellulose (DP > 1000) dissolves totally after activation in aqueous alkaline solutions. The degree of substitution can be controlled over a wide range for all investigated reactions. High yields of the reagents have been achieved for acid anhydrides, acid chlorides, isocyanates and epoxides. Ketoesters are generated readily from fatty acid chlorides and tertiary amines. Deoxycellulose derivatives can be synthesized easily from cellulose organosulfonic acid esters in the presence of halogenic or pseudohalogenic anions. Potential applications of the products as absorbents and medical membranes are described.

1 Introduction

The known technical processes for derivatising cellulose proceed heterogeneously or start heterogeneously and are completed homogeneous when during the reaction soluble products are generated. The synthesis of cellulose acetate in methylene chloride is a well known example. The expected advantages of the homogeneous reactions compared to heterogeneous reactions are:

- the control of the desired degree of substitution (DS),
- a uniform distribution of substituents along the polymer chain,
- a high yield of the reactants,
- negligible side-reactions and
- new derivatives.

Only a few of the multitude of solvents of cellulose mentioned in the literature are practically suitable for the following reasons: Many solvents react with the chemicals which are required for modifying cellulose, others degrade cellulose extensively. Philipp¹ reviews in detail solvents for cellulose and their suitability as reaction media. Some examples shall be mentioned here:

- N_2O_4 in aprotic dipolar solvents like DMSO, DMF, Pyridine,
- Formaldehyde or paraformaldehyde in DMSO, DMF, DMAc or NMP,
- Quaternary ammonium salts like N-ethylpyridiniumchloride,
- Amine oxides of various tertiary amines like N-methylmorpholine-N-oxide,
- Dimethylacetamide/LiCl or N-methylpyrrolidone/LiCl.

To us, the solvent system consisting of dimethylacetamide or N-methylpyrrolidone and lithium chloride (DMAc/LiCl and NMP/LiCl) seemed to be most promising as both solvents are highly suitable media for chemical reactions and cellulose is dissolved only physically. We have studied the reaction of cellulose to

- * carboxylic acid esters and ketoesters,
- * organosulfonic acid esters,
- * deoxycellulose derivatives,
- * carbamates and,
- * ethers

in these solvent systems² in the last few years and some new results will be reported.

2 Preparation of cellulose solutions and their properties

For dissolving cellulose in DMAc/LiCl or NMP/LiCl it is important to preactivate the polysaccharide. Water (liquid or vaporous), liquid ammonia, DMAc or NMP are therefore described in the literature³. These fluids are well suited for activating cellulose with an average degree of polymerization (DP) below 1000. High molecular weight cellulose (DP > 1000) dissolves only partly under these conditions. Therefore, we searched for an activation method suitable for a fast and total dissolution of cellulose of a wide range of DP. Aqueous solutions of various organic and inorganic bases as well as inorganic salts have been evaluated and compared with the known activating media. We have tested the various agents by dissolving the activated cellulose in DMAc/LiCl (below 60 °C) and are inspecting the solutions with a view to clarity and change of the DP of cellulose.

By microscopic inspection of cellulose solutions it is difficult to define representative samples and quantify the results. Measuring the turbidity of cellulosic solutions in DMAc/LiCl proved to be suitable. (Instrument: Turbidity photometer LTP 3, Dr. Lange, Germany; measuring range: 0 to 100 turbidity units; measurements against a standard solution: 10 grams hexamethylenetetramine p.a. or 1 gram hydrazinium sulfate p.a. in 100 ml of distilled water. The state of dissolution is better the lower the measured units are.)

Representative results are shown in table 1. Low molecular weight cellulose (DP < 1000) is sufficiently activated by the known agents. Typically, after 5 h the turbidity has decreased to 10 to 4 units. The solution of cellulose of DP > 1300 preactivated in these media contains a lot of undissolved fibrils even after 24 h, and at a low concentration of cellulose of 2.5 % . If such a cellulose is preactivated in 20 % aqueous NaOH at 20 °C for 4 h, it dissolves nearly totally within 5 h. The dissolution can be further improved by milling the cellulose beforehand. In all cases the DP of the activated and dissolved celluloses decreases hardly compared to the original material.

The solution viscosity rises dramatically when the DP or the concentrations of cellulose or the concentration of lithium chloride are increased. The solution viscosity strongly declines as the temperature rises. Thus, at an appropriate temperature relatively concentrated cellulosic

solutions (DP < 600, concentration up to 12 %) can be obtained and handled by standard laboratory equipment. Extruders or kneaders are not required. However, it has to be kept in

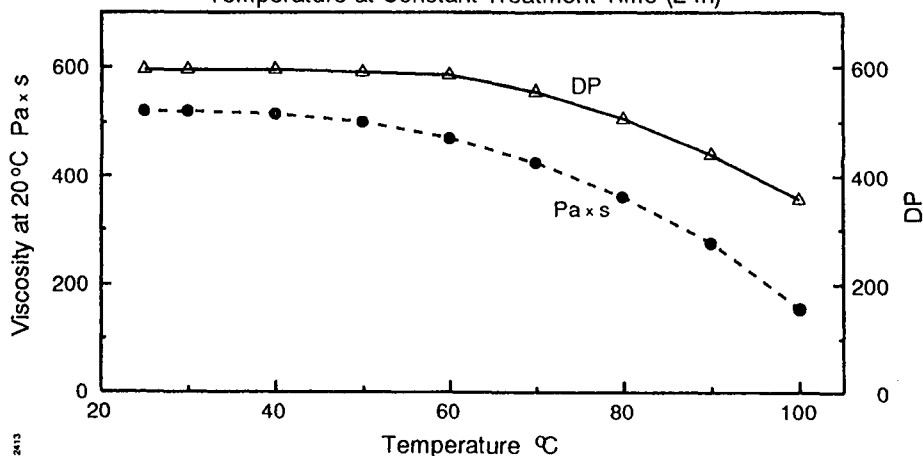
Table 1. Activation media and solubility of cellulose.

Cellulose type	Activation medium (1)		Concentration of solution/ %			Turbidity after time elapsed (1)				DP (Cuen) after 5 h
	type	Conc./%	Cellulose	LiCl	DMAc	5 h	1 d	2 d	3 d	
Pulp DP = 675	DMAc	—	5	7	88	8	—	—	—	640
	water	—	5	7	88	7	—	—	—	670
	aqueous LiOH	5	5	7	88	8	—	—	—	650
	aqueous NaOH	5	5	7	88	4	—	—	—	600
	aqueous KOH	5	5	7	88	4	—	—	—	585
	aqueous LiCl	5	5	7	88	8	—	—	—	630
	aqueous MgCl	10	5	7	88	10	—	—	—	620
	aqueous ZnCl	10	5	7	88	7	—	—	—	600
	aqueous NaSCN	10	5	7	88	9	—	—	—	660
	aq. diethanolamine	10	5	7	88	9	—	—	—	650
Linters DP = 1325	DMAc	—	2,5	7	90,5	n.m.	n.m.	n.m.	n.m.	1220
	DMAc (2)	—	2,5	7	90,5	n.m.	80	35	21	1140
	water	—	2,5	7	90,5	n.m.	n.m.	n.m.	n.m.	1320
	aqueous LiOH	10	2,5	7	90,5	20	15	12	8	1210
	aqueous NaOH	20	2,5	7	90,5	60	50	42	35	1200
	aqueous NaOH (2)	20	2,5	7	90,5	6	4	3	2	1100
	aqueous KOH	20	2,5	7	90,5	18	13	6	4	1150
	aqueous LiCl	20	2,5	7	90,5	n.m.	n.m.	95	46	1280
	aqueous MgCl	20	2,5	7	90,5	n.m.	n.m.	n.m.	n.m.	1240
	aqueous ZnCl	20	2,5	7	90,5	n.m.	n.m.	n.m.	n.m.	1150
	aqueous NaSCN	20	2,5	7	90,5	n.m.	n.m.	n.m.	n.m.	1300
aq. diethanolamine	20	2,5	7	90,5	n.m.	n.m.	n.m.	n.m.	1300	
Linters DP = 4000	DMAc (2)	—	2,5	7	90,5	n.m.	n.m.	n.m.	45	3490
	water (2)	—	2,5	7	90,5	n.m.	n.m.	n.m.	10	3870
	aqueous NaOH (2)	20	2,5	7	90,5	n.m.	n.m.	n.m.	3	3100
	aqueous KOH (2)	20	2,5	7	90,5	n.m.	n.m.	n.m.	5	3050

(1): Conditions see text. (2): Milled cellulose. DP: Degree of polymerisation. n.m.: Not measurable.

mind that cellulose solutions are stable for a longer period of time only at temperatures below 60 °C (fig. 1). Above 60 °C the degradation of the polysaccharide increases rapidly as the

Fig. 1: Viscosity and Degree of Polymerization (DP)
- Temperature at Constant Treatment Time (24h) -



temperature rises. It is therefore necessary to optimize the temperature for the reactions described below.

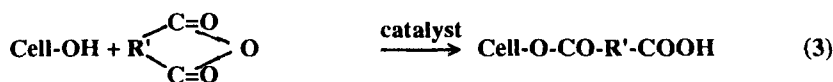
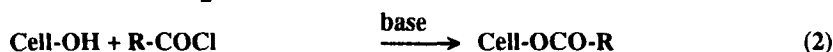
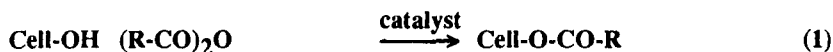
The solutions of cellulose in NMP/LiCl behave similarly to those in DMAc/LiCl. However, at 20 °C the solution viscosity for the same concentration of cellulose and the same DP is significantly higher in the NMP/LiCl solvent system. But it is more sensitive to temperature changes.

In the literature, combinations of LiCl and alkyl or alkylene ureas as well as N-methylcaprolactam are mentioned as solvents for cellulose, too. They dissolve only small quantities of cellulose and are therefore in our opinion unsuitable for technical processes.

3 Homogeneous Reactions of cellulose in DMAc/LiCl or NMP/LiCl

3.1 Carboxylic esters of cellulose

Carboxylic esters of cellulose have been synthesized in the solvent system with well known acylating agents like acid chlorides or mono or dicarboxylic acid anhydrides:



We aimed at maximizing the yield of reactants and optimizing the control on the DS over a range as wide as possible. Therefore, we have investigated the following reaction parameters:

- a) catalysts,
- b) acylating agents,
- c) reaction time and temperature and
- d) DP of cellulose.

The reaction procedure has been previously described in detail ².

The reaction is catalyzed by acidic or basic substances (table 2). The catalytic effect of acids decreases in the sequence:



Alkali acetates are efficient catalysts, too. The degree of substitution (DS) goes up with increasing basicity of the salt e.g.: lithium < sodium < potassium acetate, although sodium and potassium acetate dissolve hardly in DMAc/LiCl. Higher concentrations of alkali salts result in higher yields as shown for example for potassium acetate. The highest DS is achieved with triethylamine (TEA) and 4-dimethylaminopyridine (DMAP). However, these catalysts have to be used in stoichiometric quantities with regard to acid anhydrides. Compared to acidic catalysts the basic reactants degrade cellulose significantly less under similar reaction conditions.

The heterogeneous acylation of cellulose by known technical processes proceeds always to the triacetate which is afterwards hydrolyzed to the desired DS. In contrast to that, the

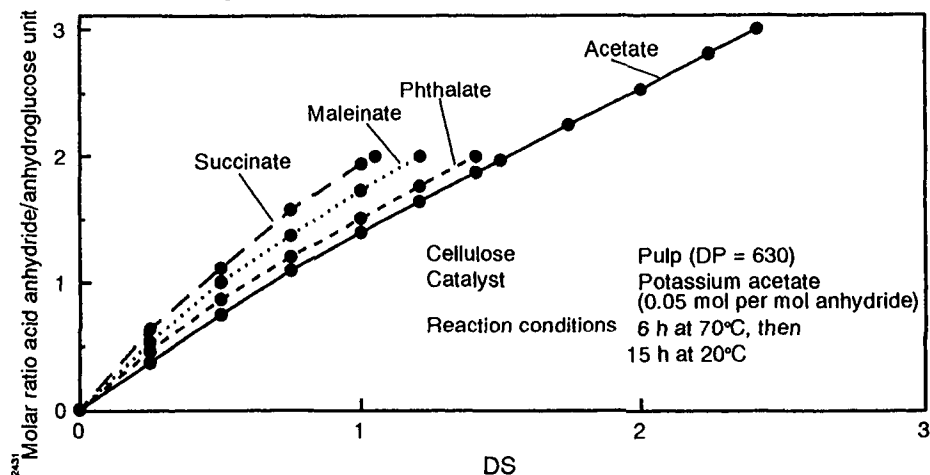
Table 2. Degree of acetylation – type and concentration of catalysts.

Cellulose:		Pulp, DP = 630.		
Reaction conditions:		1) 6 h @ 70 deg. C, 2) 15 h @ 20 deg. C.		
Molar ratio AGU : acetic anhydride	Catalyst		DS	Yield /%
	Type	Molar ratio mol/mol anhydride		
1 : 1	–	–	0,25	25
1 : 1	Formic acid	0,02	0,37	37
1 : 1	Sulfuric acid	0,02	0,43	43
1 : 1	Methanesulfonic acid	0,02	0,55	55
1 : 1	Perchloric acid	0,02	0,56	56
1 : 1	Potassium acetate	0,05	0,70	70
1 : 1	Triethylamine	1,00	0,85	85
1 : 1	4-Dimethylpyridine	1,00	0,87	87
1 : 3	–	–	1,20	40
1 : 3	Formic acid	0,02	1,57	52
1 : 3	Sulfuric acid	0,02	1,75	58
1 : 3	Perchloric acid	0,02	2,35	78
1 : 3	Lithium acetate	0,05	1,50	50
1 : 3	Sodium acetate	0,05	2,30	77
1 : 3	Potassium acetate	0,05	2,40	80
1 : 3	Potassium acetate	0,02	1,90	63
1 : 3	Triethylamine	1,00	2,85	95

AGU: Anhydroglucose unit. DP: Degree of polymerisation. DS: Degree of substitution.

homogeneous reaction can control exactly the molar ratios of acid anhydride and anhydroglucose units and therefore the DS during the esterification. We have come to this conclusion after investigating the reactions of cellulose with succinic, maleic, phthalic and acetic acid anhydride (fig. 2).

Fig. 2: Degree of Substitution and Amount of Anhydride



The acid anhydrides reveal different reactivities which increase significantly in the series:
succinic < maleic < phthalic < acetic anhydride.

The DS rises significantly with increasing reaction temperatures and levels off after some time. However, care has to be taken as cellulose degrades rapidly to rather low molecular weight derivatives above 100 °C.

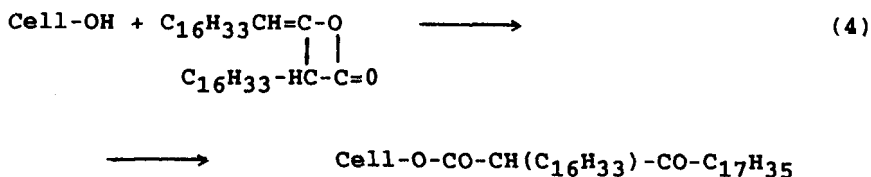
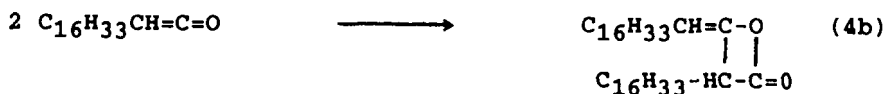
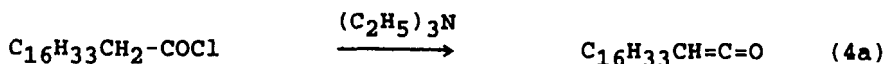
It is also possible to process high molecular weight cellulose smoothly to derivatives of high DS and DP (table 3).

Table 3. Carboxylic acid esters of cellulose vs. degree of polymerisation.

Molar ratio anhydroglucose unit : anhydride = 1 : 4.					
Catalyst: Potassium acetate, 0,08 mol/ mol anhydride.					
Reaction conditions: 1) 6 h @ 70 deg. C, 2) 15 h @ 20 deg. C.					
Cellulose		Type of ester			
Type	DP	Acetate		Propionate	
		DS	DP	DS	DP
Linters	3700	2,60	1720	2,65	1730
Linters	1140	2,80	980	2,90	1010
Pulp	1270	2,70	1020	2,95	1050
Pulp	630	2,95	570	3,00	580

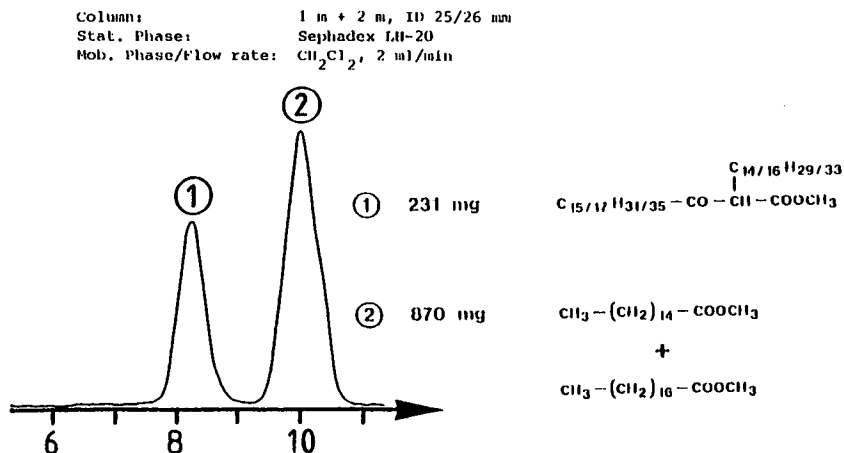
DP: Degree of polymerisation. DS: Degree of substitution.

The reaction of cellulose with stearic acid chloride in DMAC/LiCl in the presence of an inorganic or organic basic salt like lithium, sodium, potassium carbonate or lithium, sodium, potassium acetate results exclusively in the corresponding stearic ester according to eq. 2 (R = C₁₇H₃₅). If a tertiary amine like triethylamine is used, a mixture of ester and ketoester is obtained. We propose the following reaction scheme:



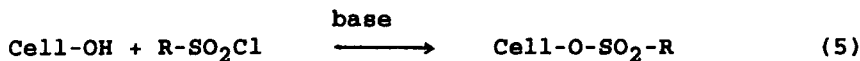
The reaction scheme is supported by the methanolysis of the mixed esters and their separation by gel chromatography (fig. 3).

Fig. 3: PREPARATIVE GELCHROMATOGRAPHY



3.2 Organosulfonic acid esters of cellulose

Alkyl or aryl sulfonic acid esters of cellulose are easily obtained by reacting the dissolved polymer with sulfonic acid chlorides in the presence of a base according to eq. 5.



The reaction of cellulose with toluene sulfonic acid chloride (TsCl) and TEA has been studied in detail.

The reaction proceeds similarly to that of carboxylic acid chlorides. However, we surprisingly detected substantial amounts of chemically bound chlorine in the products. When we varied the process conditions we observed the following behaviour: At temperatures below 15 °C and reaction times shorter than 10 h only cellulose toluenesulfonic acid ester resulted. At higher reaction temperatures and longer reaction times increasing quantities of chlorine were found in the derivative. We have come to the conclusion, that the cellulose tosylate formed initially reacts further with lithium chloride to chlorodeoxycellulose and lithium toluenesulfonate according to eq. 6.



X = Halogen or pseudohalogen

The progress of the reaction as a function of temperature and time of reaction is shown in figure 4. Increasing temperature enhances the reaction speed and the yield of both subsequent reactions. The same is true for a molar excess of TEA to TsCl (fig. 5). If other halogens or

pseudohalogen are present in the reaction mixture the respective derivatives of deoxycellulose are generated as by-products. In our opinion the high reactivity of the chloride

Fig.4: Yield of Cellulose Tosylate and Chlorodeoxycellulose

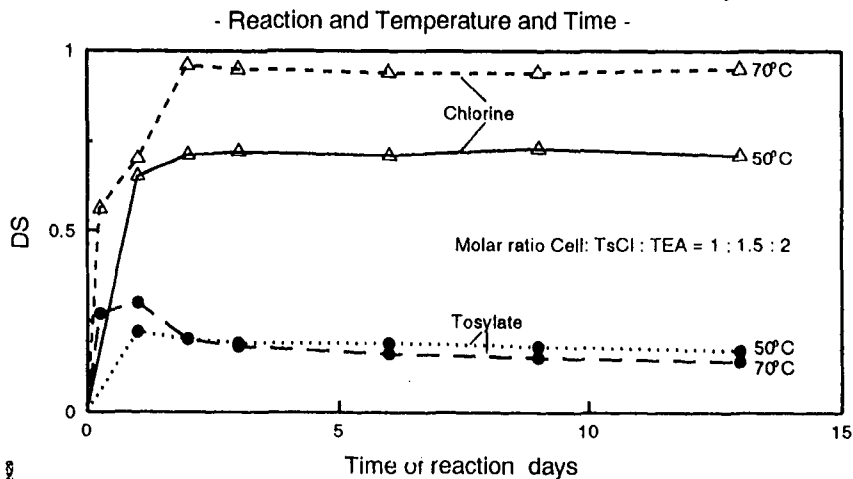
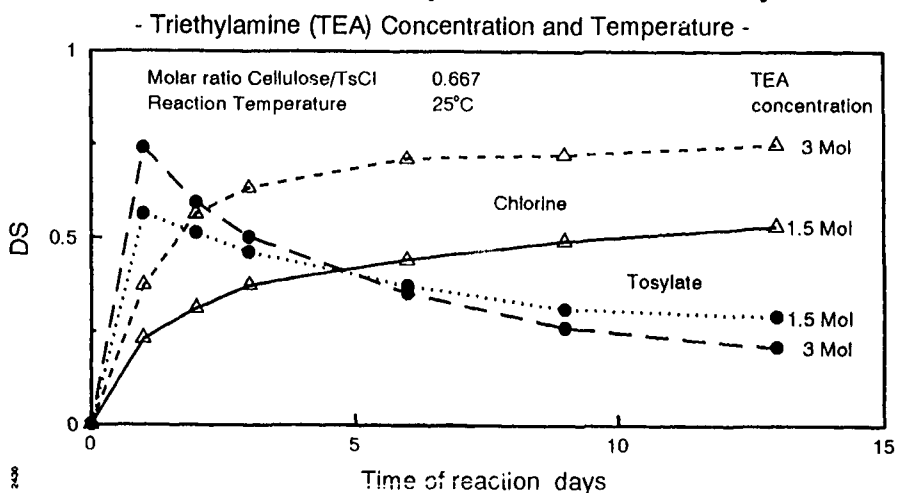


Fig 5: Yield of Cellulose Tosylate and Chlorodeoxycellulose



anion is due its poor solvation in aprotic dipolar solvents like DMAc. Chloride and similar anions then behave as strong nucleophiles.

These deoxycellulose derivatives may either directly or after their separation and purification be further processed to reactive products containing e.g. amino or mercapto groups. Thus, the

DMAC/LiCl solvent system presents a versatile method for synthesizing various deoxycellulose derivatives of rather high DS easily and of any DP desired.

3.3 Carbamates of cellulose

Cellulose carbamates should be achievable according to eq. 7. The reaction conditions are similar to those of the esterification.



We have found that mono- and diisocyanates react easily with cellulose in DMAC/LiCl to the respective carbamates, especially in the presence of a catalyst. It is obvious that diisocyanates lead to crosslinked derivatives. The DS can be controlled by choosing an appropriate molar ratio of isocyanate and anhydroglucose unit. As mentioned before, the DP of cellulose does not decline if the reaction mixture is kept at relatively low temperature and basic catalysts are used.

With monoisocyanates cellulosic carbamates of high DS have been achieved (table 4). The yields correspond to the reactivity of the isocyanates. The reaction products stay in solution. Therefore, the solutions can be directly spun e.g. into filaments or membranes according to established wet spinning procedures.

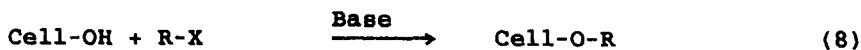
Table 4. Reaction of cellulose and isocyanates.

Cellulose:		Pulp, DP = 630.	
Molar ratio anhydroglucose unit : isocyanate = 1 : 3.			
Catalyst:		Pyridine, 10 wt. % of isocyanate.	
Reaction conditions:		24 h @ 80 deg. C.	
Isocyanate		Cellulose carbamate	
Type	Yield/ %	DS	IR wave number
Butyl-	60	1,80	1718/cm
Phenyl-	85	2,55	1726/cm
4-Tolyl-	73	1,95	1714/cm
Cyclohexyl-	45	1,35	1714/cm

DP: Degree of polymerisation. DS: Degree of substitution.

3.4 Ethers of cellulose

Ethers of cellulose should be formed by reactions according to eqs. 8 and 9.



X = Halogen



The reaction of cellulose with chloroacetic acid and a series of epoxy compounds in the presence of bases and catalysts has been investigated (table 5).

In the case of chloroacetic acid we aimed at a water soluble CMC of significantly lower DS than technical products have. Similar concentrations as in the technical but heterogeneous

Table 5. Ethers of cellulose by homogeneous reaction.

Cellulose:		Pulp, DP = 630.			
Reaction conditions:		6 to 48 h @ 70 deg. C.			
Reagent	Molar ratio	Base		Cellulose ether	
	AGU : reagent	Type	Conc./ mol	DS	Yield/ %
Chloroacetic acid	1 : 1,5	LiOH	3,0	<0,1	<7
Chloroacetic acid	1 : 1,5	NaOH	3,0	<0,1	<7
3-Hydroxypropylene oxide	1 : 1,0	NaOH	0,5	0,50	50
Propylene oxide	1 : 1,0	NaOH	0,5	0,55	55
Epichlorohydrin	1 : 1,0	TEA	2,0	0,48	48
2,3-Epoxypropyltrimethyl-ammonium chloride	1 : 1,0	NaOH	0,5	0,42	42

AGU: Anhydroglucose unit. DP: Degree of polymerization. DS: Degree of substitution.

CMC-process have been chosen. A reaction temperature of 70 °C and a reaction time of 6 h and the use of powdered NaOH or other more soluble bases like lithium hydroxide, quaternary ammonium bases like tetramethyl-, tetraethyl-, benzyltrimethyl ammoniumhydroxide or triethylamine did not lead to a water-soluble product. The DS stayed always below 0.1 compared to 0.8 of the technical CMC.

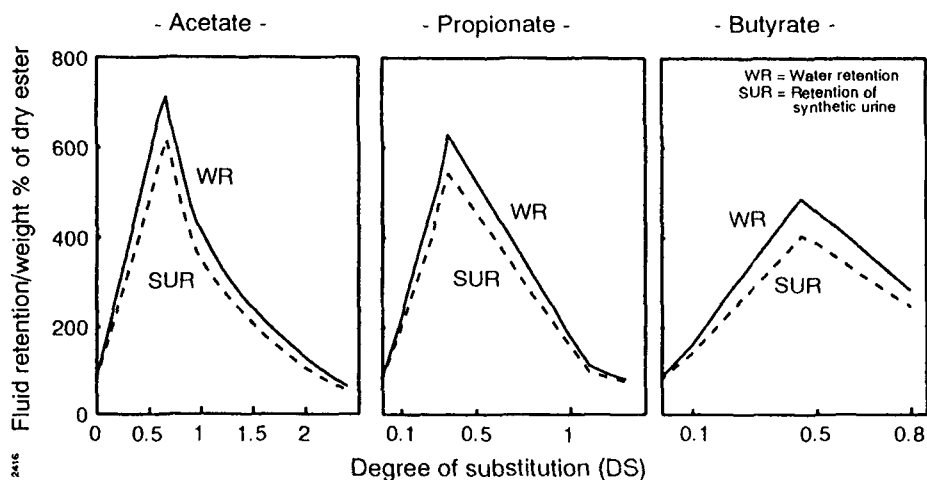
We conclude that the synthesis of cellulose ethers according to eq. 8 in the solvent system DMAc/LiCl is principally possible. However, the yields are rather limited compared to the homogeneous synthesis of cellulosic esters.

Catalysed by bases epoxy groups react significantly better with cellulose. The reaction mixtures were always gel-like at the end of the process.

4 Properties and applications of the derivatives

Cellulosic esters of monocarboxylic acids synthesized in DMAc/LiCl swell characteristically in water or physiological liquids depending on their DS. In figure 6 the retention of water and

Fig. 6: Fluid Retention of Cellulose Esters

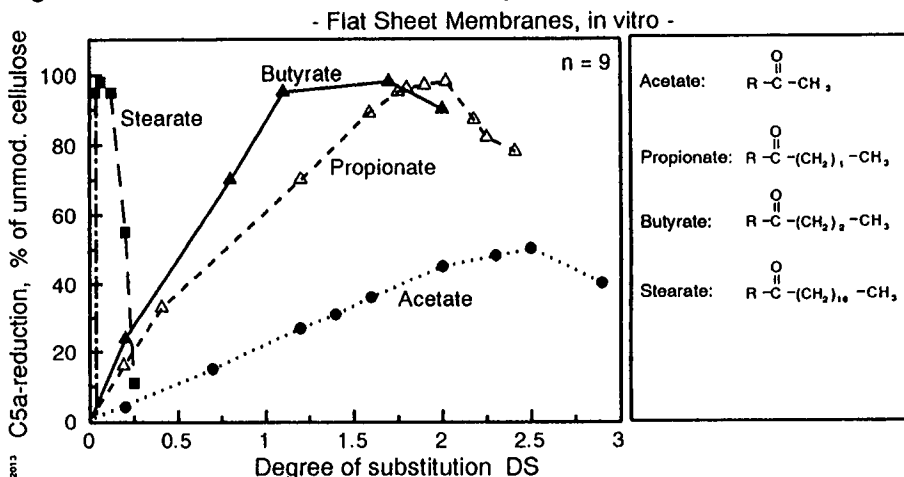


synthetic urine by cellulose acetate, propionate and butyrate is shown as a function of the DS. The measurements have been performed according to DIN 53814. At a low DS the capacity for retaining fluids increases steeply, reaches a sharp maximum, and then decreases again. The absorption maxima are specific for each substituent. The longer the chain of the carboxylic acid the lower is the maximum swelling of the corresponding cellulose ester and the DS at which the maximum occurs. Those products which swell largely in water and physiological fluids may be used as biologically degradable absorbents e.g. in hygienic applications.

Derivatives of cellulose become increasingly important for the production of membranes for hemodialysis. We have intensively investigated the biocompatibility of various cellulose derivatives as a function of the DS. The cellulosic products have been either spun to flat or capillary membranes directly from the DMAC/LiCl solution or after being isolated, purified and redissolved. Complement generation (C5a) and thrombogenicity (platelet count, TAT) have been measured as representative parameters of the biocompatibility by convenient "Elisa tests" (Behring-Werke, Germany).

The influence of the type of modification and DS has been demonstrated for cellulose acetate, propionate, butyrate and stearate (fig. 7).

Fig. 7: Reduced C5a-Generation by Neutral Cellulose Esters



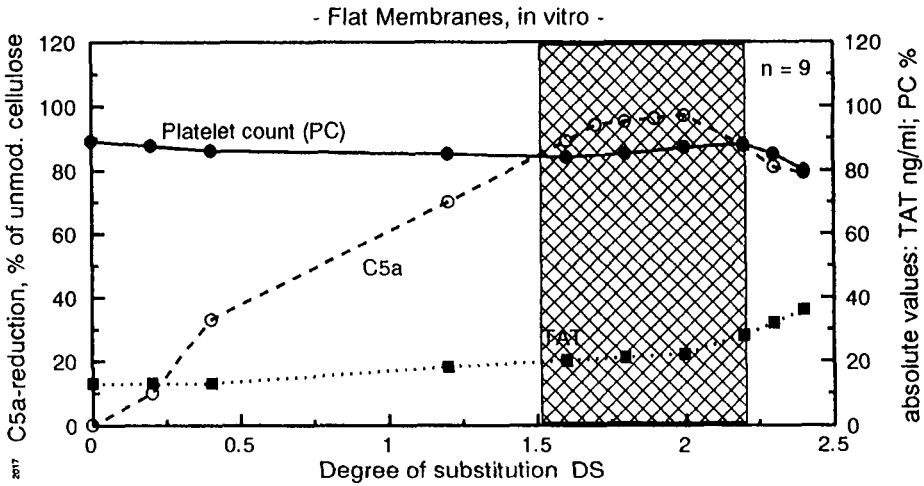
As the graph shows, C5a reduction of a membrane is strongly influenced by the modification of cellulose. At increasing degrees of acylation the C5a reduction increases to a different extent depending on the type of ester groups. Above a certain DS a C5a reduction of nearly 100 % can be achieved. The value of DS and the width of the minimum (shown in the figure as a maximum) is a characteristic for each cellulosic derivative. With increasing chain length of the ester group the C5a-minimum shifts towards lower DS. For the examples shown in figure 7 the optimal DS are:

propionate: DS = 1,8.
 butyrate: DS = 1,0.
 stearate: DS = 0,05.

At a DS beyond the optimum range the C5a activation increases again.

It is known that membranes of unmodified cellulose behave excellently with respect to thrombogenicity. Therefore, we aimed at keeping the thrombogenicity unchanged while we modified the polysaccharide. For cellulose propionate the relationship between the mentioned parameters of biocompatibility and DS are shown in fig. 8.

Fig. 8: Biocompatibility of Cellulose Propionate



Only within a specific range of DS, which for the individual esters is differently broad, the biocompatibility parameters C5a reduction, PC and TAT of the modified membranes meet the requirement. In case of the propionate the optimum is in the range of $1.5 < DS < 2.2$. The wider the range of suitable DS the safer the biocompatibility parameters can be maintained constant during the production of such membranes. Similar relations have also been found for cellulosic ethers and carbamates. We have come to the conclusion that the type of substituent and the DS are the determining factors for the biocompatibility of a cellulosic membrane.

References

- (1) Philipp, Burkardt; Lukanoff Brigitte; Schleicher, Harry; Wagenknecht, Wolfgang; *Z. Chem.*, **26** (1986), 50 ff.
- (2) Diamantoglou Michael, Kuhne Helmut; *Papier*, **42** (1986), 691 ff.
- (3) German patent DE 3027033, Deutsche ITT Industries GmbH; .

20 ^{13}C NMR spectroscopic studies on regioselective derivatization of cellulose

I Nehls*, B Philipp** and W Wagenknecht* – * Fraunhofer Institute of Applied Polymer Research, Teltow-Seehof, Germany;

** Max-Planck-Institute of Colloid and Interface Research, Teltow-Seehof, Germany

ABSTRACT

After some comments on the scope of our ^{13}C liquid NMR spectroscopic investigations as well as on advantages and problems of ^{13}C NMR application in cellulose chemistry, recent results on the regioselective sulfation and phosphatation of cellulose under homogeneous conditions of reaction are presented, employing cellulose trinitrite, trimethylsilyl cellulose of varying DS and partially substituted cellulose acetates. The effects of type of intermediate as well as of type and amount of esterifying agent on final substituent distribution are described and probable reaction mechanisms are discussed.

INTRODUCTION

Modern techniques of instrumental analysis play an increasing part in today's cellulose chemistry, requiring a close and well-balanced cooperation between the organic cellulose chemist and the method-oriented analyst. This is realized in our research on cellulose dissolution and derivatization by the joint work of our NMR group and two groups of organic cellulose chemists from Teltow-Seehof and the University of Jena.

Recent topics investigated by ^{13}C liquid NMR spectroscopy were

- (i) the course of cellulose dissolution in several derivatizing and non-derivatizing solvent systems with the results being summarized in [1],

- (ii) the determination of total and partial DS values of numerous stable cellulose esters and ethers, presented together with data published by other groups in a review now in press [2],
- (iii) the in situ study of cellulose esterification and etherification, using inorganic solvent systems under homogeneous or quasi-homogeneous conditions of reaction, centering on the problem of regioselectivity of substitution within the anhydroglucose unit (AGU).

After some comments of a more general nature on the advantages and problems of applying high resolution liquid ^{13}C NMR spectroscopy in cellulose chemistry, the subsequent contribution presents recent NMR spectroscopic results on regioselective sulfation and phosphatation of cellulose under homogeneous conditions via unstable intermediate derivatives.

SOME COMMENTS ON ADVANTAGES AND LIMITATIONS OF ^{13}C NMR APPLICATION IN CELLULOSE RESEARCH

The cellulose molecule which is composed of C, H and O atoms is very suitable for the investigations by ^1H and ^{13}C NMR spectroscopy in the solid state as well as in the liquid state after dissolution.

Our subsequent investigations were carried out by ^{13}C NMR measurements in the liquid state only.

In contrast with the complicated and overlapping signals in the ^1H NMR spectra of dissolved cellulose in the ^{13}C NMR spectrum only six signals are observed for the anhydroglucose unit.

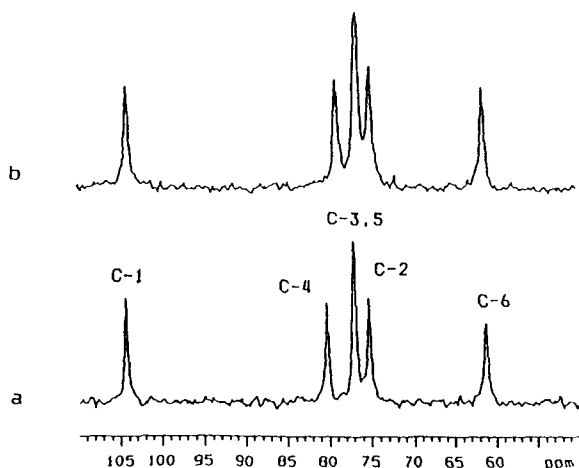


Figure 1. ^{13}C NMR spectra of cellulose dissolved in LiCl/DMAC and cadoxen (a: cellulose in LiCl/DMAC, b: cellulose in cadoxen)

For example, in the ^{13}C NMR spectrum of unsubstituted cellulose dissolved in

a non-derivatizing solvent like LiCl/dimethylacetamide or cadoxen (see Fig. 1) we find signals only at characteristic chemical shifts: the C-1 signal on the lowest field about 103 ppm, the C-4 signal at 80 ppm, the signal for the C-2, C-3 and C-5 groups in the range between 74 and 77 ppm and for the C-6 signal at the highest group field at 60 ppm.

For NMR investigations we used cadoxen especially for cellulose derivatives which are not completely soluble in water.

The derivatization of cellulose by etherification and esterification leads to significant changes in the chemical shifts of the cellulose C-atoms. The signals of the directly bound C-atoms 2, 3 and 6 are moved downfield between 2 and 10 ppm depending on the nature of the substituent.

But also the signals of the neighbouring C-atoms 1, 4 and 5 show a change in chemical shift, in this case an upfield shift between 1 and 4 ppm. Only after complete substitution in the positions C-2, C-3 and/or C-6 we find six signals again in the spectrum. But more frequently the situation of partial substitutions at the different sites of the AGU is given. This results in an increase of the number of signals in the spectrum corresponding to the existence of substituted and unsubstituted positions.

Two problems limit the use of the ¹³C NMR spectroscopy in cellulose chemistry: the limited solubility of the cellulose materials and the high viscosity of the cellulose solutions. These lead to long accumulation times due to low polymer concentration and to a broadening of the signals.

Principally two routes for the reduction of viscosity and for the improvement of the solubility were employed. The first one is the degradation of stable cellulose ethers by means of acid hydrolysis with trifluoro acetic acid. In the ¹³C NMR spectrum of the degraded cellulose sample we can observe a mixture of substituted and unsubstituted monomer units which used for cellulose esters with DS up to 1. This partial degradation appear as α and β anomers. The second is the mild enzymatic degradation results in a mixture of monomer and oligomer fragments and therefore in an increase of the number of signals in the spectrum.

The principal information available from the ¹³C NMR spectra in cellulose chemistry are

- (i) to confirm whether or not a covalent substitution has occurred,
- (ii) the determination of the position and distribution of substituents within the anhydroglucose unit,
- (iii) the calculation of the total and partial degree of substitution (DS) on the basis of quantitative signal evaluation.

Furthermore ¹³C NMR spectroscopy can help to elucidate the mechanism of reaction depending on the conditions of the synthesis.

¹³C NMR INVESTIGATION ON REGIOSELECTIVE DERIVATIZATION OF CELLULOSE VIA UNSTABLE CELLULOSE INTERMEDIATES

The central topic of our recent work was a study of homogeneous derivatization of cellulose via unstable cellulose intermediates. The main point of this work was the formation of water-soluble cellulose sulfates. Cellulose sulfates can be obtained by use of three different unstable cellulose intermediates, namely cellulose nitrite, silyl cellulose and cellulose acetate.

By means of ¹³C NMR spectroscopy we investigated the intermediates, the reaction systems after esterification in situ and the isolated final products dissolved in water or aqueous sodium hydroxide.

Our ¹³C NMR results on the formation of cellulose trinitrite on the dissolution of cellulose in the aprotic system N₂O₄/DMF and the subsequent sulfation with SO₃ via transesterification have already been presented in several publications [3, 4, 5].

Homogeneous sulfation of cellulose in the silyl cellulose system

The formation of silyl cellulose of different DS takes place on the dissolution of cellulose in the (CH₃)₃SiCl/NH₃/DMF system [6].

The result is a preferential substitution in the C-6 position and after complete C-6 substitution the secondary positions were attacked by the reagent. For the subsequent homogeneous sulfation in this system we discuss an insertion mechanism. The silyl ether group is the direct place of reaction. We assumed that the SO₃ group occupies the position between cellulose and the TMS group. Therefore the DS and the distribution of the substituents of cellulose sulfate is determined by the DS and the distribution of the silyl groups in the TMS cellulose.

By means of our ¹³C NMR investigation of the reaction mixture in situ we obtained strong evidence for the insertion mechanism.

In Figure 2 the ¹³C NMR spectra of TMS cellulose and of the reaction mixture are presented. The ¹³C NMR spectrum of TMS cellulose in DMF with DS ≈ 1.5 shows a complete C-6 substitution and a partial substitution in C-2 (see Fig. 2a). In the spectrum of the reaction mixture of TMS cellulose in DMF and SO₃/DMF in situ before desilylation, we can observe changes in the chemical shifts especially at the C-6 signal compared to the spectra of TMS cellulose and cellulose sulfate (see Fig. 2b). So we find in addition to a small signal of the C-6_{TMS} also a large signal of the insertion species for C-6_{S-TMS}. In comparison with the ¹³C NMR spectrum of the isolated cellulose sulfate the signal of the C-6 position in the reaction mixture shows an upfield shift of 1.5 ppm. The reason for this upfield shift is obviously the +I-effect of the TMS substituent which leads to an increase of the electron density and therefore to a higher shielding at the nuclear site.

The formation of cellulose sulfates occurs after subsequent desilylation in the presence of water.

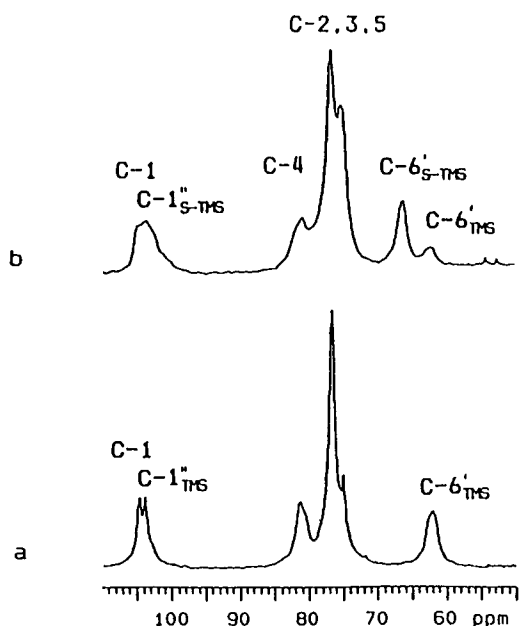


Figure 2. Comparison of the ^{13}C NMR spectra of TMS cellulose in DMF and the reaction mixture of TMS cellulose and SO_3/DMF in situ (a: TMS cellulose, b: reaction mixture)

The ^{13}C NMR spectra of a sulfation series of TMS cellulose with DS of 2.4 and different amounts of sulfating agent (SO_3) dissolved in THF demonstrate that the amount of sulfating agent determines the DS and the distribution of substituents in the cellulose sulfates also (see Fig. 3). So we can recognize the increase of the substitution in C-6 and in C-2 indicated also by the splitting of the C-1 signal, with the amount of SO_3 . In Figure 3a the ^{13}C NMR spectrum of cellulose sulfate shows only a preferential C-6 substitution. At twice the amount of sulfating agent a complete substitution in C-6 and a partial substitution in C-2 can be observed (see Fig. 3b). A considerable increase of sulfating agent leads to a complete substitution in the positions C-2, C-3 and C-6 and therefore also to an attack of the free OH groups (see Fig. 3d).

Homogeneous sulfation of cellulose in the acetate system

Cellulose acetate is the borderline case between unstable and stable derivatives which we used as an intermediate for the homogeneous sulfation and phosphatation of cellulose.

The ^{13}C NMR spectra of commercial cellulose acetates with DS of 2.0 and 2.5 show a rather equal distribution of substituents in the positions C-2, C-3 and C-6. A subsequent sulfation with SO_3 results also in a rather equal substituent distribution without regioselectivity [7].

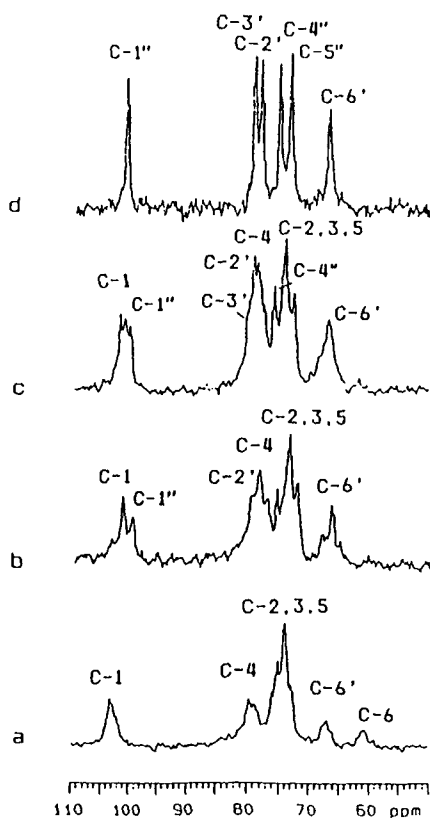


Figure 3. ^{13}C NMR spectra of cellulose sulfates produced from TMS cellulose and different amounts of sulfating agent SO_3 (a: 1.65 mol SO_3 , b: 3.3 mol SO_3 , c: 5.8 mol SO_3 , d: 9 mol SO_3)

The acetate substituents act here as **protecting groups** and only the free OH-groups were esterified.

Starting from cellulose triacetate we succeeded in regioselective deacetylation in the positions C-2 and C-3. On this basis we can prepare regioselective cellulose sulfates substituted in C-2 and C-3 positions.

Figure 4 shows the comparison of the ^{13}C NMR spectra of regioselective deacetylated cellulose acetate with DS of 0.55 (see Fig. 4a) and the corresponding cellulose sulfate with DS of 1.9 after complete deacetylation (see Fig. 4b). The sulfation of the deacetylated product with its residual acetate groups mainly in the C-6 position leads to a cellulose sulfate with complete substitution in the C-2 position and a partial substitution in the C-3 and the C-6 positions. As a special advantage of this route the introduction of sulfate groups in the C-3 position must be mentioned.

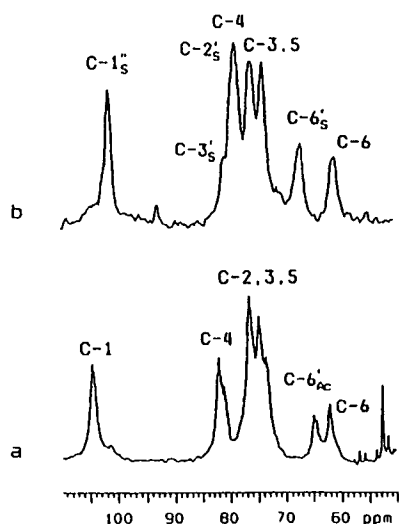


Figure 4. ¹³C NMR spectra of regioselective deacetylated cellulose acetate and the corresponding cellulose sulfate (a: cellulose acetate, b: cellulose sulfate)

Cellulose phosphates

Water-soluble cellulose phosphates were obtained for the first time by homogeneous phosphorylation of commercial cellulose acetates with DS of 2 with poly phosphoric acid as the phosphating agent.

From the ¹³C NMR spectrum in Figure 5 a preferential C-6 substitution can be observed by means of the additional signal for the substituted C-6 atom at 63 ppm while the C-2/C-3 region remains unchanged.

The phosphorylation of regioselective deacetylated cellulose acetates did not lead to water-soluble products.

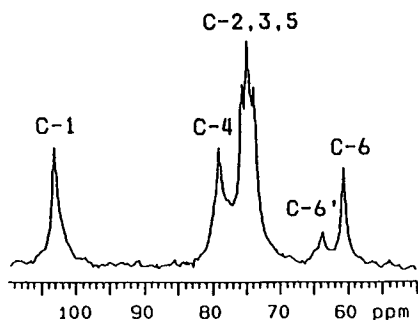


Figure 5. ¹³C NMR spectrum of cellulose phosphate dissolved in D₂O

CONCLUSIONS

Our investigations on homogeneous sulfation and phosphorylation of cellulose demonstrate the efficiency of conventional ^{13}C liquid NMR spectroscopic techniques for studying regioselective cellulose derivatization in situ. By the ^{13}C NMR spectroscopic determination of partial DS values a quantitative assessment of the degree of regioselectivity depending on reaction conditions can be performed as a basis for deriving a suitable route of synthesis to realize the substituent distribution intended. Furthermore, via the changes in number and position of the signals and via the partial DS values information on the probable mechanism of reaction becomes available.

A still open problem is the distribution of substituents along the cellulose chain. As a promising route to solve this problem we consider a combination of the NMR spectroscopy with the modern methods of chromatography.

REFERENCES

1. I. Nehls, B. Philipp, W. Wagenknecht, D. Klemm, M. Schnabelrauch, A. Stein, T. Heinze: *Papier* 44 (1990) 633-640
2. I. Nehls, W. Wagenknecht, B. Philipp, D. Stscherbina: *Progress in Polymer Science* 19 (1994) 29-78
3. I. Nehls, W. Wagenknecht, B. Philipp: *Acta Polymerica* 37 (1986) 610-613
4. B. Philipp, I. Nehls, W. Wagenknecht: *Carbohydr. Res.* 164 (1987) 107-116
5. W. Wagenknecht, I. Nehls, B. Philipp: *Carbohydr. Res.* 237 (1992) 211-222
6. W. Wagenknecht, I. Nehls, A. Stein, D. Klemm, B. Philipp: *Acta Polymerica* 43 (1992) 266-269
7. W. Wagenknecht, I. Nehls, J. Kötz, B. Philipp, J. Ludwig: *Cell. Chem. Technol.* 25 (1991) 343-354

21 Investigations on homogeneous synthesis of carboxy group-containing cellulose derivatives and the determination of the substituent distribution using HPLC

T J Heinze, U Erler and D Klemm – Friedrich Schiller University of Jena, Humboldtstrasse 10, D-07743 Jena, Germany

ABSTRACT

A new procedure for the determination of the substituent pattern of carboxymethyl cellulose (CMC) by means of high-performance liquid chromatography is described. CMC samples synthesized in the cellulose solvent LiCl/N,N-dimethylacetamide contain a significantly higher amount of tricarboxymethylated as well as unsubstituted units in the cellulose chain than those obtained in a slurry of cellulose in isopropanol/water. The heterogeneous carboxymethylation is mainly determined by statistics. Regioselectively 2,3-O-substituted CMC are available for the first time by carboxymethylation of 6-O trityl cellulose and subsequent detritylation.

INTRODUCTION

The carboxymethylation of cellulose represents the most versatile method for the synthesis of carboxy group-containing cellulose derivatives. Commercial carboxymethyl celluloses (CMC) with a degree of substitution (DS) in the range from 0.4 to 1.3 have already found a widespread use in the food and coatings industry, for example. At present, they are manufactured under heterogeneous reaction conditions in a slurry of isopropanol/water with monochloroacetate and sodium hydroxide [1].

The aim of this work was the determination of the substituent pattern of CMC by means of high-performance liquid chromatography (HPLC) as well as the synthesis of CMC samples with different substituent distribution. Such CMC should provide a better understanding of structure-property relations.

METHODS

HPLC equipment: a pump with analytical head, an injection valve with 20 μl sample loop and a differential refractometer for analytical use, all manufactured by KNAUER. The data control and analysis system was a HPLC software/hardware package (KNAUER) with interface, 12 bit analog/digital converter and personal computer. For the HPLC analysis the CMC was hydrolyzed with 80 % (v/v) H_2SO_4 within 12 h at room temperature and after tenfold dilution with water 5 h at 100 $^\circ\text{C}$. The solution was neutralized with CaCO_3 , and the CaSO_4 formed separated by filtration.

For the **homogeneous carboxymethylation** 1 g of cellulose (spruce sulfite pulp) was dried at 100 $^\circ\text{C}$ for 1 h and suspended in 60 ml DMAc. The suspension was kept at 130 $^\circ\text{C}$ for 2 h under stirring. The slurry was allowed to cool to 100 $^\circ\text{C}$ where 3 g of anhydrous LiCl was added. By cooling down to room temperature under stirring the cellulose dissolved completely. After standing overnight, a suspension of dried NaOH powder in DMAc, followed by a suspension of dried $\text{ClCH}_2\text{COONa}$. After various reaction times (see table 1) at 70 $^\circ\text{C}$ (bath temperature) the reaction mixture was cooled down and precipitated into 300 ml ethanol. The precipitates were filtered off, dissolved in water, neutralized with acetic acid and reprecipitated into ethanol, separated, washed with ethanol and dried in vacuum at 50 $^\circ\text{C}$.

For the **carboxymethylation of trityl cellulose** 10 g of trityl cellulose was dried at 55 $^\circ\text{C}$ in vacuum and dissolved in 250 ml DMSO under stirring. After standing overnight a suspension of 24 g NaOH powder in DMSO, followed by a suspension of 56 g $\text{ClCH}_2\text{COONa}$ in DMSO were added. After various reaction times (15 - 33 h) at 70 $^\circ\text{C}$ (bath temperature) the reaction mixture was cooled down and precipitated in 2000 ml acetone. The precipitates were filtered off, suspended in water and neutralized with dilute HCl. After centrifugation the product was washed with water as well as with ethanol and dried in vacuum.

RESULTS AND DISCUSSION

High-performance liquid chromatography (HPLC)

In a previous paper we have reported that the HPLC analysis of hydrolyzed cellulose methyl ethers represents a rapid and convenient method for the determination of the substituent pattern of the polymer [2]. Based on these results we examined this method for analysing CMC. For this purpose a controlled degradation of the polymer chain to the corresponding monomeric units was achieved by solvolysis with sulfuric acid. Subsequent removing of most of the H_2SO_4 as CaSO_4 after neutralization with CaCO_3 gives solutes which were analyzed directly by HPLC. A separation on a polystyrene-based strong cation-exchange resin with 0.01 M H_2SO_4 as the eluent results in the elution pattern shown in figure 1.

As confirmed by comparison with standard compounds, separation of 2,3,6-tri-O-carboxymethyl D-glucose (figure 1, **1**), groups of di-O-carboxymethyl (2,3-, 2,6-, and 3,6-O-substituted, **2**) and mono-O-carboxymethyl D-glucoses (2-, 3-, and 6-O-substituted, **3**) as well as of unsubstituted D-glucose (**4**) was achieved. Additional peaks

in the range from 5.17 to 5.45 min result from inorganic salts. Furthermore, 3 minor additional peaks were observed which originate from O-carboxymethyl glucose lactones. The lactones may be formed during hydrolysis and/or sample concentration.

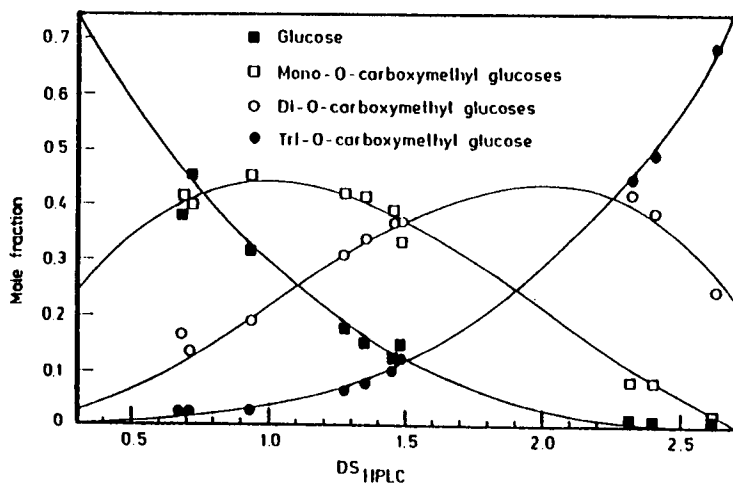
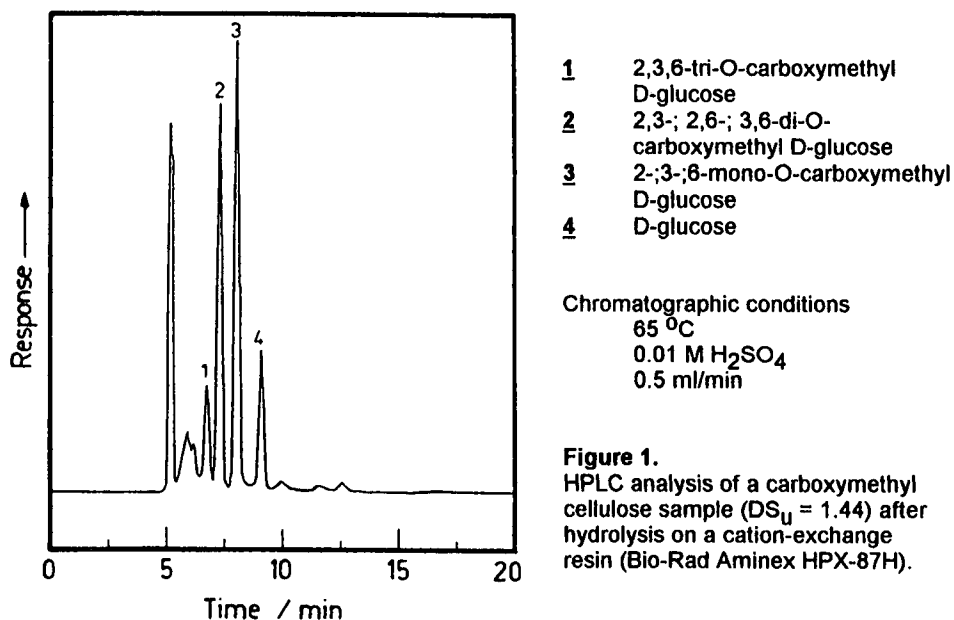


Figure 2. The mole fractions of D-glucose, the mono-O-carboxymethyl D-glucoses, the di-O-carboxymethyl D-glucoses, and the 2,3,6-tri-O-carboxymethyl D-glucose in hydrolyzed CMC samples (heterogeneous synthesis) plotted as a function of the total DS_{HPLC} . The curves are calculated (see text).

The quantitative analysis of the mole fractions obtained with 10 CMC samples [3] are graphically displayed as a function of the total DS (figure 2).

The curves in figure 2 are calculated on the basis of a statistical model for the arrangement of substituents in cellulose derivatives proposed first by *Spurlin* in 1939 [4]. The model assumes that no preference of any hydroxyl group exists and the relative reactivities of the three hydroxyl groups in the anhydroglucose unit (AGU) are constant throughout the reaction and are independent of the DS of the cellulose chain or of the state of substitution of another position within the same AGU. Summarizing these assumptions, the following binomial distribution results:

$$c_i = \binom{3}{k} (DS/3)^k (1-DS/3)^{3-k}$$

c_i : mole fractions

k : number of substituents per AGU

DS: average degree of substitution of the CMC

The good agreement of the mole fractions determined with those attained by the model indicates that the heterogeneous carboxymethylation is mainly determined by statistics.

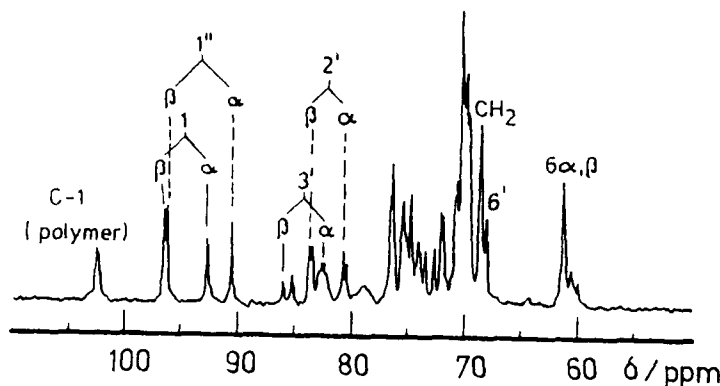


Figure 3.
 ^{13}C -NMR spectrum of a hydrolysate of a CMC sample (heterogeneous synthesis).

At present, ^{13}C - as well as ^1H -NMR spectroscopy of hydrolysates of CMC are the most common methods for the determination of the substituent pattern. This method results in direct information on the substituent distribution within the AGU at the O-2, O-3 and O-6 atom [5]. From a typical spectrum it can be concluded that the CMC synthesized under heterogeneous conditions possesses a distribution in the order O-2 > O-6 > O-3 (figure 3). These findings agree well with the results of other research groups [6].

For the determination of the mole fractions, however, an additional complicated mathematical process with the 120-line ^{13}C -NMR spectra has to be carried out [7]. From this point of view the two methods complement each other very well.

Carboxymethylation of cellulose dissolved in LiCl/N,N-dimethylacetamide

As listed in table 1 the carboxymethylation of cellulose dissolved in LiCl/N,N-

dimethylacetamide (DMAc) was carried out by reacting cellulose with a 2 to 5 molar excess of monochloroacetate and with a 2 to 10 molar excess of NaOH powder which were slurried in the reaction mixture usually at 70 °C for 10 to 72 h. The reaction starts as a homogeneous one and proceeds further in a highly swollen state.

Table 1. Degree of substitution and polymer content of CMC obtained by carboxymethylation of spruce sulfite pulp dissolved in LiCl/DMAc (reaction temperature 70 °C).

Molar ratio AGU:ClCH ₂ COONa: NaOH	Reaction time (h)	Degree of substitution Uranyl- method	HPLC	Polymer content (%)
1:2:4	10	0.24	0.33	92
1:2:4	48	0.90	1.13	66
1:2:6	27	0.60	0.68	84
1:3:6	48	1.44	1.67	82
1:4:2	67	0.65	0.92	72
1:4:8	24	0.99	1.29	91
1:4:8	48	1.47	1.88	73
1:4:8	72	1.60	1.84	69
1:5:10	48	1.62	2.07	73

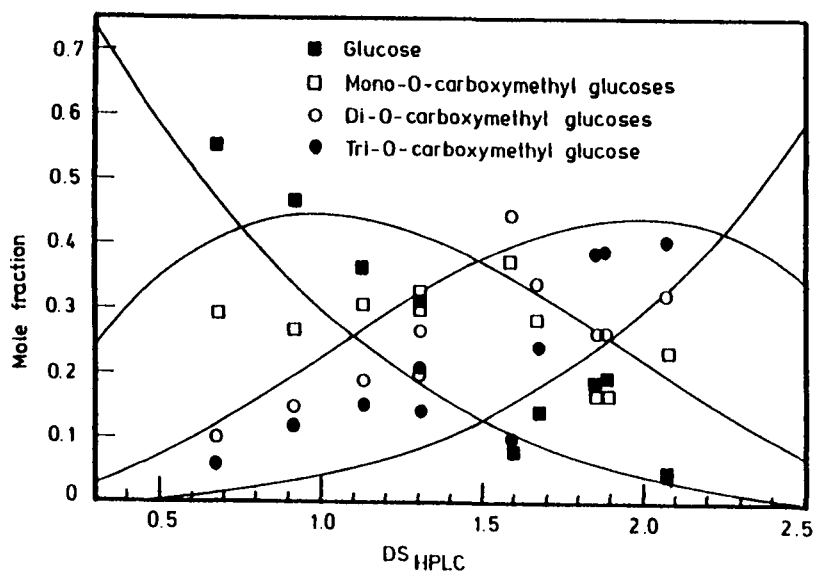


Figure 4. The mole fractions of D-glucose, the mono-O-carboxymethyl D-glucoses, the di-O-carboxymethyl D-glucoses, and the 2,3,6-tri-O-carboxymethyl D-glucose in hydrolyzed CMC samples (carboxymethylation of cellulose dissolved in LiCl/DMAc) as a function of the total DS_{HPLC}. The curves are calculated (see text).

In order to investigate the influence of this reaction condition on the substituent pattern, we examined the CMC samples with the help of the HPLC method described. In

comparison with the CMC synthesized under heterogeneous conditions a significant increase in the formation of tricarboxymethylated units occurs (figure 4). On the other hand, the mono- and di-O-carboxymethylated units are formed in a smaller amount. As a consequence, a higher content of unsubstituted units exists provided comparable DS values are considered. That means that the reaction conditions drastically influence the proportion of the mole fractions. The comparison of the substituent distribution within the AGU as revealed by ^{13}C -NMR spectroscopy shows, however, no significant differences between samples obtained in heterogeneous and homogeneous carboxymethylation reactions.

Carboxymethylation of cellulose via 6-O-triphenylmethyl cellulose

For the synthesis of CMC with a uniform distribution of substituents within the AGU we therefore investigated carboxymethylation reactions of organo-soluble 6-O-triphenylmethyl cellulose (trityl cellulose, figure 5).

The tritylation of cellulose was carried out in LiCl/ DMAc at 70 °C using pyridine as a base according to [8]. The selectively O-6 tritylated products were carboxymethylated in dimethyl sulfoxide in the presence of NaOH powder within 15 to 30 h at 70 °C. Under these reaction conditions the trityl ether bonds are stable. Subsequent detritylation with gaseous HCl in methylene chloride within 45 min yields the corresponding carboxymethyl celluloses. The products obtained are soluble in dilute aqueous sodium hydroxide yielding the corresponding sodium salts which are water-soluble.

The mixed ethers (carboxymethyl trityl celluloses) are insoluble in water as well as in the common organic solvents, but swell strong in ethanol. In the FTIR spectra they show the typical peaks at 1610 and 1410 cm^{-1} of the carboxylate group as well as at 3085, 3055 and 1500 cm^{-1} of the aromatics. In the detritylated product the peaks of the aromatics do not exist any more. Furthermore, the detritylation yields to the conversion of the carboxylate group to the free carboxylic acid form shifting its IR adsorption from 1610 cm^{-1} to 1720 cm^{-1} .

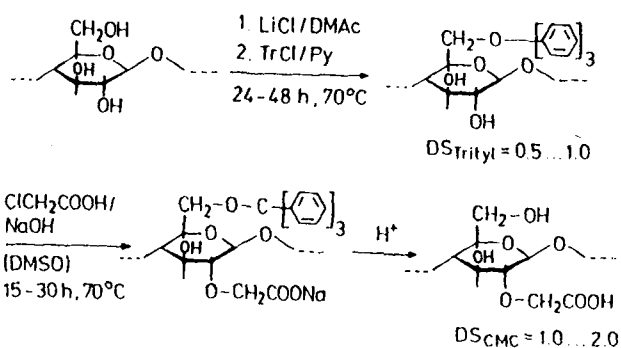


Figure 5. Reaction scheme of the carboxymethylation via 6-O-triphenylmethyl cellulose.

In order to get information on the substituent pattern using the HPLC method described a detritylation is not necessary. During hydrolysis of the polymer chain with sulfuric acid a simultaneous removal of the trityl ether group takes place.

Figure 6 shows examples of the elution pattern obtained. It can be concluded that the carboxymethylation of trityl cellulose yields to a preferred formation of disubstituted units as observed at the high intensity of peak 2. A remarkable presence of tricarboxymethylated units can be detected if the DS_{Trityl} is smaller than 1. In the case of a complete protection of the primary OH-group only a very small amount of trisubstituted units of 1.5 mol % according to a DS_{CMC} at the O-6 atom of 0.01 can be observed. It should be mentioned that the HPLC analysis is suitable for the determination of very small contents of substituents.

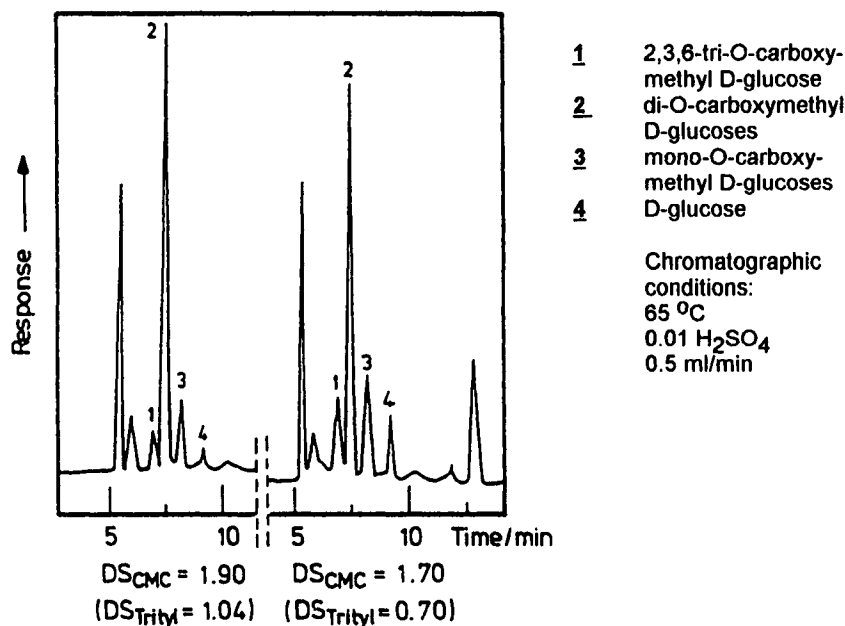


Figure 6. Examples of the HPLC analysis of O-carboxymethyl-6-O-triphenylmethyl celluloses.

In the ^{13}C -NMR spectrum of the water-soluble sodium salt of the CMC two signals in the range of the C=O signals at about 178 ppm occur (figure 7). In addition, a down-field shift of both the C-2 and the C-3 atoms takes place. It can be concluded that a preferred 2,3-O carboxymethylation was achieved. The additional very small peak in the C=O double bond region may indicate a small 6-O carboxymethylation in agreement with the results of the HPLC analysis. So, a 2,3-di-O-carboxymethyl cellulose is available for the first time.

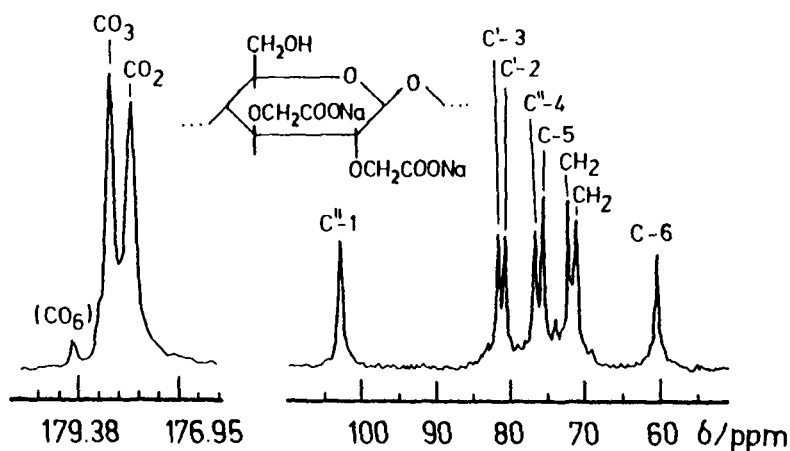


Figure 7. ^{13}C -NMR spectrum of a 2,3-di-O-carboxymethyl cellulose sample in D_2O recorded on a VARIAN Unity 400 spectrometer (accumulation number: 4000).

ACKNOWLEDGEMENTS

The authors thank Dr. I. Nehls, Fraunhofer Institute for Applied Polymer Research, Teltow-Seehof, Germany, who measured the NMR spectra.

This work was supported by the Bundesministerium für Forschung und Technologie.

Dr. Th. J. Heinze wishes to thank the Stifterverband für die Deutsche Wissenschaft for financial support.

REFERENCES

- [1] Just, E.K., Majewicz, T.G., In: *Encyclopedia of Polymer Science and Engineering*, Ed. H.F. Mark, N.M. Bikales, C.G. Overberger, G. Menges, J. Wiley & Sons, New York, Chichester, Brisbane, Toronto, Singapore 1985, Vol. 3, p. 239.
- [2] Erler, U., Mischnick, P., Stein, A., Klemm, D., *Polymer Bull.* **29** (1992) 349.
- [3] The CMC samples were synthesized under heterogeneous reaction conditions in isopropanol/water with monochloroacetic acid and NaOH according to Jiyama, K., Bach Tuyet, L.T., *Mokuzai Gakkaishi* **32** (1986) 184.
- [4] Spurlin, H.M., *J. Am. Chem. Soc.* **61** (1939) 2222.
- [5] Yalpani, M., *Polysaccharide: Syntheses, Modifications and Structure/Property Relations*, Elsevier, Amsterdam, Oxford, New York, Tokyo 1988, p. 197.
- [6] Abdel-Malik, M.N., Yalpani, M., In: *Cellulose: Structural and Functional Aspects*, Ed. J.F. Kennedy, G.O. Phillips, P.A. Williams, E. Horwood, New York 1990, p. 263.
- [7] Reuben, J., Conner, H.T., *Carbohydr. Res.* **115** (1983) 1.
- [8] Erler, U., Klemm, D., *Makromol. Chem., Rapid Commun.* **13** (1992) 195.

22 Preparation of new unsaturated polysaccharide derivatives and investigation of crosslinking reactions

D Klemm and S Vogt – Friedrich Schiller University of Jena,
D-07743 Jena, Germany

ABSTRACT

Soluble unsaturated polysaccharide esters and ethers have been prepared by homogeneous acylation of cellulose acetate and amylose with alkylhalf esters of maleic acid in presence of tosyl chloride as well as by addition of acetylenedicarboxylic acid methyl ester onto cellulose and amylose dissolved in DMAc/LiCl. The acylation of sodium carboxymethyl cellulose was carried out with maleic anhydride in a swelling system of p-toluenesulfonic acid and aprotic dipolar solvents. Layers and gels of the unsaturated polysaccharide derivatives are crosslinkable by radical initiation as well as by UV irradiation.

INTRODUCTION

Cellulose esters and ethers are important polymer materials in lacquers, biocompatible coating compositions, separation membranes and thin films for sensor applications. To modify typical properties of these materials we are interested in the synthesis and characterization of unsaturated soluble and film-forming polysaccharide esters and ethers crosslinkable by chemical reactions or irradiation. As unsaturated units in polysaccharide modification we used especially furanes, sorbates, acrylates and maleates. The presence of a second carboxyl function in the maleic acid derivatives is of importance in view of the modification of the polymer

properties by introduction of further substituents as well as by subsequent reactions.

The present paper reports synthesis pathways to maleic acid derivatives of common polysaccharides and initial investigations of their crosslinking behaviour. As shown briefly in figure 1 new unsaturated esters and ethers of cellulose, celluloseacetate, carboxymethyl cellulose and amylose have been prepared under homogeneous conditions or in a high swollen state starting from maleic acid half esters, maleic anhydride and acetylenedicarboxylic acid methyl ester.

To obtain analytical information by conventional NMR spectroscopy polysaccharides with low DP-values in the range of 120 to 300 have been preferably used.

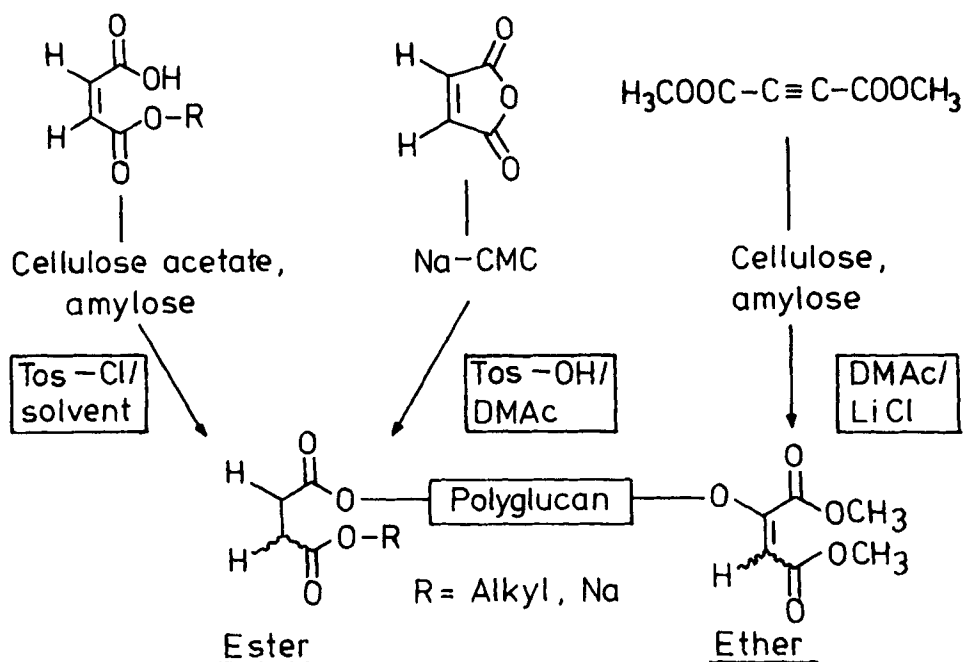


Figure 1. Synthesis pathways and types of prepared unsaturated polyglucan derivatives.

CELLULOSE AND AMYLOSE ESTERS OF MALEIC ACID HALF ESTERS

Commercial cellulose acetate (DS 0.96) dissolved in DMF (1 g in 13 ml) reacts in the presence of tosyl chloride with the free carboxyl groups of

maleic acid half esters prepared from maleic anhydride and aliphatic alcohols with different length of the alkyl groups. The esterification reactions were carried out with 2 mole equivalents of maleic esters per anhydroglucose unit at 60 °C (figure 2).

The products were isolated by precipitation in ethanol, purified by washing with ethanol, reprecipitated from DMSO in ethanol and dried at 25 °C in vacuum. They are soluble in organic solvents like DMF, DMSO, DMAc and acetone (except benzyl ester). The acetate groups of the mixed cellulose esters are essential for the solubility.

The IR spectra show the typical signals of the C=C and the C=O bonds. A wide signal is formed by the acetate (1740 cm^{-1}) and maleate (1720 cm^{-1}) ester groups. From the ^{13}C -NMR spectra we conclude - in comparison with the starting cellulose acetate - that the additional unsaturated groups are preferably located in position 3 and 6 of the anhydroglucose unit. The ^1H -NMR spectra show a signal in the range of 6.7 ppm typical for a high content of fumarate structural units in the polymers.

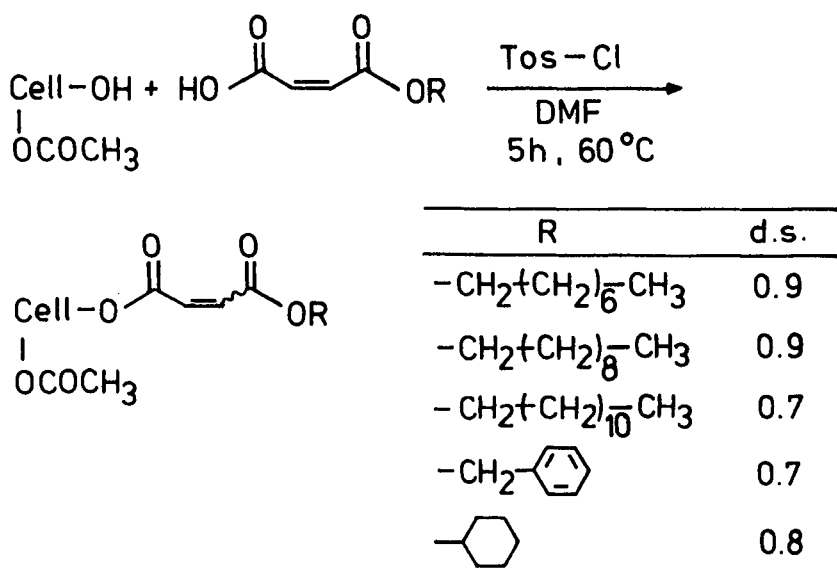


Figure 2. Synthesis of unsaturated derivatives of cellulose acetate starting from maleic acid half esters.

The acylation reaction used represents an effective synthesis of cellulose esters by esterification with free carboxylic acids. Basic work in this field was published by Shimizu and Hayashi in 1989 [1]. In low molecular

chemistry the esterification of hydroxy groups with carboxylic acids in the presence of tosyl chloride has been known since 1955 [2]. The authors describe the mixed anhydride of the carboxylic and *p*-toluenesulfonic acid as the acylation reagent.

Starting from commercial amylose (from potato starch, DP 900) and the described maleic acid half esters we combine the well known DMAc/LiCl solvent system with the tosyl chloride esterification method. Within 1 h at 60 °C the corresponding amylose esters were formed (DS 0.2 - 0.4) soluble in DMF, DMSO and DMAc.

WATER-SOLUBLE MALEATES OF SODIUM CARBOXYMETHYL CELLULOSE IN THE SWELLING SYSTEM P-TOLUENESULFONIC ACID / N,N-DIMETHYLACETAMIDE

Sodium carboxymethyl cellulose (Na-CMC) is insoluble or low-swellable in most organic solvents useful for acylation. To prepare water-soluble CMC-maleates we developed a new swelling system to activate Na-CMC. This swelling system consists of a mixture of water-free *p*-toluenesulfonic acid (Tos-OH) and a dipolar aprotic solvent like DMAc, DMF or DMSO (1 g in 15 ml). In this system Na-CMC forms a stirrable suspension of high swollen gel particles. We assume an interaction between the carboxylate groups of Na-CMC and the HO₃S-groups of the sulfonic acid with a rapid exchange of the acidic hydrogen as well as an interaction of the lipophilic toluene unit of the *p*-toluenesulfonic acid with the solvent. The model system sodium acetate and Tos-OH/DMSO forms a clear solution in a molar ratio of 1:1. The ¹H-NMR spectrum of this system shows no signal of the acidic hydrogen of the sulfonic acid and no signal of the hydrogen of possibly formed acetic acid.

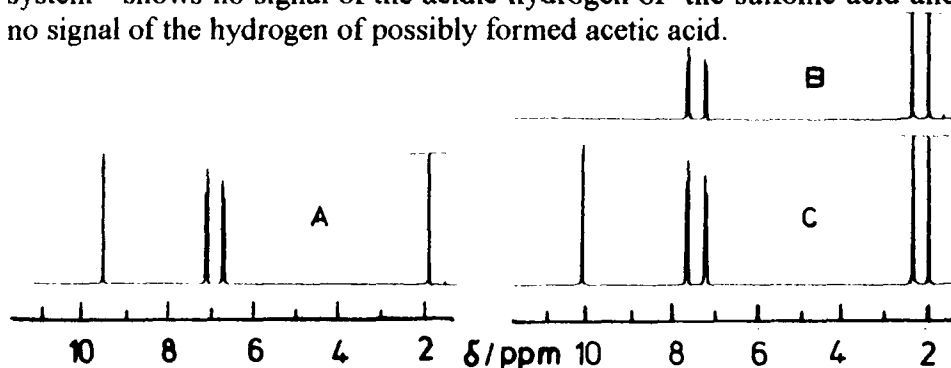
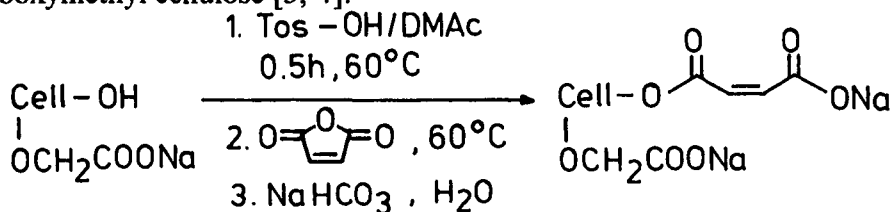


Figure 3. ¹H-NMR spectra of the model system CH₃COONa and Tos-OH (DMSO-d₆) in a molar ratio of 0:1 (A), 1:1 (B) and 1:2 (C).

In a molar ratio of 1:2 the signal of the acidic hydrogen appears once again (figure 3).

The described swelling system has been used to prepare CMC-maleates. The acylation of Na-CMC (DP 310, DS 0.76 and DP 120, DS 1.28) took place in DMAc at 60 °C in the presence of 2 mole equivalents of p-toluenesulfonic acid and maleic anhydride as the reagent. After a work-up procedure with NaHCO₃, the corresponding sodium salts resulted (figure 4). The water soluble polymers form spherical gels by addition of aluminium salt solutions, well known from unmodified sodium carboxymethyl cellulose [3, 4].

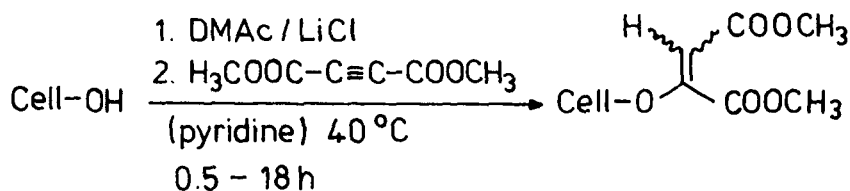


Na-CMC	Reaction conditions		CMC maleates	
DS	reagent/mol	AGU/time	DS	solubility in H ₂ O
1.28	4	4	0.3	+
1.28	8	4	0.4	+
0.76	2	4	0.3	+
0.76	4	4	0.3	±
0.76	6	14	0.9	-

Figure 4. Reaction conditions and properties of CMC-maleates.

CELLULOSE AND AMYLOSE ETHERS PREPARED FROM ACETYLENEDICARBOXYLIC ACID METHYL ESTER

A second type of maleate/fumarate-containing polysaccharides has been prepared by nucleophilic addition of cellulose onto the dimethyl ester of acetylenedicarboxylic acid. The synthesis took place as a homogeneous reaction of cellulose (Avicel, DP 150) resp. amylose (from potato starch, DP 900) in DMAc/LiCl at 40 °C using tertiary amines like pyridine as a catalyst.



Reagent / AGU mol	Cellulose DS ^{b)}	ether ^{a)} solubility in		
		DMF	DMSO	H ₂ O
1	0.5	+	+	+
3	0.9	+	+	-
5	1.1	+	+	-

^{a)}Work-up procedure: Precipitating in ethanol, washing with ethanol/acetic acid at 25°C, extraction with boiling acetone, drying at 25°C in vacuum.

^{b)}DS-determination: Saponification with 0.5 N NaOH/H₂O (16 h, 60°C and 25 h, 25°C). Addition of an excess of 0.5 N HCl/H₂O. Titration with 0.5 N NaOH/H₂O.

Figure 5. Unsaturated cellulose ethers from acetylenedicarboxylic acid methyl ester.

Under the reaction conditions the DS-values did not depend on the reaction temperature. At 70 °C and 90 °C DS-values in the same interval have been obtained. The final values have been reached within 30 min. Figure 5 demonstrates the reaction conditions and properties of the unsaturated cellulose ethers.

The IR spectra of the purified polymers show typical signals of the ester ($\nu \text{ C=O } 1710\text{-}1730 \text{ cm}^{-1}$) and the alkene ($\nu \text{ C=C } 1630\text{-}1640 \text{ cm}^{-1}$) units. In the presence of 0.5 N sodium hydroxide in water (25 °C, 48 h) the dimethyl ester groups of the unsaturated cellulose ethers are saponified forming water soluble sodium salts of the corresponding carboxy group-containing polymers.

Starting from amylose and acetylenedicarboxylic acid methyl ester we prepared unsaturated amylose ethers in a DS-range of 0.3 to 1.3 under the

same conditions. These polymers are soluble in DMF, DMSO and water (DS 0.3-0.4). Further investigations by NMR spectroscopy are directed to the content of maleate and fumarate units as well as on the substituent distribution in the polymers.

INITIAL INVESTIGATIONS OF THE CROSSLINKING BEHAVIOUR

The synthesized soluble esters of cellulose acetate resp. amylose and maleic acid half esters form layers crosslinkable by UV-irradiation and radical initiation. In the same way a mixture of these polymers in organic solvents leads to thin layers and crosslinked insoluble films (figure 6).

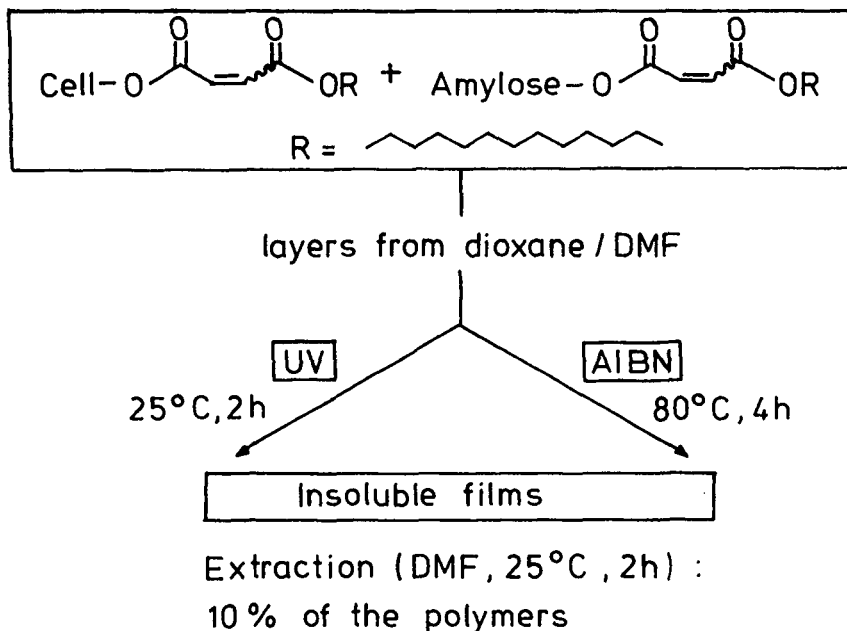


Figure 6. Crosslinking of layers of the synthesized unsaturated cellulose and amylose esters.

Further details of the crosslinking reactions as well as of the properties of the films formed are under investigation.

ACKNOWLEDGEMENTS

The authors gratefully acknowledge the financial support of the Deutsche Forschungsgemeinschaft. They also thank K. Muchina for analytical measurements.

REFERENCES

- [1] Shimizu, Y.; Hayashi, J.: *Cellulose Chem. Technol.* **23** (1989) 661 .
- [2] Brewster, J.W.; Ciotti, C.J.: *J. Am. Chem. Soc.* **77** (1955) 6214 .
- [3] Ganslaw, S.H.; Katz, G.H.: DE 2609 144 (1976), *C.A.* **85** (1976) 178 639h.
- [4] Heinze, T.; Klemm, D.; Loth, F.; Philipp, B.: *Acta Polymerica* **41** (1990) 259.

23 Analysis of carboxymethyl cellulose heterogeneity by sedimentation transport in water cadoxen

P N Lavrenko, O V Okatova – Institute of Macromolecular Compounds, Russian Academy of Sciences, 199004 St Petersburg, Russia; B Philipp – Max-Planck-Institute für Kolloid- und Grenzflächenforschung, D-14513 Teltow, Germany and H Dautzenberg – WIP-Forschungsgruppe für Polyelektrolytkomplexstrukturen, Universität Potsdam, D-14513, Teltow, Germany

ABSTRACT

Sedimentation velocity data obtained for mono-substituted carboxymethyl cellulose (CMC) samples with molecular weights from 1.2×10^5 to 3.8×10^5 were used to evaluate the heterogeneity parameters. Linear dependence has been established for the x -spectrum standard deviation of the macromolecules distribution in ultracentrifugal field, as a function of the sedimenting boundary shift. Using the recent method for the elimination of diffusion and concentration effects, parameters M_z/M_w for different polymer samples were determined to lie in the range from 1.8 to 3.5. Data are compared with the similar properties of acetate hydroxypropyl cellulose (AHOPC) samples.

RESULTS AND DISCUSSION

Determination of the inhomogeneity of cellulose and cellulose derivatives samples is an important question which can be solved most reliably by an analytical ultracentrifugation method, when an appropriate solvent is found. Recently, the aqueous cadoxen (AC) (water/cadoxen mixture, 10:1) was shown to be the most suitable solvent for sedimentation analysis of molecular heterogeneity of CMC [1] with $DS=0.9 \pm 0.1$. In this solvent, sufficient values of the buoyancy factor, $(1 - v\rho_0) = 0.52$, refractive index increment 0.15 mL/g , and practical absence of charge effects and noticeable complexation, provide reliable sedimentation

data suitable for general statistical treatment.

However, in this system CMC-AC, there are significant concentration effects shown in Fig.1, where s is the sedi-

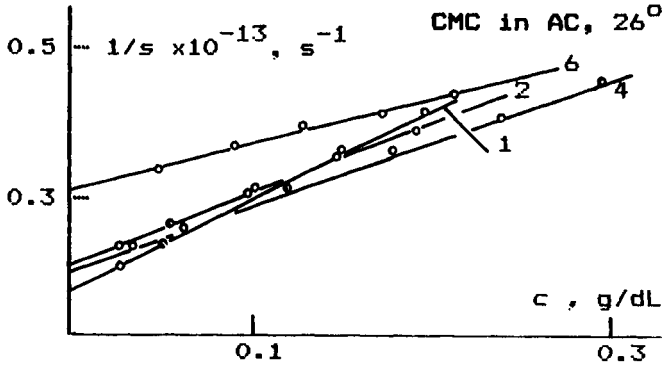


Fig.1

mentation coefficient, c concentration, and numbers on the curves correspond to CMC sample numbers. This $s(c)$ function may be described by eq. $1/s = (1/s_0) \times (1 + k_s c)$ with $s_0 = s$ at $c \rightarrow 0$. The k_s parameter was related to s_0 by $k_s = 13(s_0 \times 10^{13})^{2.2}$ mL/g s with coefficients close to that of other cellulose derivatives [2]. The relation $s_0 = 2.8 \times 10^{14} Z^{0.41} s$ with Z as degree of polymerization was also obtained [1].

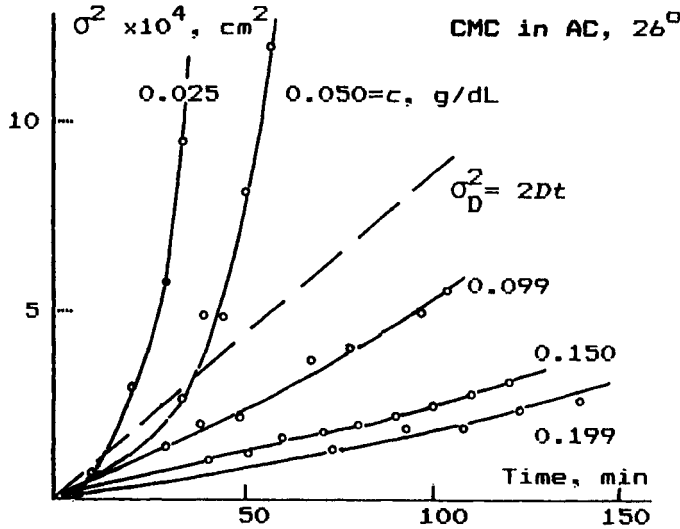


Fig.2

Table 1 lists values of s , diffusion coefficient D measured by the conventional method, and mol.wt M_{SD} by Svedberg equation.

For CMC in AC, the sedimentation curve $(1/c_0)dc/dx$ (c_0 initial concentration, x distance from rotation axis) was strongly affected by concentration effects. The second ce-

Table 1. CMC (DS=0.9) in aqueous cadoxen, 26°

Sample	$M_{SD} \times 10^{-3}$	$s_0 \times 10^{13}$	k_s	$D \times 10^7$	$(\partial\sigma/\partial x_m)_0$	σ/s_0	M_z/M_w
1	380	5.68	686	0.71	0.66	0.63	3.50
2	260	4.76	452	0.89	0.39	0.37	1.86
4	230	4.88	415	1.00	0.38	0.36	1.81
6	120	3.28	221	1.36	0.50	0.47	2.39

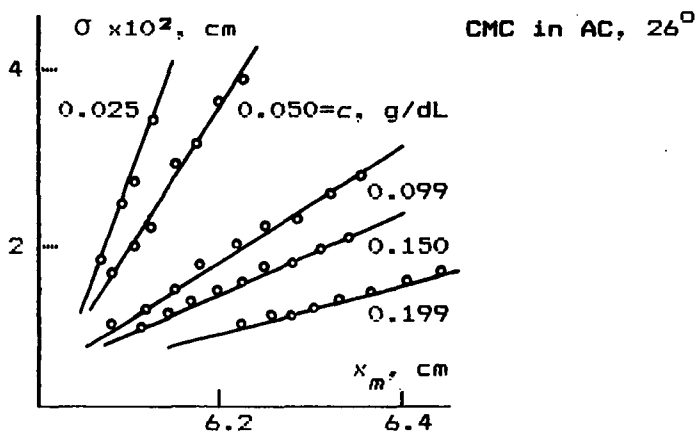


Fig.3.

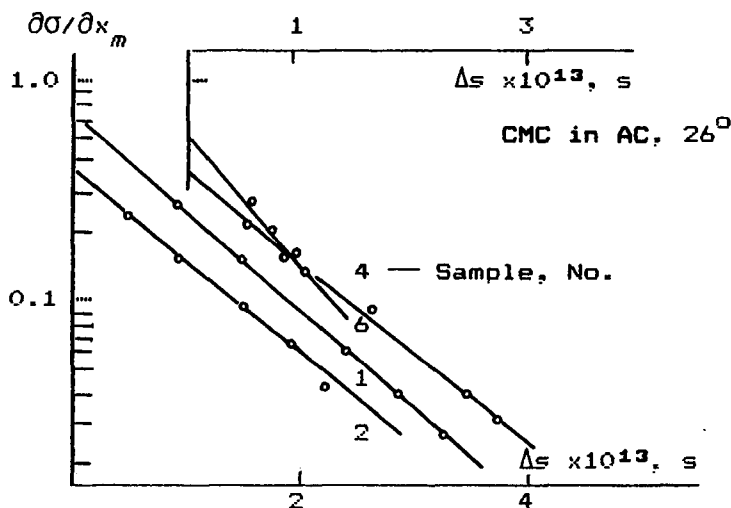


Fig.4

ntral moment σ^2 (dispersion) of the sedimentation boundary in solutions at $c \geq 0.07$ g/dL (Fig.2) lies lower even than the same value of diffusion process, σ_D^2 . Hence, polymolecularity and diffusion spreading are both suppressed by concentration effects, and experimental data cannot be treated by the Galen-Eriksson method [3] at these c values. Another method proposed recently [4] was used. Fig.3 shows σ (1st moment of the boundary curve) vs x_m for the same data as in Fig.2. Each of dependences in Fig.3 is

well approximated by a straight line with slope $\partial\sigma/\partial x_m$ which was then extrapolated linearly to infinite dilution^m (Fig.4), and the intercept $(\partial\sigma/\partial x_m)_0$ was determined reliably.

Inhomogeneity with respect to s_0 was evaluated by [4]: $\sigma_s^2/s_0^2 = 0.95(\partial\sigma/\partial x_m)_0 - D/(\omega^2 s_0)$, and parameter M_z/M_w was then calculated by $(M_z/M_w)-1 = (1-b)^{-2} \sigma_s^2/s_0^2$ with $(1-b)$ as coefficient in $s_0 = K M^{1-b}$, equal to 0.41. Results are listed in Table 1.

However, linearity of σ on x_m , being a major requisite for applicability of the method used, may be particular for the polymer in such specific solvent as cadoxen is. Really, during centrifugation of cadoxen, sedimentation pattern (Fig.5) is continuously deforming. This reflects a

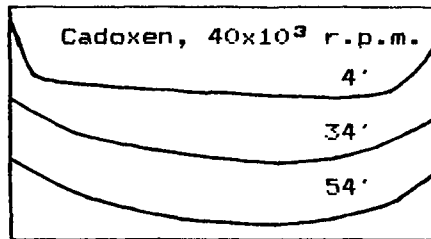


Fig.5

re-distribution of the species of cadoxen being a complex solvent. Hence, the noticeable composition solvent gradient is forming in the ultracentrifuge cell. That is why the other cellulose ether, in organic solvent, was also examined by means of the same treatment.

Sedimentation properties of acetate hydroxypropyl cellulose (AHOPC) in *N,N*-dimethylacetamide (DMA) are also subjected to strong concentration effects. Fig.6 shows $1/s$ vs c for three AHOPC fractions studied at higher c as far as dn/dc here is lower, 0.042 mL/g, with $(1-v\rho_0) = 0.229$. For AHOPC in DMA, the relations $k_s = 10(s_0 \times 10^{13})^{2.9}$ mL/g, and $s_0 = 1.84 \times 10^{-14} z^{0.44}$ s were obtained [5]. Data are listed in Table 2.

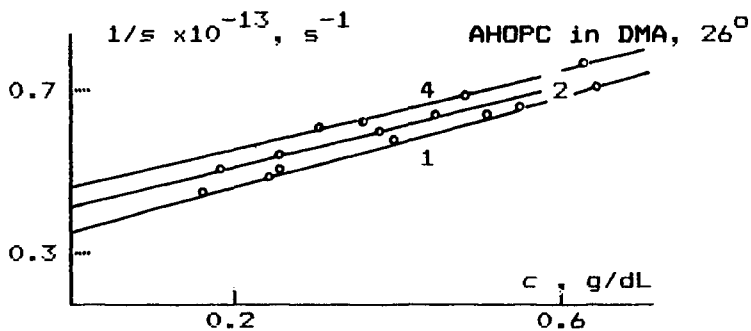


Fig.6

Table 2. AHOPC (DS=2.25) in DMA, 26°

Fract.	$M_{SD} \times 10^{-3}$	$s_o \times 10^{13}$	k_s	$D \times 10^7$	$(\partial \sigma / \partial x)_m$	σ / s_o	M_z / M_w
1	202	2.7	150	1.45	1.0	0.96	7±2
2	152	2.3	112	1.65	0.8	0.76	4±1
4	99	2.1	95	2.30	0.65	0.60	3±1

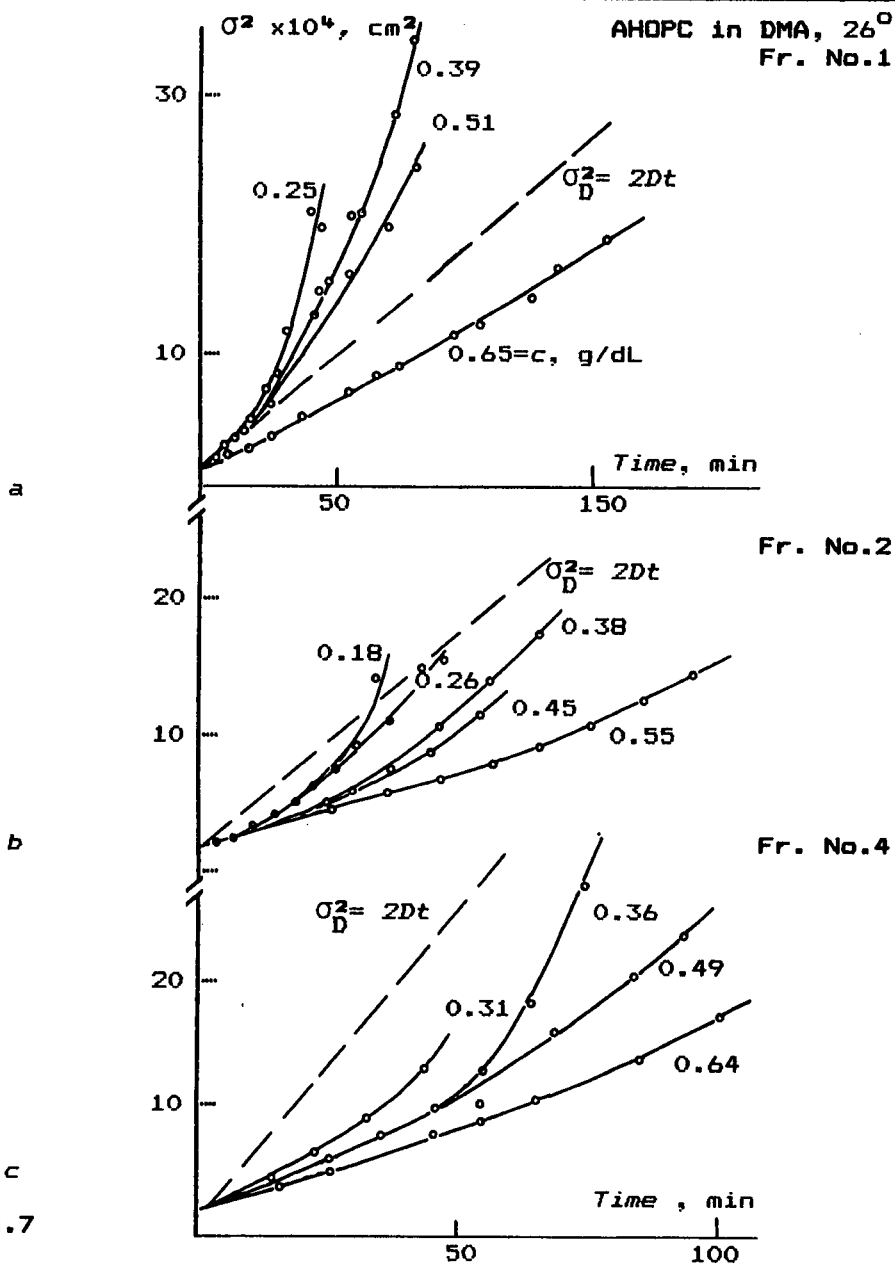


Fig.7

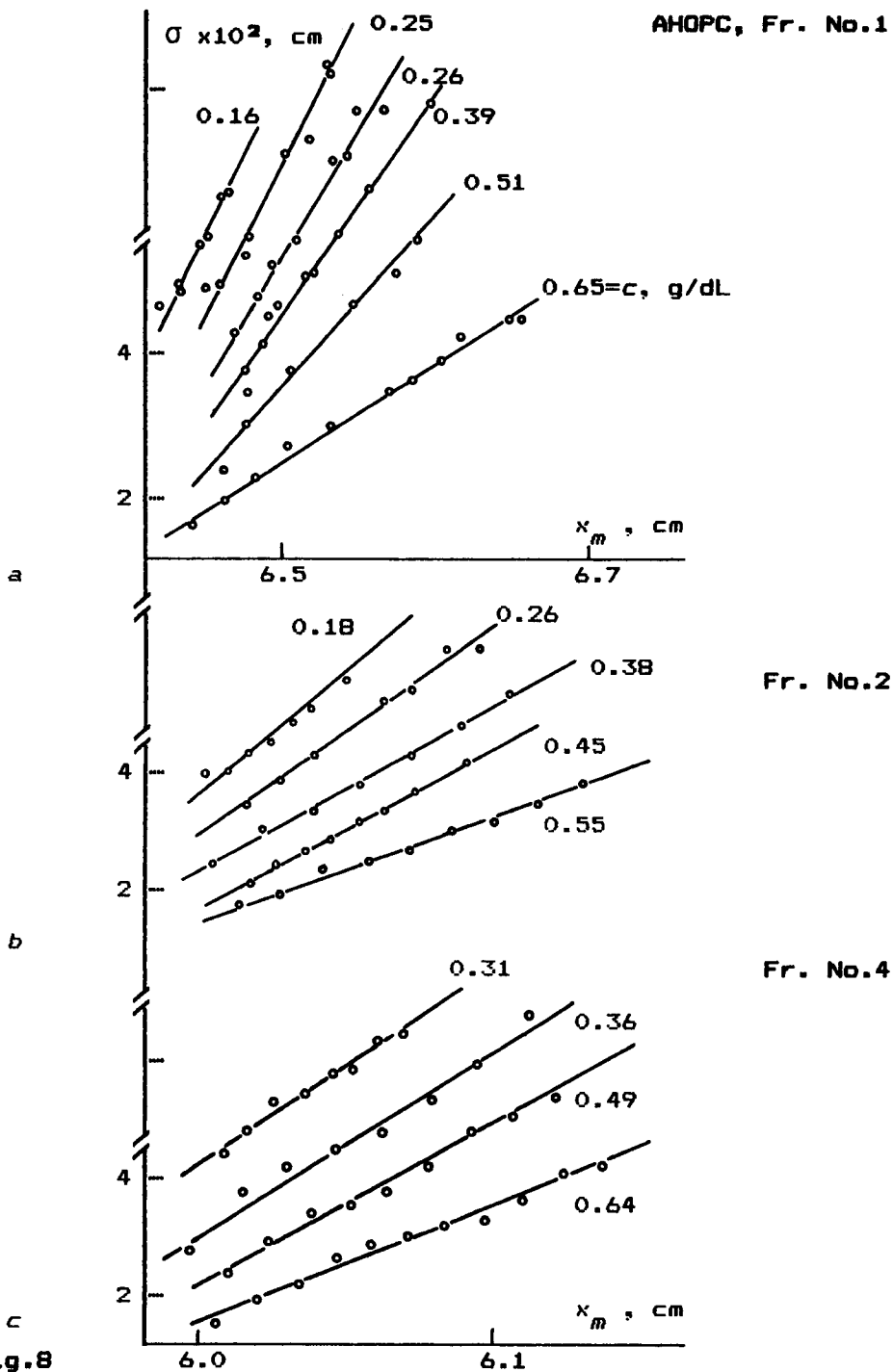
Fig.7 shows that, like CMC in AC, concentration effects in the system AHOFC-DMA are very strong. This is true for both, the most inhomogeneous fraction No.1 (Fig. 7,a) where the experimental $\sigma^2(t)$ curves lie above the curve $\sigma_D^2(t)$, and most homogeneous fraction No.4 (Fig.7,c) where all the $\sigma^2(t)$ curves are below the dependences $\sigma_D^2(t)$. This was very important that for all fractions, the dependences $\sigma(x)$ could be well approximated (Fig.8) by straight lines m to extrapolate the slope $\partial\sigma/\partial x$ to infinite dilution (Fig.9), and, hence, to evaluate the m intercept $(\partial\sigma/\partial x)_0$. A sufficiently wide collection of experimental data m is represented here in graphical form in Figs.7 and 8 specially (the first time, for AHOFC) to illustrate the linear dependence of σ on x . The comparison of experimental points with straight m solid lines in Figs.8 and 9 enables anyone to judge the degree of reliability of both the proposed method [4] and the inhomogeneity parameters based on them.

The treatment of experimental sedimentation data, obtained for AHOFC in DMA, similar to that used above for CMC, leads to inhomogeneity parameters σ/s_0 and M_z/M_w listed in Table 2. The M_z/M_w values seem s to be too z high. Probably, not only z polymolecularity (inhomogeneity in M) must be taken into account but also significant inhomogeneity in DS and structural inhomogeneity. Hence, only parameter σ/s_0 may be considered to be reliably determined, and transformation to M_z/M_w to be very questionable.

On other hand, the knowledge of a molecular inhomogeneity of the fractions is very desirable at fractionation data treatment. For instance, for two initial AHOFC samples (No. I and II in Fig.10) MWD curves were determined by means of fractionation (partial precipitation) data treated by both (1) adopted Schulz' method neglecting the overlapping of the fractions MWDs (dotted curves in Fig.10) and (2) by summarizing the partial MWDs curves for fractions (solid curves).

Fig.10 clearly shows that neglecting the overlapping of the fractions MWDs distorts significantly the MWD curve for the initial (unfractionated) sample, and noticeably (few times) lowers the $(M_z/M_w)-1$ and $(M_w/M_n)-1$ parameters of inhomogeneity.

Finally, we can conclude that sedimentation properties of CMC in AC are similar to that of other cellulose derivatives studied in organic solvents, and novel method for the sedimentation data treatment may be successfully applied to characterization of the CMC samples inhomogeneity.



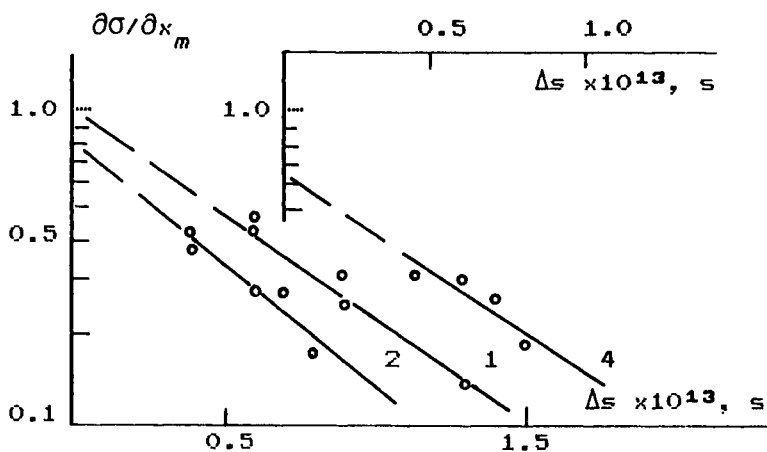


Fig.9

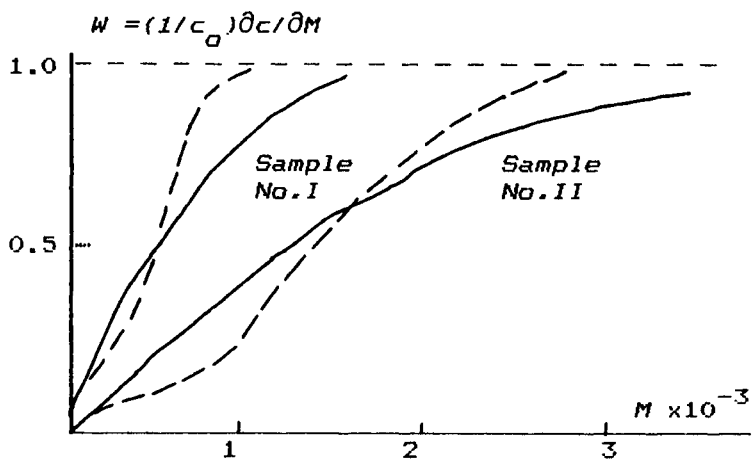


Fig.10

References

1. Lavrenko P.N., Okatova O.V., Dautzenberg H., Philipp B. *Vysokomol. Soedin. (A)* 1991, **33**, 1026.
2. Lavrenko P.N., Linow K.J., Gornitz E. The concentration dependence of the sedimentation coefficient of some polysaccharides in very dilute solution. *In: Analytical ultracentrifugation in biochemistry and polymer science.* Harding S.E., Rowe A.J., Horton J.C., Ed., Royal Soc. Chem., Cambridge, 1992, p. 517-531.
3. Eriksson A.F.V. *Acta Chem. Scand.* 1953, **7**, 623.
4. Lavrenko P.N. *Polymer*, 1994 (accepted).
5. Shtennikova I.N., Korneeva E.V., Kolbina G.F., Strelina I.A., Lavrenko P.N., Shibaev V.P., Ekaeva I.V. *Eur. Polym. J.* 1992, **28**, 353.

24 New metallic derivatives of cellulose. Compounds of microcrystalline cellulose and potassium

N E Kotelnikova, D Fengel*, V P Kotelnikov, M Stoll* – Institute of Macromolecular Compounds of the Russian Academy of Sciences, Bolshoi pr 31, St Petersburg 199004, Russia; * Institute for Wood Research, University of Munich, Winzererstrasse 45, D-80797 München, Germany

SUMMARY

Potassium derivatives of cellulose were prepared by treating microcrystalline cellulose (MCC) with complexes of potassium (K) with ethylene diamine (EDA) and K and hexamethylphosphoric triamide (HMPT). The reaction products were characterized by X-ray diffraction, ¹³C NMR and FTIR spectroscopy as well as by SEM and EDXA.

INTRODUCTION

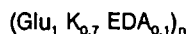
The search for preparation methods of new cellulose derivatives is often complicated by the morphology and the supramolecular structure of cellulose. In recent years new types of cellulose derivatives were prepared under heterogeneous conditions using the destabilizing action of various solvents on the cellulose structure (1-3). These studies resulted in cellulose derivatives which contain alkali metals such as lithium and sodium (4, 5). In the present contribution the synthesis of cellulose derivatives with potassium in organic solvents was studied. Microcrystalline cellulose (MCC) was chosen as the starting material.

Cellulose is known to form crystal-like molecular complexes with various solvents such as water, bases, alcohols, monoamines and polyamines (6). Ethylene diamine (EDA) and hexamethylphosphoric triamide (HMPT) were used as solvents for the synthesis of modifications of MCC. The former can form inclusion compounds with MCC whereas the interaction between the latter and cellulose has not yet been studied.

RESULTS AND DISCUSSION

The reaction of MCC with potassium takes place using the previously prepared complex of the solvent and potassium. The kinetics of the heterogeneous reaction of MCC with the K-EDA complex (Fig. 1a) reveals the insertion of potassium into the cellulose molecule reaching a limit of about 14 wt.% or 0.7 mole K/glucose unit almost independent of the molar ratio K : MCC applied for the reaction (Fig. 1b).

The resulting compound shows the crystal lattice of cellulose III with a crystallinity index of 0.50 according to X-ray diffraction (Fig. 2a). The specific feature of the diffraction pattern is the appearance of 4 additional peaks belonging to the crystalline complex of K and EDA. Comparable complexes containing EDA and other metals are assumed to possess a rhombic lattice (7). Previously it was found that small amounts of EDA are retained by MCC after treating MCC with EDA (3). The amount of EDA is 0.1 mole per glucose unit in the case of the cellulose-potassium compound. Its total formula can be given as:



The ^{13}C NMR spectra indicate that the steric environment of all carbon atoms in the K containing reaction product differs from that in the original MCC (Fig. 3a). This effect is particularly remarkable for the C(4) and C(6) atoms. The chemical shift of the C(4) atoms is caused by the rotation of the units around the C(4)-O(1) bond whereas that of the C(6) atom is induced by the rotameric variation of the oxymethyl groups (8). It is also of interest that the signals of C(4) almost disappear which is characteristic of amorphous cellulose such as cellulose recovered from solution.

The IR spectra of the K derivative of MCC reveal some new bands compared to the spectrum of MCC (Fig. 4). Some of these bands are connected with deformation vibrations of N-H groups ($700, 830 \text{ cm}^{-1}$), stretching vibrations N-H groups ($1600 - 1700 \text{ cm}^{-1}$) and deformation vibrations of C-N groups (9, 10). After deconvoluting the OH valency range (11) a band at 2730 cm^{-1} appears which is characteristic of the stretching vibrations of the N-H groups in the form of cations (9). The doublet in the range of $2870 - 2930 \text{ cm}^{-1}$ is obviously connected with the reaction at the C(6)OH group. The smoothening within the range of the OH valency vibrations ($3000-3600 \text{ cm}^{-1}$) indicates a decrease in crystallinity. The change of the band positions compared to the original MCC reveals a variation of the H bond system in cellulose.

Valuable information was obtained by scanning electron microscopy (SEM). The K derivative of cellulose shows considerable changes in fibre structure compared to the original MCC. No fibrils can be observed at the surface of the fibres (Fig. 6). The diameter of the fibres increases 1.5 times. The ends of the fibres look swollen and small particles belonging to the fibres appear at the surfaces. The potassium distribution along the fibres is completely uniform as indicated by X-ray analysis (EDXA).

In contrast to the results obtained with K-EDA the treatment of MCC with K-HMPT complex does not change the crystal lattice of cellulose I. At a low K content ($\approx 4 \text{ wt.}\%$) the crystallinity is not reduced whereas with a K content of $13.7 \text{ wt.}\%$ the cellulose is amorphized (Fig. 2b). The ^{13}C NMR spectra indicate a reduction in crystallinity by the decrease in the C(4) signal and a change in the C(6) signal range as a result of the reaction at the OH group in this position (Fig. 3b). The latter finding is confirmed by the IR spectra in the range of $2800-3000 \text{ cm}^{-1}$ (Fig. 5). According to the kinetic studies a maximum uptake of K of 0.7 mole/glucose unit can be reached (Fig. 1b). HMPT is not retained by cellulose during this reaction.

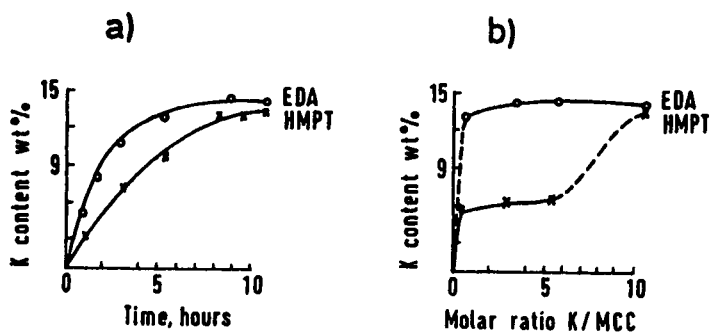


Fig. 1. Kinetics of the reaction of MCC with complexes of K and EDA or K and HMPT

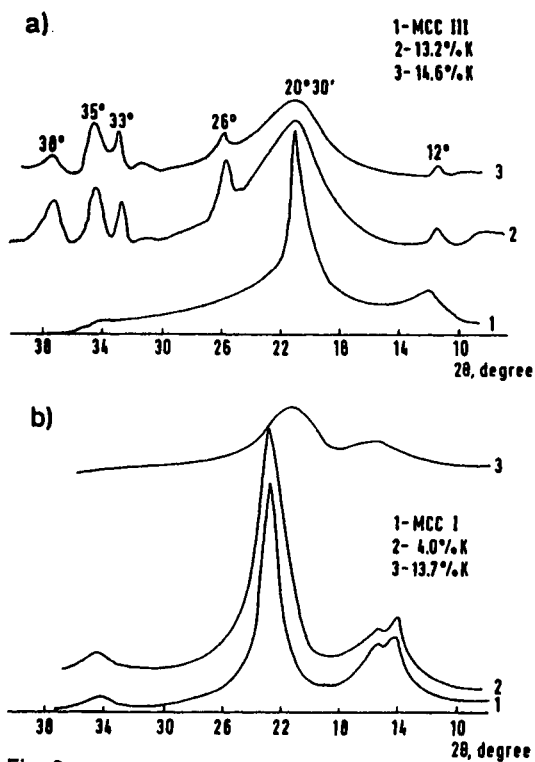


Fig. 2. X-ray diffractograms of K derivatives of cellulose prepared in EDA (a) and HMPT (b), compared with MCC of different lattice modifications

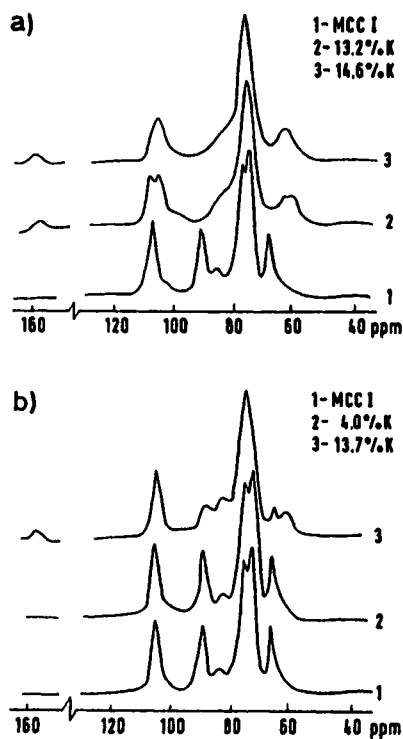


Fig. 3. Solid state ¹³C NMR spectra of K derivatives of cellulose prepared in EDA (a) and HMPT (b), compared with the original MCC

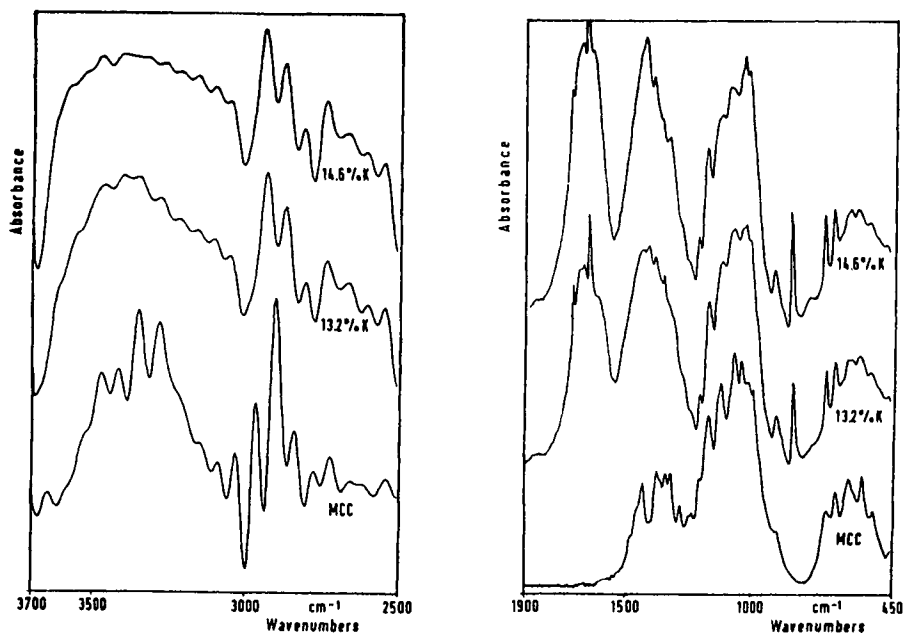


Fig. 4. FTIR spectra of K derivatives of cellulose prepared in EDA, compared with the original MCC. Fingerprint range (450 - 1900 cm^{-1}) and deconvoluted CH_2/OH range (2500-3700 cm^{-1})

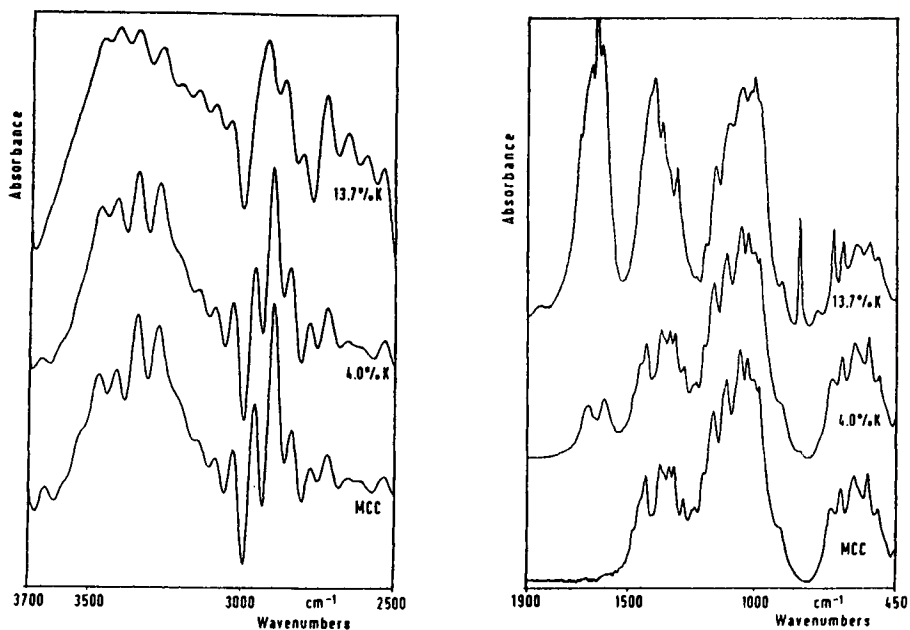


Fig. 5. FTIR spectra of K derivatives of cellulose prepared in HMPT, compared with the original MCC. Fingerprint range (450-1900 cm^{-1}) and deconvoluted CH_2/OH range (2500-3700 cm^{-1})

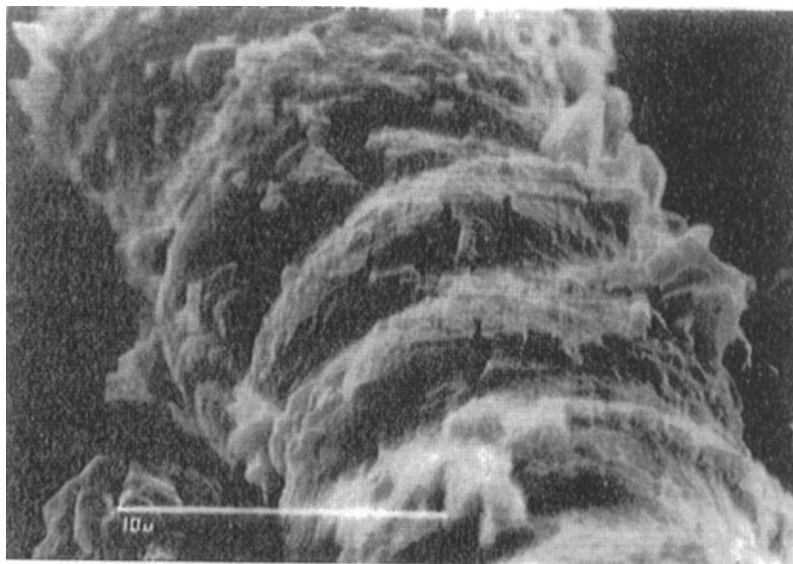


Fig. 6. Fibre of K derivative of cellulose prepared in EDA containing 14.6 % K. SEM micrograph

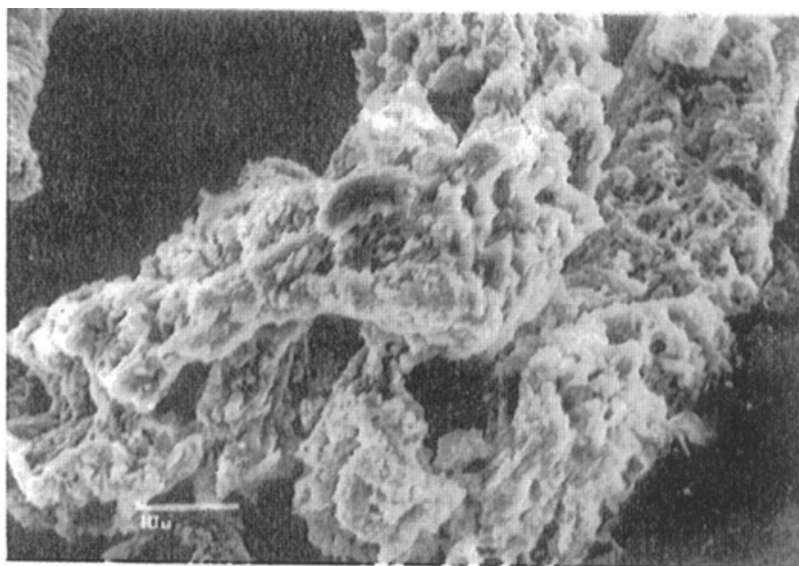


Fig. 7. Fibre of K derivative of cellulose prepared in HMPT, containing 13.7 % K. SEM micrograph

SEM studies show a beginning swelling of the fibres at low K content. At high K content an irregular swelling combined with a deformation of the fibre surfaces indicate the amorphization of the cellulose (Fig. 7). EDXA results in a uniform distribution of potassium at the fibre surface.

CONCLUSION

The introduction of potassium into the cellulose molecule results in a chemical, supramolecular and morphological change of the fibres. Using EDA as solvent a change in the crystal lattice and a reduction in crystallinity is observed. In this case EDA seems to be involved in the cellulose-K compound. Using HMPT the lattice modification of the original MCC is maintained whereas the crystallinity is greatly reduced. With both kinds of treatment a preferred reaction at the C(6)OH group of cellulose seems very likely.

ACKNOWLEDGEMENT

Many thanks to Dr. A.A. Shashilov and Dr. A.V. Griбанov for X-ray diffraction and ¹³C NMR measurements.

The financial support of the Deutsche Forschungsgemeinschaft is greatly appreciated.

REFERENCES

1. Petropavlovsky, G.A.; Kotelnikova, N.E.: Cell.Chem.Techn. **19** (1985), 591-600
2. Petropavlovsky, G.A.; Kotelnikova, N.E.; Arslanov, Sh.S.: Zh.Prikl.Khim. **62** (1989), 2803-2808
3. Petropavlovsky, G.A.; Kotelnikova, N.E.; Arslanov, Sh.S.: Khim.Drev. (1988) No.6., 3-8
4. Kotelnikova, N.E.; Kotelnikov, V.P.: Abstr. "Cellulose '91", New Orleans, USA, 1991, p. 222
5. Kotelnikova, N.E.; Kotelnikov, V.P.: Abstr. Symp.Cellulose and Lignocellulose Chemistry, Guangzhou, China 1991, pp. 227-228
6. Golhman, A.Sh.; Solomko, V.P.: Macromolecular Inclusion Compounds, Kiev, 1982
7. Nakahara, A.; Saito, Y.; Kuroya, H.: Bull.Chem.Soc.Japan **25** (1952) 331-336
8. Kotelnikova, N.E.; Elkin, A.U.; Koltzov, A.I.; et al.: In "Methods of cellulose research", Riga, "Zinatne", 1988, pp. 61-65
9. Hediger, H.J.: Infrarotspektroskopie. Grundlagen, Anwendungen, Interpretation. Akadem.Verlagsges., Frankfurt/M., 1971
10. Nakamoto, K.: Infrared and Raman Spectra of Inorganic and Coordination Compounds, 4th Ed., Wiley-Intersci.Publ., 1986
11. Fengel, D.; Holzforschung **46** (1992) 283-288

25 Structure of cellulose-polyacrylamide graft copolymers

S I Klenin, E N Bykova, S F Petrova, V A Molotkov – Institute of Macromolecular Compounds, Russian Academy of Sciences, Bol'shoi Prospect 31, St Petersburg, 199004, Russia

ABSTRACT

The molecular structure of graft copolymers were determined by the seldom applied but the most informative and the most reliable approach consisting of the comparative study of molecular parameters (diffusion and sedimentation coefficients, intrinsic viscosity, and MW) of the main and side chains and those of the final product.

The small number of grafted chains per cellulose derivatives molecule was explained by the degradation of the backbones occurring on exposure to Co^{3+} ions simultaneously with their initiation. The possible degradation types are discussed.

INTRODUCTION

Water-soluble graft copolymers based on acrylamide are of interest as highly effective flocculants, in oil production, drag reduction and others. It should be noted that one of the main conditions of high polymer efficiency in these technological processes is the high molecular weight (MW) of polymers, and graft polymerisation is one of the methods available to attain it. On the other hand, investigating the structure of

graft copolymers based on cellulose (C) and its derivatives (CD) can give additional information about the features of the C macromolecular structure.

EXPERIMENTAL

The polymerization of acrylamide initiated by Co^{3+} salts conducted in the presence of C or CD results in the formation of graft copolymers. We used carboxymethyl (CMC), hydroxyethyl (HEC), and hydroxypropyl (HPC) celluloses as backbones and isolated grafted chains by acidic hydrolysis. These processes have been discussed in greater detail in Refs.[1-3]. To prepare the solutions, distilled water was used for HEC and HPC, and 10% NaCl was employed for other samples. The diffusion D_o and sedimentation S_o coefficients, the intrinsic viscosity $[\eta]$, light scattering and flow birefringence of the samples were measured as described in [2-5]. Mainly, the MW values of samples were calculated using equations :

$$M_{SD} = \frac{S_o R T}{D_o (1 - \bar{v}\rho_o)} \quad (1) \quad M_{S\eta}^{2/3} = \frac{\eta_o [\eta]^{1/3} S_o R}{A_o (1 - \bar{v}\rho_o)} \quad (2)$$

where R is the universal gas constant , $A_o = (3.4 \pm 0.2) \times 10^{-10} \text{ g cm}^2 \text{ sec}^{-2} \text{ deg}^{-1} \text{ mol}^{-1/3}$ is the hydrodynamic invariant [6]. $T = 293^\circ\text{K}$, ρ_o and η_o are the solvent density and viscosity respectively, and \bar{v} is the specific partial volume.

The average number of grafted chains per CD molecule was calculated on the basis of comparison of MW of the main and the side chains and of the graft copolymer:

$$\bar{n} = \frac{M_{SD}^{gc} - M_{SD}^b}{M_{SD}^{sc}} \quad (3)$$

RESULTS AND DISCUSSION

The data obtained (Table 1) shows that: (1) the molecular structures of the graft copolymers synthesized do not depend on the nature of CD and one can use the star-shaped model to describe them, (2) the average minimum distance between branching points is ~ 200 glucoside units, (3) an increase in MW of main chains (CMC, HEC), other conditions being equal, does not lead to

Table 1. Molecular parameters of graft copolymers synthesized and their components.

Sample	$[\eta]$ dl/g	$D_o \cdot 10^8$ cm^2/s	$S \cdot 10^{13}$ 1/s	$M \cdot 10^{-6}$ SD	\bar{n}
CMC-1	3.5	13.0	2.65	0.15	—
PAM-1	7.0	3.2	6.1	2.0	—
GC-1	14.4	2.1	8.7	4.4	2.1
CMC-2	8.8	7.9	3.85	0.37	—
PAM-2	9.3	2.6	9.0	3.7	—
GC-2	19.0	1.4	9.1	7.0	1.8
HEC-1	1.4	22.6	2.15	0.08	—
PAM-E1	9.8	2.9	7.7	2.8	—
GC-3	11.3	2.2	10.5	6.1	1.8
HEC-2	6.9	8.9	2.75	0.25	—
PAM-E2	10.2	3.0	6.7	2.4	—
GC-4	14.4	2.0	10.0	5.3	2.2
PAM-E22	5.7	3.3	6.2	2.2	—
GC-5	14.6	1.4	16.7	12.8	6.0
HEC-3	8.5	7.4	4.2	0.45	—
PAM-E3	12.4	2.4	8.0	3.5	—
GC-6	14.5	1.45	15.4	11.3	3.2
HEC-4	12.2	6.4	4.65	0.65	—
PAM-E4	8.0	3.2	5.8	1.9	—
GC-7	13.5	1.75	11.8	7.2	3.8

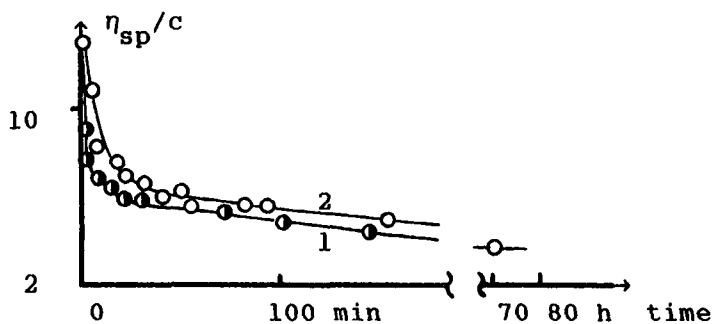


Figure 1. Time dependencies of the specific viscosity of CMC-1 (1) and CMC-2 (2) in the process of oxidation with trivalent cobalt salts. The polymer concentration 0.12% .

Table 2. Molecular parameters of water-soluble cellulose derivatives (CMC, HEC, and HPC), initial and oxidized with trivalent cobalt salts (a - d)

sample	reaction time, min	t °C	$[\eta]$ dl/g	$D_o \cdot 10^8$ cm ² sec ⁻¹	$S_o \cdot 10^{13}$ sec ⁻¹	$M \cdot 10^{-3}$ SD	$M \cdot 10^{-3}$ S η
CMC-1	---	--	3.5	13.0	2.65	150	--
CMC-1a	120	12	1.0	30.0	1.6	40	--
CMC-2	---	--	8.8	7.9	3.85	370	--
CMC-2a	120	12	1.0	30.0	1.7	40	--
HEC-1	---	--	1.4	22.6	2.25	80	70
HEC-1a	120	12	0.63	31.0	1.9	50	40
HEC-1b	120	0	1.1	29.0	2.9	80	90
HEC-2	---	--	6.9	8.9	2.75	250	240
HEC-3	---	--	8.5	7.4	4.2	450	490
HEC-3a	120	12	1.5	----	1.5	--	40
HEC-4	---	--	12.2	6.4	4.65	650	690
HEC-4a	120	20	3.0	16.0	1.3	60	50
HEC-4b	120	0	5.0	12.4	3.6	235	290
HEC-4c	15	20	3.3	----	----	---	---
HEC-4d	15	0	5.2	----	----	---	---
HPC	---	--	3.2	----	2.8	---	160
HPCa	120	0	1.6	----	1.5	---	50

a proportional increase in the average number of grafted chains [2,3].

One can suggest that the reason for this behaviour is the degradation of the backbones proceeding under the influence of Co^{3+} ions. As a result of the special experiments (Figure 1, Table 2), it was established that:

(1) the degradation of CD proceeds on exposure to Co^{3+} ions. The time dependence of specific viscosity of CMC indicates that the dramatic decrease in the degree of polymerization (DP) of the samples occurs during the first 15 minutes, (2) when CMC, HEC, and HPC of different MW interact with Co^{3+} ions at 12 or 20°C, their fragments are formed at approximately the same degree of polymerization, LODP = 200 (3) if CD interacts with Co^{3+} ions at 0 °C (conditions of graft polymerization reaction) LODP depends on the initial DP and is higher than 200. The second conclusion confirms the hypothesis about regularly located weak bonds in C. There are no common opinions about the nature of "weak bonds" [7-9], and frequency of their location along C macromolecules [10,11], but this concept successfully explains the

two-stage process of chemical degradation of C and CD.

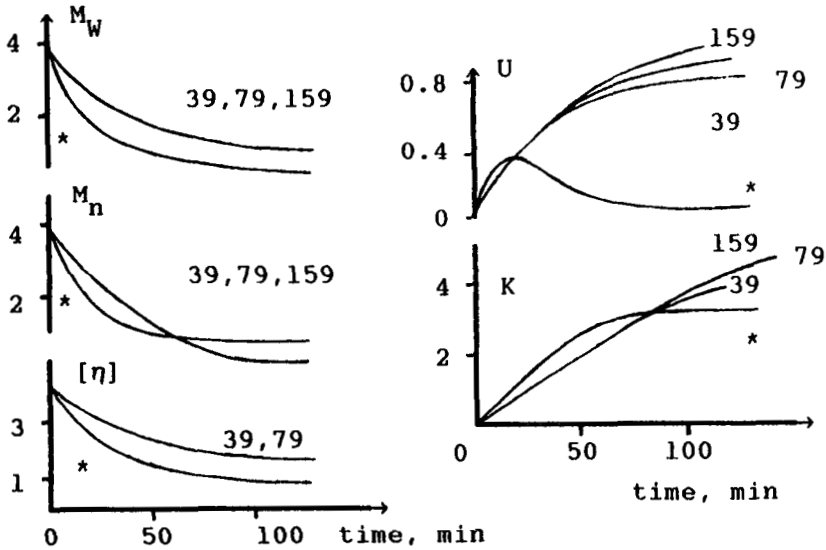


Figure 2. Time dependencies of the number-average MW

$$\bar{M}_n(t) = \frac{\sum_{n=1}^N n Y(n,t)}{\sum_{n=1}^N Y(n,t)}, \text{ the weight - average MW}$$

$$\bar{M}_w(t) = \frac{\sum_{n=1}^N n^2 Y(n,t)}{\sum_{n=1}^N n Y(n,t)}, \text{ the polydispersity para-}$$

$$\text{meter } U = \bar{M}_w(t) / \bar{M}_n(t) - 1, [\eta] = \frac{\sum_{n=1}^N [\eta] n Y(n,t)}{\sum_{n=1}^N n Y(n,t)},$$

and the number of scissions per one molecule $K(t) =$

$$= \frac{\sum_{n=1}^N (Y(n,t) - Y(n,0))}{\sum_{n=1}^N Y(n,0)} \text{ for molecules of equal}$$

initial lengths degraded regularly (* : $N-1=3, \alpha = 0,03$) and randomly ($N-1 = 39$ or 79 or $159, \alpha=10^{-3}, 5 \cdot 10^{-4}, 2.5 \cdot 10^{-4}$, respectively).

Let us consider a molecule consisting of n units of equal length and degraded irreversibly at each $(n - 1)$ bond with equal probability. This process may be described by a kinetic equation [12]:

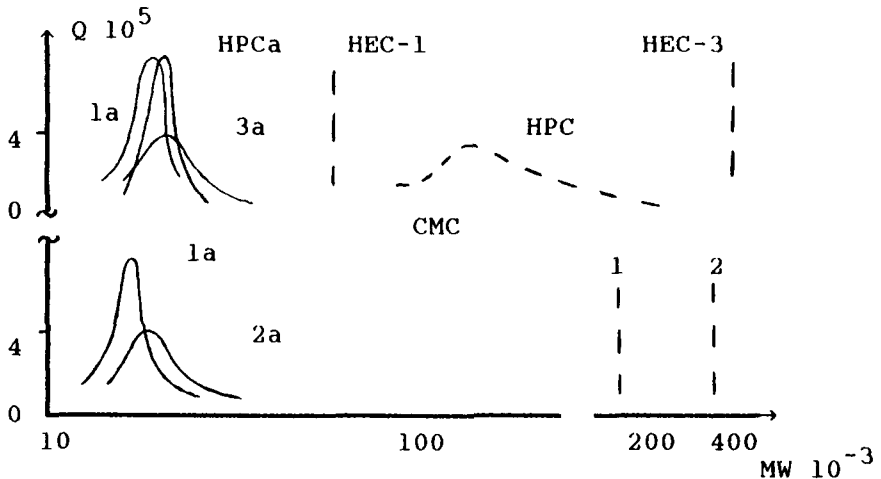


Figure 3. Differential MWD of CMC, HEC, and HPC, oxidized with trivalent cobalt salts (b). The MWD of the initial samples are shown by broken lines.

$$dY(n,t)/dt = -x(n-1) Y(n,t) + 2x \sum_{i=1}^N Y(i,t) \quad (4)$$

where $Y(n,t)$ is the concentration of molecules consisting of n units at the time moment t , x is a constant for bond breaking rate, and $(N-1)$ is the number of bonds in the longest molecule of the given ensemble at the initial time moment.

Numerical differentiation of equation system (4) was carried by the prediction and subsequent correction method. This approach has been discussed in greater detail in Ref. [13].

To solve the problem about the degradation type of CD, oxidizing with trivalent cobalt salts allows one more precisely to compare random (distance between "weak bonds" $Z \ll \text{LODP}$) and regular ($Z = \text{LODP}$) degradations to show their characteristic features. Figure 2 shows that: (1) the change in \bar{M}_w , \bar{M}_n , and $[\eta]$ with variations in t is sharper for the molecules, degraded regularly (2) if $K(t)$ is small, $U(t)$ value virtually does not depend on the degradation type, (3) there is such range of $K(t)$ in which $U(t) \rightarrow 0$ for regular degradation and $U(t) \rightarrow 1$ for random degradation.

Hence, to determine the degradation type actually occurring, we estimated the MW distribution (MWD) of

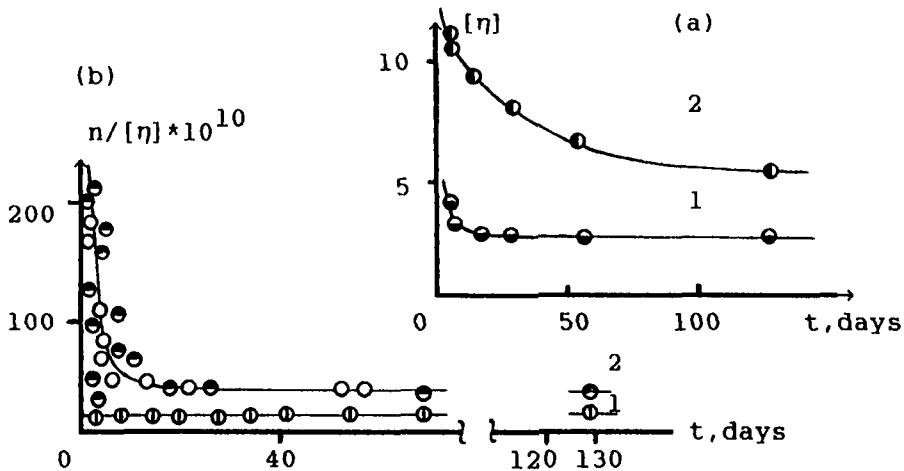


Figure 4. Plot of $[\eta]$ (a) and optical anisotropy (b) versus time of a cellulose in cadoxen; (1) initial and (2) regenerated from trifluoroacetic acid.

the samples. To determine MWD of CMC, HEC, and HPC, velocity sedimentation was used [5] (Figure 3)

It was established that when CD's of different MW and different MWD interact with Co^{3+} ions, their fragments are formed at approximately the same degree of polymerization $\text{LODP} \sim 200$ and, which is especially important, at narrow MWD $\bar{M}_w / \bar{M}_n = 1.1-1.2$. This is in agreement with the hypothesis about regularly located weak bonds in C.

Another corroboration of structural periodicity of C macromolecules is provided by experiments fixing the intramolecular organization of C during its dissolution. When C interacts with trifluoroacetic acid, the values of $[\eta]$ and optical anisotropy $n/[\eta]$ decrease considerably with time although MW is retained invariably [4], Figure 4. This may be interpreted as the dissolution of some elements of the C native structure retained in the macromolecule. This fact may be considered as a confirmation of the folded chain model of native C [8] and, hence, of the periodicity of its structure.

References

1. Kurlyankina V.I., Molotkov V.A., Klenin S.J., Lubina S.Ya., *J Polym.Sci. Polym.Chem.Ed.* 10, 3369 (1980).
2. Klenin S.J., Bartoshevich S.F., Revelskaya L.G., Kurlyankina V.I., *Vysokomol.Soed.(in Russ.)* 28 B, 534 (1986).
3. Bartoshevich S.F., Bykova E.N., Molotkov V.A., Klenin S.J., *Vysokomol.Soed.(in Russ.)*, 31 B, 747 (1989).
4. Klenin S.J., Lyubina S.Ya., Chripunov A.K., Bezrukova M.A., Bykova E.N., *Chemistry of Wood (in Russ.)* N 6, 8 (1986).
5. Tsvetkov V.N., Eskin V.Ye., Frenkel S.Ya., *Macromolecular structures in solution - (in Russ.)*, Nauka, Moscow (1964).
6. Tsvetkov V.N., Klenin S.J., *Dokl.Akad.Nauk SSSR (in Russ)* 88, 49 (1953).
7. *Cellulose Chemistry and its Applications / Ed. by Nevel T.P. Wiley, N.Y. (1985).*
8. Chang M., *J.Polym.Sci. Part C* , N 36, 343 (1971).
9. Simon I., Sheraga H.A. and Manley R.St.J., *Macromolecules.* 21, 983 (1988).
10. Marx-Figini M., *Macromol. Chem. Macromol.Symp.* , 89 , (1986).
11. Yachi T., Hayashi J., Takai M., Shimisu Y., *J.of Appl.Polym.Sci.* 37, 325 (1983).
12. Montroll E.W., Simha R.J., *J.Polym.Phys.* 8, 721, (1940).
13. Bartoshevich S.F., Nemchinov I.A., Molotkov V.A., Klenin S.J. , *Vysokomol.Soed.(in Russ.)* 33 A, 1639 (1991).

26 Hydrogels of carboxymethylcellulose and bischloroformiate diethylene glycol

R Pernikis and B Lazdina – Latvian State Institute of Wood Chemistry, 27 Dzerbenes Str, LV-1006, Riga, Latvia

The great practical interest shown worldwide in the production and investigation of the properties of high-hydrophilic materials has resulted in intensifying the research activities carried out in this direction. The analysis of the research shows that there are two major methods for the production of polymeric materials exhibiting an enhanced wetting ability: partial cross-linkage of cellulose and its derivatives, as well as the reactions of grafting to starch, cellulose and other polysaccharides of non-saturated monomers.

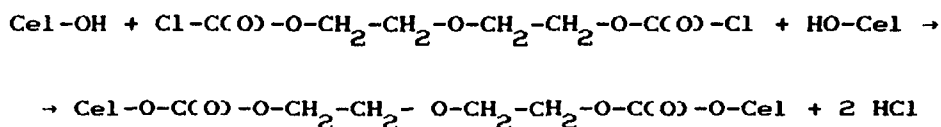
Practically all the ethers of cellulose may be cross-linked. Oligomeric and polymeric compounds may be used as cross-linking agents [1, 2].

Carboxymethylcellulose (CMC) may be subjected to cross-linkage both at the expense of the existing hydroxylic and carboxylic groups, and their interaction with different bifunctional compounds. Such a cross-linkage results in a change of CMC properties, which enables its use as a supersorbent in biology, medicine,

and agriculture.

The present work is dedicated to the study of chemically cross-linking CMC with bischloroformate diethylene glycol (BCFD).

The reaction between CMC and BCFD is performed at the expense of the hydroxylic groups of cellulose according to the scheme:



Since Na-CMC is insoluble in organic solvents, an attempt has been made to perform the reaction at the water-methylchloride interface. Na-CMC with MM 89000, C3-75 (brand 70-450) and degraded Na-CMC with MM 30000 were used for the reaction; sodium hydroxide or triethylamine were used as HCl acceptor. The reaction was performed at the ratio of the initial reagents Na-CMC:BCFD:NaOH = 1:1:2:0.66:2 (moles).

For example, 4.8 g Na-CMC and 3.5 ml BCFD were dissolved in 160 ml water and 100 ml CH_2Cl_2 , respectively. After intensive mixing, 1.68 ml of a 10% NaOH solution were gradually added. In 10 minutes, a homogeneous emulsion was formed, which was left for 1 hour; during this period of time the pH dropped from 10 to 8.5.

To purify the product, it was precipitated in 80% ethanol. To obtain a powder-like product, it was precipitated in isopropyl alcohol and washed thoroughly with methanol.

The determination of the molecular weight per cross-linked unit in cross-linked CMC (Mc) was performed by alkaline hydrolysis chemically.

The degree of swelling was determined according to the formula:

$$Q = 1 + (m_{\text{swel.}} / m_{\text{dry}} - 1) \rho_2 / \rho_p$$

where:

$m_{\text{swel.}}$, m_{dry} - weight of swollen and dry cross-linked

Na-CMC; ρ_2 - product density; ρ_p - solvent density

Table 1 lists the yield and properties of the products obtained, depending on the ratio of the initial reagents.

Table 1

Conditions of the production and the properties of cross-linked Na-CMC*

Mole ratio Na-CMC: BCFD: NaOH	Yield, %	Q_{max}	Solubility in water, %
1:1.5:1.6	44.5	25.70	17.8
1:1.0:1.6	43.3	25.26	27.9
1:0.75:1.5	46.0	28.26	80.0
1.0.5:1.0	42.7	64.80	91.0
1:1:2.00	45.3	16.87	16.1
1:1:1.32	47.1	39.25	46.6
1:1:0.66	42.7	57.00	44.0

*Reaction time 60 min

As can be seen from the data obtained, the increase in the quantity of BCFD from 0.5 to 1.5 moles does not actually affect the yield of the final product, however the degree of its swelling as well as solubility in water decrease. At a decrease of the amount of BCFD below 0.5 moles, no hydrogel formation is observed, but the viscosity of water solution increases which is, obviously, connected with the formation of cross-linked CMC macromolecules still soluble in water. The same situation

is observed when degraded CMC with MM 30,000 is used.

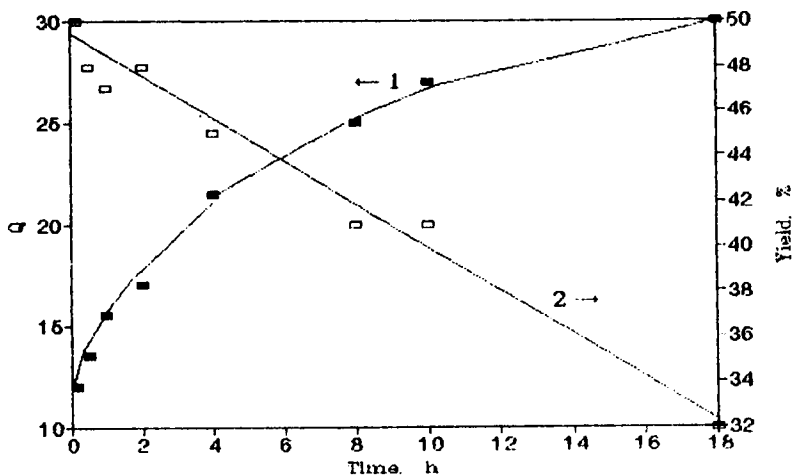


Fig. 1. Variations in swelling degree (1) and hydrogel yield (2) depending on the reaction time

An increase in the reaction time (Fig. 1) results in a gradual decrease in the product yield and an increase in the swelling degree, which is connected with the hydrolysis of the carbonate linkages formed during the reaction with BCFD. The analysis of cross-linked Na-CMC showed a 0.2 - 0.4% Cl content in the samples, which is indicative of the presence of the Cl-CO-C groups remaining from the non-reacted BCFD. The stability of cross-linked Na-CMC was determined in water and phosphate buffer (Table 2). The solubility of gel in water at the beginning of swelling was conditioned by non-reacted Na-CMC (approximately 20%) and that with low density of cross-linkage. The increase in the solubility of gel in water and phosphate buffer, conditioned by the hydrolysis of carbonate groups was observed in 3 days of enduring the gel in these media. In 7-10 days of enduring the gel in phosphate buffer, its complete decomposition took place.

Table 2

Stability of cross-linked Na-CMC depending on the endurance time in water and phosphate buffer (pH 7.4) at 310°K

Medium	Solubility, %						
	day	1	3	5	7	10	92
Water		24.7*	27.5	30.1	35.7	-	47.8
Phosphate buffer		1.7*	4.5	12.5	22.4	decompo-	100.0
		0.3**	0.4	36.5	decompo-	-	100.0
					sition		

* Q_{\max} in water 17.5; ** Q_{\max} in water 64.5

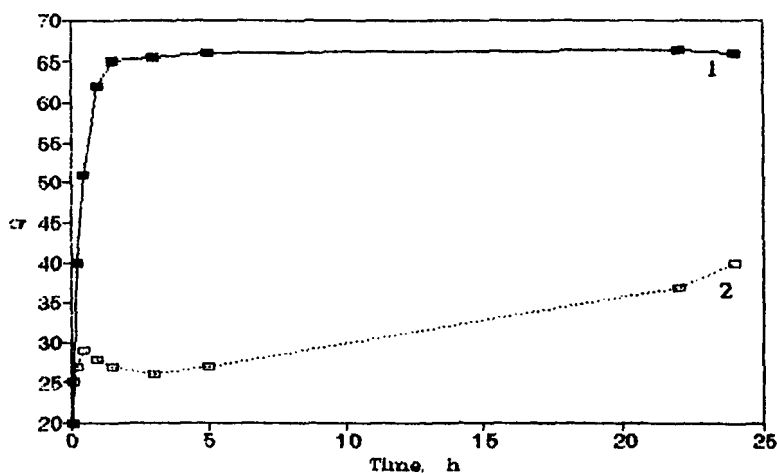


Fig. 2. Swelling kinetics of hydrogels with swelling degree $Q_{\max} = 65$ (1) and $Q_{\max} = 39$ (2).

It is known that the swelling of hydrogel is directly connected with the degree of cross-linking. The study of the swelling kinetics of cross-linked CMC in water (Fig.2)

enables characterization of the cross-linkage parameter M_c .

As can be seen from Fig. 2, maximum swelling (Q_{\max}) is reached in 24 hours of enduring the sample in water, depending on M_c .

The structure of the gels formed is characterized using the Flory-Huggins equation [3].

Table 3

Characteristics of the gel structure of cross-linked Na-CMC

Parameters	Samples			
	I	II	III	IV
Equilibrium swelling degree, Q_{\max}	72.7	27.9	20.5	6.2
Polymer fraction in swollen gel, V_2	0.014	0.037	0.047	0.161
Molecular weight per cross-link unit, M_c in terms of swelling	548.898	56.372	34.679	5.012
the chemical method	-	-	17.990	5.980
Cross-link density, mol/cm^3	2.0×10^{-6}	2.0×10^{-5}	3.0×10^{-5}	3.9×10^{-4}

As can be seen from Table 3, the lack of coincidence of the qualitative characteristics of M_c calculated in terms of swelling and obtained experimentally is accounted for by the fact that, firstly, the addition of the bifunctional reagent takes place mainly to high molecular fractions [3], and the heterogeneity of the resultant product arises for the cellulose ether in terms of molecular weight, and secondly, hydrolysis of the BFCO regions connected by one end to the CMC chain takes place.

The equilibrium degree of gel swelling, exceeding 20

confirms that the cross-linked CMC obtained has the qualities of a superabsorbent.

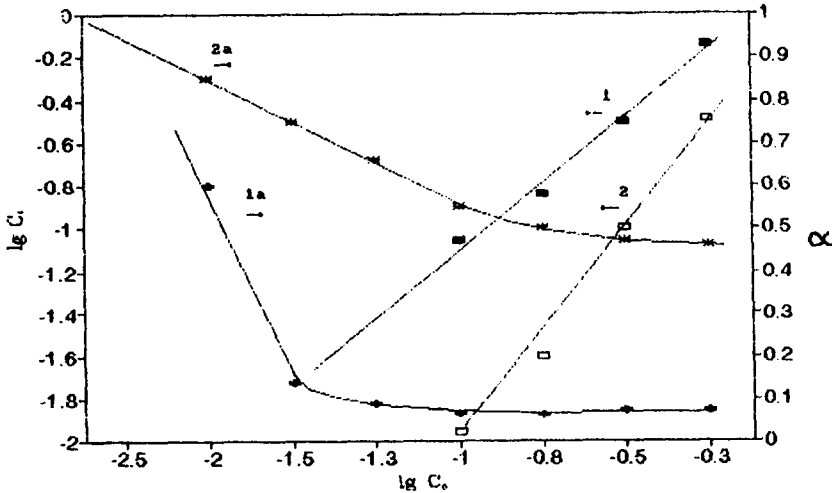


Fig. 3. Dependence of the degree of gel collapse and CuSO_4 concentration in solution outside the hydrogel after the interaction hydrogel - salt solution depending on the initial concentration of salt: 1, 1a - Q_{\max} 24.5; 2, 2a - Q_{\max} 6.2

It is known that in salt solutions the water absorption of ionic polyesters decreases dramatically. At the same time, the study of the mutual influence of hydrogels and aqueous solutions of bivalent metal salts presents a considerable interest both from the scientific and practical points of view [4], since the regularities which take place in this case may serve as a base, for example, for purification or enrichment technologies. In the present work we have studied the behaviour of the gels obtained with a degree of swelling of 24.5 and 6.2 in cuprum sulphate solutions (in concentrations from 0.001M to 0.5M), for which the gel collapse degree (α) (i.e. the ratio between the sample volume in salt solution and its

volume in distilled water in the equilibrium state) as a function of the initial concentration of the salt solution c_0 is determined (Fig. 3).

The concentration of CuSO_4 (c_1) in the solution outside the gel after the interaction hydrogel - salt solution, depending on c_0 has been studied, and, as can be seen in Fig. 3, a linear dependence has been obtained. Already at a CuSO_4 concentration of 0.01 mole/litre, an abrupt collapse of the gel takes place, however the maximum concentration of cuprum in the gel is in 0.1M CuSO_4 solution.

REFERENCES

1. M.Katalevskaya, V.Tribunsky, V.Menko, *Khimiya Drevesiny* (Wood Chemistry), 1987, 4, 22.
2. L.Westman, T.Lindstrom, *J. Appl. Polym. Sci.*, 1981, 26, 2573.
3. G.Petropavlovsky, *Hydrophilic partially substituted cellulose ethers and their modification by chemical cross-linkage*, Nauka, Leningrad, 1988, p. 240.
4. T.Butova, S.Frenkel, *Vys. mol. soed.* (High-molecular compounds), 1991, 33 (B), 856.

27 Some aspects of cellulose carbamate

H Struszczyk and A Urbanowski – Institute of Chemical Fibres,
ul M C Skłodowska 19/27, 90-570 Lodz, Poland

ABSTRACT

An entirely new method for the production of cellulose carbamate (CC) has been developed at the Institute of Chemical Fibres, Łódź, Poland. The method allowed manufacture of CC suitable for further processing into useful commodities such as fibres, film, beads, binding agents and microcrystalline cellulose and cellulose carbamate. Fibres obtained from CC resemble viscose fibres; other products made of CC proved to be useful in a number of applications.

1. Cellulose carbamate (CC).

To replace the hazardous viscose technology new processes are proposed by some leading companies [1-2]. One of the possible new routes is the CC technology. Cellulose

carbamate is formed in the reaction of cellulose and urea at about 135-140°C.

To accomplish the synthesis the average degree of polymerization (DP) of cellulose should be lowered to about 400. Furthermore the cellulose should be activated. Even distribution of the carbamate groups along the cellulose chain is desirable.

In the eighties Neste Oy of Finland introduced the cellulosic fibre made from CC under a name of Cellca [3-14]. In that process, liquid ammonia were employed for activation and irradiation for lowering the DP. After some time Neste withdrew from the process.

2. A new route for the manufacture of CC.

At the Institute of Chemical Fibres, Lodz, Poland a new method for the manufacture of CC has been developed. The new process entirely eliminates the inconvenience of liquid ammonia and irradiation, as proposed by Neste. Chemical treatment provides both for activation and for lowering of the DP and consequently for a homogeneous intercalation of urea in cellulose. The new process allows the manufacture of CC with both good yield and quality [15]. Characteristics of the CC produced are given in Table 1.

3. Possible application of CC.

Cellulose carbamate can be used to manufacture of products made by coagulation and/or regeneration processes (Fig. 1) The main target of cellulose carbamate use is to make fibres. Spinning trials are being run in cooperation with viscose mills both in Poland and abroad.

Table 1. Properties of CC form pilot scale industrial manufacture.

Property	Parameter
Form	pulp
Colour	white to light beige
Nitrogen content, %	2.0 - 3.0
Moisture content, %	7.9 - 9.0
Solubility in 9 % w/w NaOH in -5 °C	very good with concentration up to 7 - 9 wt%
K_w^*	about 10
Stability of KC solution in 0 °C	up to 120 h
Decomposition temp., °C	365
Stability of dry cellulose carbamate	stable

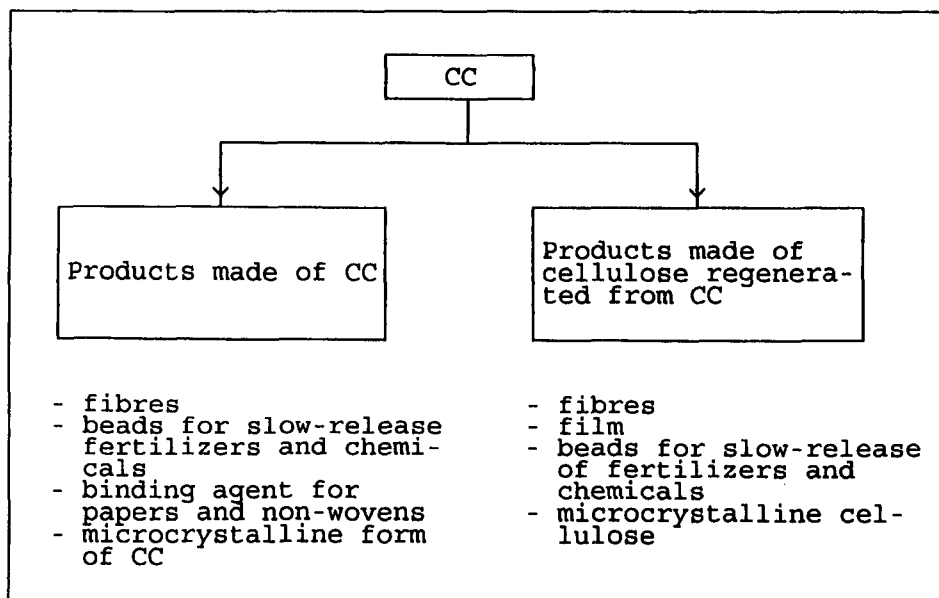


Figure 1. Scheme of products made on a base of cellulose carbamate.

Table 2. The properties of fibres made from cellulose carbamate.

Property	Parameter
Titre, dtex	1.5 - 2.0
Tenacity, cN/tex	15 - 20
Elongation, %	16 - 22
Loop tenacity, cN/tex	3.8 - 5.5
Nitrogen cont., %	1.0 - 1.2* or 0.3 - 0.5**

* - cellulose carbamate

** - cellulose

CONCLUSIONS

The new procedure allows for the manufacture of cellulose carbamate. An industrial pilot plant has been put on stream with an output of about 10 tons of CC per month. The product is stable, has good quality and dissolves well in sodium hydroxide. The alkaline solution can easily be converted into useful products such as fibres, film, beads.

ACKNOWLEDGMENTS

The work presented in this paper is a result of team work. The team included also Dr. W.Mikołajczyk, Dr. A.Bodek, Mr D.Wawro, Mr P.Starostka, Mr J.Roman.

REFERENCES

1. Chemiefasern/Textilind., 1990, 40/92, 742.

2. Chemiefasern/Textilind., Man-Made Fiber Year Book, 1991.
3. K.Meinander, V.Eklund, J.Fors, L.Mandell, J.F.Selin, O.T.Turunen, Kemira News, 1987, 2, 8.
4. H.Ekman, V.Eklund, J.Fors, J.H.Huttinen, J.F.Selin, O.T.Turunen, "Cellulose Structure Modification and Hydrolysis", John Wiley & Sons Inc., New York, 1986, p.131.
5. O.T.Turunen, K.Meinander, L.Mandell, J.Fors, R. Nousiainen, J.H.Huttinen, L.Pakkala, R.Taurio, Proceedings of the 14th IFATOC Congress p II Tampere, Finland, 1987.
6. O.T.Turunen, J.Fors, J.H.Huttinen, Proceedings of 23rd International Man-Made Congress, Dornbirn, Austria, 1984.
7. Chemiefasern/Textilind., 1987, 37/89, 778.
8. H.Struszczyk: Włókna Chemiczne, 1988, 14/4, 356; 1989, 15/1, 7; 1989, 15/2, 8.
9. US Patent 2134825 (1983).
10. British Patent 2164941 (1984).
11. Finnish Patent 61033 (1982).
12. German DDR Patent 201908 (1981).
13. German DDR Patent 214135 (1982).
14. US Patent 4404369 (1983).
15. Polish Patent Applications: P-280952; P-281342; P-284488; P-289567; P-294156; P-290948; P-291517; P-295657.

28 Investigations of amidation of C-6-carboxycellulose

K Rahn, T Heinze* and D Klemm – Friedrich Schiller University of Jena, Humboldtstraße 10, D-07743 Jena, Germany

ABSTRACT

C-6-Carboxycellulose (COC, degree of oxidation 0.52) a glucoglucuronan, which can be activated by the precipitation of an aqueous polymer solution in DMF yielding a highly swollen gel, reacts with SOCl_2 to the corresponding acid chloride with a nearly complete conversion of 91%. The subsequent reaction with benzyl amine/ pyridine yields COC benzyl amides with additional glucuronic acid and glucose residues in the polymer backbone. The cellulose derivatives are characterized by IR- and ^{13}C -NMR spectroscopy.

INTRODUCTION

The oxidation of cotton linters with $\text{NaNO}_2/ \text{H}_3\text{PO}_4$ yields C-6-carboxycellulose with a degree of polymerization of about 80 [1, 2]. These ionic lignocellulosics are interesting materials for further modifications both of the COOH-groups and of the remaining OH-groups. In a previous paper we have reported the sulphation reaction of the OH-groups yielding a polyelectrolyte with two different ionic groups [3]. Now we want to report on our first results on amidation reactions of the COOH-groups.

EXPERIMENTAL

C-6-Carboxycellulose was prepared by adding finely powdered NaNO_2 to a

* Correspondence author

solution of cotton linters in aqueous 85% H_3PO_4 and a subsequent treatment with NaBH_4 according to [2].

Methods of characterization

Infrared spectra were recorded in KBr disks with a M 80 spectrophotometer (CARL ZEISS JENA). The ^{13}C -NMR spectra were recorded on a BRUKER MSL 400 spectrometer operating at 100.63MHz in the pulsed Fourier-transform mode with proton decoupling after dissolving in 0.5M NaOH/ D_2O at 20°C. 12000- 30000 scans were accumulated.

Carboxycellulose acid chlorides (COCCl)

The sodium salt of the C-6-carboxycellulose (1.0g, 5.5mmol) was dissolved in distilled H_2O and precipitated into DMF followed by distillative removal of H_2O from the highly swollen gel under reduced pressure. To a stirred suspension of the activated polymer in ice-cooled pyridine (25ml, 313mmol) was added SOCl_2 dropwise (15ml, 207mmol). The mixture reacted for 1h at 0°C, 2h at room temperature and a further 6h at 70°C. The carboxycellulose acid chlorides (COCCl) formed can be isolated by precipitation into acetone and drying in vacuum at 40°C (method A) or used without isolation (method B) for the following amidation reactions. The halogen contents of the COCCl samples are given in Table 1. IR (KBr): 1744 cm^{-1} (COCl), 752 cm^{-1} and 680 cm^{-1} (CCl)

Carboxycellulose benzyl amides (COCBA)

The isolated COCCl prepared according to method A was suspended in pyridine (26ml, 325mmol), and then benzyl amine (3.1ml, 28mmol) was added under stirring. After a reaction time of 6 h at 70°C the resulting solution was evaporated approximately to a half of the key volume. After acidification with diluted HCl the carboxycellulose benzyl amide (COCBA) was precipitated into distilled H_2O , washed with distilled H_2O and dried in vacuum at 40°C.

If the COCCl was not isolated (method B), the synthesis was carried out as follows: To the stirred COCCl solution pyridine (10ml, 125mmol) and then a mixture of benzyl amine (4.1ml, 37mmol) in pyridine (10ml, 125mmol) was added. The reaction mixture was heated for 6h at 70°C and the formed carboxycellulose benzyl amide (COCBA) was isolated by precipitation into distilled H_2O . After washing with distilled H_2O the COCBA samples were dried in vacuum at 40°C. The nitrogen contents of the COCBA samples are given in Table 2. IR (KBr): 3288 cm^{-1} (NH), 3080-3030 cm^{-1} (ar-CH), 1656 cm^{-1} and 1528 cm^{-1} (NC=O), 700 cm^{-1} (NH)

RESULTS AND DISCUSSION

The amidation of the C-6-carboxycellulose (COC) is impossible without activation of the COOH-group. For this reason we investigate the activation of the carboxy groups of COC by the well-known acid chloride formation with chlorinating agents like SOCl_2 in DMF/ pyridine mixtures according to a procedure used for carboxymethyl cellulose (CMC) [4].

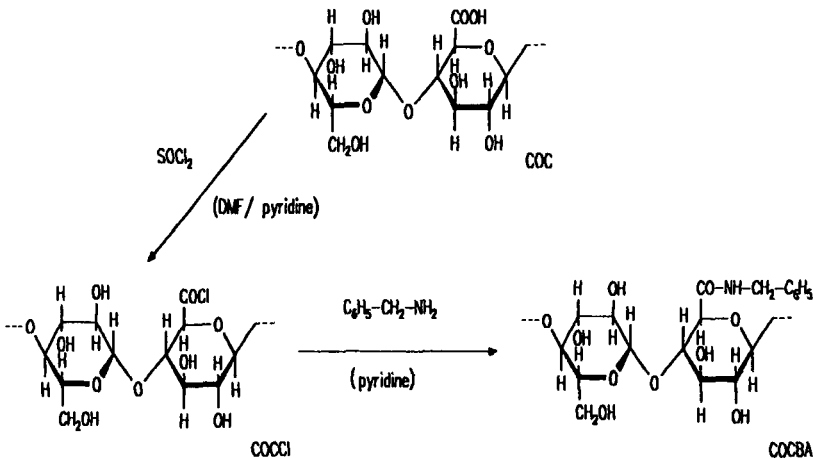


Figure 1. Reaction scheme

After a suitable pretreatment consisting of the precipitation of an aqueous sodium COC solution in DMF and the removal of H_2O from the highly swollen gel by distillation under reduced pressure the chlorination of the carboxy group with SOCl_2 in a DMF/ pyridine mixture yields the easily hydrolyzable carboxy cellulose acid chloride (COCCI, Figure 1.).

Upon addition of SOCl_2 to the mixtures of carboxycellulose and pyridine solution an exothermal reaction takes place and the mixture gradually darkens. This color change increases with increasing temperature from 0°C (yellow) to 70°C (red-brown). It was found that a molar ratio of $\text{NaCOC} : \text{SOCl}_2 : \text{pyridine} = 1 : 38 : 57$ is the most effective one investigated for a nearly complete conversion of the COONa-groups into the corresponding acid chloride (Table 1.). It is remarkable that a high conversion up to $\sim 91\%$ of the total amount of the COONa-groups is reached, if the polymer dissolves in the reaction mixture during the reaction.

It is known that the reaction of cellulose with SOCl_2 yields chlorodeoxy cellulose. For that reason we examined the possibility of this side reaction for the acyl chloride formation of COC by the following experiment. The isolated COCCI samples were hydrolyzed with H_2O for 48h at room temperature and characterized by the subsequent determination of the residual chlorine content. Under these conditions a complete hydrolysis of acyl chlorides takes place, but the deoxychloride bonds are stable. The

residual amount reaches values of 0.41 to 2.7%Cl according to degree of substitution of the replacement of OH by a Cl atom of 0.02 to 0.15 (Table 2.).

Table 1. Formation of the carboxycellulose acid chlorides (COCCI) in dependence on the molar ratio anhydro glucose unit (AGU): SOCl_2 : pyridine.

COCCI-sample (method A)	Molar ratio AGU: SOCl_2 : pyridine	Cl- content (%) ^a	Conversion of the COONa- group (%)
1	1 : 15 : 23	12.29	62.0
2	1 : 25 : 37	14.27	72.0
3	1 : 38 : 57	18.03	91.0

^a Determined by elemental analysis (19.81% Cl = 100%conversion).

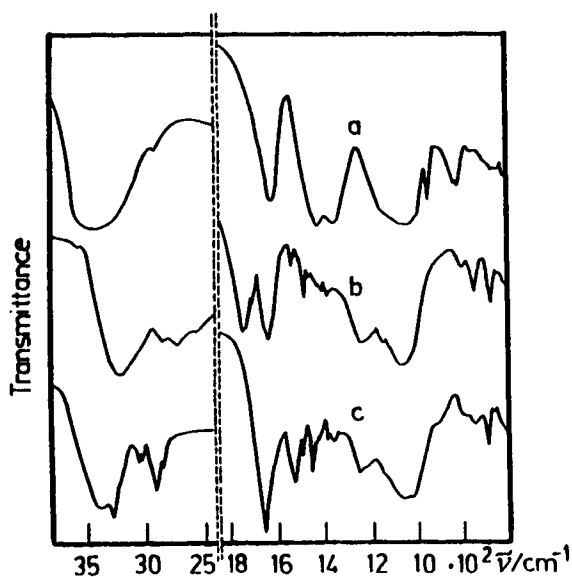


Figure 2. IR spectra of sodium carboxycellulose (a), carboxycellulose acid chloride (COCCI, b) and carboxycellulose benzyl amide (COCBA, c)

Figure 2. shows the IR spectra of the COCCI obtained (e.g. sample 2, curve b) in comparison with that of the starting COC in the sodium salt form (curve a). For the COCCI samples a new absorption appears in the $\nu_{\text{C=O}}$ region at 1744cm^{-1} indicating the conversion of COONa- into COCl- groups. Furthermore, two new signals can be observed at 752cm^{-1} and 680cm^{-1} , respectively. These adsorptions are due to $\nu_{\text{C-Cl}}$ vibrations

whereby the adsorption at 752cm^{-1} can be assigned to chlorodeoxy carboxycelluloses according to the results obtained by hydrolysis. As concluded from the work of Sakamoto [5], the chlorination takes place especially at the OH-group in the C-6 position. The peak at 680cm^{-1} can be assigned to the C-Cl valence vibration at the COCl-group. After amidation (see curve c) this signal is not detectable as result of the reaction of the acyl chloride with the amine.

The COC-chlorides are decomposed in the presence of humidity yielding a black gum-like product. The decomposition of COCCL samples occurs significantly faster than that of the CMC-chlorides.

The amidation of the COCCL samples with benzyl amine was carried out both with the isolated COCCL (preparation according to method A - see Experimental) and without isolation (method B) for 6h at 70°C in pyridine. The carboxy cellulose benzyl amides (COCBA) formed can be isolated by precipitation with distilled H_2O after evaporation to a half of the key volume and acidification with diluted HCl.

In Table 2. all COCBA samples synthesized are summarized. A high conversion up to 92% of all COCl-groups (sample 6) takes place, as a homogeneous reaction mixture is formed. In this case water-insoluble products are isolated in accordance to a high content of amide groups (Table 2.). The products isolated were soluble in DMF as well as DMSO, but insoluble in H_2O .

Table 2. Amidation of COC-chlorides with benzyl amine (BA) in pyridine for 6h at 70°C .

COCBA-sample	COCl-prepn. method	Molar ratio BA: pyridine	Precipitant	N-content (%) ^a	Conversion of the COCl-groups (%)	Residual Cl-content (%)
1	A	1: 11.6	H_2O	5.12	78.8	— ^b
2	A	1: 11.6	acetone	0.60	9.2	0.41
3	A	1: 11.6	acetone	2.73	42.0	2.22
4	B	1: 6.8	H_2O	4.36	67.1	2.74
5	B	1: 6.8	H_2O	3.08	47.4	2.04
6	B	1: 6.8	H_2O	5.98	92.0	1.15

^a Determined by elemental analysis (6.5%N = 100% conversion).

^b Not determined.

It is obvious that the amidation reaction without isolation of the COCCL yields a higher conversion (homogeneous reaction) in comparison with that carried out with isolated COCCL samples. Therefore the following reactions should be carried out preferably without isolation of the COCCL derivatives. Figure 2. shows a typical IR-spectra of COCBA (e.g. sample 1, curve c). The absorptions at 3288cm^{-1} (ν_{NH}), $3080\text{-}3030\text{cm}^{-1}$ ($\nu_{\text{ar-CH}}$), 1656cm^{-1}

($\nu_{C=O}$ amide I) and 1528cm^{-1} (δ_{N-H} amide II) indicate the presence of amide groups.

In the ^{13}C -NMR spectra of COCBA the typical peaks of COC occurs and, in addition, signals which can be assigned to the benzyl amide structure. The signals at 175.5 (C-6') and 149.1/ 149.6ppm (C-6'') may be attributed to C-6 carbon atoms of the anhydroglucose unit bearing a carboxy- and an amide group, resp. (Figure 3.). Peaks at 125.2, 127.5, 129.6 and 138.4ppm can be assigned to the carbon atoms C-(8-11) of the aromatics. From ^{13}C -NMR it can be concluded that the polymer consists of 3 different repeating units: glucose, C-6-carboxyglucose, and C-6-carboxyglucose benzyl amide.

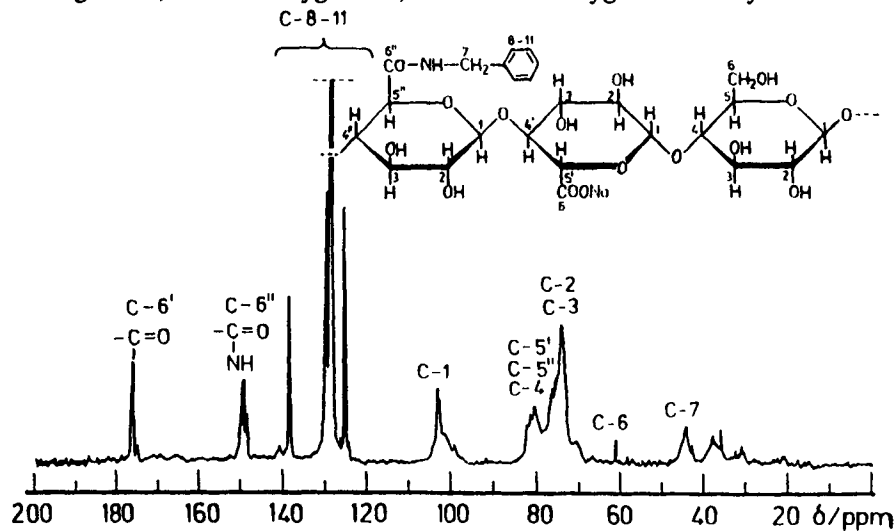


Figure 3. ^{13}C -NMR spectra of C-6-carboxycellulose benzyl amide

REFERENCES

- [1] T.J. Painter *Carbohydr. Res.* **55** (1977) 95
- [2] Th. Heinze, D. Klemm, F. Loth, I. Nehls *Angew. Makromol. Chem.* **178** (1990) 95
- [3] M. Schnabelrauch, Th. Heinze, D. Klemm, I. Nehls, J. Kötz *Polymer Bull.* **27** (1991) 147
- [4] G. Csanady, P. Narayanan, K. Müller, W. Wegscheider, G. Knapp *Angew. Makromol. Chem.* **170** (1989) 159
- [5] M. Sakamoto, K. Furuhata, H. S. Chang, N. Aoki *Carbohydr. Res.* **230** (1992) 151

ACKNOWLEDGEMENT

K. Rahn wish to thank the "Stifterverband für die Deutsche Wissenschaft" for financial support.

29 Effects of solvent addition to acetylation medium on cellulose triacetate prepared from low-grade dissolving pulp

S Saka and T Takahashi – Department of Wood & Paper Science, Faculty of Agriculture, Kyoto University, Kyoto, Japan 606-01

Shiro Saka and Tadashi Takahashi— Department of Wood & Paper Science, Faculty of Agriculture, Kyoto University, Kyoto, Japan 606-01

ABSTRACT

As cellulose triacetate is prepared from low-grade dissolving pulp, a considerable amount of the insoluble residue is present in the acetylation medium of the acetic acid / acetic anhydride / sulfuric acid system. As one of the remedies for reducing the insoluble residue, a solvent was added to the acetylation medium and the effects of the solvent addition on the amount of insoluble residue formed were studied. To do so, 17 different solvents were selected so as to cover a wide range of solubility parameters. The obtained results clearly indicated that the addition of the solvent affects the amount of insoluble residue and that nitromethane, nitroethane, dichloroacetic acid and methylene chloride were very effective for its reduction. A new acetylation system with such an appropriate solvent would provide a clue as to an industrial usage of the low-grade dissolving pulps for cellulose acetate production.

INTRODUCTION

Cellulose triacetate being important in the fiber and textile industries requires high quality cellulose as a starting material.¹⁾ This is because the low-grade dissolving pulps contain more hemicelluloses and the formation of hemicellulose acetates such as xylan acetate and glucomannan acetate, results in industrial problems such as filterability, turbidity (haze) and false viscosity. Although a considerable effort has been made since the mid-1950s to explain the relationships between the solution properties of the cellulose acetate and contaminated hemicellulose acetate,²⁻⁸⁾ viscose grade wood pulps with an α -cellulose content of less than 90% still cannot be used for manufacturing cellulose acetate.

In our previous work,^{9, 10)} we have studied cellulose triacetate prepared from softwood sulfite dissolving pulps with an α -cellulose content of 87.5%. The first problem faced was a substantial amount of insoluble residue present in the acetylation medium of the acetic acid / acetic anhydride / sulfuric acid system. This insoluble residue retained a fiber structure of swollen form, resulting in one of the industrial problems, filterability.

Characterization of the insoluble residue⁹⁾ showed that it was composed of cellulose triacetate (CTA) and glucomannan triacetate (GTA) in aggregate with each other in the acetylation medium due to their compatible nature. In addition to such chemical effects of the molecular interactions, ultrastructural effects of glucomannan distribution in pulp fibers were found to be involved in the formation of insoluble residues. Therefore, the amount of insoluble residue can be expected to be reduced if chemical effects and/or ultrastructural effects are decreased during acetylation.

As one of remedies, the pretreatment of low-grade dissolving pulps with mixtures of acetic acid and sulfuric acid was found to reduce both the chemical and ultrastructural effects of pulp fibers in the following acetylation, resulting in reducing the amount of the insoluble residue.¹⁰⁾ The use of higher amounts of sulfuric acid as a catalyst was also found to reduce the insoluble residue formed.¹⁰⁾

In this study, a solvent was added to the acetylation medium of acetic acid / acetic anhydride / sulfuric acid system and the effects of the solvent addition on the amount of the insoluble residue formed were studied. To do so, seventeen different solvents were selected to cover a wide range of solubility parameters of the solvents.

EXPERIMENTAL

Sulfite softwood dissolving pulp with an α -cellulose content of 87.5% was used for preparing cellulose triacetate as described in the previous paper.⁹⁾ As cellulose triacetate was prepared from this pulp, a large amount of insoluble residue was present in the acetylation medium of an acetic acid / acetic anhydride / sulfuric acid system.⁹⁾ Therefore, in this work, a solvent was added to this acetylation medium to study the effects of the solvent on the amount of insoluble residue formed. The solvents used in this study are given in Table 1.

The low-grade dissolving pulps (1 part) were thus acetylated with a solution of acetic acid (160 parts), acetic anhydride (7parts) and sulfuric acid (0.1 part) with a solvent (51 parts) for 3 h at 40 °C, followed by stirring overnight at 20 °C. The solutions were then spun in a centrifuge at 7000 rpm for 30 min. After the tubes were removed carefully, the supernatants pipetted away and precipitated substances were washed repeatedly with mixtures of fresh acetic acid and the solvent used in the system (160:51 in a weight ratio) by centrifugation to obtain the insoluble portions. The supernatants collected were, on the other hand, concentrated and poured into deionized water to precipitate the soluble portions. The insoluble and soluble portions were washed as described previously.⁹⁾

The degree of substitution (DS) of these samples was determined by a titration method,¹¹⁾ while neutral sugar compositions were determined by an alditol-acetate procedure¹²⁾ using conditions described in a previous paper.⁹⁾ For structural observations, some micrographs of the insoluble residues were taken in an acetylation system with a different solvent.

RESULTS AND DISCUSSION

It has been known in our previous work⁹⁾ that, when cellulose triacetate is prepared from low-grade sulfite dissolving pulp, a substantial amount of insoluble residue is present in the acetylation medium of the acetic acid / acetic anhydride / sulfuric acid system. Therefore, in this study, a solvent was added to the above acetylation medium with 1:3 weight ratio of solvent to acetic acid to study the effects of the solvent addition on the reduction of the insoluble residue content in the acetylation medium.

Table 1 shows selected solvents excluding the alkaline, unstable and reactive solvents in the reaction medium. The acetylation system with acetic acid (No.10 in Table 1) was also included just for comparison as a control reaction system without any addition of the solvent. Compared with acetic acid, 20.7 (MPa)^{1/2} in its solubility parameter (SP), the selected solvents could cover a wide range of the SP values from 16.6 to 26.0 (MPa)^{1/2}. Also included in Table 1 is the insoluble residue content in the acetylation medium with a designated solvent.

Figure 1 shows a relationship between the amount of insoluble residue and the SP of the solvent added to the acetylation medium. Numbers correspond to solvents as in Table 1. It is very apparent that compared with 15.1% in a control reaction system (acetic acid, No.10), the results are varied from 0.6% to 36.2% in insoluble residue contents, indicating that large effects of the solvent addition exist on the amount of the insoluble residue in the acetylation medium. Furthermore, it is noted that with an increase in the SP

Table 1 The insoluble residue content in the acetylation medium with a solvent added and its chemical compositions.

Solvent	Solubility parameter (MPa) ^{1/2}	Insoluble residue (wt%)	Chemical Compositions (mol%)		
			Glucose	Mannose	Xylose
1. <i>n</i> -Butyl chloride	16.6	36.2	80.0	18.9	1.1
2. 4-Chlorotoluene	18.0	28.1	79.4	20.6	—
3. 1,2-Dichloroethane	18.2	9.2	55.2	44.8	—
4. Methylcellosolve acetate	18.8	29.3	78.7	21.3	—
5. Ethylbromide	19.6	19.9	66.5	33.5	—
6. Methylene chloride	19.8	4.8	58.2	29.9	11.9
7. 2-Nitropropane	20.3	9.1	71.8	28.2	—
8. Bromobenzene	20.3	17.2	73.6	25.3	1.1
9. Nitrobenzene	20.5	7.4	57.9	42.1	—
10. Acetic acid	20.7	15.1	71.1	28.2	0.7
11. 1-Nitropropane	21.1	7.1	70.3	29.7	—
12. Methylbenzoate	21.5	24.1	80.1	19.9	—
13. 1-Bromonaphtalene	21.7	20.2	68.3	26.8	4.9
14. Dimethyl phthalate	21.9	15.6	70.5	29.5	—
15. Dichloroacetic acid	22.5	0.8	—	—	—
16. Nitroethane	22.7	3.0	69.2	30.8	—
17. Nitromethane	26.0	0.6	42.6	57.4	—

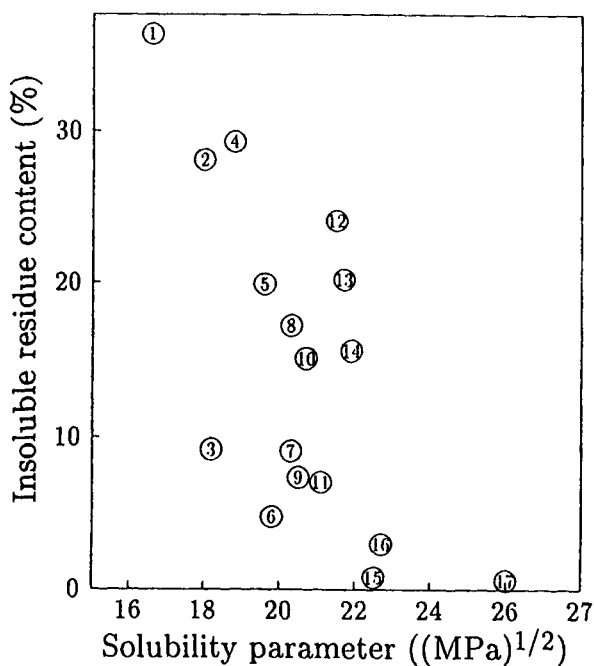


Fig. 1 The soluble residue content vs. solubility parameter of the solvent added to the acetylation medium. Numbers correspond to the solvents as in Table 1.

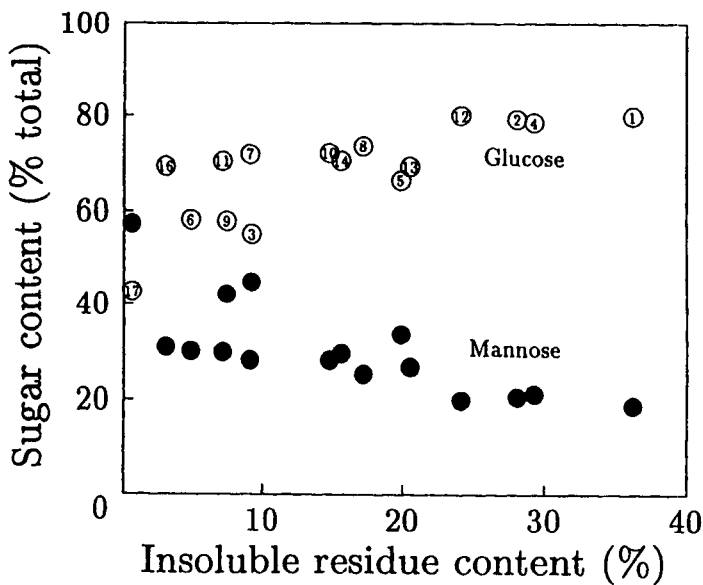


Fig. 2 The sugar content vs. insoluble residue content for acetylation medium with a solvent added. Numbers correspond to solvents as in Table 1.

values, the amount of insoluble residue has a tendency to decrease.

The effective solvents for reducing the insoluble residue are, therefore, nitromethane (0.6%), dichloroacetic acid (0.8%), nitroethane (3.0%), methylene chloride (4.8%), 1-nitropropane (7.1%), nitrobenzene (7.4%), 2-nitropropane (9.1%) and 1,2-dichloroethane (9.2%).

The chemical compositions of the insoluble residue in each reaction system are also given in Table 1. It is apparent that, in addition to glucose, the insoluble residue contains a high proportion of mannose, with a limited amount of xylose except for the reaction system with methylene chloride. This result is in good agreement with the findings of our previous work⁹⁾ that the insoluble residue is composed of cellulose triacetate (CTA) and glucomannan triacetate (GTA) in aggregate with each other at the molecular level by their mutual interactions. Therefore, GTA is involved in the formation of the insoluble residue for all acetylation systems studied.

However, a closer inspection of the results in Table 1 shows a large variation in mannose content from a maximum of 57.4% to a minimum of 18.9%. Therefore, a relationship between the insoluble residue content and its sugar content for glucose and mannose was studied (Fig. 2). From Fig. 2, it is apparent that the glucose content decreases with a decrease in the insoluble residue content, whereas the mannose content increases.

Based on a study on the chemical compositions of the isolated glucomannan from the low-grade pulp used in this study, the molar ratio of mannose to glucose is known to be 3.2:1.⁹⁾ With the value of 3.2, therefore, the contents of the GTA and CTA can be computed. Figure 3 shows the obtained ratio of CTA to GTA against the insoluble residue content. It is apparent that with a decrease in the insoluble residue content, the ratio of CTA to GTA decreases.

Comparative studies of acetylation in the model experiments¹⁰⁾ indicated that the insoluble residue from the low-grade dissolving pulp is formed by

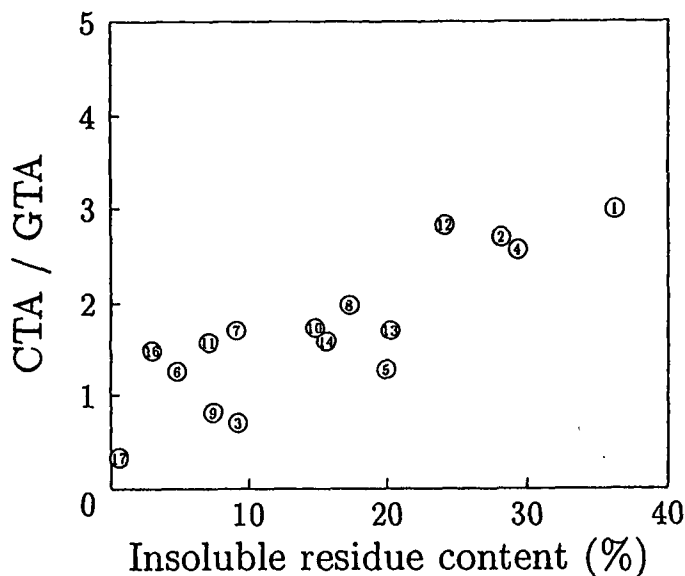


Fig. 3 The ratio of the CTA to GTA content in the insoluble residue vs. insoluble residue content. Numbers correspond to solvents as in Table 1.

ultrastructural effects of the pulp fibers and the chemical effects of the molecular interactions of CTA and GTA. The former effects originate from the ultrastructural distribution of residual glucomannan in the dissolving pulp, whereas the latter effects are due to molecular aggregation of CTA and GTA by their compatible nature. It is, therefore, possible to get a reduction in the amount of insoluble residue if chemical effects and/or ultrastructural effects are decreased during acetylation. Furthermore, our previous study¹⁰⁾ indicated that as the ultrastructural effects are decreased, the ratio of CTA to GTA content in the insoluble residue is decreased. Therefore, the results in Fig.3 suggest the reduction of the ultrastructural effects as the insoluble residue content decreases.

Figure 4 shows the light micrographs of the insoluble residue after acetylation. The structural changes are evident as the insoluble residue content decreases; the residues in the acetylation system with 4-chlorotoluene with the residual content of 28.1% are more likely to be original pulp fibers with a limited swelling. However, fiber residues in the control acetylation system with acetic acid (15.1%) are greatly swollen with retaining the fiber structure. In the acetylation system with 2-nitropropane with the lower residual content of 9.1%, the acetylated fibers are reduced to fiber fractions and finally such fiber fractions disappear in the reaction system with nitromethane (0.6%). Such changes of the fiber structure would make the pulp fibers swell more readily during acetylation and allow them to solubilize greater to the acetylation medium. These lines of evidence seem to be parallel to a process to reduce the ultrastructural effects of the pulp fibers, thus supporting the suggestion above from Fig.3.

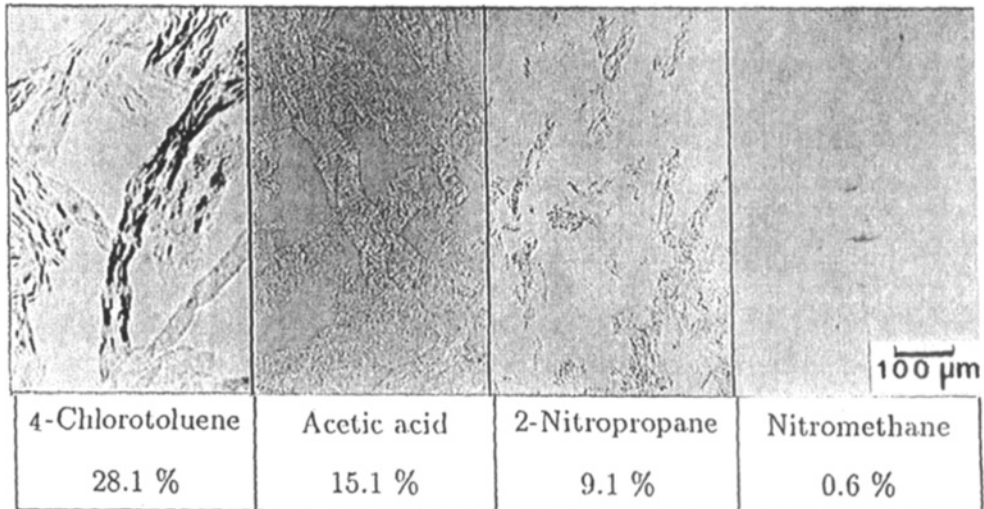


Fig. 4 Light micrographs of the insoluble residue after acetylation with a solvent designated. The value shows the insoluble residue content.

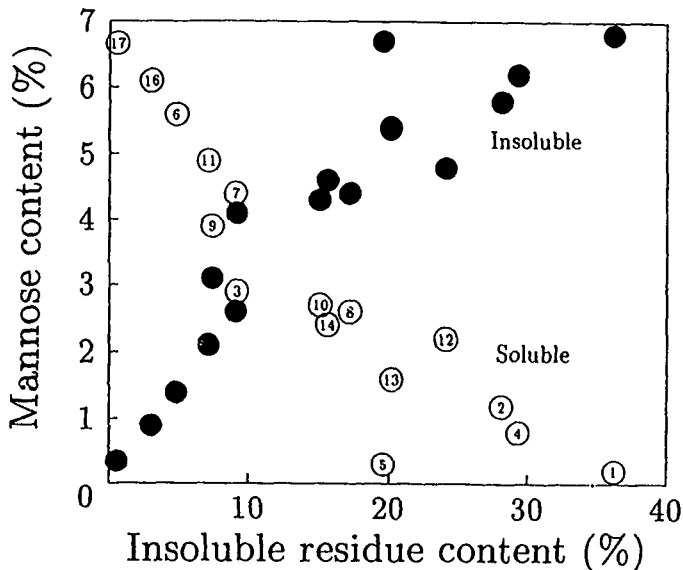


Fig. 5 Insoluble residue content vs. mannose content of the original pulp (7.0%) divided into soluble and insoluble portions.

Based on these results, it may be concluded that, in the reaction system with a small insoluble residue content, the great reduction of the insoluble residue is not only due to the ultrastructural effects reduced as proved above but also due to the chemical effects reduced in which the solubilities of CTA and GTA are improved with mixtures of the acetylation medium with the solvent added.

The determination of the chemical compositions of the original pulps used in this study indicated that it contains 7.0% mannose. Thus, the proportions of the total mannose in the soluble portion and insoluble residue were computed as shown in Fig. 5. It is apparent from Fig. 5 that as the insoluble residue decreases in content, the proportion of the mannose in the insoluble portion decreases, whereas that in the soluble portion, in turn, increases. This implies that some of the GTA which has formed the insoluble residue in the acetylation medium is no longer involved in its formation and moved to the soluble portion. Therefore, the addition of the appropriate solvent to the acetylation medium could solve a problem on the formation of the insoluble residue as the low-grade dissolving pulps are used for cellulose acetate preparation.

In conclusion, a new acetylation system with an appropriate solvent can provide a clue as to an industrial usage of the low-grade dissolving pulps for cellulose acetate production.

REFERENCES

- 1) Ichino, M.: *Nikkakyo Geppo*, 39, 25-32 (1986).
- 2) Steinmann, H.W.; White, B.B.: *TAPPI*, 37, 225-232 (1954).
- 3) Bradway, K.E.: *ibid.*, 37, 440-446 (1954).
- 4) Wells, F.L.; Schattner, W.C.; Walker, A.Jr.: *ibid.*, 46, 581-586 (1963).

- 5) Neal, J.L.: *J. Appl. Polym. Sci.* 9, 947-961 (1965).
- 6) Wilson, J.D.; Tabke, R.S.: *ibid.*, 57, 77-80 (1974).
- 7) Ueda, K.; Saka, S.; Funaki, Y.; Soejima, S.: *Mokuzai Gakkaishi*, 34, 346-353 (1988).
- 8) Ueda, K.; Saka, S.; Soejima, S.: *TAPPI*, 71, 183-187 (1988).
- 9) Matsumura, H.; Saka, S.: *Mokuzai Gakkaishi*, 38, 270-276 (1992).
- 10) Matsumura, H.; Saka, S.: *ibid.*, 38, 862-868 (1992).
- 11) Atsuki, K.: "Sen'isokagaku oyobi Kogyo" Maruzen 1956, p.418-419.
- 12) Borchardt, L.G.; Piper, C.V.: *TAPPI*, 53, 257-260 (1970).

30 Photofunctional cellulosic materials

K Arai and S Sano – Faculty of Engineering, Gunma University,
Kiryu, Gunma 376, Japan

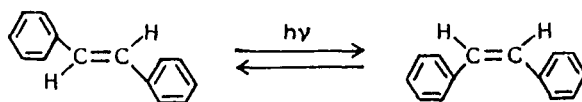
Abstract

As photofunctional materials, cellulose stilbene-4-carboxylate (SB-cellulose) and cellulose 2-methylstilbene-5-carboxylate (MSB-cellulose) were prepared and photoregulation of functions of the derivatives under irradiation with UV lights was investigated. Stilbene moieties in the SB-cellulose were found to undergo only irreversible isomerization from the trans to cis form under irradiation with UV light. However, 2-methylstilbene moieties in the MSB-cellulose do reversible isomerizations from the trans to cis form under irradiation with UV light above 290nm and the cis to trans form with about 250nm, although the cis to trans isomerization was not complete. Regulation of swelling abilities of MSB-cellulose in water and in benzene was examined under irradiation with UV light. The swelling ability in water was found to increase under irradiation with UV light above 290nm and decrease with about 250nm. On the other hand, that in benzene decreased under irradiation with UV light above 290nm and increased with about 250nm. Width of changes in the swelling ability under alternate irradiations with UV light was found to decrease only slightly even after 5 times of repeated alternate irradiation.

Introduction

Photoregulation of functions of polymers containing photochromic moieties, such as azobenzene, spiropyran, stilbene, and fulgides has been the subject of many investigations¹⁻¹⁰⁾. In the present paper, we report on the preparation of cellulose

derivatives containing stilbene and 2-methylstilbene moieties, and on the photoregulation of swelling abilities of the derivatives obtained. Stilbene is known to undergo a photo-induced trans-cis isomerization resulting in a change in the dipole moment:



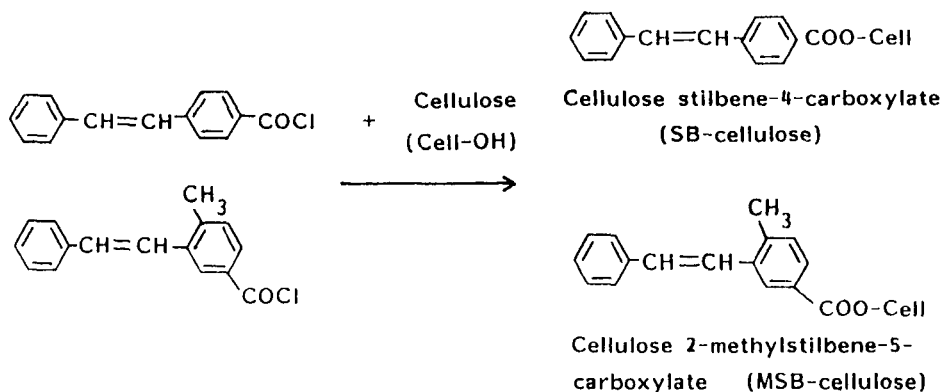
Photoregulation of the polarity of the stilbene moieties in the cellulose derivatives under irradiation with UV light was expected to make possible the reversible regulation of swelling ability of the derivatives. In this case, however, the isomerization of trans-stilbene is known to be accompanied by side reactions such as formation of dihydrophenanthrene. Thus we prepared a cellulose derivative containing the 2-methylstilbene moiety, which was expected to prevent the side reaction, as well as that containing the simple stilbene moiety.

Experimental

Microcrystalline cellulose (DP=120) was dissolved in copper(II) hydroxide-ethylenediamine aqueous solution and then poured into an excess volume of ammonium sulfate aqueous solution to be regenerated, and used as cellulose.

The cellulose was reacted with stilbene carbonyl chloride or 2-methylstilbene carbonyl chloride in pyridine-dichlorobenzene (1:1 by volume) mixture at 120 °C to produce the corresponding cellulose derivatives. The derivatives are called as SB-cellulose and MSB-cellulose, respectively.

Reaction scheme for the preparation of SB- and MSB-cellulose are shown below:



Degree of substitution(DS) of the derivatives was determined by elemental analysis.

Swelling ability was determined as follows: Cellulose derivative was suspended in water or in benzene and irradiated with UV light for a given time, and then filtered and pressed in a sintered glass filter to obtain a wet mat. Swelling ability was calculated from the weights of the mat before and after drying.

Results and Discussion

Typical changes in DS of SB-cellulose and MSB-cellulose with the reaction time are shown in Fig. 1. The DS's are found to increase with the reaction time, but they show a tendency to level-off at about 1.9 for SB-cellulose and at 1.7 for MSB-cellulose, respectively. The MSB-cellulose with DS of 1.7 was insoluble in all solvents. Repeating the same reaction to the cellulose once more increased the DS's to 2.4 for SB-cellulose and to 2.2 for MSB-cellulose, respectively. They were soluble in some organic solvents.

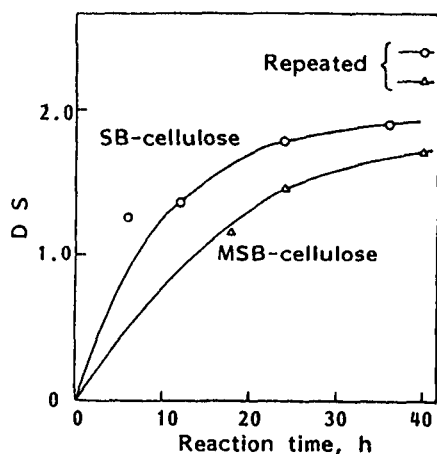


Fig.1 Typical changes in degree of substitution(DS) with reaction time. [cellulose] 0.012mol/l as AGU. [stilbenecarbonyl chloride] 0.039mol/l

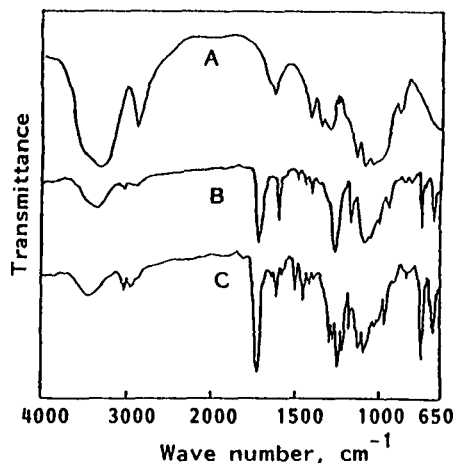


Fig.2 IR absorption spectra of microcrystalline cellulose(A), SB- and MSB-celluloses(B and C) with DS of 1.7 and 1.9

Fig.2 shows IR absorption spectra of the cellulose derivatives together with that of original cellulose. In the spectra of the derivatives, specific absorption peaks assigned to ester bonds, alkenyl double bonds, and benzene derivatives are found, and the products are confirmed to be SB-cellulose and MSB-cellulose, respectively.

Fig.3 shows changes in the UV absorption spectrum of SB-cellulose dissolved in chloroform after irradiation with UV light above 290nm. An absorption peak at

around 250nm, which is assigned to the cis form, increases. These changes suggest that the trans stilbene moieties in SB-cellulose are isomerized under irradiation with UV light to the cis form. Lack of an isosbestic point for the spectrum in the figure is thought to be due to the coexistence of side reactions. Isomerization of the cis stilbene moiety to the trans form was also examined under irradiation with UV light of around 250nm. However, the absorption spectrum was not changed. Thus the isomerization of the trans stilbene moiety in SB-cellulose to the cis form was supposed to be irreversible.

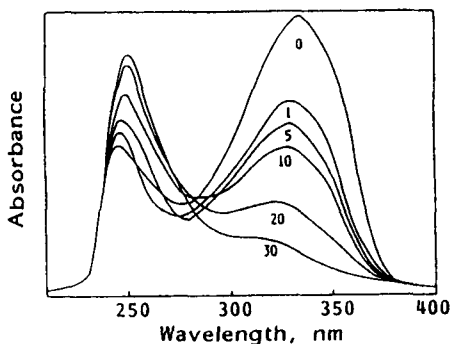


Fig.3 Changes in UV absorption spectrum of SB-cellulose (DS=1.8) dissolved in chloroform under irradiation with UV light above 290 nm. Numbers in figure indicate the irradiation time in minutes

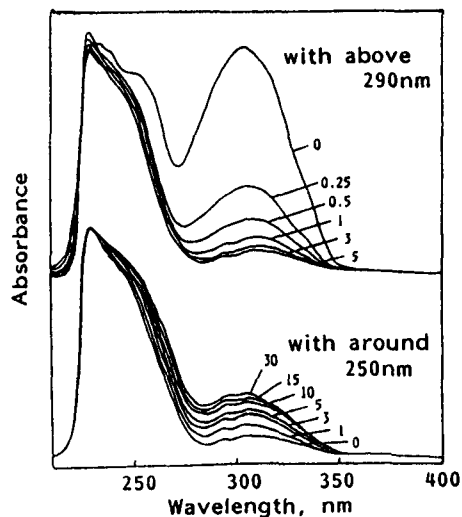


Fig.4 Changes in UV absorption spectrum of MSB-cellulose (DS=2.2) dissolved in 1,2-dichloroethane under irradiation with UV light above 290nm (above) and subsequent irradiation with that of about 250nm (below)

Fig.4 shows the changes in UV absorption spectrum of MSB-cellulose dissolved in 1,2-dichloromethane after irradiation with UV light. In the above group of the spectra, an absorption peak at around 300nm, which is assigned to the trans form of the 2-methylstilbene moiety, is found to decrease under irradiation with UV light above 290nm, with the irradiation time. This change indicates the isomerization of the trans 2-methylstilbene moieties in MSB-cellulose to the cis form. The MSB-cellulose irradiated with UV light above 290nm for 5 minutes was then irradiated with that of around 250nm. The change in the spectrum is shown below in the figure. The peak at around 300nm in the spectrum is found to increase with the irradiation time, indicating that the cis 2-methylstilbene moieties are isomerized to the trans form with the irradiation, although the isomerization is not complete

compared with the original peak height of the trans form.

Fig.5 shows the photo-induced reversible changes in an absorption peak at around 300nm in the UV spectrum of MSB-cellulose under alternate irradiations with UV light above 290nm and of around 250nm. The peak height is found to be changed reversibly with alternate irradiation, but the width of the changes in the absorption peak decreases.

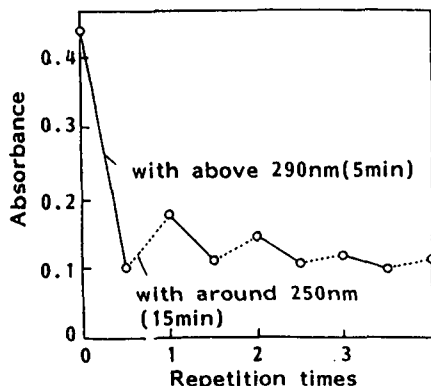


Fig.5 Photo-induced reversible changes in an absorption peak at about 300nm in UV spectrum of MSB-cellulose under alternate irradiations with UV lights above 290nm and of around 250nm

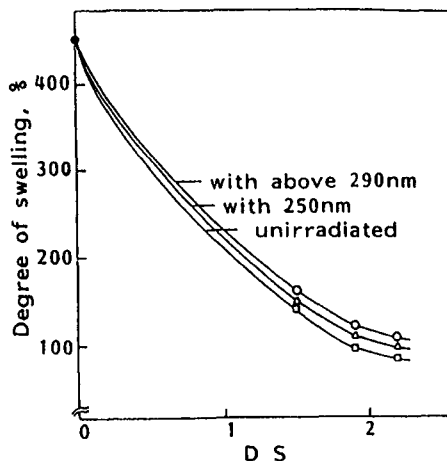


Fig.6 Changes in degree of swelling of MSB-cellulose in water with increasing degree of substitution (DS), and under irradiation with UV lights above 290nm for 60 min. and of around 250nm for 120 min.

Photoregulation of swelling abilities of MSB-cellulose in water and in benzene was examined. Fig.6 shows the changes in degree of swelling of MSB-cellulose in water with increasing DS of MSB-cellulose and under irradiation with UV light. The degree of swelling is found to decrease considerably with increasing DS, due to substitution of hydrophilic hydroxyl group by 2-methylstilbenecarboxylate. The degree of swelling increases after irradiation with UV light above 290nm and decreases after subsequent irradiation with that of around 250nm. These changes are believed to result from the changes in polarity of the 2-methylstilbene moieties in the MSB-cellulose, due to the isomerizations.

Fig.7 shows the changes in degree of swelling of MSB-cellulose in benzene with increasing DS and under irradiation with UV light. The degree of swelling in benzene is found to increase considerably with the increasing DS. This increase is also explained by the substitution of hydroxyl group by the hydrophobic 2-methylstilbenecarboxylate group. The degree of swelling decreases after irradiation with UV light above 290nm and increases after subsequent irradiation with that around 250nm. These changes again result from the changes in polarity of the 2-methyl-

stilbene moieties in MSB-cellulose, due to the isomerizations.

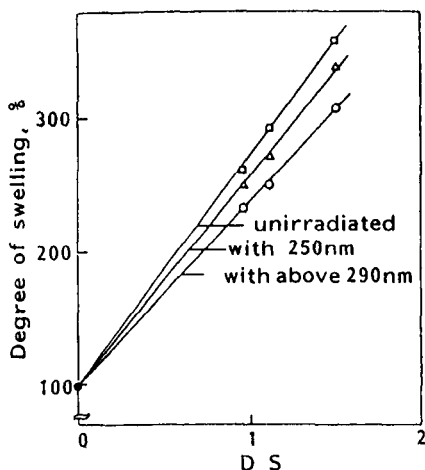


Fig.7 Changes in degree of swelling of MSB-cellulose in benzene with increasing DS, and under irradiation with UV lights above 290nm for 60min. and around 250nm for 120min.

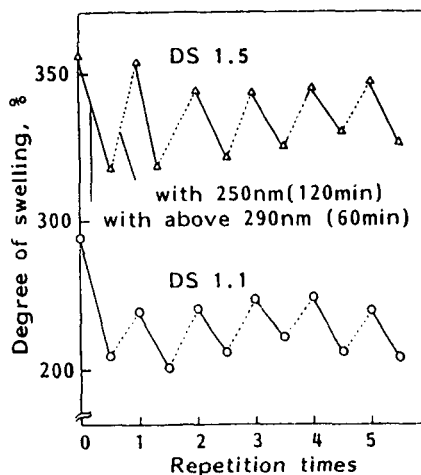


Fig.8 Photo-induced reversible changes in degree of swelling of MSB-cellulose in benzene under alternate irradiations with UV lights above 290nm and around 250 nm

Fig.8 shows the photo-induced reversible changes in degree of swelling of MSB-cellulose in benzene after alternate irradiations with UV light above 290nm and around 250nm. The degree of swelling is found to be changed reversibly with the alternate irradiations and the width of the change in the degree of swelling decreases only slightly even after 5 times of the repeated alternate irradiations. Also for swelling ability of MSB-cellulose in water, similar, but less changes were found with the alternate irradiations.

References

- 1)K. Ishihara et al., *J. Polym. Sci., Polym. Chem. Ed.*, 1984, 22, 121, 617, 3687
- 2)M. Irie and W. Schnabel, *Macromolecules*, 1985, 18, 394
- 3)H. Yamamoto and A. Nishida, *Macromolecules*, 1986, 19, 944
- 4)O. Pieroni et al., *J. Am. Chem. Soc.*, 1985, 107, 2990
- 5)H. G. Heller and J. R. Langan, *J. Chem. Soc., Perkin Trans. 2*, 1981, 341
- 6)P. J. Darcy et al., *J. Chem. Soc., Perkin Trans. 1*, 1981, 202
- 7)K. Arai and H. Udagawa, *Makromol. Chem., Rapid Commun.*, 1988, 9, 797
- 8)K. Arai and H. Udagawa, *J. Soc. Fiber Sci. Tech. Jpn.*, 1990, 46, 150, 491
- 9)K. Arai and H. Satoh, *J. Appl. Polym. Sci.*, 1992, 45, 387
- 10)K. Arai, S. Sano and H. Satoh, *J. Mater. Chem.*, 1992, 2, 1257

31 Reactions of bromodeoxycellulose with various thiols in lithium bromide/*N,N*-dimethylacetamide

N Aoki, K Furuhata and M Sakamoto – Department of Organic and Polymeric Materials, Tokyo Institute of Technology, O-okayama, Meguro-ku, Tokyo, 152 Japan

Abstract

6-Bromo-6-deoxycelluloses of a high degree of substitution were treated with various thiols under homogeneous conditions in lithium bromide/*N,N*-dimethylacetamide in the presence of triethylamine. At high temperatures, appreciable unfavorable side reaction, dehydrobromination yielding 3,6-anhydroglucose and/or 5,6-glucosene units took place. Under favorable conditions, more than 50% of bromine was substituted with thiols. Thiols used in this work include 2-hydroxyethanethiol, 2-aminoethanethiol, 4-aminobenzenethiol, 3-mercapto-propionic acid, 2-mercaptosuccinic acid, 2-mercaptobenzoic acid and cysteine. Solubilities of the products containing carboxyl, amino and/or hydroxyl groups were studied. Aminophenylthio-deoxycellulose was treated with nitrous acid followed by diazo coupling with *N,N*-dimethylaniline to yield a cellulosic dye.

Introduction

Chlorodeoxycellulose (Cell-Cl) has been used for the syntheses of various deoxycellulose derivatives by nucleophilic substitution reactions [1, 2]. Bromodeoxycellulose (Cell-Br) could be a better starting material for the preparation of exotic cellulose derivatives than Cell-Cl because in general bromine is a better leaving group than chlorine in nucleophilic substitution. However, only a few studies have been reported for the cellulose derivatization via Cell-Br and this is probably because no easy synthetic method had been proposed for Cell-Br until recently. In previous papers [3, 4], we reported

the bromination of cellulose in LiBr/*N,N*-dimethylacetamide (DMA) with *N*-bromosuccinimide and triphenylphosphine. The reaction proceeded under homogeneous conditions and Cell-Br with degree of substitution (DS) by bromine up to 0.9 was easily obtained. The substitution by bromine selectively took place at C-6 positions. The reactions of Cell-Br with various inorganic nucleophiles were compared under homogeneous conditions with those of Cell-Cl [3, 5]. The reactions of Cell-Br with thiols and amines were studied under heterogeneous conditions in aqueous alkali [3]. Cell-Br was more reactive towards those organic nucleophiles than Cell-Cl and thiols were more reactive than amines. The substitutions of Cell-Br with the thiols were not high, however, and the low reactivity was considered to be due to the heterogeneous reaction conditions employed.

In this paper, we report the reactions of Cell-Br with thiols in LiBr/DMA in the presence of a tertiary amine as catalyst. The reactions proceeded under homogeneous conditions. Thiols used contained carboxyl, amine and/or hydroxyl groups. Solubilities of cellulose derivatives thus obtained were studied in water at various pH.

Experimental

Preparation of Cell-Br: Microcrystalline cellulose was brominated [4], and was treated with dilute alkali, dialyzed against water, and freeze-dried.

Reactions of Cell-Br with Thiols: Cell-Br samples were dissolved by stirring in 220 g/L solution of LiBr in DMA at 70 °C for 1 h. The solution was set at a prescribed temperature, and a thiol, and triethylamine when necessary, were added to the solution. After the treatment, the solution was poured into a large excess of acetone and precipitates obtained were washed with acetone, dialyzed against water, and freeze-dried. The reaction product with cysteine (Cys), because of poor solubility of Cys, was dialyzed firstly against dilute sodium carbonate before the usual treatments for other reaction products.

Diazotization: The reaction product of Cell-Br with 4-aminobenzenethiol was treated with NaNO₂ and HCl [6]. The diazotized sample was put into a pH 9.0 buffer and to the mixture was added *N,N*-dimethylaniline. The suspension was stirred for a few minutes at 0 °C and filtered. The colored material was washed with water and ethanol and dried under reduced pressure.

Analyses: Analyses were made as reported previously [4].

Results and Discussion

Cell-Br samples with DS by bromine ($DS_{Br,0}$) of 0.52 ~ 0.87 were prepared at 70 °C and purified by the treatment with dilute alkali according to the method reported earlier [4]. These Cell-Br samples were found soluble in 220 g/L solution of LiBr in DMA with triethylamine (TEA) (0 ~ 40 v/v% of DMA). Reactions of Cell-Br with various thiols were studied in the LiBr/DMA solution in the presence or absence of TEA.

Reaction with Cysteine

Cys was not soluble in DMA but soluble in LiBr/DMA with or without TEA. The reaction of Cell-Br ($DS_{Br,0}$, 0.70 ~ 0.86) with Cys in LiBr/DMA in the presence of TEA (20 v/v% of DMA) was studied at different temperatures (Fig. 1).

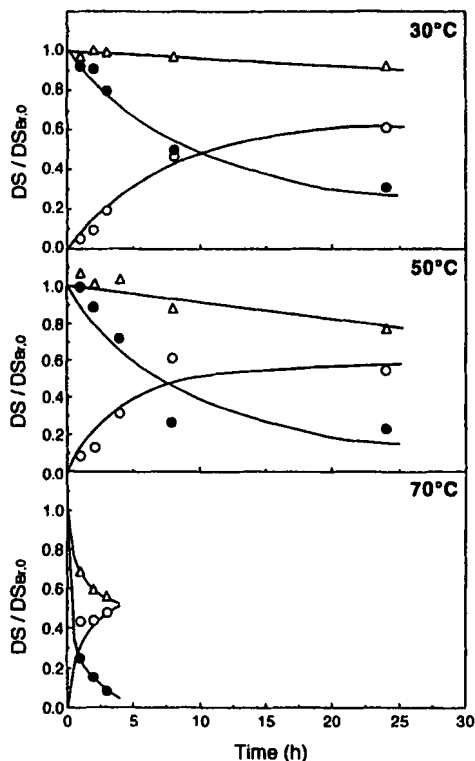


Fig. 1 Time course of the reaction in the presence of TEA (20 v/v% of DMA): ●, $DS_{Br}/DS_{Br,0}$; ○, $DS_S/DS_{Br,0}$; Δ, $(DS_{Br}+DS_S)/DS_{Br,0}$.

Thiol group in Cys selectively reacts with Cell-Br and carboxyl and amino groups do not react. From the sulfur and bromine contents of the product, the degrees of substitution by bromine (DS_{Br}) and by Cys (DS_S) were calculated as follows:

$$DS_{Br} = \frac{(M_{Glc} - M_{H_2O} \times DS_{Br,0}) - M_S \times Br\%/100}{M_S \times (M_{Br} - M_{HBr} \times Br\%/100) - M_{Br} \times M_{Cys} \times S\%/100}$$

$$DS_S = \frac{(M_{Glc} - M_{H_2O} \times DS_{Br,0}) - M_{Br} \times S\%/100}{M_S \times (M_{Br} - M_{HBr} \times Br\%/100) - M_{Br} \times M_{Cys} \times S\%/100}$$

where M_{Glc} , $M_{\text{H}_2\text{O}}$, M_{Br} , M_{HBr} , M_{S} and M_{Cys} are atomic or molecular weights of glucose unit, H_2O , bromine, hydrogen bromide, sulfur and Cys, respectively. The possible side reaction is the elimination of hydrogen bromide from Cell-Br to yield 3,6-anhydroglucose and/or 5,6-glucosene units. Fig. 1 shows that the rate of introduction of sulfur increases with increasing reaction temperature. However, the reaction reaches an equilibrium in 10 to 20 h and the final conversion to the thio derivatives is between 55 and 60%. The plot of $(\text{DS}_{\text{Br}} + \text{DS}_{\text{S}})/\text{DS}_{\text{Br},0}$ shows that the value decreases only slowly at 30 °C but very rapidly at 70 °C, where the side reaction (elimination of HBr) takes place as much as the nucleophilic substitution. The effect of TEA was studied at 30 °C (Table 1). Without TEA, the nucleophilic substitution takes place only a little and the addition of TEA (10 v/v% of DMA) causes much increase in the efficiency of the nucleophilic substitution.

Table 1 Effect of triethylamine on the substitution at 30 °C

TEA/DMA (v/v%)	Cell-Br $\text{DS}_{\text{Br},0}$	Recovery (Wt%)	DS		
			DS_{S}	DS_{Br}	$\text{DS}_{\text{S}}/\text{DS}_{\text{Br},0}$
0	0.70	39	0.03	0.45	0.04
10	0.86	59	0.44	0.20	0.51
20	0.86	78	0.53	0.27	0.62
30	0.86	98	0.40	0.13	0.47

Reactions with Other Thiols

Reactions of Cell-Br with 2-aminoethanethiol (AET), 4-aminobenzenethiol (ABT), 2-hydroxyethanethiol (HET), 3-mercaptopropionic acid (MPA), 2-mercaptobenzoic acid (MBA) and 2-mercaptosuccinic acid (MSA) were studied at 30 °C (Table 2). Functional groups present in the thiols effect the catalytic action of TEA. AET reacts with Cell-Br easily even in the absence of TEA. Aliphatic thiols with carboxyl group(s) do not react much with Cell-Br in the absence or presence of TEA (20 v/v% of DMA).

The reactivities of various thiols were compared under identical conditions in the presence of a fixed amount of TEA at 30 °C for 24 h. Fig. 2 shows plots of $\text{DS}_{\text{S}}/\text{DS}_{\text{Br},0}$ versus pKa of mercapto groups in the thiols. The $\text{DS}_{\text{S}}/\text{DS}_{\text{Br},0}$ value decreases linearly with increasing pKa of the mercapto groups.

Gas chromatographic-mass spectrometric analysis of the hydrolyzate (hydrolyzed with sulfuric acid) of the reaction products after being converted into (methyl ester of) trifluoroacetyl derivatives showed that the nucleophilic substitution at C-6 position actually took place in all cases. Infrared spectra of the reaction products also showed that the expected functional groups such as carboxyl were incorporated in the reaction products.

Table 2 Reactions of Cell-Br with various thiols at 30°C

Thiol	Cell-Br		TEA/DMA (v/v%)	Product		
	DS _{Br,0}	[SH]/[Br]		DS _S	DS _{Br}	DS _S /DS _{Br}
MPA	0.87	29	40	0.51	0.11	0.59
	0.86	29	20	0.09	0.64	0.11
	0.83	2.0	20	0.06	0.85	0.0
AET	0.87	2.1	20	0.57	0.10	0.66
	0.86	21	20	0.93	0.09	-
	0.83	8.0	20	0.53	0.33	0.64
	0.83	2.0	0	0.66	0.27	0.80
HET	0.86	36	20	0.64	0.12	0.74
	0.83	2.0	20	0.36	0.49	0.43
MSA	0.83	2.0	20	0.08	0.76	0.10
	0.83	2.0	40	0.48	0.24	0.58
MBA	0.83	2.0	20	0.60	0.26	0.72
	0.83	2.0	40	0.55	0.26	0.66
ABT	0.83	2.0	20	0.77	0.10	0.93
	0.52	3.9	20	0.39	0.04	0.75
	0.52	9.9	20	0.43	0.03	0.83

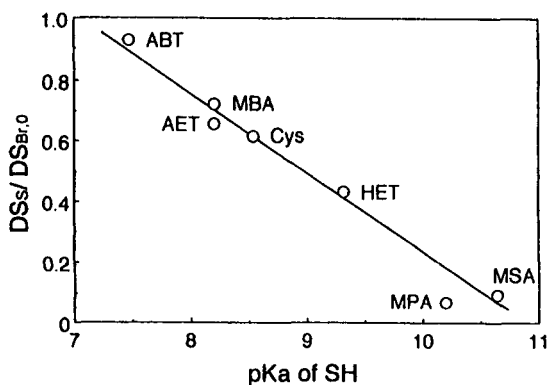


Fig.2 Relation between pKa [6] and $DS_S/DS_{Br,0}$: Samples were obtained in the presence of TEA (20 v/v% of DMA) in LiBr/DMA at 30°C for 24 h.

Solubilities

Solubilities of the thio derivatives of cellulose in aqueous media were studied (Table 3). The reaction products with MSA and MBA are the most soluble and only insoluble in a strongly acidic medium while the reaction product with MPA is only partially soluble in a strongly alkaline medium. The

reaction products with AET, ABT and HET are insoluble in all the media but the product with Cys which contains both carboxyl and amino groups are partially soluble in both strongly acidic and alkaline media.

Table 3 Solubilities^a of the reaction products with various thiols

Thiol	group	1 N HCl	pH 5.0	H ₂ O	pH 9.0	1 N NaOH
MPA	COOH	-	-	-	-	±
MSA	2COOH	-	+	+	+	+
MBA	COOH	-	+	+	+	+
Cys	COOH NH ₂	±	-	-	-	±
AET	NH ₂	-	-	-	-	-
ABT	NH ₂	-	-	-	-	-
HET	OH	-	-	-	-	-

^a +, Soluble; ±, partially soluble; -, insoluble.

Diazo Coupling of *p*-Aminophenylthiodeoxycellulose

The reaction product of Cell-Br with ABT was treated with nitrous acid and the resulting diazo compound was treated with *N, N*-dimethylaniline. The product, which contains pendant groups of Methyl Orange structure, shows a reversible change in color with pH: black at pH=1.7, brown at pH=4.0 and orange at pH 6.9. This material is insoluble in water at pH 1.7 ~ 9.0.

References

1. A. Ishizu, "Wood and Cellulosic Chemistry" (D. N.-S. Hon and N. Shirai, Eds.), Marcel Dekker, New York, Chap. 16 (1991).
2. R. G. Krylova, *Russ. Chem. Rev.*, **56**, 97 (1987).
3. K. Furuhashi, H.-S. Chang, K. Koganei, and M. Sakamoto, "Cellulose Structural and Functional Aspects" (J. F. Kennedy, G. O. Phillips, and P. A. Williams, Eds.), Ellis Horwood, Chichester, Chap. 23 (1989).
4. K. Furuhashi, K. Koganei, H.-S. Chang, N. Aoki, and M. Sakamoto, *Carbohydr. Res.*, **230**, 165 (1992).
5. K. Furuhashi, H.-S. Chang, K. Koganei, and M. Sakamoto, *Sen'i Gakkaishi*, **48**, 602 (1992).
6. For example, J. P. Danehy and K. N. Parameswaran, *J. Chem. Eng. Data.*, **13**, 386 (1968).
7. D. H. Campbell, F. Luescher, and L. S. Lerman, *Proc. Nat. Acad. Sci. U. S.*, **37**, 575 (1951).

32 Investigation of cellulose derivatives. Method of obtaining the whole molecular characteristics by velocity ultracentrifugation

E B Tarabukina, G M Pavlov and S Ya Frenkel – Institute of Macromolecular Compounds, St Petersburg State University, St Petersburg, Russia

ABSTRACT

Macromolecular properties of nitrocellulose with a degree of substitution of $\gamma=2.7$ in acetone and butylacetate and of methylcellulose with $\gamma=1.65$ in water have been analyzed. Velocity ultracentrifugation without preliminary fractionation of the polymer samples and without use of any additional methods was employed.

INTRODUCTION

Molecular characteristics of polymers can be studied by means of velocity sedimentation without any additional methods or calibration of apparatus and without preliminary fractionation of polymer sample. Such an approach is based on the analysis of two hydrodynamic characteristics which can be obtained from a series of velocity sedimentation experiments for solutions of different concentrations. Those characteristics are the sedimentation con-

stant S_0 and concentration Gralen's coefficient k_s [1] obtained from the semiempirical equation $S^{-1} = S_0^{-1}(1 + k_s c)$, S being a sedimentation coefficient corresponding to concentration c . S_0 and k_s depend differently on size, and shape, and molecular weight of a macromolecule. Direct comparison of S_0 and k_s gives an opportunity to determine molecular weight M . The relationship for the determination of M by means of S_0 and k_s was suggested by Wales and van Holde [2]. Recently Frenkel and Pavlov [3] suggested a general equation connecting S_0 and k_s with M . They introduced a sedimentation parameter $\beta_s = N_a [S] k_s^{1/3} M^{-2/3}$ of a similar type to the Flory-Mandelkern invariant [4], N_a being the Avogadro's number, $[S]$ a characteristic sedimentation constant.

The analysis of a large amount of experimental data permitted authors to establish an invariance of their parameter β_s with respect to the contour length of the macromolecule (i.e. M) and the structure of the repeating chain unit [3,5,6]. For cellulose, its derivatives and some polysaccharides an average value of $\beta_s = (1.00 \pm 0.18) \cdot 10^7 \text{ mole}^{1/3}$ was obtained.

Furthermore, taking into account the fractionation (molecular-mass-spectrometric) effect of the ultracentrifuge and using the parameter β_s one can obtain not only the average hydrodynamic M of a polymer sample, but as well M of "graphic" fractions obtained by means of transformation of the spectrum of shifts (which is the starting information from the ultracentrifuge) to the spectrum of sedimentation constants (spectrum of masses).

"Graphic" fractions, first proposed by Kinell and Rånby [7] can be obtained using the extrapolation procedure of the sedimentation coefficients distributions to zero concentration. Each "graphic" fraction can be characterized by S_0 , k_s and consequently M_{ks} . Comparing S_0 , k_s and M_{ks} of "graphic" fractions one can receive the whole quanti-

tative information for macromolecules, such as the parameters K' , K'' , b , α of the Kuhn-Mark-Houwink equations for S_0 and k_s , $S_0 = K'M^{1-b}$ (1), $k_s = K''S_0^\alpha$ (2), the Kuhn segment length A , the effective hydrodynamic diameter d . A and d can be calculated by the application of the theories of the translational friction of macromolecules to the set of the "graphic" fractions.

EXPERIMENTAL

An unfractionated sample of nitrocellulose (NC) with $\gamma=2.7$ in acetone (Ac) was investigated by the suggested method. Velocity sedimentation experiments were carried out in the analytical MOM 3170 ultracentrifuge with an Al cell of length $h=30\text{mm}$. The use of a thick rotor and cell enabled the study of the sedimentation in the low concentration range ($c=0.098\dots 0.030\text{ g}/100\text{cm}^3$). The rotor speed was 40000rev./min . The sedimentation boundary was fixed by the Philpot-Svensson optical system. The average temperature of experiments was $(18.6\pm 0.8)^\circ\text{C}$.

RESULTS AND DISCUSSION

Integral distributions of the sedimentation coefficients $G(S,t)$ depending on time t were calculated from the differential distributions of shifts taking into account a sectorial dilution. Diffusion effects were eliminated by the extrapolation of $G(S,t)$ to $t^{-1}=0$. $G(S)$ corresponding to different concentrations at $t^{-1}=0$ were extrapolated to $G(S_0)$ corresponding to zero concentration by means of the "graphic" fractionation, and then S_0 , k_s and M_{ks} of "graphic" fractions, and consequently the molecular weight distribution $G(M)$ were calculated.

The parameters of equations (1) and (2) were calculated from the logarithmic dependencies of k_s vs S_0 and S_0

vs M_{ks} shown in Fig.1. Both dependencies exhibit a definite tendency towards a change of slope on passing into the range of low M . The character of this change corresponds to the case of draining macromolecules in the absence of volume effects. The parameters K' , K'' , b and α of eqs.(1) and (2) for NC in Ac were estimated for two ranges of S_0 : $S_0 < S^*$ and $S_0 > S^*$, $S^* \approx 13$ Svedberg units (see table 1).

The conformational characteristics of NC may be calculated by the use of the theory of the translational friction of persistent chains in the absence of volume effects [8]. The dependence corresponding to this theory is shown in Fig.2. In addition to the data obtained for "graphic" fractions the data obtained by different authors for real fractions of NC with γ close to $\gamma=2.7$ were reconsidered (Figs.1,2). Data for graphic and real fractions were proceeded separately. The results expressed in Angström units are: $A=360 \pm 13$, $d=4.8 \pm 0.4$ for "graphic" fractions and $A=410 \pm 60$, $d=3.5 \pm 1.4$ for real fractions. (from the published data). The results for both sys-

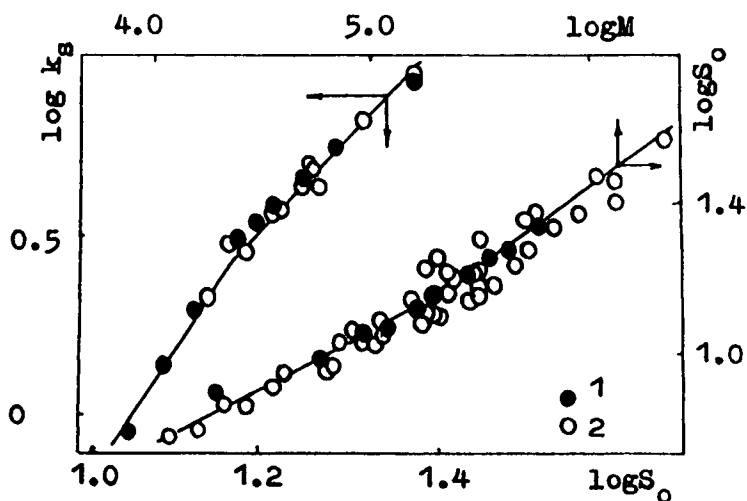


Fig.1. Logarithmic dependencies of k_s vs S_0 and S_0 vs M for NC in Ac: 1 - "graphic" fractions, 2 - real fractions from published data [9].

Table 1. Hydrodynamic and molecular characteristics of cellulose derivatives.

Polymer system		NC - Ac	NC - BAC	MC - water
M_{sd}		312000	370000	117000
M_{ks}		245000	350000	80000
$\beta_s \cdot 10^{-7} \text{mole}^{1/3}$		0.87	0.85	0.87
$A, \text{\AA}$		360	300	190
$d, \text{\AA}$		5	16	12
$S_o >$	$k_s, 100\text{cm}^3/\text{g}$	$0.63 \cdot 10^{-6} S_o^{7.7}$	$0.016 S_o^{3.1}$	
	$S_o \cdot 10^{13}, \text{s}$	$1.59 M^{0.18}$	$0.10 M^{0.33}$	
$S_o <$	$k_s, 100\text{cm}^3/\text{g}$	$0.37 S_o^{2.48}$	$0.18 S_o^{3.1}$	$0.68 S_o^{1.75}$
	$S_o \cdot 10^{13}, \text{s}$	$0.18 M^{0.36}$	$0.033 M^{0.36}$	

tems are in fair agreement.

The same sample of NC in butylacetate (BAC) and also an unfractionated sample of methylcellulose (MC, $\gamma=1.65$)

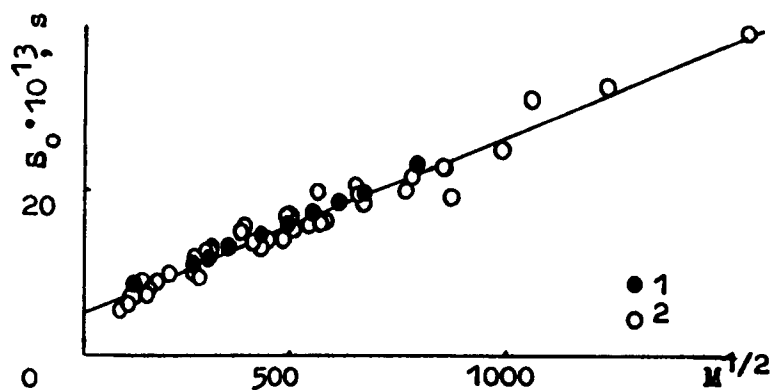


Fig.2. The dependence of S_o vs $M^{1/2}$: 1 - "graphic" fractions, 2 - real fractions from the published data [9].

in water were studied by the suggested method. The results obtained for these polymers are listed in Table 1. $G(M)$ calculated for NC in Ac and BAC practically coincide. This fact confirms the validity of the obtained results. The agreement with the available published data is also to be pointed out.

CONCLUSIONS

A new approach to obtain a whole molecular characterization of polymer in solution based on the study of the concentration dependence of the sedimentation coefficient is suggested. Investigation of cellulose derivatives by this method shows rather satisfactory results, confirming the increased rigidity of cellulose derivatives.

This study was carried out under the support of the Russian Foundation for fundamental studies (93-03-5791 PPM).

References

1. Svedberg T., Pedersen K.O., The Ultracentrifuge, Oxford, Clarendon Press, 1940.
2. Wales M., van Holde K., J. Polym. Sci., 14, 81 (1954).
3. Pavlov G.M., Frenkel S.Ya., Acta Polymerica, 39, 107 (1988).
4. Mandelkern L., Flory P.J., J. Chem. Phys., 20, 212 (1952)
5. Pavlov G.M., Frenkel S.Ya., Ukrainian Polym. J., I, 157 (1992).
6. Tarabukina E.B., Slavina Z.N., Frenkel S.Ya., Acta Polymerica, 42, 266 (1991).
7. Kinell P.O., Rånby B.G., Adv. Coll. Sci., 3, 161 (1950).
8. Yamakawa H., Fujii M., Macromolecules, 6, 407, (1973).
9. Polymer Handbook, Ed. by Immergut I.H., Brandrup J., 2nd ed., Wiley Intersci., N.Y., 1975.

33 The degradation of cellulose nitrate in composite museum artefacts: isolation, replica cellulose replacement and regular inspection in storage and on display

M A Robson – Studio, 29 Park Avenue, Birmingham B18 5ND, UK

ABSTRACT

During the nineteenth century composite museum artefacts circa 1850's contained cellulose nitrate which will cause serious problems to the conservator and curator. A case study of an imitation tortoiseshell and ostrich feather fan c.1850 demonstrates the rapid degradation of the substantial damage to the ostrich feather. An infra-red reflectance with ATR attachment provided a non-destructive method for identifying the plastic as cellulose nitrate and the white surface deposit as a plasticiser from within the plastic. The latter was removed from the surface with swabs of cotton wool moistened in distilled water. The metal pin was replaced with an acrylic plastic substitute. The ostrich feathers were detached from the cellulose nitrate spines and where possible housed separately to safeguard risk of contamination to other plastics in close proximity both in storage and on display. Replica blank spines were manufactured in wood to replace the degraded plastic. Regular inspection of such collections is vital to ensure the long term preservation of this somewhat relatively modern aspect of our heritage.

HISTORICAL BACKGROUND

Through the ages, from as far back as Primitive man, wood has been a readily available resource for the shaping of both utilitarian and decorative artefacts. Less readily available (and therefore luxury items) were products like

tortoiseshell and horn which reached the peak of their popularity during the Victorian era. With the development of the plastics industry, cellulose nitrate emerged as a cheaper substitute. It often occurs in composite museum artefacts circa 1850's and will cause serious problems to the conservator and curator. Such a problem is illustrated in a case study of an imitation tortoiseshell and ostrich feather fan c1850.

INTRODUCTION

A recent examination of this composite artefact revealed the presence of a white deposit smelling strongly of camphor on the resin spines. At only a slight touch, the ostrich feather was degrading into strands. These are classic symptoms of the degradation perception of cellulose nitrate as largely experienced in the film industry. In addition, an iron pin attaching all the spines had corroded, producing a phial of corrosion dust, and which had subsequently caused spinal damage as seen in hairline cracks in the resin spines around the pin.

EXAMINATION

An infra red spectroscopic examination produced a characteristic pattern for a cellulose nitrate compound. In addition the corrosion dust was identified as ferric oxide. A small sample of the resin dust was put into the sample preparation to compress it to a disc thin enough to allow infra red radiation to pass through it. It exploded characteristically and provides a warning for its immediate isolation/disposal (?) from the collections in storage and on display in the Birmingham Museums & Art Gallery.

An infra red spectroscopic examination of both spines and feather confirmed the presence of cellulose nitrate. This is but one example of a problem which is becoming increasingly common in recent Social History and Applied Art collections where the cellulose nitrate in several composite artefacts is reaching the end of its useful life.

ENVIRONMENTAL CONTROL

There are however, various methods for the long term preservation of such materials.

Isolation of the artefact in airtight flameproof containers will inhibit further contamination of the collections in storage and on display, but will accentuate the degradation of the confined artefact due to the build up of harmful contaminating vapours in an enclosed space. If the artefact is displayed on open shelving in a well ventilated storage/display area the emitting pollutants may harm other materials within its vicinity. Removal of the affected component part and its replacement with a more suitable and stable material may be the only choice to encourage the long term preservation of the composite artefact.

REPLICA CELLULOSE REPLACEMENT

With the degradation of cellulose nitrate, a white deposit (presumably a plasticiser from within the plastic) had oozed to the surface and smelt strongly of camphor. Nitric acid vapour is released and will seriously harm organic materials eg feather. In order to maintain the condition of the artefact in the long term, replica cellulose replacement was considered a viable solution. It fulfils those criteria which may be considered to have governed the choice of cellulose nitrate by the Victorians. It is commercially available, light in weight and will easily colour match. Indeed, a recent development is the use of modern stains and varnishes (polymeric surface finishes) to imitate any desired surface appearance. Duplicate spines were reproduced from a suitable wood eg bamboo, sandalwood and stained to a near colour match to that of the original.

CONSERVATION

The white surface deposits on the resin spines were removed with swabs of cotton wool moistened in distilled water. The feather was detached and stabilised by application of a fine mist of deionised water and allowed to dry in ambient temperatures. The feather was attached to the cellulose replacement spines with Paraloid B72 (an acrylic polymer) avoiding HMG (cellulose nitrate adhesive) as this may eventually give rise to similar problems. Cellulose nitrate lacquers eg Incralac for the protection of the metal pin is also to be avoided. A protective acrylic lacquer or a replacement acrylic pin is preferred.

DISCUSSION

Cellulose nitrate from the 1850's to 1920's has indeed contributed significantly to our heritage today. Its life span is now perceived to be relatively short and

precautionary measures are essential if the artefact is to survive in its physical form. Replica cellulose replacement will ensure that the artefact is safely preserved and can be maintained in the long term under suitable environmental conditions. As far as the artefact is concerned it makes the difference between "life or death". This does provide the curator with the choice of either retraining the exhibit or its subsequent disposal.

Computerised documentation will ensure its future knowledge providing the plastic discs are not manufactured from cellulose nitrate. Photographic film made from cellulose nitrate is, at present, at risk and such documentation requires urgent transfer to a more suitable photographic format to survive in the long term. A shared dialogue between the conservator, curator, private collector, technologist, chemist and industrialist will provide an opportunity of exchanging current ideas and findings on both the cellulose science and technology, and the plastics industry which will ensure an early diagnosis and a suitable up-to-date long term preservation of such collections which will provide important social statements for our heritage today and in the future.

ACKNOWLEDGEMENT

The author wishes to thank the following for their discussion, encouragement and support: David Bailey, Leo Biek, Debbie Bolton, Pat Brown, Andrew Carson, Eileen Collins and Christopher Radbourne, Richard Green and Alan Mitchell, Anne Hudson, Hilda Smith, Jane Thompson and Pauline Timmins, and Dr W.C. Thompson and Simon Lawson, S. P. Tyres UK Limited, Fort Dunlop, Birmingham for F.T.I.R. analysis, to Wendy Firmin, Editorial critic and Cathie Mair secretariat, Kevin and Robert Brown, Directors of Advance Offices for practical assistance and professional advice.

34 Water sorption by sulfonic and carboxylic cellulose derivatives as a function of counterions and relative humidity

J Berthold*, J Desbrières**, M Rinaudo** and L Salmén* – * STFI, Box 5604, S-114 86 Stockholm, Sweden; ** CERMAV-CNRS, BP 53X, F-38041 Grenoble Cedex, France

INTRODUCTION

It is well known that water sorption has a great influence on the physical properties of ligno-cellulosic materials affecting both swelling and softening of the material. The water sorption is also affected by the number of ionic groups in the materials as well as the nature of these ionic groups and the type of counterions. Water sorption has been studied for some cellulosic derivatives in order to shed more light on the role of the ionic groups and their counterions on the amount and type of water adsorbed.

EXPERIMENTAL

Materials

Carboxymethylcellulose fibres (CMC-fibres, Buckeye, USA) with a degree of substitution (DS) of 0.7, carboxymethylcellulose powder (CMC) DS = 1.6 and cellulose sulphate (CS) (KELCO, USA), DS = 2.1 were used. These cellulose derivatives were ionexchanged into their sodium, calcium and protonated forms by 0.1 M NaOH, Ca(OH)₂ and HCl respectively.

Procedures

The cellulose derivatives were ionexchanged, thoroughly washed and partially dried before being placed in desiccators with different atmospheres (98%, 92%, 76%, 44%, 22% and 0% for CMC-fibres; 98%, 92%, 76%, 56%, 35% and 0% for CMC and CS, established by saturated salt solutions (1)). The materials were conditioned until equilibrium was established (ca. 3 weeks). Samples of 5-15 mg were used for the analyses. The total amount of adsorbed water in the cellulosic systems was analysed with a Thermogravimetric Analyser (TGA). The amount of freezing water was determined by Differential Scanning Calorimetry (DSC) and the level of adsorbed non-freezing water was determined as the difference in adsorption between the total and the freezing bound water (2).

All DSC analyses were performed during heating with a heating speed of 1 or 2°C/min.. Samples were cooled down to the starting temperature at a rate of 200 °C/min.. TGA samples were held at 130 °C until the second derivative of the weight loss curve equalled zero. All water was then considered evaporated.

RESULTS

Water sorption isotherms

The total water adsorption isotherms for CMC fibres under different ionic environments (H^+ , Na^+ , Ca^{2+}) are shown in Figure 1. The nature of the counterion appears to have little influence on the moisture content when the relative humidity is less than about 80%. Above this RH the counterion has a large influence on the total water adsorbed. counterions favour water adsorption at high RH for CMC fibres in the following order: $Na^+ > Ca^{2+} > H^+$.

Figure 2 shows the total water adsorption isotherms for CS. The influence of the counterions Na^+ and Ca^{2+} is insignificant for RH less than about 80%. The protonated form, however, adsorbed more water throughout the whole RH range tested. The order in which the counterions favour water adsorption at high levels of RH is different from that of the CMC-fibres.

For the CS it is seen that the protonated form gives a higher level of adsorption than does the sodium form. The opposite was the case for the CMC-fibres. The calcium form does in all cases give poor adsorption. The following sequence of counterions favouring water adsorption was obtained for CS: $H^+ > Na^+ > Ca^{2+}$. It is interesting to see that the sequences here found for water adsorption in the gas phase are the same as those in the liquid water phase (3).

Freezing water

Water that freezes can be observed with DSC. In Figure 3 the development of this freezing water for a CMC- Na^+ sample may be followed over relative humidities between 76% to 98%. As a reference the melting peak for bulk water has been added. The total water content (W_c , obtained from TGA) is given for each sample. At 76% RH no peak is observed when the temperature is increased from -45°C to 25°C. At 92% RH, two peaks are observed, peak I ($T_m \approx -20$ °C) and peak II ($T_m \approx -9$ °C). Peak I is still detectable at -20 °C for 98% RH while the size of peak II has increased and its maximum moved closer to that of bulk water.

DISCUSSION

Water adsorption

The two different cellulose derivatives that have been examined differ mainly in the nature of their ionic groups, in one case (CMC) we have weak carboxylic acid groups and in the other (CS) we have strong sulfonic acid groups. The nature of the ionic site is known to have a large influence on swelling and other physical properties (4) for ion

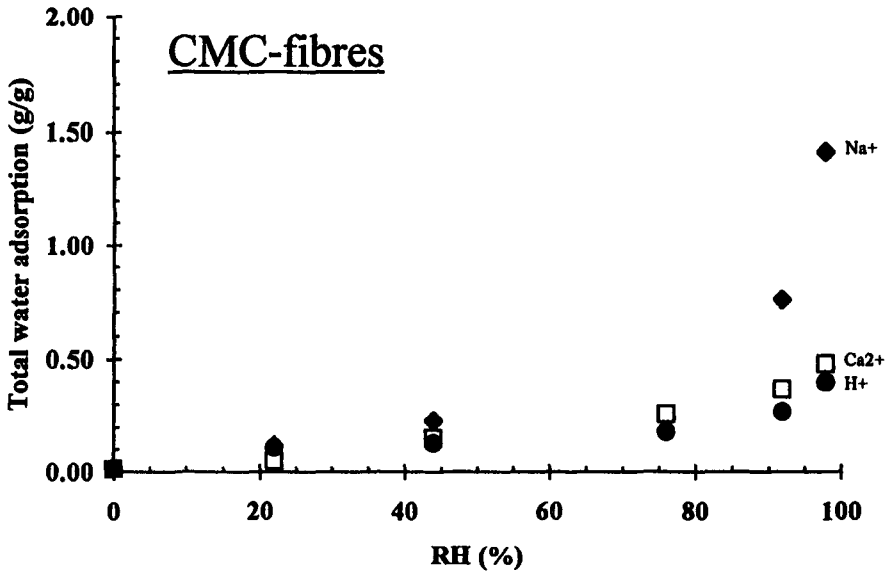


Figure 1 The total water adsorption isotherms for carboxymethylcellulose fibres as a function of relative humidity and counterion type.

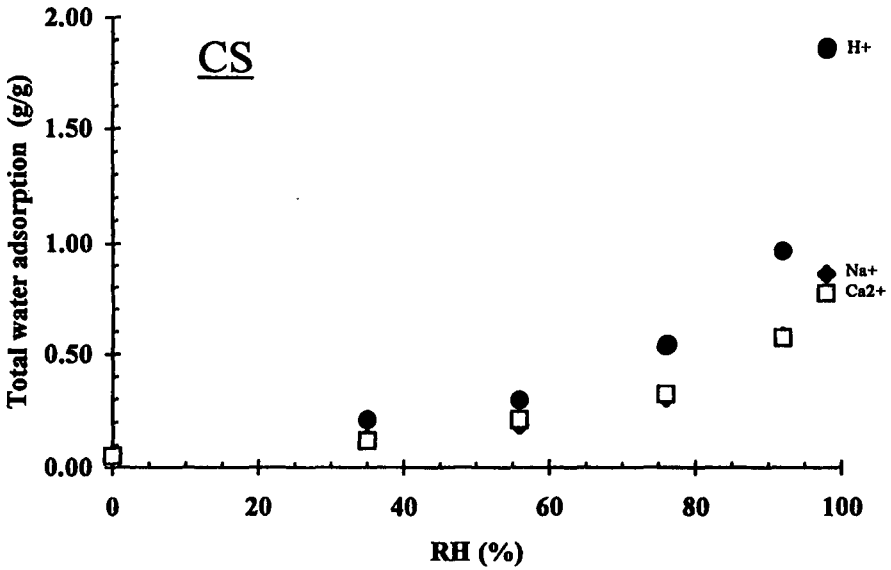


Figure 2. Total amount of adsorbed water on sulfonated cellulose as a function of relative humidity and counterion type.

exchangers. These effects are however less evident at moisture contents lower than 100% relative humidity.

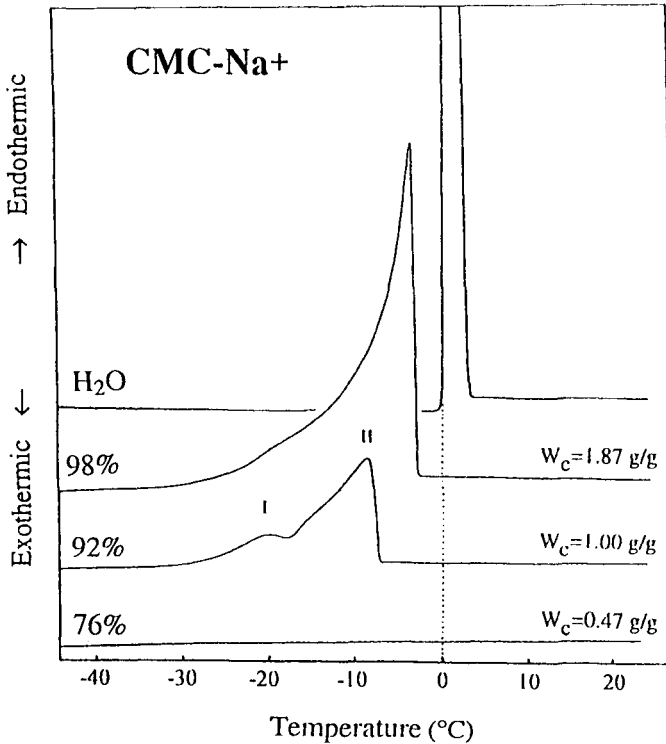


Figure 3. DSC-curves for carboxymethylcellulose powder in the sodium form (CMC-Na⁺). The effect on the freezing water as a function of the relative humidity between 76 to 98% is shown. The effect on the total water content (W_c) determined by TGA is indicated for each RH.

The observed sequence favouring total water adsorption for CMC-fibres i.e. $\text{Na}^+ > \text{Ca}^{2+} > \text{H}^+$, is however the same as for a weak acid polymer in an electrolyte (4). The protonated form adsorbs little water due to the low degree of dissociation. The opposite is true for the CS case due to the strong acid group giving a high degree of dissociation in the protonated form (5). This explains the high levels of swelling or water sorption for the protonated form. The bivalent calcium ion can interact with more than one ionic site per ion. The effect of the ionic sites on the surrounding water molecules is reduced thereby (6).

Types of water

At 76% RH CMC-fibres adsorb 0.47 g water/g dry gel (Figure 3), this water being non-detectable by DSC. The DSC detects different types of phase transitions in a

system. In this case it is the melting of solid water. The non detectable water molecules are the first water molecules adsorbed on hydroxyl groups and ionic groups and their counterions. The water molecules experience attractive forces that are strong enough to reduce their mobility to such an extent that they do not undergo any phase transition although the molecules are still mobile as detected by NMR (1). This type of water is commonly called non-freezing water (2).

At about 80% relative humidity the occurrence of peaks I and II in Figure 3 indicates that freezing water appears. This type of water only occurs in the presence of ionic groups at high degrees of relative humidity (7). In the cases where non modified cellulose has been tested no freezing water was detected at levels of relative humidity less than 99% (7).

Peak I could indicate water that has a structure, less organised than the ice-type structure, due to the influence of the ionic group and the counterions. The influence of the ionic groups with counterions on the interacting water molecules should decrease as the distance between these ionic groups and the adsorbed water molecules increases. This could then explain why peak II appears closer to 0°C, indicating a water structure that is less disordered due to less influence from the ionic sites. As the RH increases more water molecules are added to the system. These new water molecules will have a successively larger distance to the ionic groups and the counterions, thus will experience weaker attractive forces. This may explain why the difference between 92 and 98% RH is seen as an increase in the size of peak II and a shift of the maximum of peak II towards that of normal ice ($T_m = 0^\circ\text{C}$). The last molecules sorbed have thermodynamic parameters closer to those of bulk water. These different types of water are discussed further in (7)

CONCLUSIONS

It may be concluded that water adsorption and the type of water adsorbed is influenced by the nature of the ionic groups and their counterions already at moisture levels less than 100% relative humidity. The presence of ionic groups with counterions is necessary for freezing water to appear when RH is less than 100%.

ACKNOWLEDGEMENT

The authors thank Jacob Wallenbergs Research foundation, Lars-Erik Thunholms Research foundation and STORA for their financial support.

REFERENCES

- (1) CRC Handbook of Chemistry and Physics, 69th edn, (Ed) Weast,RC, CRC, Boca Raton, (1988-89), Florida, p. E-41.
- (2) Hatakeyama,H; Iwata,H; Hatakeyama,T : H and NMR studies of the interaction between water and cellulose sulphate sodium salt by DSC and NMR. Chap. 21. In:Cellulose and its derivatives. (Eds: Kennidy,JF; PhillipsGO; Wedlock,DJ; Williams,PA) Ellis Horwood Ltd.,(1985), Chichester.

- (3) Helffrich, F (Ed); Ionexchange, 1st edn, McGraw-Hill, (1962), New York.
- (4) Rinaudo, M., Swelling of polyelectric gels and thermodynamic parameters of solvation, in Charged gels and membranes, Ed: Sélégny, E. D. Reidel Publishing company, (1976), Dordrecht-Holland, p. 91-120.
- (5) CRC Handbook of Chemistry and Physics, (Ed) Weast, R.C., 63rd edn, CRC, Boca Raton, (1982), Florida, p. D-171.
- (6) Zundel, G (Ed); Hydration and intermolecular interactions., 1st edn, Academic press Inc., (1969), London.
- (7) Berthold, J; Desbrières, J; Rinaudo, M; Salmén, L. Types of water adsorbed as determined by the ionic group and its counterion. Submitted to Polymer.

Part 4:
Association thickening and gelation
of cellulosics, etc.

35 Comparative behaviour of cellulose derivatives and microbial polysaccharides. Relation between stiffness and rheological properties

M Rinaudo – Centre de Recherche sur les Macromolécules Végétales, CNRS, affiliated with Joseph Fourier University, BP 53 X, 38041 Grenoble Cedex, France

ABSTRACT

This paper describes the main rheological characteristics of polysaccharide solutions. When there is no specific interaction in solution, they behave as synthetic polymers. The main characteristic concerns their stiffness which causes a large hydrodynamic volume. The ionic charges also induce an increase in viscosity and in the chain dimensions.

INTRODUCTION

The rheological properties of polysaccharide solutions are unique in some respect compared to synthetic polymers due to their wormlike chain behaviour. Their usual properties concern mainly their thickening effect as additives in aqueous solution depending on the experimental conditions.

This paper concerns the water soluble polysaccharides and especially cellulose and cellulose derivatives in comparison with some microbial polysaccharides. Due to their structural regularity these polymers may be considered as good models for a fundamental approach and were used in our previous work. From their behaviour, one is able to draw predictions on the behaviour of other polysaccharides in solution.

The viscosity of an aqueous solution is directly related with the polymer stiffness, its molar mass and concentration, temperature, ionic strength and pH, and shear rate adopted for measurements. Whatever the polymer is, one observes a Newtonian behaviour followed by a pseudoplastic regime when the viscosity is tested as a function of shear rate; this transition will be discussed as well as the comparison between dynamic and flow determination of viscosity.

The viscosity in the Newtonian regime is directly related to the hydrodynamic parameter $[\eta]$ (the intrinsic viscosity) and to the overlap parameter $C[\eta]$; the persistence length of the molecule (taking into account the electrostatic contribution for ionic derivatives) directly controls the intrinsic viscosity.

The role of ionic charges (i.e. in carboxymethylcellulose) is important first to bring about good solubility in water but also to induce stretching of the molecule at least in moderate ionic strength and then an increase of the viscosity.

When there are no secondary intermolecular interactions in solution, the behaviour of cellulose and cellulose derivatives is the same as other polymers. If H-bonds or hydrophobic interactions exist in solution, then the behaviour will especially depend on temperature and external salt concentration.

RESULTS AND DISCUSSION

General viscometric behaviour of cellulosics.

The increase of viscosity of a fluid (i.e water) is directly related to the concentration of polymer dissolved (C), to the molecular weight of this polymer (M) and to the experimental conditions for the measurements (ionic concentration, pH, shear rate, temperature, ...).

Influence of polymer concentration

The specific viscosity η_{sp} determined at zero shear rate ($\eta_{sp} = \frac{\eta - \eta_0}{\eta_0}$ with η_0 the viscosity of the solvent and η the viscosity at a

given polymer concentration) is usually expressed by the relation :

$$\eta_{sp}/c \rightarrow 0 = C[\eta] + k'(C[\eta])^2 + B(C[\eta])^n \quad (1)$$

in which $[\eta]$ is the intrinsic viscosity. The product $c[\eta]$ is the overlap parameter. For polymeric solutions, the critical overlap concentration is approximated by $C^* \sim [\eta]^{-1}$ and C^* separates the dilute regime ($C < C^*$) where the molecules are well dispersed and separated in the solvent from the semi-dilute regime where they begin to form entanglements. This value of C^* is higher than that determined from the radius of gyration. The relation (1) indicates that one must obtain a unique curve when $\log \eta_{sp}$ is plotted as a function of $\log C[\eta]$ for different polymer concentrations and different molecular weights (or $[\eta]$ which is directly connected) as soon as k' , the Huggins constant, remains the same for all the samples (then for a series of polymer of the same chemical structure in the same solvent). This curve was previously discussed for xanthan (1,2) and for hyaluronic acid sodium salt form (3,4). In the dilute regime, η_{sp} is controlled by the product $c[\eta]$ but in the semi-dilute regime for the domain of higher concentrations it seems that η_{sp} follows the variation of $(C M)^{3.7-4}$ at least when $C[\eta]$ is larger than 10. With polysaccharides, the exponents found exceeded the value of 3-3.4 usually predicted for flexible polymers in concentrated solutions or in the melt. With interacting polymers the exponent increases as well as the gel like behaviour character.

Influence of the molecular weight

For polysaccharides, the intrinsic viscosity is usually relatively high for a given molecular weight then C^* is low. This is the first characteristic of cellulosic derivatives; the equation of Mark Houwink relating $[\eta]$ to the molecular weight :

$$[\eta] = KM^a \quad (2)$$

is characterized by an "a" exponent which is always larger than 0.5- 0.6 (even for neutral polysaccharides) as usually found for flexible synthetic polymers; some data are given in Table 1. This point was discussed for different polysaccharides in our last papers (5-7); it was attributed to their wormlike chain character.

Table 1 - Some Mark-Howink "a" parameters determined on cellulose and cellulose derivatives.

Polysaccharide	Solvent	a	Reference
Cellulose	cadoxen	0.77	(9)
Cellulose triacetate	acetone	0.82 → 1	(9)
Cellulose trinitrate	acetone	0.78 → 1	(9)
Hydroxyethyl cellulose	water	0.87	(9)
Xanthan	NaCl	1-1.14	(10)

The exponent "a" depends directly on the reduced length $L_r = L/2 L_p$ with L the contour length and L_p the persistence length. In fact L_r equals the number of Kuhn segments. Considering the theoretical model of Yamakawa-Fujii (8), one can predict the intrinsic viscosity of a given polymer in θ -conditions following the relation

$$[\eta]_{\theta} = \phi(L_r, dr) \left(\frac{M_L}{2L_p}\right)^{-3/2} M \quad (3)$$

ϕ is a function which takes into account the draining effects; dr is the reduced diameter with $dr = d_H/2 L_p$ (d_H is the hydrodynamic radius); M is the molecular weight and M_L the mass per unit length.

The exponent "a" in θ -conditions is calculated from the derivative

$$d \log [\eta]_{\theta} / d \log M \quad (4)$$

for each L_p . The function $\phi(L_r, dr)$ is also very sensitive to L_r and usually lower than the Flory constant $\phi \sim 2.5 \times 10^{23}$ only valid when $L_r \rightarrow \infty$.

This model justifies the higher "a" exponent found with cellulosics based on the semi-flexible character of the $\beta 1 \rightarrow 4$ D- glucan chains. From the literature the persistence length found on different derivatives is often in the range of 50 Å (Table 2); this value was also very recently determined for the D-glucosamine chain of chitosan (11). In Figure 1, the prediction of $[\eta]$ (M) is given for CMC with DS = 0.5 and 1 respectively assuming $L_p = 50$ Å.

Table 2 - Persistence length (L_p) of cellulose and cellulose derivatives.

Polysaccharide	L_p (Å)	Reference
Different cellulose derivatives	30 to 80	(12)
CMC	10^{-3} g/ml \rightarrow 47.6	(13)
	2.57×10^{-2} g/ml \rightarrow 27.7	
CMC	54 ($C_s \rightarrow \infty$)	(14)
Cellulose acetate	80 (depending on solvent)	(15)
Chitosan	50	(11)

Influence of the shear rate

For low shear rate, at low concentration and moderate molecular weight, a Newtonian behaviour is observed. Then over a critical value of $\gamma(\gamma_r)$ the viscosity decreases when γ continues to increase. This viscoelastic regime is characterized by the slope n which depends in first approach on the product $C[\eta]$ (2); the value of n decreases and goes to -0.8 when $C[\eta]$ increases.

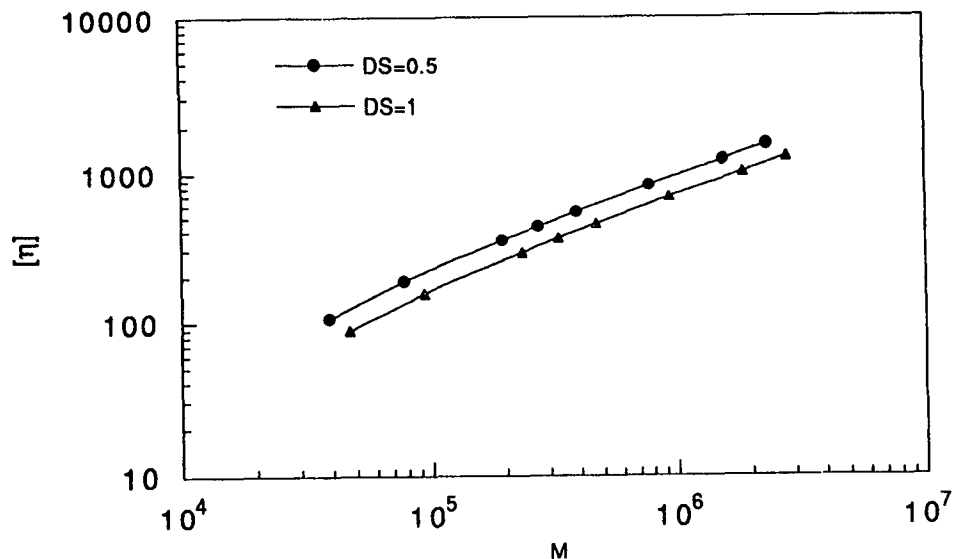


Figure 1. Prediction of the dependence of $[\eta]$ with the molecular weight for Na-CMC DS = 0.5 and 1 (relation 3)

Behaviour of ionic derivatives

Ionic derivatives such as CMC behave as polyelectrolytes and they follow the usual behaviour of charged molecules just depending mainly on their charge density (proportional to the number of ionic sites per unit length of the main chain), of the counter ions and external salt concentrations.

Comparative behaviour of CMC and xanthan was developed previously; due to the large stiffness of xanthan, the sensitivity of viscosity is lower in the presence of salt excess for monovalent as well as divalent electrolytes (16). The dependence of $[\eta]_{CS}$ with the external salt concentration (C_s) is reflected by the relation

$$[\eta]_{CS} = [\eta]_{\infty} + S C_s^{-1/2} \quad (5)$$

The slope of the linear dependence of $[\eta]$ with $C_s^{-1/2}$ is directly related to the screening effect of salt on the intrachain electrostatic repulsion; $[\eta]_{\infty}$ is the value of the intrinsic viscosity extrapolated to infinite C_s and may be assumed as representative of the θ -conditions (6). Particularly the persistence length, which characterizes the stiffness of the molecule, decreases in the presence of external salt which screens the electrostatic interaction (17).

For semi-flexible chains, with moderate persistence length, the decrease of the viscosity is more important when divalent electrolyte (i.e. $CaCl_2$) is added than when monovalent is (i.e. $NaCl$).

Steady and dynamic shear properties

The steady shear viscosity $\eta(\dot{\gamma})$ and the complex dynamic viscosity $\eta^*(\omega)$ were compared on semi-dilute solutions of xanthan in excess salt to screen the electrostatic interaction. The agreement was found to be good. The dynamic experiments determine the storage modulus (G') and the loss modulus (G'') with :

$$\eta^*(\omega) = [(G'^2 + G''^2)]^{1/2} / \omega \quad (6)$$

G' and G'' intercept for a frequency ω which decreases when the polymer concentration increases following the same dependence as $\dot{\gamma}_T$ the critical shear rate for the transition from the Newtonian to

viscoelastic domain.

This value depends on the molecular weight and polymer concentration; γ_r is usually related to the longest relaxation time of the Rouse spectrum for a polymeric solution. Recently the calculated values were compared with the experimental one for hyaluronic acid (4) as previously performed for xanthan (2).

The following relations were considered :

$$\begin{aligned} (\gamma_r)^{-1} \sim \tau_{r,0} &= 6 \eta_0 [\eta] M / \pi^2 R T \quad C < C^* \\ \tau_r &= 6 (\eta - \eta_0) M / \pi^2 C R T \quad C > C^* \end{aligned} \quad (7)$$

It is usually found that γ_r is independent of C in the dilute regime and then decreases following a dependency in C^{-3} for large polymer concentrations in agreement with the reptation concept.

The reduced values G'/C and $G'' - \omega \eta_0 / C$ can be represented as a function of the generalized frequency $\omega \tau_r$. All the points for xanthan are on two curves with slope values 2 and 1 respectively in the range of lower concentration values corresponding to the Newtonian regime. Above the crossover frequency, the two slopes decrease (2). This is a general behaviour observed on semi-dilute solutions.

CONCLUSION

This paper describes the main rheological properties of polysaccharides in solution. The aqueous solvent is mainly considered in which electrostatic interactions take a large importance.

Some characteristics were pointed out taking as reference xanthan and hyaluronan. The cellulose derivatives are characterized by a persistence length around 50 Å in θ -conditions; they behave as semi-flexible chain. Their contribution to the viscosity of a fluid will be larger than with usual synthetic polymers causing also the Mark Houwink parameter a to be > 0.5 . The important parameters to control the intrinsic viscosity are the contour length and the mass per unit length M_L .

The chemical modifications which introduce ionic charge usually cause an increase of the viscosity but also of the salt sensitivity. The viscometric behaviour of these polysaccharides just looks like that of synthetic polymer controlled by $C[\eta]$ parameter.

REFERENCES

- (1) M. Milas, M. Rinaudo, B. Tinland, *Polym. Bull.* **14**, 157-164 (1985).
- (2) M. Milas, M. Rinaudo, M. Knipper, J.L. Schuppiser, *Macromolecules* **23**, 2506-2511 (1990).
- (3) E. Fouissac, Thesis, Grenoble, 1992.
- (4) E. Fouissac, M. Milas, M. Rinaudo, *Macromolecules* (submitted).
- (5) M. Rinaudo, *Polymer* **27**, 585-589 (1992).
- (6) M. Rinaudo, in "Gum and Stabilizers for Food Industry", Eds. G.O Phillips, D.J. Wedlock, P.A. Williams, Elsevier Sciences, 51-61 (1992).
- (7) M. Rinaudo, in Proceedings of 34th IUPAC International Symposium on Macromolecules, Prague (1992) Ed. J. Kahovec (in press).
- (8) H. Yamakawa, M. Fujii, *Macromolecules* **7**, 128 (1974).
- (9) J. Brandrup, E. H. Immergut, *Polymer Handbook*, 2nd Edition John Wiley Publish. (1975).
- (10) M. Milas, M. Rinaudo, in "Industrial Polysaccharides, Genetic engineering, structure/property relations and applications", Ed. M. Yalpani, Elsevier Publish., 217-223 (1987).
- (11) M. Rinaudo, M. Milas, P. Le Dung, *Int. J. Bio. Macromol.* in press (1993).
- (12) M. Saito, *Polymer Journal* **15**, 213-223 (1983).
- (13) M. Moan, C. Wolff, *Polymer* **16**, 777-780 (1975).
- (14) R. M. Davis, *Macromolecules* **24**, 1149-1155 (1991).
- (15) Y. Itoh, Communication at Cellucon 93 Symposium, Lund, June 93 (Sweden).
- (16) M. Rinaudo, M. Milas, *Biopolymers* **17**, 2663-2678 (1978).
- (17) T. Odijk, A.C. Houwaart, *J. Polym. Sci. Polym. Phys. Ed.* **16**, 627 (1978).

36 Xanthan—The natural water soluble cellulose derivative

B E Christensen*, B T Stokke** and O Smidsrød* – Norwegian Biopolymer Laboratory, * Department of Biotechnology and ** Department of Physics, NTH, University of Trondheim, Norway

ABSTRACT

Xanthan exists under most conditions in an extended double-stranded conformation, but may dissociate into disordered, single strands. The influence of both the chemical structure and the conformational state on properties such as solubility, viscosity, salt tolerance, stability towards chemical degradation, depolymerization kinetics and gel formation, are briefly discussed.

INTRODUCTION

Xanthan (Figure 1) is a cellulose derivative in the sense that it consists of a 1,4-linked β -D-glucan (i.e. cellulosic) backbone with side-chains linked to it. Unlike the semisynthetic cellulose derivatives, where native cellulose is chemically modified, xanthan is a natural product produced by bacteria of the genus *Xanthomonas*. A further difference is that xanthan is not synthesized by modification of cellulosic chains. Instead, the xanthan-producing bacteria produce a lipid-linked intermediate

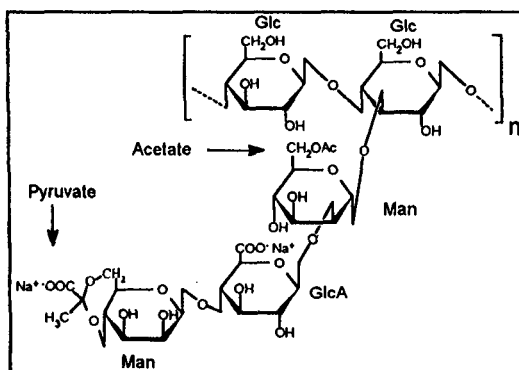


Figure 1 Pentasaccharide repeating unit of xanthan

containing the pentasaccharide repeating unit. This unit is subsequently added to the growing xanthan chain with a concomitant release of the lipid. As a result of the biosynthetic pathway, the side chains of xanthan are distributed along the backbone in a strictly *regular* pattern, substituting *O*-3 of every second glucose residue. The regularity of xanthan is in contrast to derivatized cellulose, where all of the three vacant hydroxyl groups (*O*-2, *O*-3 and *O*-6) in all glucose residues in principle may be

substituted. This suggests that the substituents are distributed in a simple statistical pattern, and that the relative content of all possible sequences, e.g. regions devoid of substituents, can be calculated directly from the degree of substitution in each of the three positions. However, analysis of unsubstituted glucose residues in carboxymethyl-cellulose (CMC) gives lower values than those calculated on a statistical basis [1].

The side chains of xanthan can be truncated to yield xanthan variants. Through genetic modification of xanthan-producing cells it has been reported that xanthan variants can be produced where each of the sugars in the side chains are successively removed [2]. The resulting variants, from the poly-pentamer to the poly-trimer (Figure 2, A-C), are therefore novel types of cellulose derivatives. In addition to the variants shown in Figure 2, variations with respect to pyruvate and acetate substitution may be produced. It is assumed, but not yet proven, that all side chains are identical and that they are regularly distributed along the backbone. However, except for the extensive genetic work which has been successfully carried out, little is so far known regarding the physical properties of these variants. An exception is the X-ray fibre diffraction study of the poly-tetramer, suggesting that its helical structure does not differ from native xanthan [3].

Another and fundamentally different way to produce changes in the side chains is by partial acid hydrolysis [4,5]. Following rapid removal of pyruvate and acetate, the terminal β -D-mannose is preferentially removed, in addition to a slow hydrolysis of the inner α -D-mannose (with concomitant loss of the entire side chain) and the cellulosic backbone. Such changes give rise to a continuous series of xanthan variants with different chemical compositions. In particular, both the regularity in the composition and in the lateral distribution of the side chains are perturbed. The resulting properties of these variants will be discussed in some detail later in this chapter. Finally, enzymes (β -D-mannosidases and β -D-glucuronidases) may potentially be employed to produce controlled removal of individual sugars from the side chains [6], although such techniques have apparently not yet been fully developed.

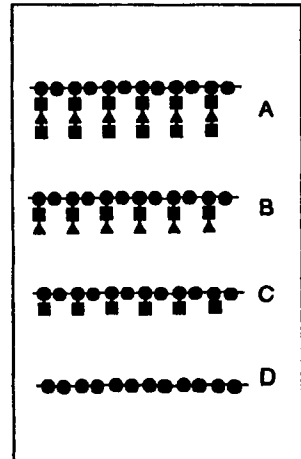


Figure 2 Xanthan variants which may be produced through genetic engineering. Symbols: ●: Glc; ■: Man; ▲: GlcA.

XANTHAN IN AQUEOUS SOLUTIONS.

As in most cellulose derivatives, the presence of side chains in xanthan ensures a high solubility in water. Xanthan may be precipitated from aqueous solutions by adding organic solvents (alcohols, acetone etc.), but is not precipitated by monovalent or divalent cations which are known to induce precipitation or gelation in other charged polysaccharides. Trivalent cations like Cr^{3+} , Al^{3+} or Fe^{3+} do, on the other hand, lead

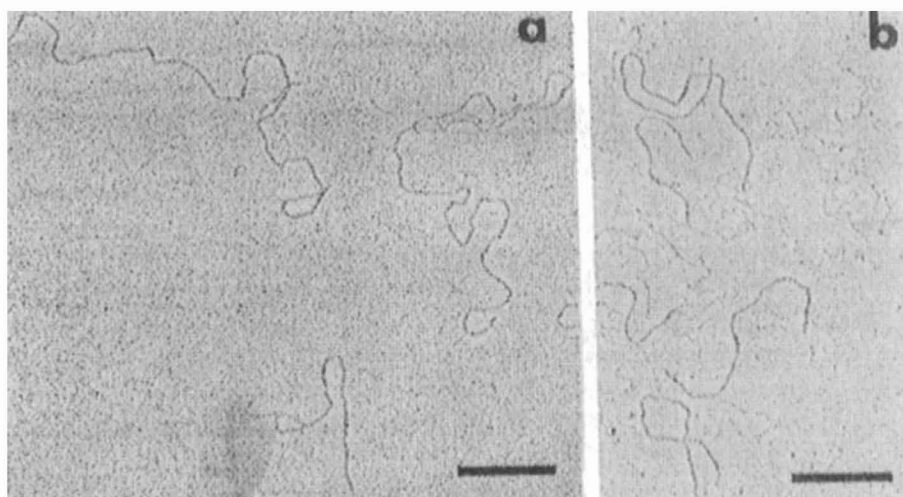


Figure 3 Electron micrograph of xanthan prepared under ordering (a) and disordering (b) conditions. Scale bar: 200 nm.

to precipitation or gelation (see below). Unlike many acidic polysaccharides, including CMC, xanthan is water soluble also in its acidic form ($\text{pH} < 3$). The ionization of the glucuronic acid (or, if present, the pyruvate) is therefore not required to obtain solubility in water. It seems therefore that the solubility is mainly linked to the ability of the side chains to prevent packing of the chains in crystals. Modifications of the side chains such as removal of acetate and pyruvate, removal of the terminal β -D-mannose, or even removal of at least up to 40% of the side chains, all have minor effects on the solubility in water. At present, it is not known whether or not it is possible to induce precipitation from aqueous solutions by forming long unsubstituted sequences along the cellulosic backbone, corresponding to that seen in some cellulose derivatives.

A certain degree of slow self-association in xanthan solution has been identified through dynamic light scattering studies [7]. However, the resulting aggregates are still water soluble, but may lead to a significant overestimation of the molecular weight. The aggregation is apparently prevented by the addition of urea.

As a water-soluble polymer, xanthan possesses many technologically useful physical properties such as:

- High viscosifying ability of aqueous solutions and 'weak gel' properties
- High stability towards chemical and biological degradation
- Low sensitivity towards pH and added salts
- Shear thinning (pseudoplasticity)

These, and other features, are consequences of essentially two molecular features. First, xanthan molecules are stiff and extended molecules, with persistence lengths in the range of 100 nm. This is about five times the values found for cellulose derivatives (see below). Secondly, the molecular weight of most commercial xanthans is well above 10^6 . In the following, the conformational properties of xanthan will be discussed somewhat more in detail.

DOUBLE-STRANDED XANTHAN (ORDERED STATE)

At moderate temperatures and ionic strengths xanthan exists in an ordered structure, giving rise to most of the observed physical properties. The nature of the ordered state has been much debated, but the double-stranded model has in recent years been most widely accepted, although some results are more adequately explained in terms of single-stranded conformations [8,9].

The most direct evidence for the double-stranded structure comes from electron micrographs of heavy-metal shadowed replicas made from aqueous solutions containing glycerol. This technique, which also has provided valuable information about the shape and conformation of other biopolymers such as collagen and scleroglucan [10], makes it possible to investigate a large number of individual molecules. For xanthan replicas prepared under *ordering* conditions (Figure 3a) the molecules appear as 'wormlike chains' of uniform thickness. Polydispersity in contour lengths is generally observed. The double-stranded nature of xanthan can be directly visualized under conditions of partial strand separation as seen in Figure 3b. Quantitative evidence for a double-stranded structure comes from estimation of the mass per unit length, M_L , which is obtained from the ratio between the molecular weight (M_w) and the contour length (L_w). All xanthans investigated under ordering conditions by this method have yielded values of M_L in the range of 1800-2000 nm^{-1} . For a fully extended single chain M_L should be around 1000 nm^{-1} , since the five-sugar repeating unit of xanthan has an equivalent weight of 850-970 (depending on the content of pyruvate and acetate), and the axial translation of one repeating unit is 0.94 nm (as determined by X-ray diffraction). Therefore, experimental values of 2000 nm^{-1} are in agreement with a double-stranded model.

For stiff and extended macromolecules like xanthan M_L can also be obtained by independent methods such as light scattering by investigating the scattering behaviour in the high-angle asymptotic domain. Results from such investigations have indeed yielded M_L -values near 2000 nm^{-1} [11,12], in agreement with the results from electron microscopy.

X-ray diffraction studies of oriented xanthan fibres were originally interpreted in favour of a 5_1 single helix [13]. Later X-ray studies have led to the conclusion that xanthan has a double-helical conformation [14,15], with a pitch of 4.7 nm, which corresponds to 0.47 nm per glucose residue. Sato *et al.* then used light scattering data in combination with a rigid-rod model (R_G - M relationship) to obtain linear mass

densities which corresponded to the same pitch [16]. On this basis they concluded that the same double-helical conformation of xanthan exists both in oriented fibres and in solution. Even though results from electron microscopy indicate that xanthan is double-stranded, the resolution of the method is not sufficient to distinguish between various types of double-strands, e.g. double-helices or side-by-side dimers.

The stiffness of double-stranded xanthan chains is usually expressed by means of the persistence length, q . This parameter can be determined in several ways, the most common being the use of the wormlike chain model for analysing the relationship between the intrinsic viscosity $[\eta]$ (at zero shear rate) and the molecular weight, or between the radius of gyration (R_G) and the molecular weight [17]. Results from such analyses have yielded q -values of 120 ± 20 nm [18].

The persistence length can alternatively be estimated from electron micrographs by statistical analysis of the local tangent-direction followed by correction for the dimensionality [19]. Values thus obtained for xanthan are in fair agreement with values obtained by other methods.

In comparison with q -values obtained for other polysaccharides xanthan belongs to the stiffest polysaccharides known, almost as stiff as triple-stranded β -D-glucans like scleroglucan and schizophyllan [19-22]. Cellulose derivatives are, on the other hand, more flexible than double-stranded xanthan, with q -values near 20 nm [12].

A direct comparison of chain stiffness in different polymers is also possible in terms of the parameters in the Mark-Houwink-Sakurada equation, linking $[\eta]$ to M through the exponent α :

$$[\eta] = KM^\alpha \quad (1)$$

For solid spheres $\alpha = 0$, and for rigid rods $\alpha = 1.8$. Random coils give values between 0.5 and 0.8. For flexible polymers α also depends on factors which may affect the extension and flexibility. For xanthan [23] the rodlike behaviour for $M_w < 2.5 \cdot 10^5$ results in an α -value of 1.5, at higher molecular weights a gradually more coil-like character leads to values closer to 1.0.

The increased chain stiffness of xanthan compared to cellulose derivatives is also well reflected in the salt tolerance, which expresses the flexibility changes and, hence, intrinsic viscosity changes, when varying the ionic strength (I). For coil-like polyelectrolytes, the salt tolerance is quantitatively expressed as the B-parameter [24] according to Equation 2:

$$B = \{\Delta[\eta]/\Delta(I^{1/2})\}/[\eta]_{I=0.1}^\nu \quad (2)$$

The term $[\eta]_{I=0.1}$ (intrinsic viscosity at an ionic strength of 0.1 M) is incorporated to cancel out effects due to different molecular weights, and the exponent ν is between 1.2-1.4. B is directly related to the Kuhn statistical length, A_m , (for a chain under θ -conditions), which for infinitely long chains is twice the persistence length. Figure 4 shows the B- A_m relationship for a series of biopolymers. The chain stiffness of CMC

is close to that of alginate, which also contains 1,4 diequatorial linkages, whereas double-stranded xanthan is much less flexible. The intrinsic viscosity of xanthan is almost independent of the salt concentration, except at very low ionic strengths, and in particular at elevated temperatures, where xanthan undergoes a conformational transition (see below).

For many carboxyl-containing polysaccharides the same intrinsic viscosity is obtained at 'infinite' ionic strength and in the acid form. In both cases the polymer is effectively neutralized. Xanthan, on the other hand, shows a characteristic and reversible decrease in $[\eta]$ when pH decreases below pK_a (~ 3) [25]. A concomitant decrease in R_G and reduction in persistence length (from 120 to 68 nm) indicates an increase in chain flexibility. At the same time the molecular weight remains constant, suggesting that the double-stranded structure is not affected. A detailed explanation of this behaviour in terms of the conformation of the glucan backbone and the role of the side chains, has so far not been presented.

The conformation of double-stranded xanthan also gives rise to a range of rheological properties which are of particular interest in many industrial uses. In addition to a high low-shear viscosity xanthan displays pronounced non-Newtonian behaviour, or shear-thinning. Typically, the relative viscosity of a 0.1% (w/v) xanthan solution in sea water may decrease from 110 at a shear rate of 1 s^{-1} to 10 at 100 s^{-1} [26]. The intrinsic viscosity shows a corresponding dependence upon the shear rate, and the Newtonian plateau is normally reached below $1\text{--}3 \text{ s}^{-1}$ for xanthans with $[\eta]$ up to 10.000 ml/g. The shear-thinning properties, which are ascribed to the partial alignment of the rodlike polymers upon shear, are of relevance during processing and pumping of polymer solutions. Once low shear conditions prevail, such as in oil bearing formations, the pumped solutions instantaneously regain their high viscosities. It may be noted that CMC may be tailored to give similar rheological properties [27]. This is apparently obtained through a more blockwise distribution of substituents where the unsubstituted regions associate to form multistranded CMC colloidal fibres.

THE CONFORMATIONAL TRANSITION

Xanthan undergoes a cooperative conformational transition upon heating and/or lowering the ionic strength. The transition is easily detected by chiroptical methods such

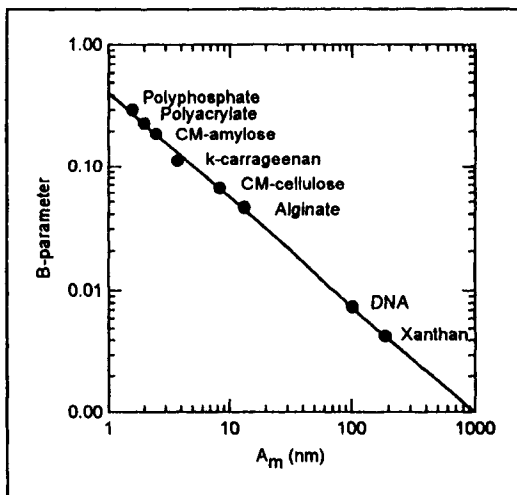


Figure 4 Relationship between the Kuhn statistical length (A_m) and the salt tolerance parameter (B)

as optical rotation or circular dichroism, or by differential scanning calorimetry (DSC). An example is given in Figure 5. The temperature at the midpoint of the transition is usually termed the melting temperature, T_m . As in most polyelectrolytes, T_m depends strongly upon both the ionic strength (Figure 6) and pH, since screening of the fixed charges by adding salt or lowering the pH (around pK_a) stabilizes the ordered conformation which has the highest charge density. In addition, the content of pyruvate (containing a charge) and acetate influences the transition by destabilizing or stabilizing the ordered conformation, respectively. It may be noted that heterogeneity in the distribution of pyruvate broadens the transition. Samples apparently displaying more than one transition are probably mixtures of xanthans with quite different pyruvate contents [28].

More drastic changes in the side chains such as complete removal of the terminal β -D-mannose or partial (up to 40%) removal of the entire side chains have relatively small effects on the conformational properties [5]. In particular, T_m and the ionic strength dependence of T_m are only marginally affected by such changes. However, the difference in optical rotation between the disordered and ordered state decreases linearly with a decrease in the content of β -D-mannose. Also, the transition enthalpy (ΔH_{cal}) decreases in the same way. This indicates that optical rotation and DSC mainly reflects conformational changes in the side chains rather than in the backbone. Nevertheless, it seems that the double helix of xanthan is quite robust, and is not affected by the mentioned changes in the side chains [3]. Further, electron micrographs of the partially hydrolyzed xanthans demonstrate that the basic conformational properties are largely unaffected, with an exception for an increase in the flexibility of the double-strands [29].

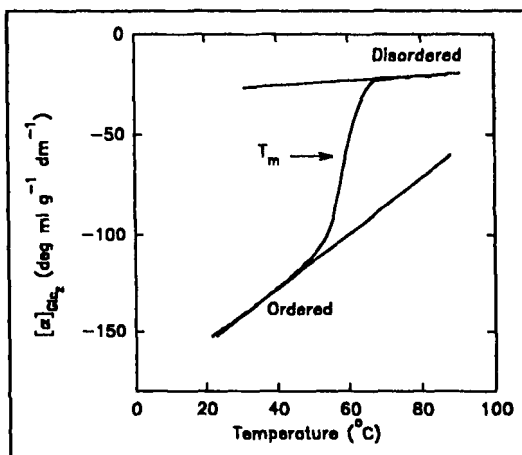


Figure 5 Temperature-driven conformational change of a xanthan sample in 10 mM NaCl.

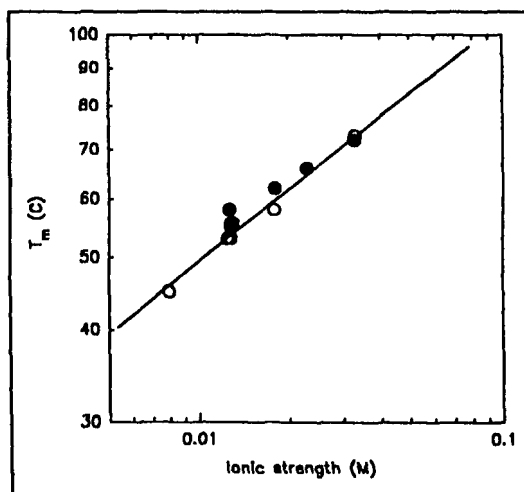


Figure 6 Ionic strength dependence of the transition temperature (T_m).

SINGLE-STRANDED XANTHAN (DISORDERED STATE)

Exposure of xanthan to low ionic strengths and high temperatures induces the cooperative transition from the ordered to the disordered state (Figure 5). Chiroptical methods give primarily information about local conformational changes, i.e. on the level of individual monosaccharide residues and glycosidic linkages. Strand separation, on the other hand, requires that *all* interchain segment-segment (non-covalent) bonds must be inactivated. It has consequently been quite difficult to obtain completely dispersed single chains in aqueous solutions within the range of polymer concentrations and temperatures which correspond to common experimental conditions. Even well above (typically 10-20°C) the chiroptically defined T_m , a small fraction of the residues in the glucan backbone are in the ordered state. Consequently, xanthan may pass through the chiroptically defined transition *without* the expected decrease in molecular weight [30-32]. It has actually been proposed that the dynamic equilibrium existing near T_m will lead to the formation of clusters consisting of more than two chains, thus explaining the observed increase in M_w and R_G with increasing temperature [31]. Characteristically, from the temperature-dependence of the second virial coefficient (A'_2), a second transition temperature (T'_m) is observed which lies 10°C above the optically determined T_m for a xanthan with $M_w \approx 2 \cdot 10^5$ [31]. Liu *et al.* [32] propose that the disordered conformation can be represented as a star-shaped, partially dissociated double chain under these conditions. A larger degree of chain dissociation (70%) has been reported in salt-free solutions at 95°C [33].

The difficulties in obtaining complete strand separation in water can apparently be circumvented by the use of cadoxen [tris(ethylenediamine) cadmium dihydroxide] [16,18,34,35]. In cadoxen, M_w values of nearly monodisperse xanthan fractions ($M_z/M_w = 1.1$) are very close to one-half of the values obtained in water. Further, a Mark-Houwink-Sakurada exponent of 0.87 is close to the values observed for CMC [36,37]. The use of cadoxen to determine strandedness of xanthan has been questioned, since degradation of the polymer can occur [38]. The latter authors also found $M_w(0.1 \text{ M NaCl})/M_w(\text{cadoxen})$ -values of 1.13-1.6 for enzymatically depolymerized samples. It should be noted, however, that the latter samples were depolymerized in the *disordered* conformation and then renatured to the ordered form. The renaturation of xanthan is apparently a complex process, as discussed below.

More conclusive results on single-stranded xanthan have in our opinion been obtained by electron microscopy, where it is possible to operate at very low polymer concentrations. This results in correspondingly low ionic strengths, with estimated T_m values well below 0°. Consequently, a large number of completely dissociated chains are observed, in addition to partially dissociated chains as well as various types of aggregates [39].

RENATURATION FROM THE DISORDERED STATE

A typical feature of xanthan solutions is the chiroptically detected hysteresis that is observed when heating above T_m followed by cooling [23]. More pronounced hysteresis is observed in viscosity measurements. At high concentrations (2%) re-natured xanthans even form highly viscoelastic solutions [40]. The latter has been interpreted in terms of the double-stranded model, where the partly dissociated single chains upon rapid cooling are prevented from returning to perfectly matched double-strands. Instead, the system becomes 'kinetically trapped' in a network where each chain can form several shorter double-stranded junctions with neighbouring chains.

An electron microscopic study [39] of more carefully renatured (ionic strength 10^{-5} M, polymer conc. 0.2 mg/ml, no heating) xanthans showed, on the other hand, that apparently perfectly matched double-strands could indeed reform, albeit slowly. Moreover, such treatment appeared to reduce the degree of aggregation found in the undenatured or native samples.

STABILITY

The salt tolerance of xanthan is an example of the physical stability of xanthan solutions. The double-stranded structure is quite robust, and the wormlike character of xanthan is maintained under most conditions, except at low ionic strength or at very high temperatures.

This picture is also reflected in the stability towards chemical degradation. When exposed to polymer degrading conditions (e.g. oxygen radicals, acids), double-stranded xanthan displays properties which are very different from single-stranded polymers such as cellulose derivatives. When passing above T_m , either by increasing the temperature or decreasing the ionic strength, the degradation rate increases rapidly. The degradation kinetics of ordered xanthan is incompatible with the single-chain model, for which a linear relationship between $1/M$ and the degradation time, t , is predicted for a random depolymerization process. This has been verified for several single-stranded polysaccharides, including hydroxyethylcellulose (HEC) as seen in Figure 7. Xanthan, on the other hand, shows an initial

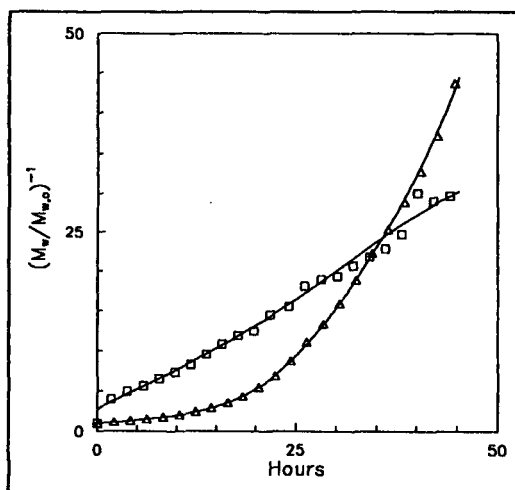


Figure 7 Degradation of xanthan (Δ) and HEC (\square) by H_2O_2 in the presence of Fe^{2+} .

phase with marginal changes in M_w , followed by a transition to a second time domain, where more rapid degradation apparently takes place. This is in qualitative accordance with the behaviour found in double-helical DNA.

In order to develop a quantitative model for the degradation of multiple-stranded polymers in general, a Monte Carlo analysis has been performed [41]. The key feature which determines the molecular weight decay is, in addition to the rate of cleavage of glycosidic bonds in the backbone, the cooperative character of the conformational transition. According to the theory, a minimum chain length (DP_{min} , in terms of sugar residues in the backbone) is needed to stabilize the ordered, double-stranded conformation. Quantitatively, DP_{min} depends on ΔH_{cal} and the cooperativity parameter, σ [42].

The simulation is carried out by introducing random breaks (at a defined rate) between adjacent backbone residues (glycosidic linkages). The structure remains intact if breaks in the same chain are separated by a distance larger than DP_{min} . (Figure 8A).

A break in the total structure only

occurs if both of the involved strands are broken in positions not separated by a distance larger than DP_{min} (Figure 8B). In addition, oligomers with DP less than DP_{min} may be released as shown in Figure 8C. Oligomers larger than DP_{min} may be released under quite special circumstances, as shown in Figure 8D. The degradation thus generates a complex distribution of macromolecular species. From the entire distribution, the relevant parameters (e.g. M_w) are calculated. By this method a time domain, occurring when $M_{w,t}/M_{w,t=0} < 0.1$, was identified, where M_w varied with time according to Equation 3:

$$M_{w,t} = M_{w,t=0} kt^\varepsilon \quad (3)$$

The parameter ε was found to be $2.3 (\pm 0.1)$ for a triple-stranded polymer, $1.66 (\pm 0.06)$ in the double-stranded case, and 1 (as expected) for single-strands, provided that (DP_{min}) was below 15.

When xanthan was subjected to partial acid hydrolysis, the results obtained with respect to ε were in fair agreement with the double-stranded model [29]. A main problem was to obtain enough data for $M_{w,t}/M_{w,t=0} < 0.1$, since an increasing amount of single-stranded oligomers are released in this time domain. These oligomers are probably more rapidly degraded, and the ε -value is expected to differ from those above.

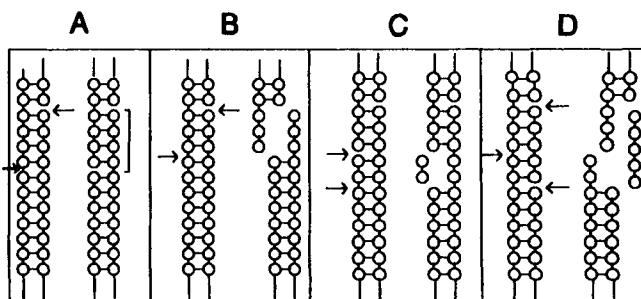


Figure 8 Schematic illustration of the consequences of cleaving linkages (arrow) in a double-stranded polymer

The release of oligomers is conveniently monitored by HPLC or gel filtration. Figure 8 shows the gel filtration elution profile for a sample degraded to $M_w = 67000$. The sample consists of two distinct fractions. The high M_w -fraction (I) was isolated, and it was subsequently shown by optical rotation that the fraction was in the ordered conformation, whereas fraction II indeed was disordered [29].

The amount of disordered oligomers released depends also on DP_{min} , and may be calculated by the Monte Carlo analysis for various values of DP_{min} . Comparison to experimental data for a series of hydrolysed xanthans suggested that DP_{min} corresponded to 10-15 glucose residues [29].

In degradation experiments such as those described above, changes occur also in the side chains. In acid hydrolysis, the terminal β -D-mannose is rapidly cleaved due to intramolecular catalysis by the glucuronic acid [4]. In the sample shown in Figure 9 all of the β -D-mannose and about 40% of the remaining side chains are hydrolysed. Nevertheless, the double-stranded form of xanthan is so robust that the conformational properties (except for the released oligomers) are largely retained [5,29].

As a biopolymer xanthan is biodegradable. However, under laboratory conditions, xanthan is unusually stable as long as it is maintained in the ordered form. In contrast, aqueous solutions of single-stranded polysaccharides easily become contaminated by microorganisms with polysaccharide degrading enzymes. The use of standard microbiological enrichment techniques has, however, provided bacterial cultures capable of producing 'xanthanases' which cleave linkages both in the side chains and in the backbone of xanthan [43].

The cellulosic backbone of single-stranded xanthan may be degraded by cellulases [43,44,47], yielding a mixture of oligomers and, in some cases, a cellulase-resistant high- M_w fraction. This reaction is inhibited by salt, which induces the ordered, double-stranded conformation. It has been speculated that regions of the backbone that are devoid of side chains are the main targets for cellulases [43]. This view is supported by recent observations using xanthans where the side chains have been partly removed (unpublished results).

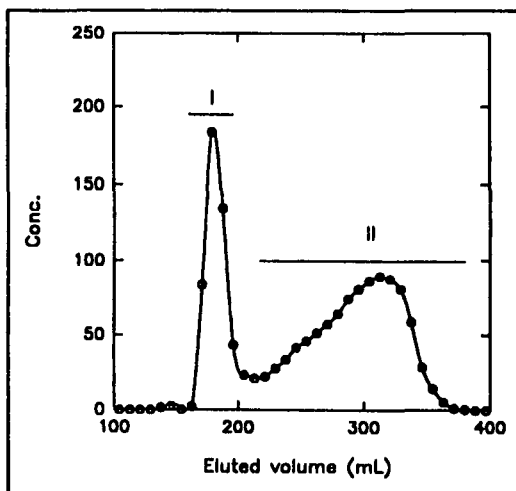


Figure 9 Gel filtration of a xanthan sample hydrolyzed to $M_w = 67000$.

GELATION

In the presence of metal ions Cr^{3+} , Al^{3+} and Fe^{3+} , xanthan may produce firm gels [45,46]. Cr-xanthan gels have been investigated in some detail because of their potential to block the water flooding of unproductive permeable zones in stratified oil reservoirs. An important property of such gels is that the gelation kinetics can be controlled by varying the concentration of Cr(III). For oil field operations, delayed gelation is a prerequisite, since gels should start to form once they are placed in the proper subterranean formation, but not during pumping and transport in the formations.

The mechanisms for the formation of Cr-xanthan gels are not known in detail. One reason is that Cr(III) forms oleates, i.e. inorganic oligomers, which may have different cross-linking properties. In the pH-range where the strongest gels are formed (pH ~ 5), the major Cr-species is the dimer, and it is believed that this component is the primary cross-linker [46].

The nature of the junction, i.e. the xanthan-Cr(III) 'bond', is thought to be of the ligand type. The Cr-species bind ligands, including water, strongly. Ligand exchange is also a slow process and the use of competing ligands such as acetate may therefore be used as an additional means to obtain delayed gelation.

The major polymer alternatives to Cr-xanthan gels in oil production are gels formed between Cr(III) or Al(III) and partially hydrolysed polyacrylamide (PAM). However, PAM or other single-stranded polymers are not as stable as double-stranded xanthan in saline formation water.

Although xanthan is commonly used in many food products, Cr-xanthan gels are obviously not suitable as food ingredients. Instead, the synergism between xanthan and certain galactomannans can be utilized [47]. The nature of these gels, e.g. the junction type, is not fully understood. It is believed that unsubstituted regions in the mannan backbone interact with xanthan, but it seems to be less clear whether it is the ordered or disordered form of xanthan that is involved in cross-linking.

REFERENCES

1. M.G. Wirick. *J. Polym. Sci.*, A-1, 1988, 6, 1965-1974.
2. R.W. Vanderslice, D.H. Doherty, M.A. Capage, M.R. Betlach, R.A. Hassler, N.M. Henderson, J. Ryan-Graniero and M. Tecklenburg. In: *Biomedical and Biotechnological Advances in Industrial Polysaccharides*. (Eds. V. Crescenzi, I.C.M. Dea, S. Paoletti, S.S. Stivala and I.W. Sutherland) Gordon and Breach Science Publ., New York, 1989, 45-156.
3. R.P. Millane and T.V. Narasaiah. *Carbohydr. Polym.* 1990, 12, 315-321.
4. B.E. Christensen and O. Smidsrød. *Carbohydr. Res.*, 1991, 214, 55-69.
5. B.E. Christensen, K.D. Knudsen, O. Smidsrød, S. Kitamura and K. Takeo. *Biopolymers*, 1993, 33, 151-161.

6. M.I. Tait and I.W. Sutherland. *J. Appl. Bacteriol.*, 1989, 66, 457-460.
7. J.G. Southwick, H. Lee, A.M. Jamieson and J. Blackwell. *Carbohydr. Res.*, 1980, 84, 287-295.
8. F. Lambert, M. Milas and M. Rinaudo. *Int. J. Biol. Macromol.*, 1985, 7, 49-52.
9. S.A. Jones, D.M. Goodall, A.N. Cutler and I.T. Norton. *Eur. Biophys. J.*, 1987, 15, 185-191.
10. B.T. Stokke and A. Elgsæter. In: *Advances in Carbohydrate Analysis*, Ed. C.A. White, JAI Press, Birmingham, 1991, 195-247.
11. G. Paradossi and D.A. Brant. *Macromolecules*, 1982, 15, 874-879.
12. T. Coviello, K. Kajiwara, W. Burchard, M. Dentini and V. Crescenzi. *Macromolecules*, 1986, 19, 2826-2831.
13. R. Moorhouse, M.D. Walkinshaw and S. Arnott. *ACS Symp. Ser.*, 1977, 45, 90-102.
14. K. Okuyama, S. Arnott, R. Moorhouse, M.D. Walkinshaw. *ACS Symp. Ser.*, 1980, 141, 411-427.
15. E.D.T. Atkins. *NATO ASI Ser, Ser E*. 1990, 186, 371-386.
16. T. Sato, T. Norisuye and H. Fujita. *Polym. J.*, 1984, 16, 341-350.
17. H. Yamakawa and T. Yoshizaki. *Macromolecules*, 1980, 13, 633-643.
18. T. Sato, T. Norisuye and H. Fujita. *Macromolecules*, 1984, 17, 2696-2700.
19. B.T. Stokke and D.A. Brant. *Biopolymers*, 1990, 30, 1161-1181.
20. T. Yanaki, T. Norisuye and H. Fujita. *Macromolecules*, 1980, 13, 1462-1466.
21. Y. Kashiwagi, T. Norisuye and H. Fujita. *Macromolecules*, 1981, 14, 1220-1225.
22. C.J. Carriere, E.J. Amis, J.L. Schrag and J.D. Ferry. *Macromolecules*, 1985, 18, 2019--2023.
23. W. Liu, T. Sato, T. Norisuye and H. Fujita. *Carbohydr. Res.*, 1987, 160, 267-281.
24. O. Smidsrød and A. Haug. *Biopolymers*, 1971, 10, 1213-1227.
25. L. Zhang, W. Liu, T. Norisuye and H. Fujita. *Biopolymers*, 1987, 26, 333-341.
26. B.T. Stokke, A. Elgsæter, E.Ø. Bjørnstad and T. Lund. *Carbohydr. Polym.*, 1992, 17, 209-220.
27. J.G. Westra. *Macromolecules*, 1989, 22, 367-370.
28. S. Kitamura, K. Takeo, T. Kuge and B.T. Stokke. *Biopolymers*, 1991, 31, 1243-1255.
29. B.E. Christensen, O. Smidsrød, A. Elgsæter and B.T. Stokke. *Macromolecules*, 1993, 26, 6111-6120.
30. I.T. Norton, D.M. Goodall, S.A. Frangou, E.R. Morris and D.A. Rees. *J. Mol. Biol.*, 1984, 175, 371-394.

31. L.S. Hacche, G.E. Washington and D.A. Brant. *Macromolecules*, 1987, 20, 2179-2187.
32. W. Liu and T. Norisuye. *Biopolymers*, 1988, 27, 1641-1654.
33. K. Kawakami, Y. Okabe and T. Norisuye. *Carbohydr. Polym.*, 1991, 14, 189-203.
34. T. Sato, S. Kojima, T. Norisuye and H. Fujita. *Polym. J.*, 1984, 16, 423-429.
35. T. Sato, T. Norisuye and H. Fujita. *Polym. J.*, 1985, 17, 729-735.
36. W. Brown, D. Henley and J. Ohman. *Ark. Kemi.*, 1964, 22, 189-205.
37. H. Estenbauer, J. Schurz and A. Wirtl. *Cellulose Chem. Technol.*, 1985, 19, 341-355.
38. M. Milas and B. Tinland. *Carbohydr. Polym.*, 1990, 13, 47-56.
39. B.T. Stokke, O. Smidsrød and A. Elgsæter. *Biopolymers*, 1989, 28, 617-637.
40. H.W. Oviatt and D.A. Brant. *Int. J. Biol. Macromol.*, 1993, 15, 3-10.
41. B.T. Stokke, B.E. Christensen and O. Smidsrød. *Macromolecules*, 1992, 25, 2209-2214.
42. J. Applequist and V. Damle. *J. Am. Chem. Soc.*, 1965, 87, 1450-1458.
43. I.W. Sutherland. *Carbohydr. Res.*, 1984, 131, 93-104.
44. M. Rinaudo and M. Milas. *Int. J. Biol. Macromol.*, 1980, 2, 45-48
45. T. Lund, O. Smidsrød, B.T. Stokke and A. Elgsæter. *Carbohydr. Polym.*, 1988, 8, 245-256.
46. H. Nolte, S. John, O. Smidsrød and B.T. Stokke. *Carbohydr. Polym.*, 1992, 18, 243-251.
47. N.W.H. Cheetham and E.N.M. Mashimba. *Carbohydr. Polym.*, 1991, 15, 195-206.
48. R.O. Mannion, C.D. Melia, B. Launay, G. Cuvelier, S.E. Hill, S.E. Harding and J.R. Mitchell. *Carbohydr. Polym.*, 1992, 19, 91-97.

37 Effect of temperature on high-methoxyl pectin gelation

J A Lopes da Silva* and M P Gonçalves** – * Escola Superior de Biotecnologia, UCP, Rua Dr António Bernardino de Almeida, 4200 Porto, Portugal; ** Departamento de Engenharia Química, Faculdade de Engenharia, Rua dos Bragas, 4099 Porto Codex, Portugal

ABSTRACT

High methoxyl pectin (HMP) gelation was investigated by small amplitude oscillatory experiments. The system studied was 1% HMP + 60% sucrose (citrate buffer, pH 3). Time sweep experiments and mechanical spectra were performed at different temperatures between 5°C and 60°C. The gel time and the shear modulus have a complex dependence on temperature, which could be explained by the opposing effects of increasing temperature on both types of interactions that stabilise the HMP gels. The "final" viscoelastic behaviour of the HMP gels also changes with the ageing temperature at which the system has been submitted. Between 15-50°C the behaviour is typical of a true gel, but for lower and higher temperatures, the behaviour changes to that of weak gels, with higher dependence on frequency for the dynamic moduli.

INTRODUCTION

Pectins are anionic structural polysaccharides extracted from the primary plant cell wall. They consist of a linear backbone of randomly connected (1→4)- α -D-galacturonic acid residues partially esterified with methoxyl groups. Neutral sugars are also present, as side-chains bound to the galacturonate chain or inserted into the main chain (rhamnose), usually in amounts of about 5-10% of the galacturonic acid. Pectins with degrees of methylation (DM) (molar ratio of methoxyl groups to galacturonic acid) higher than 50%, or high-methoxyl pectins, form gels at pH lower than

about 3.5 and when the water activity is reduced by addition of a cosolute, typically sucrose, at a concentration higher than 55% by weight.

The properties of HMP gels have been extensively studied, mainly by using empirical methods based on internal strength/breaking measurements and SAG techniques (Crandall & Wicker, 1986), and also some fundamental measurements by static viscoelastic methods, like creep compliance (Kawabata, 1977; Plashchina et al., 1979; Dahme, 1985) and stress relaxation (Comby et al., 1986). In comparison to the studies that have been done on fully set gels, only a few measurements have been reported during the HMP sol-gel transition, including small amplitude oscillatory rheological tests (Ikkala, 1986; Beveridge & Timbers, 1989; Dahme, 1992; Rao et al., 1993).

High-methoxyl pectin gelation is quite a complex process, in which several kinds of intermolecular interactions are involved. Complications arise also from polyelectrolyte effects. The available results suggest that in gels of high methoxyl pectins the junction zones are stabilised by hydrogen bonds and also by hydrophobic interactions between the ester methyl groups (Walkinshaw & Arnott, 1981; Oakenfull & Scott, 1984).

The role of hydrophobic interactions in stabilizing polysaccharide networks has been studied by different techniques: the relative effects of organic solvents (Oakenfull & Scott, 1984), temperature effects (Oakenfull & Scott, 1984, 1986), and the relative influence of the lyotropic series of salts (Case et al., 1992).

In this study we investigated the influence of temperature on the viscoelastic properties of HMP gels, near the gelation point and after maturation of the gels, by using dynamic rheological methods. Our purpose was to use the variation on temperature as a tool to know the relative influence of hydrophobic interactions and hydrogen bonds on the evolution of the viscoelastic properties of HMP gels.

MATERIALS & METHODS

Pectin sample

The pectin sample used was a commercial citrus pectin obtained from Bulmer (England). The DM was 64% as determined by gas chromatography and the percentage of anhydrogalacturonic acid (AGA) was 82% as determined colorimetrically. The intrinsic viscosity was 4.8 dl/g in 0.1M NaCl at 25°C. Details of the analytical procedures have been described elsewhere (da Silva et al., 1992).

Preparation of the gels

The pectin was previously dispersed overnight in 0.1M citrate buffer (pH 3.0) at room temperature, and then centrifuged for 1 hour at 28000 g. The dispersion was heated at 105°C in a paraffin bath for 3 min. and then the required amount of sucrose was added under stirring. The heating was

continued for 7 min., the lost water was replaced and the sample was transferred to the instrument plate at the desired test temperature. The time elapsed from the beginning of the heating process (total of 10 min at $105\pm 2^\circ\text{C}$) to the commencement of the test was exactly 15 min.

Rheological experiments

Dynamic rheological measurements were performed using a Carri-Med CS-50 controlled-stress rheometer with a temperature-regulated cone-plate device (radius 25 mm, cone-plate angle 4°).

After the sample was transferred to the instrument plate, the exposed surface of the sample was covered with a thin layer of low viscosity paraffin oil to avoid solvent evaporation. The kinetics of gel formation at different temperatures were monitored by measuring the storage (G') and the loss (G'') moduli at 0.5 Hz at a low deformation of 0.03, for about 48 h. Mechanical spectra were recorded in a constant strain mode with the same low deformation of 0.03 maintained over the frequency range explored, between 0.005 and 5 Hz.

RESULTS & DISCUSSION

Gel cure experiments have been performed on the HMP+sucrose systems (1% HMP, 60% sucrose, citrate buffer pH 3.0) at several ageing temperatures. Some of the cure curves obtained are shown in Figure 1. The general behaviour is typical of biopolymer gel systems. Both moduli increase as a result of the increasing junction zones density, with the elastic component (storage modulus, G') rising more sharply than the viscous component (loss modulus, G''), rapidly at first and then more slowly reaching an apparent plateau.

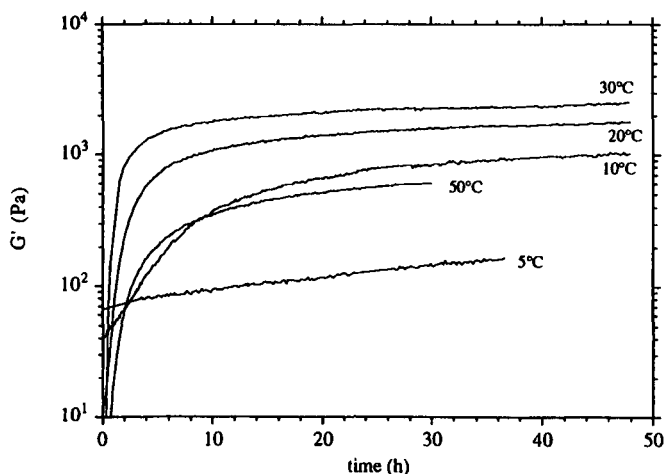


Figure 1. Storage modulus (G') vs. time for a 1% HMP sol/gel (pH 3.0, 60% (w/w) sucrose), at several ageing temperatures.

The particular behaviour at low temperatures should be noted. In the beginning of the cure experiment at 5°C, G' is higher than G'' . Aggregation phenomena, possibly controlled by hydrogen bonding, must be responsible for the high values of G' in this initial phase of the gellation process. However, the ageing process evolves slowly and monotonously. After the 48 h ageing period, the gel modulus reached a lower value than at higher temperatures, and the difference between the dynamic moduli was smaller. The storage modulus continued to increase as a function of time for all the temperatures studied, but this was more evident at 5°C.

The gel time (t_g) was determined for each ageing temperature (Fig. 2a).

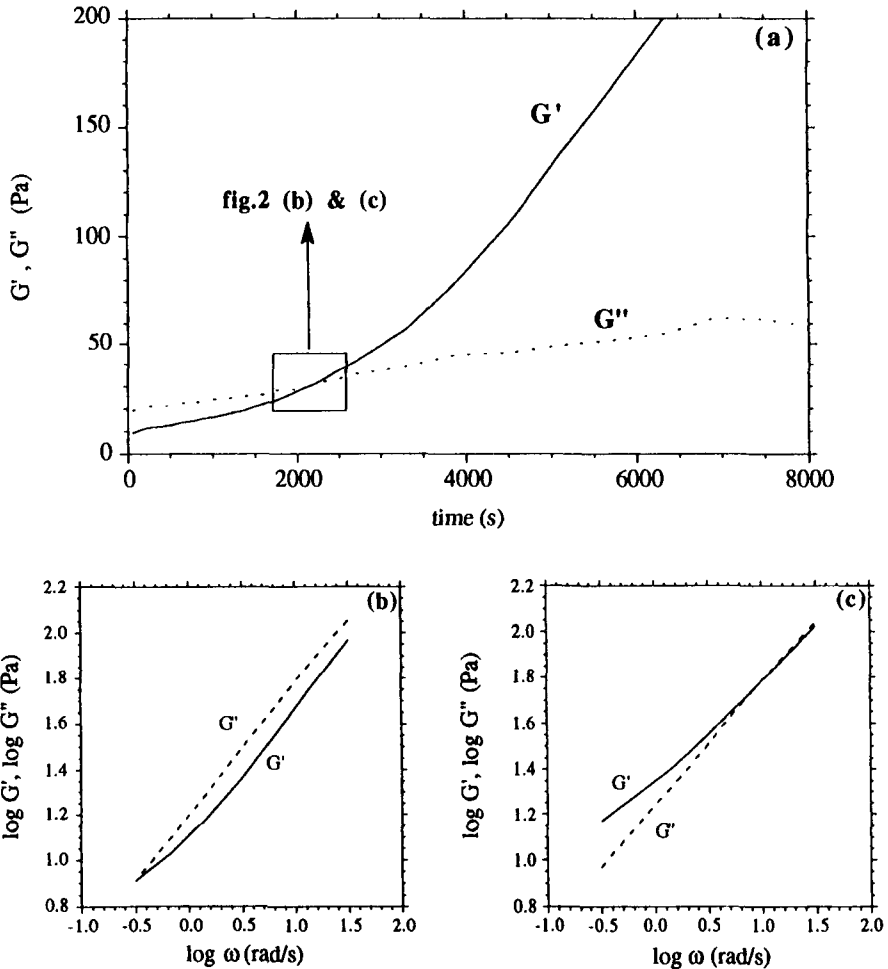


Figure 2. Sol-gel transition for 1% HMP (pH 3.0, 60%(w/w) sucrose), at 20°C and 0.5 Hz: (a) cross-over of the storage (G') and loss (G'') moduli, defining a gel time (t_g) of 36 min; (b) mechanical spectra measured at $t=28-31$ min, and (c) measured at $t=39-42$ min.

The gel time was considered as the time elapsed from the moment when the sample reached the study temperature until the cross-over of the storage (G') and loss (G'') moduli,

For temperatures lower than 10°C or higher than 70°C , important macromolecular aggregation occurred in our systems, and the gel times could not be estimated because they were shorter than the time elapsed before the beginning of the cure experiments.

Frequency sweeps were performed at different stages of the pectin network formation. Frequency sweeps performed in the vicinity of the gel point are shown in Figures 2b and 2c. Shortly before t_g the system is still a liquid, with G' and G'' having about the same slope of 0.58, but with G' tending to a limiting value at low frequencies. The tendency to an elastic plateau at low frequencies is more evident shortly after t_g , with $G' > G''$ at low frequencies and G' and G'' superimposed at higher frequencies.

Some frequency sweeps recorded for aged gels are shown in Figure 3.

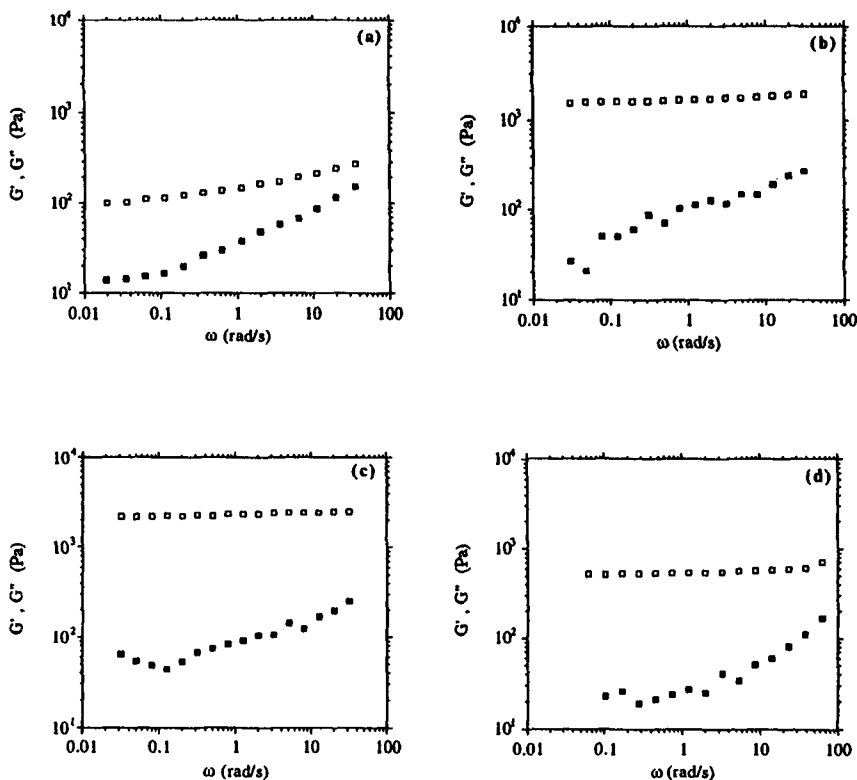


Figure 3. Mechanical spectra for a 1% HMP gel (pH 3.0, 60% (w/w) sucrose) measured at 36 h ageing time, for different ageing temperatures: (a) 5°C , (b) 20°C , (c) 30°C , and (d) 50°C . Open squares - storage modulus (G'); filled squares - loss modulus (G'').

The "final" viscoelastic behaviour of the HMP gels changes with the ageing temperature at which the system has been submitted. Between 15-50°C the behaviour is characteristic of a biopolymer gel: no molecular rearrangements take place within the network on time scales in the range of 0.003 to 32 seconds, G' is higher than G'' throughout the frequency range, and is almost independent of frequency (ω), and a power law dependence of the complex viscosity upon ω is observed. For lower and higher temperatures, the behaviour changes to that of weak gels, with higher dependence on frequency for the dynamic moduli. An increase of the loss modulus can be seen at higher frequencies, possibly related to the effect of dynamic entanglements (Clark & Ross-Murphy, 1987).

The gelation rate and the shear modulus have a complex dependence on temperature (Figure 4). This was also observed by Oakenfull and Scott (1986) for the gelation rate of similar systems. The differences we found, especially in the lower and higher temperature ranges, could be explained in terms of the different method used by those authors to describe the gel point.

Usually, for disordered biopolymers, the aggregation process leading to the building of the gelled network shows a different temperature dependence, with the storage modulus and the rate of gelation decreasing when the temperature increases. Some examples are the studies on gelatin gelation of te Nijenhuis (1981), where the mechanism is regulated by intermolecular triple helix formation, and the work of Durand and coworkers (1990) on low-methoxyl pectin gelation mediated by ionic complexation with calcium cations.

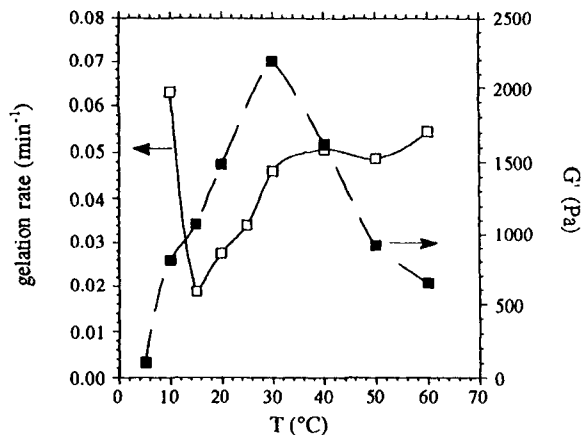


Figure 4. Effect of the ageing temperature on the gelation rate and on the storage modulus measured at 0.005 Hz for a 36 h aged 1% HMP gel (pH 3.0, 60% (w/w) sucrose).

The different behaviour of the HMP-sucrose systems could be explained by the opposing effects of temperature on both types of interactions that stabilise these kind of gels. Hydrophobic interactions increases when the temperature increases (Oakenfull & Fenwick, 1977), whereas hydrogen bonds decrease with increasing temperature. Hydrogen bonding at low temperatures or hydrophobic interactions at high temperatures could be responsible for important aggregation phenomena, but alone they are not strong enough to build up a stable HMP network.

REFERENCES

- Beveridge, T. and Timbers, G.E. (1989). *J. Texture Stud.*, **20**, 317-324.
- Case, S.E., Knopp, J.A., Hamann, D.D. and Schwartz, S.J. (1992). In "Gums and Stabilisers for the Food Industry 6", G.O. Phillips, P.A. Williams & D.J. Wedlock (eds.), pp. 489-500, Oxford University Press, London, UK.
- Clark, A.H. and Ross-Murphy, S.B. (1987). *Adv. Polym. Sci.*, **83**, 57-192.
- Comby, S., Doublier, J.L. and Lefebvre, J. (1986). In "Gums and Stabilisers for the Food Industry 3", G.O. Phillips, D.J. Wedlock & P.A. Williams (eds.), pp. 203-212, Elsevier, London, UK.
- Crandall, P.G. and Wicker, L. (1986). In "Chemistry and Function of Pectins", M.L. Fishman & J.J. Jen (eds.), pp. 88-102, American Chemical Society, Washington, USA.
- da Silva, J.A.L., Gonçalves, M.P. and Rao, M.A. (1992). *J. Food Sci.*, **57**, 443-448.
- Dahme, A. (1985). *J. Texture Stud.*, **16**, 227-239.
- Dahme, A. (1992). *J. Texture Stud.*, **23**, 1-11.
- Durand, D., Bertrand, C., Busnel, J.-P., Emery, J.R., Axelos, M.A.V., Thibault, J.F., Lefebvre, J., Doublier, J.L., Clark, A.H. and Lips, A. (1990). In "Physical Networks: Polymers and Gels", W. Burchard & S.B. Ross-Murphy (eds.), pp. 283-300, Elsevier, London, UK.
- Ikkala, P. (1986). In "Gums and Stabilisers for the Food Industry 3", G.O. Phillips, D.J. Wedlock & P.A. Williams (eds.), pp. 253-267, Elsevier, London, UK.
- Kawabata, A. (1977). *Memoirs of the Tokyo University of Agriculture*, **19**, 115-200.
- Oakenfull, D. and Fenwick, D.E. (1977). *Aust. J. Chem.*, **30**, 741-752.
- Oakenfull, D. and Scott, A. (1984). *J. Food Sci.*, **49**, 1093-1098.
- Oakenfull, D. and Scott, A. (1986). In "Gums and Stabilisers for the Food Industry 3", G.O. Phillips, D.J. Wedlock & P.A. Williams (eds.), pp. 465-475, Elsevier, London, UK.
- Plashchina, I.G., Fomina, O.A., Braudo, E.E. and Tolstoguzov, V.B. (1979). *Colloid Polym. Sci.*, **257**, 1180-1187.
- Rao, M.A., Van Buren, J.P. and Cooley, H.J. (1993). *J. Food Sci.*, **58**, 173-176, 185.
- te Nijenhuis, K. (1981). *Colloid & Polym. Sci.*, **259**, 522-535.
- Walkinshaw, M.D. and Arnott, S. (1981). *J. Mol. Biol.*, **153**, 1075-1085.

38 Phase behaviour of mixtures of associative polyelectrolyte with oppositely charged surfactant

F Guillemet, L Piculell, S Nilsson and B Lindman – Physical Chemistry 1, Chemical Center, University of Lund, PO Box 124, S-221 00 Lund, Sweden

ABSTRACT

The interaction of a hydrophobically modified cationic cellulose polymer with an anionic surfactant (SDS) has been studied by means of phase diagrams and viscometry. Over a wide range of compositions, an 'associative' phase separation occurs, resulting in the formation of two isotropic phases in equilibrium, one dilute and one concentrated in both surfactant and polyelectrolyte. Since the polymer charges are located at its hydrophobic side chains, a delicate balance between electrostatic and hydrophobic interactions is expected. A strong sensitivity to added salt was also detected.

INTRODUCTION

Water soluble polymers containing a small number of hydrophobic substituents are often referred to as hydrophobically modified polymers (HM polymers)¹. The contact between the hydrophobic groups and water is energetically unfavourable², so that these polymers have a strong tendency to associate. Because of this amphiphilic behaviour, HM polymers are also called 'polymeric surfactants' or 'associative thickeners'. Since they may act as powerful rheology modifiers, even at low concentration, they can be used in various industrial applications such as enhanced oil recovery, paints, foods, *etcetera*...

HM polymers are also of considerable interest owing to their strong interaction with surfactants³. Indeed, upon surfactant addition, a dramatic increase in viscosity is observed, due to the cross-linking of the polymer chains by the surfactant micelles. The formation of the cross-links is facilitated by the presence of strongly hydrophobic groups on the polymer backbone. At higher surfactant concentrations, the number of polymer groups per micelle decreases until the cross-links vanish. This

close to that of pure water, while the bottom phases were highly viscous and sometimes hazy.

The concentration of polymer in the supernatant phase was determined by a colorimetric method¹¹ using a UV-Visible Perkin-Elmer spectrophotometer. The total amount of polymer and surfactant in the bottom phase was obtained by weighing after freeze drying. Then, it was possible to calculate the concentrations of polymer and surfactant in both phases.

The viscometric measurements were performed at 25°C with an Ostwald capillary viscometer (the flow time of water was about 130 s in a 0.7 mm diameter tube). The samples were mixed for one day and not centrifuged.

RESULTS AND DISCUSSION

Figure 2 illustrates the phase diagram of the pseudo-ternary LM200-SDS-water system. A droplet shaped two-phase region is located in the water corner, with two isotropic phases in equilibrium. The supernatant phase is of low viscosity and the bottom phase is rich in both polymer and surfactant. Since the charge density of the polymer is low, the two-phase region exhibits a strong asymmetry with respect to the bisector of the water corner. Addition of small amounts of SDS to a polymer solution causes coacervation (liquid-liquid phase separation) while some polymer can still be soluble in a more concentrated micellar solution.

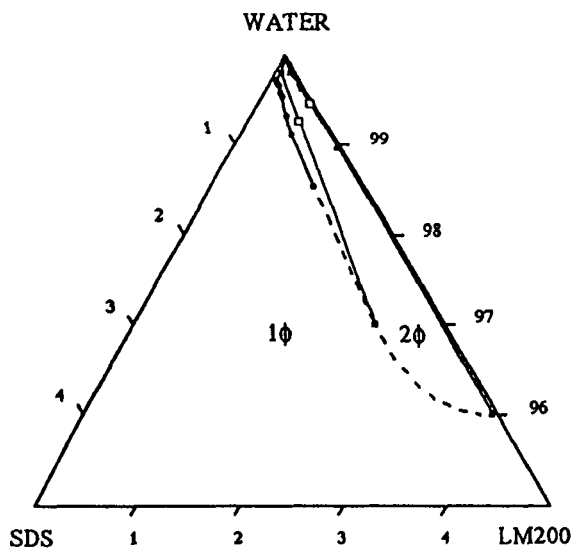


Figure 2. Experimental pseudo three-component phase diagram for the LM200-SDS-water system. The dashed part of the phase boundary indicates uncertainty in this region. The composition (in wt%) of two samples located in the two-phase region is indicated. Open squares refer to initial sample compositions, and filled squares connected by the tie lines refer to the compositions of the two phases in equilibrium.

Figure 3 is another representation of the phase diagram for the LM200-SDS-Water system, without salt and with 10 mM NaCl. The two-phase region is delineated by two boundaries, one at low surfactant concentrations, referred to as the

coacervation line, and the other at high surfactant concentrations, referred to as the resolubilization line. The coacervation line is in good agreement with the charge neutralisation line, which corresponds to systems containing equal amounts of polymer and surfactant charges. With salt addition, the coacervation line is shifted to lower surfactant concentrations but retains its shape, while the resolubilization line is moved to higher surfactant concentrations. It is interesting to notice the very low surfactant concentration needed to induce the phase separation.

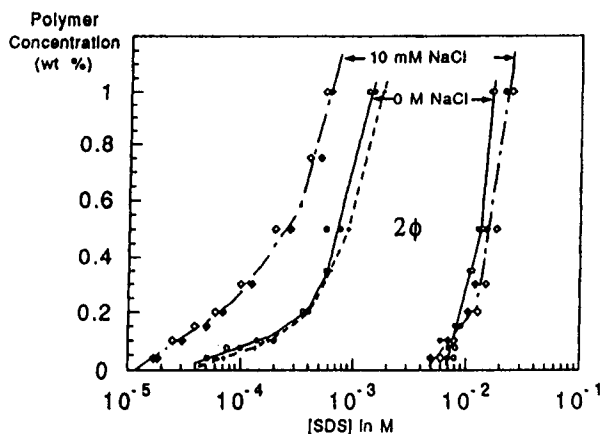


Figure 3. Phase diagram of the system LM200-SDS-Water, without salt (—) and with 10 mM NaCl (— · —). The charge neutralisation line (— · — · —) corresponds to an equal amount of polymer and surfactant charges.

Coacervation. Upon surfactant addition, the surfactant molecules bind to the cationic hydrophobic side chains of LM200, forming a complex with a reduced overall charge and a higher hydrophobicity. The tendency toward association can be explained both by the electrostatic attraction¹² and the formation of hydrophobic 'bonds' between the surfactant and the polymer alkyl chains⁵. Due to the decrease in the electrostatic repulsions and in the hydrophilicity, the complex starts to aggregate at a certain degree of surfactant binding. The solution becomes opalescent and, if the polymer concentration is high enough, a macroscopic phase separation occurs. For polymer concentrations lower than 0.2 wt%, the solutions turn opalescent and are stable over several weeks or even months. However, centrifugation of these samples induces a macroscopic phase separation, with a neat boundary between the two phases. The near coincidence of the coacervation and the charge neutralisation lines indicates that phase separation may be expected at a binding ratio close to one surfactant ion per charged polymer segment.

Resolubilization. With excess of surfactant, the polymer-surfactant complex becomes negatively charged so that electrostatic repulsions lead to a resolubilization of the complex. However, the detail of this mechanism has to be clarified. A certain part of the added surfactant molecules may not adsorb on the hydrophobic polymer side chains and then act as free ions in the solution. Thereby, the ionic strength of the solution increases and the electrostatic repulsions needed to resolubilize the complex are screened. This may explain why the resolubilization occurs at surfactant concentrations much higher than the concentration corresponding to the stoichiometric charge reversal of the complex.

Salt effect. A striking feature occurs in these mixtures of HM polymer with oppositely charged surfactant: in the presence of NaCl the two-phase region becomes

larger. The opposite trend is observed in mixtures of oppositely charged water soluble polyelectrolytes. Thalberg et al.¹³ have reported a suppression of the two-phase region when sufficiently high salt amounts were added in mixtures of hyaluronan and oppositely charged surfactants. As is evident from figure 4, LM200 derives its solubility from the presence of charges. For a 0.1 wt% polymer solution, the polymer chain exhibits a more compact conformation at salt concentrations as low as 10^{-4} M NaCl and is not soluble any more above 15 mM NaCl. Therefore, LM200 is an intrinsically water insoluble polymer (in the absence of charges). Salt addition decreases its solubility and hence phase separation occurs at lower surfactant concentrations. The resolubilization in the presence of salt requires higher surfactant concentrations. Again, this can be ascribed to the screening by the salt of the electrostatic repulsions responsible for the resolubilization of the polymer-surfactant complex.

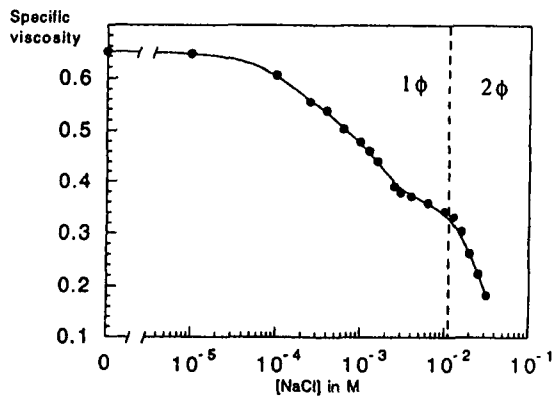


Figure 4. Specific viscosity of a 0.1 wt% solution of LM200 versus NaCl concentration at 25°C. In the two-phase region, the viscosity of the supernatant phase has been measured.

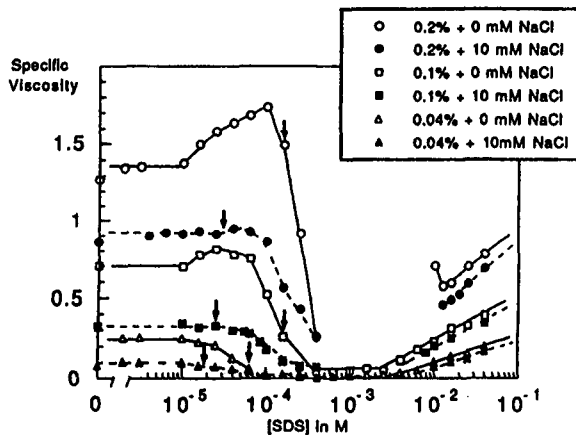


Figure 5. Specific viscosity versus SDS concentration, at 25°C, for different polymer concentrations, without salt (open symbols) and with 10 mM NaCl (filled symbols). The arrows correspond to the onset of phase separation as determined independently (cf fig. 3).

Viscosity. Figure 5 shows the viscosity of different polymer solutions versus surfactant concentration with and without salt. In all cases, a drop in the viscosity near the coacervation line is observed, corresponding to the onset of phase separation. It has to be noted that these samples, which had not been centrifuged, represent metastable dispersions. Nevertheless, these hazy samples can be stable for weeks or months, without appearance of a macroscopic phase separation.

At surfactant concentrations above the resolubilization line, the viscosity increases slightly. The elevation in viscosity is larger than the expected contribution from free micelles in solution. Hence this effect may result from a polyelectrolyte swelling of the complex, due to a continuous binding of the surfactant molecules to the polymer chains.

The lowering of the viscosity upon salt addition indicates a reinforcement of intramolecular interactions. The salt screens the repulsion between the polymer charges and promotes hydrophobic intramolecular association¹⁴. The polymer chains exhibit a more compact conformation.

For the salt free solutions containing more than 0.1 wt% LM200, intermolecular associations occur around 10^{-5} M SDS, giving an increase in viscosity. With salt addition, this rise vanishes. The formation of cross-links between the polymer chains is promoted by both hydrophobic interaction and electrostatic attraction between SDS molecules and the cationic alkyl tails of LM200 (at higher polymer concentration, ≥ 0.5 wt%, very viscous solutions are observed in this range of SDS concentrations). On the one hand, salt addition screens the favourable electrostatic interaction between SDS and LM200. On the other hand, the polymer chain exhibits a more compact conformation, which may lead to a transition from the overlap to the dilute regime¹⁵ (the overlap concentration, c^* , of the LM200 + 10 mM NaCl system was determined to 0.2 wt% by viscometry).

CONCLUSIONS

An 'associative' phase separation occurs in mixtures of cationic hydrophobically modified cellulose polymer and oppositely charged surfactant. This coacervation results from the binding of surfactant molecules to the hydrophobic side chains of the polymer, leading to the formation of an uncharged water insoluble complex. With excess of surfactant, electrostatic repulsions lead to the resolubilization of the complex. Salt addition induces an increase of the two-phase region. This has been attributed to the intrinsically water-insoluble character of the HM polyelectrolyte. Finally, it has been shown that salt addition could modulate the inter- and intra-molecular association of polymer chains in the presence of surfactant.

ACKNOWLEDGEMENTS

This work is part of a joint project with Dr. Christian Colette and Dr. Shu Rong Rebre from ELF ATOCHEM. We are grateful for all fruitful discussions and financial support. Krister Thuresson is acknowledged for valuable comments.

REFERENCES

1. Polymers in Aqueous Media, Glass J. E., Ed., ACS Symposium Series 223, American Chemical Society, Washington DC, 1989.

2. Tanford, C., *The Hydrophobic Effect : Formation of Micelles and Biological Membranes*, 2nd ed., John Wiley & Sons, New York, 1980.
3. B. Lindman and K. Thalberg, *Interaction of Surfactants with Polymers and Proteins*, Goddard, E. D., and Ananthapadmanabhan, K. P., Eds, CRC Press, 1993, 203.
4. Winnik, F. M., Ringsdorf, H., and Venzmer, J., *Langmuir*, 7, 905 and 912, 1991. Tanaka, R., Meadows, J., Phillips, G. O., and Williams, P. A., *Macromolecules*, 25, 1304, 1992. Dualeh, A. J. and Steiner, C. A., *Macromolecules*, 23, 251, 1990. Hu, Y. Z., Zhao, C. E., and Winnik, M. A., *Langmuir*, 6, 80, 1990. Biggs, S., Selb, J., and Candau, F., *Langmuir*, 8, 838, 1992. Thuresson, K., Nilsson, S., and Lindman, B., to be published in the conference proceeding of Cellucon'93, Lund.
5. Iliopoulos, I., Wang, T. K., and Audebert, R., *Langmuir*, 7, 617, 1991. Peiffer, D. G., *Polymer*, 31, 2353, 1990.
6. Cabane, B. and Duplessix, R., *Colloids Surf.*, 13, 19, 1985.
7. Hayakawa, K. and Kwak, J. C. T., in *Cationic Surfactants*, Rubingh, D. N. and Holland, P. M., Eds., Marcel Dekker, New York, 1991, 189.
8. Goddard, E. D., *Colloids Surf.*, 19, 301, 1986. Thalberg, K., Lindman, B., and Karlström, G., *J. Phys. Chem.*, 94, 4289, 1990. Dubin, P. L. and Oteri, R., *J. Colloid Interf. Sci.*, 95, 453, 1983.
9. Goddard, E. D. and Leung, P. S., *Colloids Surf.*, 65, 211, 1992.
10. Brode, G., Goddard, E. D., Harris, W. C., and Salensky, G. A., *Polym. Mater. Sci. Eng.*, 63, 696, 1990.
11. Dubois, M., Gilles, K. A., Hamilton, J. K., Rebers, P. A., and Smith, F., *Analytical Chem.*, 28, 350, 1956.
12. Piculell, L. and Lindman, B., *Adv. Colloid Interf. Sci.*, 41, 149, 1992.
13. Thalberg, K., Lindman, B., and Karlström, G., *J. Phys. Chem.*, 95, 6004, 1991.
14. Magny, B., Thèse, Université Paris VI, France, 1992.
15. Rauscher, A. and Hoffmann, H., *Tenside Surf. Det.*, 29, 101, 1992.

39 The interaction of amphiphiles with polysaccharides

K Shirahama, S Sato, L Yang and N Takisawa – Department of Chemistry, Faculty of Science and Engineering, Saga University, Saga 480, Japan

ABSTRACT

Amphiphiles such as surfactants, drugs, and dyes interact with polysaccharides. Such interactions were studied using binding isotherms obtained by means of amphiphile-sensitive electrodes. It was found that the amphiphiles were strongly bound to polysaccharides with electrical charge opposite to the amphiphiles implying the importance of electrostatic effects. On the other hand, amylose and some modified celluloses showed affinity to some amphiphiles. Thus polysaccharides provide an interesting field where a variety of interactions occur.

INTRODUCTION

Amphiphiles are a class of compound having both hydrophilic and hydrophobic groups. Thus biomolecules such as amino acids, lipids, and others fall into this category. Furthermore surfactants also belong to this class, and may be the most interesting not only because of their use as detergents in daily life and surface-treatment agents in industry but because of their typical amphiphilic character, on which a tremendous amount of academic research has been carried out[1,2]. It is noteworthy to point out that drugs and dyes are also classified as amphiphiles. Amphiphiles show intriguing phenomena: self-aggregation, adsorption, and interaction with other entities.

There are many papers on the interaction of amphiphiles with polymers both synthetic and natural, and ionic and non-ionic[3-6].

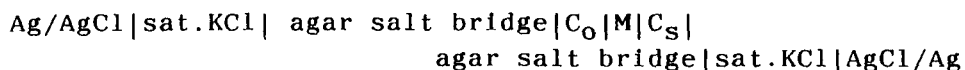
In this paper, we report some aspects of interactions of amphiphiles with polysaccharides. Polysaccharides might not be thought to interact with amphiphiles, because of their apparent hydrophilicity, but actually show affinity toward amphiphilic compounds under certain circumstances.

The interaction is best described using binding isotherms, which are conveniently obtained by amphiphile-selective electrodes developed in our laboratory.

EXPERIMENTAL SECTION

Amphiphile-selective electrodes

We have been developing various types of electrode for sensing amphiphiles, and we will describe here the most recent version of them. Our electrode is based upon the concentration cell:



where M is a membrane sensitive to an amphiphilic ion, C_0 a concentration of standard solution, and C_S that of sample solution. The electrode membrane has to be hydrophobic enough and to contain a small amount of charged group opposite to the amphiphilic ion in question. For this purpose, poly(vinyl chloride) is used together with an appropriate plasticizer which is either low molecular weight or polymer. A small amount of negative charge is implanted in the electrode membrane by either copolymerizing a monomer with a sulfonate group, or using persulfate as a polymerization catalyst which automatically introduces negative charge to the hydrophobic membrane[7]. In contrast with cationic amphiphile electrodes, it is usually difficult to produce an electrode sensitive to anionic amphiphiles, but we found that a tricresylphosphate-plasticized copoly(VCl, VAc(5%)) membrane containing 0.7% hexadecyltrimethylammonium dodecyl sulfate as an ion-exchanger was useful for sensing sodium dodecyl sulfate[8].

A typical electrode performance is shown in Figure 1, where electromotive force(E_m) is plotted against logarithm of dodecylpyridinium bromide concentration(C_S). In the absence of polymer, the electrode shows a response in accordance with the Nernst equation,

$$E_m = [RT/zF]\ln(C_S/C_0) \quad [1]$$

When sodium dextran sulfate($C_p = 0.1$ mM sulfate residue) is present, a deviation appears which is caused by a partial uptake of surfactant by the polymer. By following the arrows, an equilibrium surfactant concentration, C_f and an amount of bound surfactant($\Delta C = C_S - C_f$) are easily obtained, and, in turn, are used for constructing a binding isotherm($\Delta C/C_p$ vs. C_f).

All polysaccharides were dialyzed before use.

RESULTS AND DISCUSSION

Binding of surfactants to charged polysaccharides

Ionic polysaccharides strongly interact with oppositely charged surfactants. Examples are shown in Figure 2, where two binding isotherms are shown; one for the dodecylpyridinium bromide-sodium dextran sulfate system, and the other for the sodium dodecyl sulfate-N-methylglycolchitosan system.

Both systems are characteristic of cooperative binding: there is actually no binding at low surfactant concentration, and with increase in equilibrium concentration, there is a sudden occurrence of surfactant take-up, which is soon saturated within a very narrow surfactant concentration. The highly cooperative nature is brought about by interaction between alkyl chains of bound surfactants. It is noted that a cationic surfactant is strongly bound to an anionic polyelectrolyte and vice versa. It is seen that there is a symmetry with respect to the signs electric charges of the interaction systems. This symmetry is, however, broken when polymers are neutral. Methylcellulose is markedly interactive with sodium dodecyl sulfate, but not with dodecyltrimethylammonium nor with dodecylpyridinium bromides. This asymmetry is still to be studied[3]. Ethylhydroxyethylcellulose (EHEC) binds exceptionally, although very weakly, tetradecylpyridinium bromide, a cationic surfactant as seen in Figure 3[9]. The binding seems to proceed in a very weakly cooperative manner, but soon is suppressed by onset of ordinary micelle formation. Amylose is another exception from the above mentioned asymmetry. Amylose, although neutral, binds cationic surfactants as seen in Figure 4 [10]. The binding mode is not cooperative, but of the Langmuir type. Amylose forms helical cavities which form the binding sites. In contrast although anionic surfactants are also bound to amylose, the binding mechanism seems to depend strongly on both alkyl chain-length of surfactant and molecular weight of amylose[11].

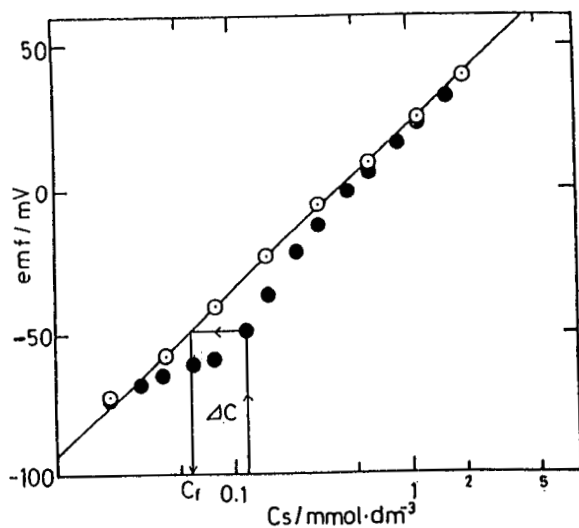


Figure 1. A potentiogram for dodecylpyridinium bromide-sodium dextran sulfate system in 20 mM NaBr at 25°C, polymer concentration, $C_n = 0.1$ mM sulfate residue.

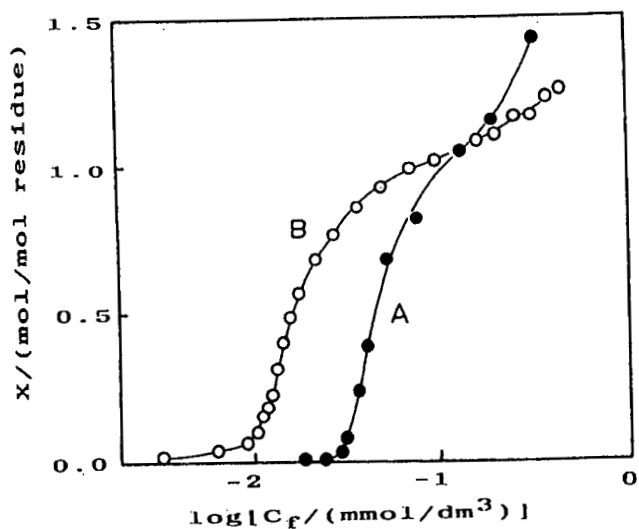


Figure 2. Binding isotherms. A: the same as in Figure 1, B: N-methylglycolchitosan chloride system in 20 mM NaCl at 25°C.

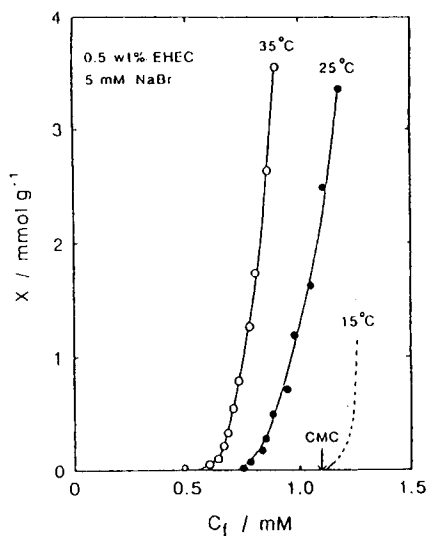


Figure 3. Binding isotherms for ethylhydroxyethyl-cellulose(EHEC)-tetradecylpyridinium bromide system in 5 mmol/dm^3 NaBr, EHEC concentration = 0.5%

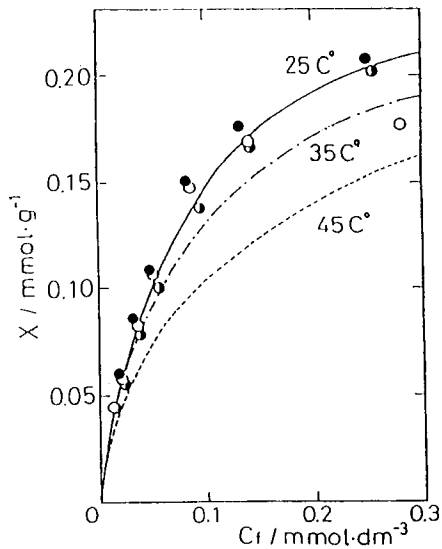


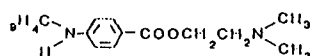
Figure 4. Binding isotherms for amylose-tetradecylpyridinium bromide system in 5 mmol/dm^3 NaBr.

Binding of drugs to dextran sulfate

Most drugs are amphiphilic ions, and so it is interesting to see how they interact with polysaccharides. Among many drugs, local anesthetics(LA) are chosen, since their solution properties are very similar to surfactants, the model amphiphiles: e.g., they form micelles. Local anesthetics are cations with aromatic hydrophobic groups connected to ternary ammonium groups through a polar(amide or ester)group. The molecular structures of LA used are listed in Figure 5. The surface activity (and anesthetic



procaine (PCH)



tetracaine (TCH)



dibucaine (DCH)

Figure 5. The Chemical structures of local anesthetics(LA)

All the ternary amines are protonated to be ammonium cations in a neutral pH medium.

potency) increases in the order of procaine(PCH), tetracaine(TCH), and dibucaine(DCH). The binding isotherms for LA-sodium dextran sulfate systems are shown in Figure 6. The interaction is characterized with a cooperative binding for a more surface active LA(DCH) to a comparable extent with the systems including ionic surfactants. The cooperativity originates from the interaction between aromatic groups of bound anesthetic molecules, which is very similar to the surfactant systems.

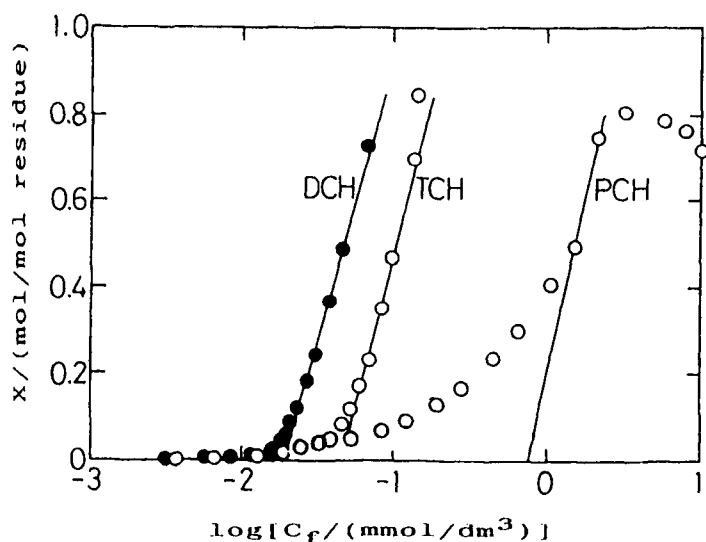


Figure 6. Binding isotherms for local anesthetics-sodium dextran sulfate systems. Salt not added, temperature 25°C.

Furthermore there is additional binding before the cooperative binding starts. This primary binding is more marked with a less surface active LA(PCH). This interaction is not found in the ionic surfactant systems with a simple hydrophobic group. In contrast, LA has a little more complex chemical structure which a simple hydrocarbon group in surfactant lacks, interacting with hydroxyl, sulfate groups, and other parts of dextran sulfate. This two-step binding mechanism can be seen transitionally in the present systems[12].

Gellan gum

Pseudomonas elodea, a kind of bacteria produces a polysaccharide with a very unfamiliar(to us) chemical structure; a repeat unit of D-glucose, D-glucuronic acid, D-glucose, and L-rhamnose with average molecular weight of $90,000 \pm 2,000$ (Figure 7). It is reported to form a left-hand double helix[13]. This polymer is called "gellan gum" named after its effective gelling property. So we

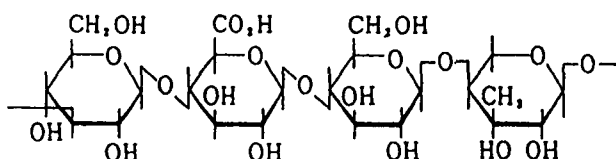


Figure 7. The chemical structure of gellan gum.

looked at the interaction of a cationic surfactant with this polysaccharide in solution. A binding isotherm of the dodecylpyridinium chloride-gellan gum system is shown in Figure 8, where the logarithm of amount of bound surfactant per carboxyl group in gellan gum is plotted against the logarithm of equilibrium concentration. It is noted that there are at least two binding modes.

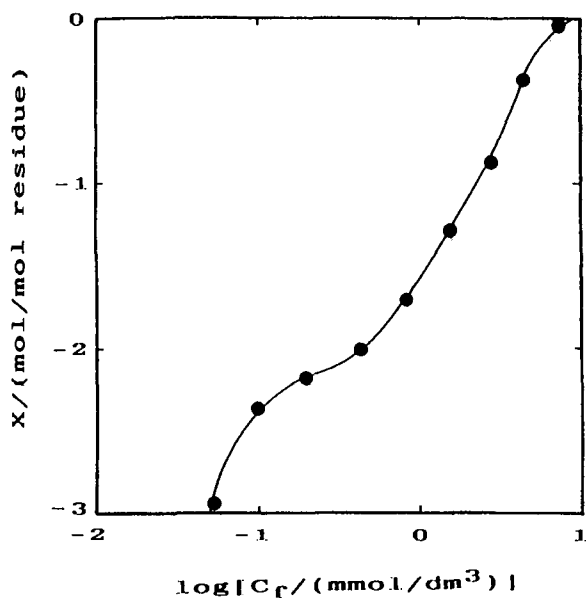


Figure 8. Binding isotherm for the gellan gum-dodecylpyridinium chloride system at 25°C. $C_p = 4.7 \text{ mmol}/\text{dm}^3 \text{ COO}^-$, pH = 7.7

Actually a Scatchard plot in the lower surfactant region gives a straight line producing a binding constant = $3.65(\text{mmoldm}^3)^{-1}$, and a saturation of 0.0158 surfactant molecules/tetrasaccharide unit. It is not clear at the moment whether the helical structure accommodates the surfactant molecule, or whether some other binding sites are provided. In the higher concentration region, binding tends to $X=1$ indicating that the carboxyl group is a binding site.

Photosurfactant

An azo-compound, 4-ethyl-azobenzene-4'-oxyethyltrimethyl ammonium bromide (Figure 9) undergoes a trans/cis isomerization on UV/vis light irradiation in aqueous solution.

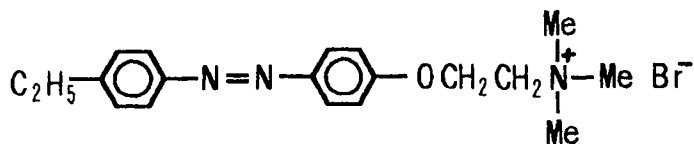


Figure 9. The chemical structure of photosurfactant.

Interestingly this compound forms micelles. The electric conductivity of the photosurfactant shows a break at a certain concentration. The break point appears to increase on UV irradiation implying that the cis form is less cohesive because of its stereostructure. Binding isotherms are shown for sodium dextran sulfate-photosurfactant (both irradiated and nonirradiated) in Figure 10. The isotherm for dodecyltrimethylammonium bromide is added for comparison. The irradiated cis-surfactant should have a little less affinity to the polysaccharide. This result means that light may be used to control binding affinity in addition to well known parameters such as temperature, pressure, added salts and organic compounds. It is also noted that the photo-

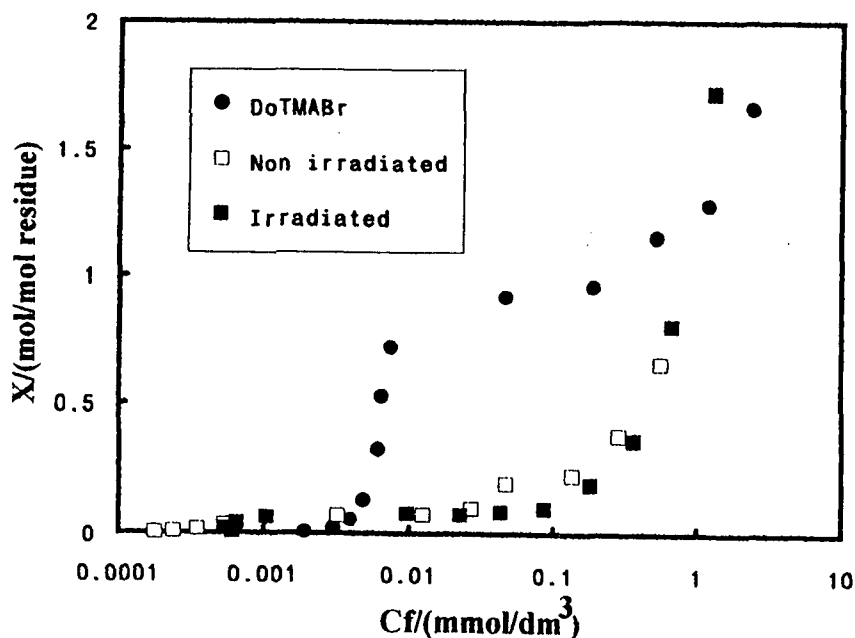


Figure 10. Binding isotherms of photosurfactant to sodium dextran sulfate at 25°C.

control of binding should be very effective because of the highly cooperative nature of the interaction.

CONCLUSIONS

Charged polysaccharides bind amphiphiles with electric charge opposite to the polysaccharides. When polysaccharides are not charged, the interactions are usually very weak or none. Amylose is an exception: its helical structure accommodates amphiphiles. Since there are various kinds of polysaccharides and even more number of amphiphiles, the interactions between the two classes of materials will show a great diversity, which may be interesting and useful.

REFERENCES

- [1] Anionic Surfactants, Physical Chemistry of Surfactant Action, ed. E.H. Lucassen-Reynders, Dekker, New York, 1981.
- [2] Cationic Surfactants, Physical Chemistry, ed. D.D. Rubingh and P.M. Holland, Dekker, New York, 1991
- [3] E.D. Goddard, Colloids Surfaces, 19, 255-300 (1986).
- [4] E.D. Goddard, Colloids Surfaces, 19, 301-329 (1986).
- [5] I.D. Robb, ref.[1], pp.109-142
- [6] K. Hayakawa and J.C.T.Kwak, ref.[2], pp189-248
- [7] S.G. Cutler, P. Mears, and D.G. Hall, J. Chem. Soc. Faraday I, 74, 1758-1767 (1978).
- [8] K. Shirahama and H. Nakamiya in "Ordering and Organisation in Ionic Solutions," ed. N. Ise and I. Sogami, World Scientific, Singapore, 1988.
- [9] A. Carlsson and B. Lindman, T. Watanabe, and K. Shirahama, Langmuir, 5, 1250-1252(1989).
- [10] K. Shirahama, T. Watanabe, and M. Harada, in "The Structure, Dynamics, and Equilibrium Properties of Colloidal Systems," ed. D.M. Bloor and E. Wyn-Jones, Kluwer, 1990, 161-172.
- [11] M. Yamamoto, T. Sano, S. Harada, and T. Yasunaga, Bull. Chem. Soc. Jpn., 56, 2643-2646(1983).
- [12] N. Takisawa et al., in preparation
- [13] G.R. Sanders and C. Clark, Food Technology, 37, 63-65(1983).

40 Interaction between nonionic polymers or surfactants and ethylhydroxyethylcellulose characterised by Fourier transform NMR self-diffusion

K Zhang*, B Lindman* and M Jonströmer** – * Physical Chemistry I, Chemical Center, University of Lund, POB 124 S-22100 Lund, Sweden; ** Astra Draco AB, Box 34, 22100 Lund, Sweden

ABSTRACT

The interactions between a nonionic surfactant, octa-ethylene glycol dodecyl ether (C₁₂E₈), or polyethylene oxide (PEO) and ethylhydroxyethyl cellulose (EHEC) have been studied by measuring the C₁₂E₈ and PEO self-diffusion coefficients in EHEC solutions at different temperatures. Two types of EHEC, one which is hydrophobic and the other hydrophilic, were used. It is shown that the self-diffusion approach can provide useful insights into the structure of the cellulose ether solutions as well as the interaction between the cosolutes and the cellulose ether.

INTRODUCTION

A deep understanding of the self-diffusion of cosolutes in macromolecular solutions is of fundamental importance in relation to many applications in biology and medicine as well as in technology. The self-diffusion coefficient of cosolutes is mainly modified by two effects. The first one is the so-called obstruction effect, which originates from the excluded volume of impenetrable particles leading to a lengthening of the diffusing paths. This effect is determined generally by the size and the geometry of the cosolute, the polymer concentration and the geometrical arrangement of the polymer chains. The second one is related to direct specific interactions between the cosolute and the polymer, which normally leads to a further retardation of the diffusion. Over the past few years, a fair amount of studies [1-5], both experimental and theoretical, on the characterisation of the diffusion process in macromolecular solutions have been

performed. It is established that investigations of the self-diffusion of cosolutes in macromolecular solutions can provide valuable information concerning the solution structure, i.e., the geometrical arrangement of the polymer chains, as well as its variations as a function of temperature or concentration. Such investigations may also give direct insights into the specific interactions between the cosolute and the polymer.

In this report, we investigate the self-diffusion of $C_{12}E_8$ and PEO in EHEC solutions. EHEC is ethylhydroxyethyl cellulose, $C_{12}E_8$ octa-ethylene glycol dodecyl ether and PEO polyethylene oxide, respectively. Two EHEC polymers differing strongly in polarity are used.

EXPERIMENTAL

Materials

$C_{12}E_8$ of high quality (>98%) was obtained from Nikko Chemicals, Tokyo, Japan and used as received. PEO of different molecular weights, 4000 (PEO₄), 20000 (PEO₂₀) and 40000 (PEO₄₀), respectively, were obtained from Merck and used as received. Samples of ethylhydroxyethyl cellulose, EHEC, with different hydrophobicities were supplied by Berol Nobel AB, Sweden. One is hydrophobic EHEC (Bermocoll CST 103, below referred to as EHEC_u) with a cloud point of about 30°C; the other is hydrophilic (Bermocoll E230G, below referred to as EHEC_p) with a cloud point of about 62°C. EHEC is a water-soluble polymer at room temperature. The number average molecular weight is 80,000 and 100,000 for EHEC_u and EHEC_p, respectively (given by the manufacturer). Dilute EHEC solutions were dialysed against pure water (Millipore water, USA) for at least 5 days to remove salt (impurity from the manufacture) which was followed by freeze-drying. 2H_2O (99.7 atom% 2H) was obtained from Norsk Hydro, Norway.

Self-diffusion measurements

Samples were prepared by mixing bulk solutions of the components in standard 5 mm NMR tubes. All the samples were made up with 2H_2O . The proton self-diffusion studies were performed at 60 MHz on a modified JEOL FX-60 FT NMR spectrometer equipped with a home made pulsed field gradient unit. The 2H_2O signal was used to lock the magnetic field externally. The temperature was determined to within 0.5 °C by a calibrated copper constantan thermocouple and measured immediately before and after the experiments. All samples were equilibrated in the NMR probe for at least 5 minutes before the measurements. For a complete description of the experimental technique, see Ref. 6.

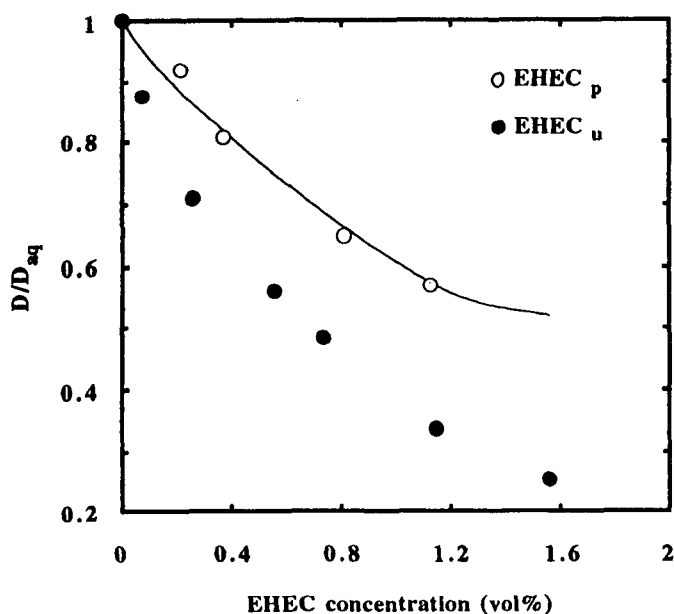


Figure 1. The relative self-diffusion, D/D_{aq} , for 1.0 wt% $C_{12}E_8$ in solutions of EHEC_p and EHEC_u as a function of the polymer concentration (vol%). The solid line is calculated according to Eq.(6) with $a=4.5 \text{ \AA}$ and $R_s=33.4 \text{ \AA}$. The volume fraction of the polymer was calculated from the partial specific volume $v = 0.75 \text{ mL/g}$. Temperature $T=298 \text{ K}$.

RESULTS AND DISCUSSION

1) Self-diffusion of $C_{12}E_8$ in EHEC solutions at 25°C

In Figure 1 we present the relative self-diffusion coefficient, D/D_{aq} , for a constant $C_{12}E_8$ concentration (1.0 wt%) in solutions of two different EHEC polymers, one hydrophilic, EHEC_p, and one hydrophobic, EHEC_u, as a function of the polymer concentration. D_{aq} is the self-diffusion coefficient of $C_{12}E_8$ measured in polymer-free solution at the same temperature. As may be inferred, the self-diffusion in EHEC_p solutions is more rapid than that in EHEC_u solutions. Due to their very similar molecular structure, the obstruction effect from the two polymers is assumed to be the same. Therefore, the different rates of diffusion with the two polymers is caused mainly by a difference in the interactions between the surfactant and the polymers. Usually there is no or very weak interaction between hydrophilic nonionic polymers, such as EHEC_p, and nonionic surfactants at normal temperatures [7]. In this case, the reduction of the surfactant mobility is attributed to the obstruction effect. However, when the hydrophobicity of the polymer is sufficiently large, for instance in the case of EHEC_u, a strong attraction between the polymer and the surfactant may occur, leading to a further decrease of the surfactant mobility. Thus, the additional retardation of the surfactant mobility in the EHEC_u solutions gives a clear demonstration of significant associative interaction between $C_{12}E_8$ and EHEC_u, which is consistent with previous phase diagram findings [8].

In order to get a closer examination of the interaction between $C_{12}E_8$ and $EHEC_u$, we need to quantify the obstruction effects from both the polymer chains and from other micelles.

Spherical micelles are formed in the binary $C_{12}E_8$ /water solutions over wide temperature and concentration ranges [9]. The reduced mobility due to obstruction between spherical nonionic micelles is well expressed by the relationship [1,2]

$$D_{aq} = D_0(1-2\phi_s) \quad (1)$$

where D_{aq} is the micellar self-diffusion coefficient in the absence of the polymer, ϕ_s the volume fraction of the micelles including the water of hydration and D_0 the self-diffusion coefficient at infinite dilution.

The obstruction effect from the polymer chains, which is represented by the reduction of the surfactant mobility in the $EHEC_p$ solutions, can be described by a model developed by Johansson et al. [10]

$$D/D_{aq} = e^{-\alpha} + \alpha^2 e^{\alpha} E_1(2\alpha) \quad (2)$$

where $\alpha = \phi_p(R_s + a)^2/a^2$, ϕ_p is the volume fraction of the polymer, R_s is the surfactant micellar radius, a is the polymer radius and E_1 is the exponential integral, i.e. $E_1(x) = \int_x^{\infty} e^{-u}/u \, du$.

The micellar radius, $R_s = 33.4 \text{ \AA}$, including the water of hydration, is taken directly from the literature [10]. The value of the polymer radius, $a = 4.5 \text{ \AA}$, is obtained by fitting Eq. (2) to the data in Figure 1 for $EHEC_p$ solutions (solid line in the Figure). The polymer radius obtained here is larger than that of K^+ - κ -carrageenan, which has a similar molecular backbone as EHEC, in coil conformation ($a = 3.3 \text{ \AA}$) but smaller than that of double helix conformation ($a = 5.1 \text{ \AA}$) [10,11]. Taking account of the fact that the EHEC molecule has large branched groups, $a = 4.5 \text{ \AA}$ is reasonable.

Assuming a distribution of the surfactant only between free micelles and micelles bound to the polymer chains, the observed self-diffusion coefficient, in the $EHEC_u$ solutions, D_{obs} , can be described with a simple two site model:

$$D_{obs} = D_f (1 - P_b) + P_b D_b \quad (3)$$

Combining with Eqs.(1) and (2), we obtain

$$D_{obs} = [D_0(1-2\phi_s)(e^{-\alpha} + \alpha^2 e^{\alpha} E_1(2\alpha))](1 - P_b) + P_b D_b \quad (4)$$

where P_b is the fraction of the surfactant micelles bound to the polymer, D_b the self-diffusion coefficients of the polymer-surfactant complex, D_f the diffusion coefficient of free micelles, and D_0 the micellar self-diffusion coefficient at infinite dilution, which is $6.6 \cdot 10^{-11} \text{ m}^2\text{s}^{-1}$. The self-diffusion coefficient of the polymer-surfactant complex, D_b , may be assumed to be negligible compared to D_{obs} (the $EHEC_u$ self-

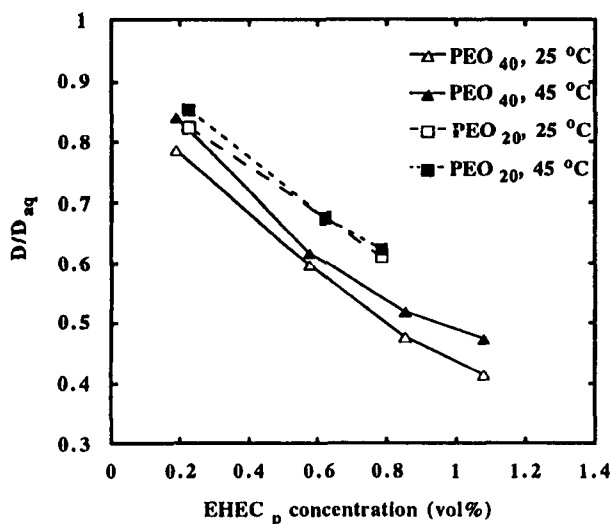


Figure 2. The relative self-diffusion, D/D_{aq} , for 1.0 wt% PEO in solutions of EHEC_p as a function of the EHEC concentration (vol%) at two different temperatures. The volume fraction of the polymer was calculated from the partial specific volume $v = 0.75$ mL/g.

diffusion coefficient was recently determined by an improved FT-NMR-PGSE technique to $6.0 \cdot 10^{-13} \text{ m}^2 \text{ s}^{-1}$ [12]). With the values of a , R_s and D_b at hand, the binding isotherm of $C_{12}E_8$ to EHEC_u can be calculated by using Eq. (4). It is found that the interaction can be described in terms of a Langmuir isotherm [13].

It is worth noting that Eq. (4) holds under conditions that the presence of the nonionic polymer does not significantly affect the nonionic micellar size. As noted, $C_{12}E_8$ micelles, in contrast to $C_{12}E_6$ micelles, have little tendency to grow [9,10].

II) Self-diffusion of PEO in EHEC_p solutions at different temperatures.

As noted, EHEC has a reduced solubility in water at higher temperatures. Above the critical point (cloud point), polymer molecules are aggregated and form a separated phase. We have reasons to expect that with increasing temperature, even well below the cloud point, polymer chains are associating leading to an increase in the available space for the diffusion of solutes in the solution [14]. Consequently, a significant increase in D/D_{aq} is expected as the temperature is raised, provided the size of the cosolute is comparable to the mesh size formed by the EHEC chains (the EHEC solutions investigated are in the semi-dilute regime and we can picture the system as a three-dimensional lattice with a mesh size ξ). In order to examine this assumption we measured the self-diffusion of PEO of different molecular weights in EHEC_p solutions at different temperatures. The reason for choosing PEO instead of $C_{12}E_8$, is that $C_{12}E_8$ micelles may grow beyond a certain temperature range [9]. PEO of different molecular weights was chosen in order to observe the size effect of the diffusing species on D/D_{aq} .

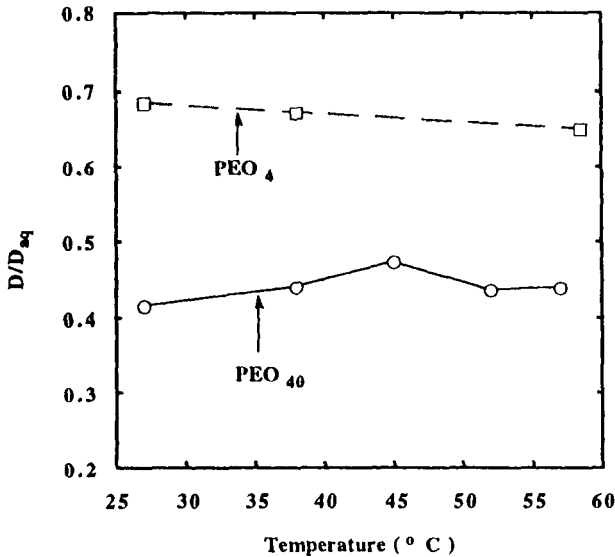


Figure 3. The relative self-diffusion, D/D_{aq} , for 1.0 wt% PEO in solutions of EHEC_p as a function of temperature. The concentrations of EHEC_p are 1.32 vol% for the PEO₄ system and 1.08 vol% for the PEO₄₀ system.

In Figure 2, we show D/D_{aq} for a constant concentration of PEO in EHEC_p solutions as a function of the EHEC_p concentration at two different temperatures. As noticed, raising the temperature from 25 to 45°C indeed induces a slight increase in D/D_{aq} . In Figure 3, D/D_{aq} is presented as a function of temperature. For PEO of low molecular weight (PEO₄) a slight decrease in D/D_{aq} is observed. Interestingly, for PEO of high molecular weight (PEO₄₀), however, D/D_{aq} passes through a maximum with increasing temperature.

Before analysing these data, it is necessary to examine if the hydrodynamic size of PEO keeps constant within the temperature range investigated or if there is some self-association. A variation of PEO size with temperature will be reflected in the temperature dependence of the diffusion, which is described by the relationship

$$D = D_{\infty} \exp(-A_D/RT) \quad (5)$$

where A_D is the activation energy of diffusion and D_{∞} the diffusion coefficient at infinitely high temperature. In Figure 4, $\ln D_{aq}$ is presented versus $1/T$ for different PEO solutions. The linear relationship between $\ln D_{aq}$ and $1/T$ demonstrates clearly that no variation of size is indicated. In other words, no appreciable aggregation between PEO molecules occurs. Furthermore, a common activation energy of the diffusion of $A_D = 21$ kJ/mole was obtained for the three PEO solutions.

It is thus clear that the temperature dependence of D/D_{aq} mainly reflects the obstruction effect from the EHEC chains and a specific interaction between PEO and

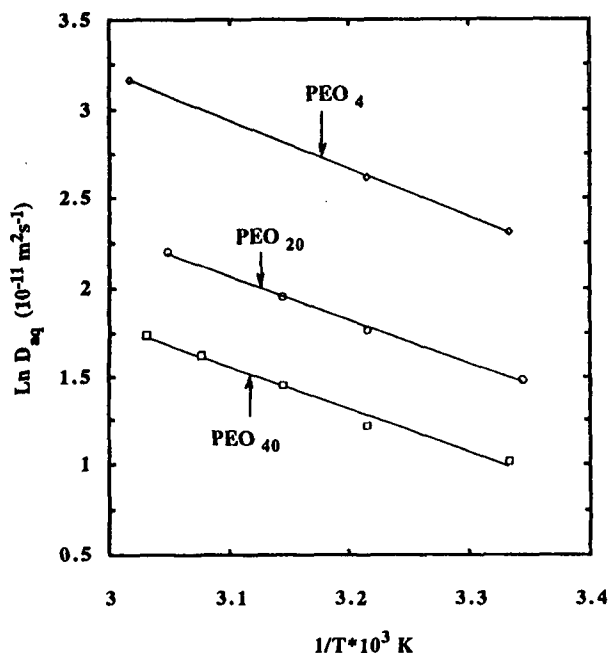


Figure 4. Temperature dependence of the self-diffusion coefficient of aqueous PEO solutions for different molecular weights of PEO (4000, 20000 and 40000). The PEO concentration is 1.0 wt%.

EHEC_p. With increasing temperature, more EHEC_p chains are bound together resulting in an increase in the available space. Moreover, at the same time the hydrophobicity of both PEO and EHEC_p increases rendering an associative interaction between PEO and EHEC_p. Obviously, the maximum of D/D_{aq} with temperature for a high molecular weight PEO is the result of an interplay between these two effects. At increasing the temperature the former effect is at first dominating leading to an increase in D/D_{aq} ; at higher temperatures, however, the interaction between PEO and EHEC_p becomes stronger leading to the reduction in D/D_{aq} . For a lower molecular weight PEO, probably because of its significantly smaller molecular size (the radius of gyration is 26 and 90 Å for PEO₄ and PEO₄₀, respectively) [15] compared to the mesh size, the variation of the available space exerts no drastic influence on D/D_{aq} . Thus, the associative interaction is dominant within the temperature range investigated. Moreover, this interaction is expected to be slightly weaker than that of PEO₄₀.

CONCLUDING REMARKS

The present study shows that the self-diffusion approach can provide useful insights into the structure of polymer solutions as well as the interaction between a cosolute and the polymer. Usually there is no significant associative interaction between nonionic surfactants and nonionic polymers. However, when the hydrophobicity of the polymer is sufficiently large, an associative interaction may become dominant.

REFERENCES

1. Ohtsuki T, Okano K (1982) *J Chem Phys* 77(3):1443
2. Jönsson B, Wennerström H, Nilsson PG, Linse P (1986) *Colloid & Polymer Sci* 264:77
3. Preston BN, Laurent TC, Comper WD, Checkley GJ (1980) *Nature* 287:499
4. de Gennes PG (1979) *Nature* 282:22
5. Aven MR, Cohen C (1990) *Polymer* 31:778
6. a) Callaghan PT (1984) *Aust. J. Phys.* 37:359
b) Ståls P (1987) *Prog. Nucl. Magn. Reson. Spectrosc.* 19:1
7. Goddard ED (1986) *Colloids Surfaces* 19:255
8. Zhang KW, Karlström G, Lindman B (1992) *Colloids Surfaces* 67:147
9. Nilsson PG, Wennerström H, Lindman B (1983) *J Phys Chem* 87:1377
10. Johansson L, Hedberg P, Löfroth JE (1993) *J Chem Phys* 97:747
11. Nilsson S, Piculell L, Jönsson B (1989) *Macromolecules* 22:2367
12. Ståls P, unpublished data.
13. Zhang KW, Jonströmer M, Lindman B, to be published
14. Johansson L, Elvingson C, Löfroth JE (1991) *Macromolecules* 24:6024
15. Kekicheff P, Cabane B, Rawiso M (1984) *J Colloid Interface Sci* 102:51

41 Formation of hydrogen-bonding polymer complex gels from carboxymethylcellulose and poly(methacrylic acid)

M Sakamoto, H J Kim, K Mimura, Y J Lee and T Inoue –
Department of Organic and Polymeric Materials, Faculty of
Engineering, Tokyo Institute of Technology, O-okayama, Meguro-ku,
Tokyo, 152 Japan

Abstract: Polymer complex gel films in "modulated structure" were prepared by placing a thin liquid film of an aqueous solution of the sodium salt of poly(methacrylic acid) (PMAA) or carboxymethylcellulose (CMC; degree of substitution, 1.16) and poly(ethylene oxide) (PEO) or poly(N-vinylpyrrolidone) (PVP) in dilute hydrochloric acid. Time-resolved light scattering profiles were measured for the gel formation and the dried films, obtained from the gel films by slow evaporation of the solvent, were observed by scanning electron microscopy. Except for PMAA-PEO system, it could be demonstrated that hydrogen-bonding polymer complex gels were formed via spinodal decomposition.

Introduction:

The importance of spinodal decomposition in phase separation of polymer blends [1] and polymer solutions [2] has been much demonstrated in recent years. Spinodal decomposition leads to a "modulated structure", i.e. a phase-separated structure with unique co-continuity and periodicity. In a previous paper [3], we reported that a soft, bulky, cotton-ball-like precipitate obtained by the freeze-defreeze method from a very dilute mixed solution of PMAA and poly(acrylamide) showed an interconnecting lacy structure similar to that [4] observed for a film made by drying a hydrogel film in the modulated structure.

In this work, gel formation by immersing thin films of the sodium salt of carboxymethylcellulose (CMC) or PMAA and poly(ethylene oxide) (PEO) or poly(N-vinylpyrrolidone) (PVP) in dilute hydrochloric acid was studied. Hydrogen ions are supposed to diffuse into the thin film, and to convert the sodium salt into the acid form. Polymer complexes will be formed at this stage and phase separation will take place via a spinodal decomposition mechanism to yield gels with modulated structure.

Experimental

Polymer samples: Sodium salt of CMC was obtained from Daicel Chem. Ind. Ltd., with degree of substitution of 1.16, and with viscosity of 47 cps (1% solution at 27°C at 60 rpm). PMMA was prepared by radical polymerization of methacrylic acid in methyl ethyl ketone; its viscosity average molecular mass (M_v) was 180×10^3 . PEO (M_v , 6×10^3) and PVP (M_v , 10×10^3 and 360×10^3) were obtained from Tokyo Kasei Kogyo Co. Ltd. PVP of lower molecular mass was used for complex formation with CMC and that of the higher one was for complex formation with PMAA. Most of the experiments were carried out at 22 or 25°C. **Gel formation:** An optical cell with a water jacket to maintain the temperature was filled with dilute hydrochloric acid pH 0.6. An aqueous solution of an acceptor polymer and sodium salt of a donor polymer was placed in a shallow cell (depth, 0.25 mm) made of a plate of cover glass and a PET film and the cell was sunk in the hydrochloric acid in the optical cell. **Light scattering experiments:** Time-resolved light scattering data were obtained with a goniometer-type apparatus (the sweep time, 3 sec; the angular range, 45 degrees.) or with a detector-array type apparatus (50 channels; the angular range, 30 degree; the time slice, 1/30 sec), both being equipped with Ar-Ne laser sources.

Results and Discussion

Early stage of spinodal decomposition (CMC complexes)

Spinodal decomposition proceeds in three stages. According to the Cahn's linear theory [5], the intensity of scattered light (I) in the early stage is described by:

$$I(q,t) = I(q,t = 0) \exp[2 R(q) t] \quad (1)$$

where q is the wavenumber of concentration fluctuation calculated from the scattering angle, t is the time after the initiation of spinodal decomposition, and $R(q)$ is the growth rate of concentration fluctuation. q is given by:

$$q = 4\pi \sin(\theta/2)/\lambda \quad (2)$$

where θ is the scattering angle and λ is the wavelength of irradiated laser light. $R(q)$ is given by:

$$R(q) = -Mq^2 \left(\frac{\partial^2 f}{\partial c^2} + 2\kappa q^2 \right) \quad (3)$$

where M is the mobility, c is the concentration and κ is the concentration-gradient energy coefficient. Then, the apparent diffusion coefficient (D_{app}) is given by:

$$D_{app} = -Mq^2 \left(\frac{\partial^2 f}{\partial c^2} \right) \quad (4)$$

And, q_m , the wavenumber of the most probable concentration fluctuation, is given by:

$$q_m = 2\pi/\Lambda_m \quad (5)$$

where Λ_m is the most probable wavelength of the periodic structure. When a solution of sodium salt of CMC and PEO was placed into the acid solution, a pale blue gel film was soon formed. The structure, when observed through an optical microscope, looked like the modulated structure. When laser light was passed onto the gel film, a ring pattern was observed. It is the so-called "spinodal ring" [6]. These results suggest that phase separation takes place via spinodal decomposition. The early stage of spinodal decomposition for the CMC/PEO(6/4) system was studied (Unit molar ratio of the two components based on their polymer recurring units is given in the parenthesis.). The total polymer concentration (TPC) was 0.2 mol/L* .

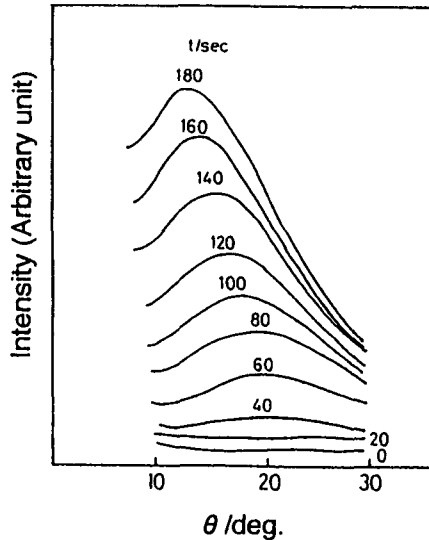


Fig. 1. Scattered light intensity versus scattering angle for phase separation of CMC/PEO(6/4) (TPC, 0.20 mol/L).

* Polymer molar concentration (mol/L) is based on the (average) mass of the polymer recurring unit.

Fig. 1 shows the time-resolved light scattering profile for this system. At earlier times, the concentration fluctuations are too small to be measured. After 40 sec, a scattering angle with the maximum scattered light intensity appears in the profile. The peak position does not change while the intensity increases with time. After 80 sec, the scattering angle with the maximum intensity starts to shift to a smaller angle and the intensity continues to increase with time. Fig. 2 shows that the scattered intensity increases exponentially with time. Plots of $R(q)/q^2$ vs q^2 in Fig. 3 show that Cahn's linear theory stands for this system. From the intercept, the apparent diffusion coefficient is calculated to be $-16 \times 10^{12}/\text{cm}^2\text{sec}^{-1}$. CMC/PEO systems with various compositions were studied in a similar way (Table 1). For a wide range of CMC/PEO ratios (from 10/0 to 4/6), similar phase separation was found to take place. Note that CMC alone underwent spinodal decomposition from its sodium salt.

Intermediate and Late Stages (CMC complexes)

Coarsening of the structure begins at the intermediate stage with self-similarity. The amplitude of concentration fluctuation still increases with time as in the early stage. At the late stage of spinodal decomposition, the amplitude reaches the equilibrium composition difference so that it does not increase any more, but the coarsening is still going on at this stage also in a self-similar manner. Intermediate and late stages of spinodal decomposition

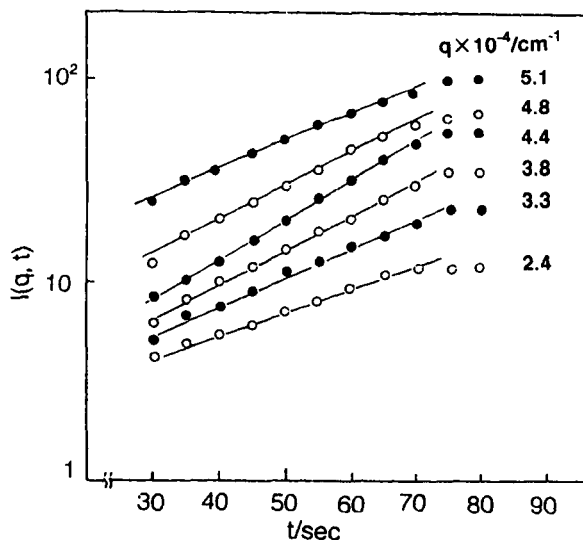


Fig. 2. Semilogarithmic plots of scattered light intensity for phase separation of CMC/PEO(6/4) (TPC, 0.20 mol/L).

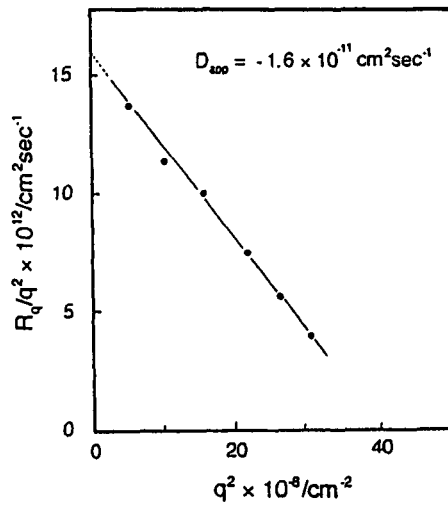


Fig. 3. R_q/q^2 versus q^2 for phase separation of CMC/PEO(6/4) (TPC, 0.20 mol/L).

Table 1 The early stage of spinodal decomposition of CMC/PEO

CMC/PEO*	10/0	9/1	8/2	7/3	6/4	5/5	4/6
$R_q \times 10^3/\text{sec}^{-1}$	7.0	7.5	14	12	17	21	23
$-D_{\text{app}} \times 10^{12}/\text{cm}^2\text{sec}^{-1}$	7.0	10	10	12	16	21	28
$\Lambda_m / \mu\text{m}$	1.3	1.2	1.1	1.2	1.5	1.6	1.7

* Unit molar ratio

have been treated with a dynamical scaling hypothesis [7]. The applicability of the scaling hypothesis can be tested by plotting scaled structure factor, $F(x,t) \equiv q_m^{-3}(t) I(x,t)$ vs reduced wavenumber (q/q_m) for different times. The structure factor increases with time and converges in the intermediate stage. In the late stage, the plot becomes independent of time.

Fig. 4 shows how the plot of the structural factor converges for the CMC/PEO(6/4) system. It is clear that spinodal decomposition proceeds from intermediate stage into late stage at 500 sec after the initiation of spinodal decomposition. Spinodal decomposition of both the CMC and CMC/PVP(6/4) systems also proceeded into the late stage. Analysis of power

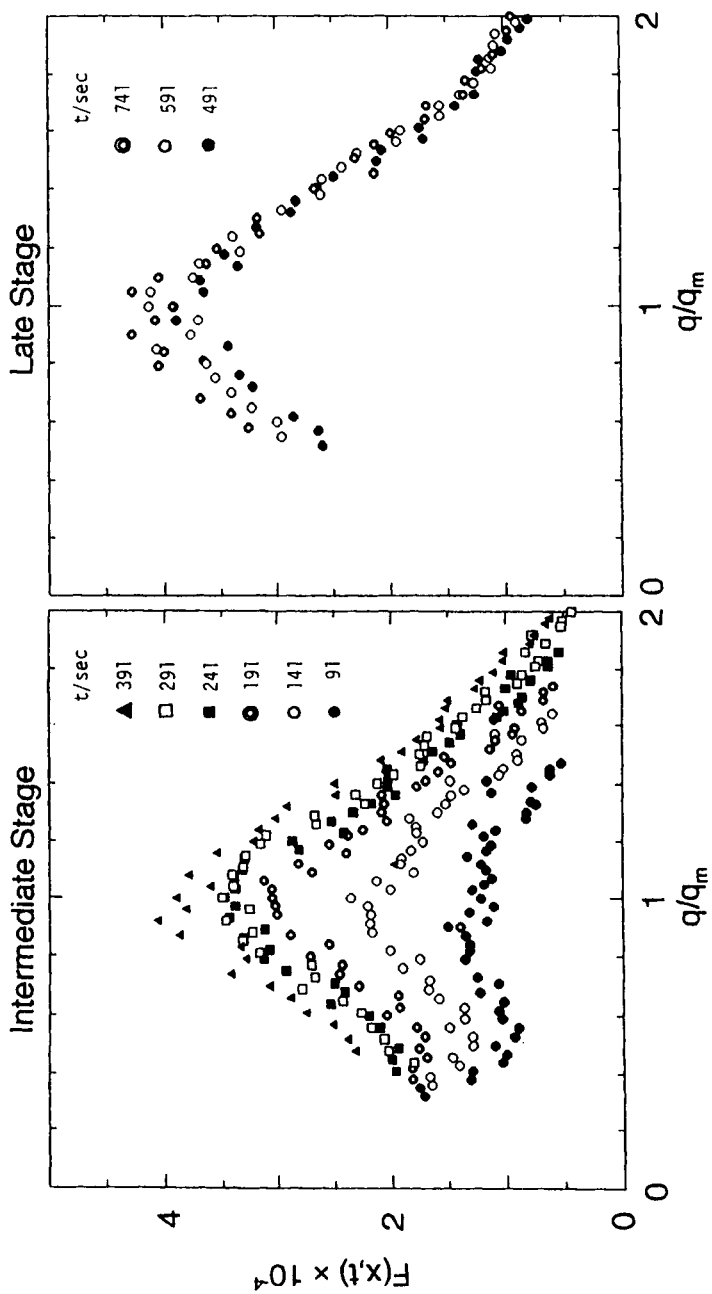


Fig. 4. Scaled structure factor versus reduced wavenumber for phase separation of CMC/PEO (6/4) (TPC, 0.20 mol/L).

law growths of q_m and I_m (I at q_m) showed the characteristic feature [7] of the late stage of spinodal decomposition.

PMAA Complexes

Light scattering experiments were done for PMAA/PVP samples of the molar ratios of PMAA to PVP between 9/1 and 5/5. R_{qm} in this system decreased with increasing molar fraction of PVP at the early stage. I_m stopped to increase as early as after 95 sec and the analysis showed that pinning took place in the intermediate stage. The phase separation of PMAA/PEO took place too fast to be followed.

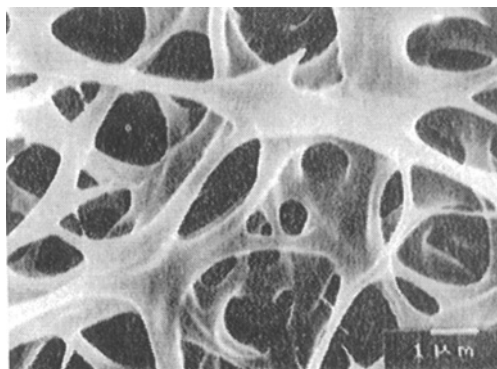


Fig. 5. A SEM picture of the surface (air) side of dried film made from CMC/PEO(2/8) (TPC, 0.20 mol/L) gel film.

Morphology of Dried Gel Films

Fig. 5 shows the surface side or air side of the film made from CMC/PEO (2/8) gel film. An interconnecting lacy structure is clearly observed. The back side, or glass side of the same dried film was covered with a thin film and through holes in the film, the lacy structure was observed. Dried films of CMC/PVP could not show the lacy structure because they were covered with thin films without holes. The surface view of a dried film of PMAA/PEO (5/5) (TPC, 0.24 mol/L) was somehow different from those of other samples and looked microporous (Fig. 6).

Conclusion:

Although the current system for gel formation is a complex process composed of diffusion of hydrogen ions, conversion of carboxylate to carboxylic acid, formation of hydrogen-bonding polymer complex, and phase separation, it was clearly demonstrated by time-resolved light scattering experiments that the phase separation in the system proceeds via spinodal decomposition mechanism, except for PMAA/PEO.

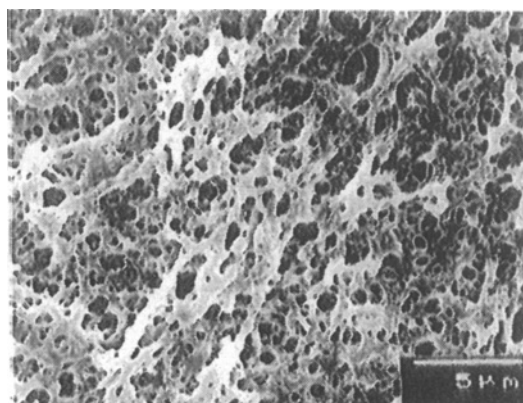


Fig. 6. A SEM picture of the surface (air) side of dried film made from PMAA/PEO(5/5) (TPC, 0.24 mol/L) gel film.

Literature:

- 1) T. Inoue, T. Ougizawa, O. Yasuda, and K. Miyasaka, *Macromolecules*, **18**, 57 (1985).
- 2) J. Lal and R. Bansil, *Macromolecules*, **24**, 290 (1991).
- 3) H. J. Kim and M. Sakamoto, *Sen'i Gakkaishi*, **47**, 424 (1991).
- 4) P.-J. Tsai, and J. M. Torkelson, *Macromolecules*, **23**, 775 (1990).
- 5) J. W. Cahn, *J. Chem. Phys.*, **42**, 93 (1965).
- 6) T. Hashimoto, K. Sakai, and H. Kawai, *Macromolecules*, **17**, 2812 (1984).
- 7) K. Binder and D. Stauffer, *Phys. Rev. Lett.*, **33**, 1006 (1974)

42 Effects on phase behaviour and viscosity of hydrophobic modification of a nonionic cellulose ether. Influence of cosolutes

K Thuresson, S Nilsson and B Lindman – Physical Chemistry 1, Chemical Center, University of Lund, PO Box 124, S-221 00 Lund, Sweden

Abstract

The phase behaviour and the viscosity have been studied as a function of added cosolutes for the two non-ionic polymers ethyl(hydroxyethyl)cellulose (EHEC), and a hydrophobically modified analogue (HMEHEC). The cosolutes used are ranging from ordinary salts and alcohols to an anionic surfactant. Only minor changes were seen in phase behaviour on hydrophobic modification of EHEC, while a major impact on the viscosity was observed. A qualitative discussion of cosolute effects relates the observations to the distribution of cosolute molecules between bulk solution and polymer surface.

Introduction

In the last decade hydrophobically modified polymers have received a great interest¹. These polymers typically consist of a hydrophilic part to which small amounts of hydrophobic groups are grafted. The hydrophilic part of the polymer can be ionic^{2,3} (anionic or cationic) or nonionic⁴. Commercially these polymers are interesting for their rheological properties. They can, for example, be used as thickeners in paints or food. Another application is enhanced oil-recovery. Scientifically they have received interest for their associative behaviour (both polymer-polymer and polymer-cosolute association) in aqueous solutions. In this study, we have focused on a non-ionic associative thickener based on cellulose, i.e. hydrophobically modified ethyl(hydroxyethyl)cellulose (HMEHEC). For comparison its unmodified analogue (EHEC) has also been investigated. The hydrophobic modification consists of branched nonylphenol groups grafted to the polymer backbone. The polymers have been investigated with respect to effects on phase behaviour and viscosity of addition of cosolutes. Despite a very low degree of hydrophobic modification of HMEHEC, the side groups affect the viscosity dramatically and, to a lower extent, also the phase behaviour. These polymers show a reversed temperature dependence: upon increasing temperature the polymers become insoluble in water, and a phase separation occurs⁵. Apart from the binary polymer/water solutions, three and four component systems have also been studied (e.g. addition of salt, alcohol, surfactant or salt and surfactant in combination).

In aqueous solutions of HMEHEC, the various cosolutes have been found to have a major effect on the viscosity. For instance, depending on surfactant concentration, the viscosity can increase by two orders of

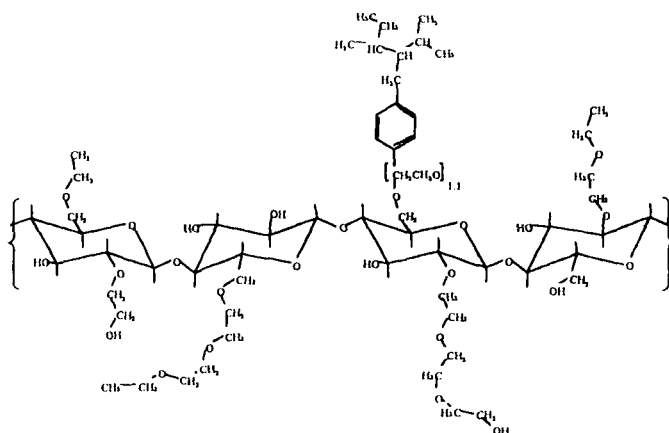


Fig. 1. The structure of HMEHEC. MW=100,000 Daltons. Substitution degree of nonylphenol ca. 1 mol%. Each polymer molecule contains ca. 5 hydrophobic tails. 1 wtw% polymer \leftrightarrow 0.4 mmolal nonylphenol.

magnitude. Another finding is that, even though the hydrophobically modified polymer is uncharged, addition of salt can either increase or decrease the viscosity, depending on the nature of the anion of the salt used.

In contrast, the viscosity of EHEC solutions shows only minor or negligible changes on addition of various cosolutes.

Experimental

Materials

The polymers used are commercial thickeners supplied by Berol Nobel AB, Stenungsund, Sweden. The unmodified polymer is an ethyl(hydroxyethyl)cellulose (EHEC). The hydrophobically modified polymer (HMEHEC) is equivalent to the EHEC sample but with approximately one mole percent branched nonylphenol covalently bonded to the polymer (fig. 1). The degree of nonylphenol substitution was measured by UV absorbance at 275 nm with a Perkin-Elmer UV-Vis spectrophotometer. Both polymers have the same molecular weight (approximately 100,000 Daltons) and degree of substitution of ethyl- and hydroxyethyl-groups ($DS_{\text{ethyl}} = 0.6-0.7$ and $MS_{\text{EO}} = 1.8$). The molecular weight, DS and MS were given by the manufacturer. Prior to use, HMEHEC was rinsed from unreacted nonylphenol by extensive extraction with acetone several times. Small amounts of free nonylphenol would have the same effects on the phase behaviour and the viscosity of HMEHEC as added alcohols (see below). After extraction, the polymer sample was dried from acetone and dissolved in water (ca. 1 w/w% of polymer). High molecular weight impurities not soluble in water were centrifuged off, leaving a clear supernatant phase. Low molecular weight impurities, such as salt, in the supernatant were removed by dialysis against Millipore water in a Filtron Ultrasette™ device. The conductivity of the expelled water was measured and when no decrease in the conductivity was obtained the dialysis was stopped. This occurred after ca. 70 hours and at a conductivity of ca. 2 $\mu\text{S}/\text{cm}$. The remaining polymer sample was freeze dried. NaCl was of pro analysi quality and obtained from Merck, NaBr and NaSCN were of analytical reagent quality and obtained from Mallinckrodt Chemical Works. The alcohols (methanol, ethanol, propanol, pentanol and hexanol) were all of pro analysi quality and supplied by Merck. The surfactant (SDS) was of specially pure grade and obtained from BDH. All cosolutes were used as received. The water used was of Millipore quality.

Methods

The samples were prepared from stock solutions of a concentration twice, with respect to polymer and cosolute, respectively, of that desired in the final samples. The samples were carefully mixed, by turning end over end for at least 24 hours in room temperature (22-25 °C), before any measurements were performed. The temperature where phase separation occurred was measured both in increasing and decreasing runs with visual detection. The average value was taken to represent the phase separation temperature.

All viscosity experiments were carried out on a Bohlin VOR rheometer in the oscillatory mode. The viscosity values presented are all obtained at 0.1 Hz. For measurements on EHEC a double gap concentric cylinder was used, while for the measurements of HMEHEC an ordinary concentric measuring system (cup and bob) was chosen.

Results and Discussion

Phase behaviour

EHEC and HMEHEC show an anomalous solution behaviour; when the temperature is increased the solubility of the polymers decreases and the solution demixes into one phase rich and one phase poor in polymer. This is a behaviour HMEHEC and EHEC have in common with several other nonionic polymers^{6,7,8}. The temperature where phase separation occurs is referred to as the cloud point (CP). In order to determine a suitable concentration of the polymer for the following investigations the CP was determined as a function of polymer concentration (fig 2). At low concentrations CP changes strongly as the polymer concentration is altered. At higher concentrations of polymer CP flattens out at approximately 50 °C. The concentration chosen for further study was 1 w/w% where only a minor concentration dependence in CP exists.

Phase diagrams were investigated in the presence of electrolyte, or alcohols, for EHEC and HMEHEC⁹. These phase diagrams are similar in appearance for the two polymers. The trends in behaviour are what one would expect according to investigations on cellulose ethers in the past¹⁰, but differences exist and can be related to the hydrophobic modification of HMEHEC. The major, and trivial, difference in phase behaviour observed between the two polymers is that CP is shifted downwards by approximately fifteen degrees. This can be ascribed to the introduction of hydrophobic side groups on HMEHEC, making it less water soluble. Phase diagrams were also obtained in the presence of SDS (fig. 3). The differences between modified and unmodified polymer were now found to be more pronounced. This can again be related to the hydrophobic

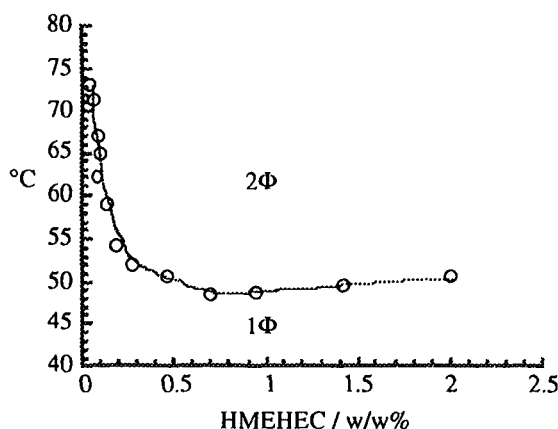


Fig. 2. CP as a function of HMEHEC concentration. 1 w/w% polymer was chosen for further investigations.

modification of HMEHEC.

Addition of salts.

On addition of salt to the polymer/water solution, CP is decreased or increased depending on which salt is added. If the added salt has an anion with a small molecular radius (e.g. chloride) a decrease in CP is seen while a salt with a large anion (thiocyanate) rather will increase CP. This can be explained in two ways. 1. Adding NaCl to the polymer/water solution results in a solvent with higher effective polarity⁵, or 2. There can either be a positive or negative excess at the polymer/water interface when a cosolute, as salt, is added to the solution. This will affect the interfacial energy^{5,11}. NaCl is depleted from the interface giving a force to minimise the polymer-solvent contact. The polymer molecules cluster together and a phase separation occurs at a lower temperature. SCN⁻ enriches at the polymer surface. This leads to a decrease in interfacial energy between the polymer and solvent, resulting in a higher solubility of the polymer and an increase in CP.

Addition of alcohols.

The effect of alcohols on the solubility of the polymers depends to a high degree on the length of the aliphatic chain. On addition of an alcohol with a short aliphatic chain the solubility increases slightly, while an alcohol with a longer hydrocarbon chain decreases CP. The large drop in CP on addition of long chain alcohols is referred to the binding of alcohol molecules to the hydrophobic parts of the polymers, making the polymer/alcohol complex more hydrophobic. As short chained alcohols have a polarity in-between those of water and EHEC, they can either enrich at the polymer surface (the polymer/alcohol complex becomes more polar) or they can lower the polarity of the solvent (water/alcohol). In both models the difference in polarity between polymer and solvent will decrease, and CP increases⁵.

Addition of surfactant.

On adding an ionic surfactant (in this case SDS), CP is decreased at low concentrations, but increased to above 100 °C at higher surfactant concentrations (fig. 3). The initial drop in CP is larger in the case of HMEHEC and starts at a lower surfactant concentration than in the case of EHEC. When surfactant molecules bind to the polymer molecule they introduce one hydrophobic part (the tails) and one hydrophilic part (the head groups). As the surfactant head group is charged the polymer/surfactant complex will act as a polyelectrolyte. The balance between these contributions determines if CP is decreased or increased. We believe that for HMEHEC no critical aggregation concentration (cac), where the surfactant molecules start to bind to the polymer molecule, exists (or it is very low). The binding of surfactant molecules is more or less noncooperative. This is possible as the hydrophobic tails can act as hydrophobic binding sites for surfactants^{4,12}. This is different from solutions of EHEC where the cac is ca. 5 mmolal¹³. The cac for EHEC is dependent on type of surfactant, polymer structure, temperature and electrolyte concentration.

As argued previously the phase behavior of ionic systems is strongly influenced by general electrostatic effects¹⁴. The phase separation should be suppressed in mixtures of a nonionic polymer and an ionic

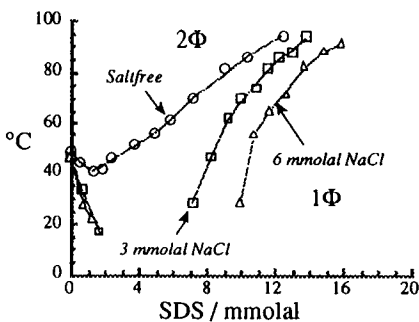


Fig. 3a. CP as a function of SDS and salt concentration for HMEHEC.

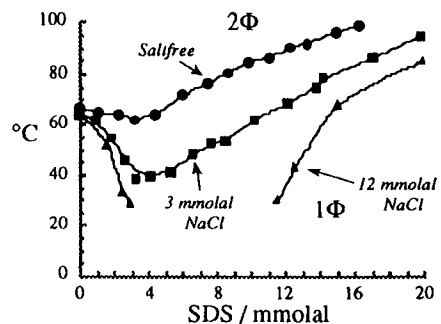


Fig. 3b. Same as fig. 3a, for EHEC.

surfactant in the absence of salt, because of the resulting loss of entropy of mixing of the surfactant counterions. Furthermore, a strong salt dependence is expected, where added salt could result in either segregative or associative phase separation. These systems are of the associative type and the tendency towards phase separation then increases (cloud point decreases) in the presence of salt. The associative interaction is stronger for HMEHEC than for EHEC explaining the quantitative differences. It should be noted that the amount of salt needed to get a shift in CP is three orders of magnitude larger in the system polymer/water than in the system polymer/water/surfactant, illustrating the significance of general electrostatic effects.

Viscosity

The phase diagrams were used to find the proper mixtures for viscosity investigations. When EHEC becomes hydrophobically modified, the viscosity of a 1 w/w% polymer solution increases by approximately a factor of ten. The hydrophobic tails tend to cluster together, forming cross links between polymer chains and a loose three dimensional network is built up in the solution.

On addition of different cosolutes, the viscosity of HMEHEC solutions changes dramatically while the viscosity of EHEC solutions is left almost unchanged⁹ (fig. 4).

Addition of surfactant.

When SDS is added to a solution of HMEHEC the viscosity starts to increase at concentrations as low as 10^{-4} molal (fig. 4) which should be compared with the cmc for SDS which is ca. 8 mM. The viscosity then increases strongly on further SDS addition. Again it seems that the surfactant binds to HMEHEC in a noncooperative way. At ca. 4 mmolal of SDS, the viscosity passes through a maximum and on further SDS addition a levelling off to a value well below the initial viscosity is seen. This is explained in terms of formation of mixed micelles, consisting of SDS molecules and hydrophobic tails of the polymers. At the viscosity maximum the ratio between surfactant molecules and hydrophobic tails is optimal for strengthening the existing network. At higher surfactant concentrations, there is on average only one hydrophobic tail (or less) per micelle and the intermolecular cross links disappear and the viscosity is decreased^{2,4}.

In fig. 4 it can be noted that the viscosity for EHEC is increased on addition of SDS^{15,16}, but the increase starts at a higher SDS concentration than in the case of HMEHEC and is much weaker. This reflects the fact that also EHEC (without nonylphenol groups) is a polymer with hydrophilic and hydrophobic parts and the surfactant molecules can interact with the latter. It also reflects the higher cac of EHEC compared to HMEHEC.

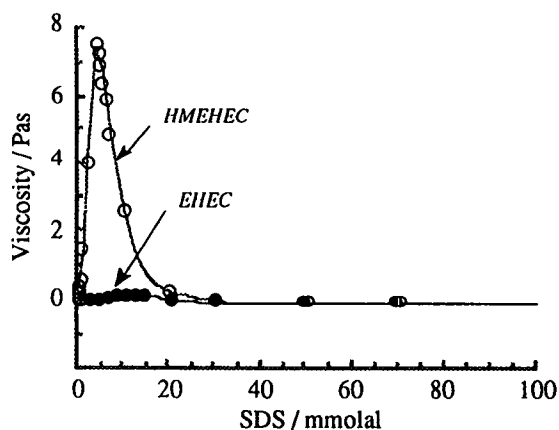


Fig. 4. The viscosity as a function of surfactant concentration for HMEHC and EHEC.

It is interesting to note that at high SDS concentrations, where the intermolecular network is disrupted, the viscosity for EHEC and HMEHEC solutions is roughly equal. The hydrophobic tails of HMEHEC do not affect the viscosity under these conditions.

Addition of alcohols.

If we add alcohols with different chain lengths we observe a viscosity increase with the longer chained alcohols (pentanol, hexanol) in the case of HMEHEC⁹, which is, however, an order of magnitude smaller than that observed with SDS. The alcohol molecules preferentially adsorb at the hydrophobic moieties and strengthen the preexisting network, but the hydrophobic interaction is weaker, than with SDS, due to the shorter hydrocarbon chains of the alcohols. Another difference compared to SDS is that there is no viscosity maximum present. This is so because the alcohol molecules are unable to form micelles and hence can not break up the interpolymer association. Rather, as the hydrophilic contribution is weaker from alcohols than for SDS, a phase separation occurs at higher alcohol concentrations.

The short chained alcohols have a higher polarity and they do not adsorb extensively to the polymer molecules. The difference in polarity between polymer and solvent decreases, the hydrophobic junction zones are weakened and hence the viscosity lowered⁹.

Addition of salts.

When salt is added, the viscosity changes in a way dependent on the anion of the salt used. Viscosity increases when NaCl is added while with NaSCN a decrease is observed⁹. The effects are qualitatively the same for both EHEC and HMEHEC but more pronounced for the latter. These observations parallel those of numerous aqueous systems associated with the so-called lyotropic series. Cl⁻ ions have an unfavourable interaction with nonpolar or weakly polar groups while for SCN⁻ a weak adsorption is expected. Therefore, Cl⁻ promotes but SCN⁻ opposes polymer-polymer association, which explains the observed viscosity effects. As the hydrophobic parts of HMEHEC are larger than for EHEC, viscosity effects are larger.

Conclusions

We demonstrate that the association of hydrophobically modified polymers is strongly affected by a wide range of cosolutes, including surfactants, alcohols and simple electrolytes, which dramatically influence the phase behaviour and the viscosity. The findings directly reflect the distribution of cosolutes between the polymer chains and the bulk solution.

Acknowledgement

The present work has been financially supported by a grant from NUTEK. Ingegerd Lind is gratefully acknowledged for obtaining some of the CP curves.

References

- (1) *Polymers in Aqueous Media Performance Through Association.*; Glass, J. E., Ed.; American Chemical Society: Washington DC., 1989.
- (2) Magny, B.; Iliopoulos, I.; Audebert, R.; Piculell, L.; Lindman, B. *Progr. Colloid Polym. Sci.* **1992**, *89*, 118.
- (3) Goddard, E. D.; Leung, P. S. *Colloids and Surfaces* **1992**, *65*, 211.
- (4) Tanaka, R.; Meadows, J.; Williams, P. A.; Phillips, G. O. *Macromolecules* **1992**, *25*, 1304.
- (5) Karlström, G.; Carlsson, A.; Lindman, B. *J. Phys. Chem.* **1990**, *94*, 5005.
- (6) Bailey, F. E., Jr; Koleske, J. V. *Poly(ethylene oxide)*; Academic Press: New York, 1976.
- (7) Winnik, F. M. *Macromolecules.* **1987**, *20*, 2745.
- (8) Heskins, M.; Guillet, J. E. *J. Macromol. Sci., Chem.* **1968**, 1441.
- (9) Thuresson, K. *Results to be published.*
- (10) Carlsson, A. Thesis, Lund University, Sweden, 1989.
- (11) Piculell, L.; Nilsson, S. *Progr. Colloid Polym. Sci.* **1990**, *82*, 198.

- (12) Sivadasan, K.; Somasundaran, P. *Colloids and Surfaces*. 1990, 49, 229.
- (13) Carlsson, A.; Karlström, G.; Lindman, B.; Stenberg, O. *Colloid Polym. Sci.* 1988, 266, 1031.
- (14) Piculell, L.; Lindman, B. *Adv. in Colloid and Interf. Sci.* 1992, 41, 149.
- (15) Carlsson, A.; Karlström, G.; Lindman, B. *Langmuir* 1986, 2, 536.
- (16) Holmberg, C.; Nilsson, S.; Singh, S. K.; Sundelöf, L.-O. *J. Phys. Chem.* 1992, 96, 871.

43 Structure and solution properties of modified hydroxyethyl cellulose

U Kästner and H Hoffmann – Universität Bayreuth, Physikalische Chemie I, D-95440 Bayreuth, Germany; R Dönges and R Ehrler – Hoechst AG, Werk Kalle-Albert, Rheingastr. 190, D-65174 Wiesbaden, Germany

Abstract

We investigated the solution behavior and the macroscopic properties of samples of hydroxyethyl cellulose (HEC) which were modified by cationic groups (cat-HEC) and perfluoro chains (F-HMHEC). The systems were characterized with rheological, electric birefringence and scanning electron microscopic measurements.

A solution of 1% HEC ($MW 5 \cdot 10^5$) had a viscosity of about 100 mPas. The chemical modification caused an increase of the viscosity up to 1000 mPas. The solutions showed shear thinning behavior. With the addition of surfactant the viscosity of the cat-HEC and F-HMHEC solutions increased even more. Such solutions showed viscoelastic behavior and a yield stress value. The results are interpreted in terms of associations of the modified groups with the surfactant molecules by forming a three-dimensional network structure. These network structures could be made visible by freeze-fracture scanning electron microscopy (FFSEM).

Introduction

Water soluble cellulose derivatives are large scale commercial products. The compounds are used in many industrial applications. Because of their compatibility hydroxyethyl cellulose (HEC) and cationically modified HEC (cat-HEC) are used in food chemistry and

cosmetics as thickeners. The hydrophobically modified perfluoro compound (F-HMHEC) is, because of its resistance to degradation by bacteria and enzymes, of particular interest for water based paints and varnish colours.

The chemical modification of the HEC causes an increase in viscosity. During the last few years it was shown by several groups¹⁾⁻³⁾ that the efficiency of HEC as a thickener can be improved considerably by hydrophobic modification. The degree of hydrophobic substitution has to be kept low. Otherwise the polymers become insoluble in water. The thickening behavior of these polymers are due to intra- and intermolecular crosslinking of their hydrophobic side chains. The addition of small amounts of surfactant increases and strengthens these crosslink points and optimizes the macroscopic properties of the compounds.

Solutions with similar properties as described can be obtained with cationically modified HEC by the addition of anionic surfactants as investigated over recent years⁴⁾⁻⁶⁾. The anionic surfactants bind to the cationic charges of the polymer and the tails of the surfactants act again as crosslinks between different polymer backbones.

Materials and Methods

Both derivatives of HEC were kindly obtained from HOECHST AG (Kalle-Albert; 6200 Wiesbaden 1, Germany) and used as supplied.

Four cationically modified HEC compounds with different molecular weights and different degrees of molar substitution of hydroxyethyl and the cationic substituent glycidyl-trimethyl-ammonium-chloride were used (see table 1).

The four hydrophobically modified samples and the unmodified HEC had the same molecular weight and degree of molar substitution of hydroxyethyl. The degree of perfluoro substitution is very low (see table 1).

For the electric birefringence measurements we placed the solution in a cell between crossed polarizer and analyser, passed a light beam (He/Ne laser) through this system and measured the light intensity that was transmitted when an electric field was applied to the solution.

All oscillatory measurements were recorded using a Bohlin CS-rheometer (measuring geometry: double gap or cone/plate).

The visualization of the expected network structure was achieved using a scanning electron microscopy (electron microscope: JEM 840-A (Jeol)). The samples are prepared by the freeze-fracture method using liquid propane as cryogen.

Results and Discussion

The HEC and cat-HEC compounds were water-soluble. The solubility of the hydrophobically modified hydroxyethyl cellulose (F-HMHEC) depended on the degree of hydrophobic substitution. For up to 4 perfluoroalkyl groups per cellulosic chain the samples were soluble in water. The presence of water soluble polymer backbones and water insoluble side chains renders the F-HMHEC a macromolecular surfactant molecule. We found a strong increase of the viscosity at a concentration, c^* , of F-HMHEC which was much lower than c^* for the HEC solution. This thickening behavior of the F-HMHEC solutions is due to intermolecular crosslinking of the polymers through hydrophobic bonds of the perfluoroalkyl groups. For the cat-HEC solutions we observed, at very low polymer concentrations, an increasing viscosity as for typical poly-electrolytes where the viscosity follows a scaling law of $(c/c^*)^{1/2}$. The concentration c^* and the measured zero shear viscosity at a polymer concentration of 1% per weight are given in table 1.

sample	M_w [g/mol]	z_s	c^* [%]	η_0 [mPas]	L_k [nm]	$l(\tau)$ [nm]
HEC	all samples 500 000	-	0,4	120	all samples 1200	82
F-HMHEC 1)		1	0,1	210		82
F-HMHEC 2)		4	0,1	723		82
F-HMHEC 3)		6	0,1	1 132*		-
F-HMHEC 4)		8	0,1	1 290*		-
cat-HEC 1)	33 000	37	0,2	260	72	80
cat-HEC 2)	43 000	41	0,2	360	102	115
cat-HEC 3)	120 000	48	0,2	615	260	160
cat-HEC 4)	150 000	63	0,2	2 900	300	185

Table 1: Some characteristic parameters of the various modified hydroxyethyl cellulose samples. M_w is determined from light scattering experiments, z_s means the number of side chains per polymer backbone unit. c^* is the critical concentration where the zero shear viscosity begins to rise abruptly. η_0 is the zero shear viscosity at a polymer concentration of 1% by weight. The contour length (L_k) is determined from the molecular weight and $l(\tau)$ is the coil dimension determined from the relaxation times of electric birefringence measurements.

* Measured zero shear viscosity after homogenization of the phase separated systems.

The time constants which were obtained from the electric birefringence decay were used to determine a length for the molecules. This length agreed for the HEC sample with that measured by light scattering. Thus it seems that the birefringence monitors the rotation of the hydrodynamic coil. For the unmodified and the hydrophobically modified HEC the

contour length L_k which is based on the molecular weight and a length of 0,63 nm for a monomer unit, is 15 times longer than the length determined from the electric birefringence decay ($l(\tau)$). These polymers are present in the solution in a coiled conformation.

In spite of the low charge density of only one cationic group per four to ten cellulosic units the cat-HEC compounds show behavior which is typical for poly-electrolytes. This can be concluded from the comparison of the contour length (L_k) for the molecules. For the cat-HEC samples 1) and 2) the dimension which is determined from the birefringence decay $l(\tau)$ is about the same as L_k . For the two samples with the highest molecular weight the contour length is somewhat larger than the length determined from the birefringence data. The difference is, however, less than a factor of two. This shows that the molecules are present in the solution in a more or less extended conformation and are not coiled. The calculated parameters L_k and $l(\tau)$ are also included in table 1.

We studied further the influence of surfactants on the modified HEC solutions. The higher modified F-HMHEC sample 3) became water soluble with small amounts of added hydrocarbon surfactant, the sample with 8 hydrophobic side chains became only soluble with perfluoroalkyl surfactants. It was found that the properties of the cat-HEC and F-HMHEC solutions became similar in the presence of anionic surfactants while the HEC solution was not influenced by the addition of surfactants. It is shown that the viscosity and the storage (G') and loss modulus (G'') of the cat-HEC and F-HMHEC solutions pass over a maximum with an increasing concentration of surfactant. This maximum occurs at a surfactant concentration which is considerable less than the critical micellar concentration (cmc). At the maximum the solutions showed viscoelastic behavior.

Figure 1 shows the measured viscosity data against the relative concentration ($c(\text{surfactant})/cmc$) for two samples of cat-HEC with added SDS, the unmodified HEC sample and a solution of F-HMHEC 3) with various anionic and cationic surfactants. Figure 2 shows the storage moduli G' at a constant frequency of 10 Hz ($G' \sim G^0$) for the same samples with various anionic surfactants.

The cat-HEC samples show a strong increase of the viscosity and the storage moduli with increasing charge compensation. The maximum is reached at 90% neutralization. After the maximum the solutions phase separate because the surfactant concentration is large enough to compensate the charge of the polymers. The two phases separated macroscopically and a sharp phase boundary was observed between them. The two phase system changed again to a single phase solution when more surfactant is added than is necessary for charge neutralization. It is likely that the excess surfactants bind on the surfactant-polymer

complexes and reverse the charge. The strongest hydrogel we found was for the highest modified sample, cat-HEC 4), which shows a yield stress value at the maximum.

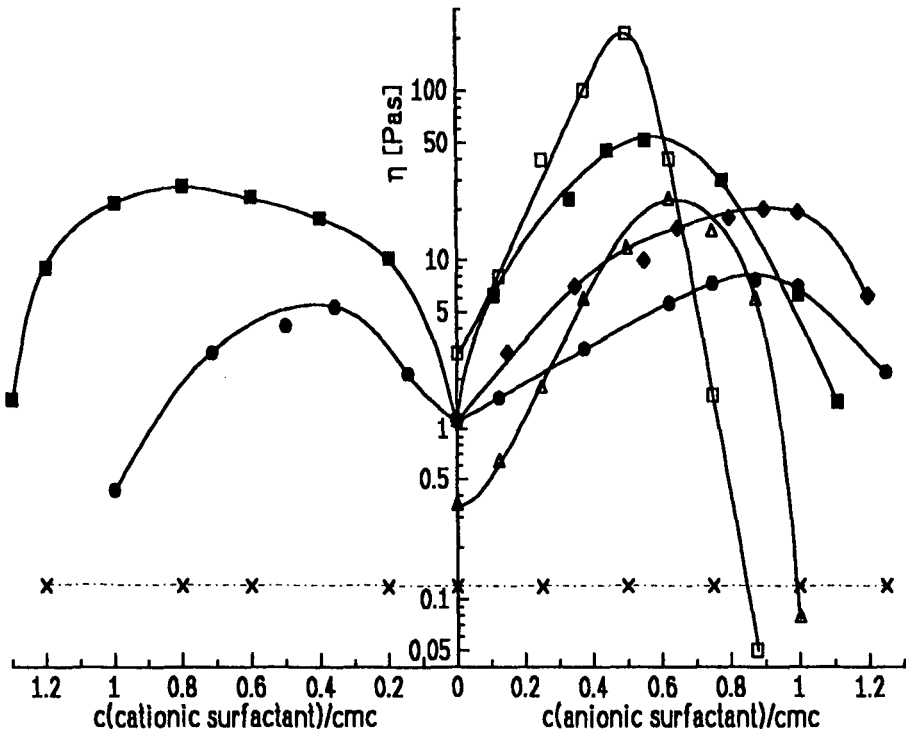


Figure 1: The viscosity at a constant shear rate of $0,5 \text{ s}^{-1}$ as a function of the relative concentration of various anionic and cationic surfactants. The samples are 1% solutions of:

- (\times) HEC with $\text{C}_8\text{F}_{17}\text{CO}_2\text{Li}$ and $\text{C}_8\text{F}_{17}\text{C}_4\text{H}_8\text{N}(\text{CH}_3)_3\text{I}$;
- (\bullet) F-HMHEC 3) with $\text{C}_{12}\text{H}_{25}\text{SO}_4\text{Na}$ and $\text{C}_{12}\text{H}_{25}\text{N}(\text{CH}_3)_3\text{Br}$;
- (\blacklozenge) F-HMHEC 3) with $\text{C}_{14}\text{H}_{29}\text{SO}_4\text{Na}$;
- (\blacksquare) F-HMHEC 3) with $\text{C}_8\text{F}_{17}\text{CO}_2\text{Li}$ and $\text{C}_8\text{F}_{17}\text{C}_4\text{H}_8\text{N}(\text{CH}_3)_3\text{I}$;
- (\triangle) cat-HEC 2) and (\square) cat-HEC 4) with added $\text{C}_{12}\text{H}_{25}\text{SO}_4\text{Na}$.

The plots of the viscosity and the storage moduli of the F-HMHEC solutions against the concentration of several cationic and anionic surfactants are not symmetrical. Anionic surfactants influence the properties of the F-HMHEC solutions much stronger than cationic surfactants. This observation might have its origin in the weak complexation of metal ions by ethylenoxide (EO) groups. The F-HMHEC samples also have EO groups which could bind a few sodium ions and thus support the binding of the anionic but not the cationic surfactants. This complexation might also be the reason that we could observe interactions

between the perfluoro polymers and hydrocarbon surfactants. The influence of anionic hydrocarbon surfactants increases with the length of the alkyl group of the surfactant (from dodecyl to tetradecyl). Longer chains of cationic hydrocarbon surfactants did not interact. However the strongest hydrogels were observed for F-HMHEC with perfluoroalkyl surfactants.

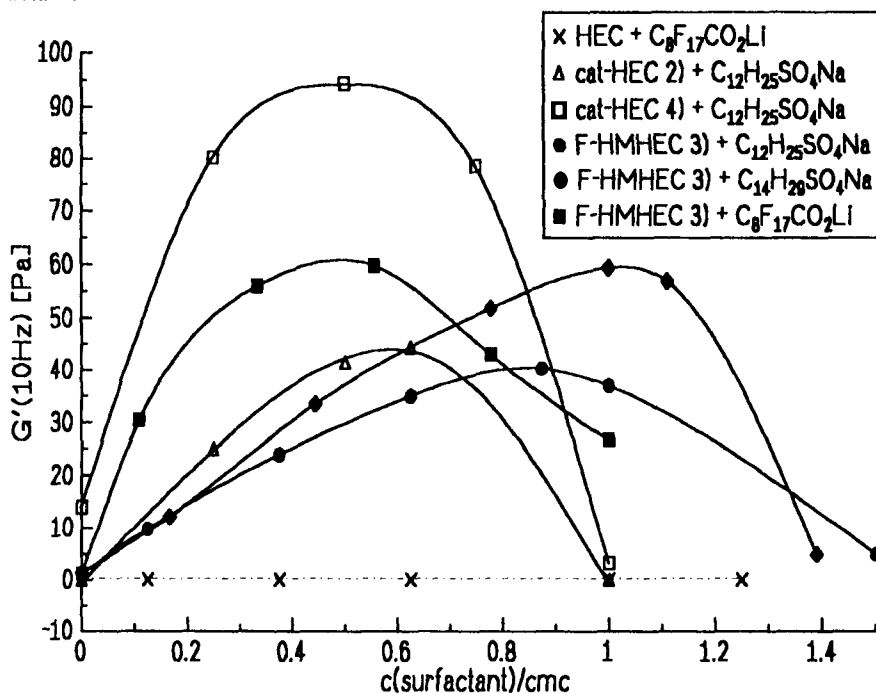


Figure 2: The storage moduli G' at a constant frequency of 10 Hz (plateau) against the relative concentration of various anionic surfactants. The samples are 1% solutions.

The behavior of both polymer types with added surfactant can be understood on the basis of associations between the polymeric side chains and the surfactant molecules. For the hydrophobically modified samples F-HMHEC the surfactant molecules are binding to the hydrophobic crosslinks. The number of association points increases with the level of added surfactant. For the cat-HEC samples the anionic surfactant molecules associate with the cationic groups of the polymer. Because of their hydrophobic tails the polymers become hydrophobic and can interact like the F-HMHEC-surfactant-systems.

These three-dimensional network structures were observed by freeze-fracture scanning electron microscopy (FFSEM). Figure 3 shows the pictures of a cat-HEC sample 4) (3a) and a F-HMHEC sample 2) (3b) at their maximum viscosity. Both network structures occur as

connected spherical particles. The size of the F-HMHEC coils corresponds to the size determined from light scattering and electric birefringence measurements. The diameter of the cat-HEC globules are about 50 nm. It thus seems that the increasing charge compensation leads to a now more coiled conformation of this compounds.

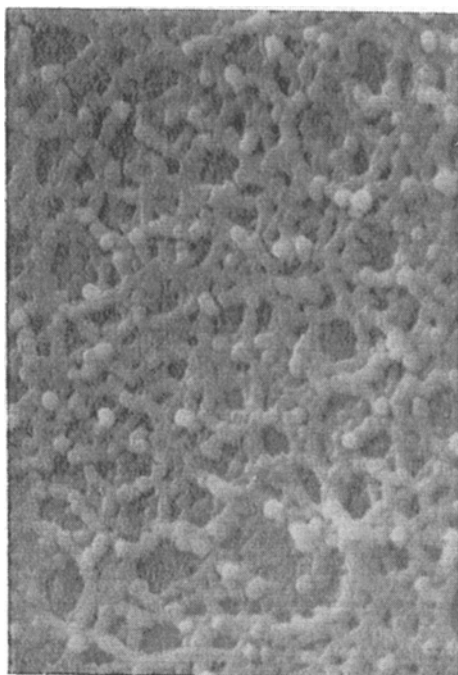


Figure 3a: FFSEM picture of a 1% cat-HEC 4) sample with 4 mmol SDS; \blacksquare = 1 μ m.

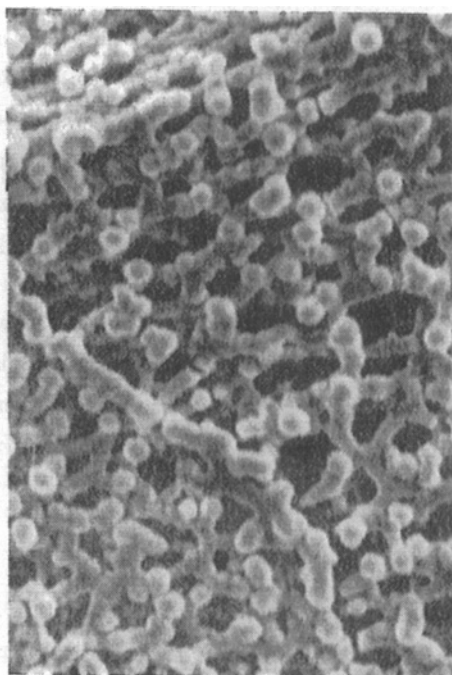


Figure 3b: FFSEM picture of a 1% F-HMHEC 2) sample with 4 mmol $C_8F_{17}CO_2Li$; \blacksquare = 1 μ m.

Conclusions

Both polymer types showed different behavior of their pure solutions above c^* . The F-HMHEC samples interacted through their hydrophobic side chains and formed spherical aggregates. The cat-HEC samples behaved like poly-electrolytes. Due to the electrostatic repulsion the chains were more or less in a stretched conformation. These chains formed above c^* interacting polymeric domains.

By the addition of surfactants the differences between the two systems disappeared. For both polymer types we found a maximum in the viscosity and the storage modulus with an

increasing surfactant concentration. It is assumed that the polymers form spherical aggregates which are connected to a three-dimensional network.

The structure of the hydrophobically modified hydroxyethyl cellulose on the addition of surfactant is interpreted as an association between the hydrophobic tails of the surfactant and the hydrophobic side chains of the polymer. Counting the junction points which form the elastic network we found that only a few percent of the hydrophobic side chains built up the network structure. It is likely that the main part of the hydrophobic side chains form intramolecular associations and form the globules as seen in the FFSEM picture.

The structure for the cationically modified hydroxyethyl cellulose with added anionic surfactant is interpreted in interactions between the charged head groups of the surfactants and the cationic substituents of the polymer. The hydrophobic tails of the surfactant molecules form the junction points of the network structure. The number of these junction points was very low while the charge neutralization was about 90%. In this case the polymer has a strong hydrophobic character and we suggest that the hydrophobic parts (the tails of the surfactants) interact in the way of forming intramolecular associations. This would cause a more coiled conformation of the polymeric backbones as seen in the FFSEM picture.

References

- 1) Sau, A.C.; Landoll, L.M. in Glass, J.E. (Ed.): *Polymers in Aqueous Media, Advances in Chemistry Series 223*, Am. Chem. Soc., Washington DC (1986) p.343.
- 2) Tanaka, R.; Meadows, J.; Phillips, G.O.; Williams P.A.: *Macromolecules 25* (1992) p.1304.
- 3) Dualeh, A.J.; Steiner, C.A.: *Macromolecules 24* (1991) p.112-116.
- 4) Dualeh, A.J., Steiner, C.A. in Harland, R.S.; Prud'homme, R.K. (Eds.): *Polyelectrolyte Gels, Advances in Chemistry Series 480*, Am. Chem. Soc., Washington DC (1992) p.42.
- 5) Goddard, E.D.; Leung, P.S.; Padmanabham, K.P.A.: *J. Soc. Cosmet. Chem. 42* (1991) p.19-34.
- 6) Goddard, E.D.; Leung, P.S.: *Colloids and Surfaces 65* (1992) p.211-219.

44 Intra- and intermolecular hydrophobic associations in aqueous solutions of amphiphilic derivatives of alginate

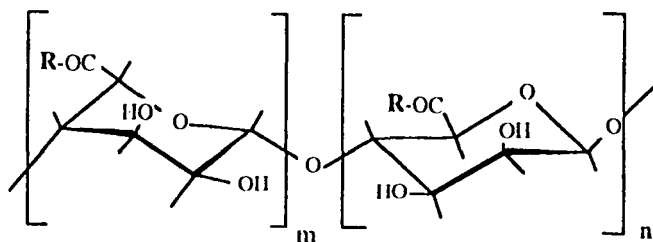
A Siquin, P Hubert and E Dellacherie – Laboratoire de Chimie-Physique Macromoléculaire, URA CNRS 494, ENSIC BP 451, 54001 Nancy Cédex, France

Hydrophobically-associating water-soluble polymers are receiving increasing attention owing to their peculiar physico-chemical properties in aqueous solution, both at low concentration and in the semi-dilute regime. Above a certain critical concentration, the chains interact intermolecularly to form aggregates of large hydrodynamic volume and accordingly very high viscosity, whereas below this critical concentration, the chains interact intramolecularly, leading to shranked conformations of the coil.

We report our preliminary results on the introduction of hydrophobic side-chains on a derivative of sodium alginate. This study has the ambition to go beyond the mere observation of uncommon physico-chemical properties of aqueous solutions, shared by many other amphiphilic derivatives, most frequently prepared from hydroxyethyl cellulose (HMHEC)(1) or acrylic monomers (2). As a matter of fact, the alginate salts exhibit a sol-gel transition when simply submitted to modifications of their ionic environment, e.g. substitution of Na^+ by divalent cations such as Ca^{2+} . This property provides an additional motivation for the preparation of amphiphilic macromolecules and their study, not only in solution but, in the near future, also in the gel state.

SYNTHESIS

The reaction consisted of a nucleophilic displacement of a propylene glycol ester of alginate (PGA), by a long chain aliphatic amine (in the present study dodecylamine), at room temperature in DMF. The final composition (moles %) of the amphiphilic polysaccharide (PGA-C₁₂) is given in the following figure :



PGA: R \equiv O⁻Na⁺ (#30%); Propylene glycol (# 70%).

PGA-C₁₂: R \equiv O⁻Na⁺(#30%); Propylene glycol (#61%);
NH-(CH₂)₁₁CH₃ (#9%).

RHEOLOGICAL MEASUREMENTS

Fig. 1 shows the concentration dependence of the solution viscosity, for PGA and PGA-C₁₂ in pure water. PGA exhibits a slow increase of its viscosity, in agreement with typical polyelectrolyte behavior when concentration is sufficiently high so that electrostatic repulsions are screened. In opposition, the viscosity of PGA-C₁₂ sharply increases with the concentration, to reach values two orders of magnitude higher than those of the precursor.

The hydrophobic nature of the phenomena observed is clearly evidenced by the effect of ionic strength on the respective viscosities of PGA and PGA-C₁₂. In the presence of salts (Fig. 2) the viscosity of PGA-C₁₂ is strongly enhanced, whereas the unmodified polysaccharide remains totally unaffected.

These results can be interpreted in terms of intermolecular hydrophobic interactions between the dodecyl chains immobilized on PGA. As the polymer concentration increases, hydrophobic domain ordering becomes important and may ultimately result in a "pseudo-reticulated" structure.

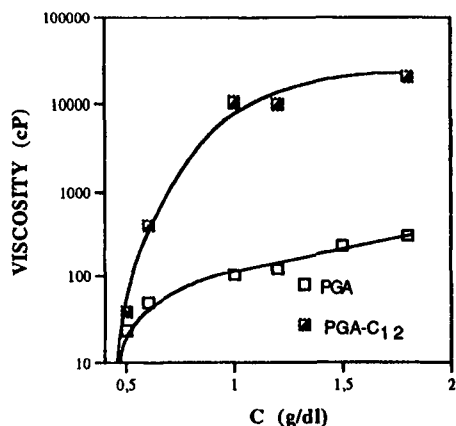


FIG. 1 : Viscosity of PGA and PGA-C₁₂ vs polymer concentration, in pure water (shear rate : 0.06 s⁻¹)

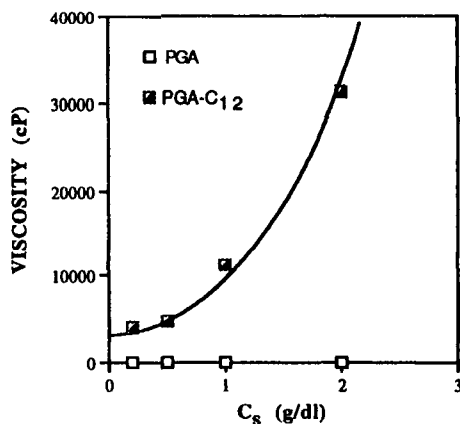


FIG. 2 : Viscosity of PGA and PGA-C₁₂ vs NaCl concentration (Cs) (polymer concentration : 1.2 g/dl; shear rate : 0.06 s⁻¹).

VISCOMETRY AT HIGH DILUTION

The measurement of the intrinsic viscosity $[\eta]$, corresponding, for neutral polymers, to the extrapolation to infinite dilution of the Flory-Huggins equation (3)

$$\eta_{sp}/c = [\eta] + k_H [\eta]^2 c$$

(where c is the polymer concentration and η_{sp} the specific viscosity of the solution) reflects the actual geometry of the coil, free from intermolecular interactions.

In dilute aqueous solution (polymer concentration < 0.2 g/dl), the dimension of an amphiphilic polyelectrolyte chain and accordingly its viscosity, is the resultant of two opposing effects : the coulombic repulsive forces between ionic charges borne by the macromolecule and the attractive interactions between its hydrophobic segments.

The effect of increasing ionic strength on PGA is limited to a progressive screening of the repulsions, leading, as expected, to a more and more compact coil. For PGA-C₁₂, in superposition to this effect on repulsive charges, the ionic strength plays a favorable role on the establishment or the reinforcement of hydrophobic interactions between dodecyl groups. The consequence for PGA-C₁₂ is that the expansion of its conformation, compared to that of PGA, is still more restricted and its viscosity further decreased (Fig. 3).

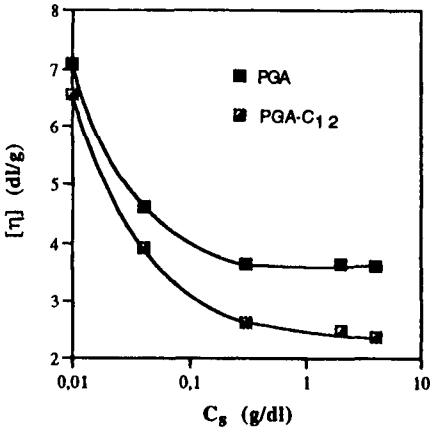


FIG. 3 : Intrinsic viscosity $[\eta]$ of PGA and PGA-C₁₂ at various NaCl (C_s) concentrations.

Since the higher the ionic strength, the stronger is the hydrophobic effect, it is not surprising to observe that the difference, $\Delta[\eta]$, between the two macromolecules is larger and larger as the salt concentration increases .

The values of the Huggins coefficient are also significantly different for PGA and PGA-C₁₂ in the whole range of ionic strength considered. For PGA, the values remain within the 0.3-0.5 range generally observed for non-associating polymers. In opposition, the high values ($k_H > 1$) obtained for PGA-C₁₂ are a qualitative indication that polymer-polymer interactions are more favored than those between the coil and the solvent. This observation is consistent with the hypothesis involving the formation of hydrophobic microdomains through intramolecular associations. In addition, the possibility of residual intermolecular interactions may as well be considered.

FLUORESCENCE

Pyrene is a hydrophobic probe with very low solubility (about $3 \cdot 10^{-7}$ M) in water. Its fluorescence spectrum at low concentration possesses a fine structure whose relative peak intensities are highly sensitive to the polarity of the microenvironment. The ratio of the intensity of the highest energy vibrational band (I_1) to that of the third highest energy vibrational band (I_3) has proved to correlate with solvent polarity. In hydrocarbon solvents, the ratio I_1/I_3 is around 0.6. It is close to 1.1 in ethanol and around 1.6 in water. This polyaromatic hydrocarbon can be used to probe the formation of hydrophobic microdomains in microheterogeneous

aqueous systems (4) and is therefore well adapted to the study of PGA-C₁₂, and appears as a complementary technique to viscometry.

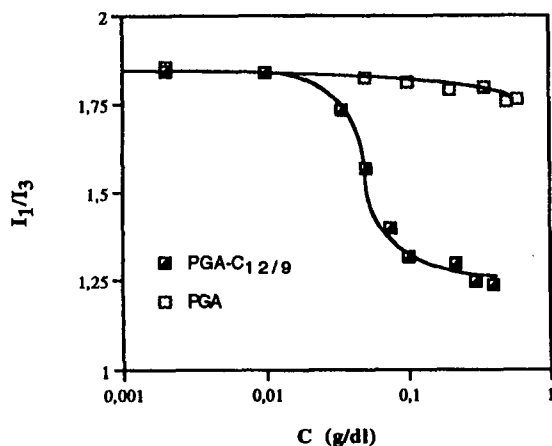


FIG. 4 : I_1/I_3 ratio of pyrene ($C = 1.1 \cdot 10^{-6}$ M) in the presence of PGA or PGA-C₁₂, vs polymer concentration, in pure water.

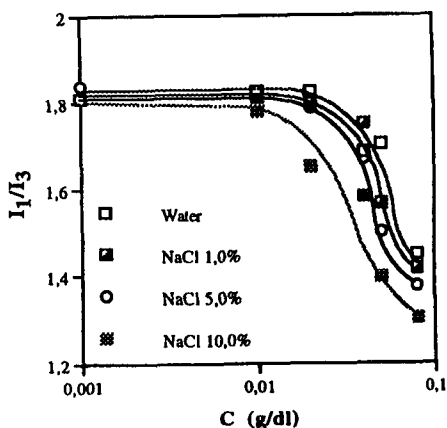


FIG. 5 : Variation of I_1/I_3 ratio of pyrene in the presence of PGA-C₁₂ vs polymer concentration, at various NaCl concentrations.

Fig. 4 shows the variation of the I_1/I_3 value vs polymer concentration, in pure water, for PGA and PGA-C₁₂.

The fluorescence spectrum of pyrene is hardly affected by the presence of PGA, in the whole concentration range tested. The value of I_1/I_3 stays above 1.8, indicating the aqueous nature of the environment probed. In contrast, in the presence of PGA-C₁₂ and for polymer concentrations as low as 0.02%, I_1/I_3 values

continuously decrease to reach finally a plateau around 1.25, i.e. rather close to that experienced with SDS micelles above their CMC (1.1). These results suggest that hydrophobic microdomains already exist in pure water for PGA-C₁₂. Considering the low amount of carboxylic groups available in ionized form on this polymer, it is not so surprising that the balance between electrostatic repulsions and hydrophobic attractions can tend so readily towards the formation of such hydrophobic microdomains.

The effect of increasing ionic strength on the variation of I₁/I₃ vs PGA-C₁₂ concentration is shown in Fig. 5. One observes that the higher the ionic strength, the lower the polymer concentration necessary for the chain to start organizing in hydrophobic microdomains. Furthermore, the I₁/I₃ value at high polymer concentration (0.1% and beyond) is lower as the salt concentration is raised, indicating, as expected, that the environment probed by pyrene is increasingly hydrophobic with the ionic strength. These results are consistent with the conclusions drawn from the viscometric experiments.

CONCLUSION

The covalent immobilization (# 9%) of an aliphatic long chain amine (dodecylamine) onto a partially esterified derivative of alginate (PGA) affords an amphiphilic polyelectrolyte. In aqueous solution, this compound exhibits peculiar physico-chemical properties resulting from intra- or intermolecular hydrophobic associations, depending on the concentration range concerned. These properties are evidenced by viscometric, rheological and fluorescence measurements.

Before approaching studies related to the gel state, physico-chemical properties of derivatives differing from PGA-C₁₂ both in the substitution ratio and the length of the immobilized alkyl chain will be investigated.

REFERENCES

- (1) Landoll, L. M., *J. Polym. Sci.*, **1982**, *20*, 443
- (2) Magny, B., Iliopoulos, I. and Audebert, R., *Polym. Commun.*, **1991**, *32*, 456
- (3) Huggins, M. L., *J. Am. Chem. Soc.*, **1942**, *64*, 2716
- (4) Nakajima, A., *J. Lumin.*, **1976**, *11*, 429

45 Fluorescence studies of cellulose ethers in aqueous solution and in films

F M Winnik – Xerox Research Center of Canada, 2660 Speakman Drive, Mississauga, Ontario, Canada, L5K 2L1

ABSTRACT

Cellulose ethers are often soluble in cold water, but when their solutions are heated above a critical temperature, the cloud point, they separate into two phases. Detailed aspects of this phase transition have been investigated by fluorescence studies of pyrene- and fluorene-labelled hydroxypropyl cellulose samples. The spectroscopy of labelled hydroxypropyl cellulose films is described for films cast from cold aqueous solutions and from solutions heated above their cloud point.

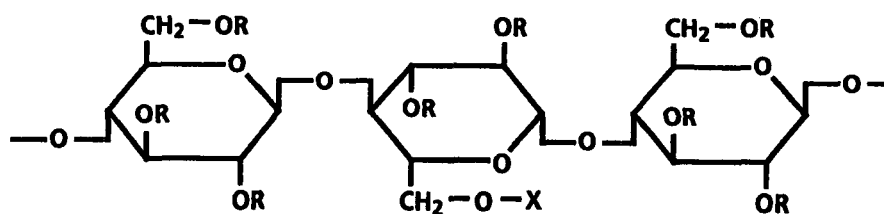
INTRODUCTION

Cellulose ethers are widely used in industry, for example as rheology modifiers in fluids or as components of composites and coatings where they help in modulating adhesion to various surfaces.¹ Most cellulose ethers are soluble in organic solvents, but they also exhibit appreciable solubility in water, at least within specific temperature and concentration domains. Given the recent trend towards replacing solvent-based industrial processes with techniques using

water-borne fluids, it can be foreseen that the applications of cellulose ethers will increase rapidly in number and diversity. In order to design materials with improved performances it is important to understand in detail the interactions taking place in aqueous solutions of cellulose ethers and how they are affected by external stimuli. In previous investigations we have demonstrated how fluorescence spectroscopy can be employed to explore the solution properties of cellulose ethers in water.^{2,3} These studies have led us to undertake a study of the morphology of polymer films prepared under various conditions. Initial results of this study are presented here. After a brief review of the structural features of the polymers studied and of the spectroscopic tools employed, experiments are described which provide information on the properties of aqueous solutions of cellulose ethers and on the morphology of films cast from these solutions. Preliminary results of measurements by Total Internal Reflectance (TIR)⁴ fluorescence are described.

THE POLYMERS

The study focuses on hydroxypropyl cellulose (HPC), a commercial polymer prepared by reaction of propylene oxide with cellulose. This reaction requires the diffusion of reactants into the cellulose fibres. It leads to a structurally inhomogeneous polymer with blocks of fully substituted glucose units interspaced by more lightly di- or mono-substituted units.⁵ The chemical structure of HPC is characterized by the degree of substitution (DS >2.8) which represents the average number of oxygens of the glucose units bearing a substituent and by the molar substitution (MS ca 5.8), which is the average number of hydroxypropyl groups linked to the glucose units. Fluorescently labelled HPC samples were prepared from a commercial material by attaching dyes to the hydroxyl groups of the polymer via ether linkages randomly distributed along the polymer chain (Figure 1).²



HPC: $X = H$, HPC-Py: $X = (CH_2)_4 - Py$, HPC-Flu: $X = CH_2 - Flu$;

$R = CH_2CH(OH)CH_3$

Figure 1: Idealized structures of hydroxypropyl cellulose and of the labelled polymers

EXPERIMENTAL

Materials. Two samples of Pyrene-labelled HPC (HPC-Py) were prepared from HPC (Klucel-L, Mw 100,000, Aldrich Chemicals Co.) as described previously.² The sample used in the pyrene excimer studies contains 5.33×10^{-5} mol of Py/g of polymer or on average 1 Py for 56 glucose units. The sample used in the non-radiative energy transfer (NRET) experiments contains 6.80×10^{-6} mol of Py/g of polymer or on average 1 Py per 438 glucose units. The Fluorene-labelled HPC (HPC-Flu) contains 8.9×10^{-5} mol of Flu/g of polymer or on average 1 Flu per 33 glucose units.

Fluorescence measurements. The solution spectra were recorded on a SPEX Fluorolog 212 spectrometer equipped with a DM3000F data system. Measurements of the fluorescence of films were performed with a home-built spectrophotometer described in detail elsewhere.⁶ For TIR experiments the incident angle of the excitation light was set at 68° . The excitation wavelength was set at 330 nm for the pyrene excimer experiments and at 310 or 290 nm for the NRET experiments.

Sample Preparation. Solutions for analysis were prepared by allowing each polymer to dissolve in water over 24 h. Solutions containing HPC-Py and

They were kept at room temperature for at least 2 hr prior to spectroscopic measurements. Polymer films (thickness *ca* 50 μm) were cast on sapphire ($n = 1.81$ at 310 nm) plates from a solution of labelled HPC in water (1 mL, polymer concentration: 2 g L⁻¹, [Flu]/[Py] = 2). They were dried at room temperature, then kept in vacuo at 25°C for 24 hr. The films obtained from phase-separated aqueous solutions were prepared by casting a preheated solution (1 hr at 50°C) onto sapphire plates kept at 50°C. The films were cooled to room temperature, dried, and evacuated for 24 hr.

RESULTS AND DISCUSSION

Solution properties. In dilute aqueous solution HPC exhibits a thermoreversible phase transition: it is soluble in cold water, but separates from solution upon heating above a critical temperature, the cloud point (CP, 42°C).⁷ The solubility of HPC in cold water can be attributed to the ability of the polymer to form H-bonds with water while inducing considerable ordering of the solvent through its apolar substituents. The enhancement of water structure takes place around the methyl and methylene groups of HPC and around the hydrophobic dyes of labelled HPC. This water structuring brings about large negative contributions to both the enthalpy ΔH_M and the entropy ΔS_M of mixing. At a sufficiently high temperature the entropic term of the free energy of mixing will overcome the negative enthalpy of solution, resulting in a positive free energy. Thus at this temperature phase separation occurs. The phase separation phenomena of aqueous HPC have been studied in detail by light scattering and calorimetry,⁸ as well as by spectroscopic tools, such as ¹³C NMR⁹ and fluorescence. In experiments with fluorescently labelled polymers it is possible to exploit the association of hydrophobic chromophores in water. For example one can probe short-range (4 to 5 Å) interactions between identical chromophores capable of excimer emission, or one can monitor interactions between pairs of different dyes capable of undergoing non-radiative energy transfer.¹⁰ In this case the critical separation distance between chromophores undergoing this process is larger (20 to 50 Å).

non-radiative energy transfer.¹⁰ In this case the critical separation distance between chromophores undergoing this process is larger (20 to 50 Å).

Pyrene excimer experiments in solutions. The fluorescence spectrum of HPC-Py in cold water exhibits an emission due to locally excited Py, with the (0,0) band located at 376 nm ('monomer' emission) and a broad featureless emission centred at 480 nm attributed to pyrene excimers. The latter originates from preformed Py dimers or higher aggregates.¹¹ Upon warming a solution of HPC-Py from 10°C to 45°C, the intensity of excimer emission increases gradually to reach a maximum value at ca 38°C. It undergoes a sharp decrease as the solution reaches the cloud point temperature (Figure 2). Thus the pyrene excimer experiments reveal a disruption of the hydrophobic aggregates upon macroscopic phase separation. In the anisotropic phase formed above the cloud point the chromophores are accommodated as isolated entities within the polymer-rich phase.

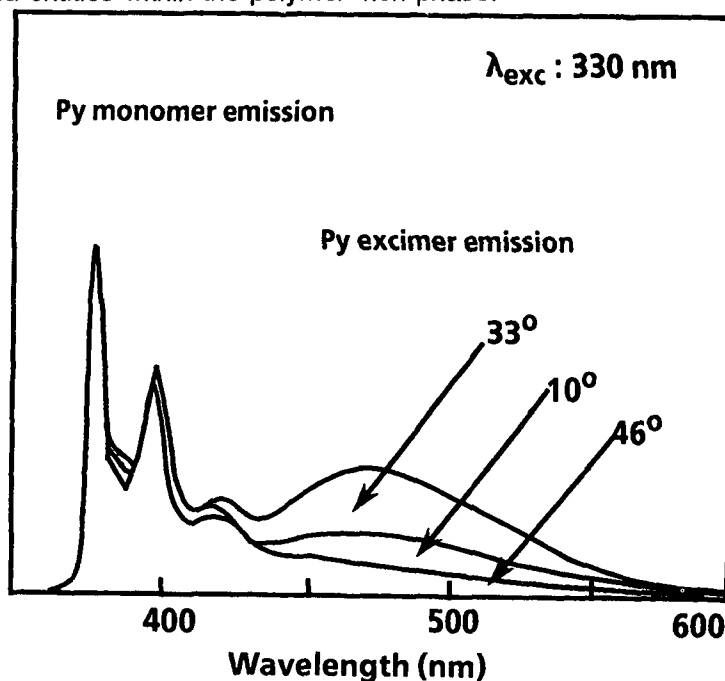


Figure 2: Fluorescence spectra of aqueous solutions of HPC-Py (0.15 g L⁻¹) at several temperatures.

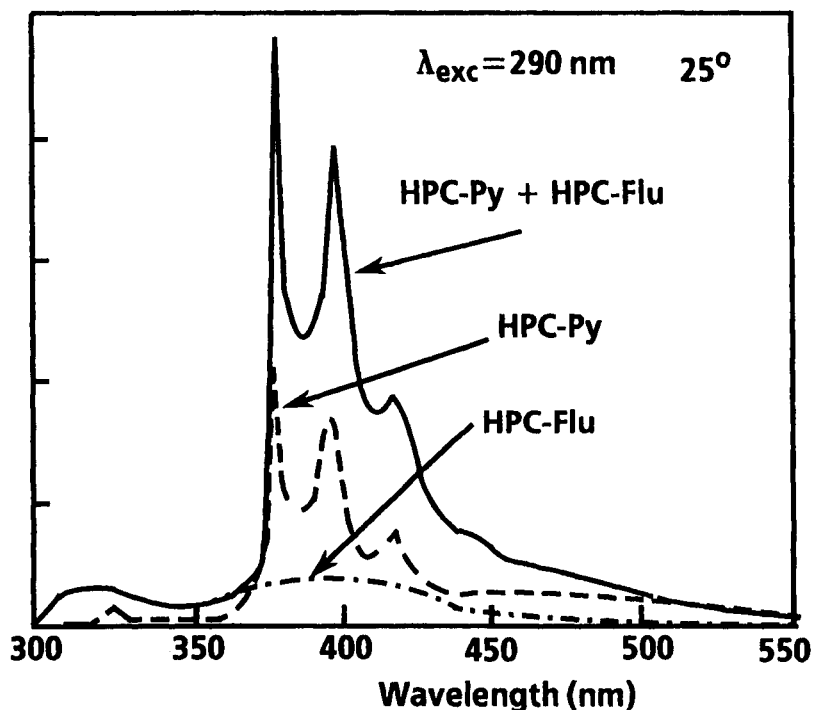


Figure 3. Fluorescence spectra of aqueous solutions of HPC-Py (0.15 gL^{-1}), HPC-Flu (0.05 gL^{-1}) and a mixture of the two polymers.

Non-radiative energy transfer (NRET) experiments in solution. The NRET process is an extremely powerful tool to characterize distances between pairs of interacting chromophores.¹⁰ Spectroscopically, the fluorene-pyrene pair is well suited for NRET experiments, since the emission spectrum of Flu (energy donor) overlaps well with the absorption of Py (energy acceptor) and there exists a window in the UV spectrum where absorption of Flu is much stronger than that of Py, thus allowing selective excitation of Flu in the presence of Py. Experiments were carried out with aqueous solutions of HPC-Py and HPC-Flu of varying total polymer concentration and at different temperatures. The emission spectra of cold aqueous solutions of HPC-Py, HPC-Flu, and a mixture of the two polymers at the same concentration are shown in Figure 3. The pyrene emission intensity is greatly enhanced in the presence of HPC-Flu, indicative of the occurrence of NRET between chromophores

dependence of the efficiency of NRET in this system revealed that interpolymeric association takes place at concentrations as low as 0.05 g L^{-1} .³ Upon heating a mixed polymer solution above its cloud point, the fluorene emission decreased while the Py emission increased, revealing a modest enhancement of NRET efficiency. This observation suggests that in the phase separated domains the chromophores are brought into closer proximity. However since the characteristic distance of the Flu-Py pair is 20 \AA the process does not report on the changes in chromophore aggregation revealed so dramatically by the Py excimer experiments discussed in the previous section.

Non-radiative energy transfer experiments in films. Next, a series of NRET measurements were performed with labelled-HPC films cast onto sapphire from aqueous solutions, below the cloud point and as phase separated mixtures (50°C). When light travelling in a material with higher refractive index (n_1) is incident upon an interface at an angle greater than the critical angle, although the light undergoes total reflection, there is some penetration of the excitation light into the material with the lower refractive index in the form of an evanescent wave.⁴ This evanescent wave can be used to excite selectively chromophores located in the vicinity of the interface (ca 30 nm in these experiments). In films cast from solutions below their cloud point, the efficiency of energy transfer between Flu and Py labels was very high. Only little differences could be detected between the efficiency of NRET in the bulk of the film and at the substrate/polymer interface. However in films cast from solutions above their cloud point, significant differences were observed (Figure 4): the NRET efficiency measured at the interface (TIR) was weaker than that of the bulk of the film. Under both conditions, though, the NRET efficiency was estimated to be much weaker than in films cast at room temperature, implying a higher degree of segregation between polymer chains in films cast from phase-separated mixtures. The differences between interface and bulk interactions or to the existence of domains of liquid crystallinity formed during the drying process.¹²

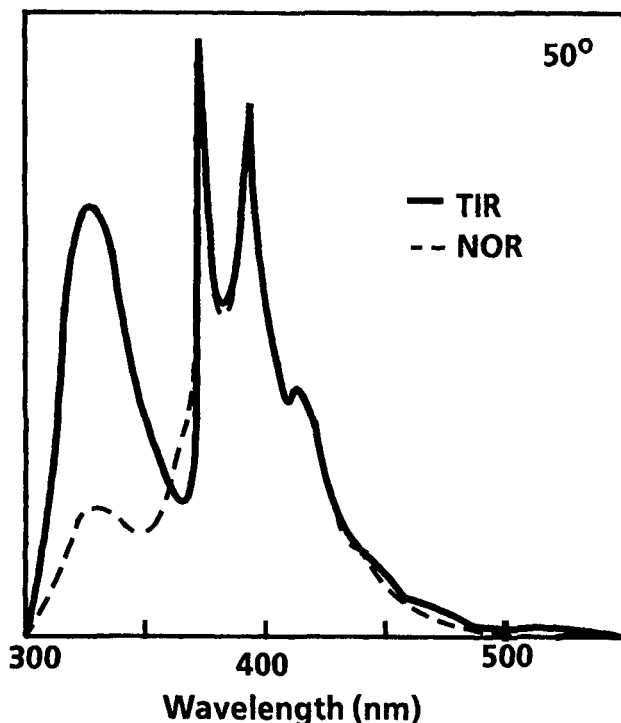


Figure 4: Fluorescence spectra of a HPC-Py/HPC-Flu film cast at 50°C and measured under normal conditions (NOR) and (TIR).

REFERENCES.

1. For a recent review, see Doelker, E. in *Biopolymers I, Advances in Polymer Science*, 107, Peppas, N. A.; Langer, R. S., Ed., Springer-Verlag, Berlin, 1993, pp 199-264.
2. Winnik, F. M.; Winnik, M. A.; Tazuke, S.; Ober, C.K. *Macromolecules* **1987**, *20*, 38.
3. Winnik, F. M. *Macromolecules* **1989** *22*, 734.
4. Masuhara, H.; Itaya, A. in *Lasers in Polymer Science and Technology: Applications, Volume 2*, Fouassier, J.-P.; Rabek, J. F., Ed.; CRC Press, Boca Raton, USA (1990); chapter 10.
5. Takahashi, S.; Fujimoto, T.; Miyamoto, T.; Inagaki, H. *J. Polym. Sci., Polym. Chem. Edn*, **1987**, *25*, 987.
6. Itaya, A.; Yamada, T.; Tokuda, K.; Masuhara, H. *Polymer J.*, **1990**, *22*, 987.

7. For a description of the water-HPC phase diagram, see: Fortin S.; Charlet, G. *Macromolecules* **1991**, *24*, 2413.
8. Robitaille, L.; Turcotte, N.; Fortin, S.; Charlet, G. *Macromolecules* **1991**, *24*, 2413.
9. Ibbett, R. N.; Philp, K.; Price, D. M. *Polymers* **1992**, *33*, 4087.
10. Lakowicz, J. R, *Principles of Fluorescence Spectroscopy*, Plenum Press, New York, 1982.
11. Winnik, F. M. *Chem. Rev.* **1993**, *93*, 587.
12. The TIR experiments were carried out in the laboratory of Professor A. Itaya (Kyoto Institute of Technology, Kyoto, Japan).

46 Modification of cellulose-based polyelectrolyte adlayer by surfactant. Null ellipsometry and SFA study

V Shubin* and P Petrov – Physical Chemistry I, Chemical Centre, University of Lund, PO Box 124, S-221 00 Lund, Sweden

Abstract

The effect of addition of anionic (SDS) and non ionic ($C_{12}E_5$) surfactants on the structure and composition of layers of cationic hydrophobically modified hydroxyethylcellulose Quatrisoft® LM 200, adsorbed on negatively charged surfaces (mica and SiO_2), was studied by surface force apparatus (SFA) and *in situ* null ellipsometry. It is shown that associative binding of surfactant to the polymer results in a variety of interfacial behaviour depending on the nature and concentration of added surfactant.

Introduction

Chemically modified, natural polysaccharides (starch, cellulose, etc.) are a large and important class of industrial polymers. Due to their unique rheological behaviour they are widely used as thickeners in a variety of water-based formulations, such as latex paints, building materials, drilling muds, etc. Being non toxic, they find increasingly wide application in foods and cosmetics. Adsorption of these polymers at solid - liquid interfaces is used to control stability of colloidal dispersions as well as other interfacial properties such as wettability and adhesion. In a number of applications, the polymers are used in combination with surfactants. It is well recognized that interaction between polymers and amphiphiles strongly affects phase behaviour, rheological and other bulk

* On leave from: Department of Colloid Chemistry, Chemical Faculty, St. Petersburg University, St. Petersburg, Russia

properties of polymer solutions, as well as polymers' behaviour at interfaces (Goddard and Ananthapadmanabhan, 1993).

In this paper we present an experimental study of interfacial behaviour of a cationic hydrophobically modified hydroxyethylcellulose Quatrisoft® LM 200 in the presence of anionic and non ionic surfactants. The influence of surfactant addition on the structure and composition of the adsorbed polymer layers as well as on the interaction between them was studied via surface force apparatus and *in situ* null ellipsometry.

Experimental

Materials and chemicals

Water used in this study was purified by the following consecutive steps: distillation, percolation through a Millipore Water System and final double distillation in an all-Pyrex apparatus. The mica used in our SFA experiments was best quality, optically clear muscovite green mica, obtained from Mica Supplies Ltd.(England). Si/SiO₂ plates for ellipsometry were prepared and cleaned as described elsewhere (Tiberg and Landgren, 1993). Sodium dodecyl sulfate (specially pure, from BDH) was purified by triple recrystallisation from pure water. Penta-ethyleneglycol mono *n*-dodecyl ether (C₁₂E₅) was purchased from Nikko Chemicals (Japan) and was used as supplied. QUATRISOFT® LM 200 was obtained from Union Carbide Chemicals and Plastics Co., Inc. It was purified by extensive dialysis and freeze-dried. The polymer is an *N,N*-dimethyl-*N*-dodecylammonium derivative of hydroxyethylcellulose with molecular weight of approximately 100,000.

Surface force measurements

The forces between mica surfaces bearing adsorbed layers were measured using a Mark IV surface force apparatus (Parker et al., 1989). The technique allows an accurate determination of forces, $F(D)$, acting between two mica sheets, mounted in the apparatus in a crossed cylinder configuration, as a function of surface separation D (Israelachvili and Adams, 1978). The measured forces were scaled with the mean local radius of curvature R of the curved mica sheets.

At the beginning of each experiment mica surfaces were brought into contact in air and then in water to verify the absence of debris and other types of surface contamination. Contact position, as measured in water, was used throughout subsequent experiments as a zero distance reference. An aliquot of concentrated polymer solution was then injected into the apparatus with a syringe to obtain a final polymer concentration of 34ppm. The interaction forces between polymer layers were also measured in the presence of added surfactants. At least two reproducible runs were recorded for each system composition. Force measurements were conducted both on approach (compression) and separation (decompression) and the separation was changed with a rate of 0.47nm/s. All measurements were performed at 22°C in a thermostated room.

Ellipsometry

An automated Rudolf Research thin-film null ellipsometer, type 43603 - 200E, was used in this study. A detailed description of our experimental set-up can be found elsewhere (Landgren and Jönsson, 1993). The substrate (Si/SiO₂ plates) optical characteristics were determined at the beginning of each experiment by ellipsometric measurements in two ambient media as discussed in (Landgren and Jönsson, 1993).

Then a certain amount of polymer was injected into the cuvette, which primarily contained 5ml H₂O, and the ellipsometric angles Ψ and Δ were recorded continuously until an equilibrium was reached. Then the system composition was changed either by addition of a desired amount of surfactant or by pumping (20ml/min) preheated pure water through the cuvette (rinsing). All measurements were conducted at the wavelength $\lambda = 401.5\text{nm}$ and the angle of incidence $\phi = 67.2^\circ$ in a thermostated cuvette at $25 \pm 0.1^\circ\text{C}$ under continuous stirring by a magnetic stirrer at about 300rpm.

The results of Ψ and Δ measurements were interpreted within the framework of an optical four layer model, assuming isotropic media and planar interfaces. The mean refractive index n_f and the average thickness d_f of the adsorbed layer were calculated using the numerical procedure described in (Tiberg and Landgren, 1993). The adsorbed amount (Γ) was calculated from n_f and d_f according to (de Feijter et al., 1978) using $dn/dc = 0.152\text{cm}^3/\text{g}$.

Results

Fig. 1 shows the force-distance profiles measured after equilibration of mica surfaces with 34ppm aqueous solution of Quatrisoft alone and in the presence of $4 \cdot 10^{-5}\text{M}$ SDS. In the pure polymer case the measurable repulsive force extends to separation of about 60nm. Upon compression the repulsion rises gradually and reaches $F/R=10\text{mN/m}$ at separation of about 14nm. The measured force-distance profile is in remarkable agreement with that reported by (Argillier et al., 1991). Both decay and the magnitude of the force are indicative of the nonelectrostatic nature of the repulsion, the latter being dominated, apparently, by osmotic and steric contributions. Under large applied load the adsorbed layer of Quatrisoft can be compressed down to 8nm but cannot be squeezed out. A shallow, but distinctive and reproducible, minimum was observed on separation (not shown). This attractive minimum can be attributed to non equilibrium effects induced by compression and interpenetration of adsorbed layers.

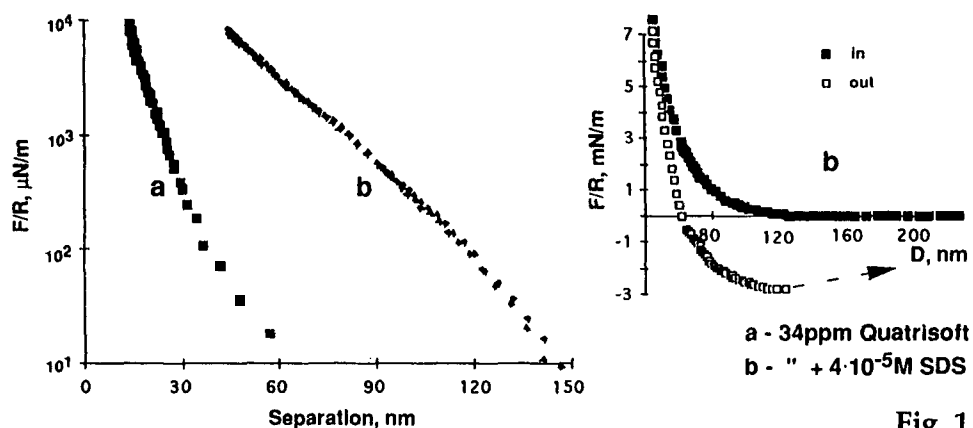


Fig. 1

Upon addition of $4 \cdot 10^{-5}\text{M}$ SDS to the system the force profile changes dramatically. On approach the onset of an increasing monotonic repulsion was observed when the surfaces were some 145nm from water contact, i.e. at separations substantially larger than in pure polymer case (60nm). With an applied force of about 10mN/m , a

separation of $D=43\text{nm}$ was reached, and under strong compression the polymer/surfactant layers could be squeezed down to 18nm . Thus, addition of small amounts of anionic surfactant changes considerably both the extent and compressibility of the adsorbed layers. The latter can result from an increase in the amount of material in the gap and/or in strength of intralayer repulsive interactions. In the insert we show comparison of forces measured on approach and separation in the presence of $4\cdot 10^{-5}\text{M}$ SDS. A deep attractive minimum ($F/R=-2.8\text{mN/m}$ at $D=130\text{nm}$) was observed on decompression in this case, indicative of a strong affinity between adsorbed layers. It is noteworthy that when more SDS was added to the system, giving a final concentration of $2\cdot 10^{-3}\text{M}$, a further increase of the repulsive interaction extent was observed with a long-range interaction setting in at *ca.* 250nm (see Fig. 2, curve b).

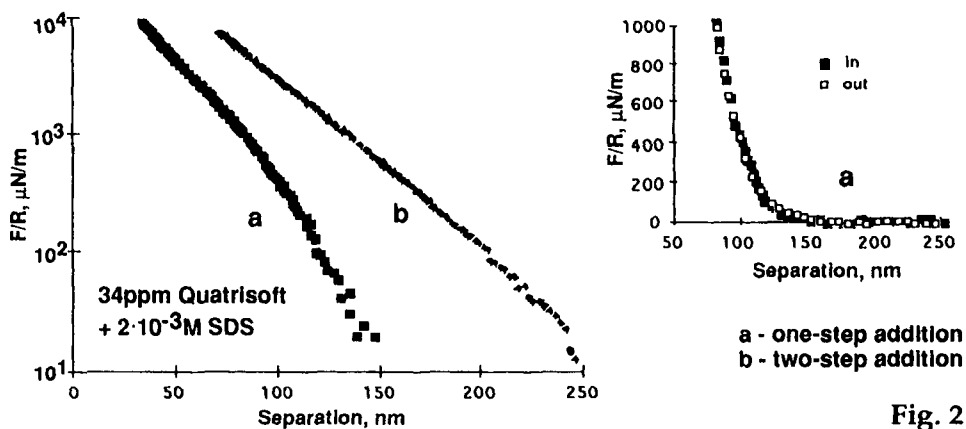


Fig. 2

In another experiment the polymer adsorption was followed by a single addition of SDS, giving a final concentration of $2\cdot 10^{-3}\text{M}$. The force-distance profile measured after equilibration is shown in Fig. 2, curve a. At first sight, the force appears to be rather similar to that measured in the presence of $4\cdot 10^{-5}\text{M}$ SDS, at least in respect to the onset of repulsion (c.f. Fig. 1, curve b). However, a number of differences are evident. A less steep increase in repulsion at distances below 100nm results in a shorter separation attained at $F/R=10\text{mN/m}$, namely 31nm , compared to 43nm in the previous case. Further compression led to a 12nm thick bilayer, again thinner than at $4\cdot 10^{-5}\text{M}$ SDS. Furthermore, as can be seen from the insert, a purely repulsive interaction identical to the compression curve, was observed on decompression. This indicates an absence of any interlayer association at this relatively high surfactant concentration. All these features, together with the above mentioned expansion of the adsorbed layer, formed at $c_{\text{SDS}}=4\cdot 10^{-5}\text{M}$, upon addition of $2\cdot 10^{-3}\text{M}$ of surfactant, give strong evidence that, although exhibiting the same range of repulsive interaction, the polymer/surfactant layers formed at low and high SDS concentration are substantially different.

Force measurements in systems containing non ionic surfactant showed that, unlike SDS, C_{12}E_5 does not cause dramatic changes in either the range or the magnitude of interaction between Quatrisoft adlayers. Even above the CMC

($6.5 \cdot 10^{-5} \text{M}$) addition of the surfactant causes only a slight increase in the force magnitude. At concentrations far above CMC a somewhat stronger repulsion was observed with no major change in the interaction range.

A summary of experimental results on the structure of an adsorbed layer, obtained via ellipsometry, is presented in the table below.

	at equilibrium:			after rinsing:		
	Γ , mg/m^2	d_f , nm	n_f	Γ , mg/m^2	d_f , nm	n_f
Quatrisoft	1.6	7	1.375	1.6	7	1.375
+ SDS						
$2 \cdot 10^{-5} \text{M}$	2.5	14	1.369	2.1	10	1.374
$4 \cdot 10^{-5} \text{M}$	4.0	36.5	1.359	2.8	23	1.361
$2 \cdot 10^{-3} \text{M}^*$	4.5	90	1.350	3.1	26	1.361
$1 \cdot 10^{-4} \text{M}$	2.8	25	1.359	2.3	17	1.363
$2 \cdot 10^{-4} \text{M}$	2.1	15	1.363	1.9	12	1.366
$2 \cdot 10^{-3} \text{M}$	1.8	57	1.347	1.5	7.5	1.372
$9 \cdot 10^{-3} \text{M}$	0.2	62	1.343	-	-	-
+ C_{12}E_5						
$5 \cdot 10^{-5} \text{M}$	1.7	7	1.379	1.6	7	1.375
$2 \cdot 10^{-4} \text{M}$	2.5	7	1.396	"	"	"
$5 \cdot 10^{-4} \text{M}$	3.2	11	1.386	"	"	"
$2 \cdot 10^{-3} \text{M}$	3.8	19	1.373	"	"	"

*addition on top of $4 \cdot 10^{-5} \text{M}$

We first point out that rinsing has no effect on the characteristics of the adsorbed Quatrisoft layer. This feature reveals irreversibility (or quasi irreversibility) of adsorption of the cationic polymer onto the negatively charged silica surface. As can be seen from the table, in the case of SDS the adsorbed amount is a nonmonotonic function of surfactant concentration with a maximum at around $c_{\text{SDS}} = 4 \cdot 10^{-5} \text{M}$. Up to about the CMC, Γ values exceed those measured in the absence of SDS, which means that upon addition of surfactant more material is brought into the interfacial region. This can be SDS alone or in combination with the polymer. The fact that Γ is maximal at rather low surfactant concentrations is strong evidence that at low c_{SDS} the supplementary adsorption is dominated by the polymer. An analysis of the system behaviour upon rinsing gives further support to this idea. Indeed, rinsing after addition of $2 \cdot 10^{-3} \text{M}$ SDS brings the system back to its initial state, whereas at low surfactant levels only partial removal of supplementary adsorbed material was observed. Taking into account effective irreversibility of the polymer binding to the surface, this finding reveals that in the former case the increase in Γ upon surfactant addition is due to a reversible surfactant binding to the polymer, while in the latter one a substantial extra amount of polymer is adsorbed. Both at low and high SDS concentrations, addition of the surfactant leads to the increase in the ellipsometrically measured adlayer thickness, that is to say to the layer expansion, which is in qualitative accordance with SFA findings.

Clearly different was the effect of addition of nonionic surfactant on the structure of adsorbed Quatrisoft layer. Up to concentration about ten times the CMC, addition of $C_{12}E_5$ results in a gradual increase in Γ , with no changes in d_f . For $c > 5 \cdot 10^{-4} M$ adsorption is accompanied by an increase in the layer optical thickness. At all studied $C_{12}E_5$ concentrations (up to $10^{-2} M$) rinsing led to a quick removal of adsorbed material down to pure polymer level which indicates that neither supplementary polymer adsorption nor polymer displacement by surfactant was involved in this case.

Discussion

The results obtained in the present study show that Quatrisoft molecules adsorb strongly onto the negative surfaces in a rather expanded conformation. The adsorption is expected to be limited by steric and electrostatic repulsion between adsorbed molecules. Addition of surfactants causes substantial changes in the structure and composition of the adsorbed layer. These changes can be interpreted in terms of associative binding of surfactant to the polymer. This model assumes formation of micellar-type surfactant aggregates on hydrophobic side chains of the polymer and has been successful in explaining unusual rheological behaviour of hydrophobically modified polymers in the presence of surfactants (Magny *et al.*, 1992).

Anionic surfactant association with cationic polymer starts at concentrations far below the CMC and is favoured by electrostatic forces. At low SDS concentrations when few "micelles" are formed on polymer chains, effective neutralisation of the polycation both in bulk and at the interface makes possible supplementary adsorption of the polymer/surfactant complex. The incorporation of additional macromolecules into the adsorbed layer can be promoted by formation of intermolecular micellar bridges. This bridge formation shows itself in the occurrence of a deep attractive minimum on decompression at $c_{SDS} = 4 \cdot 10^{-5} M$. Expansion of the adsorbed layer at this concentration is caused mainly by steric intralayer repulsion. Upon increasing the SDS bulk concentration, progressive binding of surfactant aggregates leads to an increase of the macromolecule net negative charge and decrease of number of free cationic groups. This results in a drop of additional polymer adsorption down to zero at $c_{SDS} > 5 \cdot 10^{-4} M$. The adlayer expansion observed at $c_{SDS} = 2 \cdot 10^{-3} M$ can be attributed to electrostatic repulsion between polymer molecules bearing bound SDS micellar aggregates. Note also the absence of an attractive minimum on the corresponding force profile. Beyond the CMC the anionic surfactant wins its competition with the surface for the polymer and highly negatively charged polymer/surfactant complex desorbs from the surface.

Unlike SDS, non ionic amphiphile $C_{12}E_5$, does not cause visible changes in the configuration of adsorbed macromolecules, although it aggregates on Quatrisoft's hydrophobes. Up to a $C_{12}E_5$ concentration of about $5 \cdot 10^{-4} M$ no changes in adlayer thickness were detected by either SFA or ellipsometry. At higher surfactant concentrations ellipsometrically measured layer thickness increases, while interaction range is not affected. This inconsistency turns out to be rather misleading since the change in d_f , calculated without a true account of the density distribution in the surface film, can mean a qualitative change in the density profile at a constant total layer

extent. It is known that $C_{12}E_5$ has a tendency to form large nonspherical micelles at high concentrations. Thus, the feature observed can be rationalized by assuming formation of such large surfactant aggregates preferably in the outer part of the adsorbed polymer layer where steric constraints are less pronounced.

The above example demonstrates that comparative interpretation of SFA and ellipsometric results should be undertaken with a proper account of the character of material distribution within the adlayer. Thus, for example, a simple analysis shows that $d_f=7\text{nm}$ measured by ellipsometry in the case of pure Quatrisoft layer corresponds to the layer extension of *ca.* 27-30nm if an exponentially decreasing polymer density profile is assumed. This latter estimate is in good accord with the force onset, observed with SFA. An exact quantitative agreement, however, can hardly be expected due to the certain difference in the chemical nature and charging behaviour of the two substrate surfaces used.

References

- Argillier, J. F., R. Ramachandran, W. C. Harris and M. Tirrell. 1991. Polymer-surfactant interactions studied with the surface force apparatus. *J. Colloid Interface Sci.* 146: 242-250.
- de Feijter, J. A., J. Benjamins and F. A. Veer. 1978. Ellipsometry as a tool to study the adsorption behavior of synthetic and biopolymers at the air-water interface. *Biopolymers* 17: 1759-1772.
- Goddard, E. D. and K. P. Ananthapadmanabhan, Ed. (1993). Interactions of surfactants with polymers and proteins. Boca Raton, CRC Press.
- Israelachvili, J. N. and G. E. Adams. 1978. Measurement of forces between two mica surfaces in aqueous electrolyte solutions in the range 0-100 nm. *J. Chem. Soc. Farad. Trans. 1* 74: 975-1001.
- Landgren, M. and B. Jönsson. 1993. Determination of the optical properties of Si/SiO₂ surfaces by means of ellipsometry, using different ambient media. *Journal of Physical Chemistry* 97: 1656-1660.
- Magny, B., I. Iliopoulos, R. Audebert, L. Piculell and B. Lindman. 1992. Interactions between hydrophobically modified polymers and surfactants. *Progress in Colloid and Polymer Science* 89: 118-121.
- Parker, J. L., H. K. Christenson and B. W. Ninham. 1989. Device for measuring the force and separation between two surfaces down to molecular separations. *Rev. Sci. Instrum.* 60: 3135-3138.
- Tiberg, F. and M. Landgren. 1993. Characterization of thin nonionic surfactant films at the silica/water interface by means of ellipsometry. *Langmuir* 9: 927-932.

47 Ellipsometry studies of the interfacial behaviour of ethyl(hydroxyethyl)cellulose

F Tiberg and M Malmsten – Physical Chemistry I, Chemical Centre, University of Lund, PO Box 124, S-221 00 Lund, Sweden and The Institute for Surface Chemistry, PO Box 5607, S-114 86 Stockholm, Sweden

ABSTRACT

We report on the temperature-dependent adsorption of ethyl(hydroxyethyl)cellulose (EHEC) at the polystyrene-water interface revealed by ellipsometry. This technique allows separate determinations of the optical mean thickness, the average refractive index and the adsorbed amount of an adsorbed polymer film. The low optical contrast of the water-EHEC-polystyrene system makes measurements of these quantities difficult, but we show that they can be determined with sufficient accuracy by using a modern high precision ellipsometer.

At room temperature, EHEC adsorbs sparsely on polystyrene surfaces ($\Gamma \approx 1 \text{ mg/m}^2$), forming layers with an optical mean thickness that slightly exceeds 30 nm. Raising the temperature results in increasing adsorption and a simultaneous contraction of the adsorbed layer. The conjunction of these opposing trends leads to a strong decrease of the ellipsometric thickness near the bulk phase separation temperature at this surface. The adsorbed layer contains a fraction highly extended but dilute tails, reflected by its large hydrodynamic extension, as observed by photon correlation spectroscopy measurements ($\delta_h \approx 110 \text{ nm}$ at 20°C). This fraction, however, does not significantly affect the interaction forces between two EHEC coated surfaces.

INTRODUCTION

The phenomenon of polymer adsorption underlies many important processes. Frequently, the practical problem is to stabilise colloids or to avoid adsorption of

biopolymers or other unwanted material (c.f. Napper, 1983). Ethyl(hydroxyethyl)cellulose has proven very effective for these purposes and it is of fundamental interest to correlate this efficiency to the behaviour of this polymer at the solid/liquid interface (Malmsten et al., 1990; Malmsten et al., 1991a and b; Malmsten and Tiberg, 1993).

Numerous techniques are today available for studies of interfacial properties of polymers and the progress in the development of these have during the past few years indeed been tremendous. Ellipsometry is one among the techniques that appear increasingly promising. This is a consequence of the rapidness, flexibility and non-destructive character of this technique, as well as of recent instrumental and methodological improvements, which further has expanded its applicability (Azzam and Bashara, 1989; Tiberg and Landgren, 1993). The present work explores the possibility of using ellipsometry for separate measurements of the thickness and the adsorbed amount of adsorbed layers with low optical contrast to the surrounding media. This is a difficult task, since these parameters are very sensitive to errors in the applied optical model, as well as to those associated with the experimental set-up (Tiberg and Landgren, 1993). We hope to show, however, that such measurements can indeed be performed with a modern high-performance instrument and that the results obtained provide information that is of fundamental interest for the understanding of EHEC's efficiency as a protein rejecting and stabilising agent.

EXPERIMENTAL

The ethyl(hydroxyethyl)cellulose (EHEC) used in this study was kindly provided by Berol Nobel AB, Sweden. The two fractions used have molecular weights of 250 000 (EHEC 1) and 475 000 (EHEC 2), as determined by light scattering. The cloud points (CP's) of EHEC 1 and EHEC 2 are 39°C and 35°C, respectively. The radii of gyration at 20°C and 0.2 mM NaCl is 80 nm for EHEC 1 and 85 nm for EHEC 2.

The adsorption was monitored in situ by a high precision null ellipsometer. The instrument used was an automated Rudolf Research thin-film ellipsometer, type 43603-200E, equipped with Berger-Lahr stepper motors, and controlled by a personal computer. A xenon lamp filtered to 401.5 nm was used as a light source. The optical contrast of the system is better at this wavelength than that at, say, 600 nm. The set-up and measurement procedure has been described previously (Tiberg and Landgren, 1993). To summarise, the average optical thickness and the amount adsorbed are

obtained after first determining the optical properties of the the bare substrate. The complex refractive index for a homogeneous substrate like polystyrene can easily be determined from a single set of ellipsometric angles, ψ and Δ , which in turn are derived directly from the ellipsometric polariser and analyser readings. The polymers are added to the temperature controlled cuvette after the substrate characterisation, and the ellipsometric angles ψ and Δ are then monitored continuously. The mean ellipsometric thickness (δ_e) and the average refractive index (n_e) are then calculated numerically (cf. Azzam and Bashara, 1989). The calculation of the adsorbed amount (Γ) from the latter parameters is then straight forward (de Feijters et al., 1978).

RESULTS AND DISCUSSION.

Figure 1 shows the time-evolution of the adsorption of EHEC 2 on polystyrene at 20°C. The adsorption on polystyrene is rather fast and plateau values are generally reached within 1500 seconds. This feature is seen in both the mean optical thickness and the adsorbed amount. Small fluctuations on the order of a few percent are observed in Γ , while larger effects, with fluctuations up to $\pm 15\%$, are observed in δ_e . This is a direct consequence of uncertainties in the determination of the ellipsometric angles ($\sigma(\psi, \Delta) < (\pm 0.002^\circ, \pm 0.004^\circ)$). These result in relatively large errors in thickness and refractive index, which due to covariance largely cancel out when the adsorbed amount is calculated (Tiberg and Landgren, 1993).

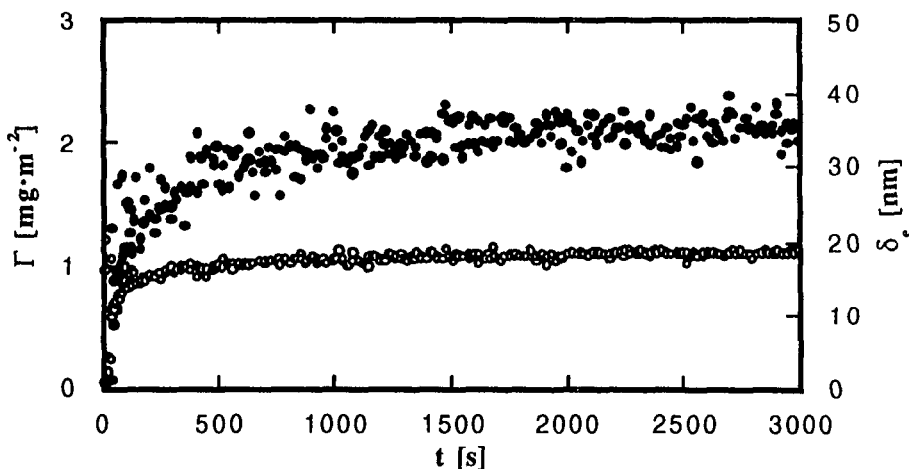


Figure 1. Time evolution of the adsorbed amount (Γ , open circles) and the average ellipsometric layer thickness (δ_e , closed circles) for EHEC 2 at polystyrene at 20°C.

The magnitude of the fluctuations is enhanced by the low optical contrast between the adsorbed layer and the polystyrene surface. The latter can be optimised by using light of shorter wavelengths, but we found the precision in the measured parameters sufficient for our needs and did not go further into this problem.

Figures 1 and 2 show that both EHEC fractions adsorb rather sparsely at polystyrene at low temperatures. The adsorbed amount on polystyrene is around $1 \text{ mg}\cdot\text{m}^{-2}$ at room temperature. This is less than half the value observed on hydrophobised silica at the same temperature (Malmsten and Tiberg, 1993). Raising the temperature towards the cloud point (CP), i. e. worsening the solvency conditions of the polymer, results in marked changes of the adsorbed layer properties, as can be seen in figures 2 and 3.

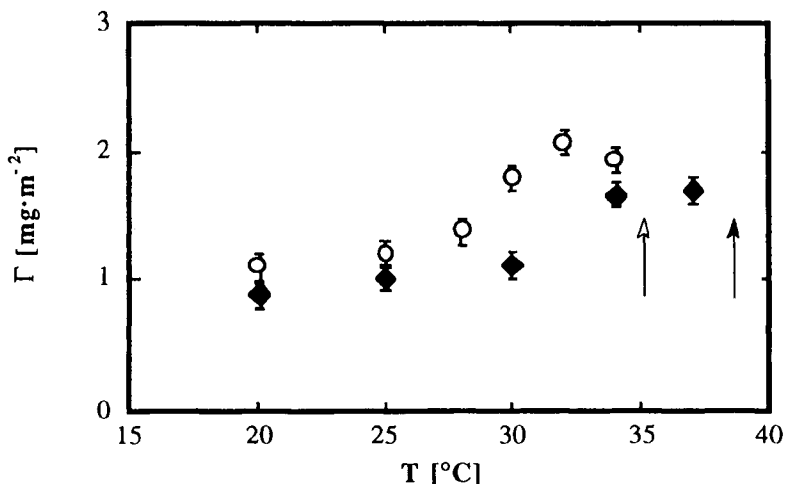


Figure 2. Adsorbed amount (Γ) of EHEC 1 (closed diamonds) and 2 (open circles) at polystyrene as a function of temperature. Cloud points (CP's) are indicated by closed and open arrows, respectively.

The adsorbed amount increases strongly in the region just prior to the CP and then levels off and seems to reach more or less constant values around the CP. This increase of the adsorbed amount is correlated with the solvency conditions of the polymer.

An explanation of the "plateau" region observed at higher temperatures is less straight forward, but involves the orientation of this copolymer at hydrophobic surfaces. Hence,

due to orientation, the segments of the outer region of the adsorbed layer may experience good solvency conditions, despite the overall solvency conditions being poor. The outer adsorbed layer region then acts as a steric barrier for further adsorption. The behaviour is somewhat unexpected, but agrees well with results obtained by means of the surface force technique, where the force between two EHEC layers remains monotonically repulsive even at temperatures above the bulk phase separation temperature (Malmsten et al., 1990). Flocculation studies performed with EHEC-stabilised polystyrene particles, showing that the dispersion remains stable at least 15 degrees above the CP, further confirm this notion (Malmsten and Tiberg, 1993).

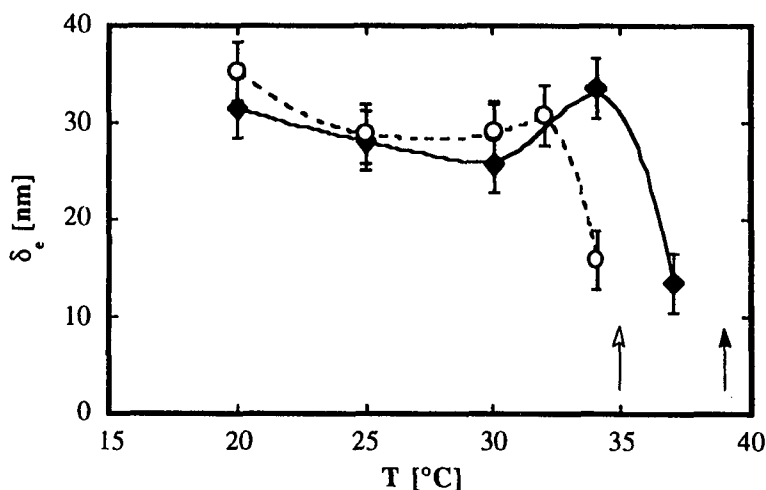


Figure 3. Average ellipsometric layer thickness (δ_e) of EHEC 1 (closed diamonds) and 2 (open circles) at polystyrene as a function of temperature. Cloud points (CP's) are indicated by closed and open arrows, respectively.

The effect of temperature on the ellipsometric thickness is more complex, since increasing the temperature results in a concomitant tendency of increasing the adsorbed amount and contracting the adsorbed layer. The outcome of this competition depends on the conjunction of these events. A slight decrease of δ_e and a moderate increase of Γ is initially observed as the temperature is raised. This is followed by a small increase of δ_e , indicating that the contracting tendency is masked by the relatively strong increase of Γ observed in this region. As Γ finally levels off, contraction once more becomes the dominant effect. Note, however, that since the outcome of the competition depends on

the adsorbed amount, as well as on its temperature dependence, this will vary between surfaces. For example, at very hydrophobic surfaces, the increase in Γ with temperature is so strong, that a monotonic increase in the adsorbed layer thickness is observed (Malmsten and Claesson, 1991a).

The average ellipsometric thickness (δ_e) is around 30 nm for both EHEC 1 and EHEC 2 at 25°C. The hydrodynamic thickness (δ_h) observed by photon correlation spectroscopy is around 110 nm at the same temperature. The finding that δ_e is much smaller than δ_h is in agreement with previous experimental and theoretical findings (cf., Takahashi and Kawaguchi, 1982; de Gennes, 1990). The reason for this is that δ_e pertains to a step-like segment density profile of the adsorbed layer. Thus, ellipsometry primarily monitors the dense loop and train fractions of the adsorbed layer, while the hydrodynamic thickness is sensitive to the often dilute tail fraction. This indicates that a region with extended but dilute tails is present in the adsorbed EHEC layer. The onset distance for repulsive interactions is much smaller than $2\delta_h$, but corresponds rather well with twice the average ellipsometric thickness (see Figure 4).

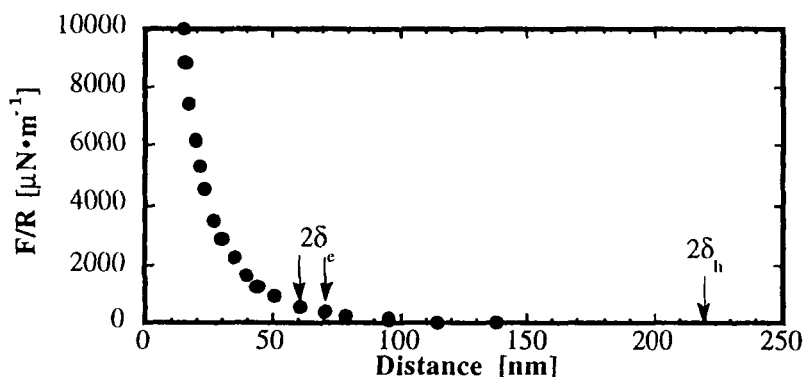


Figure 4. The ellipsometric (δ_e) and hydrodynamic (δ_h) thickness obtained for EHEC 2 at polystyrene ($\Gamma \approx 1 \text{ mg}\cdot\text{m}^{-2}$) and the interaction forces obtained at hydrophobised mica surfaces ($\Gamma \approx 5 \text{ mg}\cdot\text{m}^{-2}$). Shown also is the value of δ_e at hydrophobised silica ($\Gamma \approx 2.7 \text{ mg}\cdot\text{m}^{-2}$). All measurements were performed at room temperature.

This shows that the dilute tail region plays a limited roll for the steric stabilising forces induced by the adsorption of EHEC on hydrophobic surfaces.

REFERENCES

- Azzam, R. M. A. and Bashara, N. M. *Ellipsometry and Polarized Light*, North-Holland, Amsterdam, 1989.
- de Feijter, J. A., Benjamins, J. and Veer, F. A. *Biopolymers* 17, 1759 (1978).
- de Gennes, P.G., in *Liquids at Interfaces*; Charvolin, J., Joanny, J. F., Zinn-Justin, J., Eds., North-Holland, Amsterdam, 1990.
- Malmsten, M., Claesson, P. M., Pezron, E. and Pezron, I. *Langmuir* 6, 1572 (1990).
- Malmsten, M. and Claesson, P. M. *Langmuir* 7, 988 (1991a).
- Malmsten, M., Lindman, B., Holmberg, K., and Brink, C. *Langmuir* 7, 2412 (1991b).
- Malmsten, M. and Tiberg, F. *Langmuir* 9, 1098 (1993).
- Napper, D. H., *Polymeric Stabilization of Colloidal Dispersions*, Academic Press, New York, 1983.
- Takahashi, A. and Kawagushi, M., *Adv. Polym. Sci.* 46, 1 (1982).
- Tiberg, F. and Landgren, M., *Langmuir* 9, 927 (1993).

Part 5:

Applications of cellulosics

48 Chiral nematic suspensions of cellulose

J-F Revol, L Godbout, X-M Dong and D G Gray – Paprican and Department of Chemistry, Pulp and Paper Research Centre, McGill University, Montreal, Canada

ABSTRACT

The phase separation of suspensions of anisotropic rod-like species such as tobacco mosaic virus, DNA fragments and collagen into fluids displaying nematic or chiral nematic order is a widely observed phenomenon. Suspensions of rod-like cellulose crystallites also can form a chiral nematic phase. The rodlets of crystalline cellulose were prepared by sulphuric acid hydrolysis of natural cellulose fibres from several sources. The suspensions are thought to be stabilized by the charged sulphate ester groups on the surface of the crystallites. Well-formed textures and disclinations characteristic of chiral nematic liquid crystals, readily formed by these dilute suspensions, are observed. Preliminary results indicate that the critical volume fraction for phase separation of salt-free suspensions can be as low as 0.03, with a relatively narrow biphasic region. The phase separation is sensitive to the ionic strength of the medium. Some effects of magnetic fields on the orientation of the ordered phase will also be described.

INTRODUCTION

Colloidal suspensions of certain rod-like species such as tobacco mosaic virus¹, DNA fragments², and collagen³ form ordered phases above some critical concentration. The phase separations resemble those observed for stiff-chain polypeptide⁴ and polysaccharide^{5,6} macromolecules, and are essentially entropy-driven due to shape anisotropy⁷. Many of the species forming ordered phases are

optically active, and the resulting ordered phases display chiral nematic properties with a characteristic handedness. The species themselves are usually complex molecules, with the rod-like properties resulting from multiple helical conformation of the molecular chains. Recently, suspensions of acid-degraded crystallites of cellulose⁸ have also been found to form *chiral* nematic phases at low concentrations. The properties of the cellulose suspensions⁹ seem to depend on the source (which may be wood pulp, cotton, bacterial or algal cellulose) and on the hydrolysis conditions. The formation of highly ordered chiral nematic phases from these readily accessible materials seems noteworthy. These phases differ from the colloidal crystallization observed for charged spherical colloidal particles at low ionic strengths¹⁰ in that the particles are highly anisotropic and the order is orientational rather than positional. In this paper, experimental results on the characterization and phase separation of cellulose suspensions prepared from cotton filter paper are presented.

EXPERIMENTAL

As reported previously⁸, the suspensions are prepared by acid-catalysed hydrolysis of natural cellulose fibres. In this case, Whatman No. 1 filter paper was ground to <20 mesh in a Wiley mill. The powder (20 g) was mixed with 175 mL of 64% sulphuric acid and stirred at 45° C for 1 h. The acid was removed by prolonged dialysis with water, and then by treatment with a mixed-bed ion exchange resin. This removed all ionic material except the H⁺ counterions associated with the sulphate groups on the surface of the crystallites. The crystallites were dispersed by a brief ultrasonic treatment. The suspension was then fractionated by means of the observed phase separation¹¹; for a biphasic sample, the crystallites with larger axial ratios preferentially migrate into the ordered phase. By continuous evaporation of an isotropic sample, the first anisotropic phase to separate was discarded, and the final isotropic phase was also discarded ($\approx 10\%$).

The sulphur content of the suspension was determined by elemental analysis as 0.7% of the total dry weight of the suspension. If it is assumed that all the sulphur is in the form of sulphate groups, and that all these groups are on the surface of the crystallites, then the surface charge due to sulphate groups is about 0.36 e/nm².

RESULTS AND DISCUSSION

For an ideal suspension of non-interacting rods of length L and diameter d , Onsager⁷ predicted that the critical concentrations for ordered phase formation would depend only on the axial ratio L/d of rods of length L and diameter d . For

volume fractions of rods $c < c_i$, the solution is completely isotropic, for $c > c_a$ it is completely anisotropic, and for $c_i < c < c_a$, the solution separates into isotropic and anisotropic phases, where:

$$c_i = 3.3 \text{ d/L and } c_a = 4.5 \text{ d/L.} \quad (1)$$

Here, c_i and c_a are the concentrations in the isotropic and anisotropic phases, respectively, in volume fraction units. In the biphasic region, the concentration of rods in each phase remains constant with increasing overall concentration; the volume of the ordered phase increases relative to the total volume of ordered and disordered phases. The volume fraction of the ordered phase, Φ , thus increases linearly with total concentration of rods.

Above a critical concentration c_i , suspensions of cellulose crystallites form a biphasic region, where the lower anisotropic phase shows optical properties characteristic of chiral nematic liquid crystals (Figure 1).

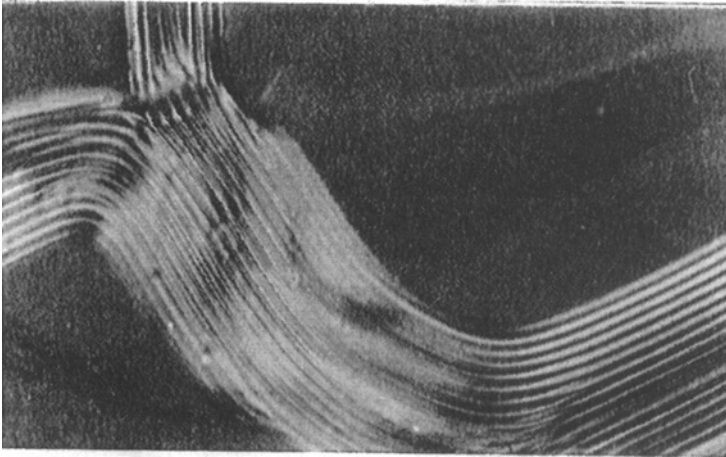


Figure 1. Photomicrograph showing chiral nematic texture of a suspension of crystallites made from filter paper. The spacing between the parallel lines ($6.2 \mu\text{m}$) is equal to half the chiral nematic pitch.

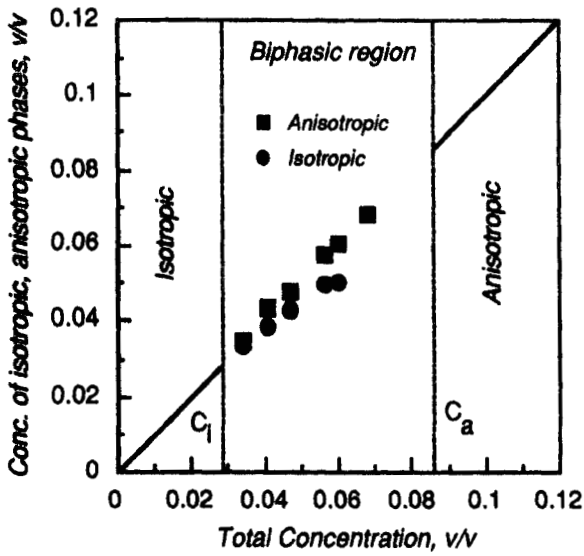


Figure 2. Cellulose suspension in water. Concentration of isotropic and anisotropic phases in biphasic region against total concentration.

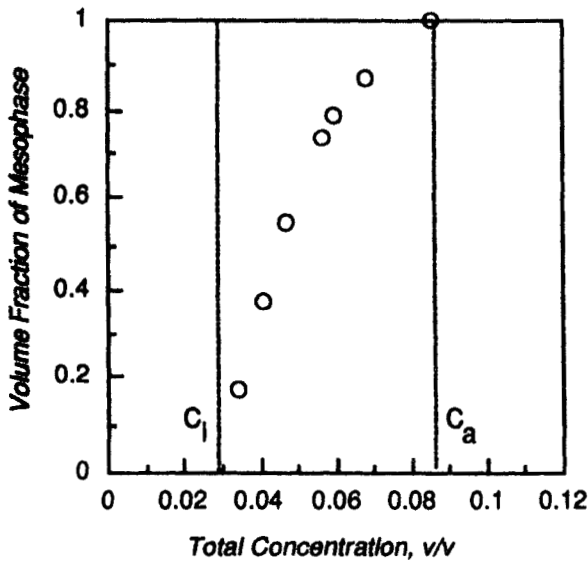


Figure 3. Cellulose suspension in water. Volume fraction of anisotropic phase in total sample volume as a function of total concentration.

As the total concentration of the suspension is increased, the volume fraction, Φ , of the ordered phase (concentration c_a) increases, while the volume fraction of the isotropic phase ($1-\Phi$), of concentration c_i decreases. The concentrations in both phases for a sample dialyzed extensively against pure water are shown as a function of total concentration in Figure 2, and the relative volumes of the two phases are shown in Figure 3. The situation differs from that predicted by the simple Onsager theory; the concentrations in the isotropic and anisotropic phases do not remain constant across the biphasic region, but increase with increasing concentration, and the corresponding change in Φ with total concentration is not linear. Furthermore, the anisotropic phases form at volume fractions of around 0.03. From the dimensions of the crystallites (200-300 nm long and ≈ 7 nm wide), the anisotropic phase requires a concentration of more than 0.1, according to eq.1. However, the equations assume only hard-core repulsion between the rods, whereas the cellulose suspensions are stabilized by electrostatic repulsive forces. This may be viewed as causing an increase in the effective diameter and volume of the rods. The repulsive forces are particularly effective when no ions other than the counterions associated with the surface sulphate groups on the cellulose are present. Furthermore, the electrostatic screening due to these counterions will increase as the concentration of suspension increases, so that the effective rod diameter also changes with concentration.

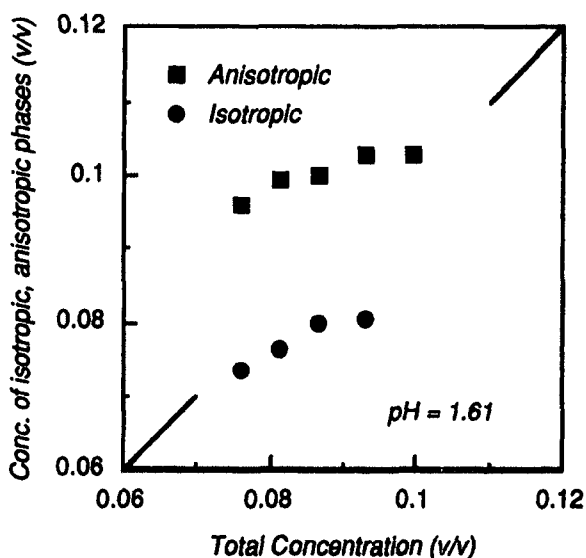


Figure 4. Concentrations in each phase of biphasic region for cellulose suspensions at constant pH = 1.61.

As a qualitative test of the effects of ionic strength on the phase separation process, a sample of the suspension was dialysed exhaustively against 0.01M HCl solution, and a range of concentrations was prepared by dilution with HCl solutions to give the same final measured pH of 1.61. The measured concentrations of suspensions in the isotropic and anisotropic phases at increasing total concentrations is shown in Figure 4. In the presence of added electrolyte, more suspension is required to form an ordered phase, and the difference in concentration between the isotropic and anisotropic phases is much larger than in the case where only counterions are present (Figure 2). Although far from constant, the concentration in the two phases increases less steeply than in the absence of added electrolyte. The reason for the observed increase is not certain yet, but it may well be an effect of polydispersity in the axial ratio or charge density of the cellulose crystallites. Based on a lattice theory for the phase separation of rod-like species, Moscicki and Williams¹² showed that increasing the width of the distribution of rod lengths causes a curvature in the relationship between total concentration of rods and volume fraction of anisotropic phase, and an increase in the concentrations in the isotropic and anisotropic phases with increasing total concentration.

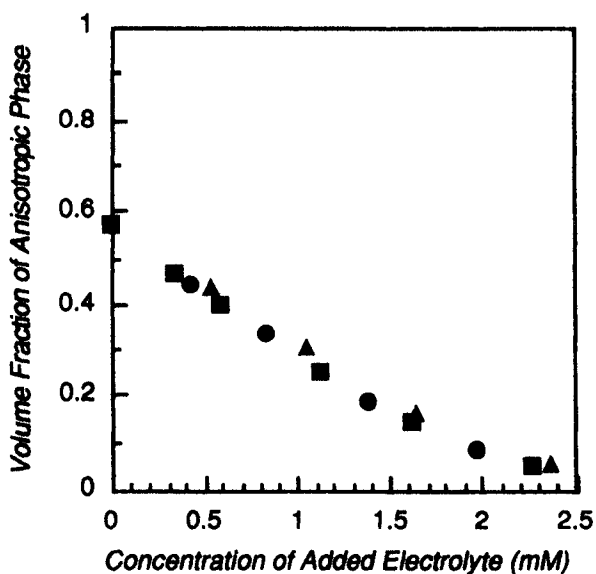


Figure 5. Effect of electrolyte concentration on volume fraction of anisotropic phase in biphasic sample for a constant total concentration of cellulose (0.052 v/v).

The effect of electrolyte concentration on the phase separation are also shown in Figure 5, which presents the effect of added HCl, NaCl and KCl on phases formed

from a fixed total concentration of cellulose crystallites. The volume fraction of ordered phase in the biphasic sample decreases with increasing electrolyte concentration. The difference in cellulose concentration between the two phases remains fairly constant with electrolyte content, with the concentration in both phases increasing slightly with electrolyte content (Figure 6). The three electrolytes behave similarly, and the tendency to form a chiral nematic ordered phase is suppressed as the electrolyte concentration is increased.

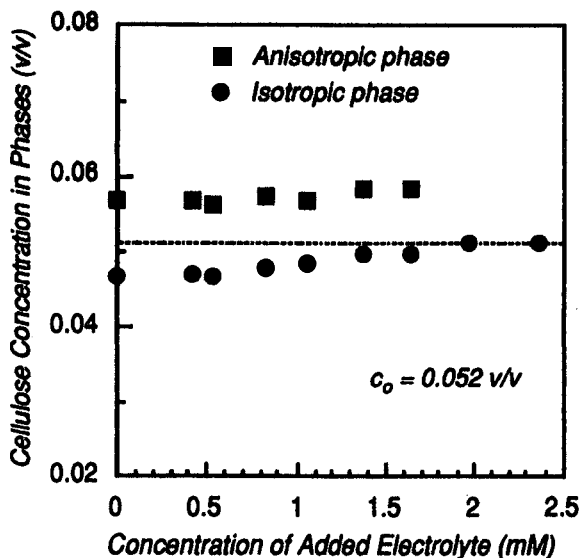


Figure 6. Effect of electrolyte concentration (NaCl and KCl) on cellulose concentrations in both phases of samples with a constant total concentration of cellulose (0.052 v/v, dotted line).

The chiral interaction between the crystallites are also sensitive to electrolyte content. Figure 7 shows that the chiral nematic pitch of the anisotropic phase at a fixed total cellulose content decreases markedly with electrolyte content. As the pitch decreases, the chiral twisting interactions between the crystallites increases. The chiral twisting power, defined as $1/P$, where P is the pitch, doubles in value as the electrolyte content is increased. Evidently, the chiral interactions are not screened by the increasing ionic strength, and it seems unlikely that the slight increase in concentration evident in Figure 6 is responsible for the effect.

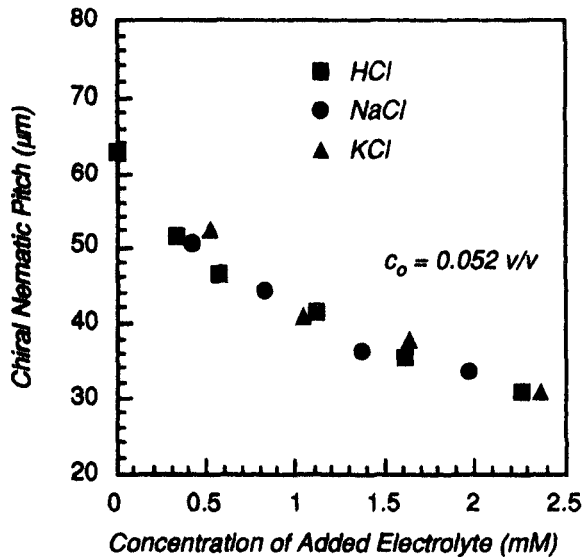


Figure 7. Effect of electrolyte concentration on chiral nematic pitch for the anisotropic part of biphasic suspensions of fixed total cellulose content (0.052 v/v).

ACKNOWLEDGEMENTS

We thank the Natural Sciences and Engineering Research Council of Canada and the Paprican graduate student program for support. X.-M.D. thanks the Pall Corporation for a scholarship.

REFERENCES

1. F.C. Bawden and N.W. Pirie, *Proc. R. Soc. Lond.(B)* **123**, 274 (1937).
2. C. Robinson, *Tetrahedron*, **13**, 219 (1961).
3. M.-M. Giraud-Guille, *Biol. Cell*, **67**, 97 (1989).
4. C. Robinson, *Faraday Soc. Trans.*, **52**, 571 (1956).
5. G. Maret, M. Milas and M. Rinaudo, *Polym. Bull.*, **4**, 291 (1981).
6. K. Van and A. Teramoto, *Polym. J.*, **14**, 999 (1982).
7. L. Onsager, *Ann. N.Y. Acad. Sci.*, **51**, 627 (1949).
8. J.-F. Revol, H. Bradford, J. Giasson, R.H. Marchessault and D.G. Gray, *Int.J.Biol.Macromol.*, **14**, 170 (1992).
9. J.-F. Revol, L. Godbout, X.-M. Dong, D.G. Gray, H. Chanzy and G. Maret *Liquid Crystals*, **16**, 127 (1994).
10. S. Hachisu, Y. Kobayashi and A. Kose, *J. Colloid Interface Sci.*, **42**, 342 (1973).
11. T. Sato, T. Kakiyama and A. Teramoto, *Polymer*, **31**, 11 (1990).
12. J.K. Moscicki and G. Williams, *Polymer*, **23**, 558 (1982).

49 Novel results of structural investigations on crystalline and liquid crystalline cellulose derivatives and their potential application

P Zugenmaier – Institute of Physical Chemistry, Technical University of Clausthal, D-38678 Clausthal-Zellerfeld, Germany

ABSTRACT

The crystal and molecular structure of homogeneously and heterogeneously derived cellulose tribenzoate (CTB) was solved. The most probable structure for two differently prepared samples appears to be a trigonal unit cell, space group $P 3_2$, $a = b = 12.2 \text{ \AA}$, c (fiber axis) = 15.2 \AA , $\gamma = 120^\circ$ with one chain passing through the unit cell. A three-fold helical (3/2, lefthanded) conformation of the chain leads to an unusual parallel chain arrangement also for solution grown crystals. The morphology of the fibrils was simulated by a statistical method by computer modeling, a probability parameter introduced by which the two limiting cases of antiparallel and parallel packing arrangements, as well as all cases of up and down chains can be studied for a trigonal lattice.

An investigation of polymer-solvent interaction, most probably causing the unusual chain arrangements in cellulose and which may play an important role in application, has been undertaken for the cellulose tricarbonylate/methyl acetoacetate system in the semi-dilute and liquid crystalline state.

INTRODUCTION

The chain polarity in cellulose crystalline structures have been controversially discussed for more than 60 years and experiments performed including those on cellulose derivatives which suggest a parallel arrangement of chain on one side and antiparallel arrangements on the other side for the same material. But it is generally accepted that the chains of solution grown polymeric crystals arrange in an antiparallel fashion.

CRYSTAL STRUCTURE OF CELLULOSE TRIBENZOATE (CTB)

The starting material for a structural investigation was native cellulose (Ramie fibers) which was derivatized in a heterogeneous fashion without distortion of the original morphology on one side and homogeneously produced compounds, totally dissolved, recrystallized as a film and stretched to obtain fibers on the other side. X-ray fiber diffraction experiments with a flat film camera leads to essentially the same diffraction pattern with a third order meridional reflection for both differently prepared CTB samples [1] pointing to the same crystal structure. Conformation analysis prefers a lefthanded (3/2) helical conformation. Packing analysis performed on a variety of unit cell sizes, derived from a basic trigonal lattice ($a = b = 12.2 \text{ \AA}$, c (fiber axis) = 15.2 \AA ; $\gamma = 120^\circ$) and symmetries was undertaken of which the two most favorable packing arrangements with parallel (space group $P 3_2$) and antiparallel (space group $P 2_1$) neighboring chains are depicted in Figs. 1-3. A close packing of the chain requires the bond C6-O6 gauche to C5-O5 and gauche to C5-C4 (gg). The grid in the a, b-plane onto which the chains are placed is the same in both figures 1 and 2. Fig. 3 represents two chains in parallel and antiparallel arrangement of which the parallel packing is slightly favored in contact energy. X-ray refinement results in the lowest R value for the crystal structure with the trigonal, one chain unit cell of Fig. 2, space group $P 3_2$, and this solution is also supported by the fact that the X-ray pattern can completely be indexed with this small one chain unit cell. A one chain unit cell requires parallel packing

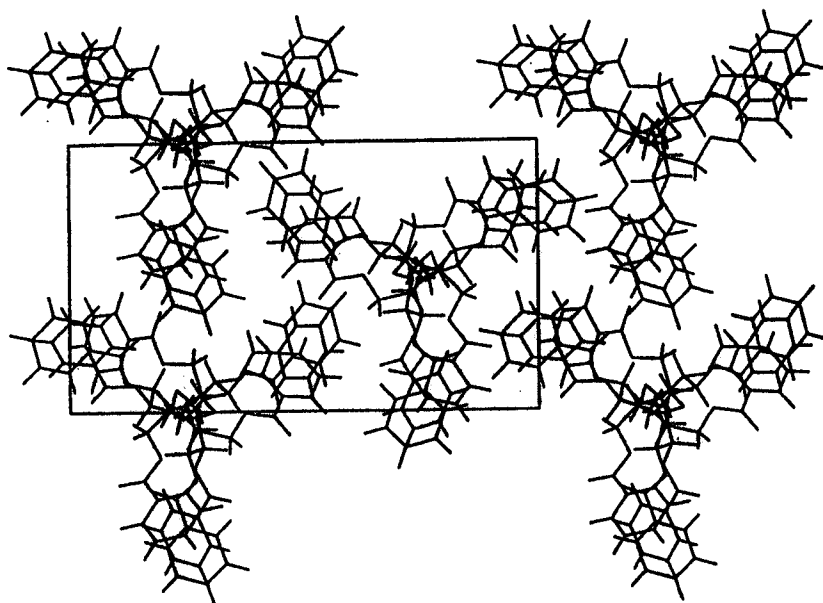


Fig. 1. Antiparallel packing model for cellulose tribenzoate viewed along the helix axes.

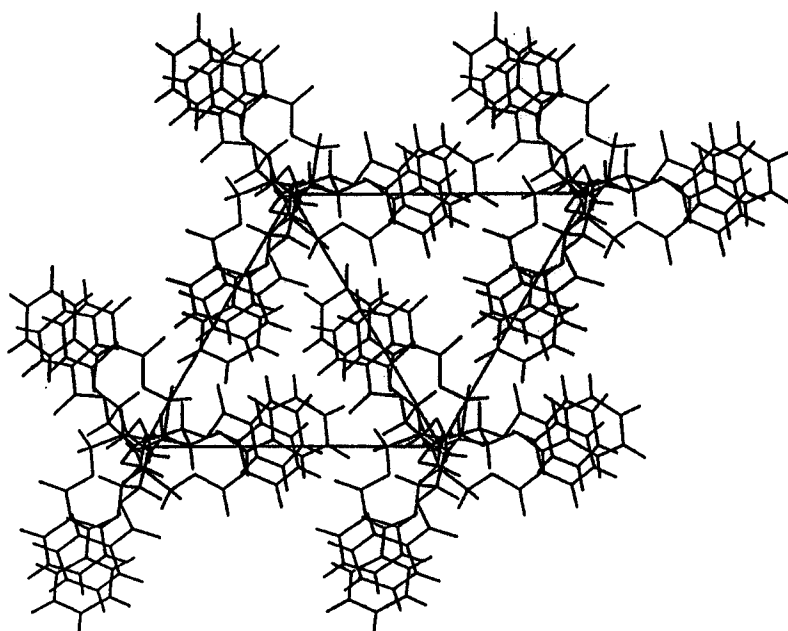


Fig. 2. Parallel packing model for cellulose tribenzoate viewed along the helix axes.

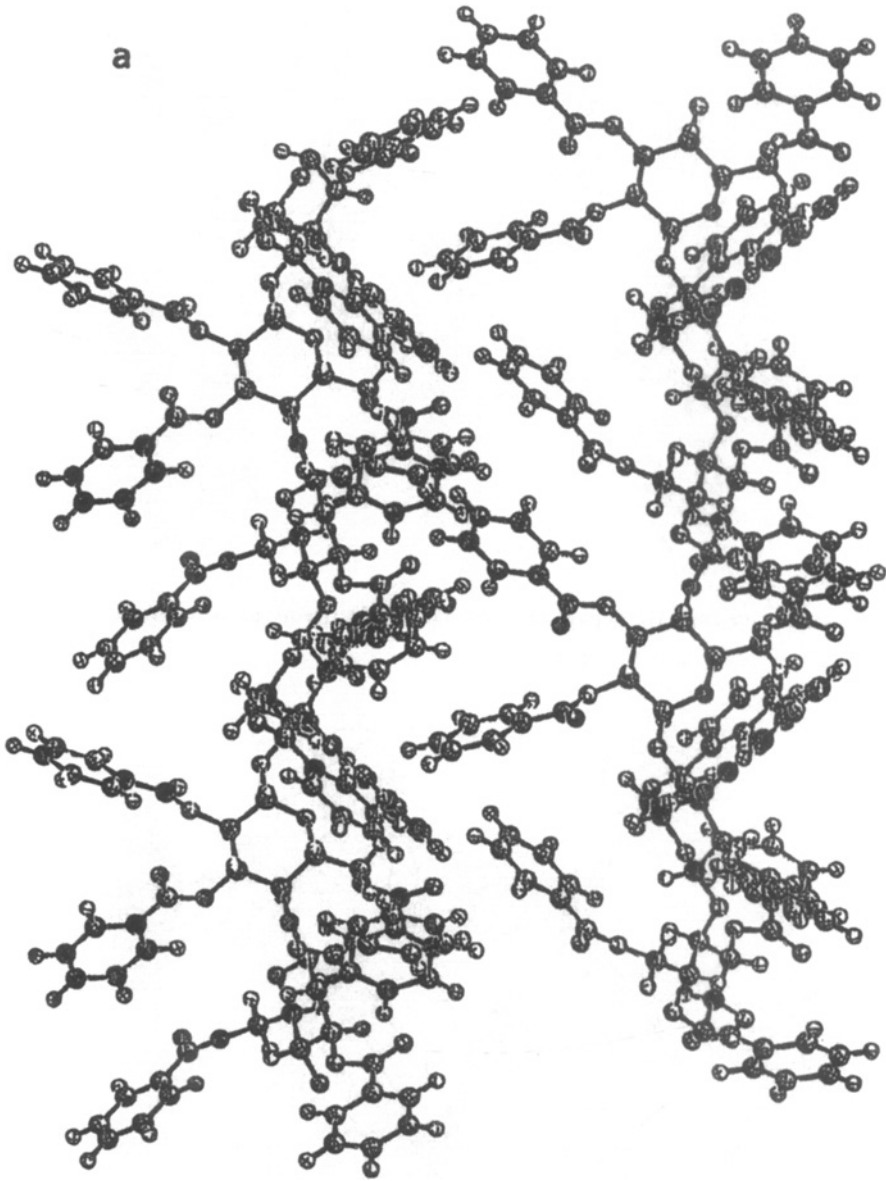


Fig. 3a. Representation of two neighboring chains of an antiparallel packing model viewed towards the helix axes.

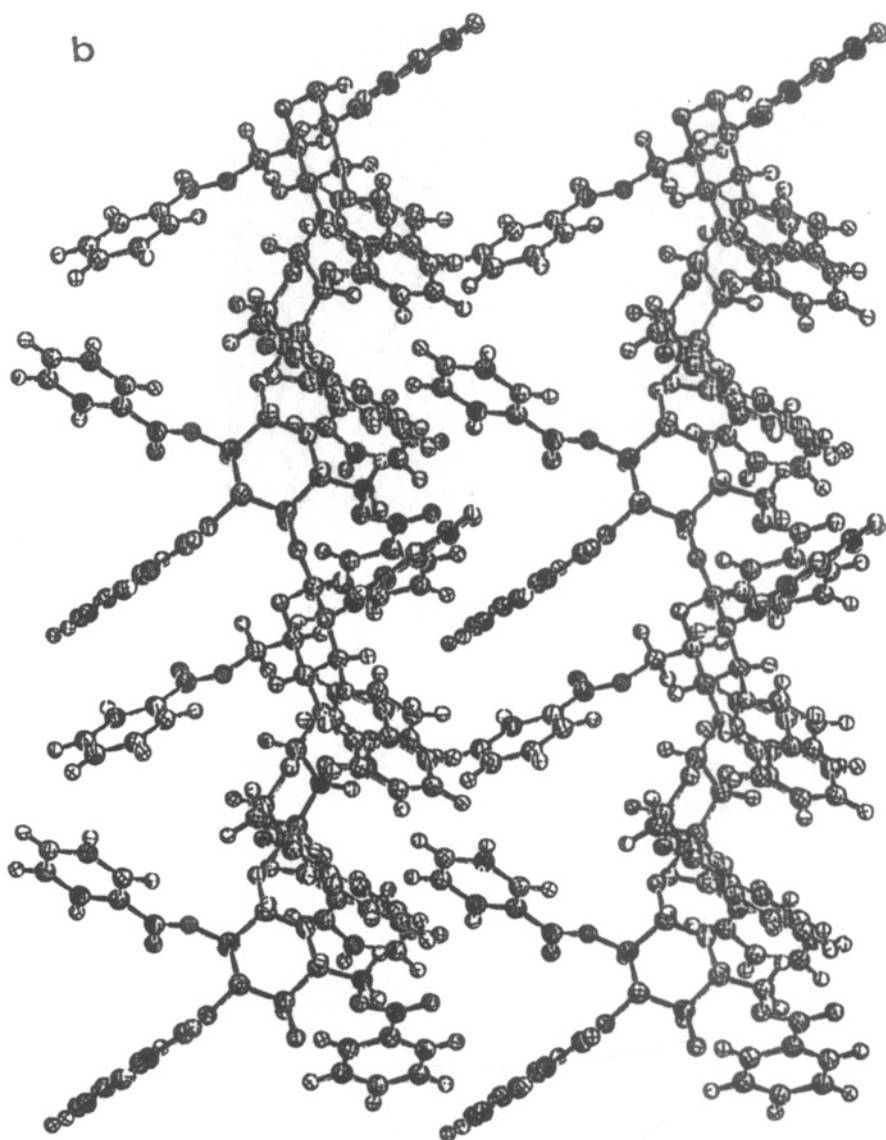


Fig. 3b. Representation of two neighboring chains of a parallel packing model viewed towards the helix axes.

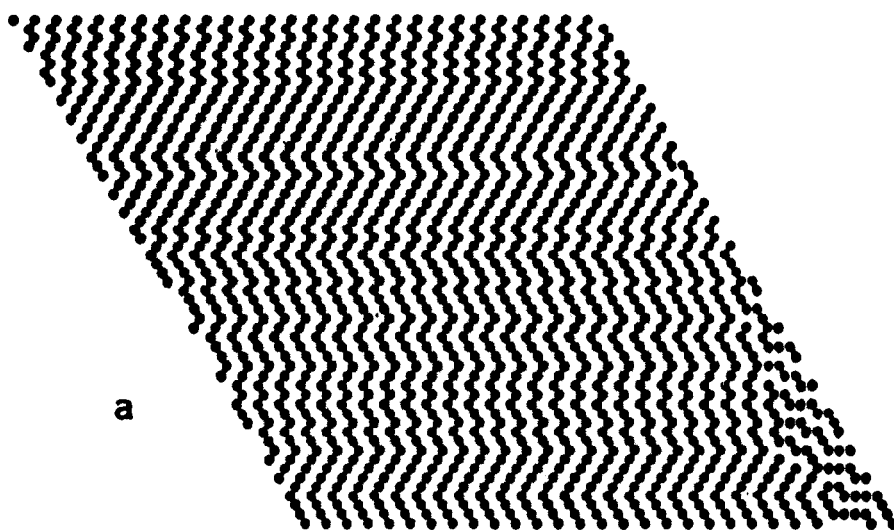


Fig. 4a. Model for chain packing with $r = 0.0$.

●: up chains, in between down chains

arrangements as a consequence for both heterogeneously and homogeneously derivatized CTB. The coordinates of this structure are given in reference 2 and will be published elsewhere.

CRYSTALLINE DOMAINS OF CTB

The parallel chain arrangement of solution grown crystals of CTB seems to contradict the basic idea that an equal number of chains should run in either direction in a solution which then leads to an antiparallel packing arrangement during crystallization. Therefore, a study was undertaken to simulate the crystallization procedure on a very basic scale with potential energy considerations, omitting any constraint implied by the system. The trigonal lattice established for CTB was used onto which the chains are positioned. If an antiparallel chain arrangement is strongly preferred, up and down chains crystallize in an alternating manner onto the nucleus. For a preferred

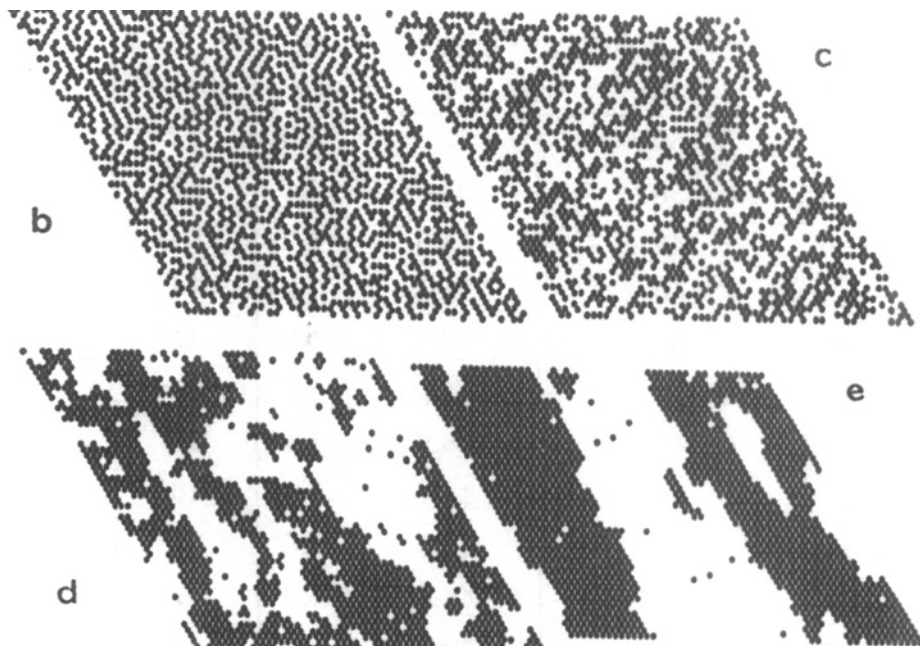
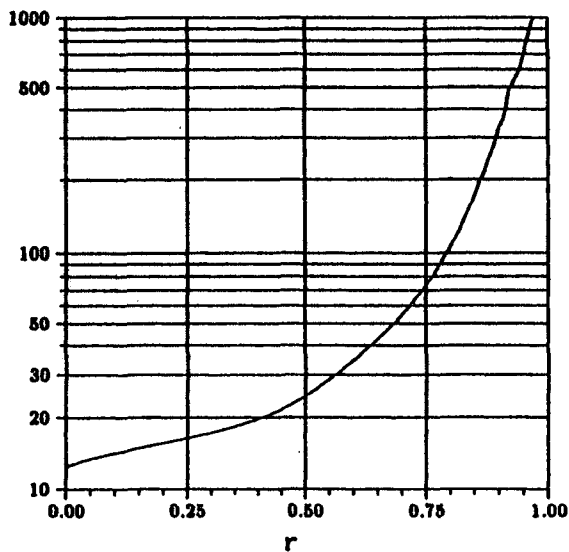


Fig. 4b-e. Models for chain packing, ●: up chains, in between down chains (b: $r = 0.25$, c: $r = 0.5$, d: $r = 0.75$, e: $r = 0.85$).

Fig.5.
Size of parallel domains as a function of parameter r for a chain cross section of 12.2 \AA (CTB)



r	Overall Polarity	Parallelism	Fibrillar Size	
	%	%	rel.	abs./Å
0.00	50	33.3	1.0	12
0.05	50	33.8	1.1	13
0.10	49	34.6	1.2	14
0.15	50	35.4	1.2	14
0.20	50	36.4	1.3	15
0.25	49	37.5	1.3	16
0.30	49	38.9	1.4	17
0.35	50	40.7	1.5	18
0.40	50	42.9	1.6	19
0.45	50	45.8	1.8	21
0.50	50	50.0	2.0	24
0.55	49	55.3	2.3	28
0.60	49	61.1	2.8	34
0.65	49	67.1	3.5	42
0.70	50	73.5	4.5	54
0.75	50	79.6	6.0	72
0.80	50	85.5	8.7	105
0.85	48	90.8	13.9	169
0.90	46	94.9	25.8	314
0.95	36	97.7	56.8	692
1.00	0	100.0	∞	∞

Table 1.

Computer simulations of fibrillar crystallization

Fig. 6.
DSC thermograms of CTC/MAA solutions of various concentrations (in wt% CTC). Heating rate 10°C/min.

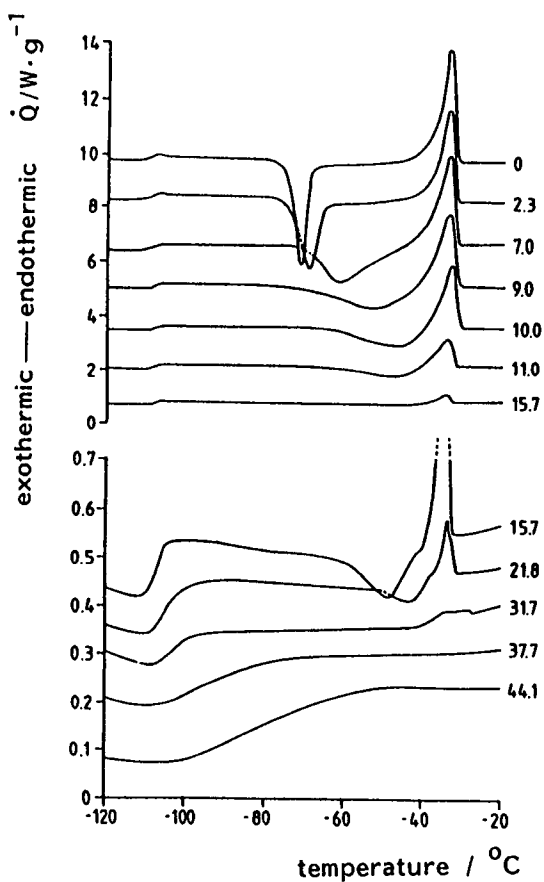
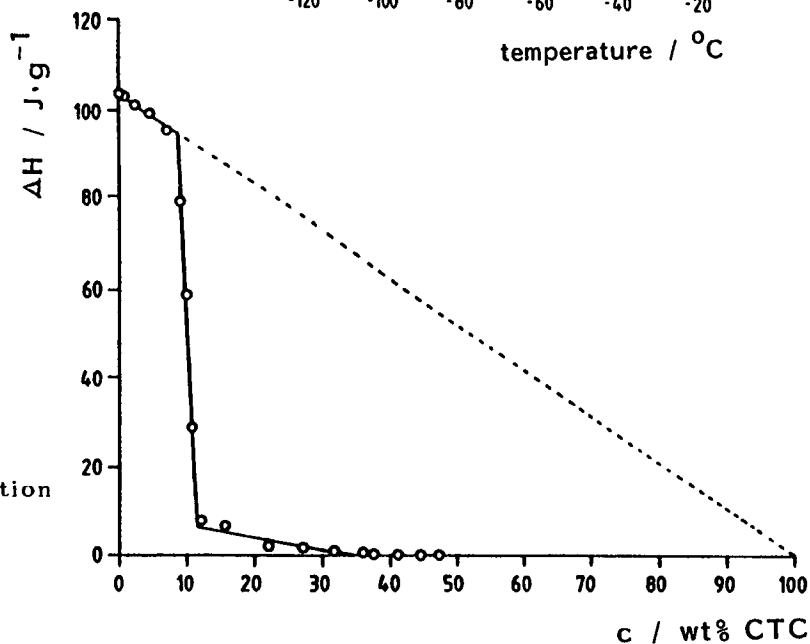


Fig.7.
Melting enthalpy ΔH [J/g] of free MAA as a function of a CTC concentration



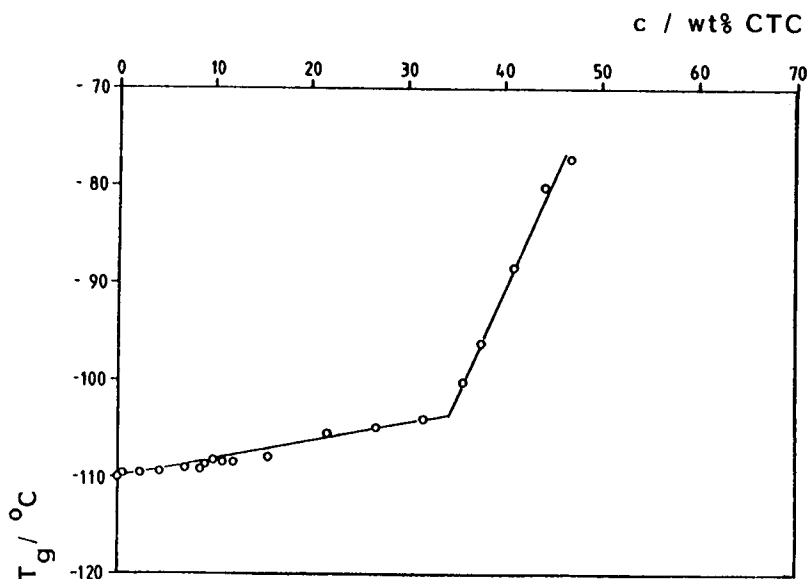


Fig. 8. Dependence of the glass transition temperature T_g on CTC concentration c of CTC/MAA solutions.

parallel packing, only chains with one single directional sense, which is determined by the nucleus, will be crystallized to the growing domain. However, if the energy gained by the system is the same for either an up or a down chain independent of the direction of adjacent chains a statistical array of up and down chains will be expected.

A probability parameter r was introduced to describe the chain directions on the two-dimensional lattice perpendicular to the chain axes: $r = 0$ for antiparallel packing, $r = 1$ for parallel packing and $0 < r < 1$ for statistical packing with increasing preference for parallel packing with growing r values. (For further details see ref. 2.)

The results of this simulation are presented in Figures 4, 5 and Table 1. Fig. 4 demonstrates that large uniform domains appear with increasing r containing up and down chains, respectively. An equal number of chains pointing in either direction results up to $r = 0.85$ as concluded from the calculated overall polarity of Table 1. The average size of domains of parallel running chains D is presented in Table 1 in relative and absolute values. A chain diameter of 12.2 \AA was assumed according to the cross section of CTB and D plotted in Fig. 5 as a

function of the r value. Although the simulation was carried out for the crystallization process, the results may be similar for a treatment of a fibrillar metastable morphology driven towards the equilibrium state.

LIQUID CRYSTALLINE STATE

The morphology of fibrillar material depends strongly on the interaction between chains as shown by the simulation of the crystallization process. How can this interaction be changed? Experiments with lyotropic cholesteric cellulose derivatives reveal that the polymer solvent interaction plays an important role in establishing the supermolecular structure.

A thermal analysis for the system cellulose triphenylcarbamate (CTC)/methyl acetoacetate (MAA) was carried out from the dilute and semi-dilute to the liquid crystalline state with regard to the polymer solvent interaction. The results are presented in Figures 6-8 [3]. Figure 6 depicts DSC experiments on quenched CTC/MAA solutions of various CTC concentrations ranging from 0 to 44.1 wt%. Pure MAA shows a glass transition at 110°C followed by a crystallization and subsequent melting. At higher CTC concentrations the crystallization of the solvent disappears as does consequently the melting. A plot of the melting enthalpy ΔH [J/g] versus CTC concentration exhibit some unexpected behavior of the system. If only free solvent is present the normalized ΔH (per g solution) should follow the dashed line in Figure 7. However, a strong drop in ΔH occurs already at 11 wt% and ΔH disappears completely at the isotropic - liquid crystalline phase transition. T_g as a function of CTC concentration changes its behavior abruptly at this phase transition only (Fig. 8). This investigation shows that according to Hatakeyama et al. [4] some solvent is bound to the polymer chain at relative low concentration and free solvent is no longer present at the phase transition into the cholesteric state. A small biphasic region in the phase diagram of the same system [5] and the existence of crystalline solvent/cellulosic complexes point also to strongly bound solvent by the cellulosic chain. It seems likely that the interaction of cellulosic chains with different bound solvent

may behave differently during the crystallization process and thus various morphologies of the fibrillar material are obtained.

CONCLUSION AND POTENTIAL APPLICATION

A simple model simulation is able to explain parallel and antiparallel chain packing arrangements as well as the conversion from parallel to antiparallel packing of chains and vice versa, long debated in the mercerization process from cellulose I to cellulose II or the transformation of cellulose triacetate I to cellulose triacetate II through the cellulose triacetate/nitromethane complex, if an equal number of up and down chains are present.

It is important to notice that depending on fiber and film forming processes various structures, parallel, antiparallel or statistical chain arrangements, may evolve with different properties driven by external and internal parameters. Domains of various sizes may play an important role in wet spinning from dilute solution. It is also expected that a different morphology will be formed by the spinning process from a liquid crystalline solution or dry spinning dependent on the chain interaction and constraints implied.

This work was supported in part by a grant from Bundesministerium für Forschung und Technologie.

REFERENCES

1. Steinmeier, H., Zugenmaier, P., Carbohydrate Research 1987, 164, 97.
2. Riehl, K., Dissertation, TU Clausthal, Clausthal-Zellerfeld, 1992.
3. Haurand, P., Dissertation, TU Clausthal, Clausthal-Zellerfeld, 1990.
4. Hatakeyama, T., Ikeda, Y., Hatakeyama, H., Makromol. Chem. 1987, 188, 1875.
5. Haurand, P., Zugenmaier, P., Polymer, 1991, 32, 3026.

50 Flow-induced structures in isotropic and anisotropic cellulose derivative blends

S G James, J Schatzle, V Tsakalos, E Peuvrel-Disdier and P Navard –
Ecole des Mines de Paris, Centre de Mise en Forme des Matériaux
BP207, 06904 Sophia-Antipolis, France

ABSTRACT:

The shear flow behaviour of cellulose derivative-based incompatible blends has been studied using rheological and rheo-optical (polarizing microscopy) methods. Two types of model systems were used, one with a high interfacial tension (hydroxypropylcellulose in water / polydimethylsiloxane) and one with a low interfacial tension (two cellulose derivatives in a common solvent).

This study shows the importance of coupling rheological investigations with morphological observations in order to understand the behaviour during flow:

- positive deviation of the viscosity from the ideal mixing law when the morphology is globular,
- negative deviation of the viscosity with a fibrillar morphology.

This final morphology clearly results from the competition between the interfacial and viscous forces (globular when the interfacial tension dominates, fibrillar for dominating viscous forces).

Almost no effect is observed when changing the minor component from an isotropic to a liquid crystalline (anisotropic) phase.

1. INTRODUCTION

The field of cellulose and cellulose derivative blends is one of growing interest. In addition, to have a liquid crystalline polymer (LCP) in the blend can give improved mechanical properties compared with those of conventional blends [1] and the LCP often acts as a processing aid by

lowering the bulk viscosity of the blend [2]. The purpose of this paper is to understand the rheology of isotropic and anisotropic cellulose derivative based blends in relation to their morphology by using rheo-optical techniques. The kind of morphology which can be attained and the importance of having an anisotropic phase are questions which will be addressed.

2. EXPERIMENTAL

Materials:

Two kinds of systems will be studied:

System 1: Solutions of hydroxypropylcellulose in water / Polydimethylsiloxanes.

Hydroxypropylcellulose (HPC): Type L ($M_w=100000$) from Aqualon
 50% by weight of HPC_L in water: anisotropic solution (HPC_L50)
 30% by weight of HPC_L in water: isotropic solution (HPC_L30).

Polydimethylsiloxanes (PDMS): Rhodorsil 48V175000 (PDMS₁)
 or Rhodorsil H47V1000000 (PDMS₂) from Rhône-Poulenc.

The viscosity of the HPC solutions ($\eta(\text{HPC}_{L30}) = 420$ Pa.s, the viscosity curve of HPC_L50 being presented in Ref 3) is in between the two PDMS viscosities ($\eta(\text{PDMS}_1) = 160$ Pa.s and $\eta(\text{PDMS}_2) = 1100$ Pa.s).

System 2: Mixtures of cellulose derivatives in a common solvent.

In each series the total polymer concentration was kept constant and the ratio of the polymers was varied. The composition and the total polymer concentration C are indicated below:

2a. HPC_E + EC in acetic acid, C=35 wt%

2b. HPC_E + EC in acetic acid, C=25 wt%

2c. HPC_E + CA in acetone, C=29 wt%

HPC_E: hydroxypropylcellulose type E ($M_w=60000$) from Aqualon.

EC: ethylcellulose, Ethocel from Fluka.

CA: cellulose acetate from Rhodia.

The solutions were prepared by mixing the three compounds at room temperature, followed by stirring over a few days.

In case 2a., an anisotropic phase was observed for the phase rich in HPC_E, coexisting with an isotropic phase rich in EC. In cases 2b. and 2c., two isotropic phases are present.

Rheological measurements and rheo-optical observations:

The observations of the morphology of all the blends during shear flow were made with the rheo-optical system described in detail elsewhere [3]. The observations during shear were performed using an optical polarizing microscope.

The viscosities were measured with an Instron 3250 rheometer and a Rheometrics Stress Rheometer (RSR) in the cone-and-plate geometry.

Because of the vapour pressure of acetone, measurements on system 2c. were performed in a couette fixture (RSR and a Haake RV2 rheometer). To allow an easy comparison of the results of different blends, the rheological measurements can be presented in terms of normalized viscosity (measured viscosity divided by the value calculated from the ideal mixing law).

Measurement of the interfacial tension:

The interfacial tension was measured using a dynamic method called "the thread break-up method". This method is based on the observation of the time relaxation of a thread imbedded in another polymer. If the thread is long, sinusoidal distortions (Rayleigh instabilities) appear along the thread due to the interfacial tension. They then grow up and lead to the break-up of the thread. Following the growth of the distortions as a function of time enable to determine the interfacial tension (theory of Tomotika [4]). An example of the different steps leading to the break-up of the thread is given in Figure 1. This method was first applied to molten polymers [5] and extended to the case of polymer solutions by Tsakalos [6].

This method was applied to the system HPC_L30 / PDMS (Rhodorsil 47V600000). The interfacial tension for this system is equal to 12.2 ± 1 mN/m. This high value was expected as the two polymers of system 1 are known to be incompatible. The interfacial tensions of system 2 were not measured, but their close chemical structure should lead to a low interfacial tension.

3. RESULTS AND DISCUSSION

System 1:

The two blends show identical steady state morphology during shear, which is globular due to the high interfacial tension of the system. In both cases increasing the shear rate leads to a decrease in the average size of the inclusions up to a critical size (Figure 2).

Looking at the time necessary to reach this stable morphology, it appears that this time is very different for the two blends.

In the case where $\eta(\text{HPC}_L)/\eta(\text{PDMS}_2) < 1$, it takes up to 30 minutes to reach the steady state. Different stages are observed during the transient regime. At rest, the inclusions are large and spherical, but as soon as the shear is started they are elongated into fibres, over a period of 20 s. After this time the fibres start to break following the same mechanism as the one observed at rest for the measurement of the interfacial tension (see Figure 1). After about 30 minutes there are very few fibres

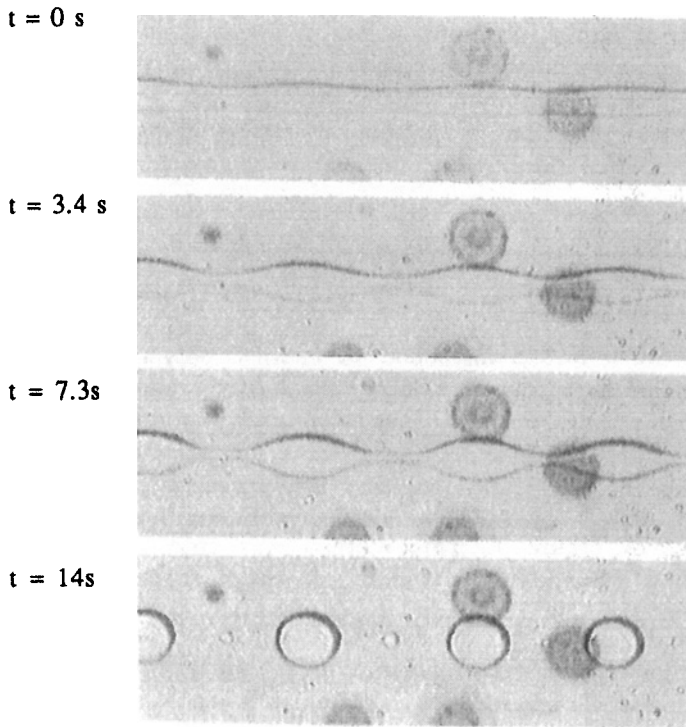


Figure 1: Development of the Rayleigh instabilities for the system HPC_L30 / PDMS (initial diameter of the thread = 21 μm).

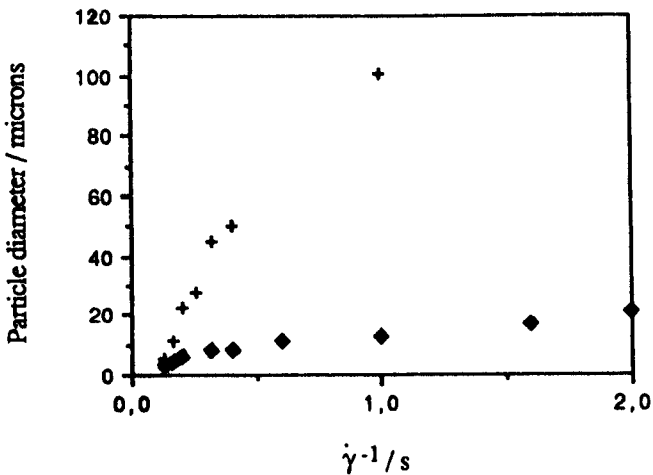


Figure 2: Average diameter of the inclusions as a function of $1/\text{shear rate } (\dot{\gamma}^{-1})$ for the systems: 10% HPC_L50 / PDMS₁ (+) and 10% HPC_L50 / PDMS₂ (◆)

left and the morphology consists mainly of small droplets of HPC which are slightly deformed from perfect spheres by the flow field.

For the system $\text{HPC}_L/\text{PDMS}_1$, where the matrix has a lower viscosity than the one of the inclusions, the elongation and break-up stages of the inclusions occur in 30 s. The average resulting size of the droplets is of course much larger than in the other system (Figure 2) (deformation and break-up being easier for system 2).

This necessary time to reach a steady state morphology is also observed when measuring the viscosity of the blends, which means that it takes 30 minutes to reach a stable measurement in the system $\text{HPC}_L/\text{PDMS}_2$, whereas the establishment of the steady state viscosity for $\text{HPC}_L/\text{PDMS}_1$ is almost instantaneous.

The viscosities of blends as a function of concentration were also investigated (Figure 3). The morphology being globular, these values were compared to Taylor model predictions [7] (model of spherical droplets (slightly deformed) of a Newtonian component in a Newtonian matrix). The comparison shows that the experimental measurements are in reasonably good agreement with the Taylor model predictions.

In this figure, two experimental measurements are reported, one where both phases are isotropic, one where one phase is anisotropic. It appears that changing the minor component from an isotropic to an anisotropic phase has almost no effect on the blend viscosity.

System 2:

The behaviour of the second type of systems, where the interfacial tension is low, is different. Two different types of morphology are observed during shear:

- globular at low shear rates
- fibrillar at high shear rates.

In fact this clearly shows the competition between the viscous and the interfacial forces on the resulting morphology. At low shear rates, the viscous forces are weak and the interfacial tension is dominating, which results in a globular morphology. As the shear rate increases, the viscous forces become dominant, leading to the deformation of the inclusions in fibrils.

This difference in morphology is clearly seen looking at the viscosity of the blends (Figure 4). When the morphology is globular, the viscosity is above the ideal law of mixing. As the shear rate is increased, the morphology becomes more and more elongated leading to a diminution in the viscosity of the blend. This morphological evolution during shear explains the appearance of a peak in the viscosity curves (Figure 4).

In the case where the morphology is always fibrillar (viscosity always

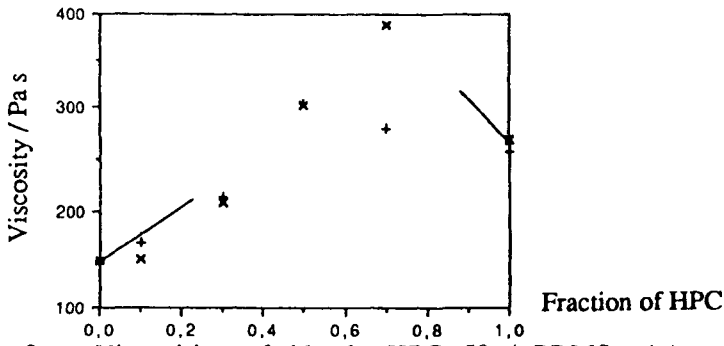


Figure 3: Viscosities of blends HPC_L50 / PDMS₁ (+) and HPC_L30 / PDMS₂ (x) as a function of the concentration at a shear rate of 1 s⁻¹. The solid lines are the viscosities predicted by the theory of Taylor [7] for Newtonian fluids.

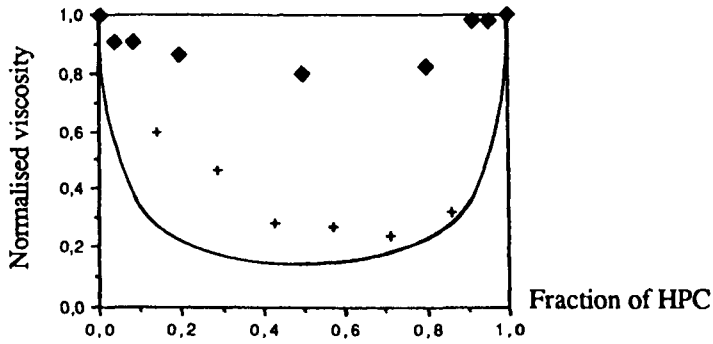


Figure 4: Normalized viscosities of systems 2a.(+) and 2b.(◆) as a function of polymer fraction of HPC_E at a shear rate of 1 s⁻¹. The solid lines are the viscosities predicted by the Heitmiller layer model [8].

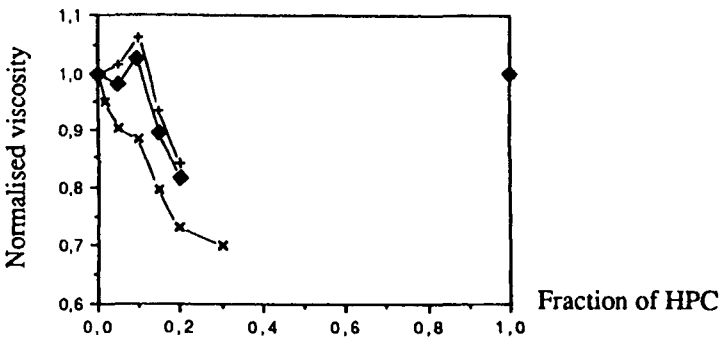


Figure 5: Normalized viscosities of system 2c. as a function of polymer fraction of HPC_E at shear rates of 0.03 s⁻¹(+), 0.05 s⁻¹(◆) and 0.7 s⁻¹(x).

lower than the ideal mixing law), the normalized viscosities of blends as a function of concentration are reported for the systems 2a. and 2b. (Figure 5). These experimental values are compared with the layer model of Heitmiller (alternating layers of two components, parallel to the plate surface) [8]. In agreement with the layer model, one finds a negative deviation of the experimental results from the ideal mixing law. The divergence can be explained by the imperfection of the developed layer structure (in our case, a fibrillar structure instead of layers).

Comparing the two experimental curves (system 2a. where one phase is anisotropic, and system 2b. where the two phases are isotropic) shows that a negative deviation is obtained in both cases, but a stronger negative deviation is found for the blend where one phase is anisotropic.

4. CONCLUSION

We have examined two types of blend systems, both of which contain HPC blended with another immiscible polymer. The choice of the systems have enabled us to investigate the influence of:

- the interfacial tension,
 - the viscosity ratio,
 - having an anisotropic phase,
- on the morphology of the blends.

We have found that the two first parameters have a strong influence on the final morphology of the blends. In the first system, where the interfacial tension is high, a globular morphology is found, once the equilibrium has been reached during flow. With the second system, where the interfacial tension is low, a fibrillar structure is, at most shear rates, favoured during flow.

The viscosity of the blends has been shown to depend strongly on the morphology present during flow. In the case of a globular morphology, the blend viscosity always shows a positive deviation from the viscosity given by the rule of mixtures. When the morphology is fibrillar, a negative deviation from the ideal behaviour is found. The transition from a morphology of discrete inclusions to a fibrillar structure is accompanied by a decrease in the viscosity.

We have also observed that in some cases, the time necessary to reach a steady state viscosity might be long (around 30 minutes), which was correlated to an evolution of the morphology. The variation of viscosity over long periods of time has important implications for viscosity measurements of blends especially at high temperatures (it is not always possible to shear for long times due to degradation of the polymer).

With the systems studied in this paper, it appears that changing the minor component from an isotropic to an anisotropic phase (same viscosity range and assumed same interfacial tension with the matrix as the chemical structure did not change) has almost no effect on the blend behaviour.

REFERENCES:

1. G. Crevecoeur, G. Groenincks, LCP-Seminar'91 in Neste Oy, Kulloo, 28-29 November 1991.
2. D. Dutta, H. Fruitwala, A. Kohli, R.A. Weiss, *Polym. Eng. Sci.* **30** N°17 (1990) 1005
3. B. Ernst, P. Navard, *Macromolecules* **22** (1989) 1419.
4. S. Tomotika, *Proc. R. Soc. London Ser. A* **150** (1935) 322.
5. D.C. Chappellear, *Polym. Prepr.* **5** (1964) 363.
6. V. Tsakalos, rapport de DEA, Ecole des Mines de Paris, Sophia-Antipolis (1992).
7. G.I. Taylor, *Proc. Roy. Soc.(London)* **A138** (1932) 41.
8. R.F. Heitmiller, R.Z. Naar, H.H. Zabusky, *J. Appl. Polym. Sci.* **8** (1964) 873.

51 Shear induced texture of lyotropic hydroxypropyl cellulose in flexible polyester resin

M Mucha and Z Kotarski – Faculty of Process and Environmental Engineering, Technical University, 90-924 Łódź, Poland

ABSTRACT

A variety of morphological textures of the heterogeneous blends: HPC/AcA, HPC/polyester resin and (HPC/AcA) /polyester resin is presented. The graphs taken from thermo-optical analysis and differential scanning calorimetry allow observation the phase behaviour of the samples.

INTRODUCTION

The study of cellulose and cellulose derivatives blends with synthetic polymers is now the subject of increasing investigation (Nishio et al., 1985a, 1989b; Paillet et al., 1993; Sakellariou et al., 1993; Wang et al., 1991) and has importance in relation to practical applications. The occurrence of the lyotropic phase with a cholesteric liquid-crystalline order in concentrated aqueous and acetic acid (AcA) solutions of hydroxypropyl cellulose (HPC) was reported (Mitchell et al., 1992; Schone et al., 1991; Werbowyj et al., 1976). The morphological textures and the thermal properties of HPC blends with flexible crosslinked polyester resin is presented here. The solid sheared and nonsheared heterogeneous blends were prepared by the photopolymerization of a liquid oligoester containing lyotropic HPC prepared by dissolution in acetic acid. The critical concentration necessary for the formation of an anisotropic-lyotropic phase at room temperature has been investigated for HPC, the most investigated cellulose derivative,

varying in their molar mass and the nature of the solvent (Bheda et al., 1980). For example the value of 0.30 weight fraction as the minimum concentration of a HPC sample in acetic acid was found. The heterogeneous inclusions of lyotropic HPC in the oligoester tend to elongate under shear to form a variety of supermolecular fibrous honey-comb line textures, which can be stabilized by the fast polymerization of the polyester matrix. The resulting morphology and the phase behaviour of the blends is altered by the conditions of their preparation and applied shearing stress.

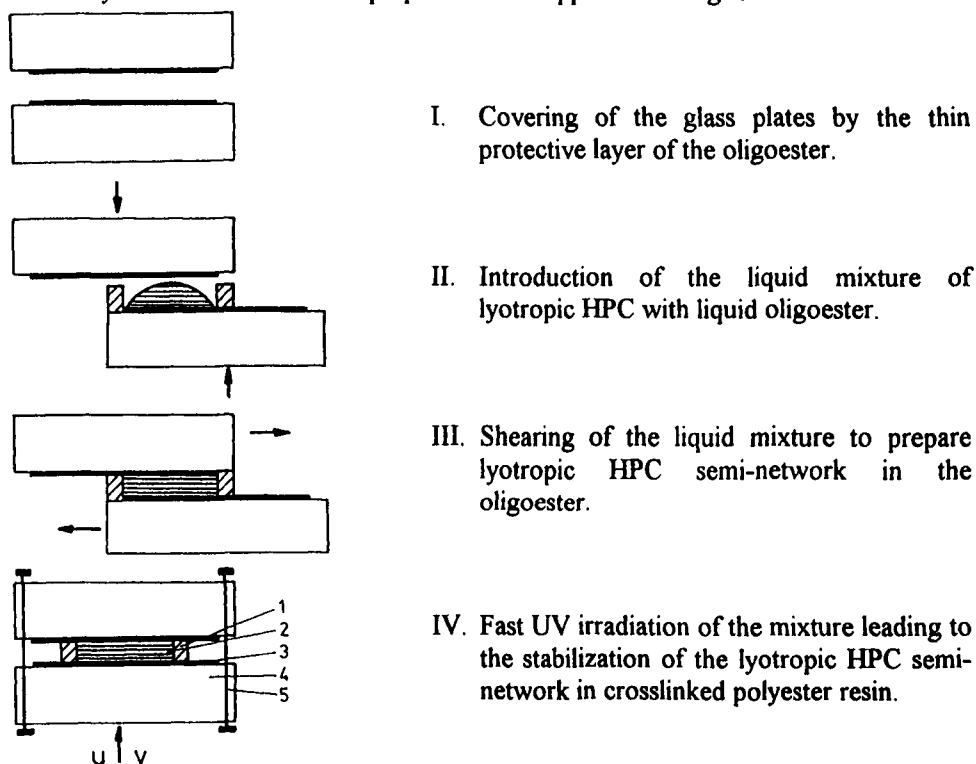


Fig.1. Sample preparation by shear. 1.distance film, 130 μ m 2. sample, 3. protective layer, 4. glass plates, 5. screws for tightening

EXPERIMENTAL

Components:

Pure hydroxypropyl cellulose was taken from Scientific Polymer Production Inc, USA. UV cured oligoester resin was a three component commercial mixture with styrene and a cure agent.

Blends:

40 % [wt/wt] solution of HPC in acetic acid was prepared. Thin layers of the lyotropic HPC solution were birefringent in the quiescent state (Fig. 2a) and depending on the extent of shear stress applied presents a so called banded structure with a clear periodic

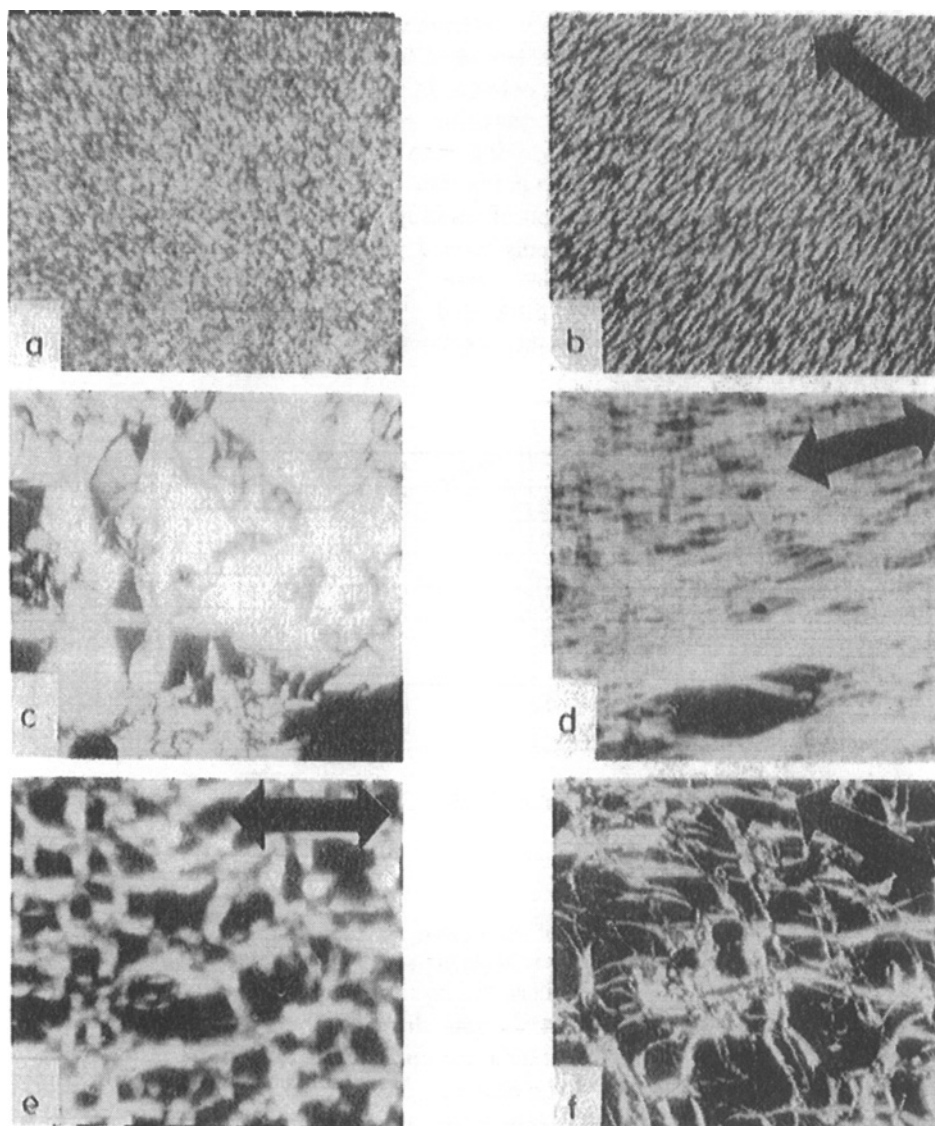


Fig.2. Crosspolarized light micrographs of: a. and b. - thin lyotropic layer of HPC (40 wt% solution in acetic acid) in quiescent and shearing conditions, c. and d. - 20 wt% of lyotropic HPC blended with polyester resin (in d. shearing is induced by fast mixing of liquid blend), e. and f. - shear induced textures of lyotropic HPC (40 wt% and 60 wt%) in the blends with polyester resin. \longleftrightarrow 0.1 mm

arrangement along the direction of shear (Fig. 2b) in crosspolarized light. The optical anisotropy in the banded structure can be interpreted (Nishio et al., 1985a) in terms of a model in which optical axes are alternately tilted from band to band at an angle to the shearing direction. The 40 % HPC solution in acetic acid was taken as a base to prepare the blends with the liquid oligoester resin in the following ratios: 20% (HPC/AcA) / 80% resin and 40% (HPC/AcA) / 60% resin. Lower than 20% concentration of lyotropic (HPC/AcA) in the resin does not create the semi-network of lyotropic HPC, too high a concentration of liquid lyotropic HPC/AcA does not allow a film of good quality with the photopolymerized polyester resin to be obtained. The samples under study are presented in Table 1. In Fig. 1 the method of sample preparation by shear between glass plates and photopolymerization of the matrix is presented. Also the methods of the studies are described.

Table 1. Samples and methods

Nr	Samples	wt% HPC	DSC	TOA	Mech.	Photo
1.	pure resin	0	+	+	+	-
2.	pure HPC	100	+	+	-	-
3.	HPC/resin	20	+	+	-	+
4.	HPC/AcA	40	+	+	-	+
5.	(HPC/AcA)/resin 40/60	16	+	+	+	+
6.	(HPC/AcA)/resin 20/80	8	+	+	+	+

Heating rate $\beta=10/\text{min}$ (DSC) and $7/\text{min}$ (TOA)

RESULTS AND DISCUSSION

A variety of morphological textures of the heterogeneous blends: HPC with polyester resin and (HPC+AcA) with polyester is presented in the following micrographs (Fig. 1c-f) taken from the polarized optical microscope. Honey-comb like textures of lyotropic HPC prepared in quiescent and under shear are observed. The graphs taken from thermo-optical analysis, and differential scanning calorimetry (Fig. 3 and 4) allow the phase behaviour of the samples to be observed. The temperatures T_1 (~150 C) and T_2 (~200 C) are taken as the phase transition temperatures to mesomorphic and isotropic phases of the pure HPC. The HPC introduced to polyester still exhibits both lyotropic (with solvent) or thermotropic behaviour. After evaporating of AcA from the lyotropic HPC (curve 4 in Fig. 3) in the vicinity of 120 C, both thermotropic and isotropic transitions of pure crystallized HPC are exhibited. The isotropisation of the lyotropic HPC included in crosslinked polyester resin occurs at 170 C (curve 5 in Fig. 3). DSC thermograms show the presence of a broad endotherm associated with the transitions and attributed to evaporation of acetic acid with a maximum at around 120 C. Glass transition temperature T_g of HPC in the same range 80-110 C was found elsewhere

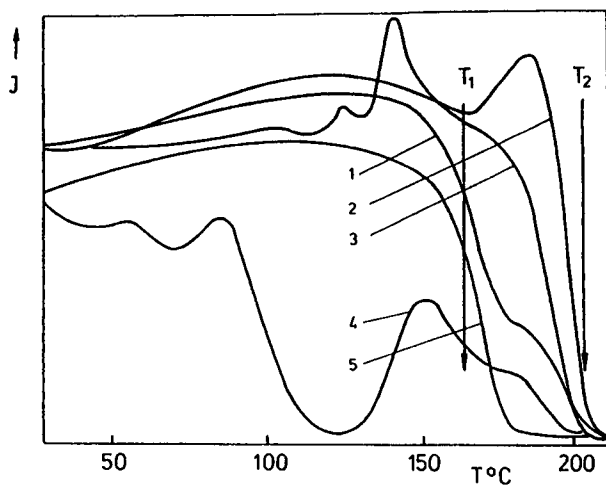


Fig.3. Thermo-optical curves of HPC-polyester resin blends taken for: 1. and 2. pure HPC-first and second run, 3. 20% HPC in polyester resin, 4. 40% in acetic acid (AcA), 5. 40% (HPC+AcA) in polyester resin, T_1 , T_2 phase transition temperatures.

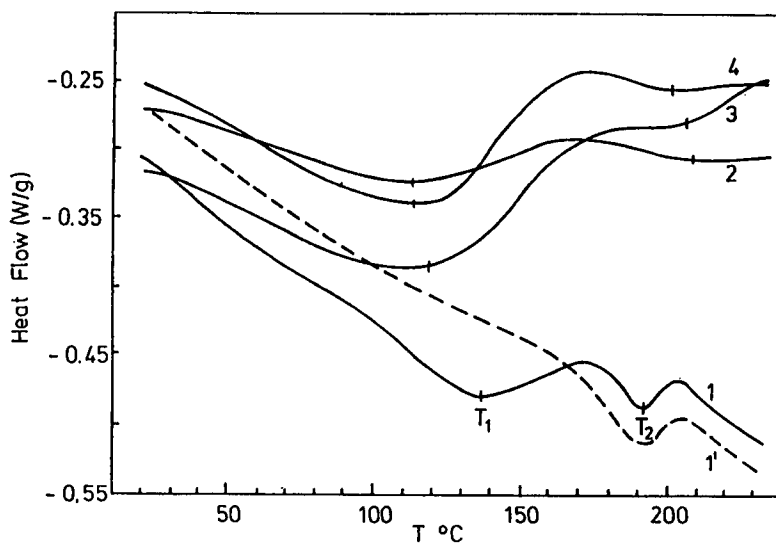


Fig.4. DSC curves of HPC-polyester resin taken for: 1. and 1.- pure HPC first and second run after fast cooling, 2. 20% HPC in polyester resin, 3. 20% (HPC+AcA) in polyester resin, 4. 40% (HPC+AcA) in polyester resin, T_1 , T_2 phase transition temperatures.

(Rials et al., 1988; Suto et al., 1986). from DSC and DMA studies. Here T_g was difficult to distinguish from the broad DSC peak of the first phase transition- T_1 . The mechanical properties of the shear induced blends of lyotropic HPC with polyester resin were investigated. The strain-stress behaviour and the Young's modulus values of the blends are varied in the comparison with the pure polyester resin. Additional work is planned to characterize more fully the properties of these liquid crystalline HPC with photopolymerized polyester resin blends.

CONCLUSIONS

1. The two phase morphological structure of the blends of lyotropic HPC in oligoester and polyester is exhibited.
2. The banded or semi-network, honey-comb like textures are produced by the shearing procedure between glass plates of the thin liquid layer of lyotropic HPC or blended with the liquid oligoester respectively.
3. The shear induced structure of the blends is stabilized by the fast photopolymerization of the polyester matrix.
4. The optical and thermal behaviour of the HPC blends differs from the pure polymer, but HPC included in polyester still exhibits both lyotropic (with solvent) and thermotropic behaviour.

REFERENCES

- Bheda J., J.F.Felleris and J.L.White (1980), *Colloid Polymer Sci.*, **258**, 1335.
 Mitchell G.R., W.Guo and F.J.Davis (1992), *Polymer*, **33**, 68.
 Nishio Y., T.Yamane and T.Takahashi (1985a), *J. Polymer Sci., Polymer Phys. Ed.*, **23**, 1053.
 Nishio Y. (1989b), *Polymer J.*, **21**, 347.
 Paillet M., J.Y.Cavaille, J.Desbrieres, D.Dapeyre and A.Pegny (1993), *Colloid and Polymer Sci.*, **271**, 311.
 Rials T.G. and W.G.Glasser (1988), *J. Appl. Polymer Sci.*, **36**, 749.
 Sakellariou P., A.Hassan and R.C.Rowe (1993), *Polymer*, **34**, 1240.
 Schone A., B.Morgenstern, W.Berger and H.W.Kammer (1991), *Polymer Network Blends* **1**, 109.
 Suto S., M.Kudo and M.J.Karasawa (1986), *J. Appl. Polym. Sci.*, **31**, 1327.
 Wang L.F., E.M.Pearce and T.K.Kwei (1991), *Polymer*, **32**, 249.
 Werbowyj R.S. and D.G.Gray (1976), *Mol. Cryst. Liq. Cryst.* **34**, 97.

52 Studies on membranes blended with cellulose cuoxam/casein

L Zhang, G Yang and L Xiao – Department of Chemistry, Wuhan University, Wuhan 430072, China

ABSTRACT

Blend membranes of cellulose cuoxam with casein were prepared and characterized by SEM, X-ray diffraction, IR, solid-state NMR, element and amino-acid analysis. The blends were miscible, when the casein content was smaller than 15% by weight. Young's modulus, tensile strengths, right-angle tearing strengths and breaking elongations were measured, and these values of both the dry and wet blend membranes were superior to that of regenerated cellulose membranes nonblended. Their mean pore diameters and permeabilities were improved. The interaction between the hydroxyl groups of cellulose and peptide bonds of casein in blend membranes was discussed.

INTRODUCTION

Regenerated cellulose membranes have been widely applied to membrane separation techniques such as dialysis, ultrafiltration and fractionation of mixtures. Even now in some fields they are considered superior due to their hydrophilicity and solute permeability. The permeation of solutes in aqueous solution is carried out in water swollen membranes. Therefore, the water

content in membranes is an important parameter concerning with permeability. However, the increase of water content usually causes a decrease in the mechanical strength of the membranes^[1]. In order to produce membranes having good permeability and excellent mechanical strengths, there have been many studies on blends of cellulose with e. g. polyacrylonitrile in N, N-dimethylacetamide-lithium chloride (DMAC-LiCl)^[2], poly(4-vinylpyridine) in dimethyl sulfoxide-paraformaldehyde (DMSO-PF)^[3] and so on. Much attention has been focussed on the cellulose/synthetic polymers blends prepared using nonaqueous solvent systems, but there are few reports describing blends from cellulose cuoxam and other polymers. In previous work^[4], regenerated cellulose membranes blended from cuoxam/zincoxene have been made and their mechanical properties were significantly improved. In this work, regenerated cellulose membrane having outstanding mechanical strength in a water-swollen state, were prepared by blends of cellulose cuoxam with a natural polymer-casein. The miscibility of the binary blends, their mechanical properties and porosities have been studied.

EXPERIMENTAL

Preparation of membranes

The linters used were supplied by Hubei Chemical Fiber Manufacture. The viscosity average molecular weight $M\eta$ was determined to be 1.96×10^5 from its intrinsic viscosity $[\eta]$ in cadoxen solution at 25°C by $[\eta] = 3.85 \times 10^{-2} M_w^{0.76}$ ^[5]. The casein was purchased from Shanghai Chemical Reagent Factory, and its components analysed by amino acid analyzer (Waters PICO, TAG) are shown in Table I. The average molecular weight was determined by electrophoresis and found to be 1.8×10^4 .

The 8 wt% cellulose solution in cuoxam (I) was prepared according to our patent^[6]. The casein was dissolved in aqueous ammonia solution to a concentration of 20 wt% (II). A mixture of I and II was spread over a glass plate, and then placed in a coagulation bath. The clear blend membranes obtained were washed in running water for 10 minutes, followed by drying in air. By changing the weight ratio of I to II to 100:1, 50:1, 25:1 and 5:1, a series of blend membranes coded as RC-S1, RC-S2, RC-S3 and RC-S4 were prepared. The membrane obtained from pure cellulose cuoxam was coded as RC-0.

Characterization of membranes

The nitrogen contents in the membranes were determined by the model PE-240B elemental analyzer. IR spectra of the membranes were recorded with a Nicolet FT-IR Spectrometer. Solid-state NMR spectra were obtained with a Bruker MSL-400 instrument. Scanning-electron micrographs (SEM) were made on a Jeol-JXA-840 microscope (Hitachi, Japan). The membranes were coated with carbon and gold, subsequently their surfaces were observed and photographed. The X-ray diffractions were measured with an X-ray diffractometer Rigaku 3015. The X-ray diffraction patterns with $\text{CuK}\alpha$ at 35 kV and 25 mA were recorded in the region of $2\theta = 5-35^\circ$. The degree of crystallinity (X_c) was calculated according to the usual method^[7].

Tensile strength (σ_b), right-angle tearing strength (σ_{tr}) and breaking elongation (ϵ_b) of dry and wet membranes were measured by an electronic strength tester XLD-0.1 according to the Chinese standard method (GB4456-84). Young's moduli (E') were measured on a Instron 3710-016 at 25°C.

An improved Bruss osmometer, based on the flow rate method reported in our previous work^[8], was used for measuring the mean pore radius ($2\bar{r}_t$), and ethanol permeabilities (G) through the membranes were evaluated by Kuhn's equation^[9].

Table 1 Analytical results of the casein components

No.	1	2	3	4	5	6	7	8	9
Component	Asp	Glu	Ser	Gly	His	Arg	Thr	Ala	Pro
Content (wt. %)	6.34	22.71	3.49	1.76	2.76	3.36	3.60	2.75	10.00
No.	10	11	12	13	14	15	16	17	18
Component	NH_2	Tyr	Val	Met	Cys	Ile	Leu	Phe	Lys
Content (wt. %)	3.28	4.91	6.54	2.39	0.05	5.18	9.30	4.76	7.28

Table II. The results of elemental analysis

Membranes No.	(Values calculated)					
	N wt%	C wt%	H wt%	N wt%	C wt%	H wt%
Casein	12.24	48.53	7.38	15.1	45.1	4.56
RC-0	0	38.57	6.15	0	44.4	6.2
RC-S1	0.53	38.42	6.25	0.58	39.04	6.21
RC-S2	1.02	39.08	6.26	1.11	39.48	6.26
RC-S3	2.57	39.52	6.34	2.04	40.23	6.36
RC-S4	3.96	40.27	6.43	4.08	41.89	6.56

RESULTS AND DISCUSSION

Analytical results of the nitrogen, hydrogen and carbon contents of the casein, regenerated cellulose and their blend membranes are summarized in Table I. The experimental values of nitrogen in the blend membranes are in good agreement with calculations based on the components in the starting mixture solution. Figure 1 shows IR spectra of the membranes coded RC-0, RC-S4 and casein. N-H and C-N of peptide bonds in the casein have bending vibrations and stretching vibrations at 1550 cm^{-1} , and the strong stretching vibration of C=O at 1640 cm^{-1} . As shown in the IR spectrum of RC-S4 membrane, absorbance occurs at $1530\text{--}1550\text{ cm}^{-1}$ and is markedly enhanced at 1650 cm^{-1} indicating that the blend membranes consist of cellulose and casein. The slight shifting of the C=O vibration in RC-S4 is due to the effect of their strong inter- or intra- hydrogen bond between peptide bonds of casein and hydroxyl of cellulose.

Figure 2 shows scanning electron micrographs of the membranes. The membranes of RC-0 and RC-S3 display smooth surfaces with homogeneous pore distribution. In contrast, the RC-S4 membrane shows a very rough surface with globules resulting from the phase separation on mixing. It implies that when the casein content of the blend was smaller than 15% by weight, the cellulose cuoxam with casein solution are miscible, giving homogeneous blend.

Table III. NMR peak assignments for casein, regenerated cellulose and blend membranes

samples	peak position (ppm)					source
	C (—C—O)	C ₁	C ₄	C ₂ C ₃ C ₅	C ₆	
BRC-1	—	107.3, 105.4	87.9, 83.8	75.1 ^a	63.1, 61.0	[10]
		97.5	81.7		60.0	
$\begin{array}{c} \text{O} \\ \\ \text{—C—NH}_2 \end{array}$	177.5	—	—	—	—	[9]
casein	173.5	—	—	—	—	This work
RC-0	—	105.0 ^a	—	75.0 ^a	62.0 ^a	This work
	182.0 ^b , 173.0, 171.0 ^b	104.0 ^a	—	74.5 ^a	62.0 ^a	This work
RC-S4	181 ^b , 173.5	104.5 ^a	—	74.5 ^a	63.5, 60.0 ^b	This work

a. denotes a broad peak; b. denotes the shoulder peak

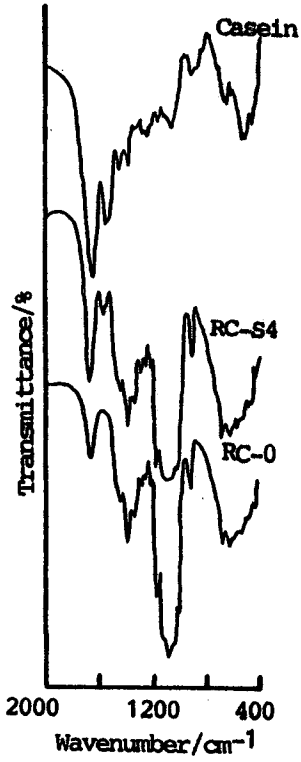


Fig 1. IR spectra of the membranes and casein.

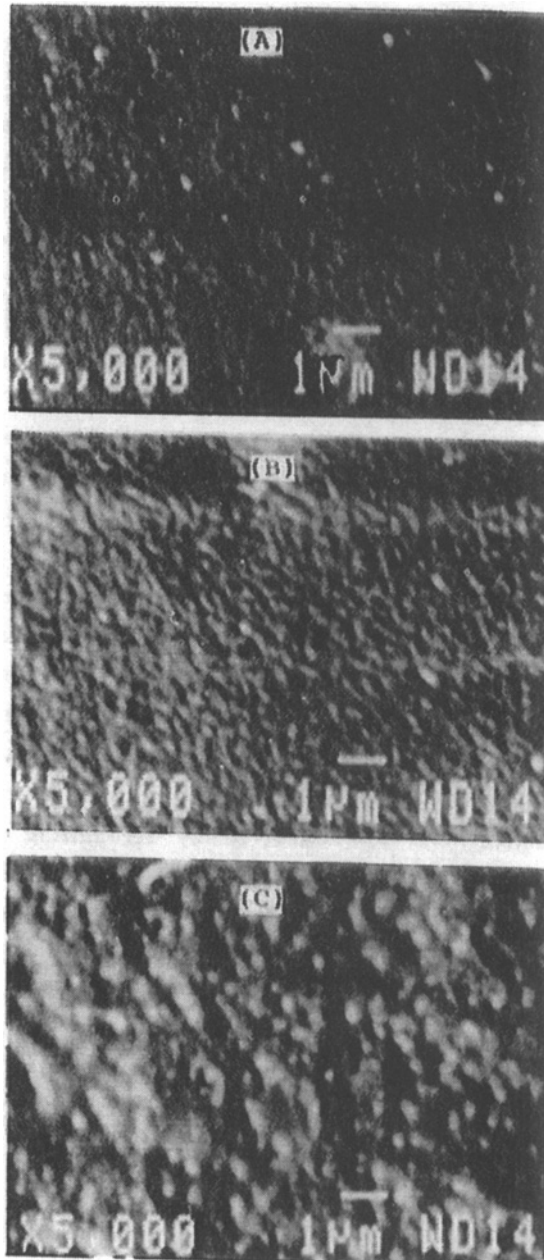


Fig 2. Scanning electron micrographs of the surface of the membranes for RC-0 (A), RC-S3 (B), RC-S4 (C).

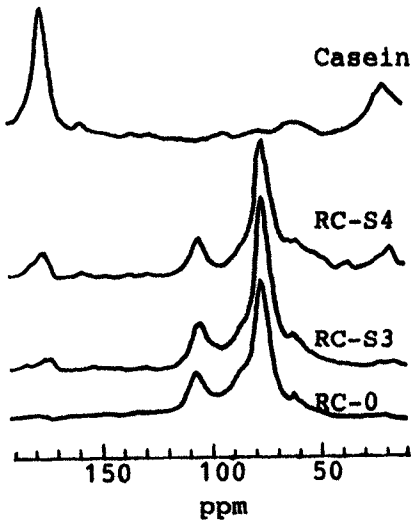


Fig 3. CP—MAS ^{13}C NMR spectra of the membranes and casein.

interacting and noninteracting hydroxyl groups, are apparent on the spectra for the blends. It is noted that the casein portion and C_6 of cellulose of the spectrum for RC-S4 blend show peaks at 173.5 ppm and 63.5, 60.0 ppm respectively as was expected by recognizing that the portion of phase separation occurs between the cellulose and casein. The results support the conclusions that were obtained by SEM. In the blends, the carbons which bear a hydroxyl group ($\text{C}_2, \text{C}_3, \text{C}_4$) and those that do not (C_1, C_6) show the shift in their resonance peak. We think that it results from the induced electron withdrawing effect caused by the interaction of the hydrogen of their hydroxyl groups with the carboxylate groups of the casein, and by the action of peptide bonds. If enough functionalities of the respective blend components interact to produce homogeneous mixing on a molecular scale and cause the electron density around the carbons bearing the interacting groups to be perturbed, then the ^{13}C resonance peak of these carbons will show changes in line shape or a chemical shift^[12]. Thus the good miscibility of the RC-S3 blend was understood by SEM and ^{13}C CP-MAS NMR.

The degrees of crystallinity described in Figure 4 and mechanical properties of the membranes are summarized in Table V. It is clear that tensile

Figure 3 shows the relevant portions of the ^{13}C CP-MAS NMR spectra for casein material and the membranes of RC-0, RC-S3 and RC-S4. Assignment of the resonance peaks was made with the aid of published NMR spectra^[10,11], and is given in Table III. The peaks ($\text{C}_1, \text{C}_2, \text{C}_3, \text{C}_6$) of the cellulose portion for the blend membranes are shifted to the right. The broader peaks (C) of the casein portion, resulting from the suggested partial superposition of the carbon resonances for the

strengths (σ_b), right-angle tearing strengths (σ_{tr}) and breaking elongations (ϵ_b) of both the dry and wet blend membranes are higher than those of the nonblends. The values of σ_b , σ_{tr} and ϵ_b of RC-S4 are lower than that of other blends because of its inhomogeneity as seen from Figure 2. The degrees of crystallinity (X_c) and Young's modulus (E') of RC-S1, RC-S2 and RC-S3 blend membranes are significantly higher than those of the nonblend. It implies that the molecules are arranged more compactly in the blend membranes.

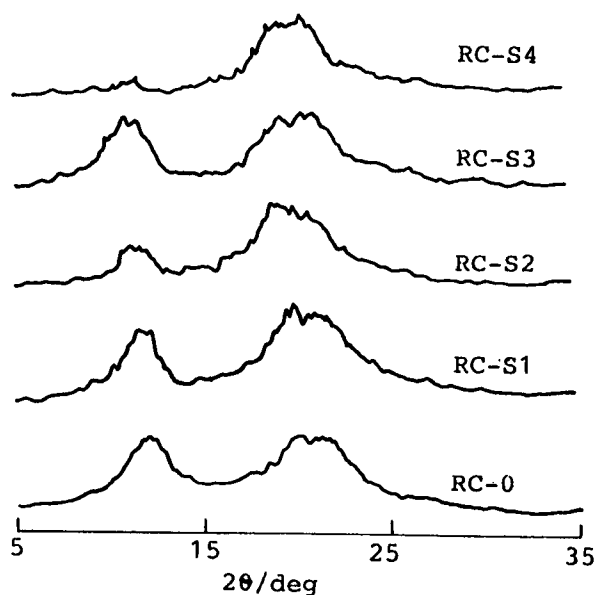


Fig 4. X-ray diffractograms of the membranes.

CONCLUSIONS

The membranes blended with cellulose cuoxam / casein were satisfactorily prepared. When the casein content of the mixture was smaller than 15%, the blend membranes were miscible. The good state of miscibility of the blends is due to the chemical interactions between the hydroxyl groups of cellulose and peptide bonds of casein as examined by IR, ^{13}C CP-MAS NMR, SEM. The strengths, Young's modulus and degrees of crystallinity for the blend

The experimental results of the mean pore diameter ($2\bar{r}_f$) and ethanol permeability (G) through the membranes are shown in table IV. The values of $2\bar{r}_f$ and G for the blends are higher than that of the nonblend. It is possible to produce the fine micro-phase separated structure of the nonpolar R group in the casein and increase the free volume, which provides it with correspondingly greater permeability and higher strength.

membranes in both dry and wet state are markedly higher than that of the nonblend. The permeability through the blend membranes are superior to the regenerated nonblended cellulose membrane.

Table N. The experimental results of structure, porosities and mechanical properties for the membranes

Membranes No.	σ_b (kg. cm ⁻²)		ϵ_b (%)		σ_r (kg. cm ⁻²)		$E' \times 10^{-10}$	$2r_f$	$G \times 10^{13}$	X_c
	dry	wet	dry	wet	dry	wet	dyne. cm ⁻²	Å	cm ³ . sec. g ⁻¹	%
RC-0	1040	316	17	44	329	80	4.7	72	6.7	32
RC-S1	1504	450	30	55	507	141	4.8	68	6.1	42
RC-S2	1597	371	32	73	433	122	5.2	89	9.6	46
RC-S3	1444	395	25	66	273	119	4.2	87	8.1	44
RC-S4	1254	316	10	44	309	99	3.9	101	11.3	35

ACKNOWLEDGMENTS

This project was supported by grants from Polymer Physics Laboratory, Changchun Institute of Applied Chemistry, Academis Sinica. We thank Dr. N. H. Young of Wuhan Institute of Physics, Academia Sinica, and Dr N. Yao of Hubei Research Institute of Chemistry for their assistance in performing the NMR and X-ray diffraction experiments.

REFERENCES

1. N. Nishioka, K. Watase, K. Arimura, K. Kosai, M. Uno, *Polymer J.* 16 (12), 867 (1984)
2. Y. Nishio, S. K. Roy, R. S. J. Manley, *Polymer*, 28, 1385 (1987)
3. J. F. Masson and R. S. J. Manley, *Macromolecules*, 24, 5914, (1991)
4. L. Zhang, G. Yang, W. Fang, *J. Membrane Sci.*, 56, 207 (1991)
5. W. Brown and R. Wikström, *Eur. Polym. J.*, 1, 1 (1965)
6. L. Zhang, G. Yang, S. Yan and H. Liu, Chinese Patent, Application CN 93101825.0, 14, Feb. 1993.
7. J. F. Rabek, *Experimental Methods in Polymer Chemistry: Applications of wide-angle x-ray diffraction (WAXS) to the study of the structure of polymers*, Wiley Interscience, Chichester, 1980, P. 505
8. L. Zhang, G. Yang, *Chinese J. Appl. Chem.*, 8 (3), 17 (1991)

9. W. Kuhn, Z. Electrochem., Ber. Bunsenges. Physik. chem., 55, 207 (1951)
10. Sadtler Standard Carbon-13 NMR spectra, Vol. 18, 3491C, Researchers, USA, 1978.
11. K. Kamide, K. Okajima, T. Matsui, K. Kowsaka, Polymer J., 16(12), 857 (1984).
12. J. F. Masson and R. S. J. Manley, Macromolecules, 25, 589. (1992)

53 On the use of clouding polymers for purifying chemical systems

G Karlström*, H-O Johansson** and F Tjerneld** – * Department of Theoretical Chemistry, ** Department of Biochemistry, Chemical Centre, University of Lund, S-221 00 Lund, Sweden

ABSTRACT

The possibility of using clouding polymer - water systems for purification of chemical systems is investigated by both theoretical and experimental means. It is found that the most important parameter governing the purifying capacity of the polymer - water system with respect to the additive is the difference in interaction between the additive and the polymer and the additive and water. The importance of the degree of polymerization and the distance from the critical point in the phase diagram is also investigated. In particular it is shown that it is easier to remove high molecular weight compounds than low molecular weight compounds, and that it is optimal to work at a temperature well above the clouding temperature of the polymer water system. The theoretical results can be applied to experimental results from aqueous solutions of PEO (poly(ethylene oxide)), UCON (a random copolymer of ethylene oxide and propylene oxide) and EHEC (ethyl (hydroxyethyl) cellulose) as polymers, and different ionic and nonionic substances as additive.

INTRODUCTION

Aqueous polymer solutions have been used for purifying chemical systems for a long time, and a good introduction to the subject is given by Albertsson (Albertsson 1986). In that work the thermodynamical background for the partitioning of a substance between two polymer phases is given based on a phenomenological approach together with a set of empirical rules describing the partition of a substance between two phases. The theoretical background for these rules is not always fully understood.

The main use of these systems are in biochemical applications and thus the solvent normally is water and frequently one of the two polymers used to create the two phase system contains ethylene oxide groups. Typical examples of such polymers are polyethylene oxide (PEO), copolymers of ethylene oxide and propylene oxide (UCON and Pluronic) and substituted cellulose derivatives such as e.g. ethyl (hydroxyethyl)-cellulose (EHEC). Many of these ethylene oxide containing groups have the common

property of a decreased solubility in water at elevated temperatures. Thus at a certain temperature (the clouding temperature) an aqueous polymer solution phase separates into two isotropic phases. This process depends on addition of cosolutes to the water, and in a recent work we showed (Zhang et al 1992) that if the cosolute preferred to interact with either the solvent or the polymer strong enough, then the cosolute induced phase separation, whereas the opposite condition stabilized a one phase system. This property actually makes the clouding polymer solutions a good tool to study effective intermolecular interactions in aqueous solutions.

Unfortunately the fact that the additive affects the phase equilibrium, and thus the length of the tielines, complicates the rationalization of the forces governing the purifying process. In the next section we will first briefly discuss the relation between the phase behaviour of a system consisting of water and a clouding polymer and the intermolecular interactions in the system. That section will also deal with the partitioning of the additive between the two phases in such systems above the clouding temperature. In the last section the partitioning of an additive between the two phases in an "ordinary two polymer system" will be discussed.

THEORETICAL BACKGROUND AND APPLICATION FOR A ONE POLYMER SOLVENT SYSTEM.

The purpose of this section is to present the necessary theoretical background for analyzing how an additive is distributed between two phases. The starting point is the Flory-Huggins polymer theory and a two conformational description of the polymer (Karlström 1985). The basic assumption here is that each segment of the polymer may exist either in a polar or a nonpolar conformation. The polar conformations are energetically favored and the nonpolar are entropically favored. The polar conformations interact favorably with water whereas the nonpolar ones interact less favorably with water. Using these assumptions it is possible to write the entropy and energy of the system according to (Zhang et al 1992)

$$S = -nR \left(\sum_{i=1}^m \left(\frac{\phi_i}{M_i} \ln \phi_i + \phi_i \sum_{j=1}^{l(i)} P_{i,j} \ln \frac{P_{i,j}}{F_{i,j}} \right) \right) \quad (1)$$

and

$$U = n \sum_{i=1}^m \phi_i \sum_{j=1}^{l(i)} P_{i,j} \sum_{i'=1}^m \phi_{i'} \sum_{j'=1}^{l(i')} P_{i',j'} w_{i,j,i',j'} \quad (2)$$

In these equations n equals the total number of moles in the system and R the gas constant. The ϕ is the mole fraction of the components and M the degree of polymerization of the components, the P specifies the amount of different types of conformations of each component, the F specifies the ratio of the abundance of different types of conformations and finally w is the interaction parameter. The interested reader is referred to the original work for more details. Assuming equations 1 and 2, the free energy of the system can be calculated according to $A = U - TS$. Using these equations one can derive the effect on the phase behaviour of an additive. This was previously

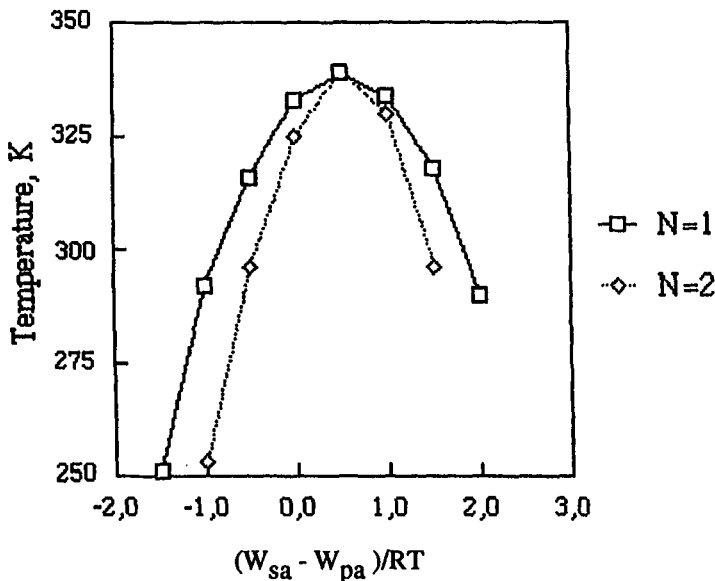
done for a polymer with only one conformation and with infinite chain length. The following relation was obtained

$$-0.5 RT > (w_{sa} - w_{pa}) > 1.5 RT \quad (3)$$

In equation 3 w is an interaction parameter and subscripts s , a and p stands for solvent, additive and polymer respectively.

In figure 1 we show variation of the clouding temperature obtained for a typical clouding polymer with a degree of polymerization of 78 as a function of the interaction between the polymer and the additive and the solvent and the additive. The effect of doubling the degree of polymerization for the additive is also shown. For an infinite chain length on the additive one obtains a cloud point lowering for all differences between $w_{sa} - w_{pa}$ except when the difference is $0.5RT$. Formally there is one interaction parameter between the polar polymer conformation and the additive and one between the nonpolar polymer conformation and the additive. These are in all applications discussed in this work chosen to be the same.

Figure 1. Cloud point in studied system as a function of interaction parameter and degree of polymerization of the additive.



The degree of polymerization of the polymer is 78. N is the degree of polymerization of the additive. The system composition is 72% water, 24% polymer and 4% additive (mol%). The clouding temperature of the pure polymer - water system is 323 K.

We have now seen how the additive affects the phase equilibrium in the system and will now investigate the partitioning of an additive between two phases of different composition in terms of an entropic and an energetic contribution. It will be assumed

that the amount of the additive is infinitely small and that the additive has a degree of polymerization of M_a . Under these assumptions we may derive an apparent entropy of solvation in a phase which is independent of the conformational equilibrium in the system.

$$\frac{dS}{dn_a} = -R \left[\frac{1}{M_a} (1 + \ln \phi_a) - \phi_s - \frac{\phi_p}{M_p} \right] \quad (4)$$

and an apparent energy of solvation equal to

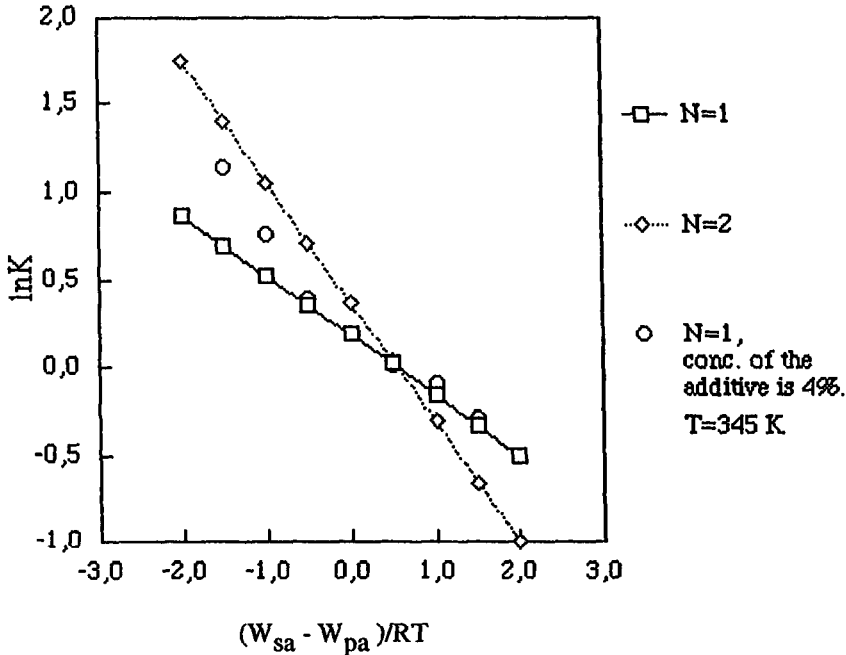
$$\begin{aligned} \frac{dU}{dn_a} = & -[\phi_s \phi_p (P w_{sp} + (1-P) w_{su}) + \phi_p^2 (1-P) (P w_{pu} + (1-P) w_{uu}/2)] \\ & + \phi_s w_{sa} + \phi_p (P w_{pa} + (1-P) w_{ua}) \end{aligned} \quad (5)$$

In equation 4 and 5, ϕ is the mole fraction. P in equation 5 is a measure of the probability of finding a polymer segment in a polar conformation and $(1-P)$ is the probability for finding it in a nonpolar conformation. The subscripts p and u refer to these conformations. Similar expressions have been determined for the partition of a molecule between two polymer rich phases without internal degrees of freedom (Walter et al 1985). From equation 4 we see that the additive prefers a phase consisting of monomeric species. This corresponds to what is often called the excluded volume effect. Equation 4 indicates that there is no excluded volume, rather that the available volume is larger in a monomeric solvent than in a polymeric one. Phases where the dU/dn_a is as small as possible are energetically favored, and this means that close to the critical point, where the $w_{sp\text{ eff}}$ reaches its maximum value $0.5RT$ in a stable phase, the energy is as favorable as possible for dissolving the additive with constant interaction parameters between the solvent and the additive as well as between the polymer and the additive. If however the preference of the additive for either the polymer or for the solvent is too large (see equation 3) then the additive will induce phase separation.

In practice this means that if we have a real system made up from water and a clouding polymer and the additive is a moderately hydrophobic substance and if we are interested in where the additive is found at temperatures above the clouding temperature, the entropic contribution would favor the water phase whereas the energetic contribution favors the polymer rich phase. If the additive is more polar than water (a salt) then both the energetic and the entropic contributions favor the water phase as the solvent phase. In figure 2 we show the variation of the partition coefficient K as a function of the variation of the interaction parameters for a model system (see Johansson et al 1993 for more details). The theoretically derived results obtained from equations 4 and 5 at infinite dilution are shown as straight lines in the figure. The difference in slope for M_a equals 1 and 2 comes from the fact that both the entropy and the energy contributions for two "monomeric units" are twice that for one "monomeric unit". If the additive is a salt one must calculate the contribution from each of the ions independently and then make sure that both phases are electrically neutral.

If the polymer in the system phase separates out of the solution at higher temperatures then one must treat the problem of phase behaviour and distribution simultaneously but the results can easily be understood in terms of the mechanisms discussed above. In table 1 we show the distribution of an additive between the two phases in a system consisting of a solvent and a clouding polymer for different values of interaction parameters and

Figure 2. $\ln K$ for additives as a function of interaction parameter and degree of polymerisation used for the additive.



The system composition is: 75% water, 24% polymer and 0.01 % additive (conc in mol%). The temperature is 338K, i.e. 15 K above the cloud point

temperature. Table 1 shows the clouding temperature and the composition of the different phases at different temperatures and different effective interaction parameters for the additive. From table 1 it is clear that most additives prefer the water rich phase unless the additive is unpolar. This is to a large extent due to the larger entropy of mixing for the additive in the polymer free phase.

PARTITIONING OF AN ADDITIVE BETWEEN TWO POLYMER PHASES.

In the previous section we discussed the partitioning of an additive between a solvent rich phase (water) and a polymer rich phase. Having solved this problem it is an easy task to establish the equilibrium between two phases each containing mainly one of the two considered polymers and solvent. The procedure to follow is to first establish the phase diagram for the system and then to use generalizations of equations 4 and 5 to calculate the entropy and the energy of solvation in each of the phases.

In practice the rules governing the partitioning are simple: the additive prefers the phase with as little polymer with as low molecular weight as possible from an entropic point of view and prefers the phase with the most attractive interaction parameters from an energetic point of view.

When clouding polymers are used one has the possibility to use the temperature as a parameter, and in particular one may choose to remove the phase containing the clouding polymer if it contains the additive. When this phase is heated above the clouding

temperature the additive is frequently found in the small water phase which is formed. The clouded polymer can then be recycled and used to extract more of the additive from the bulk phase (Harris, Karlström, Tjerneld). Since the additive is found in the small water phase one has obtained a concentrated water solution of the additive.

Table 1. Calculated partition coefficient as a function of temperature and interaction parameters

	Effective interaction parameter $(w_{sa} - w_{pa})/R^* 323$			
	-1	0.	1.	2.
clouding temperature (K)	291	332	334	290
partitioning data at $C_p + 5$ K				
polymer conc in phase 1	12.70%	15.71%	15.28 %	16.12%
polymer conc in phase 2	42.13%	36.31%	33.62%	40.46%
partition coefficient ^a	1.63	1.12	0.93	0.68
partitioning data at $C_p + 10$ K				
polymer conc in phase 1	9.03%	12.35%	12.11 %	12.51%
polymer conc in phase 2	45.92%	38.80%	36.05%	42.81%
partition coefficient ^a	1.83	1.15	0.91	0.63
partitioning data at $C_p + 20$ K				
polymer conc in phase 1	5.18%	8.45%	8.46%	7.92%
polymer conc in phase 2	50.16%	41.45%	38.62%	45.60%
partition coefficient ^a	2.06	1.19	0.89	0.57

a) partition coefficient is the ratio of the concentrations of the additive in the water rich and the polymer rich phases.

The opportunity to recycle one of the polymers and use it in a new purification step opens up a new possibility, since this enables the use of more expensive polymers in the purification process. One tempting procedure would be to use a chemically modified polymer, which e.g. contains a ligand that binds a molecule which one wants to remove from the solution (Alred et al 1992).

REFERENCES

- Albertsson P-Å. (1986) Partition of Cell Particles and Macromolecules, 3 rd ed. Wiley, New York.
- Alred P.A., Tjerneld F., Kozlowski A. and Harris J.M. (1992) Bioseparation, 3,363.
- Harris P.A., Karlström G. and Tjerneld F., (1991) Bioseparation, 2,237.
- Johansson H-O., Karlström G. and Tjerneld F. (1993) submitted for publication.

Karlström G., (1985), *J. Phys. Chem.* 89,4962.

Walter H., Brooks D.E., and Fisher D. *Partitioning in Two Phase Aqueous Systems* (1985) Academic, Orlando, FL, 1985

Zhang K-W., Karlström G.and Lindman B.(1992), *Colloids and Surfaces*, 67,147.

54 Surfaces coated with ethyl(hydroxyethyl) cellulose: Temperature effects on adsorption and interaction

P M Claesson and M Malmsten – The Laboratory for Chemical Surface Science, Department of Physical Chemistry, The Royal Institute of Technology, S-100 44 Stockholm, Sweden and The Institute for Surface Chemistry, Box 5607, S-114 86 Stockholm, Sweden

ABSTRACT

The temperature dependence of the forces acting between hydrophobic surfaces coated by a layer of ethyl(hydroxyethyl) cellulose, (EHEC), has been studied as a function of separation and temperature. Both the situation where the adsorbed amount is kept constant and where the adsorbed amount is allowed to vary with temperature have been explored. In both cases the surface interaction is very temperature sensitive due to the temperature dependent interactions between ethylene oxide groups and water. The results are discussed and related to the protein repelling properties of EHEC coated surfaces and EHEC as a steric stabilizer.

INTRODUCTION

The properties of polymers at interfaces are of great importance in many practical situations. For instance for determining polymers ability to act as stabilizers in e.g. paints and foodstuff, and as "biocompatible" or "protein repellent" coatings in medical applications. For these applications it is important that the polymer is firmly anchored to the surface and yet form a layer that extends sufficiently far out in the solution to give rise to a strong long-range steric repulsion that prevents unwanted flocculation or adsorption. These requirements are often at odds with each other since polymers adsorb strongly when the segment-surface affinity is high and the solvency bad. Under these conditions, however, the adsorbed layer is likely to give rise to no, or a very limited, barrier against flocculation. The situation can be improved by using random- or block-copolymers which contain some segments or blocks

that are firmly anchored to the surface while other segments have a high affinity for water and provide the steric repulsion. One example of such a heterogeneous co-polymer is ethyl(hydroxyethyl)cellulose (EHEC), a nonionic cellulose ether that consists of a cellulose backbone which is substituted with ethyl groups and oligo(ethylene oxide) chains.

The adsorption properties of EHEC, especially regarding the effects of temperature, cosolutes and surface hydrophobicity, have been studied by in situ ellipsometry (Malmsten and Lindman, 1990). It was found that the adsorbed amount increased with temperature and with the hydrophobicity of the substrate surface. In this paper we review some of our data concerned with the temperature dependent interactions between adsorbed layers of EHEC (Malmsten et al., 1990b; Malmsten et al., 1991; Claesson et al., 1991; Pezron et al., 1991).

MATERIALS AND METHODS

Polymer characteristics

EHEC polymers were supplied by Berol Nobel AB, Sweden. Two fractions of EHEC were used. Both fractions are polydisperse but the average properties of the EHEC samples are given in table 1. On heating, EHEC shows a lower consolute temperature. Hence, at low temperature, aqueous EHEC solutions are clear, isotropic one phase systems, whereas EHEC solutions at higher temperatures separate into two phases. The lower temperature phase boundary is usually referred to as the cloud point (CP). The cloud points for the EHEC fractions used are given in table 1. A similar phase behaviour is observed for ethylene oxide polymers and ethylene oxide surfactants. Force measurements have demonstrated that the interactions between ethylene oxide surfactants adsorbed on hydrophobic surfaces (Claesson et al., 1986, 1991) are strongly temperature dependent, consistent with the observed phase behaviour.

	EHEC 1	EHEC 2
Molecular weight	250.000 g/mol	475.000 g/mol
Radius of gyration at 20°C, 0.2 M NaCl	800 Å	850 Å
Molar substitution of ethyl groups	1.4	1.7
Molar substitution of ethylene oxide groups	0.9	1.0
Cloud point	39° C	35° C

Table 1. Some average properties of the EHEC fractions used

Surface preparation

Mica surfaces were rendered hydrophobic by deposition of a monolayer consisting of a 1:1 mixture of eicosylamine and eicosanol (EA/EO) dissolved in a chloroform/ethanol mixture (49:1). The deposition was

done with a computerized Langmuir trough system (KSV Chemicals, Helsinki) enclosed in a laminar flow cabinet. Details of the properties of this mixed monolayer have been reported elsewhere (Yaminsky et al, 1993, Berg et al. 1993) and the deposition procedure has been described (Malmsten et al. 1990). The advancing and receding contact angle on the hydrophobic surface was about 112° and 80°, respectively.

The surface force apparatus

Measurements of the forces acting between two hydrophobic substrate surfaces coated with EHEC were carried out with a surface force apparatus Mark II (Israelachvili and Adams, 1978) or Mark IV (Parker et al., 1989). The two interacting surfaces are mounted in a crossed cylinder geometry. This geometry is experimentally suitable, and the measured force, F_c , divided by the local geometric mean radius of the cylinders, R , is related to the free energy of interaction per unit area between two flat surfaces, G_f (Derjaguin, 1934)

$$F_c(D)/R = 2\pi G_f(D) \quad [1]$$

This relation is valid provided that the radius of the cylinders (about 2 cm) is much larger than the surface separation (D), and provided that the surface radius does not change with surface separation (Parker and Attard, 1992). The latter requirement is not fulfilled for the strongest forces reported in this publication. The distance between the surfaces is determined with an accuracy of 0.2 nm using multiple beam interferometry. The force is measured from deflections of a double variable cantilever spring supporting the lower surface. The detection limit is about 10^{-7} N.

RESULTS AND DISCUSSION

Forces at room-temperature

The forces measured between hydrophobic surfaces coated with EHEC 1 and with EHEC 2 about 15°C below the cloud point are illustrated in figure 1. The EHEC concentration is such that the adsorption plateau value has been reached (Malmsten and Lindman, 1990). No significant forces are measured until the separation is less than 1500 Å. At smaller distances the force increases nearly exponentially with decreasing separation. Two things are worth noticing: First, the range of the repulsive force is significantly lower than four times the radius of gyration (3200 Å). This shows that the polymer does not adsorb as a random coil but in a significantly more flat conformation. Secondly, despite the fact that EHEC 2 has about twice the molecular weight compared to EHEC 1 the range of the forces is similar for the two EHEC fractions. The distance dependence of the force is also very similar for the two fractions.

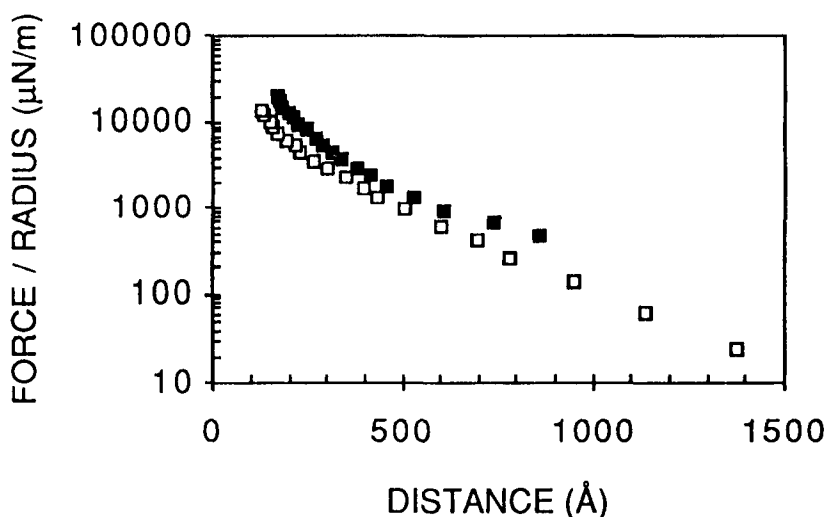


Figure 1. Force normalized by radius as a function of separation for EHEC coated surfaces at 15° C below the cloud point. ■ represent forces between surfaces coated with EHEC 1 across a 0.1 wt% aqueous EHEC solution. □ represent forces between surfaces coated with EHEC 2 across a 0.25 wt% EHEC solution

These results support the idea that EHEC adsorbs in a rather flat conformation on these hydrophobic surfaces. It also appears that the polydispersity of the system is not very important for the measured force profile in these cases with a rather strong segment-surface affinity. The same forces were measured on approach and on separation (Malmsten et al., 1990b, 1991), indicating that the measurements were carried out under quasiequilibrium conditions. This means that all changes in the layer occur slowly (e.g. desorption/adsorption) or rapidly (e.g. conformational changes) compared to the time scale of the measurement.

Temperature-dependent forces, constant adsorbed amount

These experiments were performed with EHEC 1. A droplet of 0.1wt% EHEC solution was placed between the surfaces and the force measured as a function of surface separation (see figure 1). In the next step, the apparatus was filled with water, the adsorbed polymer layer was allowed to equilibrate according to the new situation (EHEC concentration about 0.0001%), and the forces were measured again at different temperatures. It was found that the range of the forces at 25°C decreased slightly upon dilution during the first hour but after that remained constant (figure 2). We interpret this as a slight initial desorption of EHEC, consistent with ellipsometric data (Malmsten and Lindman, 1990). The range of the

forces decrease strongly as the temperature is increased to 44°C, demonstrating that the adsorbed layer contracts significantly (figure 2).

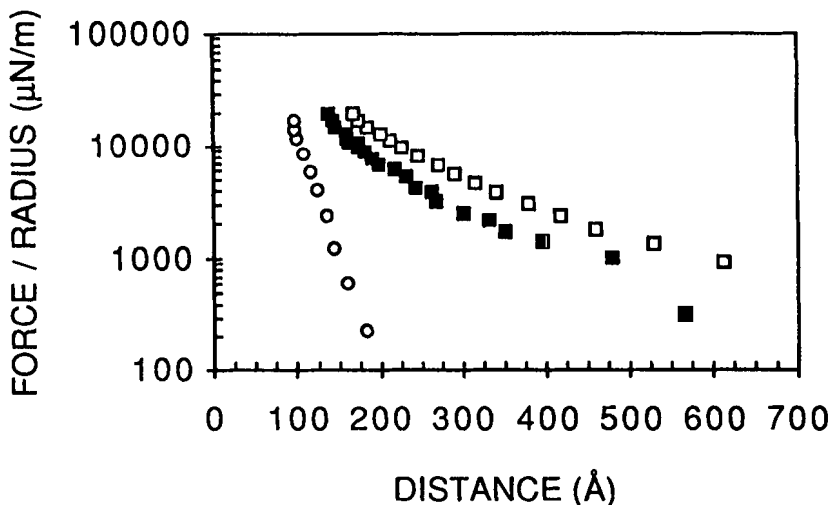


Figure 2. Force normalized by radius as a function of separation for surfaces coated with EHEC 1. □ represent forces measured across a 0.1 wt% solution at 25°C, ■ represent forces measured after dilution at 25°C, ○ represent forces measured after dilution at 44°C.

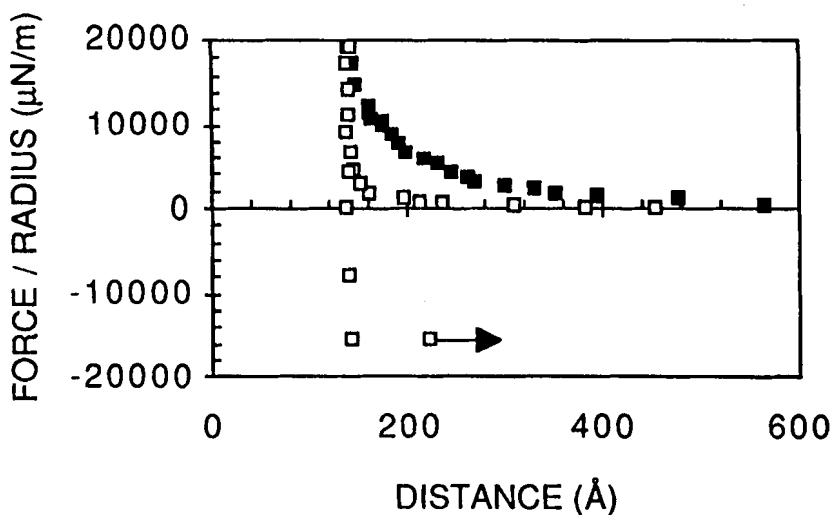


Figure 3. Force normalized by radius as a function of separation for surfaces coated with EHEC 1. ■ represent forces measured at 25°C and □ forces at 55°C

It is worth noting that despite the fact that the temperature is 5°C above the cloud point the force remains purely repulsive and the same on approach and on separation. It is only when the temperature is increased significantly above the cloud point that an attractive force component is observed. This situation is illustrated in figure 3, which compares the forces measured at 55°C with those observed at 25°C. It should be noted that all changes observed with temperature are reversible.

The contraction of the EHEC layer with increasing temperature is related to the temperature dependence of the interaction between ethylene oxide groups and water (Kjellander, 1982; Karlström, 1985). Hence, EHEC will have a more hydrophobic character at higher temperatures resulting in an increasing train fraction whereas the population and average length of loops and tails decrease with increasing temperature (Scheutjens and Fleer 1979, 1980). Since EHEC is a heterogeneous polymer we suggest that segregation occurs with hydrophobic segments close to the surface and hydrophilic segments preferentially oriented towards the bulk solution. This orientation of hydrophilic groups towards the solution lowers the local χ -parameter and thus is one important reason why no attraction is observed at 44°C (5°C above the cloud point). The other reason is that at this temperature the polymer layer is very compact which results in a significant entropic repulsion, due to low interpenetration of the polymer layers. It is only well above the cloud point (55°C, figure 3) that also the outermost segments experience poor solvency conditions and thus a short-range (but strong) attraction develops. On further compression the entropic repulsion dominates.

The possibility that polymers may stabilize dispersions at worse than θ -conditions, so called 'enhanced steric stabilization', has been discussed previously (Dobbie et al., 1973; Lambe et al. 1978). In particular it has been observed that EHEC has the ability to stabilize polystyrene particles at temperatures well above the cloud point (Malmsten and Tiberg, 1993), consistent with the findings reported here.

A second consequence of the contraction of the EHEC layer and the decreasing steric repulsion is that adsorption onto EHEC-coated surfaces will occur more easily at higher temperatures provided that the amount of EHEC on the surface remains constant. The same is true for other poly(ethylene oxide) containing polymers (Gölander, 1992). This phenomenon has recently been discussed in more detail (Claesson, 1993).

Temperature-dependent forces, variable adsorbed amount

The adsorption of EHEC onto hydrophobic surfaces increases strongly when the temperature is increased up to the cloud point (Malmsten and Lindman 1990; Malmsten and Claesson 1991) For EHEC 2 on hydrophobised mica the adsorbed amount increases from 5 mg/m² at 20 °C to 15 mg/m² at 52°C. This means that when the adsorbed amount is

allowed to vary with temperature the compressed layer thickness and the repulsive forces observed at distances below about 800 Å increase significantly (figure 4).

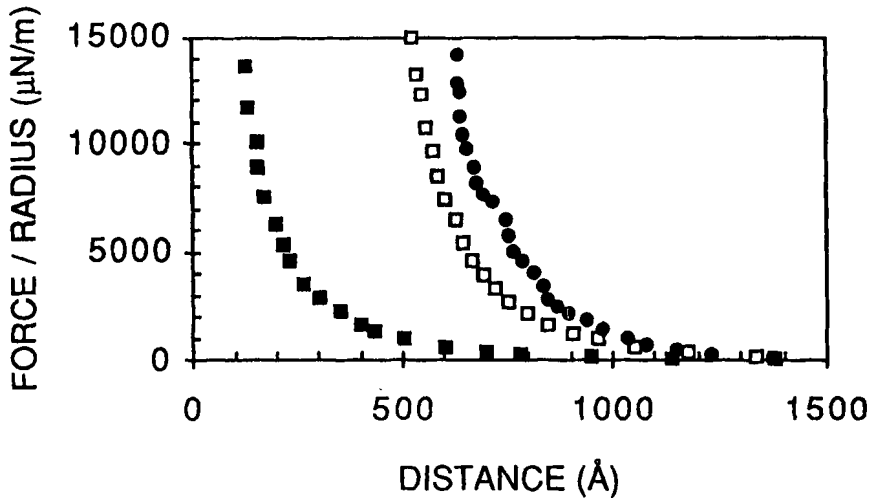


Figure 4. Force normalized by radius as a function of separation for surfaces coated with EHEC 2 across a 0.25 wt% EHEC solution. The temperature was 20°C (■); 37°C (□); and 41°C (●)

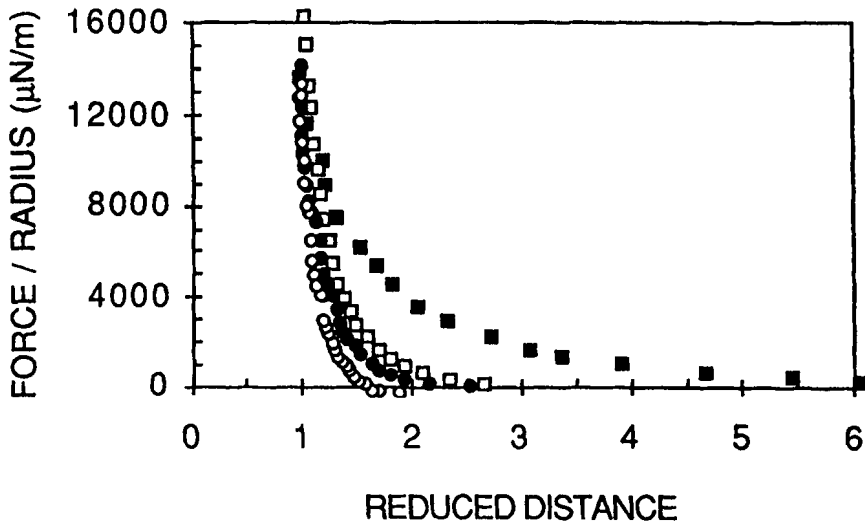


Figure 5. Force normalized by radius as a function of reduced distance for surfaces coated with EHEC 2 across a 0.25 wt% EHEC solution. The temperature was 20°C (■); 37°C (□); 41°C (●); and 52°C (○)

However, it is clear that also in this case the decreased solvency results in an adsorbed layer that is more compact at the higher temperatures. This can clearly be seen when the force curve is plotted against the normalized separation, i.e. the separation divided by the layer thickness obtained under a high load ($F/R \geq 20.000 \mu\text{N/m}$). Such a plot, which provides information about how far polymer tails and loops extend relative to the compact part of the adsorbed layer, is shown in figure 5.

This type of presentation of the force curves demonstrates a remarkable resemblance of the forces obtained at different temperatures for EHEC layers having a constant adsorbed amount (5 mg/m^2) and those obtained when the adsorbed amount is allowed to vary (the adsorbed amount is about 15 mg/m^2 at $40\text{-}55^\circ\text{C}$). This is clearly seen in figure 6.

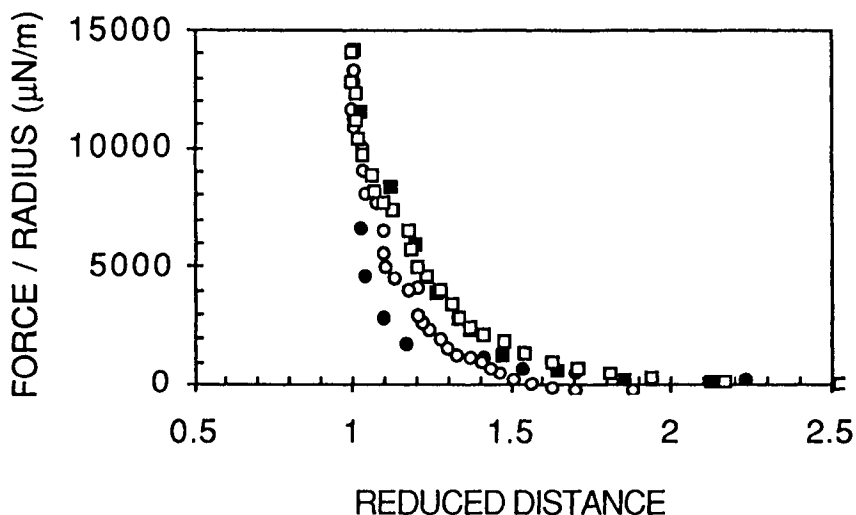


Figure 6. Force normalized by radius as a function of reduced distance for surfaces coated with EHEC 2 across a 0.25 wt% EHEC 2 solution. The temperature was 41°C (\square); and 52°C (\circ). Surfaces precoated with EHEC 1 across water. The temperature was 44°C (\blacksquare); and 55°C (\bullet)

For a given temperature the force is determined by the segment distribution profile away from the surface. Hence, the fact that the force law scales very closely with the compressed layer thickness indicates that for these compact adsorbed layers the decay of the segment distribution profile scales similarly.

REFERENCES

Berg, J. 1993 "Molecular Films on Mica Surfaces", PhD-thesis, Royal Institute of Technology, Stockholm, Sweden

Claesson, P.M.; Kjellander, R.; Stenius, P.; Christensson, H.K.; **1986** *J. Chem. Soc. Faraday Trans. I* 82, 2735

Claesson, P.M.; Bergenståhl, B.A.; Eriksson, J.C.; Herder, C.E.; Pezron, E.; Pezron, I.; and Stenius, P., **1990** *Faraday Discuss Chem. Soc.* 90, 129

Claesson, P.M.; Malmsten, M.; Lindman, B. **1991** *Langmuir* 7, 1441

Claesson, P.M. **1993** *Colloid and Surfaces A* 77, 109

Derjaguin, B.V. **1934** *Kolloid-Z.* 69, 155

Dobbie, J.W.; Evans, R.; Gibson, D.V.; Smitham, J.B.; Napper, D.H. **1973** *J. Colloid Interface Sci.* 45, 557

Gölander, C.G.; Herron, J.; Lim, K.; Claesson, P.M.; Stenius, P.; Andrade, J.D.; **1992** in J.M. Harris (Ed), "Biomedical applications of polyethyleneglycol chemistry", Plenum Press

Israelachvili, J.N.; Adams, G.E. **1978** *J. Chem. Soc. Faraday Trans. I* 74, 975

Kjellander, R. **1982** *J. Chem. Soc. Faraday Trans 2* 78, 2025

Karlström, G. **1985** *J. Phys. Chem.* 89, 4962

Lambe, R.; Tadros, Th.F.; Vincent, B. **1978** *J. Colloid Interface Sci.* 66, 77

Malmsten, M.; Lindman, B. **1990** *Langmuir* 6, 357

Malmsten, M.; Claesson, P.M.; Pezron, E.; Pezron, I. **1990b** *Langmuir* 6, 1572

Malmsten, M.; Claesson, P.M., **1991** *Langmuir* 7, 988

Malmsten, M.; Tiberg, F. **1993** *Langmuir* 9, 1098

Parker, J.L.; Christenson, H.K.; Ninham, B.V. **1989** *Rev. Sci. Instrum.* 60, 3135

Parker, J.L.; Attard, P. **1992** *J. Phys. Chem.* 96, 10398

Pezron, I.; Pezron, E.; Claesson, P.M.; Malmsten, M. **1991** *Langmuir* 7, 2248

Scheutjens, J.M.H.M.; FLeer, G.J. **1979** *J. Phys. Chem.* 83, 1619.

Scheutjens, J.M.H.M.; FLeer, G.J. **1980** *J. Phys. Chem.* 84, 178.

Yaminsky, V.V.; Claesson, P.M.; and Eriksson, J.C. **1993** *J. Colloid Interface Sci.*, 161, 91

55 Sodium cellulose sulphate as a component for polyelectrolyte complex formation—preparation, characterisation, testing

H Dautzenberg, B Lukanoff and K Neubauer – Research group 'Polyelectrolyte Complexes', University Potsdam, Kantstr 55, 14513 Teltow, Germany

Abstract

Heterogeneous sulphation of cellulose with a mixture of H_2SO_4 /propanol has been studied as a possible method for obtaining sodium cellulose sulphate suitable for the preparation of capsules by polyelectrolyte complex formation. Product parameters like water solubility and DS as well as viscosity of the water soluble parts of the sodium cellulose sulphate preparations have been investigated for their dependence on reaction conditions like time, temperature, or molar ratio H_2SO_4 /propanol. Capsule formation was tested with poly-(diallyldimethyl ammonium chloride) as cationic counterpart. Capsule properties such as size, mechanical strength, or dry mass and thickness of the capsule wall were compared with those of capsules generated from cellulose sulphate preparations obtained under homogeneous reaction conditions.

Introduction

The reaction between countercharged polyelectrolytes in highly diluted solution mostly yields irregular particular precipitates. Polyelectrolyte complex (PEC) formation, however, can also result in membrane-like polymer network structures. As we found some years ago (Dautzenberg et al., 1980) microcapsules consisting of a semipermeable capsule wall and a liquid core are obtained by introducing droplets of the solution containing the anionic polymer into a precipitation bath containing the cationic polymer. Sodium cellulose sulphate (NaCS) with poly-(diallyldimethyl ammonium chloride) (Poly-DADMAC) as counterpart (Dautzenberg et al., 1985) has

proved to be one of the best combinations for that process of capsule formation. Investigations into several fields of application carried out so far confirmed that by encapsulation of proteins, enzymes, cells, or tissue without any noticeable loss in their activity, a variety of functioning biologically active systems useful in biotechnology and medicine can be created (Braun et al., 1985; Förster, 1991).

The first experiments were performed with homogeneously prepared NaCS samples (according to Wagenknecht et al., 1978). Despite the very promising results we eventually achieved with homogeneously prepared NaCS, we decided to stop using this type of NaCS because we saw very little chance for developing and implementing the necessary technical process for its production. We looked for possibilities to produce NaCS in an easier way and with less toxic and aggressive chemicals than $\text{SO}_2 / \text{N}_2\text{O}_4$. From the various alternatives reported in the literature, we selected the heterogeneous sulphating process of cellulose with H_2SO_4 /propanol as sulphating agent (Petropavlovskij, 1973, Lukanoff et al., 1990) for further investigations.

The aim of the present work was to find out whether it would be possible to prepare NaCS suitable for capsule formation by this heterogeneous sulphation process despite the well known unavoidable high hydrolytic chain length degradation of the cellulose in protic solvents. For that we investigated in detail how main product parameters like DS, water solubility and viscosity depend on the reaction conditions like time, temperature and molar ratio H_2SO_4 /propanol, on the reaction regime as well as on the cellulose starting material. Products obtained as water soluble sodium cellulose sulphates were tested with respect to their behaviour in the process of capsule formation using Poly-DADMAC as cationic counterpart of PEC formation. As far as possible correlation between capsule properties, such as size, mechanical strength, dry mass (polymer content) and thickness of the capsule wall, and product characteristics of the NaCS samples were studied. Results were compared with those found with homogeneously prepared NaCS samples.

Experimental

Sulphation

Cellulose starting materials were cotton linters ($\text{DP}_{\text{Cuoxam}} = 1400$), VHV (very high viscosity) pulp ($\text{DP}_{\text{Cuoxam}} = 1550$) and activated linters (treatment with 18 % NaOH, neutralisation with acetic acid, washing with water, substitution of water by propanol). The sulphating mixture was prepared separately by adding slowly precooled propanol to sulphuric acid (96 %) below 15 °C (molar ratio H_2SO_4 /propanol 0.9 to 3). After bringing the mixture to the reaction temperature (-10 to 22 °C) cellulose (30 to 90 g) was added (molar ratio H_2SO_4 /cellulose 11 to 32). To stop the reaction (after 15 min up to several days) the resulting sulphuric acid half ester of the cellulose was separated by filtration, washed with cold propanol/water (10/1 v/v) and neutralised with NaOH either in ethanol or water. Accompanying Na_2SO_4 was removed from the products by rinsing them with ethanol containing up to 40 % (v/v) water.

The final products were characterised by their DS (elemental analysis S, Na, or precipitation titration with Poly-DADMAC1, see capsule formation), by their amounts of the insoluble residue or the water soluble part, and by the viscosities of the soluble part dissolved in water (1 wt-%). In selected cases intrinsic viscosities (as measure for molar mass) were determined or elugrams were taken by SE chromatography (as measure for molar mass distribution).

Capsule formation

As cationic counterparts, two Poly-DADMAC samples of low molecular mass (LMM), $M < 10,000$ and one sample of higher molecular mass (HMM), $M \sim 30,000$ were used. Capsules were prepared by pressing the NaCS solution (4 wt-%) through a syringe needle and introducing the droplets into the stirred precipitation bath (PB) containing 2 wt-% Poly-DADMAC. The capsule formation was observed up to 6 hours either in water or in 0.12M NaCl solution as reaction medium. In every case mechanical strength and capsule mass were measured. In selected cases comprehensive characterisation comprised the additional determination of NaCS conversion, capsule size and shape, thickness and polymer content of the capsule wall (for experimental details see Dautzenberg et al., 1993).

Results and discussion

The experimental results of investigating the sulphating process are summarised in Figs. 1 to 5. At optimal molar ratio H_2SO_4 /propanol between 1.75 and 2.0 sulphation proceeds very fast already at low temperatures (Fig.1). For better control of the reaction it is advisable to choose a reaction temperature below $0^\circ C$. Maximum DS is at all temperatures below or about 1.0. DS values obtained at different temperatures are not markedly affected by changing the alcohol (2-propanol instead of 1-propanol) or addition of toluene as inert diluent (Fig.2). The reactivity of the sulphating system slightly increases by using 1-propanol instead of 2-propanol and decreases in presence of an diluent.

Under the aspect of product synthesis, correlation between DS, product solubility and viscosity of the water soluble part is of main interest. Fig.3 shows how these 3 parameters depend on the molar ratio H_2SO_4 /propanol (MR) at otherwise constant reaction conditions ($0^\circ C$, 2 hrs.). A noticeable conversion of linters only takes place if MR is above 1. DS steeply increases in the region above 1.5. Full water solubility is reached under these conditions at MR 2.0 or so and needs high DS (0.6), which is connected with high chain length degradation down to low viscosity (about 10 mPas). Activation strongly increases cellulose reactivity, thus causing a shift of the DS curve to much lower MR. The steep increase starts as early as $MR < 1$. The curves of the other two parameters show a similar shift. Full water solubility is already achieved at DS less than 0.4.

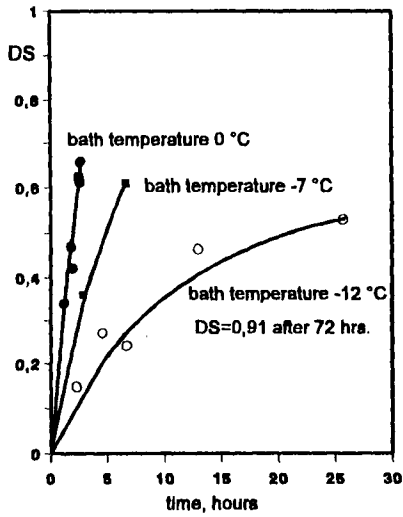


Fig.1. DS vs. reaction temperature (molar ratio $H_2SO_4/1$ -propanol: 0 °C ...2.0, -7 °C and -12 °C...1.75)

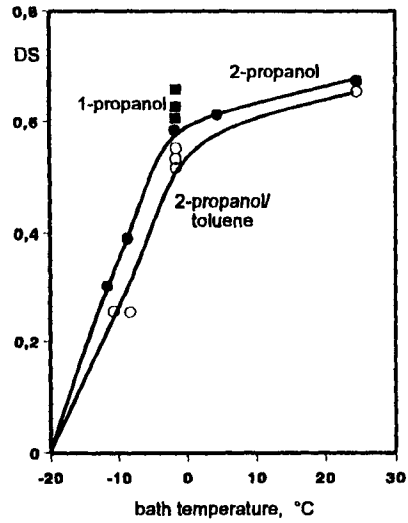


Fig.2. Sulphation of linters in presence of and absence from toluene as diluent (molar ratio H_2SO_4 /propanol: 2.0, 2 hrs.)

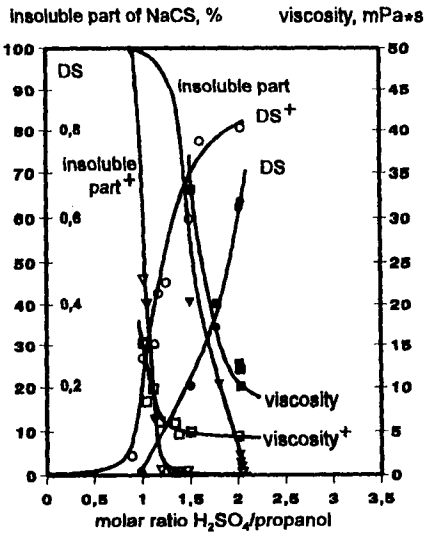


Fig.3. Product parameters of NaCS in dependence on the molar ratio $H_2SO_4/1$ -propanol (0 °C, 2 hrs.)

† cotton linters activated

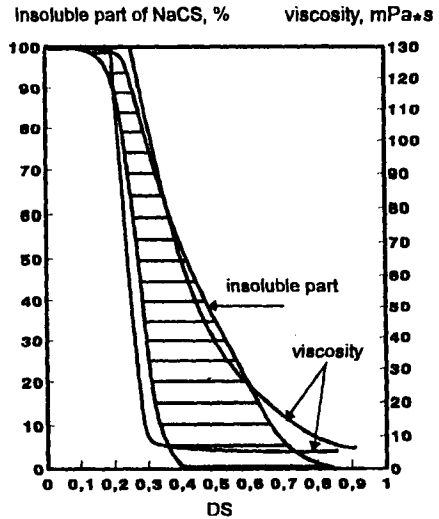


Fig.4. Correlation between DS, solubility and viscosity of NaCS samples prepared under different reaction conditions

Unfortunately, the competitive hydrolytic chain splitting reaction is obviously still more accelerated than esterification. This can be concluded from the very low viscosities obtained for sodium sulphates prepared from activated linters. As Fig.3 convincingly demonstrates, no fixed correlation exists between the three product parameters. It is therefore a question of optimising the process to find the reaction conditions that lead to maximum water solubility at lowest DS and a wanted high viscosity of the water soluble part.

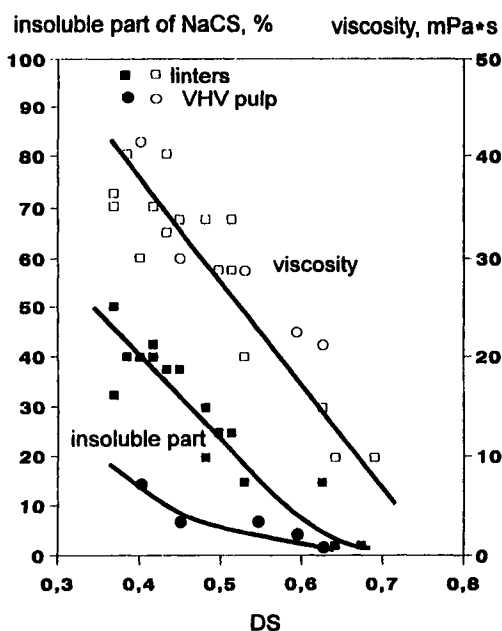


Fig.5. Effect of the cellulose starting material on the correlation between DS, solubility and viscosity of NaCS (molar ratio $H_2SO_4/1$ -propanol 1.6.....2.0, $-5^\circ C$, 2hrs.)

When all single correlation values found so far under various reaction conditions with different starting materials and under variation of the reaction regime are collected in one Figure, they stretch over the marked areas in Fig.4. From Fig.5 we learn that VHV pulp gives most promising results. It allows the maintenance of the same correlation between DS and viscosity as with linters, but reduction of the insoluble part at a given DS value. Fig.6 demonstrates that full water solubility of the product is generally connected with low product viscosities (below 10 mPas) independent of the DS necessary for reaching 100% solubility. Medium viscosity products (15 to 50 mPas) are attainable with different DS values (0.3 to 0.6) and various amounts of insoluble part (50 to 90 %) in dependence on the way chosen for preparing the NaCS.

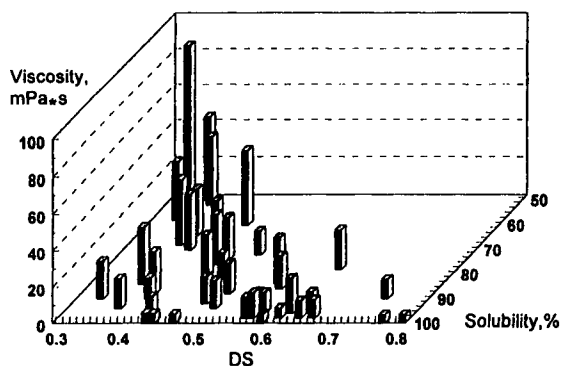


Fig.6. Correlation between water solubility of heterogeneously prepared NaCS samples and DS and viscosity of the soluble parts (prepared under variation of the cellulose starting material and the sulphating conditions)

Unexpectedly, it is even possible to get soluble parts having viscosities higher than 100 mPas. In that case, however, a low yield of the final product (water soluble part) has to be accepted. As far as insoluble parts have been analytically investigated, independent of their amount, low DS values between 0.05 and 0.1 and surprisingly low degrees of chain degradation (DP_{Cuoxam} up to 1000) are found.

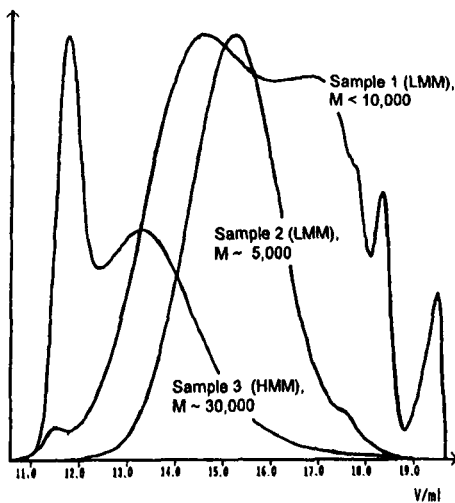


Fig. 7. Elugrams of Poly-DADMAC samples used for capsule formation with heterogeneously prepared NaCS samples (Column HEMA BIO 100, EM 0.5 M NaCl, flow rate 0.8 ml/min., RI detector)

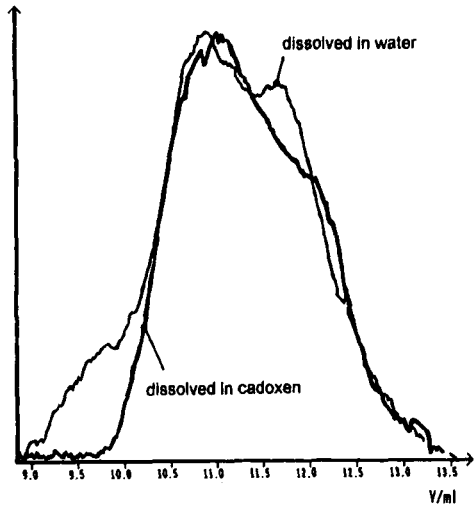


Fig. 8. Test elugram of sodium carboxymethyl cellulose (NaCMC) (Column HEMA BIO 40/ HEMA BIO linear, EM 0.05 M NaCl, flow rate 0.8 ml/min., RI detector)

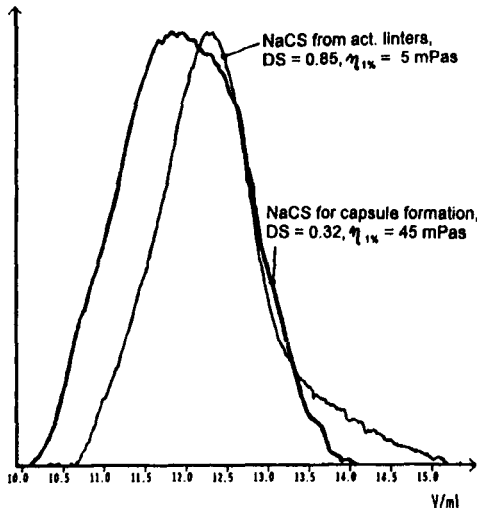


Fig. 9. Elugram of a heterogeneously prepared NaCS sample suitable for capsule formation in comparison to that of NaCS obtained from activated linters (Column HEMA BIO 40/ HEMA BIO linear, EM 0.05 M NaCl, flow rate 0.8 ml/min., RI detector)

Some preliminary SE chromatographic results are given in Figs. 7 to 9. Fig. 7 shows the elugrams of the Poly-DADMAC samples used for capsule formation. Fig. 8 reveals using sodium carboxymethyl cellulose as model substance the necessity of using a cellulose solvent in the dissolution step of the sample, because otherwise the elugram is disturbed by aggregates occurring in solution. Fig. 9 shows the elugram of a sample suitable for capsule formation in comparison to that of a low viscosity product obtained from activated linters.

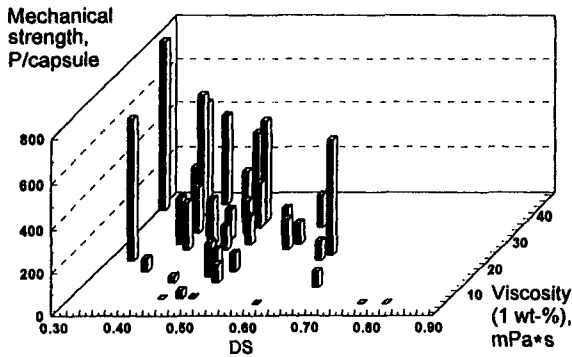


Fig.10. Mechanical strength of capsules in dependence on the DS and the viscosity of the NaCS samples used for capsule formation (Conditions of capsule preparation: 4wt-% heterogeneously prepared NaCS, 2wt-% Poly-DADMAC, reaction time 60 min., 23°C, reaction medium water)

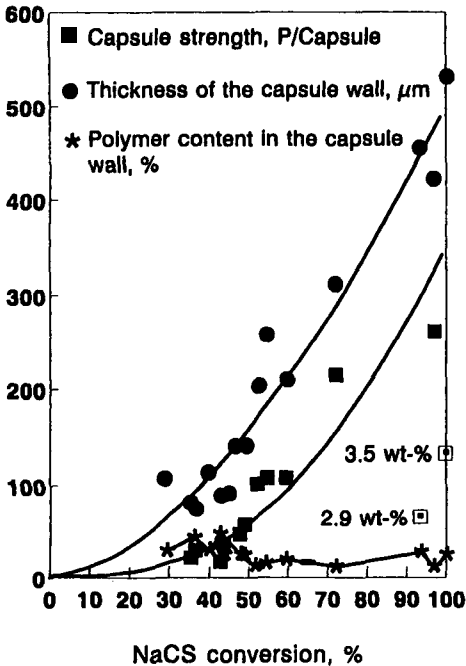


Fig.11. Parameters of capsules obtained from heterogeneously prepared NaCS samples as function of the NaCS conversion (Conditions of the capsule preparation: 4wt-% NaCS, 2wt-% Poly-DADMAC 1, reaction time 30 min. 23°C, reaction medium water)

As Fig.10 demonstrates, formation of capsules with heterogeneously prepared NaCS samples is possible. Their mechanical strength can reach a very high level. Viscosities above 15 mPas are necessary in order to obtain sufficient capsule strength, which further increases with increasing viscosity and decreasing DS. But due to the connection between DS and viscosity mentioned before, a dependence of capsule strength on DS can not be concluded. A quite close correlation seems to exist between capsule strength and the degree of NaCS conversion (Fig.11). This appears reasonable. Differences in NaCS conversion are brought about by differences in the properties of the NaCS samples used. It is worth mentioning that capsule strength is not necessarily lower if the NaCS concentration in the starting droplet is reduced to avoid too high solution viscosities with high viscosity products. In that case the same mechanical strength can result

despite the much lower thickness of the capsule wall (marked points in Fig.11). Because of the complexity of the process of capsule formation further data will not be discussed in detail here. In Fig.12 the behaviour with respect to capsule formation

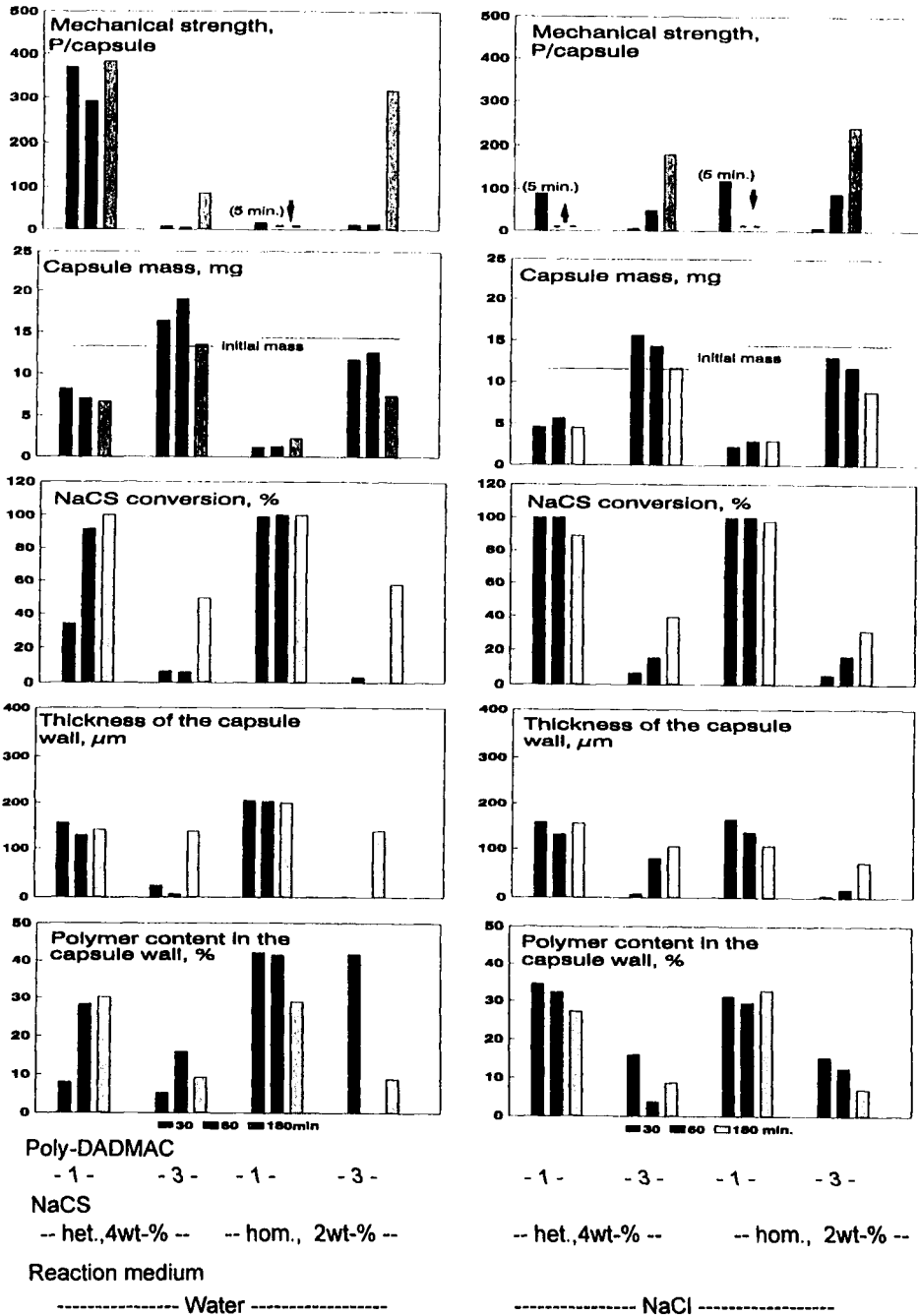
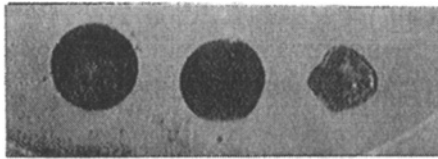


Fig. 12. Comparison of capsules obtained at 23°C with different NaCS and Poly-DADMAC samples (heterogeneously prepared NaCS: LMM, homogeneously prepared NaCS: HMM; Poly-DADMAC sample 1: LMM, sample 3: HMM) after different residence times in the precipitation bath

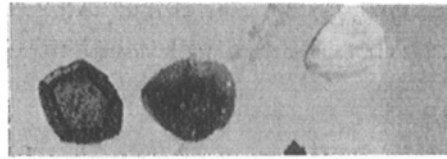
Although therefore a direct comparison of the data is difficult, we can draw the following conclusions. LMM Poly-DADMAC fits better the low viscosity NaCS, while HMM Poly-DADMAC is better suited as counterpart for high viscosity NaCS. Differences occur in the rate of NaCS conversion. Different NaCS concentrations are probably partly responsible for this.

Fig.13 presents the size and the shape of capsules obtained in water as reaction medium (according to the first group of diagrams in Fig.12).

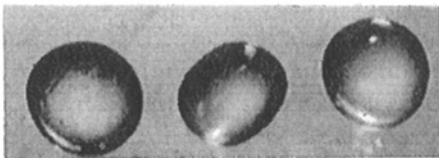
Fig.14 gives an impression of the asymmetric capsule wall structure .



Poly-DADMAC 1 (LMM)

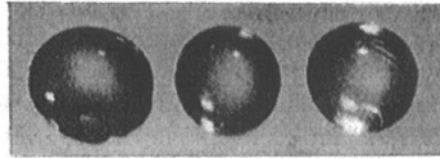


Poly-DADMAC 1 (LMM)



Heterogeneously prepared NaCS (LMM)

Residence time in the precipitation bath, min.
30 60 180



Homogeneously prepared NaCS (HMM)

30 60 180

Fig.13. Size and shape of capsules obtained with different NaCS and Poly-DADMAC samples in water as reaction medium in dependence on their residence time in the precipitation bath

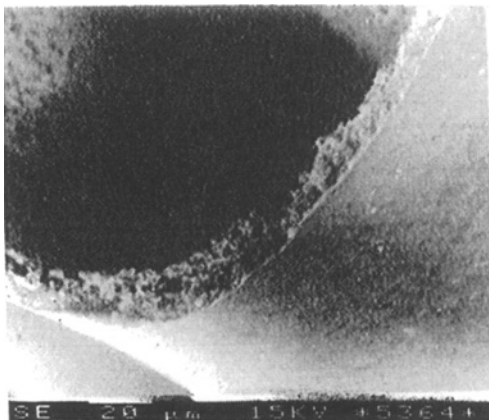


Fig. 14. SE micrograph of a capsule wall obtained with heterogeneously prepared NaCS

Acknowledgement

We gratefully acknowledge the funding of parts of this work by the German "Arbeitsgemeinschaft für industrielle Forschungsvereinigungen", "Fond der chemischen Industrie", and the "Bundesministerium für Forschung und Technologie". We wish to thank Mrs. B. Tiersch for carrying out EM investigations.

References

- Braun, K.; Besch, W.; Jahr, H.; Loth, F.; Dautzenberg, H. and Hahn, H.-J.,
Biomed. Biochem. Acta 44(1985) 143.
- Dautzenberg, H.; Loth, F.; Pommerening, K.; Linow, K.-J. and Bartsch, D.,
DD WP 160 393 (1980).
- Dautzenberg, H.; Loth, F.; Wagenknecht, W. and Philipp, B.,
Das Papier 39(1985)601.
- Dautzenberg, H.; Loth, F.; Fechner, K.; Mehlis, B. and Pommerening, K.,
Makromol. Chem. Suppl. 9(1985) 203.
- Dautzenberg, H.; Holzapfel, G. and Lukanoff, B.,
J. Biomaterials, Artificial Cells, Immobilization and Biotechnology 21(1993) 399.
- Förster, M., Dissertation, MLU Halle (1991).
- Lukanoff, B.; Dautzenberg, H. and Holzapfel, G., DE OS 40 21 049 (1990).
- Petropavlovskij, G., Faserforsch. und Textiltech. 24(1973) 49.
- Wagenknecht, W.; Philipp, B. and Plaschnik, D., DD WP 152 565 (1978).

56 Porous cellulose matrices—A novel excipient in pharmaceutical formulation

R Davidson, H Nyqvist and G Regnarsson – Kabi Pharmacia AB, S-11287 Stockholm, Sweden

INTRODUCTION

In solid pharmaceutical formulation there is often the need to reduce the dosage form to a series of almost identical small discrete units in order to achieve a more reproducible and efficient oral delivery of the drug substance. These are collectively known as Multiple-Unit dosage forms, and usually consist of a bead-like core which has been modified (e.g. by coating it with a barrier film) or possesses intrinsically the required properties (hydrophilic matrix effect, low rate of disintegration) to produce the desired drug-release profile. The traditional methods of producing such beads inevitably lead to some wastage from sizing operations, as well as release of drug-containing dusts.

In order to circumvent some of these disadvantages the authors are developing a carrier system based on a well known excipient substance - cellulose. The overall concept is to produce highly porous cellulose matrices, select the required size fraction, and only then load them with drug substance possibly as part of the drug raw material manufacturing process and not as an independent operation.

MATERIALS AND METHODS

The matrices are produced from a special grade of fibrous cellulose (satisfying USP/NF *Powdered Cellulose*, and described in Int. Pat. App. WO91/18590, 1991, henceforth referred to as S.C.) by mixing with water (quoted in table 2 as % of the dry cellulose weight) in a planetary mixer, extruding the mass through an oscillating granulator, and subjecting the material to partial drying in a high velocity air vortex for a given time. This

time corresponds to a reduction of the water content to about 180% of the dry weight of cellulose. The material is then removed and dried at 80° C for 2 hours. There is no binder used, and the process will also function satisfactorily with commercial grades of powdery cellulose although yielding distinct results. The specifications of the raw materials employed and the characterization of the matrix types under discussion are presented in tables 1 and 2.

TABLE 1 - SPECIFICATIONS OF RAW MATERIALS

	SOLKA-FLOC	AVICEL	S. C.	S. C.	UNIT
	BW-20	PH101	S-20	S-10	
FIBRE LENGTH	powdery	powdery	0,29/0,35	0,48/0,66	mm
FIBRE WIDTH	powdery	powdery	38,2/38,6	37,7/37,3	µm
D.O.P.(a)	1345	331	2517	3380	n
SED. VOLUME(b)	87	43	160	270	ml
He DENSITY	not determined	1,5520	1,5600	1,5708	g/cc

(a)-according to SCAN-CM 15:88 (b)-10g cellulose suspended in 500ml water, 24h at rest.

TABLE 2 - CELLULOSE MATRICES - MANUFACTURING DATA

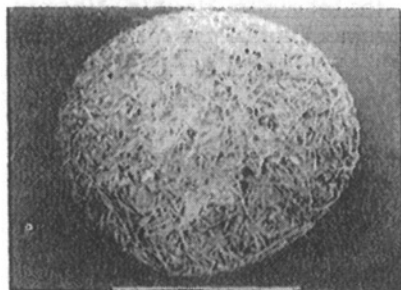
TYPE	CELLULOSE	% MIX. WATER	TYPE	CELLULOSE	% MIX. WATER
Standard	S.C. S-20	~300	High water	S.C. S-20	~440
Low water	S.C. S-20	~220	Long fibre	S.C. S-10	~300
Avicel	Avicel	~130	Solka-Floc	Solka-Floc	~160

With Solka-Floc and Avicel the initial water content is more critical, with the S.C.'s a considerable variation is possible leading to different particle size distributions. The mesh size of the screen in the oscillating granulator has very little influence on the particle size distribution but has to be selected in order to allow effective spheronization to take place in the vortex apparatus.

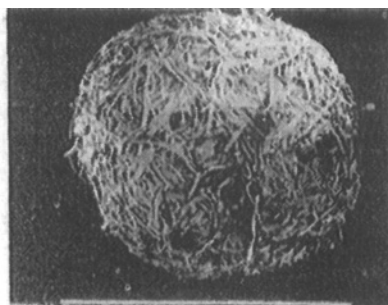
The **morphology** of these matrices may best be described as a tangle of fibres which is sufficiently coherent to resist prolonged agitation in aqueous or organic solvents. Beads manufactured from Avicel have quite a different appearance and are much more compact. Solka-Floc beads resemble S.C. beads although the fibrous structure is finer and the beads are harder. Beads from S.C. S-10 are more fibrous (Figure 1).

If we section the beads we can observe the most important differences between the various types, the section of a large Avicel bead by abrasion reveals a large irregular cavity in an otherwise very compact structure. The section of the S.C. bead reveals a roughly uniform fibrous interior. These beads are very difficult to cut as they crush easily whilst Avicel beads crumble. Solka-Floc beads are similar to S.C. beads but more compact. Smaller Avicel beads normally have cracks rather than cavities (Figure 2).

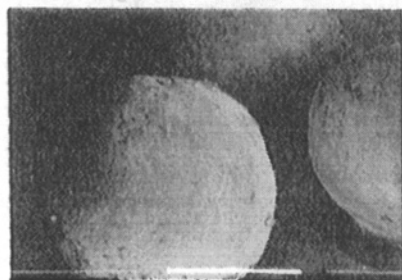
FIGURE 1 - MATRICES MADE FROM DIFFERENT TYPES OF CELLULOSE (Scale bars = 1mm)



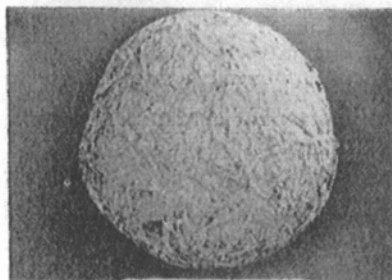
S. C. S-20



S. C. S-10

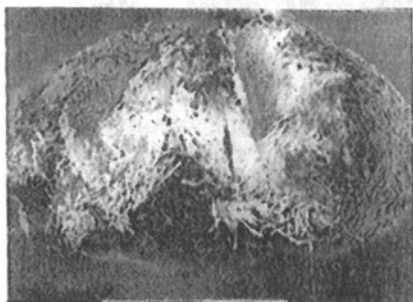


AVICEL PH101

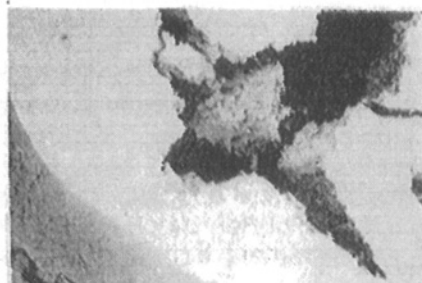


SOLKA-FLOC BW20

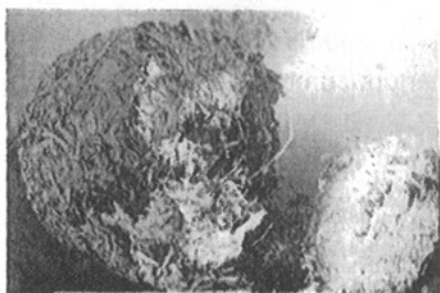
FIGURE 2 - S. C. AND AVICEL MATRICES CUT OPEN (Scale bar=1mm)



S. C. S-20



AVICEL



SOLKA-FLOC

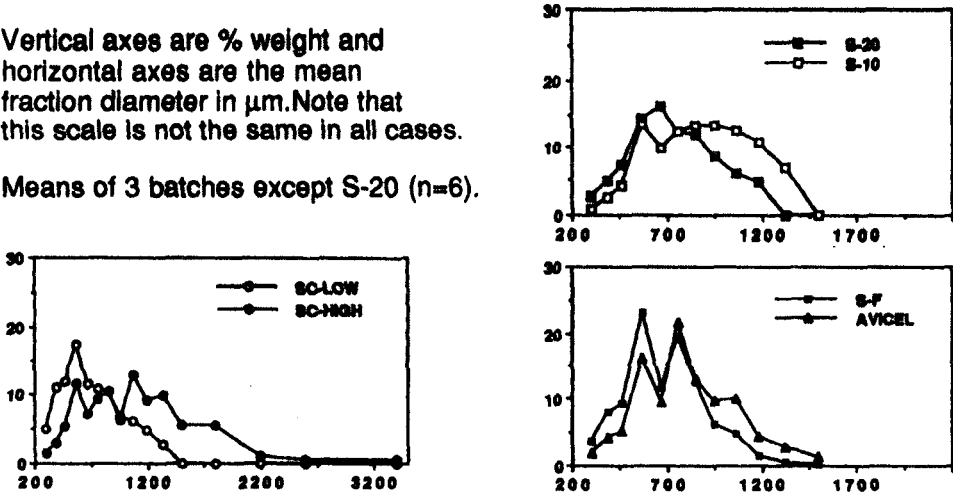
RESULTS

The **particle size distribution** appears to follow a double Normal distribution, presenting two peaks for most cases. Probit lines from these distributions have a distinct "break" between two straight lines. In the case of S.C. S-20 the distribution was closer to Normal leading us to suggest that in certain circumstances the two populations would coincide. The particle diameter median value for these conditions was $679 \pm 11,3 \mu\text{m}$ (1 S.D. $n=6$).

FIGURE 3 - PARTICLE SIZE DISTRIBUTIONS

Vertical axes are % weight and horizontal axes are the mean fraction diameter in μm . Note that this scale is not the same in all cases.

Means of 3 batches except S-20 ($n=6$).



The **total porosity** expressed as cc/g of dry matrices is given in brackets in the **pore size distribution** curve legends (Fig. 4) as total volume below $\approx 100\mu\text{m}$ nominal diameter. It can be seen that the pore size distribution is similar between S.C. and Solka-Floc, but Avicel is completely different. Also the porosity of low and high water matrices and long fibre cellulose matrices is given. All curves relate to beads 0,71-0,8 mm diameter. Matrices of different diameters from standard batches were also analyzed, the results are shown in the final 2 curves and should be compared to the S.C.S-20 curve. There is a substantial increase in porosity in the 5-10 μm size bracket.

In order to determine the **expansion** of these matrices in water, a special cell was constructed and the matrices fixed to a glass slide so that individual measurements (image analysis) could be performed on a significant number of matrices in the dry and wet state. A steel ball was used as the standard. Cyclohexane was also tried in some cases as a non-aqueous solvent, it produced no significant dimensional change. The results of 48 hour expansions (% increase in projected area) are presented related to material type and size of matrix in figure 5, with the mean expansions related to the D.O.P. of the raw material.

FIGURE 4 - PORE SIZE DISTRIBUTIONS (Mercury penetrometry)
 Horizontal axes are the mean nominal pore diameter (μm), vertical axes the equivalent pore volume in cubic centimetres per gram of dry matrices.

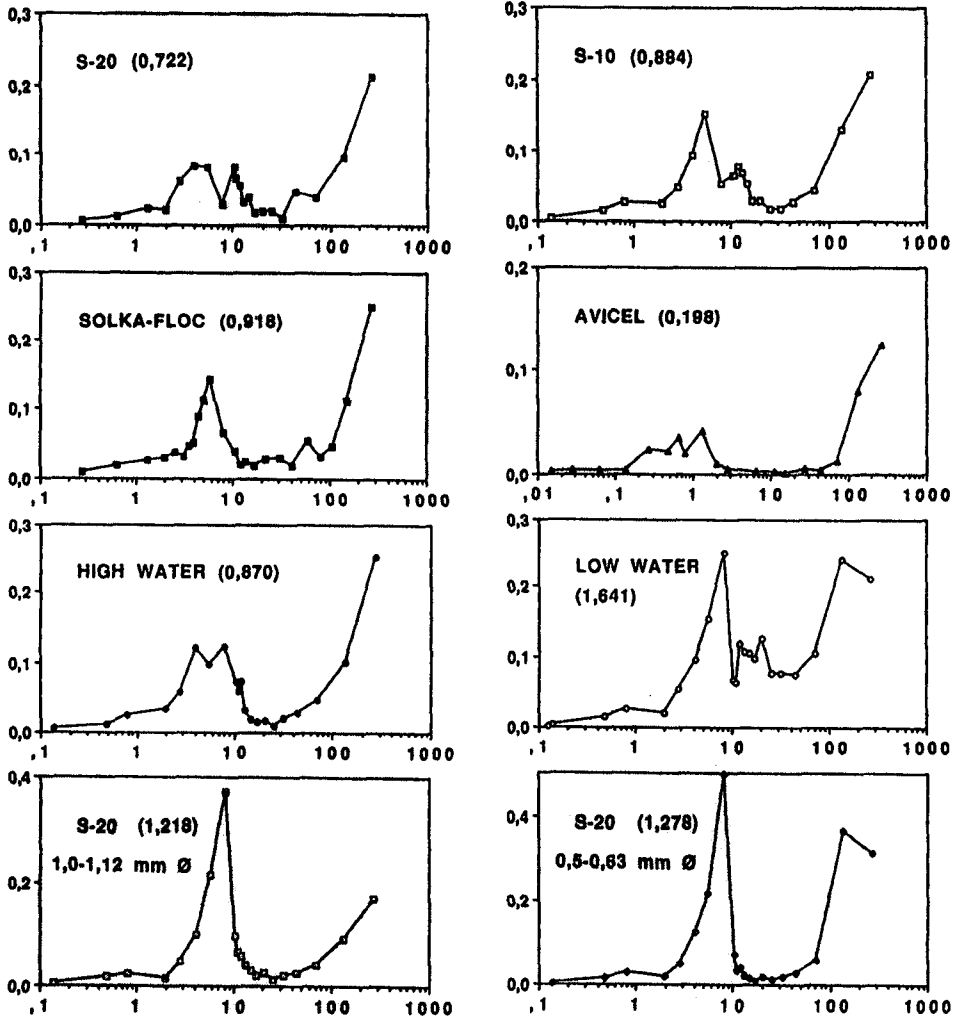
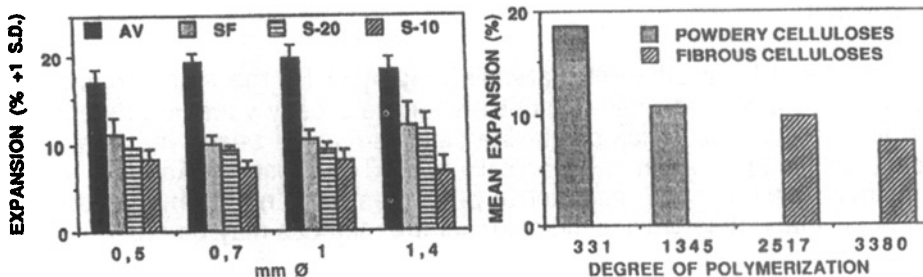


FIGURE 5 - PROJECTED AREA EXPANSIONS OF MATRICES IN WATER



The expansion with respect to time revealed an approximately linear relationship between the projected area expansion and the logarithm of time, some expansion being detectable up to 5 days after bringing the material into contact with water. The bulk of the expansion however took place within the first 30 minutes, too fast to be accurately followed by this method.

The **mechanical properties** of these matrices are also very different between Avicel and S.C., Solka-Floc and S.C. S-10 matrices have not been investigated in detail yet. S.C. S-20 matrices deform in a plastic fashion whilst Avicel matrices tend to crumble into flakes and powder.

Standard S-20 matrices have also been successfully loaded with paracetamol as a model water-soluble drug, and drug contents of about 30% w/w have been achieved in a single loading. These loaded beads are shown in figure 6. We do not have any quantification of the distribution within the matrices, however figure 7 shows a loaded bead cut open revealing a compact apparently well-loaded interior. The loading of 30% w/w is equivalent to an occupation of about half the available matrix voidage (porosity).

FIGURE 6 -
LOADED MATRIX SURFACE VIEW
Scale bar = 100 μ m

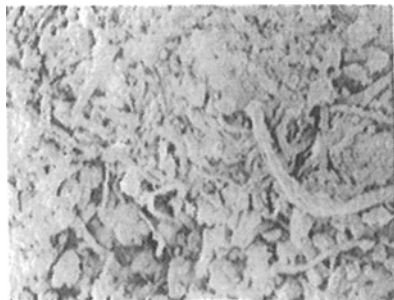
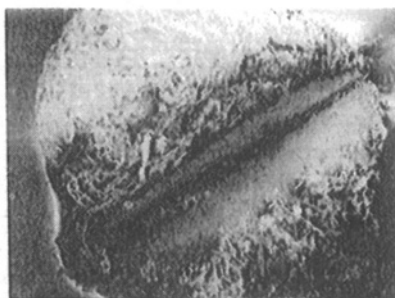


FIGURE 7 -
LOADED MATRIX CUT OPEN
Scale bar = 1 mm



DISCUSSION

The properties of the different materials employed for the manufacture of these matrices are essentially responsible for the greatly variable properties of the finished product. Microcrystalline cellulose yields beads that are too compact for this application, mechanically treated cellulose (Solka-Floc) may be employed although the mechanical properties have not been studied in detail, preliminary observations indicate that the matrices may be too fragile.

The special cellulose material certainly seems to produce the highest yields and the potentially most useful porous matrices. The results presented demonstrate that it is possible to produce these matrices with good reproducibility in terms of particle size. The mercury porosimetry data are single batch readings that were mostly confirmed by repetition. One should bear in mind that the nominal pore diameter tells us the size of the access pore to a given volume as if it were round. These results are most useful from a comparative point of view and as a measurement of total voidage rather than as precise pore measurements. Some results are paradoxical, such as the high porosity of S.C. matrices manufactured with higher or lower amounts of water when compared to the standard situation. If one may speculate a little, one could suggest that the more or less optimal conditions that lead to a high yield and Normal particle size distribution also allow the formation of a tighter bundle of fibres. Conditions departing from these would lead to a more imperfect structure with greater voidage.

The expansions in water are revealing in that the most crystalline material is the one that expands the most. One could suggest that as the material is not entirely crystalline, and water interacts primarily with the amorphous part, the crystalline fraction would act as an inert filler forcing the whole structure to swell. In the case of the fibrous materials, the greater voidage and flexibility of the fibres would absorb the expansion possibly with a loss of voidage. As well as the alterations of voidage one must bear in mind the risk that the expansion would split a controlled delivery coating layer and render the barrier useless.

The loading results are most encouraging in that the process employed was simple and effective, yielding a drug loading with an apparently satisfactory size range and distribution, although some individual matrices appeared to have a heavier surface coating, such as the one shown on figure 7.

APPLICATIONS

These porous matrices were originally conceived as possible drug carriers, although other uses have been suggested.

One such alternative application is as a tableting aid for other beads which due to their fragility may be difficult to formulate as a tablet.

The application of these matrices as drug carriers is particularly interesting if they are to be loaded by the raw material manufacturer. Their use in solid formulation would be advantageous as one could obtain a granular free-flowing intermediary without having to undergo a granulation step.

In terms of economy there could be a considerable process saving, and there would be virtually no waste of drug as the material would be sized before loading. The reduced dust generating potential would also make handling safer. These advantages would become most evident when handling very expensive or toxic drugs. Also, drugs that have unfavourable crystallization properties could be formulated more conveniently.

From the point of view of Controlled Drug Delivery there are three distinct approaches possible. In the first place, drugs with favourable solubility characteristics could undergo release from these matrices as from a hydrophilic matrix, control being achieved by a combination of low solubility and a porous cellulose structure through which the drug would have to diffuse. Secondly, there is the coating approach, the matrix itself would have a relatively small influence on the release profile, the rate of diffusion through a well-supported membrane of known properties being the important factor. Finally there is the possibility of loading these matrices with drug and another substance, which would have the role of a rate-reducer. Essentially, by means of its own solubility, this third substance would govern the porosity of the system.

ACKNOWLEDGMENTS

Håkan Nyqvist is presently at Astra Arcus AB, Södertälje, Sweden. Ricardo Davidson is a guest researcher supported by a grant from the "Ciência" program, J.N.I.C.T. Portugal. The authors are grateful to Mr. S. Karlsson of the Swedish Ceramic Institute for the mercury porosimetry studies, and to Ms. M. Nordensvan of the STFI, for part of the raw material characterization. Part of these results are due for publication soon in the International Journal of Pharmaceutics.

REFERENCES

International Patent Application WO91 / 18590 / 1991

57 Cellulose ethers for cement extrusion

D Schweizer and C Sorg – Hercules GmbH, Düsseldorf, Germany

Introduction

Industrial cellulose ethers represent a significant aspect of the cellulose chemistry. The worldwide annual production is estimated to be over 300.000 metric tons. The cellulose ethers are made by activation of wood pulp or linters with sodium hydroxide followed by reaction with an etherifying agent. In most cases the crude cellulose ethers are purified to remove salts that are formed as by-products. Table 1 shows the most important industrial cellulose ethers and their common abbreviations.

Table 1
Industrial most important cellulose ethers

type	abbreviation
Na-carboxymethylcellulose	CMC
Na-carboxymethylhydroxyethylcellulose	CMHEC
Hydroxyethylcellulose	HEC
Methylcellulose	MC
Methylhydroxyethylcellulose	MHEC
Methylhydroxypropylcellulose	MHPC
Hydroxypropylcellulose	HPC
Ethylhydroxyethylcellulose	EHEC
Ethylcellulose	EC

A substantial outlet for the application of cellulose ethers are formulations used by the building industry. Generally speaking these formulations are made up from binders e.g. cement, gypsum, or synthetic latex, aggregates as silica sand, limestone, kaolin as well as additives and water. Water plays a dominant role in these formulations. Gypsum and cement need water for hydration and water control is essential to achieve good final properties after setting and hardening. Excessive water loss to the substrate results in incomplete binder hydration of gypsum or cement which negatively affects adhesion, cohesion, compressive and flexural strength. For latex binders, water loss disturbs film formation thereby reducing binder properties. For control of the water balance cellulose ethers are added. Besides providing water retention they also improve workability and increase adhesion. To investigate the performance of cellulose ethers in building formulations we focussed on cement extrusion.

Results and discussion

The continuous extrusion of cement is an economical and efficient way to produce slabs, pipes, bricks, spacers and similar objects. In the process cement is dry mixed with aggregates and additives. Upon addition of water the mixture is plastisized in kneaders and subsequently extruded. Cellulose ethers as additives can either be dry blended with cement/aggregates or predissolved in the make-up water.

Table 2 Typical formulations for cement extrusion

Formulation	1	2	3
Portland cement	65	46	62,1
Silica sand, medium diameter 0,28mm	24 - 31,5	50	37,3
Limestone flour	3,5 - 11	-	-
Fibres	-	4	0,6
Cellulose ether *	0,5 - 1	0,5 - 1	0,5 - 1
Water *	11,5 - 13,6	11,5 - 13,6	11,5 - 13,6

* on 100 parts of mixture

As can be seen these systems are strongly water deficient in order to keep their shape after extrusion by imparting high green strength, to achieve strong compressive and flexural strength after setting and hardening and to reduce numbers of cracks. Without an extrusion aid plastification and extrusion would be impossible. Furthermore extrusion aids should provide good water retention and workability, reduce extrusion pressure, prevent de-watering during extrusion, increase green strength of extruded species, prevent cracks and fissures and finally improve flexural and compressive strength of the end products.

Cellulose ethers have been used for many years as an extrusion aid. In order to learn more about the scope and limits of the products we first screened which types would function in the formulations. For the evaluation we used a high shear torque rheometer and a double screw lab extruder to extrude rods with a diameter of 20 mm. The high shear rheometer is a mixing chamber with two counter rotating cam blades. The prewetted mix is fed to the mixing chamber. The rotation of the cam blades is preset and under high shear the mix starts to plastify. To keep the rotation at preset conditions different electrical input is required depending on the consistency of the mass. In such a way torque over time can be monitored. The extrudability was judged by the extrusion pressure and visual inspections of the rods. Table 3 shows the results with different type of cellulose ethers.

Table 3 Screening of cellulose ethers for cement extrusion

Type	2 % viscosity (mPas) 2)	methoxyl (%)	EOOH (%) 3)	POOH (%) 3)	DS CM 3)	plastifi- cation	extruda- bility
CMC	35.000				0,7	no	no
HPC	13.000			72		no	no
MHPC	66.000	23,3		9,3		yes	yes, firm extr.
MHEC	30.000	26,0	5,3			yes	yes, firm extr.
HEC-1	36.100		56,1			yes	yes, soft extr.
HEC-2	29.000		65,6			no	no

1) Use level cellulose 1,0 %, water ratio 12,5 %

2) Brookfield RVT 20 °C, 20 rpm

3) EOOH: hydroxyethoxyl

POOH: hydroxypropoxyl

DS CM: Degree of substitution carboxymethylgroups

As can be seen only MHEC, MHPC and HEC-1 lead to plastification and extrudability. The result for CMC is not too surprising since CMC as the sodium salt of an anionic cellulose ether is sensitive towards calcium-ions. In the presence of these divalent cations CMC cannot hydrate and is rather converted to calcium-CMC with a low solubility. HPC is in this series the cellulose ether with the lowest hydrophilicity. Therefore hydration rate is insufficient to go into solution in such a water deficient system. Results are surprising for the two HEC-types. As can be seen the one product with the lower hydroxyethoxyl-content already gives a soft extrudate that is judged to be at the borderline with respect to green strength and shape retention. The explanation lies in the molecular structure of the two HEC products. The HEC-1 type has longer branching ethyleneoxide sidechains compared to the HEC-2 type where the length of the sidechains is shorter yet the number is higher. This is best expressed by the degree of substitution of ethyleneoxide per anhydroglucose-unit. For the HEC-1 type the DS is approx. 1.1, for the HEC-2 type the value is approx. 1.8. This means that for the HEC-1 product the cellulose backbone is more open for interaction with cement than the HEC-2 type.

After having screened which types of cellulose ether are in general suitable for plastification and extrusion we looked closer at the torque versus time recording generated with the high shear rheometer, figure 1.

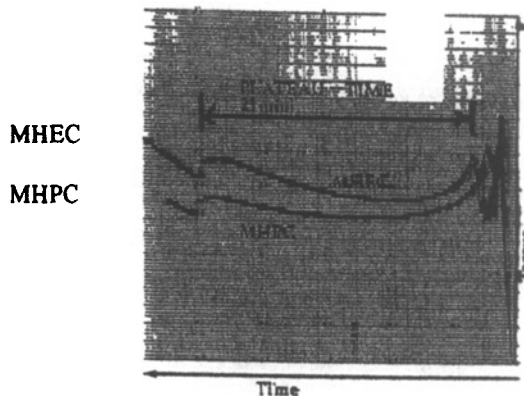


Fig. 1. Plastification of cement in the high shear rheometer. Torque as a function of time.

Immediately after filling plastification starts as is noticed by the presence of a peak. This peak is due to maximum swelling of the system in the aqueous phase to give plastification. Torque drops after plastification to a state of maximum disaggregation and remains rather constant before it increases again. This increase is the result of setting and hardening of the cement, which would finally lead to an unworkable solid mass. Therefore we define the time after peak drop till increase of torque due to hardening of the cement as the plateau time. Plateau time is the time available for plastification and extrusion and all precaution has to be taken that the system when shaped is within the plateau time.

We assumed that plateau time is influenced by the availability of make-up water for cement hydration. If the cellulose ether controls the water balance and releases water for cement hydration then setting of cement will be extended. This means that plateau time can be influenced by the viscosity of the cellulose ether, the particle size and the amount of water available for hydration i.e. the water ratio.

For all the upcoming tests we focussed on MHEC-types knowing from other lab tests that similar results would be obtained with MHPC. The HEC-1 type was not included because as already said plastification was at the borderline.

First we checked the influence of cellulose ether viscosity and water ratio on plateau time and torque.

We used three types of MHEC with the same substitution level and particle size distribution yet different viscosity. In that run we also varied water ratio. Results are shown in figures 2 and 3.

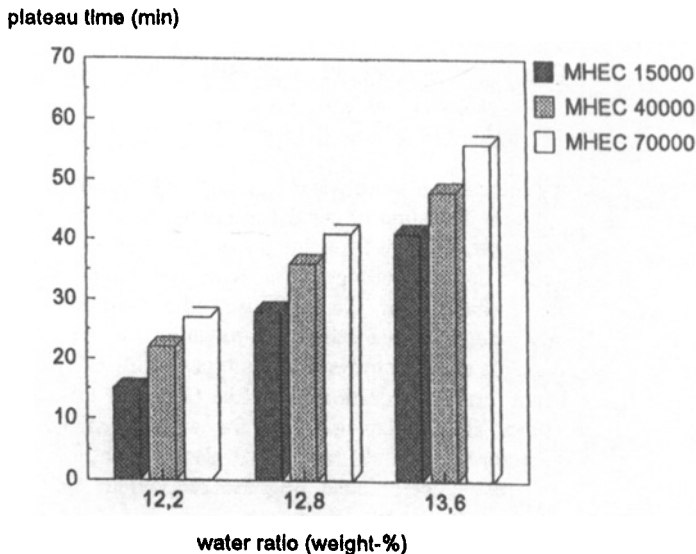


Fig. 2 Influence of MHEC viscosity and water ratio on plateau time (use level MHEC: 0,92 weight-%)

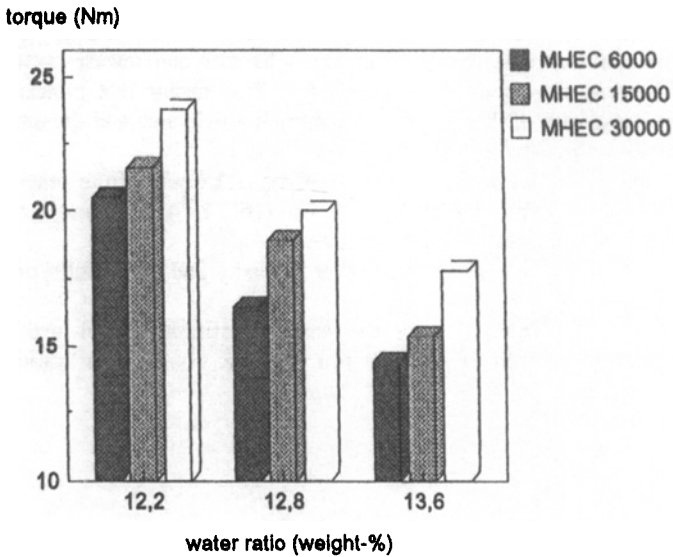


Fig. 3 Torque as a function of MHEC viscosity and water ratio
(Use level MHEC: 0,92 weight-%)

Not surprisingly plateau time increases if more water is available for hydration. The cement gel particles that are formed upon hydration of cement are more distant from each other in a system with higher water content. Since it takes longer for the crystals to bridge the gap the plateau time will increase before setting starts with the build-up of the three-dimensional network. The influence of the cellulose ether viscosity is also very pronounced. Higher viscosity types have a better water retention i.e. they hold the water stronger and make it less available than the lower viscous types of lower molecular weight. Therefore at a given water ratio cement hydration should be faster for lower viscous types leading to shorter plateau time. This explanation asks for a dissolved or at least partly dissolved cellulose ether. Therefore one would expect that also the torque of the system is higher for higher viscous cellulose ether because the dissolved cellulose ether contributes by its viscosity to a stiffer consistency of a plastified mass.

Figure 3 shows that the results are in line with the ones of plateau time. As can be seen torque is higher with lower water ratio because the solid content gets higher with less water present. It is also obvious that at a given water ratio torque is higher for the higher viscous MHEC-type due to contribution of the higher aqueous viscosity.

The assumption that the properties of the plastified cement mixture is controlled by the properties of the dissolved cellulose ether is further supported by investigating the influence of particle size and of temperature on plateau time, figures 4 and 5.

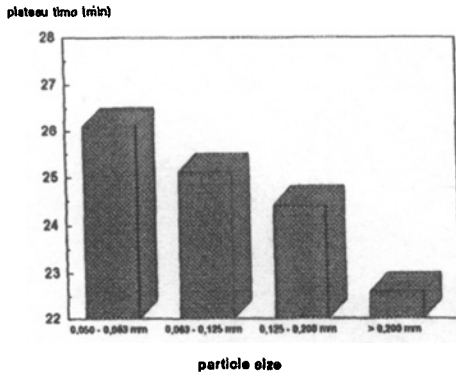


Fig. 4 Influence of MHEC 40.000 particle size on plateau time
(water ratio: 12,2 weight-%, use level MHEC: 0,92 weight-%)

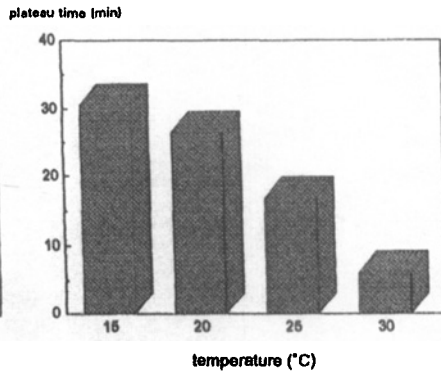


Fig. 5 Influence of temperature on plateau time
(water ratio: 12.2 weight-%, use level MHEC 50000: 1 weight-%)

The finer the particle size the faster the hydration rate of the cellulose ether. Therefore the sieve fraction between 0,05 - 0,063 mm hydrates faster than the coarse fraction larger than 0,2 mm. Fast hydration leads to longer plateau time, figure 4.

The higher the temperature the lower is the solubility of a cellulose ether. It is also known that setting of cement is accelerated by temperature increase. Combining both facts easily explains the reduction of plateau time with increasing temperature, figure 5.

After having evaluated how plastification is influenced by the cellulose ethers, water ratio and temperature we were interested in how this would translate to extrusion of plastified cement. As already noted, plastified cement was extruded with a double screw lab extruder to rods of 20 mm diameter. For flexural strength values the rods were stored 7 days at 23 °C / 50 % relative humidity.

At first we looked at the influence of water ratio on extrusion pressure and flexural strength, figure 6.

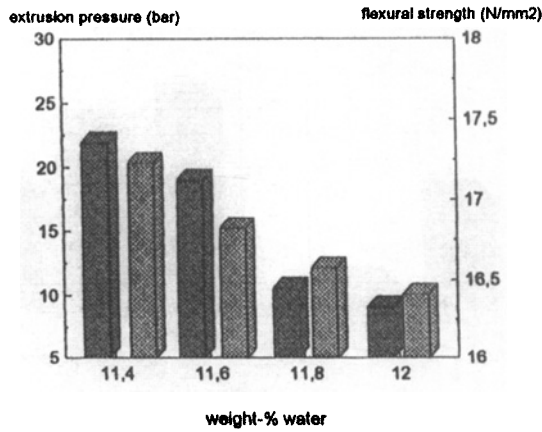


Fig. 6 Influence of water ratio on extrusion pressure and flexural strength
(Use level MHEC 30000: 1 weight-%)

The results are in line with the plastification data from the high shear rheometer. With more water available the consistency is softer which leads to lower extrusion pressure and also to lower flexural strength because the system is less densely packed.

If the cellulose ethers act as water retention agents, plastiziser and adhesive, then the extrusion properties should be influenced by the use level of cellulotics as is shown in figure 7.

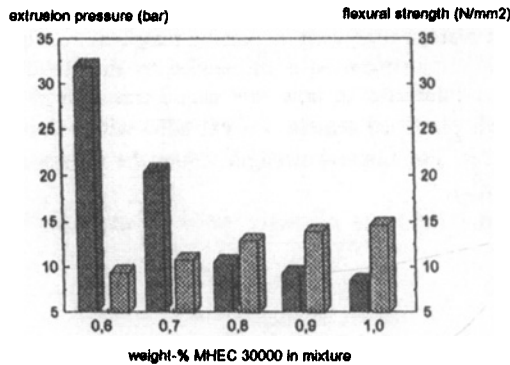


Fig. 7 Influence of use level cellulose ether on extrusion pressure and flexural strength
(water ratio 12 weight-%)

The cellulose ether functions indeed as lubricant and adhesive because by increasing use level extrusion pressure drops yet flexural strength increases.

Another support of this assumption would be that at a given use level of cellulose ether and constant water ratio higher viscous types should give higher flexural strength.

This is actually the case as demonstrated in figure 8.

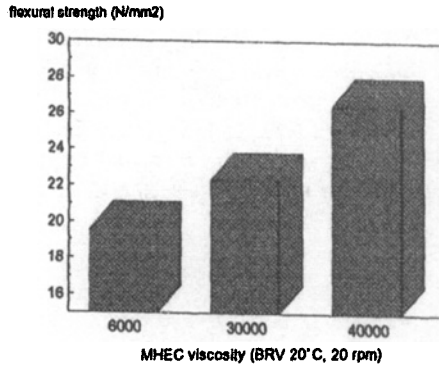


Fig. 8 Influence of MHEC viscosity on flexural strength
(water ratio 12,5 weight%, use level MHEC: 1 weight-%)

As it was shown all parameters on plastification and extrusion could be linked to the properties of an aqueous cellulose ether solution. This means that the cellulose ether hydrates in the make-up water to go at least partially into solution. It also means that adsorption on the cement or sand surface and/or flocculation does not happen to a great extent. If this is true then cellulose ethers should be extractable from the reaction mixture. To prove the point we added a cellulose ether solution to cement, centrifuged after 10 min and determined the concentration of cellulose ether in the supernatant liquid by addition of phenol/sulfuric acid. The reagent forms a yellow complex with the colour intensity being dependent on the cellulose ether concentration in the solution. By recording the colour intensity at 487 nm using a UV/VIS spectrometer we found 88 % of the original cellulose ether in the supernatant solution. It has to be mentioned that the water ratio was increased from originally 12 % to 70 % in order to get separation of the layers by centrifuging. But even if the conditions are not identical with the ones for cement extrusion the result fits into the pattern. On the other hand we do not totally exclude interaction between cellulose ethers and cement because we assume that this is the explanation why HEC-2 does not plastify in contrast with HEC-1.

Summary

It was shown that among the various cellulose ethers MHEC, MHPC and to a certain extent HEC are suitable for cement extrusion. CMC and HPC did not plastify.

The properties of the cellulose ethers could be linked to the properties of the aqueous solutions of cellulose ethers. The plateau time was defined as the time available for plastification and extrusion before the cement hardens. The plateau time is influenced by the ability of the cellulose ether to release water in a controlled way for cement hydration. Higher viscous cellulose ethers with higher water retention lead to a longer plateau time as does higher use level of cellulose ether or finer particle size.

Increasing use level of cellulose ethers leads to lower extrusion pressure but also to higher flexural strength. Flexural strength can also be increased by choosing a higher viscous cellulose ether. All the data indicate that cellulose ethers act as water retention agents, lubricants and adhesives.

58 Water-soluble polymers in tunnelling and slurry supported excavations

S A Jefferis – Golder Associates, Consulting Engineers,
54–70 Moorbridge Road, Maidenhead, Berkshire, England

ABSTRACT

Water soluble polymers are widely used in oil well drilling and many special materials have been developed. There are also applications for polymers in civil engineering excavation work but they are more rarely used and bentonite clay based fluids are still the norm. However, the opportunities offered by polymer systems are becoming more widely appreciated and their use is developing especially in tailored systems designed for particular applications. The paper gives an overview of the properties of polymers that are required or may be exploited in civil engineering work.

INTRODUCTION

Polymers and the swelling clay bentonite find particular application in underground work and especially deep excavations in water bearing strata. There are very many different possible applications and new processes are continually being developed. However, some of the special advantages of polymers can be highlighted by considering just three civil engineering processes: tunnelling, caisson sinking and deep foundation excavation.

TUNNELLING

Conceptually one of the simplest methods of forming a tunnel is pipe jacking. In this process sections of tunnel pipe are jacked into the ground from a thrust pit. Spoil is

excavated at the front of the tunnel either by hand or with a tunnelling machine. The excavated diameter is designed to be slightly greater than the outside diameter of the pipe sections and the annular void so created is filled with a lubricant gel injected near the excavation face and at intervals back along the tunnel. As each pipe section is jacked into the ground a further one is added at the thrust pit. Typically the maximum length of any pipe jack will be less than 100 metres but much greater lengths have been achieved. An important requirement of process is that the frictional grip of the surrounding ground on the string of pipes is not so great that the jacking thrust approaches the axial strength of the pipes. Thus the lubricant must:

- (a) be lubricious, that is it must have a low shear strength;
- (b) adhere to the pipe sections and not be scraped off by the jacking process;
- (c) not be lost into the ground by penetration or so compressed as to be ineffective as the surrounding soil closes on the pipe.

Thus the ideal lubricant should have a low shear strength and yet not be lost into the ground but maintain a stable annulus around the pipe. The necessary gel strength to limit penetration into the ground will increase with the size of the soil voids and in coarse grounds it may be necessary to add flaky materials to reduce penetration.

The lubricant will also consolidate (lose water and so reduce in volume) as the surrounding soil closes on it. This is undesirable since it will increase the shear strength and reduce the thickness of the lubricant layer. As the lubricant must be an injectable fluid some consolidation is inevitable. However, the rate of consolidation can be reduced by the addition of fluid loss control agents which reduce the rate of water loss under pressure.

Typically sodium bentonite is used as the lubricant at a concentration of about 10% by weight in water. Carboxymethyl cellulose may be added to reduce fluid loss. Many other additives have been employed to reduce shear strength and some formulations seem almost bizarre. Further work is needed on the adhesion of the lubricant to the pipe sections to limit lubricant loss and for this there would seem to be openings for bio-fluid type materials such as those that line the mouth and allow free movement of the tongue during speaking and eating etc.

EARTH PRESSURE BALANCE TUNNELLING

When excavating a tunnel in soft ground it is necessary to prevent the excavated face from collapsing or moving inwards as this will cause settlement at the ground surface. For hand excavated tunnels in dry ground the face may be boarded and worked in small sections. In wet ground water as well as soil must be held back. This may be achieved by pressurising the tunnel with compressed air so that the air pressure balances the water pressure. This is an expensive process and there are severe limitations to the pressures that can be balanced if the tunnel workers are not to be subjected to unacceptable conditions and even at quite modest depths the workers may be involved in lengthy periods of decompression. Thus in general for all but short tunnels some form of tunnelling machine will be used.

There are very many different types of machine but only a few systems for controlling ground water. It is in these systems that polymers find particular application.

In any tunnelling machine there will be a cutter-head set with teeth which is slowly rotated and cuts into the soil. The resulting spoil passes into a chamber behind the cutter-head from which it may be discharged onto a conveyor belt and thence to rail cars in the tunnel. Earth pressure balance tunnelling is a particular method for controlling ground water and soil pressures. In this procedure the machine chamber is sealed and the discharge of cut spoil from it is controlled so that the head of the machine is pressurised and thus the face kept stable and the ground water held back. The control may be achieved with a screw conveyor. This is a highly specialised piece of plant which may be over 1 m in diameter by 15 m long with separate screw and casing rotators that can be driven at variable speeds or even in reverse. The reason for this is that in wet grounds it is necessary to develop a plug in the screw with sufficient cohesion that it can hold back the water pressure in the head. In some grounds it may be easy to form a plug but in others additives are essential. Requirements are that:

- (a) the spoil is converted to a smooth cohesive paste that can build a plug;
- (b) the cohesion of this paste is relatively insensitive to the quantity of water mixed into it as grounds which yield large amounts of water may have to be excavated;
- (c) the additive is easily dispersible into the soil as the mixing action within the head of the machine will be rather poor;
- (d) the additive is lubricious and does not increase the torque on the cutter-head. Ideally it should reduce this torque.

Typically bentonite at about 5 to 10% has been used as the additive as it gives good lubricity. However, at such concentrations it has little capacity to absorb further water and in wet grounds it may be impossible to form a plug to control the ground water inflow. Water absorbent polymers such as cellulose based systems have also been used but large quantities may be necessary in wet grounds. Such materials may be more effective as part of blends with other polymers such as polyacrylamides. These have a powerful flocculating action on any clay in the soil and a spoil-polyacrylamide mix may be able to absorb substantial quantities of water without becoming a 'soup'. Polyacrylamide solutions in water at 0.2 to 1% easily can be mixed with soil to produce a spongy workable mass and water contents over 200% can be achieved even with low clay soils without the system degenerating into a soup (without polymer the maximum water content might be ~ 60%). A further feature of some polyacrylamide-spoil blends is that any clay becomes much easier to handle. It loses its stickiness and it no longer adheres to any stones in the soil and they appear clean and clay free.

However, at polyacrylamide concentrations over about 1% the behaviour can change. The solution is no longer easily miscible with spoil but tends to coat it so that the mix takes on the appearance of frog spawn with lumps of spoil in a stringy fluid.

The optimum polymer solution concentrations may be determined by laboratory trials but the rate at which the solution is injected into the face must be left to the discretion of the tunnelling machine pilot as at any time he will have many conflicting demands to balance. Polymer formulations should be designed to improve his control

and must not reduce it. The use of polymers in this type of tunnelling is still developing and there is much potential for new products. For example a dispersing agent could be included (preferably with the polymer as it would be difficult to add it to the spoil prior to the polymer - though chemically to achieve dispersion and flocculation at the same time would be a challenging task). The aim would be to disperse the fines in the soil so that other polymers could act on and bind many small particles rather than fewer but larger aggregates. This could enhance the water binding power of the polymer systems and extend their application to soils containing very limited amounts of fine material.

SLURRY TUNNELLING

In some grounds where the potential water inflows are very large or the soil is too coarse to develop a cohesive plug in a screw conveyor it is necessary to use a totally enclosed 'slurry tunnelling' system. In this system the head chamber is again sealed but a water based slurry is pumped into it at a pressure sufficient to support the ground face. The injected slurry becomes mixed with the excavated soil and the spoil laden mix is then pumped from the head to a cleaning plant at the ground surface where the spoil is removed and water returned to the face. Polymers may be added to the slurry and requirements are that:

- (a) the polymer limits fluid loss to the ground, that is it prevents filtration of water from the slurry into the soil;
- (b) the polymer should reduce settlement of solids in the spoil pipelines and preferably should reduce the pumping pressures;
- (c) the polymer should not adversely affect the separation of spoil in the cleaning plant. Ideally it should improve cleanability by inhibiting the dispersion of clays.

In the early slurry tunnelling machines bentonite clay at a concentration of 2 to 5% was used in the slurry. However, it was not ideal as it was removed at the cleaning plant with other clays naturally present in the ground. Also bentonite is sensitive to contamination by cement and salts in the ground. Severe salt contamination is rare but cement contamination can occur as a cement grout will be injected to fill the small annular space that is always left between the 'as dug' tunnel and the lining as the machine advances. Some of this grout may penetrate into the head of the machine and become mixed with the slurry. Cement causes an instant and substantial thickening of bentonite and thus an increase pumping pressures and a reduction in the efficiency of the slurry cleaning plant.

Bentonite is therefore not the ideal slurry forming material and sodium carboxymethyl cellulose (CMC) has been quite widely used. CMC is useful as it has a synergistic effect with clays and markedly reduces fluid loss and modestly develops slurry viscosity (and so improves spoil carrying capacity). Furthermore its pseudoplastic rheology means that pumping pressures may be significantly lower than with bentonite (which although thixotropic can still have a relatively high yield stress). CMC has three disadvantages: it is biodegradable; its effect is reduced by cement

contamination and it binds to clay and so is removed with any clay at the cleaning plant (this loss is probably inevitable for any material that develops synergy with natural clays). Typically CMC will be used at concentrations of 0.05 to 0.2 % by weight of slurry (the slurry could contain 35% solids by weight of slurry when leaving the tunnelling machine and 5% when returned after cleaning, most of which would be fines as the cleaning plant will preferentially remove the coarser material).

Experiments with different CMCs have shown that high viscosity grades are more cost effective than low viscosity grades in developing viscosity and reducing fluid loss. In some early applications a biocide was added to the slurry to prevent bacterial degradation and agar gel plates were used to check for bacterial fouling. As the CMCs available today are more resistant to bacteria, biocides are seldom used.

Other polymers will no doubt find application. For example hydroxyethyl celluloses are less sensitive to cement contamination than carboxymethyl celluloses and some polymers can very usefully inhibit the dispersion of clay cuttings so that they do not break down and thicken the slurry but remain as lumps which easily can be removed at the cleaning plant.

In the cleaning plant the coarse solids are removed on vibrating screens. The finer materials generally are removed using a combination of hydrocyclones and dewatering screens (these screens dewater the slurry which has been concentrated with the hydrocyclones). In soils containing a significant amount of clay it may be necessary to use a centrifuge or filter belt press. If a belt press is used the slurry must be flocculated before pressing and this will require the use of a polymer. With some soils (especially those containing significant amounts of montmorillonite clays) it may be necessary to use both inorganic and polymer flocculants. The author has had considerable success with Portland cement (that is the standard construction cement) as an inorganic flocculant. Major elements in cement are calcium, aluminium and iron and thus it can have a powerful flocculant action. In use it may be mixed with water at a water/cement ratio of about 0.5 and then poured directly into a stirred slurry tank.

CAISSON SINKING

Caisson sinking is similar to pipe jacking save that the direction of 'tunnelling' is vertical and the caisson is not jacked into the ground but sinks under its own weight. To aid sinking a lubricant is injected at the periphery as in pipe jacking. However, the maximum injection pressure is now limited as the annulus will be open at the ground surface and thus there is no possibility of holding back the soil by using and maintaining a high injection pressure (such pressures would be quite normal practice in pipe jacking). To limit closure of the annulus the lubricant may be weighted with a dense material such as calcium carbonate (limestone powder) or more rarely barium sulphate which is denser but much more expensive. It is often found that the only way to keep the annulus open is to circulate the lubricant by pumping it in near the base of the annulus and recovering it at the ground surface. The properties required for caisson lubrication are the same as those for pipe jacking save that if the lubricant is recirculated it may be necessary to add a dispersing agent to improve fluidity. Also biological stability will be important as the sinking operation may take many months.

SLURRY TRENCHING AND PILING

The birth of civil engineering excavation slurries is generally held to have been in 1949 when a clay slurry was used to stabilise a trench excavation. This was followed in about 1953 by an application to form concrete piles. The basic principle of slurry supported excavation is that if a hole is excavated in the ground to a depth of more than about 2 metres it will tend to collapse. However, if as the excavation proceeds a slurry is pumped into the hole the hydrostatic pressure of the slurry will prevent collapse. Once the hole has been excavated to the required depth a steel reinforcing cage may be lowered in and the hole then backfilled with concrete to form a pile or structural wall. Another, and currently much used variant is to excavate the trench under a cement-bentonite self hardening slurry that will set if left in the trench at the end of excavation to form an underground barrier for control pollution migration. A further development is to insert an HDPE membrane into the trench before the slurry sets. Such combination barriers are much used for the control of landfill gas migration. To date the only polymers used in cement-bentonite slurries have been to modify the behaviour of the cement (eg retarders). However, it should be noted that large volumes of slurry are used in barriers and a single job may take over 10,000 m³.

In the first slurry supported excavations for piles and structural walls the slurry was discarded after a single use. However, it was soon appreciated that the slurry could be cleaned and re-used and today cleaning plants are standard equipment. Re-use is also financially very important as the cost of slurry disposal may be several times that of slurry production (few landfill sites will accept liquid wastes). Bentonite slurries are widely used and concentrations are typically from 2.5 to 5% (though higher concentrations may be necessary if the bentonite is of limited quality). CMC has been used as has xanthan gum and proprietary blended products tailored to particular applications are becoming available. These may be blends of CMC, xanthan, polyacrylamides etc. The required properties of slurries for structural walls or piles are: fluid loss control, appropriate rheology, ease of cleaning, insensitivity to cement contamination and stability during multiple uses.

Bentonite offers a reasonable compromise for these properties but there is much potential for polymer systems. A major problem when designing polymer systems is that it is difficult to quantify the properties that are required as these will vary with the excavation plant in use and the soil to be excavated. Also in any situation there may be more than one set of properties that is acceptable and thus many different slurry formulations may be acceptable. However, the following properties are typical:

Fluid loss of order 20 ml when measured at 100 psi in the American Petroleum Institute fluid loss cell. Fluid losses above 40 ml would be regarded as high for structural walls (cut-off wall cement-bentonite slurries always show much higher losses but generally will be used in permeable ground where the water lost can rapidly dissipate without compromising the stability of the excavation).

The requirements for rheology are more complex. For good cleanability the slurry must have low viscosity and low yield stress. However, such a slurry will penetrate into any open ground and thus large losses could occur. Also as the excavation is supported only by the hydrostatic pressure of the slurry it is useful if the slurry is slightly denser than the adjacent ground water perhaps of order 1100 kg/m³. This

requires that some spoil be suspended in the slurry. Ideally this should be fine sand or silt (particles up to about 100 microns) but not clay so as to avoid excessive thickening of the slurry (thus inhibition of clay dispersion is again an advantage). At the end of excavation the base of the trench must remain clean and free from settled debris which could give a soft compressible base to a foundation pile or wall. A clean base requires that any solids either settle rapidly and so can be removed as part of the excavation cycle or not at all. The rheology that best meets this requirement is a thixotropic Bingham type fluid (eg a bentonite slurry which is fluid when agitated but develops a gel on standing for a few minutes) or a strongly pseudoplastic fluid (a fluid which shows a decreasing viscosity with increasing shear rate). Pseudoplastic fluids have the advantage that they should be more easily cleanable than Bingham fluids (shear rates in the cleaning plant will be high). Pseudoplasticity is a feature of many polymer solutions and thus they have a natural potential as excavation fluids. Xanthan gum is particularly effective for spoil suspension and blends containing xanthan or similar bio-polymers find many special applications.

A major disincentive to the use of polymer slurries is their high initial cost which can be 10 times that of comparable bentonite slurries. It could be hoped that this extra cost might be recouped by obtaining more uses from polymer slurries. Data on the relative degree of re-use (the volume of excavation achieved per unit volume of original slurry) that can be achieved with polymer and bentonite slurries are limited but in practice it is unlikely that there will be any substantial difference between the two types as the main slurry losses are similar: slurry will be lost to the ground; with the excavated spoil and as a result of dilution as any water associated with soil is dispersed in the slurry (this must be countered by regular additions of polymer or bentonite). A further and often expressed concern is that if an excavation intercepts a drain or a major cavity a substantial volume of polymer may be lost and much money may literally go down the drain.

As already noted the cost of disposal of slurry may be significantly greater than the cost of production and disposal costs may tip the financial balance between different slurry systems. In principle it should be possible to break a polymer slurry down to water viscosity for example with an oxidising agent such as calcium hypochlorite. However, if there is to be any significant saving in disposal costs the resulting liquid must be sufficiently innocuous that it can be discharged directly to public sewer. This will require that its solids content and chemistry are acceptable to the sewer authority. The requirement for acceptable chemistry could preclude the use of many breakdown agents including calcium hypochlorite.

There is a special type of underground construction that takes particular advantage of the degradability of polymer slurries. This is the drainage wall or gas venting trench. In this process a trench is excavated under a polymer slurry and backfilled with clean coarse gravel. The polymer in the backfilled trench then may be left to degrade naturally or wells may be installed and breakdown agents introduced. Ultimately a gravel filled trench is achieved which may be used as a drainage wall for example to intercept contaminated ground water or as a vent trench to intercept landfill gas. In the past the process has been seldom used but it is now gaining in popularity.

POLYMER STORAGE AND MIXING

On most sites using bentonite for major excavation work the bentonite will be delivered in bulk tankers and stored in silos. With polymers the quantities will be much smaller and usually they will be delivered and stored in bags thus avoiding costly silos. However, on construction sites covered storage can be at a premium and the author has seen bags of polymer reduced to a gelatinous mass by exposure to the elements. The packaging of polymers in weather proof bags could reduce wastage.

Polymer mixing can present some problems. Many bentonite mixers are little more than a cylindrical tank mounted above a centrifugal pump. Such systems are not well suited to the mixing of powdered polymers which may lump or stick to the walls of the tank. Producing polymers as prills can improve mixability but polymer suppliers also must be prepared to develop suitable low cost mixing plant such as in-line eductor mixers. Such mixers must be sized to achieve the required rate of mixing (perhaps 5 to 20 m³/hour) and the quantity of polymer to be added. The rate of mixing should be limited only by the availability of water and not the capacity of the mix head.

Currently many polymers are available as dispersions in non aqueous liquids. This greatly simplifies mixing and reduces the time for the development of solution properties. However, the ultimate fate of the polymer in most excavation processes is either to be left in the ground or to be dumped with the spoil. As a result municipal authorities can require guarantees that the material presents no environmental hazards. Often the polymer may pose no problems but the dispersing medium especially if based on a mineral oil may be much less acceptable and become the controlling factor.

CONCLUSIONS

There is a substantial potential market for polymers in civil engineering and a single job could use several tonnes of product. However, to date the use of polymers in civil engineering has been rather limited and there are few specialist suppliers or formulators of polymer systems. The oil industry has made much wider use of polymer systems and has been proactive in developing new polymers. The civil engineering industry generally has been content to accept the polymers that are immediately available. In part this is because many construction situations are quite tolerant of polymer properties and thus there has been no need for special systems. More importantly the lack of special development is because it is difficult to identify the parameters that are fundamental to a good product. Thus a fluid loss of 20 ml and an apparent viscosity of 15 cP might be typical for many construction slurries but doubling or halving either of these figures might have little obvious benefit or do little obvious harm. Clearly it is difficult to sell a polymer as more versatile system if versatility is not needed.

The cost of the lubricant or slurry on a construction site may be a fraction of the total budget but still every penny must be justified - especially in times of recession. If the market is to be developed polymers must be shown to achieve not only their immediate technical goals but also to give improved overall productivity which is where the real savings may be found.

59 Larch wood polysaccharides as the potential raw material for improvement of cellulosic materials and porous ceramic properties

F Kurgan and R Belodubrovskiy – 194021, St Petersburg, Shvernik ave, 49, VNIIB, Russia; V Bogdan – 665718, Bratsk, Bratsk Lespromcomplex Concern, Russia

ABSTRACT

The larch wood polysaccharide arabinogalactan (AG) and associated flavanoids have been separated by membrane methods. The surface application of different molecular mass AG solutions to cellulosic materials for various purposes were studied. The strength characteristics of pulp were improved and the folding endurance (number of double folds) also increased by ~25% as compared to a reference pulp sample. The effect of AG additives was studied as: 1. the stabilizer in the graphite industry; 2. the substitution of dextrin in the electronic industry for glueing together insulator materials; 3. the plasticizer and combustible plasticizing agent in a porous ceramics production (filter medium, porous filtration pots and et.) AG addition increases mechanical strength of ceramics and decreases the plasticizer consumption significantly compared with carboxymethylcellulose.

METHODS

The larch wood polysaccharide AG and associated flavonoids isolated by low-temperature prehydrolysis were separated by membrane methods: ultrafiltration at the first stage and reverse osmosis - at the second one (Kogan, Kurgan et al., 1989). Thus, two fractions of AG were obtained: low-molecular and high - molecular mass.

RESULTS AND DISCUSSION

In this research the potential use of AG in various industrial branches was studied. To increase strength characteristics of unbleached pulp its surface was treated with 10-15% AG solution. Thanks to AG structure (similar to that of starch) it forms additional hydrogen bonds with hydroxyl groups of cellulose molecules and binds the neighbouring cellulose molecules (Terpuhova, Antonovskiy et al., 1979).

Table 1. The comparison of arabinogalactan, dextrin and lignosulfonate as the stabilizers in graphite suspensions.

Stabilizer	Consumption, g	Concentration loss, %
Lignosulfonate	6	22
Dextrin	5	15
	2	22
Arabinogalactan	5	18
	10	17

After surface treatment of cellulose handsheets (Russian Standard - 75 g/m² and 60°SR) the strength characteristics of pulp are improved; the folding endurance (number of double folds) also increases by ~25% as compared to reference pulp sample. Similar results were obtained after AG addition into the brown stock, but only in the presence of some substances which increase the retention of AG on the fibers. In our case DSL was used.

The other direction of our research was the study of AG as a stabilizer of graphite suspensions instead of dextrin. The experimental procedure of this study was the following: graphite (10 g) with AG (5, 10 g) were finely ground then water (0.5 l) was added and the first sample was taken at a depth of 10 cm. After one hour settling a sample was taken again at the same depth. Then the relative loss of sample weight was evaluated (it is so-called loss of concentration which characterizes the suspension stability). The greater it is, the less is the suspension stability. From data presented in Table 1 we may conclude that AG having good stabilizing properties can be used as a graphite suspension stabilizer instead of expensive dextrin and non-effective lignosulfonate.

The third direction presented here is the use of AG as a plasticiser in porous ceramics production (filter medium, porous filtration pots et). 2-2.5 % of AG added to ceramics composition provides products with the same characteristics as after the addition of the more expensive carboxymethylcellulose.

Table 2. The effect of AG addition on porous ceramics characteristics with and without the use of burning additive "DSL".

Composition, %	1	2	3	4
Mixture characteristics				
Synthetic corundum	85.0	85.0	85.0	85.0
Clay	15.0	15.0	15.0	15.0
Carboxymethylcellulose (CMC)*	2.0	--	--	--
Polyvinylacetate (PVA)*	5.0	5.0	5.0	5.0
Plasticizer AG *				
Burning additive (DSL)*	--	2.0	2.5	2.0
Physical characteristics				
Water content, %	16.4	16.4	16.5	18.5
Porosity, %	36.5	41.34	41.53	46.13
Air permeability factor, m ³ .cm/cm ² .h.mmwater (Banzen)	0.24	0.23	0.25	6.07
Average diameter of pores, mm	10.37	9.58	9.86	46.5
Mechanical strength, s bending, MPa	9.12	8.39	8.85	18.57

*) Additive % of the mixed main components.

Combinations of AG and our special burning additive DSL permit not only an increase in porosity and air permeability, but also an improvement in the mechanical strength. From results presented in Table 2 we conclude that it is possible to use AG as the plasticizer instead of CMC.

CONCLUSIONS

Arabinogalactan (AG) may be used as a stabilizer in graphite industry, as plasticizing agent in porous ceramics production and as sizing agent in pulp and paper production.

REFERENCES

1. L.V.Kogan, F.B.Kurgan, Yu.N.Filimonov. The method of pulp production. Author's certificate of S.U. N 1595997, 1988.
2. A.F.Terpuhova, S.D.Antonovskiy, M.M.Chochieva. Adhesive properties of arabinogalactan. Himija i tehnologija tsellulozy. Mezhdusovskiy sbornik. Leningradskaja Lesotehnicheskaja Akademija, 1978, v.6, p.117-119.

60 Rheology of cellulose viscose

B Lönnberg, S Rosenberg and K Lönnqvist – Pulping Technology,
Åbo Akademi University, Åbo, Finland

ABSTRACT

Preparation of regenerated cellulose matrices requires that the crystalline cellulose of highly delignified and bleached wood fibres are made soluble. Solubility in weak alkali can be achieved by xanthogenation of the alkali cellulose, as was shown by Cross, Bevan and Beadle in 1891. The cellulose xanthogenate viscose obtained may then be regenerated by various means, such as mineral acid or heat.

The cellulose xanthogenate viscose can be regenerated to form thread by spinning, film by extrusion or sponge by casting. Cellulose sponges have been used for a number of years for cleaning and clinical purposes. Modern medicine and biotechnology demand specific cellulose sponge properties dependent on the application. In preparation of sponges it is thought that viscose viscosity will determine the flow of viscose around crystals and fibres mixed with the viscose to create porosity and strength of the regenerated cellulose. Therefore, attention is paid to the rheological properties of the viscose as indicated by some rheometer technique, which simulates the mixing procedure.

The rheometer used seemed to be useful for evaluation of the important parameters of the viscose preparation process including steeping/ageing, xanthogenation and ripening. Decreased degree of polymerisation achieved mainly by more effective ageing, *i.e.* longer time and higher temperature, decreased the viscose

viscosity significantly. The time of ripening conducted subsequent to xanthogenation initially decreased the viscosity to a minimum in between 30 to 50 h ripening time, but it increased again and returned to the initial viscosity level after some 150 h ripening time.

INTRODUCTION

There has been an increasing interest in man-made sponges for analytical, clinical and medical purposes. Sponges made from natural polymers like cellulose provide suitable physical and chemical properties for a variety of sponge products. Cooperation between University of Turku and Åbo Akademi University was established to improve the cellulose sponge properties aimed at monitoring the wound healing process (1, 2).

The viscose process based on xanthogenation subsequent to the steeping stage was selected as being well known from a number of applications for production of textile fibre, film and sponges. The schematical diagram in Fig. 1 (3) describes the different stages of the standard viscose process. The study reported here concentrates on the preparation of the viscose as being the raw material for the regenerated cellulose sponge. For clinical use the sponge should be pure cellulose and further it should have certain chemical and physical surface properties. Although the sponge preparation including coagulation/regeneration, bleaching and washing are significant parameters for the final sponge properties, they are not considered in this context. The aim was primarily to establish the effects of the various viscose preparation parameters to explore anomalies, if there are any, and thus forming the prerequisite for preparation of viscose viscosity suitable for mixing with salt crystals and cellulose fibres.

High viscosity viscose is supposed to flow unsufficiently round introduced particles such as crystals leaving the final sponge matrix too open, which implies low strength and low elasticity. On the contrary, low viscosity viscose will flow sufficiently forming continuous intracellular walls in the matrix and providing structures suitable for certain applications, such as that of collecting blood cells. The optimum conditions must therefore be found keeping in mind also the important chemical properties of the sponge interfaces.

THEORY OF VISCOSITY

The viscosity of viscose liquids can be determined relatively easy with a mixing device operated under controlled conditions (constant concentration, certain design for vessel and mixing rotor) by measuring for example the shaft torsion at a

certain rotational speed. This might be postulated as follows:

$$P = f(d, n, \eta) \quad /1/,$$

where P = net effect (W) introduced by the rotor as calculated from the torsional resistance, d = diameter (m) of the vessel, n = rotational speed (1/s) of the rotor and η = viscoelasticity (Ns/m²) of the liquid. This general model can be developed by application of dimensional analysis:

$$P = c d^3 \eta n^2 \quad /2/,$$

where c = constant of proportionality. The final model implies that a plot P versus n^2 would result in a linear function, the gradient of which reflects the viscoelasticity of the viscose, provided that the same vessel and rotor are used in all experiments.

EXPERIMENTAL

The evaluation of the cellulose xanthogenate viscose properties was made by measuring some properties on the cellulose sponges obtained and by measuring the viscose viscosity. The viscosity measurements are reported here. The viscosity was measured by application of a commercial rheometer, the Bohlin VOR Rheometer with the C14 measuring lid. The vessel diameter and height were 15.4 and 27.9 mm respectively. The bob in the vessel had a diameter of 14 mm and a height of 21 mm. The sample volume required is 2.0 ml. In this device the vessel is rotating, while the bob is stationary.

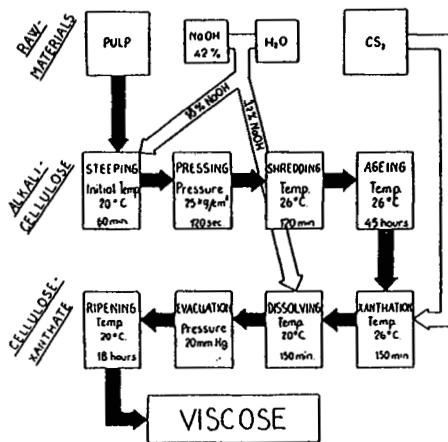


Fig.1. The viscose process (Ellefsen and Glöersen 1954).

RESULTS AND DISCUSSION

Steeping

Steeping (alkalising) of the cellulose determines the degree of polymerisation, DP. Fig. 2 indicates a clear correlation between viscose viscosity and the cellulose content of the viscose. If the steeping was conducted to generate different levels of DP, the viscosity levels obtained under certain xanthogenation conditions were also different. The DP 185 viscose was aged for 20 h at 43° C and xanthogenated by charging 26 % CS₂. The 328 DP viscose again was not aged at all, but the CS₂ charge was now 60 %. The 335 DP viscose finally was comparable with the former viscose in that it was not aged, but on the other hand it was xanthogenated in the same way as the 185 DP viscose. As visible the viscosity was much higher for the high-DP viscose evidently due to larger particles in the solution (4).

Steep 15% NaOH Age (see text) Xanth (see text)
Rheometer speed 46/s

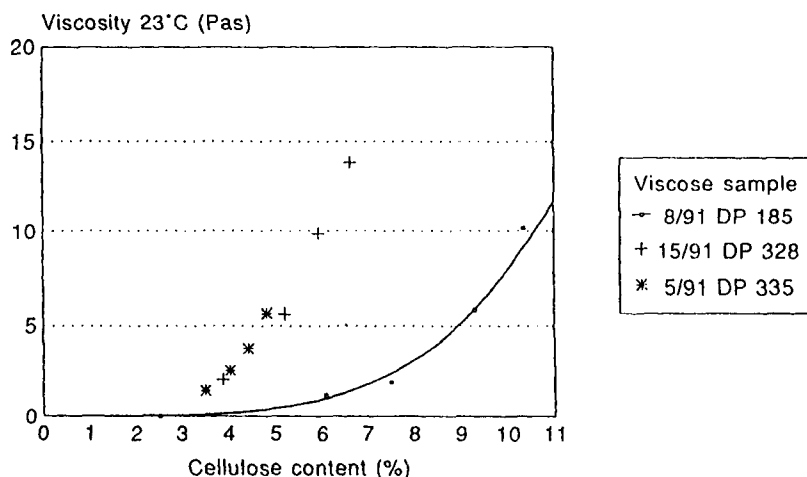


Fig.2. Viscose viscosity as a function of the cellulose content and DP.

Xanthogenation

Fig. 2 is also indicating that the influence of xanthogenation, changing from 26 % CS₂ charge to 60 %, is of minor significance for the viscose viscosity.

Ripening

The time of ripening of the xanthogenate is significant for the viscose viscosity, as is shown in Fig. 3. By increasing the ripening time the viscosity decreased initially, only to increase at a later stage and to reach the initial viscosity level. This phenomenon is known to be a result of desubstitution and resubstitution of the xanthate groups.

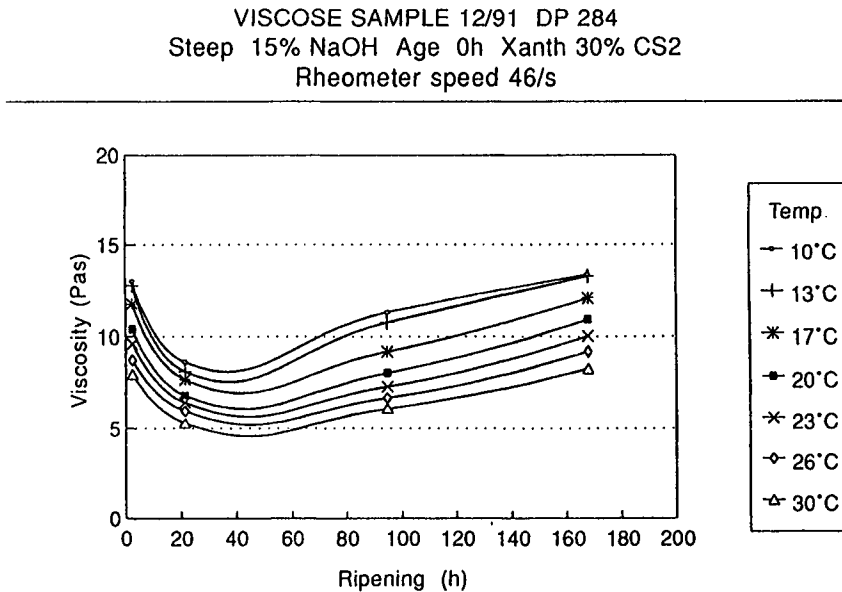


Fig.3. Viscose viscosity as a function of ripening and temperature.

Viscose parameters

As is seen from, for example Fig. 2, the higher cellulose content increased viscose viscosity under otherwise constant conditions, *i.e.* constant DP, steeping, ageing, xanthogenation and time of ripening as well as constant sodium hydroxide content of the viscose and a certain shearing rate.

Moreover, increasing temperature of the viscose decreased its viscosity, as is illustrated in Fig. 4.

VISCOSE SAMPLE 8/91 DP 185
 teep 15% NaOH Age 20h/43°C Xanth 26% CS2
 Rheometer speed 46/s

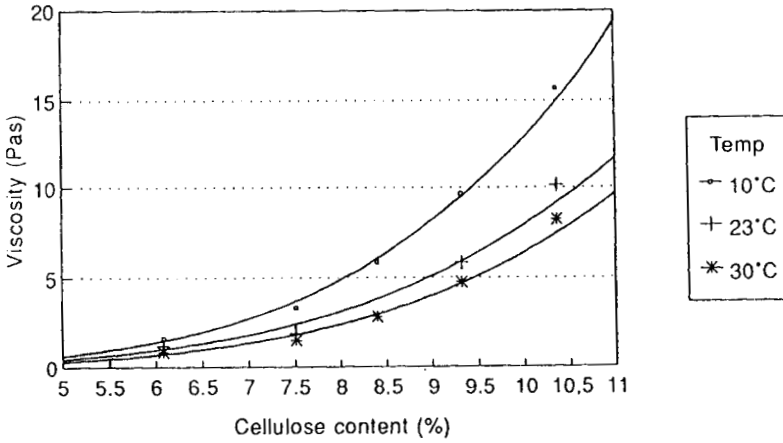


Fig. 4. Viscose viscosity as a function of cellulose content and temperature.

VISCOSE SAMPLE 15/91 DP 328
 Steep 15% NaOH Age 0h Xanth 60% CS2

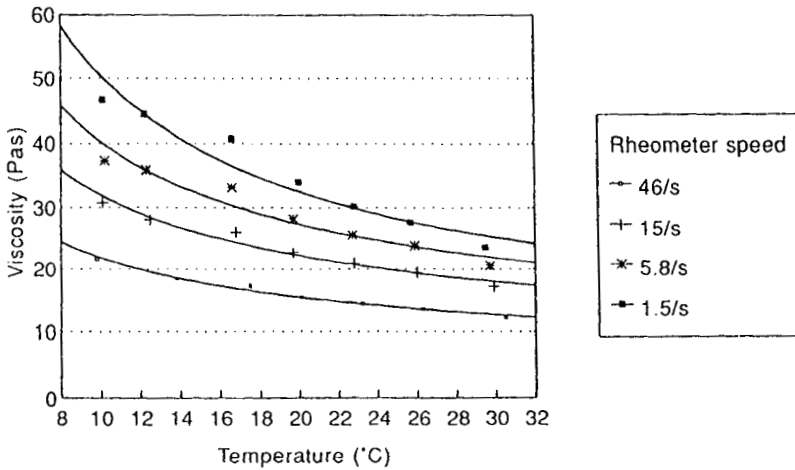


Fig. 5. Viscose viscosity as a function of temperature and rheometer speed.

Fig. 5 gives the correlation between viscose viscosity and viscose temperature at certain cellulose and sodium hydroxide concentrations of the viscose. It is evident that increased rotational speed provides lower viscosity levels of the viscose.

Finally, in the same type of diagram, Fig. 6 shows the viscose viscosity level as a function of the ripening time at a certain temperature.

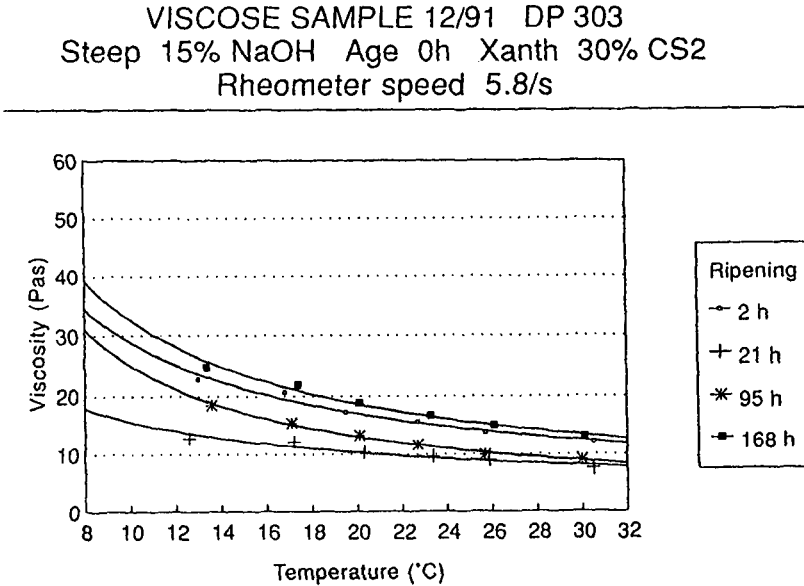


Fig. 6. Viscose viscosity as a function of temperature and ripening time.

CONCLUSIONS

This preliminary work on the correlations between the viscose viscosity and some certain viscose parameters, such as cellulose content of the final viscose, when the viscose process including steeping, xanthogenation and ripening is conducted according to standard procedures, indicate that the rheometer technique would be suitable for evaluation of the viscose properties.

Further work will focus on the search for some model for these correlations.

ACKNOWLEDGEMENTS

The financial support from the Technology Development Center of Finland (TEKES), Helsinki and Cellomeda Oy, Turku, Finland is gratefully acknowledged.

REFERENCES

- (1) Jouko A. Viljanto, Assessment of wound healing speed in man, *Clinical and Experimental Approaches to Dermal and Epidermal Repair: Normal and Chronic Wounds*, 1991 Wiley-Liss, Inc., p. 279-290.
- (2) O. Pajulo, B. Lönnberg, K. Lönnqvist and J. Viljanto, Development of a high grade viscose cellulose sponge, XXVIII Congress of The European Society for Surgical Research (ESSR), Turku, Finland, May 23-26, 1993, Abstract Book, P-156 (Eds. H. Aro and J. Niinikoski).
- (3) Ö. Ellefsen and J.G. Glöersen, Experiences with the P.F.I. Viscose Pilot Plant, *Paperi ja Puu - Papper o. Trä* (1954):9, 349-362.
- (4) M. A. Cohly, High shear rheological properties of viscose, *International Dissolving Pulps Conference 1968, Proceedings* p. 8.2.1-8.2.35

Part 6:
Wood, pulp and fibres

61 The effect of chlorine-free bleaching of dissolving pulp from Siberian wood species on structural changes and its properties

R Belodubrovskiy, V Kosheleva, O Zarudskaia, L Zvezdina and M Lazareva – 194021, St Petersburg, VNIIB, Shvernik av., 49;
V Bogdan – Bratsk Lespromcomplex Concern, Russia

ABSTRACT

Operating conditions of stepwise hydrolysis, kraft pulping and subsequent chlorine-free bleaching to produce dissolving pulp for different purposes were worked out and tested on a pilot and industrial scale. Viscose and cord pulps from softwood produced at the experimental department of Bratsk Forest Concern and bleached according to the scheme excluding elemental chlorine at the first bleaching stage are in conformity with standards. Structural and other characteristics of viscose and cord celluloses are identified with the same characteristics of these dissolving pulps bleached by traditional schemes. Several batches of cord pulp were produced at the Bratsk Forest Concern with low consumption of elemental chlorine from 40 kg/t to 19 kg/t at first stage. The pilot batches of chlorine-free dissolving pulp were processed at the chemical industry mills into viscose fiber and technical filament. Physical-mechanical characteristics of final products conform to the specification requirements.

MATERIALS AND METHODS

In this study the viscose pulp was produced from the pine and larch grown in the region of Bratsk, Siberia by two-stage prehydrolysis (the first stage - 160°C, the second stage - 170°C) followed by kraft pulping. This pulping was carried out according to the operation conditions of Bratsk Forest Complex. The viscose pulps produced by Baikal Pulp and Paper Mill and "Baikal" firm were used as reference pulp

samples. Some properties of these pulps are given in Table 1.

Table 1. Some properties of the pulps.

	Baikal sample	Bakai sample (V-60)
a-cellulose content, %	92.0	93.5
Dynamic viscosity, mp	110	96
Ash content, %	0.08	0.16
Pulp reactivity, %	80/11	80/11

RESULTS AND DISCUSSION

We worked out and tested on an industrial scale the operating conditions of stepwise prehydrolysis and subsequent kraft pulping which allow production of unbleached dissolving pulp of various purposes with lower pulp hardness (60 - 80 p.u.), higher viscosity, whilst simultaneously preserving the content of a-cellulose at 95 - 96%. Viscose and cord pulp from larch and pine wood produced at the experimental department of Bratsk Forest Complex were delignified by oxygen-alkali treatment without use of elemental chlorine at the first stage. The final bleaching was carried out with chlorine dioxide and hypochlorite. All the numbers, describing non-bleached pulps are given in Table 2.

Table 2. Unbleached pulp characteristics.

Wood species	Pulp characteristics		
	Hardness, p.u.	Viscosity, mps	a-cellulose content, %
Larch (viscose)	71	224	94.5
Pine (viscose)	65	206	94.5
Pine (cord)	82	320	95.8

All characteristics of bleached pulp are in conformity with the standards for bleached dissolving pulps. All the numbers concerning experimental bleaching are given in Table 3.

During the comparison of mass- molecular distribution of chlorine-free bleached and chlorine bleached viscose pulps it was established that it is identical: distribution is narrow enough and both pulps have a comparatively small content of low-molecular fractions with DP<200.

Data is given in Table 4.

Microscope research of swelling shapes of pulp fibers in orthophosphoric acid (characterizing indirectly the pulp reactivity to viscose formation) showed that the quantity of progressive swelling shapes (gel, grain, wood-loose and caterpillar-like shapes) is 84.5 - 89.7% for viscose pulp and 65-75% for the test batches of cord pulps as compared to 69.2% for the commercial pulp samples of Baikal pulp mill and 66.6% for the pulp of "Bakai" firm (trade mark V-65), respectively. From these results it is clearly seen that physical-chemical characteristics of dissolving pulp from Siberian soft wood treated without elemental chlorine at the first bleaching stage are identical to that of commercial pulp samples and "Bakai" firm (USA) samples with trade marks V-65, V-60. Moreover chlorine-free samples are characterized by a high processing ability. Several test batches of cord pulp were produced at the Bratsk Forest Complex with reduced chlorine consumption from 40 to 19 kg/t at the first bleaching stage. Bleaching was carried out according to the scheme C/D - E02 - H - D - D - A. Dioxide consumption was equal to 14 - 16 kg/t. The produced cord pulp was considered as the standard.

Table 3. Final product characteristics.

Characteristics	Pulp		
	Viscose		Cord
	Larch	Pine	Pine
a-cellulose content, %	92.7	93.2	~95.4*
Dynamic viscosity, mps(mPa.s)	112 (11.2)	105 (10.5)	190 (19.0)
Resin and fat content, %	0.05	0.03	0.05
Ash content, %	0.01	0.07	0.08
Brightness	89	90	88
Reactivity, CS ₂ /NaOH, %	80/11	80/11	110/11 (90/11)

*) Alkali solubility of pulp, % 10% - 5.7, 18% - 3.3

One has to point out also the decrease of organo-chlorine compounds in effluent from 3.1 kg/t to 1.7 - 1.9 kg/t. Experimental dissolving pulps (oxygen-alkaline pulps as well as pulps produced with reduced chlorine consumption) were processed at the various experimental departments and

Table 4. Mass-molecular distribution of viscose pulp.

Pulp	Fraction content (%) with DP within the limits					
	0-200	200-400	400-600	600-800	800-1000	1000-1200
Viscose (larch)	12.5	18.0	16.1	17.0	18.3	18.1
Viscose (pine)	12.0	19.6	16.4	17.0	18.0	17.0
Viscose produced at the Baikal pulp mill	14.0	19.5	21.5	22.0	13.0	10.0
Viscose produced by Bakai firm (trade mark)						
V-65	13.1	22.6	15.9	18.9	14.5	15.0
V-60	13.1	15.3	9.7	13.0	21.0	27.9

technical threads. Physical-mechanical characteristics of final products are in conformity with specifications (Table 5).

Table 5. Viscose and cord pulp characteristics.

Specifications	Pilot trials	
	Characteristics of the samples	
	1	2
Viscose fiber		
Linear density, tex	0.16-0.17	0.16
Specific tensile strength (specific breaking load), cN / tex,		
no more	21	26.5
Breaking elongation, %	19-26	25.3
Cord fiber (industrial thread)		
Specific tensile strength (specific breaking, load) cN / tex		46.4
Breaking elongation, %		11.7

CONCLUSIONS

It is clearly seen from our research that the use of chlorine-free bleaching or the bleaching at the lowered chlorine consumption allows to produce from Siberian softwood species the viscose and cord pulps which conform to the standard.

63 Thermodynamics of the wood matrix state

K Bogolitsyn – Arkhangelsk Forest Engineering Institute, Lenin Embankment 17, 163007 Arkhangelsk, Russia

Abstract

The thermodynamic miscibility of lignin, hemicellulose and cellulose has been investigated by the common solvent vapour static sorption method. This has allowed determination of the changes of free energy of the polymer mixing. Experimental results allow confirmation that the leading role of hemicellulose as a binder between cellulose and lignin microfibrils in the cell wall is not only in formation of covalent and hydrogen bonds, but also in formation of solid solutions with other components in transition layers. The physicochemical model of wood matrix formation was suggested on the basis of interconnection of changes in functional composition, redox properties and the thermodynamic state of biopolymers.

Review

The modern theories of wood matrix structure as a complex composition of natural biopolymers (lignin, hemicellulose, cellulose)

are based on common regularities of formation and properties of net polymers and polymers' compositions. The significant feature of this composition is thermodynamic compatibility of its components. It defines heterogeneity or homogeneity of the system and its thermodynamic stability. The polymer systems are thermodynamically compatible if their components are intersoluble on a molecular level. This state is in principle an exception: usually systems are microheterogeneous with a forced thermodynamic compatibility in comparison with homogeneous systems (completely compatible). The concept of structure of a ligno-carbohydrate matrix is closely connected with the idea of wood substance thermodynamic imbalance. The mechanism of its formation, incompatibility between lignin and carbohydrates, presence of valence bonds between lignin and hemicelluloses, existence of interpenetrative nets of incompatible components (which provide compatibility), indicates the quasistationary state of the cell wall. Therefore, any physical or chemical effects on the ligno-carbohydrate matrix should decrease compatibility between its components and can lead to microseparation into layers.

Thermodynamic compatibility of polymers is evaluated by different physical and chemical methods [1]. Non-thermodynamic methods include structural (radiography, optical and electronic microscopy, spectroscopical analysis) and relaxational methods (mechanical, dielectrical relaxation, nuclear magnetic resonance). However, from the quantitative point of view it is better to evaluate compatibility by means of thermodynamic methods, allowing one to determine thermodynamic parameters, which characterize reciprocal dissolution of components, thermodynamic affinity and phase diagrams "polymer-

polymer". Flory-Huggins interaction parameters, the second virial coefficient, Gibbs energy of mixing, changes in a value of chemical potential can be a measure of thermodynamic affinity between polymers.

The Flory-Huggins interaction parameter (X_{23}) can be determined by the method of static sorption of vapour of common solvent [2]. The negative value of this parameter for two polymers indicates their thermodynamic compatibility.

Thermodynamic compatibility is characterized by the negative value of Gibbs energy of mixing and positive value of its second derivative as a function of composition [3]. The methods of evaluation of thermodynamic compatibility of polymers by enthalpies of mixing of their low molecular analogues are known [4].

Comparison of physical and chemical methods of determination of thermodynamic characteristics shows that correct results can be obtained by means of direct calorimetric measurements of heats of mixing (methods of Paul and Tager [3,4]).

Priority in the field of study of thermodynamic compatibility of wood components belongs to the Institute of Wood Chemistry, Latvian Academy of Sciences. The investigations carried out by the research group lead by Prof. P. P. Erinsh in 1977-84 made it possible to use the heterogeneity of ligno-carbohydrate wood matrix as a principal example [5]. On the basis of values obtained for the Hildebrand parameter they concluded that the system of lignin-cellulose is thermodynamically incompatible, but the "hemicellulose of coniferous-hemicellulose of wood leaf", "hemicellulose-lignin" and "hemicellulose-cellulose" systems are compatible. The synergistic

effect of hemicellulose action in wood substance is revealed by increasing compatibility of incompatible biopolymers: cellulose-lignin by the formation of bonds between each of them separately and hemicelluloses.

Further, by investigations of the state of wood component mixtures by other techniques, such as the method of electronic spectroscopy [6], determination of heats of mixing of low-molecular analogues [7] and the method of static sorption of common solvent vapour [8] the authors came to the conclusion of thermodynamic incompatibility in the lignin-hemicellulose system.

Japanese researchers [9] studied the compatibility of lignin and hemicellulose by means of differential scanning calorimetry. They found out that compatibility of components in lignin-hemicellulose mixture is increased with rising temperature, thus the binodal temperature can be defined. This system has an "upper critical solubility temperature (UCST)" type of temperature-composition diagram. For the system studied UCST is reached in the range of very large and very small lignin contents. Decrease in binodal temperature by the addition of lignin-carbohydrate complex (LCC) to lignin-hemicellulose mixtures allows, according to authors' opinion one to consider the last as a "compatibilizer" of the components of the system. This corresponds to the statement, that compatibility of homopolymers can be increased by the addition of copolymer, i.e. a macromolecule which contains monomers present in the mixed homopolymers. Thus, together with results confirming the conclusion of wood components incompatibility, there are enough data that prevent one from making such a simple conclusion. The obtained data

seem to have an inner contradiction but the following explanation is offered.

Wood components are compositionally inhomogeneous polyfunctional polymers, separate fragments and groups of macromolecules which greatly differ in donor- acceptor properties [10]. The distinguished property of natural polyphenol compounds of the lignin type is their well-defined ability to oxidation with creation of the quinone form and the reduction-oxidation system phenol-quinone. That is why, according to the Cassidy and Kun definition, lignin can be referred to as a redox-polymer, which contains functional groups, which are able to reverse reduction-oxidation interactions [11].

Oxidation of carbohydrate wood component is one of the significant reactions. Besides, its condition is characterized by the presence of various functional groups in macromolecules the proportion of which defines the physicochemical properties [12]. Thus, the analyzed properties of wood components permit one to consider them as reduction-oxidation biopolymers and the wood matrix as a combination of them.

There is no doubt that factors that determine values of thermodynamic parameters of natural redox-polymer states especially in molecular and high molecular levels of their structural organization, are the presence of definite types of functional groups and structures, correlation of reduction and oxidation forms, ability to form chemical links, etc. Actually, in the process of biogenesis not only structural, but also functional, transformations of components, which form the composition of wood substance, take place [13]. In the early stages of wood formation (young wood), lignin predecessors present themselves as phenol compounds of low molecular mass, and their content in

comparison with carbohydrate component is not high. Phenol compounds can be oxidized comparatively easy, and their reduction-oxidation processes in cambial tissues are in balance, and accumulation of phenol oxidation products in cells does not occur. The mechanism of biosynthetic formation of vegetation phenol compounds and the chemical nature of components, probably defines thermodynamic compatibility in a "phenol compound-carbohydrate" system and the formation of sufficiently strong chemical links. During dying of living cells in the process of wood formation (lignification) oxidation processes begin to predominate over reduction and polyphenol oxidation products are accumulated in the quinoid forms that are catalysts of biological processes. Formation of a phenol-quinoid reduction-oxidation system of lignin components leads to thermodynamic imbalance in the wood matrix, thermodynamic incompatibility of lignin and cellulose, and as a result appearance of heterogeneity. Results obtained for thermodynamic compatibility of components in the "lignin-hemicellulose-cellulose" system by the method of static sorption of vapour of common solvent (by the changes of free energy of mixing) [14,15] can prove the approach described above of the thermodynamic state of the wood matrix. For the first time we came to the fact of the existence of two regions of compatibility in intervals of lignin content in composition at 0-10 and 85-100 mass percentage. Experimental results confirm that the leading role of hemicellulose as a binder between lignin and cellulose microfields in the cell wall is not only in formation of covalent and hydrogen bonds with them, but also in formation of solid solutions with other components in transition layers.

Consequently the approach offered for consideration of the thermodynamic state of wood matrix can be a basis for developing new technologies of chemical wood treatment, directed at separation of wood components by breaking links in the ligno-carbohydrate matrix, and also at methods of wood components production in their native state: e.g. technologies of non-reagent wood separation (biodestruction, burst autohydrolysis, electric impulse and radio treatment etc.), methods of cellulose production by use of complex systems, including organic solvents with different degree of mixing with water, and oxidation methods of delignification.

References

1. T.E.Skrebets, K.G.Bogolitsyn and A.Y.Gur'ev, *Wood Chemistry*, 1992, 4-5, 3.
2. T.K.Kwei, T.Nishi and N.F.Roberts, *Macromolecules*, 1974, 7, 667.
3. A.A.Tager, T.I.Sholochovich and I.M.Sharova, *Visokomol.soed.*, 1975, 17A, 2766.
4. C.A.Cruz, J.W.Barlow and D.R.Paul, *Macromolecules*, 1979, 12, 726.
5. P.P.Erinsh, *Khim.drev.*, 1977, 1, 8.
6. B.A.Anderson, U.L.Kallavus and J.A.Gravitis, *Khim.Drev.*, 1984, 1, 106.
7. M.K.Jakobson, G.V.Freymane and P.P.Erinsh, *Khim.drev.*, 1988, 1, 3.
8. J.A.Gravitis, B.A.Anderson, M.K.Jakobson, I.K.Dumil and P.P.Erinsh, *Khim.drev.*, 1984, 5, 99.
9. M.Shigemarsu, M.Mozita and I.Sakato, *Mokuzai Gakkaishi*, 1991, 37, 50.
10. K.G.Bogolitsyn, *Doctor's Dissertation*, Riga, 1987.

11. K.G.Bogolitsyn and V.G.Krunchak, *Abstr.Inter.Symp.Wood and Pulping Chem.*,
USA, Carolina Univ., 1989, 421.
12. K.G.Bogolitsyn, O.Brovko, A.Aizenshtadt and G.M.Poltoratsky, *Abstr.Inter.Symp. Cellulose and Lignocell.Chemistry*,Guangzhou, China, 1991, 134.
13. L.He and N.Terashima, *J.Wood Chem. and Technol.*, 1990, 10, 435.
14. K.G.Bogolitsyn, A.Y.Gur'ev and T.E.Skrebets, *Abstr.Inter.Symp.Wood and Pulping Chem.*, Beijing, China, 1993, 342.
15. A.Y.Gur'ev, K.G.Bogolitsyn, and T.E.Skrebets, *Wood Chem.*, 1993, 4, 3.

62 Some aspects of lignin modification

K Wrześniewska-Tosik, and H Struszczyk – Institute of Chemical Fibres, 90-570 Lodz, ul MC Skłodowska 19/27, Poland

ABSTRACT

The progress of development of new polymeric materials is related to the use of renewable raw materials such as lignin. The different types of lignin, both lignosulfonates and steam-explosion lignin, modified by terephthaloyl chloride, were used in these studies. The super-molecular properties and useful behaviour of modified lignin are presented. Applications of some lignin-based additives for modification of polyester fibres are also discussed.

INTRODUCTION

The progress of new polymeric materials is also related to the use of renewable raw materials such as lignin. The reactivity of lignin is concerned mainly with

the presence of hydroxyl groups, both aromatic and aliphatic, and permits production of several lignin-based modified versions for special applications [1]. Several studies dealing with modifications have recently been published [1-6]. A recent investigation of this process has produced meltable aromatic ester-like polymeric materials with a wide range of applications. The derivatives have several advantages such as a melting point between 250°C and 350°C, good hydrolytic and chemical resistance, increased thermal resistance, white to yellow colour as well as miscibility in a melt with other polymers [1-4,6].

This paper presents some new types of lignin-based polymers obtained by reaction of lignosulfonates and steam-explosion lignin with terephthaloyl chloride. The properties of the modified lignins, including their molecular weight distribution and uses for modification of polyester fibres, are discussed.

EXPERIMENTAL

MATERIALS AND METHODS

Lignosulfonates of Ultrazine NAS and Borresperse NA, Borregaard Inc., Ltd, Sapsborg, Norway, and experimental samples of steam explosion lignin coded L-2 and L-3, Virginia Tech, Blacksburg, USA (Table 1) were used. Terephthaloyl chloride with m.p. = 83-84°C, Merck, Germany was used as a reactive modifier, and the modification of lignin by this compound was carried out for 1 h at 30°C by a solution method [4] in dimethylacetamide using pyridine as hydrogen chloride acceptor. The properties of the

Table 1. Some properties of lignins used

Type of lignin	Colour and form	Moisture content %	Element content, %			Total hydroxyl groups content % wt
			C	H	S	
Ultrazine NAS	dark brown powder	4.9	44.7	5.0	2.6	15.1
Borresperse NA	light brown powder	5.1	40.7	4.8	4.1	14.9
L-2	light brown powder	10.8	58.4	6.2	-	10.0
L-3	dark brown powder	23.9	45.6	5.6	-	7.2

derivatives obtained as well as raw materials such as element content, melting point, total hydroxyl group content were determined by standard analytical methods [1-4]. Estimation of molecular weight distribution for modified lignin was carried out by GPC liquid chromatography on a HP 1050 Hewlett-Packard using a polystyrene-filled column made by Polymer Laboratories (UK). The lignin based additives were introduced during the polymerization stage using 6% w/w of lignin derivative based on dimethylterephthalate monomer weight. A standard polymerization of dimethylterephthalate with ethylene glycol was also carried out for comparison.

The polyethylene terephthalate (PET) fibres, both standard as well as modified by lignin-based additives, were manufactured by a melt-spinning method using an extruder type of spinning apparatus of Barmag, Germany equipped with spinnerets with 32 holes of 0.25 mm diameter. The dried standard PET made in ZWCh Elana, Toruń, Poland was also used to manufacture filaments for comparison. The properties of polyethylene terephthalate

and suitable fibres were determined by typical analytical methods used in the chemical fibres industry.

RESULTS AND DISCUSSION

Modification of lignin by bi-functional acid chlorides has created a chance of manufacture of multifunctional polymeric materials using renewable raw materials. Lignins modified by terephthaloyl chloride are characterized by several useful properties as summarized in Table 2. From these data it can be concluded that the products obtained during modification of lignosulfonates are characterized by suitable relation of melting point with the raw materials molar ratio. The steam explosion lignin seems also to be attractive as a raw material for chemical modification by terephthaloyl chloride, especially in the case of products with lower melting points (Table 2).

Estimates of the distribution of molecular weight of modified lignins using GPC are presented in Table 3.

The modification of steam explosion lignin has caused suitable augmentation of the average molecular weight as well as reduction of product polydispersity. The steam explosion lignin containing still some cellulose seems to be the most suitable raw material for modification to obtain products suitable for use in resins or composites.

The modified lignosulfonates were used as the additives for modification of polyester fibres. The mechanical properties of polyester fibres modified by 6% w/w of lignosulfonate-based additives as well as standard polyester fibres for comparison are presented in Table 4. Some super-molecular parameters of modified polyester fibres are presented in Table 5.

Table 2. Some properties of lignin (L) modified by terephthaloyl chloride (TC).

Type of lignin	Symbol of product	Colour and form	Molar ratio of L to TC	Element content, %			M.p. °C
				C	H	S	
Ultrazine NAS	-	d.brown	-	55.9	4.21	5.02	*
	LS -2	l.cream	1:1	56.7	4.15	4.55	278-285
	LS -4	l.cream	1:2	56.7	4.01	5.00	302-307
	LS -5	l.cream	1:3	56.0	4.04	4.06	287-292
	LS -6	l.cream	1:4	56.2	4.16	4.46	314-317
Borresperse NA	-	l.brown	-	56.0	4.20	4.09	*
	LS'-2	beige	1:1	56.8	4.00	4.00	280-295
	LS'-4	beige	1:2	57.0	4.07	3.97	301-308
	LS'-5	beige	1:3	56.0	4.09	3.77	294-298
	LS'-6	beige	1:4	56.9	4.18	3.99	315-321
L - 2	-	l.brown	-	58.4	6.20	-	*
	L2A	l.brown	1:3	60.0	4.04	-	230
L - 3	-	d.brown	-	45.6	5.60	-	*
	L3A	brown	1:3	58.5	4.20	-	230

* - non melting without decomposition, l-light, d-dark.

Table 3. Distribution of molecular weight of some lignin-based modificates.

Type of modificates	Type of lignin	M_w $\times 10^{-4}$	Polydispersity
LS-5	Ultrazine NAS	5.7	6.0
LS'-5	Borresperse NA	4.9	5.2
L-3A	Steam-explosion	11.8	4.8
L-3	" "	9.1	6.3

Table 4. Some mechanical properties of modified polyester fibres.

Sample type	Stretching	dtex	Tenacity cN/tex	Elongation %	Contraction %
Filament	3.25	66.0	21.5	65.2	35.2
with LS-5*	3.74	57.0	24.7	46.7	24.1
	4.00	52.2	28.4	32.9	18.7
	4.80	44.0	36.8	16.4	14.2

Filament	3.25	64.4	24.8	56.0	33.6
with LS'-5	3.74	55.2	30.3	36.7	13.6
	4.00	51.4	34.6	30.0	11.1
	4.80	42.9	45.7	10.3	10.2

Standard	3.25	64.9	29.0	51.0	28.8
filament	3.74	56.2	37.0	32.4	13.4
	4.00	51.6	41.7	25.4	11.8
	4.80	43.8	56.2	11.2	11.1

* - 6% w/w of additives on DMT weight

Table 5. Some super-molecular parameters of modified polyester fibres.

Sample type	Type of lignin used	Density g/cm ³	Crystallinity degree %
Filament with LS-5	Ultrazine NAS	1.3729	18.6
Filament with LS'-5	Borresperse NA	1.3732	18.7

Standard filament	-	1.3676	14.1

Application of lignosulfonate-based additives for modification of polyester fibres caused suitable

augmentation of their crystallinity degree as well as density (Table 5). This phenomenon is related to the action of additives on the super-molecular structure of the polyester fibres. The results of determination of useful properties of modified polyester fibres are summarized in Table 6.

Table 6. Some properties of modified polyester fibres.

Type of sample	Type of lignin used	Moisture content %	Electric resistance Ω	LOI %
Filament with LS-5	Ultrazine NAS	1.00	1.1×10^{14}	24
Filament with LS'-5	Borresperse NA	0.83	7.0×10^{13}	24
Standard filament	-	0.70	1.6×10^{14}	22

Modification of PET fibres by lignosulfonate-based additives caused suitable augmentation of moisture content and flame resistance (Table 6). At the same time it can be pointed out that compared with standard PET fibres the modified PET fibres are characterized by better dyeability for several types of dyes.

CONCLUSIONS

1. Modification of lignosulfonates by terephthaloyl chloride has created lignin-based polymeric derivatives with a melting point in the range of 280-321°C suitable for use as additives to improve of polyester fibre properties.

2. Polyester fibres modified by lignosulfonate-based additives are characterized by several advantages in comparison to standard polyester fibres, such as better dyeability, higher moisture content or higher flame resistance.

3. Modification of steam explosion lignin by terephthaloyl chloride has produced lignin-based derivatives with a wide range of melting point from 230°C and suitable for use in resins and composites.

REFERENCES

1. W.G.Glasser and S.Sarkanen ed., Lignin: Properties and Materials, ACS Symposium Series 397, ACS, Washington D.C., 1989.
2. H.Struszczyk, "Modification of Lignin: Present State and Development Forecast", in "Lignocellulosics: Science, Technology, Development and Use", Ellis Horwood Ltd., New York, 1992, p.791.
3. K.Wrzeńniewska-Tosik and H.Struszczyk, "Some Aspects of Lignin Modification", in "Lignocellulosics: Science, Technology, Development and Use", Ellis Horwood Ltd., Chichester, 1992, p.629.
4. Polish Patent 134256 (1982).
5. Van der Klashort, G.H. Forbes, C.P. Psotta, Holzforschung, 37(6), 279 (1983).
6. H.Struszczyk, K.Grzebieniak, K.Wrzeńniewska-Tosik and A.Wilczek, "Some Applications of Modified Lignin", in "Cellulosics: Chemical, Biochemical and Material Aspects", Ellis Horwood Ltd., 1993, p.555.

63 Thermodynamics of the wood matrix state

K Bogolitsyn – Arkhangelsk Forest Engineering Institute, Lenin Embankment 17, 163007 Arkhangelsk, Russia

Abstract

The thermodynamic miscibility of lignin, hemicellulose and cellulose has been investigated by the common solvent vapour static sorption method. This has allowed determination of the changes of free energy of the polymer mixing. Experimental results allow confirmation that the leading role of hemicellulose as a binder between cellulose and lignin microfibrils in the cell wall is not only in formation of covalent and hydrogen bonds, but also in formation of solid solutions with other components in transition layers. The physicochemical model of wood matrix formation was suggested on the basis of interconnection of changes in functional composition, redox properties and the thermodynamic state of biopolymers.

Review

The modern theories of wood matrix structure as a complex composition of natural biopolymers (lignin, hemicellulose, cellulose)

are based on common regularities of formation and properties of net polymers and polymers' compositions. The significant feature of this composition is thermodynamic compatibility of its components. It defines heterogeneity or homogeneity of the system and its thermodynamic stability. The polymer systems are thermodynamically compatible if their components are intersoluble on a molecular level. This state is in principle an exception: usually systems are microheterogeneous with a forced thermodynamic compatibility in comparison with homogeneous systems (completely compatible). The concept of structure of a ligno-carbohydrate matrix is closely connected with the idea of wood substance thermodynamic imbalance. The mechanism of its formation, incompatibility between lignin and carbohydrates, presence of valence bonds between lignin and hemicelluloses, existence of interpenetrative nets of incompatible components (which provide compatibility), indicates the quasistationary state of the cell wall. Therefore, any physical or chemical effects on the ligno-carbohydrate matrix should decrease compatibility between its components and can lead to microseparation into layers.

Thermodynamic compatibility of polymers is evaluated by different physical and chemical methods [1]. Non-thermodynamic methods include structural (radiography, optical and electronic microscopy, spectroscopical analysis) and relaxational methods (mechanical, dielectrical relaxation, nuclear magnetic resonance). However, from the quantitative point of view it is better to evaluate compatibility by means of thermodynamic methods, allowing one to determine thermodynamic parameters, which characterize reciprocal dissolution of components, thermodynamic affinity and phase diagrams "polymer-

polymer". Flory-Huggins interaction parameters, the second virial coefficient, Gibbs energy of mixing, changes in a value of chemical potential can be a measure of thermodynamic affinity between polymers.

The Flory-Huggins interaction parameter (X_{23}) can be determined by the method of static sorption of vapour of common solvent [2]. The negative value of this parameter for two polymers indicates their thermodynamic compatibility.

Thermodynamic compatibility is characterized by the negative value of Gibbs energy of mixing and positive value of its second derivative as a function of composition [3]. The methods of evaluation of thermodynamic compatibility of polymers by enthalpies of mixing of their low molecular analogues are known [4].

Comparison of physical and chemical methods of determination of thermodynamic characteristics shows that correct results can be obtained by means of direct calorimetric measurements of heats of mixing (methods of Paul and Tager [3,4]).

Priority in the field of study of thermodynamic compatibility of wood components belongs to the Institute of Wood Chemistry, Latvian Academy of Sciences. The investigations carried out by the research group lead by Prof. P. P. Erinsh in 1977-84 made it possible to use the heterogeneity of ligno-carbohydrate wood matrix as a principal example [5]. On the basis of values obtained for the Hildebrand parameter they concluded that the system of lignin-cellulose is thermodynamically incompatible, but the "hemicellulose of coniferous-hemicellulose of wood leaf", "hemicellulose-lignin" and "hemicellulose-cellulose" systems are compatible. The synergistic

effect of hemicellulose action in wood substance is revealed by increasing compatibility of incompatible biopolymers: cellulose-lignin by the formation of bonds between each of them separately and hemicelluloses.

Further, by investigations of the state of wood component mixtures by other techniques, such as the method of electronic spectroscopy [6], determination of heats of mixing of low-molecular analogues [7] and the method of static sorption of common solvent vapour [8] the authors came to the conclusion of thermodynamic incompatibility in the lignin-hemicellulose system.

Japanese researchers [9] studied the compatibility of lignin and hemicellulose by means of differential scanning calorimetry. They found out that compatibility of components in lignin-hemicellulose mixture is increased with rising temperature, thus the binodal temperature can be defined. This system has an "upper critical solubility temperature (UCST)" type of temperature-composition diagram. For the system studied UCST is reached in the range of very large and very small lignin contents. Decrease in binodal temperature by the addition of lignin-carbohydrate complex (LCC) to lignin-hemicellulose mixtures allows, according to authors' opinion one to consider the last as a "compatibilizer" of the components of the system. This corresponds to the statement, that compatibility of homopolymers can be increased by the addition of copolymer, i.e. a macromolecule which contains monomers present in the mixed homopolymers. Thus, together with results confirming the conclusion of wood components incompatibility, there are enough data that prevent one from making such a simple conclusion. The obtained data

seem to have an inner contradiction but the following explanation is offered.

Wood components are compositionally inhomogeneous polyfunctional polymers, separate fragments and groups of macromolecules which greatly differ in donor- acceptor properties [10]. The distinguished property of natural polyphenol compounds of the lignin type is their well-defined ability to oxidation with creation of the quinone form and the reduction-oxidation system phenol-quinone. That is why, according to the Cassidy and Kun definition, lignin can be referred to as a redox-polymer, which contains functional groups, which are able to reverse reduction-oxidation interactions [11].

Oxidation of carbohydrate wood component is one of the significant reactions. Besides, its condition is characterized by the presence of various functional groups in macromolecules the proportion of which defines the physicochemical properties [12]. Thus, the analyzed properties of wood components permit one to consider them as reduction-oxidation biopolymers and the wood matrix as a combination of them.

There is no doubt that factors that determine values of thermodynamic parameters of natural redox-polymer states especially in molecular and high molecular levels of their structural organization, are the presence of definite types of functional groups and structures, correlation of reduction and oxidation forms, ability to form chemical links, etc. Actually, in the process of biogenesis not only structural, but also functional, transformations of components, which form the composition of wood substance, take place [13]. In the early stages of wood formation (young wood), lignin predecessors present themselves as phenol compounds of low molecular mass, and their content in

comparison with carbohydrate component is not high. Phenol compounds can be oxidized comparatively easy, and their reduction-oxidation processes in cambial tissues are in balance, and accumulation of phenol oxidation products in cells does not occur. The mechanism of biosynthetic formation of vegetation phenol compounds and the chemical nature of components, probably defines thermodynamic compatibility in a "phenol compound-carbohydrate" system and the formation of sufficiently strong chemical links. During dying of living cells in the process of wood formation (lignification) oxidation processes begin to predominate over reduction and polyphenol oxidation products are accumulated in the quinoid forms that are catalysts of biological processes. Formation of a phenol-quinoid reduction-oxidation system of lignin components leads to thermodynamic imbalance in the wood matrix, thermodynamic incompatibility of lignin and cellulose, and as a result appearance of heterogeneity. Results obtained for thermodynamic compatibility of components in the "lignin-hemicellulose-cellulose" system by the method of static sorption of vapour of common solvent (by the changes of free energy of mixing) [14,15] can prove the approach described above of the thermodynamic state of the wood matrix. For the first time we came to the fact of the existence of two regions of compatibility in intervals of lignin content in composition at 0-10 and 85-100 mass percentage. Experimental results confirm that the leading role of hemicellulose as a binder between lignin and cellulose microfields in the cell wall is not only in formation of covalent and hydrogen bonds with them, but also in formation of solid solutions with other components in transition layers.

Consequently the approach offered for consideration of the thermodynamic state of wood matrix can be a basis for developing new technologies of chemical wood treatment, directed at separation of wood components by breaking links in the ligno-carbohydrate matrix, and also at methods of wood components production in their native state: e.g. technologies of non-reagent wood separation (biodestruction, burst autohydrolysis, electric impulse and radio treatment etc.), methods of cellulose production by use of complex systems, including organic solvents with different degree of mixing with water, and oxidation methods of delignification.

References

1. T.E.Skrebets, K.G.Bogolitsyn and A.Y.Gur'ev, *Wood Chemistry*, 1992, 4-5, 3.
2. T.K.Kwei, T.Nishi and N.F.Roberts, *Macromolecules*, 1974, 7, 667.
3. A.A.Tager, T.I.Sholochovich and I.M.Sharova, *Visokomol.soed.*, 1975, 17A, 2766.
4. C.A.Cruz, J.W.Barlow and D.R.Paul, *Macromolecules*, 1979, 12, 726.
5. P.P.Erinsh, *Khim.drev.*, 1977, 1, 8.
6. B.A.Anderson, U.L.Kallavus and J.A.Gravitis, *Khim.Drev.*, 1984, 1, 106.
7. M.K.Jakobson, G.V.Freymane and P.P.Erinsh, *Khim.drev.*, 1988, 1, 3.
8. J.A.Gravitis, B.A.Anderson, M.K.Jakobson, I.K.Dumil and P.P.Erinsh, *Khim.drev.*, 1984, 5, 99.
9. M.Shigemarsu, M.Mozita and I.Sakato, *Mokuzai Gakkaishi*, 1991, 37, 50.
10. K.G.Bogolitsyn, *Doctor's Dissertation*, Riga, 1987.

11. K.G.Bogolitsyn and V.G.Krunchak, *Abstr.Inter.Symp.Wood and Pulping Chem.*,
USA, Carolina Univ., 1989, 421.
12. K.G.Bogolitsyn, O.Brovko, A.Aizenshtadt and G.M.Poltoratsky, *Abstr.Inter.Symp. Cellulose and Lignocell.Chemistry*,Guangzhou, China, 1991, 134.
13. L.He and N.Terashima, *J.Wood Chem. and Technol.*, 1990, 10, 435.
14. K.G.Bogolitsyn, A.Y.Gur'ev and T.E.Skrebets, *Abstr.Inter.Symp.Wood and Pulping Chem.*, Beijing, China, 1993, 342.
15. A.Y.Gur'ev, K.G.Bogolitsyn, and T.E.Skrebets, *Wood Chem.*, 1993, 4, 3.

64 Effect of grinding on structure and reactivity of pulps

H Schleicher and J Kunze – Fraunhofer-Einrichtung für Angewandte Polymerforschung, D-14513 Teltow, Germany

INTRODUCTION

For some applications and several manufacturing processes of cellulose derivatives use of ground pulp is advantageous or necessary. The main purpose of grinding of pulp is the reduction of the particle size, but grinding not only reduces the particle size but also changes some structural parameters.

In the literature [1,2] a strong decrease of the crystallinity and of the degree of polymerization of cellulose by grinding in a vibration mill is described. Under extreme conditions amorphous cellulose with low DP may be prepared by this type of grinding. For industrial purposes other principles of grinding are used, mainly continuous processes, for instance cutting mills.

Up to now little information about alterations of cellulose parameters by such grinding processes has been published. For that reason the goal of our work was a comparative investigation of the influence of the type of raw material on changes of structure and properties of celluloses induced by grinding. Some orientating tests of the influence of grinding conditions on the characteristics of cellulose were also made. For the investigations we used celluloses with different native structures (linters, spruce sulphite pulp with normal viscosity, spruce sulphite pulp with high viscosity, and pine prehydrolyzed sulphate pulp). The cutting ground products were characterized in comparison with unground celluloses by

solid state high resolution ^{13}C -nmr spectroscopy, porosity, retention values for water and dimethylsulfoxide, DP and level-off DP, carbonyl content, alkali solubility, and some chemical reactions.

RESULTS

CHANGES OF STRUCTURE

As demonstrated by Figure 1, the solid state high resolution ^{13}C -nmr spectrum of cellulose was changed by grinding. Some lines are lowered and others are constant or enlarged in their intensity. Comparing the spectra of the native and of the ground celluloses, changes of the degree of order and of the conformation of cellulose by grinding are visible. A decrease in the degree of order is identified mainly by the decrease of the intensity ratio of the C-4 lines at about 89 and 84 ppm. Changes of the conformation are recognized by a decrease of the intensity of the C-2,3 lines in relation to the C-5 line. A significant decrease of the content of highly ordered regions of cotton linters by elastic deformational milling is also discussed by Bakhramov et al. on the basis of solid state high resolution ^{13}C -nmr investigations [3].

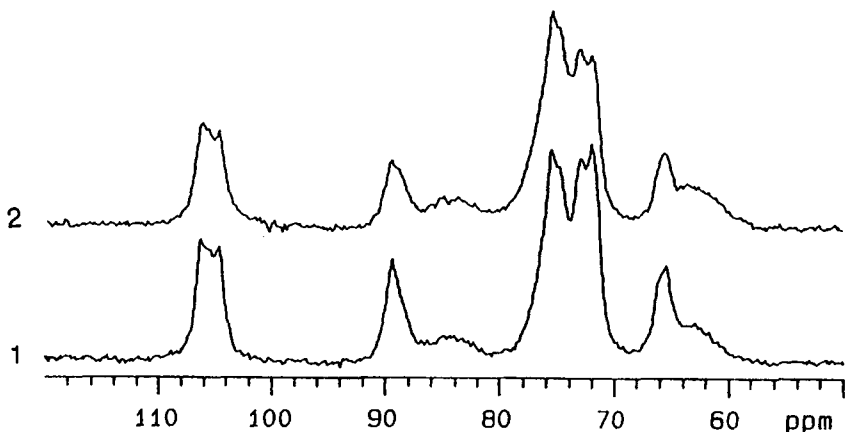


Figure 1. Solid state ^{13}C -nmr spectra of unground (1) and ground (2) linters

Comparing the same grinding conditions, the changes of the structure determined by variations of the intensity of the lines of the ^{13}C -nmr spectrum are larger for linters than for wood pulps. Diminished intensities of the C-4 line at about 89 ppm, of the C-6 line at about 65 ppm, and of the C-2,3 lines at about 73 ppm were observed for all ground cellulose materials. In the case of linters small increases of the C-4 line at about 84 ppm and of the C-6 line at about 63 ppm were additionally recognized.

For the cellulose samples investigated we calculated for each sample the ratios of the intensities of the lines C-4 89 ppm to C-4 84 ppm and C-2,3 73 ppm to C-5 75 ppm. Then we compared these ratios for the ground and unground samples and calculated values for relative changes caused by grinding by dividing the values of the ground samples by the values of the unground samples. As demonstrated by Table 1 on the basis of the C-4 lines the degree of order of linters is reduced more by grinding than that of wood pulps. The changes of the C-2,3 lines by grinding are nearly the same for all cellulose samples (Table 2).

Table 1. Influence of grinding on intensity ratios of the C-4 lines (89 ppm / 84 ppm) of solid state ^{13}C -nmr spectra of celluloses

Sample	Unground	Ground	Ratio of ground to unground cellulose
Linters	4.0	2.0	0.5
Sulphite pulp normal viscosity	2.0	1.5	0.75
Sulphite pulp high viscosity	1.9	1.35	0.71
Sulphate pulp	2.0	1.4	0.71

Table 2. Influence of grinding on intensity ratios of the C-2,3 line to the C-5 line (73ppm / 75ppm) of solid state ^{13}C -nmr spectra of celluloses

Sample	Unground	Ground	Ratio of ground to unground cellulose
Linters	1.04	0.87	0.84
Sulphite pulp normal viscosity	1.05	0.93	0.89
Sulphite pulp high viscosity	1.05	0.91	0.86
Sulphate pulp	1.10	0.98	0.89

Alterations of the solid state ^{13}C -nmr spectra of cellulose extend by a more intense influence of mechanical load on cellulose in the course of grinding. Such increased load on the cellulose may be caused by variations of the grinding conditions, for instance by changing of the

machine unit and in this way causing more disruption than cutting and grinding and by reducing the particle sizes of the ground cellulose. Figure 2 demonstrates this influence comparing the solid state ^{13}C -nmr spectra of two ground pulps with different particle sizes.

Comparing Figure 1 with Figure 3 similarities in the changes of the solid state ^{13}C -nmr spectra of cellulose caused by grinding to those caused by alkali treatment with aqueous sodium hydroxide are evident.

A measure to recognize changes in the fibrillar area of cellulose is the level-off DP determined by definite partial hydrolytic decomposition of the cellulose material

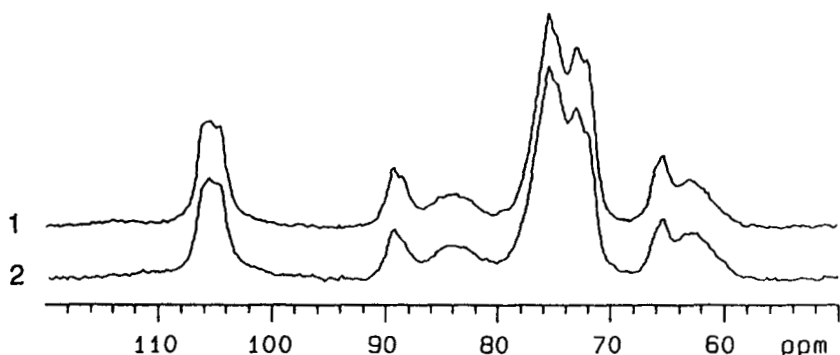


Figure 2. Solid state ^{13}C -nmr spectra of ground sulphate pulp. 1 - particle length between about 100 and 500 μm , 2 - particle length in the range of about 100 μm (besides some larger and many smaller particles)

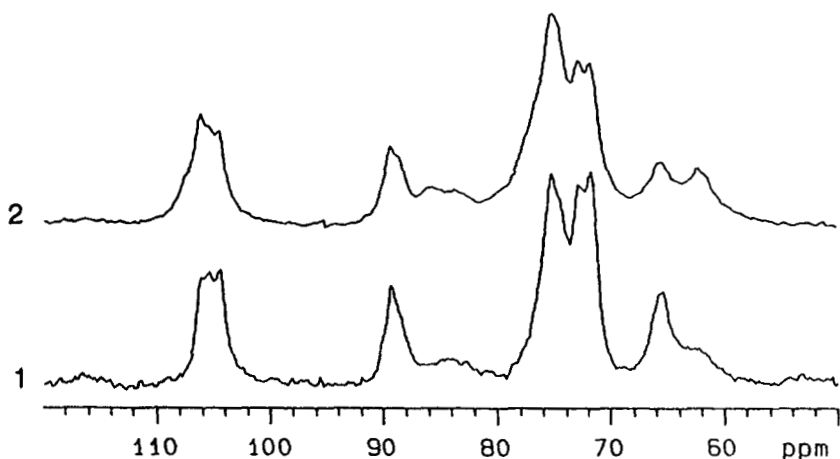


Figure 3. Solid state ^{13}C -nmr spectra of linters (1) and linters treated with 10 % w/w NaOH (2)

followed by measurement of the DP. It is known that by different treatments of pulps the level-off DP decreases. By alkali treatment of linters and wood pulps the level-off DP decreases with increasing NaOH concentration of the lye but in different ways for the various celluloses depending on the supermolecular structure of the cellulose samples [4].

Changes of the level-off DP of some cellulose materials caused by grinding are shown in Table 3. The numerical changes of the level-off DP are higher for sulphite pulps than for linters. But comparing the grinding with an alkali treatment of cellulose it is shown in Table 3 that for linters a higher sodium hydroxide concentration is necessary than for wood pulps to reach the same level-off DP as by grinding. This means that by the grinding process the fibrillar structure of linters is changed more than that of wood pulps. As is shown in Table 3 the level-off DP is changed by alterations in grinding conditions.

Table 3. Changes of the level-off DP of celluloses by grinding

Sample	Level-off DP		NaOH concentration to reach the level-off DP of ground pulp by an alkali treatment [%]
	Unground	Ground	
Linters	150	115	12
Sulphite pulp normal viscosity	175	125	8.5
Sulphite pulp high viscosity	200	120	-
Sulphate pulp	132	105	9.5
Ground sulphate pulp with low particle size		90	10.5

The pore system of the cellulose has an important influence on the course of reactions and dissolving processes of the cellulose. It is known that by various treatments of the celluloses the pores may be changed in different directions. For instance, by swelling, pores are often enlarged and by drying or heating, especially of swollen celluloses, pores may be closed.

We used mercury porosimetry and swelling values for the characterization of changes of the pores caused by grinding. The water retention values were determined after a swelling time of 1 hour followed by centrifugation of the

swollen sample. The DMSO swelling values were determined principally in the same way but with different swelling times [5].

Comparing the ground with the unground celluloses by the mercury porosimetry method we found a drastic decrease of the total porosity caused by a reduction of the large pores but connected in most cases with an increased porosity in the area of small pores ($< 0,1 \mu\text{m}$).

As is shown in Table 4, the water retention values are diminished by grinding. Corresponding to former investigations [5], larger swelling values were found with DMSO than with water. In contrast to the swelling in water the swelling values with DMSO after long swelling times (> 1 h) are higher for ground samples (Table 5). But for short swelling times (15 minutes) with some ground samples higher and with some samples ground in different ways, lower DMSO swelling values in relation to the swelling

Table 4. Changes of water retention value by grinding

Sample	Water retention value [%]	
	Unground	Ground
Linters	58	52
Sulphite pulp normal viscosity	65	57
Sulphite pulp high viscosity	74	68
Sulphate pulp	64	55
Ground sulphate pulp with low particle size		49

Table 5. Changes of DMSO swelling values by grinding
(72 hours swelling time)

Sample	DMSO swelling value [%]	
	Unground	Ground
Linters	95	117
Sulphite pulp normal viscosity	104	121
Sulphate pulp	102	113
Ground sulphate pulp with low particle size		132

values of the corresponding unground celluloses were observed. Contrary to the water retention values decreasing with increasing mechanical load of the cellulose by the grinding, the long time (72 h) DMSO swelling values increased with increasing load. But the DMSO swelling values determined after a short swelling time (15 minutes) decreased with increasing mechanical load at grinding. This is an indication that by this way the hornification of the cellulose caused by the grinding increases. In our opinion the differences between the short time and the long time DMSO swelling values, or still better the way in which the swelling values increase with the swelling time, give useful information about the accessibility of the pores.

It is known that the degree of polymerization of polymers may be reduced by mechanical treatment. We found that the extent of the reduction of the DP of cellulose by grinding is influenced more by the type of cellulose and the grinding conditions than the changes of the supermolecular structure of cellulose. As shown in Table 6 linters are more degraded than wood pulps by grinding under the same conditions. It is worth mentioning that high viscosity sulphite pulps used for the manufacture of cellulose ethers were only to a small extent reduced in their DP by grinding.

Table 6. Influence of grinding on reduction of DP

Sample	DP	
	Unground	Ground
Linters	1950	1630
Sulphite pulp normal viscosity	670	585
Sulphite pulp high viscosity	1570	1520
Sulphate pulp	750	670

By some orientation investigations of one of our partners it was found by grinding that the number average molecular weight M_n is reduced more than the weight average molecular weight M_w . That means grinding decreases the uniformity of the molecular weight distribution.

By determination of the carbonyl groups of some ground and unground pulps an increase of the carbonyl content of cellulose by grinding was found.

CHANGES OF THE REACTIVITY

It is known that the reactivity of cellulose may be increased or decreased if the structural parameters of the cellulose are changed. But it is necessary to emphasize that reactivity and accessibility of cellulose are not absolute but only relative parameters. The progress of different cellulose reactions is influenced or limited by the various parameters of the cellulose structure in different ways. The influence of the initial accessibility of the pores of the cellulose on the reactivity increases with decreasing swelling power and increasing size of the molecules of the reaction media. Splitting of hydrogen bonds between the fibrils by some treatments of the cellulose has a positive effect on many cellulose reactions. For the ground celluloses it is expected that the reduced accessibility of a part of the pores has a negative influence and the splitting of fibrillar bonds has a positive effect on the reactivity of the celluloses.

Acetylation is a reaction with a low swelling power of the reaction medium. We used the acetic acid content after an acetylation time of 3 minutes as a measure of reactivity [6]. Table 7 demonstrates a reduced acetylation velocity of the ground celluloses. The negative effect of grinding on the acetylation is especially high for linters and smallest for sulphite pulp of high DP.

Table 7. Influence of grinding on velocity of acetylation

Sample	Bound acetic acid after 3 minutes [%]	
	Unground	Ground
Linters	20	8
Sulphite pulp normal viscosity	24	17
Sulphite pulp high viscosity	59	45

The solubility of cellulose is influenced or limited by various parameters like DP, extent of interfibrillar bonds, and accessibility of the pores, in different way for the different solvents. Solvents with a strong swelling power are able to overcome a small hornification of the cellulose.

The alkali solubility of the cellulose is increased by grinding due to the decreased DP and the changed supermolecular structure. The solubility in sodium hydroxide lye of a concentration of 10 % w/w at 20 °C increased about 1 to 6 % depending on the grinding conditions and the cellulose material. The solubility in sodium hydroxide lye with

a concentration of about 10 % w/w at - 10 °C changed more than the alkali solubility at room temperature indicating an improved accessibility of the ground cellulose.

Some years ago we found that for the dissolution of cellulose in the system DMSO/paraformaldehyde for ground pulp a lower paraformaldehyde content was necessary than for the dissolution of unground pulp [7]. For many cellulose reactions alkali cellulose as an intermediate is manufactured by treatment of pulp with sodium hydroxide lye. The NaOH concentration necessary for the transformation of cellulose to alkali cellulose depends on the supermolecular structure of the cellulose samples [8]. We wanted to know whether the alkalization of cellulose is influenced by grinding.

Unground and ground pulps were treated by sodium hydroxide lye with concentrations of 9 to 12 % w/w. After regeneration of the alkali treated samples they were investigated by solid state ^{13}C -nmr spectroscopy and some other methods. Figure 4 demonstrates that by the alkali treatment of the ground pulp a larger part of cellulose is transformed to cellulose II than of the unground pulp.

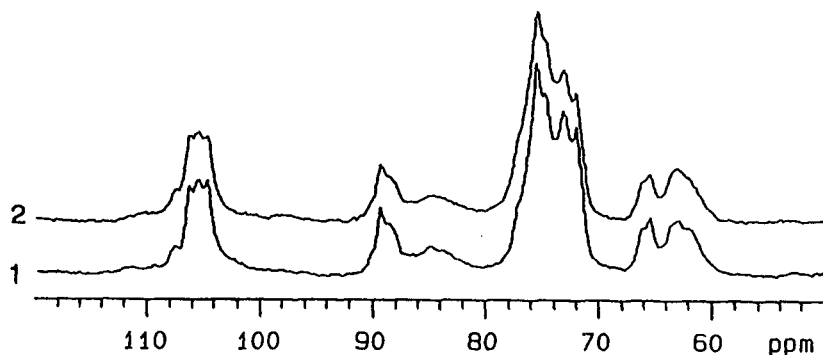


Figure 4. Solid state ^{13}C -nmr spectra of alkali treated sulphate pulps (10 % w/w NaOH). 1 - unground pulp, 2 - ground pulp

The changes of the solid state ^{13}C -nmr spectra and of the level-off DP demonstrate that by grinding of cellulose the penetration of alkali lye into cellulose is improved and a reduced sodium hydroxide concentration of the lye is necessary for structural changes of cellulose.

CONCLUSIONS

By grinding of cellulose materials beside reduction of particle size various structural parameters of the cellulose are changed, and by its depending on the following reactions the reactivity may be improved or decreased. The extent of structural alterations of cellulose increases

with increasing mechanical load of cellulose at the grinding. By grinding the parameters of linters are more changed than those of wood pulps. This may be explained by differences in the structure of the different celluloses. We suppose that the higher order and the higher density of hydrogen bonds of linters compared with wood pulps make it more difficult to split fibres in smaller particles. For that reason more principal valence bonds are disrupted by mechanical load.

REFERENCES

1. G. E. Maciel, W. L. Kolodziejcki, M. S. Bertram, B. E. Dale, *Macromolecules* 15 (1982) 686-687
2. H.-P. Fink, B. Philipp, D. Paul, R. Serimaa, T. Paakari, *Polymer* 28 (1987) 1265-1270
3. M. Bakhramov, N. V. Myagkova, B. k. Davranov, R. G. Zbankov, R. Teejaer, E. V. Korolik, S. P. Firsov, *Vysokomol. Soed.*, B 34 (1992) 75-78
4. H. Schleicher, B. Philipp, C. Ruscher, *Faserforsch. u. Textiltechnik* 18 (1967) 1-4
5. B. Philipp, H. Schleicher, W. Wagenknecht, *Faserforsch. u. Textiltechnik* 24 (1973) 106-112
6. L. Loeb, L. Segal, *Text. Res. J.* 24 (1954) 654-658
7. H. Schleicher, K. Schubert, W. Wagenknecht, DD-WP 137717
8. B. Philipp, R. Lehmann, C. Ruscher, *Faserforsch. u. Textiltechnik* 10 (1959) 22-35

65 Cellulose recrystallization in the alkaline pulping of wood

E Evstigneyev and A Shashilov – St Petersburg State Technological University of Plant Polymers, 198095 St Petersburg, Russia

ABSTRACT

The change of phase composition and structure of soft wood (spruce, pine) and hard wood (birch) cellulose has been studied by X-ray analysis of crystal structure during soda, soda-AQ, kraft, kraft-AQ, polysulphide and polysulphide-AQ pulping. It is shown that a change of cellulose structure occurs in all stages of delignification, during an increase in structure homogeneity. It is shown that high temperature (170°C), reduction of liquor activity at the end of pulping and dissolution for the majority of lignins and hemicelluloses contribute to the recrystallization process. A statistically true correlation is derived, showing that the feasibility of cellulose recrystallization is related to the extent of delignification. It is assumed that high hemicellulose content in pulp may block the recrystallization process. The specific AQ influence on cellulose structure is not available during alkaline pulping.

INTRODUCTION

Cellulose recrystallization occurs generally under hydrothermal treatment, i.e. when segmental mobility of molecular fragments of amorphous component as well as mutually ordered orientation probability increases. It is established that on hydrothermal treatment of wood pulp recrystallization proceeds in the range of 130-175°C. For this it is suggested that recrystallization occurs within crystallites at defect regions by disordered end chain groups reorientation [1].

Traditional processes of alkaline delignification occur in water at a temperature of 170°C, i.e. under the conditions promoting cellulose recrystallization, in particular in the cooking end when alkali content in a liquor greatly decreases. Our investigation showed that in soda and soda-AQ spruce chips cooking an actual increase of relative crystalline component content in pulp is observed [2]. However at the same time the work by Hattula where cellulose recrystallization on kraft cooking for pine chips was not observed [3] was published. It should be noted that the effective alkali charge chosen by Hattula, i.e. 4.4 mol/kg of wood that is 27.3% on o.d. wood as Na₂O, significantly exceeds conventional charge (16-18%).

Taking into account recorded discrepancies in the results we performed comparative studies in cellulose recrystallization under soda, kraft and polysulphide cooking of softwood and hardwood with AQ and without it. The aim of the given investigation was to find out how alkaline cooking conditions influence structural characteristics of the crystalline cellulose part and whether a mutual relationship exists between cellulose structure change and delignification as well as to what degree, under given conditions, AQ influences cellulose structure or whether such a specific effect is unavailable.

EXPERIMENTAL

The conditions of soda, soda-AQ, kraft and kraft-AQ spruce chips cooking as well as the methods of pulp preparation and analysis are described in [4]. On polysulphide cooking, active alkali charge was 15% (as Na₂O), sulphidity 25%, added elemental sulphur amount was 3% on o.d. wood. For kraft pine and birch chips the cooking active alkali charge was 17% (25% sulphidity). The liquor-wood ratio was 4:1. The temperature was increased from 80°C to 170°C for 120 min, and the temperature was held at 170°C for 60 min.

X-ray diffractometry studies were carried out with an automatic X-ray diffractometer ADP-1 computer-controlled with monochromatized CuK_α-irradiation. Pyrolytic graphite was used as a monochromator. X-ray pattern was performed with a pitch of 0.1° in the interval of 2θ from 17 to 30°. The pulp samples was prepared as pellets with diameter of 10 mm and thickness of 1.5 mm. There were 3 pellets for every sample and then parameters for every pellet was averaged for the whole sample.

Relative crystalline component content in pulp was calculated by the formula: $C=c \cdot Y/c_1$, where c and c_1 are the degree of pulp and wood crystallinity, respectively,

Y - pulp yield. Degree of delignification was determined by the formula: $A=100-L$, %, where $L=l \cdot Y/l_i$, %, where l and l_i - lignin content in pulp and wood, respectively.

RESULTS AND DISCUSSION

In Figure 1 are given the changes of relative crystalline component content (C) in pulp during cooking.

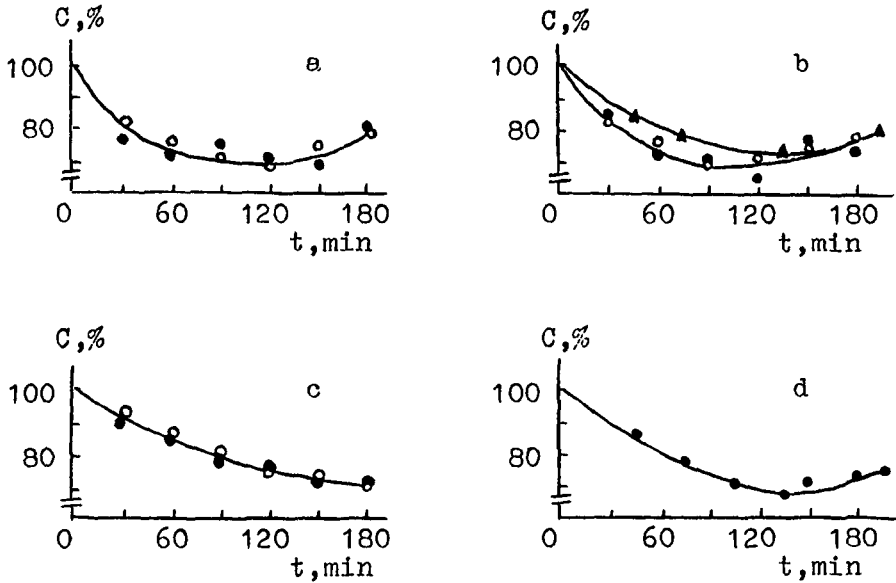


Figure 1. The change of relative crystalline content in pulp during soda (a), kraft (b) and polysulphide (c) spruce chips cooking and kraft birch chips cooking (d). (●) - without AQ, (○) - with AQ, (▲) - kraft pine wood cooking.

It may be seen that during temperature rise (0-120 min) C drops by about 70% based on a value in wood. C was determined taking into account pulp yield decrease during cooking (see Experimental). Due to this fact it may be said that at this stage up to 30% of cellulose crystallinity is lost. It is attributed to alkaline cellulose destruction although it is not excluded that under these conditions partial disordering occurs. In the subsequent period (120-180 min) at constant temperature (170°C) during all analysed cookings, except the polysulphide one, insignificant statistical increase of the relative crystalline component content in pulp may be seen. For softwood (spruce, pine) C approaches 78-80% and for hardwood (birch) 73.4%.

As for the probable cellulose recrystallization mechanism we may note the following. To recrystallization it is necessary to have plasticizing agent (water) accessibility to amorphous cellulose regions and to increase free space for molecular mobility. Both are made during cooking as lignin and hemicelluloses dissolve. The relationship between delignification and recrystallization is shown on Figure 2. It may be seen that the increase of the relative crystalline component content is initiated after dissolving over 85% of the lignin, i.e. at the final cooking stage. As for hemicelluloses they appear to be a unique "buffer zone" blocking plasticizing agent effects on cellulose. It is attributed to the fact that on polysulphide cooking there was no recrystallization (Figure 1c).

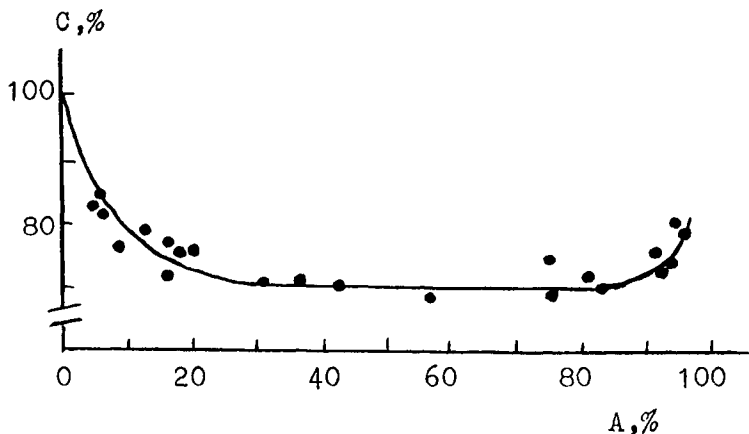


Figure 2. Relative crystalline content versus degree of delignification for soda, soda-AQ, kraft, and kraft-AQ spruce pulps.

As it is known [5], a relatively high yield of polysulphide cooking is attained due to maintaining a large hemicellulose content. Hemicelluloses dissolution during cooking favorably influences the above process in another way. Under these cooking conditions they cleave, forming a series of organic acids; due to the fact liquor alkalinity significantly decreases.

Based on the measurement results in this paper it may be possible to derive a single correlation series for analysed cooking (Figure 3). This series may be kept within common one (see [6]) as a fragment. The single series of structural states is undoubtedly a series of structural cellulose homogeneity increment. Only in this

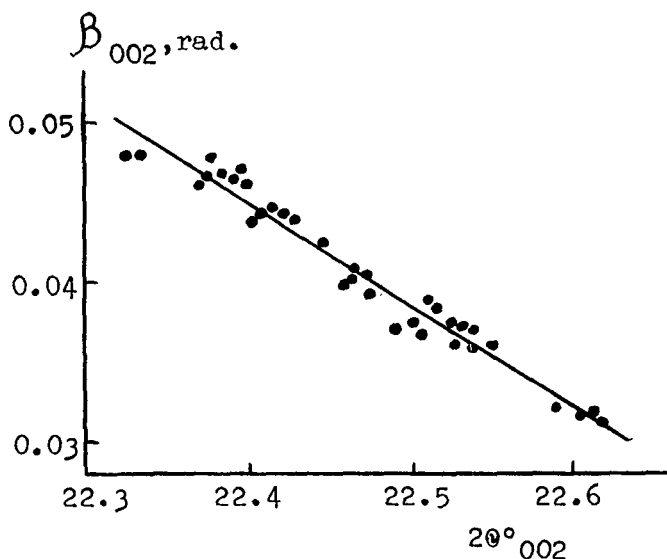


Figure 3. Correlation between position and semiwidth of 002 reflex on spruce pulps X-ray patterns for soda, soda-AQ, kraft, kraft-AQ, polysulphide, and polysulphide-AQ cookings.

sense we understand the change of crystalline cellulose part structure during delignification.

There is no specific AQ effect on cellulose structure during cooking. It is attributed to the fact that the position of the points in Figures 1-3 on cooking with AQ and without it coincide in practice.

CONCLUSION

Under alkaline cooking conditions cellulose recrystallization for both softwood and hardwood occurs. For this process high temperature (170°C), relatively low liquor alkalinity, high degree of delignification and destruction of "buffer zone" of hemicelluloses are required.

REFERENCES

1. Hattula T., ISF-85: Proc. Int. Symp. Fiber Sci. and Technol., Hakone, 20-24 Aug., 1985. Barking, (321) 1986.
2. Shashilov A.A., Evstigneyev E.I., Shalimova T.V., and Zacharov V.I., Khimiya Drevesiny N 2, 7(1986).
3. Hattula T., Paperi ja Puu 68, 926(1986).
4. Evstigneyev E., Maiyorova H., and Platonov A., Tappi J. 75, 177, (1992).

5. Lasmarias V.B., and Peterson R.C., *Cellul. Chem. and Technol.*, 14, 479(1990).
6. Ivanov M.A., and Shashilov A.A., Abstracts of 2-nd seminar, *Submicroscopic Structure of Wood and Its Role in Delignification Process*, Riga, 1983, p. 117.

66 Wide angle X-ray and solid state ^{13}C -NMR studies of cellulose alkalization

H-P Fink, E Walenta, J Kunze and G Mann – Fraunhofer-Institute of Applied Polymer Research, Kantstraße 55, D-14513 Teltow-Seehof, Germany

ABSTRACT

Alkali-celluloses prepared from linters material and spruce sulphite dissolving pulp by treatment with aqueous alkaline solutions up to 50% NaOH were investigated by WAXS and ^{13}C -CP/MAS-NMR. Results indicate (i) the formation of a uniform alkali-cellulose phase similar to sodium cellulose I completed at 16% NaOH, (ii) a basically altered state of less ordered alkali-cellulose around 25% NaOH, and (iii) a slightly varying state with diminishing order from 25% to 50% NaOH. Changes in chain conformation and spatial arrangement are discussed with regard to specific interactions of sodium cations with the different hydroxyl groups of anhydroglucose units.

INTRODUCTION

Alkali-celluloses /1/ as important intermediates in manufacture of viscose fibres and cellulose ethers have been a research topic in recent years, especially with regard to phase transitions and to specific interactions between sodium cations and hydroxyl groups of cellulose /2-8/. Particularly WAXS and NMR methods have been employed successfully to wet alkali-celluloses at low and medium steeping lye concentrations up to about 30% NaOH, whereas the interaction in the whole concentration range of aqueous alkaline solutions up to about 50% has been investigated only with dried /9/ or regenerated /10/ cellulose samples.

In our contribution we investigate wet alkali-celluloses prepared at different aqueous alkaline concentrations up to 50% NaOH by combined WAXS and ^{13}C -CP/MAS-NMR. Using different cellulosic materials we intend to give a survey of the effects of the alkalization of freely swelling pulps in a concentration range important for etherification of cellulose. Moreover, the experimental results of the aqueous alkalization should provide a reference to assess an alkalization by the isopropanol-water-NaOH system relevant for the industrial slurry process.

EXPERIMENTAL

As cellulosic materials we used commercial cotton linters pulp and spruce sulphite dissolving pulp with a DP (cuoxam) of about 2000 and 700, respectively. The samples were milled prior to alkalization reducing the DP and the crystallinity by about 10 %.

Alkalizations were performed with aqueous alkaline solutions at concentrations of 4%, 10%, 16%, 25%, 30%, 35%, 40%, 45%, and 50% by weight NaOH at room temperature for 1 h with lye in excess. After alkalization the alkali-celluloses were pressed mechanically resulting in a cellulose content usually in the range of about 30% to 50% depending on the raw material and the NaOH concentration. For comparison, a slurry alkalization with a standard composition (overall NaOH concentration < 5%) of the isopropanol-water-NaOH system was employed.

For WAXS measurement, the alkali-cellulose samples were prepared as flat cakes air tight between polyester foils, whereas for NMR investigation a rotor, sealed according to /11/, was used. X-ray scattering of the isotropic samples was measured between 4° and 104° in 2Θ -scale by a Siemens D-5000 diffractometer in Θ - 2Θ -transmission mode with CuK_α -radiation (40kV, 35mA). The measured curves were corrected for parasitic scattering including that of the polyester foils. ^{13}C -CP/MAS-NMR spectra were recorded by a UNITY 400 spectrometer operating at 100 MHz for ^{13}C with a contact time of 1ms, a sample rotation frequency of 4...5kHz, and an accumulation number of about 5000.

RESULTS

Scattering curves of alkali-celluloses produced from milled linters pulp with aqueous alkaline solutions are presented in Figure 1. At 4% NaOH the nearly unchanged WAXS-curve of the original linters material with cellulose I as the crystalline modification is preserved and also at 10% NaOH the cellulose I patterns still dominate. Above 10% NaOH a phase transition occurs from cellulose I to highly ordered alkali-cellulose. Between 16% and 25% another phase transformation takes place with a completely changed WAXS diagram at 25% NaOH, whereas with further increasing NaOH concentration up to the maximum of 50% a decreasing sharpness of the interferences may be observed.

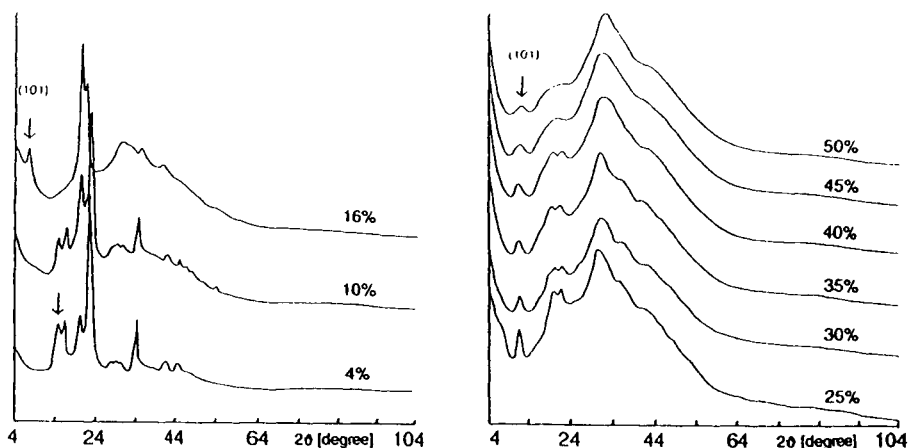


Figure 1 WAXS-curves of wet alkali-celluloses as a function of NaOH-concentration

The largest lattice spacing of the experimental alkali-celluloses (for convenience denoted by d_{101} according to Meyer/Misch convention) and the full width at half maximum (FWHM) of the appropriate interference are put together in Table 1.

Table 1 Lattice spacing d_{101} and line width FWHM_{101} from WAXS of alkali-celluloses

NaOH wt. %	linters pulp		spruce diss. pulp	
	d_{101} nm	FWHM degree	d_{101} nm	FWHM degree
16	1,27	1,31	1,25	1,34
25	0,79	1,65	0,79	1,64
30	0,79	1,71	0,79	1,73
35	0,79	1,73	0,78	1,99
45	0,79	2,44	0,78	1,84
50	0,78	3,02	0,78	2,64

Alkalization in the isopropanol-water-NaOH system results in rather disordered alkali-celluloses as described earlier /4/, with WAXS curves resembling those of high aqueous alkaline concentrations and with reduced differences between linters and wood pulp.

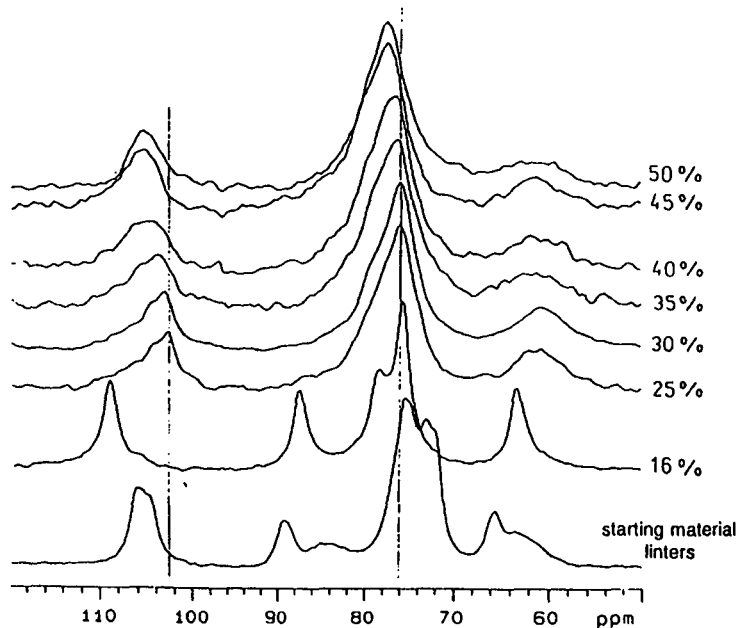


Figure 2
 ^{13}C -CP/MAS-NMR spectra of wet linters-alkali-cellulose as a function of aqueous alkaline concentration

^{13}C -CP/MAS-NMR spectra of alkali-celluloses prepared from linters in the whole possible concentration range of aqueous alkali are presented in Figure 2. In accord with our WAXS-results, the spectrum of the original material is changed completely at 16% and 25% NaOH. Above 25% NaOH the NMR spectra indicate a decreasing order with increasing concentration as already shown by WAXS, but additionally a slight shift of C(1) and C(2,3,4,5) lines to lower magnetic field can be observed. Line positions of cellulose I and alkali-celluloses are filed in Table 2.

Figure 3 shows NMR spectra of samples alkalized with a standard composition of the isopropanol-water-NaOH system. These spectra display only two broad lines in the regions 100 ... 110 ppm and 68 ... 90 ppm.

Table 2 ^{13}C -CP/MAS-NMR line positions of linters-alkali-celluloses relative to TMS = 0

aqueous NaOH concentration	average line positions in ppm			
	C(1)	C ^c (4)/C ^a (4)	C(5)/C(2,3)	C ^c (6)/C ^a (6)
original Cell.I	105	89/85	76/73	66/63
16%	109	87	76	63
25%	103	-	76	61
30%	103	-	76	61
35%	104	-	76	62
40%	105	-	76	62
45%	106	-	77	62
50%	106	-	77	62

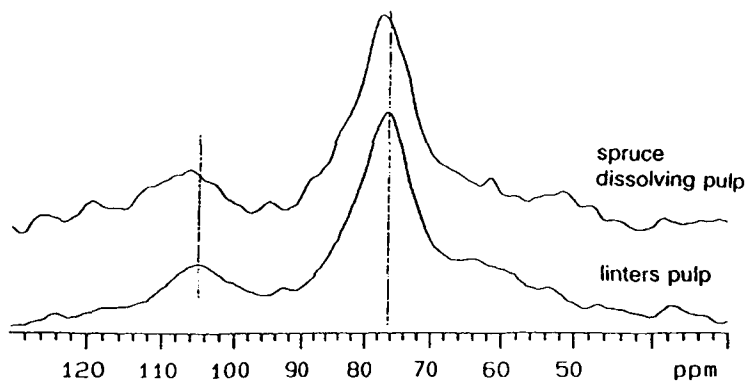


Figure 3 ^{13}C -CP/MAS-NMR-spectra of wet alkali-celluloses from the system isopropanol-water-NaOH

DISCUSSION AND CONCLUSIONS

From both WAXS-curves (Fig. 1) and NMR-spectra (Fig. 2) the series of alkali-celluloses may be classified by:

- (i) a defined state of high order achieved in the whole sample at 16% NaOH,
- (ii) a completely changed state of lower order around 25% NaOH,
- (iii) a slightly changing state with decreasing order from 25% to 50% NaOH.

A comparison of the d_{101} -values (Table 1) from WAXS-measurements with literature data */1/* shows, that the experimental states (i) and (ii) do not correspond exactly to one of the well known sodium celluloses I-V usually prepared under tension. Nevertheless, the d_{101} -values of states (i) and (ii) are close to the lattice spacings of sodium cellulose I with a twofold screw axis and to sodium cellulose II with a threefold screw axis of the chains, respectively. The increasing line width FWHM at constant d -values (Table 1) in the concentration range from 25% to 50% NaOH indicates a decreasing lateral crystallite size and/or order, while averaged lateral chain distances remain approximately unchanged.

NMR-results may be discussed with respect to specific interactions of sodium cations with hydroxyl groups of cellulose taking into account a molecular structure of cellulose I with intramolecular and intermolecular H-bridges according to */12/* (Figure 4). As compared with cellulose I, state (i) is characterized by a shift of C(1), C(2,3) and C^α(4) lines to lower field strength and of C^β(4) and C^γ(6) lines to higher magnetic field (Fig. 2, Table 2).

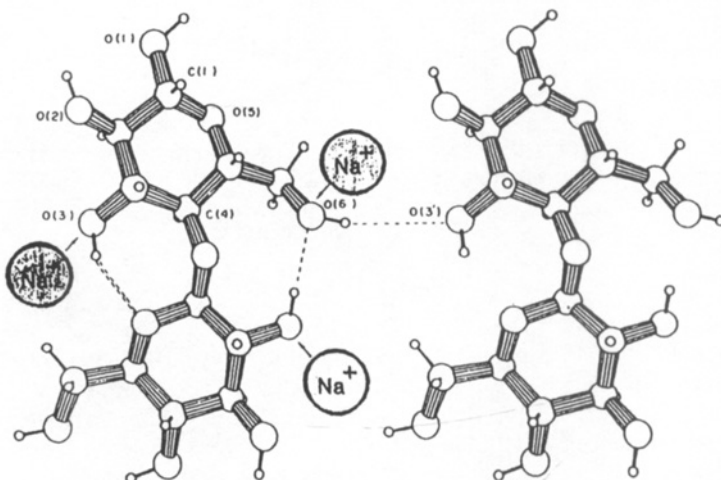


Figure 4 Cellulose I structure with intramolecular and intermolecular H-bridges

The interaction of Na^+ with a specific hydroxyl oxygen should result in a reduced electron density of the neighbouring C-atoms and in a line shift for the carbons in α - and β -position to lower magnetic field, whereas the next but one carbon's line may move to higher field by the γ -effect */6/*. Hence, state (i) is characterized by a preferred Na^+ coordination to O(2)-C(2), probably breaking the intramolecular O(2)-H(2)-O(6) bridge and influencing also the O(6) intermolecular H-bonding. The high-field-shift of the C^α(4)-line and the increased line sharpness of C(4) indicate a one phase alkali-cellulose (i) with an overall chain conformation with a twofold screw axis. According to */13/*, the C(6) line position depends on the

conformation of the C(6)H₂OH-group with tg conformation at the lowest field, gt at higher and gg at the highest magnetic field. With regard to the observed C(6) line shift we suppose a transformation of the C(6)H₂OH-group conformation from tg in crystalline cellulose I to gt in alkali-cellulose state (i) made possible by some rotational freedom of this group due to the broken O(2)-H-O(6) hydrogen bond.

The NMR spectrum of alkali-cellulose (ii) exhibits a remarkable line shift for C(1) and C(4) to higher field as compared to cellulose I and especially to state (i). According to Horii /13/ the C(1) and C(4) line positions strongly depend on the torsional angles ϕ and ψ of the 1,4- β -D-glucosidic linkage. Herefrom it seems to be clear that the twofold screw axis of state (i) molecules is altered in state (ii). Torsional freedom of ϕ and ψ may be explained by a broken O(3)-H-O(5) intramolecular bridge due to an additional coordination of Na⁺ to O(3). The position of the C(6)-line indicates a preferred gg-conformation in state (ii).

Slight changes of the broad lines for C(1) and C(2,3,4,5) to lower magnetic field indicate an increasing strength of interaction of Na⁺ with both O(2) and O(3) in stage (iii). Additional broadening of the C(6)-line may be explained by non uniform interactions and a broad conformational distribution of the C(6)H₂OH-groups.

As a conclusion, the effects of cellulose alkalization in the entire aqueous alkaline concentration range may be explained with regard to spatial and conformational changes of the cellulose chains due to specific c_{NaOH} -dependent interactions of Na⁺ with hydroxyl groups of cellulose. Furthermore, combined WAXS-curves and NMR-spectra of wet alkali-celluloses provide a sensitive scale for assessing the action of more complicated alkalizing systems as e.g. isopropanol-water-NaOH.

ACKNOWLEDGEMENT

This work has been supported by a grant of the Bundesministerium für Forschung und Technologie (BMFT) of Germany, BEO 0310377A.

REFERENCES

- /1/ Sobue, H., Kiessig, H., and Hess, K.: Z. Physikal. Chem. B43 (1939) 309
- /2/ Kunze, J., Ebert, A., Schröter, B., and Frigge, K.: Polym. Bull. 5 (1981) 399
- /3/ Fink, H.-P. and Philipp, B.: J. Appl. Polymer Sci. 30 (1985) 3779
- /4/ Philipp, B., Kunze, J., and Fink, H.-P.: in "The Structures of Cellulose", ACS Symposium series 340 (1987) p.178
- /5/ Okano, T. and Sarko, A.: J. Appl. Polymer Sci. 29 (1984) 4175
- /6/ Kamide, K., Kowsaka, K., and Okajima, K.: Polymer J. 17 (1985) 707
- /7/ Kim, N.-H., Sugiyama, J. and Okano, T.: Mokuzai Gakkaishi 35 (1989) 387
- /8/ Yokota, H., Sei, T., Horii, F., and Kitamaru, R.: J. Appl. Polym. Sci. 41 (1990) 783
- /9/ Takahashi, M., Ookubo, M., and Takenaka, H.: Polymer J. 23 (1991) 1009
- /10/ Richter, U., Krause, T., and Schempp, W.: Angew. Makromol. Chem. 185/186 (1991) 155
- /11/ Horii, F., Hirai, A., Kitamaru, R., and Sakurada, I.: Cell. Chem. Technol. 19 (1985) 513
- /12/ Gardner, K.H. and Blackwell, J.: Biopolymers 13 (1974) 1975
- /13/ Horii, F.: in "Nuclear Magnetic Resonances in Agriculture", CRC Press, Boca Ratou, Florida (1989) p. 312

67 The effect of refining in the fibre structure and properties in unbleached eucalypt pulps

J Gominho and H Pereira – Departamento de Engenharia Florestal, Instituto Superior de Agronomia, Universidade Técnica de Lisboa, 1399 Lisboa Codex, Portugal

ABSTRACT

In this paper results on the effect of PFI refining of never dried and dried eucalypt pulp, using a commercial unbleached kraft pulp from *Eucalyptus globulus* wood, are presented.

Refining did not shorten the fibres to a significant degree and in relation to wood it is the pulping process that mostly affected fibre length (1.19mm average length in wood and 0.68mm in pulp). Some shortening of fibers by end cutting occurred, mostly in the first phase of refining giving rise to approx. 20% of <0.2mm fibres; this effect was higher in never dried pulp. However, the weight of the finer fractions is small and the weighted average fibre length by weight remains fairly constant. External fibrillation was limited but refining increased microcompressions and cross-sectional slip planes and significantly fragmented the vessels. The drying of eucalypt pulp decreases the refining behaviour and the development of pulp properties. For the same beating degree, never dried pulp has higher strength (ca.20-30% higher tensile strength) and more flexibility, ensuring a better fibre bonding.

INTRODUCTION

An important step in papermaking is the mechanical beating or refining of pulp by which the sheet forming properties and the physical

characteristics of pulp will be enhanced. Important effects of refining are an increase in the swelling of the cell-wall and in cell flexibility (Lindstrom 1986), as well as fibre shortening and the creation of external/internal fibrillation and tangential fissures (Clark 1978).

Pulp drying causes an irreversible reduction in the swelling ability of cellulose. This hornification process starts at approximately the moisture content where all water occluded between the fibres has been removed. The irreversible changes during drying seem to be a general feature of many hydrogen-bonded materials, including kraft lignin and hemicelluloses. The degree of cell wall collapse on drying is generally higher for beaten fibres than for unbeaten fibres (Lindstrom 1986).

In this paper we study the effect of PFI refining in a never dried and dried eucalypt unbleached kraft pulp in relation to fibre dimensions and structure as well as to some properties.

MATERIAL AND METHODS

An industrial unbleached kraft pulp from eucalypt (*Eucalyptus globulus* Labil.) was used in this study. The pulp was collected directly in the mill after the washing stage. The pulping conditions were the following: total alkali 150g/l (NaOH), 25% sulphidity, maximum temperature 165°C, liquor:wood ratio 4:1. The pulp characteristics were the following: Kappa no. 13, 90° ISO brightness, residual alkali 0.68 g/l (NaOH) and moisture content 609% based on oven dry pulp.

The samples used in this study included the never dried pulp, as received, and a once dried pulp prepared from the former. Refining was done in a PFI with a variable number of revolutions under mild conditions with a 0.48 mm spacing between roll and bedplate. All pulp samples (30g) were processed at 10% stock concentration. Fibre length and width, as well as wall thickness, were measured in all samples using a semi-automated measurement system. Forming handsheets and their physical testing were performed according to Tappi standards. Microscopic observations were made on the handsheets and on dissociated elements under polarized light. The handsheet samples were dehydrated, embedded and sectioned for the cross-sectional observations.

RESULTS AND DISCUSSION

The beating degree in °SR and the drainage time for the never dried and the dried pulps are shown in Table 1 for different beating times. Beating degree increases regularly with the number of PFI revolutions and it is always lower for the dried pulp by approx. 4-6 °SR for the same treatment time. A similar trend was observed for the drainage time.

Table 1. Beating degree and drainage time for a never dried and a dried eucalypt pulp

Revolutions	Beating degree, °SR		Drainage time, s	
	Never dried	Dried	Never dried	Dried
0	16	16	4.0	4.0
1500	23	18	4.6	4.2
3000	26	22	5.4	4.5
6000	29	25	5.6	4.5
9000	35	31	9.5	8.2
15000	40	37	10.5	10.0
20000	47	41	11.8	10.5
25000	52	46	12.0	10.9
30000	58	49	14.0	11.0
40000		57		13.0

The average fibre length and the weighted average length by weight of the different samples are shown in Table 2. The fibre length in wood was 1.19 mm. The greatest shortening effect was noticed by the action of the pulping process, reducing the average fibre length to 0.68 mm. Refining slowly decreased the average length, more in the never dried pulp. However, if a weighted average fibre length by weight is considered, the effect of refining is very small.

Table 2. Average fibre length in never dried and dried pulps with different refining times

Revolutions	Average fibre length, mm		Weighted average fibre length by weight, mm	
	Never dried	Dried	Never dried	Dried
Wood	1.19		1.61	
Pulp	0.68		0.85	
0	0.73		0.89	
1500	0.70	0.68	0.95	0.93
3000	0.62	0.76	0.95	0.88
6000	0.66	0.73	0.94	0.88
9000	0.65	0.65	0.93	0.82
15000	0.59	0.69	0.88	0.84
20000	0.50	0.69	0.84	0.82
25000	0.53	0.64	0.84	0.84
30000	0.56	0.74	0.89	0.92
40000		0.74		0.88

The fibre length distribution is shown in Figure 1. In relation to wood, the largest effect corresponds to the pulping process, which is responsible for the shortening of fibres and for the overall movement of the curve to the right, but cutting to fragments giving rise to small dimension particles did not occur. The desintegration step in the blender

did not alter the length distribution. In the first phase of the refining process of never dried pulp appears a class of fines < 0.2 mm of some relative importance (approximately 10% for 1500 revolutions and 25-30% for higher revolution numbers), which does not change with refining time, the distribution curves remaining fairly constant. In the case of dried pulp, this class of finer material is smaller explaining the higher average fibre length of the samples.

Figure 1. Fibre length distribution in wood, pulp (—), desintegrated (....) and refined never dried pulp at 30 000 revolutions (- - -)

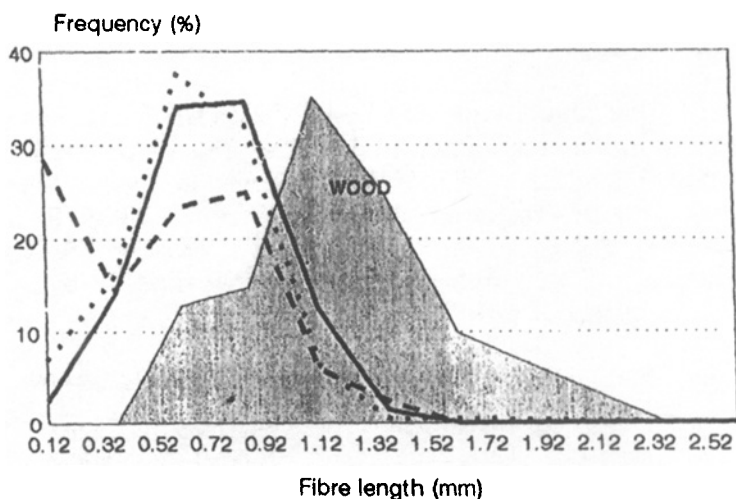
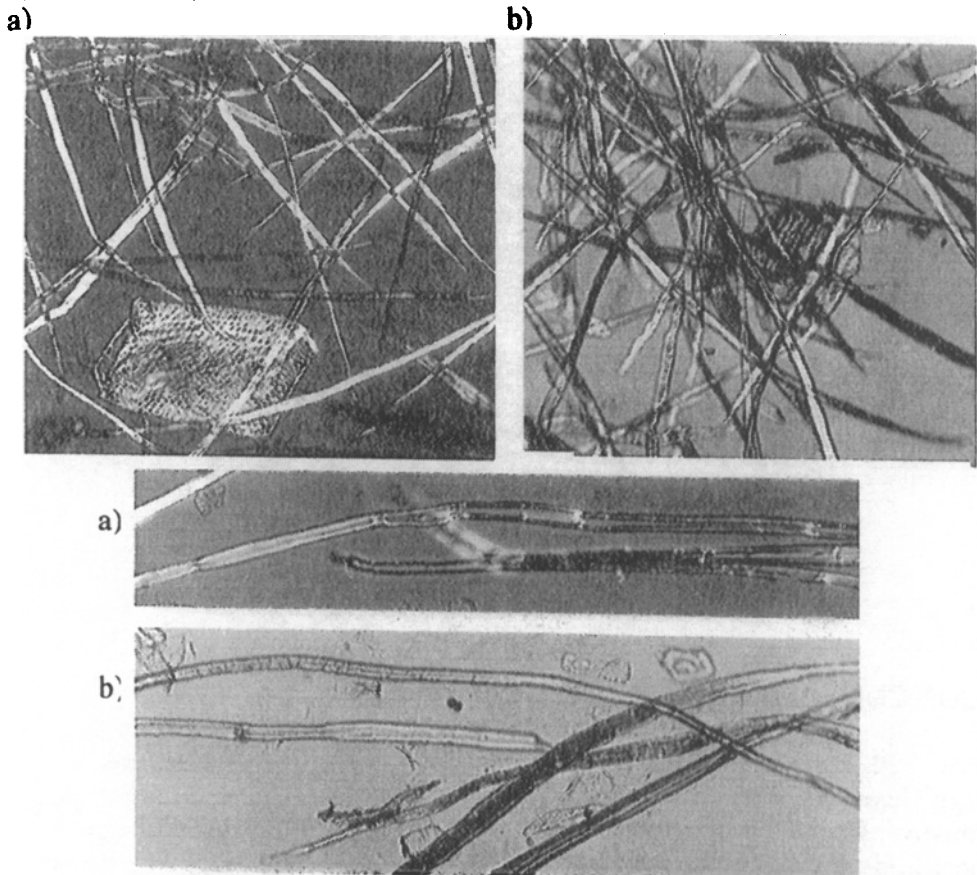


Figure 2 shows some examples of the microscopic observations under polarized light. Refining did not significantly increase external fibrillation. Transversal microcompressions and cross-sectional slip planes, already numerous in unbeaten fibres, increase with refining. In beaten pulps, vessels are fragmented.

The physical properties of handsheets are summarised in Table 3. The apparent density of unrefined handsheets was 0.569 g/cm^3 and increased with refining with approximate 10% higher values for never dried pulp handsheets. The cross-sections of two handsheets (beaten to 37 and 57 °SR) are shown in Figure 3. Strength properties are developed by refining. Never dried pulp has higher tensile strength (ca. 20-30% more) and stretch as well as burst and tear than dried pulp for the same beating degree.

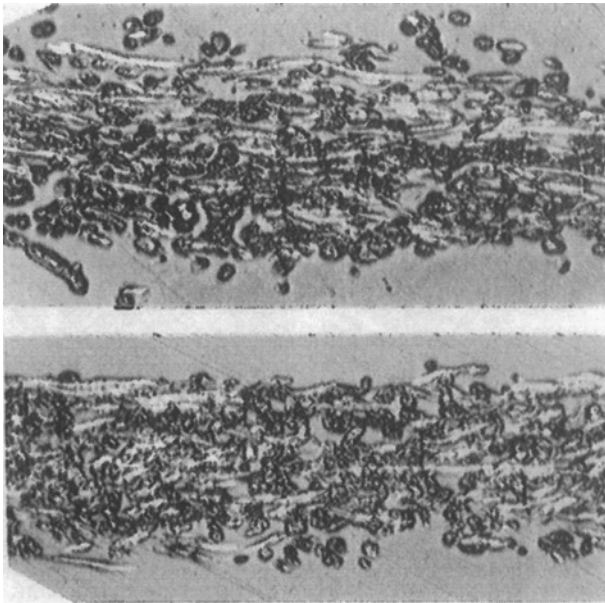
Figure 2. Microscopic observation of fibres under polarised light.

a) unrefined b) refined to 49°SR

Table 3. Physical properties of handsheets prepared from never dried and dried pulp with different refining degrees. Units: tensile index N.m/g, tear index mN.m²/g, burst index kPa.m²/g.

Beating (revolutions)	Never dried pulp				Dried pulp			
	Tensile index	Stretch %	Tear index	Burst index	Tensile index	Stretch %	Tear index	Burst index
0	56.7	0.99	7.6	2.8	56.7	0.99	7.6	2.8
1500	73.8	1.88	10.0	4.7	47.9	1.46	8.6	2.3
3000	80.0	2.38	8.1	5.2	51.2	1.80	8.2	2.7
6000	81.6	2.52	7.1	5.3	54.3	2.13	9.4	3.3
9000	81.9	2.82	11.9	5.5	59.1	2.46	10.9	3.6
12000	77.8	3.34	11.3	5.5	62.7	3.00	11.5	3.0
15000	76.3	3.10	6.8	5.7	66.7	2.90	9.4	4.2
30000	83.1	3.84	9.9	6.5	60.2	3.38	10.4	4.7

Figure 3. Microscopic observation of cross-sections of handsheets under polarised light beaten 37°SR (top) and 57°SR (bottom)



CONCLUSIONS

The PFI refining of eucalypt pulp did not shorten the fibres to a significant degree; in relation to wood it is the pulping process that mostly affects fibre length. Some shortening of fibers by end cutting occurred, mostly in the first phase of refining, and this effect was higher in never dried pulp. However, the weight of the finer fractions is small and the weighted average fibre length by weight remains fairly constant. The drying of eucalypt pulp decreases the refining behaviour and the development of pulp properties. For the same beating degree, never dried pulp has higher strength and more flexibility, ensuring a better fibre bonding.

References

- Clark, J.A. 1978. Pulp technology and treatment for paper. Miller Freeman, S.Francisco
- Lindstrom, T. 1986. The porous lamelar structure of the cell wall. In: Paper, structure and properties (Ed: J.A.Bristow & P. Kolseth), M. Dekker Inc., New York, p.99-120
- McKenzie, A.W. 1983. A comparison of the Lampen and PFI mills. Appita 37: 53-59
- Miller, P.R. 1989. Fibre and sheet properties resulting from refining stock concentration variation, Appita 42: 125-130

68 Biological delignification of Brazilian lignocellulosic residues

S P D' O Barreto¹, A C D Coelho², J F Kennedy³, J L Lima Filho¹, E H M Melo¹ and M Paterson³ – ¹ Departamento de Bioquímica/LIKA, UFPE, Recife, Pernambuco, 50670-901, Brasil; ² Departamento de Engenharia Química, UFPE, Recife Pernambuco, 50670-901, Brasil; ³ Research Laboratory for the Chemistry of Bioactive Carbohydrates and Proteins, School of Chemistry, The University of Birmingham, B15 2TT, UK

ABSTRACT

Phanerochaete chrysosporium has been grown on pieces of banana tree trunks. As a result of the semi-solid fermentation, using glucose as carbon source, it was found that the lignin peroxidase activity was 206 U/L on the fifth day of fermentation and 140 U/L on the tenth day. A reduction of 32% of the lignin content in the native banana tree trunk was observed after 15 days of fermentation. These results have shown that *P. chrysosporium* grown on banana tree trunks is a potential microorganism for an alternative process for cellulose and paper production with environmental benefits.

INTRODUCTION

Production of cellulose and paper is one of the oldest practice in the world. Paper consumption has increased considerably and at this growth rate, the need of paper in the next century will be five times higher than nowadays. The major problem for this growing demand is the replacement of all trees used for this purpose. The utilisation of agricultural residues as an alternative process for paper manufacturing is a potential route. Just in five small towns in the Northeastern region of Brazil (State of Pernambuco) there is an area of approximately 12 000-ha cultivated with banana. The amount of banana tree trunks produced in this area is approximately 31 000 tonnes/ha *per annum*. However, there is a need for an appropriate storage system for the banana tree trunks as their water content can reach 80% (w/w). An appropriate mechanism to remove the water content from the tree trunks is necessary prior to large scale storage.

Industrial chemical pulping and bleaching processes of lignocellulosic material for cellulose and paper production are highly pollutant. Studies on alternative biological pulping to either diminish or even eliminate pollution have been carried out in various research laboratories.

Several fungi in nature are capable of degrading lignin. Some of these fungi are also used for bleaching pulps, but they act very slowly (Tien and Kirk, 1984).

The presence of lignin in wood and other plant materials increases the resistance to microbial degradation. Lignin serves as a barrier between environment and wood polysaccharides. This barrier must be partly removed or at least morphologically changed before the wood polysaccharides can be attacked by their specific enzymes.

The white-rot *P. chrysosporium* is a well known ligninase producer which degrades a variety of organic compounds including lignin, vanillic acid, chlorinated aromatic compounds, etc. (Reid, 1988; Duran et al., 1987). The cultivation of *P. chrysosporium* in different liquid culture media as well as the mechanism of ligninase action and their properties have been intensively studied (Linko, 1988). However, production of ligninases by growing *P. chrysosporium* on culture media has been based on expensive chemicals, reagent grade salts and pure aromatic alcohols as enhancers of enzyme production (Asther et al., 1988). This paper has studied the use of banana tree trunks as a low cost medium for *P. chrysosporium* growth and ligninase production. Delignification of banana tree trunks was also investigated.

MATERIALS AND METHODS

Materials

The banana tree trunks (*Musa esplendida*) used were from the Northeastern region of Brazil (State of Pernambuco). All chemicals used were of analytical grade.

Microorganism

Phanerochaete chrysosporium was kindly donated by Dr. T. K. Kirk.

Inoculum

Cultures of *P. chrysosporium* were maintained on supplemented malt agar. Four days were required for production of spores in an Erlenmeyer flask (1 L). The culture medium contained basal medium (B III), glucose (10%), malt extract (10 g), peptone (2 g), yeast extract (2 g), asparagine (1 g), potassium dihydrogen orthophosphate (2 g), magnesium sulphate (1 g) and thiamin-HCl (1 mg).

Growth media

Cultures were grown under stirring conditions for delignification using glucose (2.7 mg/mL) as a carbon source and banana tree trunks (71 g). The culture medium contained sodium tartrate (20 mM) in place of the usually employed sodium 2,2-dimethyl succinate.

Enzyme production was induced by adding benzyl alcohol (final concentration of 2.5 mM).

Enzyme activity

Lignin peroxidase activity was determined spectrophotometrically (244 nm), at 28°C by measuring the rate of oxidation from benzyl alcohol to benzaldehyde. The reaction system was made up of extracellular lignin peroxidase (200 mL), benzyl alcohol (10 mM, 200 mL), sodium tartrate buffer (0.1 M, pH 3.0, 50 mL), hydrogen peroxide (0.4 mM, 200 mL) and completed with distilled water to a final volume of 1.0 mL.

Reducing sugars

The concentration of glucose was determined according to the reducing sugars method of Bernfeld (1955).

Protein concentration

The protein concentration was measured according to the method of Bradford (1976).

RESULTS AND DISCUSSION

Biodegradation of lignin has been greatly developed over the last 15 years and its interest has intensified in recent years (Umezawa and Higuchi, 1989, Hattori et al., 1992). The normal way for white-rot fungi to degrade lignocellulosic materials is by a simultaneous attack on the polysaccharides and lignin. It seems that an absolutely specific attack on the lignin is probably impossible by the microorganisms studied so far. The fungi seem to need polysaccharides or low molecular mass sugars to degrade lignin (Leisola et al., 1984; Ander and Eriksson, 1985).

Most of the studies on biodegradation of lignin by *P. chrysosporium* are based on liquid media growth. Semi-solid fermentation systems can be efficiently operated, however, they must provide suitable conditions for substrate colonisation and lignin degradation by the fungi. At the same time, the conditions should minimise carbohydrate hydrolysis by these fungi and any other organism present (Reid, 1988). As the lignin is removed and the polysaccharides become progressively more accessible to enzymic hydrolysis, the rate of carbohydrate degradation tends to increase. Thus, there will be an optimum incubation time, after which the yield of digestibility of the polysaccharides increases, although lignin degradation continues.

P. chrysosporium growing on banana tree trunks requires the presence of glucose as a carbon source. Figure 1 shows that the peak of lignin peroxidase activity on the fifth day of fermentation is characteristic of the described liquid fermentations for *P. chrysosporium*. This behaviour can be attributed to the presence of glucose, the concentration of which was reduced 40% during the first five days of fermentation. However, the peak of lignin peroxidase activity on the tenth day is characteristic of solid fermentation of the *P. chrysosporium*. At this time, the concentration of glucose was equivalent to 23% of the initial concentration. It can be

observed that on the thirteenth day, the glucose reached its lowest concentration, then beginning to increase again. This increase in the glucose concentration could be due to the degradation of cellulose by cellulase. The maxima activities of lignin peroxidase were 206 and 140 U/L at days 5 and 10, respectively (Figure 1). These values were higher than those found by Duran et al. (1987) (23.0 U/L) and Kirk and Obst (1988) (95.0 U/L).

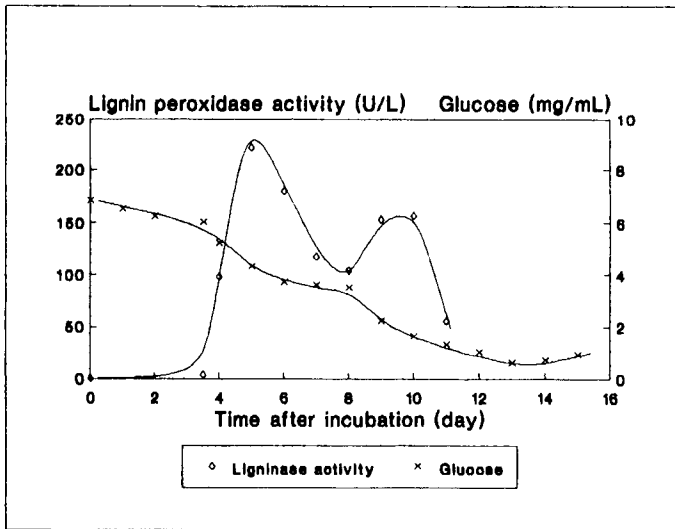


Figure 1. Lignin peroxidase activity and glucose concentration during cultivation of *P. chrysosporium* on banana tree trunks by semi-solid fermentation.

The maximum protein concentration was achieved on day 8 of the fermentation (Figure 2). The pH values were relatively constant (ca. 5.2) during the whole fermentation (Figure 2).

The percentages of lignin, Klason method (Kirk and Obst, 1988), in the native banana tree trunks and at the end of the fermentation (day 15) are shown in Table 1.

Table 1. Lignin content of native banana tree trunks and after the semi-solid fermentation with *P. chrysosporium*.

Banana tree trunk	Lignin (Klason) (%)
Native form	21.0
After 15 days of fermentation	14.4

A reduction of 32% in the lignin concentration is observed. Generally, maximum degradation of lignin in hardwoods is achieved between 3 to 8 weeks, while in softwoods this is achieved between 3 to 4 weeks.

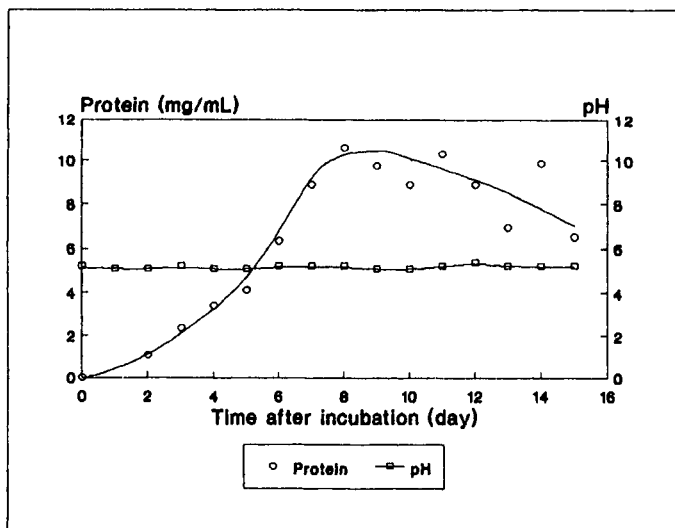


Figure 2. Protein concentration and pH during cultivation of *P. chrysosporium* on banana tree trunks.

Pulping of banana tree trunks by the classical chemical method used by the paper industries in the State of Pernambuco removed 65% of lignin (Barreto et al., 1993) (Table 2). A modified chemical method which contains urea removed 80.4% of lignin (Barreto et al. 1993) (Table 2).

Table 2. Lignin content of banana tree trunks treated by the classical chemical method and by a modified method using urea.

Banana tree trunk	Lignin (Klason) (%)
Native form	18.4
Classical chemical method	6.4
Modified chemical method (+ urea)	3.4

The delignification of banana tree trunks using *P. chrysosporium* is lower than the chemical methods. However, considering the great amount of pollution caused by the paper industries which use the chemical methods, the use of *P. chrysosporium* would cause a lesser degree of environmental damage.

CONCLUSION

The results indicate that semi-solid fermentation of banana tree trunks using *P. chrysosporium* reduces the lignin content by 32% and is therefore a potential alternative process for cellulose pulping and paper production with less pollution.

REFERENCES

- Ander, P. and Eriksson, K-E. (1985) *Appl. Microbiol. Biotechnol.*, **21**, 96-102.
- Asther, M.; Lesage, L.; Drapron, R.; Corrieu, G. and Odier, E. (1988) *Appl. Microbiol. Biotechnol.*, **27**, 393-398.
- Barreto, S. P. D' O., Melo, E. H. M., Lima Filho, J. L., Coelho, A. C. D. and Kennedy, J. F. (1993) In: *Cellulosics: Pulp, Fibre and Environmental Aspects*. J. F. Kennedy, G. O. Phillips and P. A. Williams, Eds., Ellis Horwood Ltd., Chichester, 31-36.
- Bernfeld, P. (1955) *Methods in Enzymology*, **1**, 149-158.
- Bradford, M. M. (1976) *Anal. Biochem.*, **72**, 248-254.
- Duran, N.; Rodriguez, J.; Ferraz, A. and Campos, V. (1987) *Biotechnol. Lett.* **9**, 357-360.
- Hattori, T., Umezawa, T., Shimada, T. and Higuchi, T. (1992) In: *Ligno-Cellulosics: Science, Technology, Developmente and Use*. J. F. Kennedy, G. O. Phillips and P. A. Williams, Eds., Ellis Horwood Ltd., Chichester, 73-82.
- Kirk, T. K. and Obst, J. R. (1988) In: *Methods in Enzymology*, Vol 161. W.A. Wood and S. T. Kellogg, Eds., Academic Press, San Diego, 87-100.
- Leisola, M. S. A., Ulmer, D. C.; Waldner, R. and Feichter, A. (1984) *J. Biotechnol.*, **1**, 331-339.
- Linko, S. (1988) *J. Biotechnol. Lett.*, **8**, 163-170.
- Reid, I. D. (1988) *Enzyme Microb. Technol.*, **11**, 786-802.
- Tien, M. and Kirk, T. K. (1984) *Proc. Natl. Acad. Sci. USA*, **81**, 2280.
- Umezawa, T. and Higuchi, T. (1989) *FEBBS Lett.*, **242**, 325-329.

69 Investigation of cellulose and lignins by molecular hydrodynamic methods

G Pavlov – University of St Petersburg, Institute of Physics,
St Petersburg, 198904, Russia

Cellulose investigations started a long time ago. Nevertheless, the experimental data containing independently determined molecular weights of samples (M) and data on chain dimensions remain incomplete. The main reason for this is (fortunately) the poor cellulose solubility. Cellulose dissolution probably occurs as a result of the interaction between the solvent components and the OH-groups of glucopyranose rings, which can be regarded as partial substitution. Our investigation of cellulose in alkaline solution of iron-sodium tartrate complex (FeTNa) [1] comprised the following stages: 1) investigation of the solvent, i.e. determination of the size and mass of the low molecular weight complex, 2) determination of the degree of bonding of this complex to cellulose molecules, 3) determination of the equilibrium value of density increment [2], 4) determination of hydrodynamic and molecular characteristics of cellulose in the solvent used.

The main investigation methods followed classical methods of molecular hydrodynamics: velocity sedimentation (S_0 - sedimentation coefficient and K_s - concentration sedimentation coefficient), isothermal translational diffusion (D_0 - translational diffusion coefficient), and viscometry ($[\eta]$ -intrinsic viscosity). These methods make it possible to investigate both low molecular weight compounds (D_0 and $[\eta]$) and polymer molecules (S_0 , K_s , D_0 , $[\eta]$).

The values of D_0 and ($[\eta] \cdot M$) were measured for some low molecular weight complexes. In the interpretation of experimental values hydrodynamic theories were used for the model of a non draining uncharged spheres [3] and the density increment $\Delta P/c_M = M(1 - \nu^P)$ where c_M is the complex concentration determined by an independent method and expressed in mole/cm³. In the case of diffusion, the M value of the low molecular weight complex was calculated from the equation:

$$(M - \Delta P/\Delta c_M) = (4\pi/3)(kT/6\pi\eta_0 D_0)^3 N_A P_0$$

where η_0 and P_0 are the solvent viscosity and density respectively, k is Boltzmann's constant, and N_A is Avogadro's number.

Table 1. Characteristics of low molecular weight complexes.

Complex	$D_0 10^7$ cm ² /s	$([\eta] \cdot M)$ cm ³ /mol	$\Delta P/\Delta c_M$ g/mol	M_D g/mol	M_η g/mol	$r_D 10^8$ cm	$r_\eta 10^8$ cm
FeTNa	37	1100	470	720	940	4.5	5.6
Cadoxen	-	900	109	-	470	-	5.2
CaCl ₂ +DMAA	47	-	110	375	-	4.8	-
LiCl +DMAA	50	910	38.5	250	380	4.5	5.2
LiCl +H ₂ O	124	140	23	42	79	2.0	2.8

M_D and M_η are the molecular weights and r_D and r_η are the radii of equivalent spheres calculated from diffusion and viscometric data, respectively.

By using dialysis (Vladipore membranes based on polysulfonamide) the differences Δn and ΔP were determined for two cases: 1) solutions were compared before and after dialysis, 2) solvents were compared before and after dialysis (n - refractive index and P - density). The values of $(\Delta P/Pw)$ and $(\Delta c_M/w)$ were extrapolated to the condition $(wV_1/V_2) \rightarrow 0$ where w is the weight concentration of cellulose in FeTNa, V_1 is the solution volume, and V_2 is the solvent volume against which dialysis was carried out. This condition corresponds to dialysis against infinite solvent volume. It was found for cellulose in FeTNa that

$$(\Delta P/Pw)_0 = (M_{cc}/M)(1 - \nu_{cc}P_0) = 0.75 \pm 0.03$$

$$(\Delta c_M/w)_0 = (20 \pm 2) \cdot 10^{-4} \text{ mol/cm}^3$$

The number of bonded low molecular weight complexes per cellulose monomer unit was determined from the value of $(\Delta c_M/w)_0$:

$$n_{cc} = (\Delta c/w)_0 M_0 / P_0 = 0.28$$

where M_0 is the molecular weight of the repeat cellulose unit and P_0 is the solvent density. Hence, on average one FeTNa-complex is present per 3.5 cellulose monomer units. The value of density increment $(\Delta P/Pw)$ was used in the interpretation of sedimentation-diffusion data.

Cellulose was investigated over a wide range of degrees of polymerisation in FeTNa with the following compositions:

solvent 1: $c_c = 0.10M$; $1.5M$ NaOH; 2% of sodium tartrate (TNa) ($P_0 = 1.120 \text{ g/cm}^3$; $\eta_0 = 1.71 \cdot 10^{-2}$ poises)

solvent 2: $c_c = 0.30M$; $1.5M$ NaOH ($P_0 = 1.191$, $\eta_0 = 2.94 \cdot 10^{-2}$).

The results were compared with published data for cellulose in FeTNa [4-6].

The equilibrium rigidity of cellulose chains was evaluated with the assumption of very small volume effects by using theories [7]. The factor of hindrance to internal rotation $\phi^2 = A/A_f$ was calculated on the basis of experimental (A) and theoretical (A_f) values of the Kuhn segment length. The A_f value is obtained with the assumption of a complete freedom of rotation of the cellulose chain about all OC_1 and OC_4 bonds [8]. Consequently, the calculated values of ϕ^2 greatly exceed those obtained for all other linear polymers. However, the initial model for calculating A_f does not take into account intrachain hydrogen bonds which lead to the formation of ladder structure fragments of the cellulose chain. The theoretical model was generalized to the case of identical rigid fragments inclined to each other at a valence angle θ . For an even number n of glucopyranose rings contained in a rigid fragment, the following expressions were obtained:

$$b_n = b_1; \quad d_n = 2(n-1)b_1 \cos(\theta/2) + nd_1 \sin(\theta/2);$$

$$A_{fn} \lambda_n = (d_n \sin(\theta/2))^2 + (2b_n + d_n \cos(\theta/2))^2 (1 + \cos\theta) / (1 - \cos\theta)$$

$$\lambda_n = n \lambda_1; \quad \lambda_1 = 0.515 \text{ nm}; \quad d_1 = 0.142 \text{ nm}; \quad b_1 = 0.265 \text{ nm};$$

$$(\pi - \theta) = 109.5^\circ.$$

Some cellulose derivatives were also studied: highly substituted nitrate, sulfoacetate and methylcellulose, as well as some polysaccharides of other origin: chitosan, chitin nitrate, microbial mannan, laminarin and polymaltotriose [9-12] (See table 2).

These latter polysaccharides differ from each other in the type of inclusion of the saccharide ring into the main chain, which profoundly affects the equilibrium rigidity of the chain.

Table 2. Parameters of Kuhn-Mark-Houwink equations
 ($[\eta] = K_{\eta} M^a$)

Polymer	Solvent	a	$K_{\eta} 10^2$ cm ³ /g	$M 10^{-3}$
Cellulose	FeTNa $C_c=0.10M$	0.79	2.6	6-640
Cellulose	FeTNa $C_c=0.30M$	0.89	1.05	5-440
Cellulose nitrate, DS=2.7	ethyl acetate	0.95	0.51	50-980
Cellulose sulfoacetate	0.2M NaCl	0.95	0.21	7-70
Chitosan	0.33M CH ₃ COOH+ +0.3M NaCl	1.02	0.34	13-190
Chitin nitrate, DS=1.75	DMF	1.04	0.15	11-170
Mannan	H ₂ O	0.75	2.33	20-180
Polymalto- triose	H ₂ O	0.58	6.0	3-660
Dioxan lignin	dioxan	0.27	0.49	6-100
Dioxan lignin	DMSO	0.21	1.04	6-100
Groundwood lignin	DMSO	0.25	0.72	6-60
Groundwood lignin	DMSO	0.44	0.15	0.6-6

Soluble lignin fragments: dioxan lignin and ground-wood lignin were studied. In the interpretation of molecular data on lignin the fundamental problem is its linear analog. If the properties of this analog are known, it is possible to determine the degree of branching of soluble lignin fragments. For this purpose the plot of the type Burchard-Stockmayer-Fixman is generally used [13]. In our opinion in this case it is necessary to take into account the fact that at $M < 6 \cdot 10^3$ lignin fragments are virtually linear, and the dependence used has a zero slope. This conclusion can be taken into account in determining the degree of lignin branching.

REFERENCES

1. Jayme G. in Cellulose and cellulose derivatives. 1971. Ed. N.M.Bikales and L.Segal. J. Wiley, New York.
2. Vink H., Makromol. Chemie. 1964, 76, 66.
3. Tanford Ch. Physical Chemistry of macromolecules. 1961. J. Wiley. New York.
4. Claesson S., Bergmann W., Jayme G., Svensk. papperstidn. 1959, 62, 141.
5. Valtassaari L., Makromol. Chem. 1971, 150, 117.
6. Rinaudo M., Papeterie 1968, 90, 479.
7. Yamakawa H., Fujii M., Macromolecules 1973, 6, 407; 1974, 7, 128.
8. Benoit H., J.Polym. Sci. 1948, 3, 376.
9. Pavlov G., Selunin S., Vysokomol. Soedin. 1986, ser. A, 28, 1727.
10. Pavlov G., Shildiaeva N., Komkov Yu., Khimiya Drevesiny - Wood Chemistry. 1988, N3, 26; N4, 10; N5, 46; N6, 7.
11. Pavlov G., Pertsovskii O., Khimiya Drevesiny. 1990, N 4, 10.
12. Pavlov G., Korneeva E., Michailova N., Ananyeva E., Carbohydrate Polymers. 1992, 19, 243.
13. Fla F., Robert A., Holzforschung 1984, 38, 37.

70 The reactivity of chlorine-free bleached dissolving pulp in respect to its chemical processing

**K Fischer and I Schmidt – Dresden University of Technology,
Department of Forestry, Institute of Wood and Plant Chemistry,
Piener Straße 23, 01737 Tharandt, Germany**

ABSTRACT

When bleaching dissolving pulp in a chlorine-free way it is a great problem to maintain viscosity. Some possibilities during the bleaching process and in a post-treatment have been investigated in order to degrade the cellulose up to the required level. The reactivity of these pulps has been characterized by monitoring the molecular weight distributions of the cellulose and the filterability of the viscoses processed from it.

INTRODUCTION

The reduction or removal of organically-bound chlorine from mill effluent and pulps is one of the main points of discussion for producers as well as scientists working in this field especially in Europe. Today several ways are in progress to minimize these problems which are detectable in strength, brightness and viscosity losses in producing paper pulp. The losses in pulp viscosity caused by oxygen and peroxide treatment of the pulp which are unfavourable for producing paper pulp are not easy to utilize for a definite degradation of the viscosity which is necessary for producing dissolving pulp. Nowadays bleaching processes using oxygen and peroxide only as bleaching agents are optimized very well in respect to the brightness of paper pulps. But for dissolving pulp it is also necessary to have a definite viscosity of the pulp at the end of the bleaching process. Some possibilities are given in decreasing the pulp viscosity using oxygen-containing bleaching agents only. In our laboratory some work has been done in order to control the degradation in pulp viscosity by the help of bleaching with an

acid peroxide solution, ozone, a steam-explosion treatment or a treatment with energy-rich electrons. Furthermore, the effect of such agents or post-treatments on the reactivity of the pulps has been investigated.

PULP REACTIVITY

The word *reactivity* is not a well defined term. In our opinion the reactivity of a pulp should be considered with respect to the process by which the pulp has to be processed. In these investigations the pulp reactivity is evaluated in respect to the viscose process by help of the molecular weight distribution of the pulps and the clogging values of the viscoses produced from these pulps.

As it could be learnt from the investigations carried out on oxygen bleached sulphite pulps from beech wood the best in reactivity was yielded when the pulp was delignified and its viscosity was degraded as far as possible during the acid pulping process. The residual diminution of the pulp viscosity and the required brightness can be reached during the alkaline peroxide stage. As it was shown earlier the best filterability of its viscoses is given by processing a pulp which was extensively delignified (1).

The results of the investigation of the molecular weight distributions of oxygen-bleached pulps which differ from the original unbleached pulps in the Kappa number show that the extended delignified pulp gives not only the best filterable viscose but also a higher intrinsic viscosity and a lower polydispersity (Tab. 1). A cause for the better uniformity of pulp 2 (Tab. 1)

No.	kappa number un-bleached	IV dl/g	DP _n	DP _w	M _w /M _n	R _V g/cm ²
1	16.1	169	136	1100	8.08	103
2	6.9	268	455	1750	3.84	367

Tab. 1 Data given by the molecular weight distribution from chlorine-free bleached pulps and clogging values of viscoses produced from it (IV - intrinsic viscosity) bleaching sequence: EOP P P

may be seen in a better accessibility of the bleaching agents which has been prepared during the extended delignification process. The good accessibility of the pulps could be interpreted by the help of scanning electron microscopic pictures. Such investigations have shown that the primary wall of an extended delignified sulphite pulp was completely removed and there were defects within the S₁-wall (1).

THE REACTIVITY OF CHLORINE, CHLORINE-REDUCED AND CHLORINE-FREE BLEACHED PULPS

For these investigations industrially produced pulps were used which were bleached with and without chlorine-containing agents. The bleaching sequences for the pulps were CEHH, DEHH, EOP-P-P. The ordinary pulp parameter and the clogging values are summarized in Table 2. As can be seen this table contains the values for several oxygen-bleached pulps which possess a similar α -content and brightness but have quite different clogging values. The table reveals also that the ordinary bleached pulp

(CEHH) exhibits the highest filterability. Therefore, the causes of the different behaviour of the pulps during the viscose process have to be clarified. The great differences of the filterability may not be explained from the commonly used parameters. Both chlorine-free bleached pulps possess similar values and the differences in the degree of polymerization between the chlorine and chlorine-free bleached pulps do not reflect the trend of the clogging values.

As the viscoses from all pulps were prepared with a high charge of carbon disulfide the trials were repeated at lower CS₂-charges in order to check the influence of the CS₂-charge on the filterability of the viscoses. Table 3 contains the clogging values of several pulps prepared at different amounts of CS₂.

sequence	α -Cell. %	DP	B %	R _V g/cm ²
CEHH	91.0	700	93.4	620
D/CEHH	93.3	715	93.5	465
EOP PEP	93.3	950	91.1	223
EOP PEP	93.2	1005	89.7	460

Tab. 2 Ordinary data of pulps bleached according to different sequences and clogging values of the viscoses produced from these pulps (B - brightness)

sequence	R _V at a CS ₂ charge of				
	40	36	32	28	24
CEHH	620	603	602	560	495
DEHH	465	-	640	520	350
1. EOP PEP	223	-	-	-	-
2. EOP PEP	460	290	280	250	-
3. EOP PEP	360	-	410	-	-

Tab. 3 Clogging values of several pulps in dependence on the CS₂ charge

It could be found that the common chlorine bleached pulp results in a very good filterable viscose up to a CS₂-charge of 24%. The pulp produced in a chlorine-reduced way shows a very good filterability of its viscoses also at a lowered CS₂ charge.

Investigating the chlorine-free bleached pulps it must be admitted that there are pulps

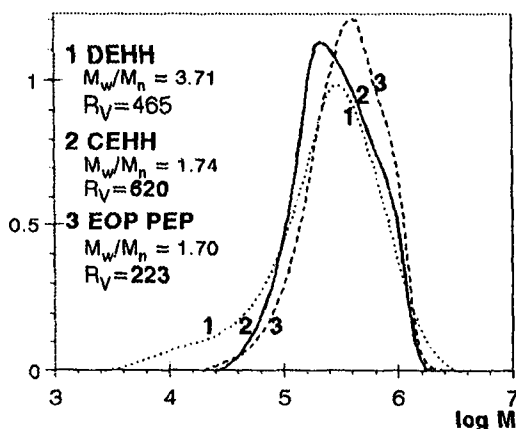


Fig. 1 Molecular weight distribution of bleached pulps

which show also a good filterability at a reduced charge of CS₂. The causes of the different behaviour of the pulps ought to be investigated. From the molecular weight distributions of the pulps as well as the pulps after alkalization and aging quite different behaviour of several pulps within these processing steps could be observed. Fig. 1 shows the molecular weight distribution of pulps which were bleached with and without chlorine. The chlorine-free bleached pulp shows the smallest distribution curve and the CEHH

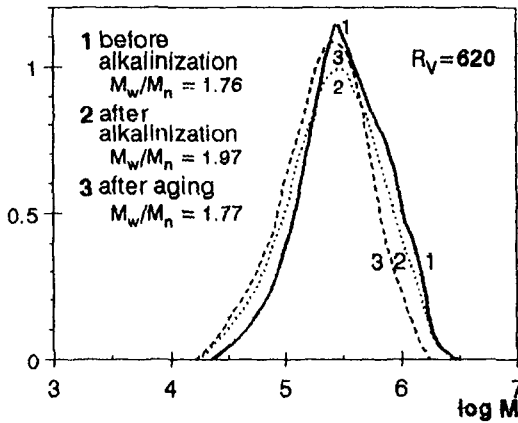


Fig. 2 Molecular weight distribution of a chlorine bleached pulp, after alkalization, and aging

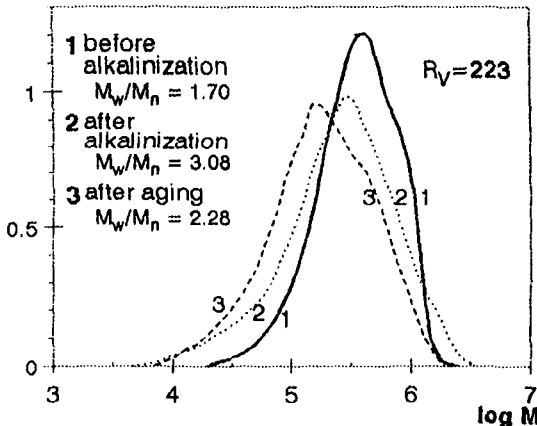


Fig. 3 Molecular weight distribution of a chlorine-free bleached pulp, after alkalization, and aging

seems to possess the most uniform one. Looking at the MWD of the chlorine bleached pulps after alkalization and after aging (Fig. 2) it is observed that the uniformity of the MWD is kept and only a small shifting of the curve towards the low molecular range can be recognized. Taking the MWD of the chlorine-free bleached pulp which results in a worse filterable viscose into consideration it must be stated that the pulp is very sensitive to the alkalization process (Fig. 3). The influence of the aging process on the MWD is not so pronounced as the alkalization process itself. The polydispersity of the pulp increases and it is higher than that of the aged chlorine bleached pulp.

Fig. 4 shows the MWDs of another chlorine-free bleached pulp which was mercerized and aged. In this case the uniformity of the distribution curve is also kept on during the processing steps and the viscose produced from this pulp shows a good filterability. From the results can be concluded that a certain stability of the pulp against alkali must be given.

In order to test the behaviour of the mercerized pulp during the aging time the aging kinetics of two different bleached pulps has

been investigated. For the chlorine bleached pulp, it could be observed that both the weight average and the number average are decreased during aging up to a certain point and afterwards both average values approach each other.

In the second case a chlorine-free bleached pulp which shows a poor reactivity was investigated. The value for the number average of polymerization was only influenced slightly, the weight average was strongly diminished, and the values did not converge. From these results it may be concluded that not only the MWDs of the bleached pulps but also the MWDs after certain aging conditions are of a special interest to the quality of the viscoses.

A consideration of the ratios of the weight average and the number average

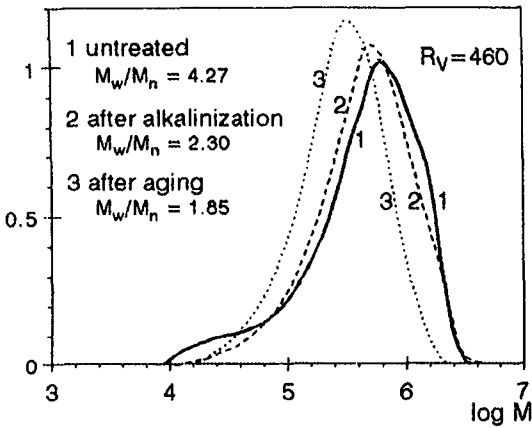


Fig. 4 Molecular weight distribution of a chlorine-free bleached pulp, after alkalization, and aging

molecular weight has shown that an enhanced filterability of the viscoses occurs along with a decreasing value for the ratios M_w/M_n (Fig. 5) determined at the aged alkali celluloses. The ratios M_w/M_n determined from the bleached pulps do not show such a strong correlation. This means that the quality of the pulp may be equalized up to a certain point by the alkalization process and thus the properties of the pulps determined after the alkalization and aging process give more probable information regarding to the viscose quality.

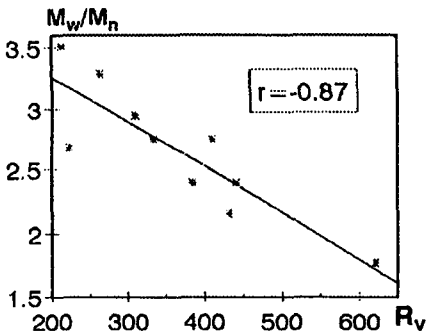


Fig. 5 The influence of M_w/M_n from alkali cellulose on the clogging values

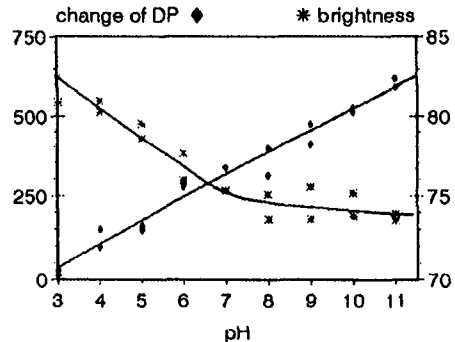


Fig. 6 Influence of the pH of the peroxide stage on the DP-changes and the brightness

Besides the problems of the strong differences in the clogging values and getting the required viscosity at the end of the bleaching process there are the problems of the brightness of pulps bleached with oxygen or peroxide only as seen in Table 2. Therefore, the influence of the pH-value of the peroxide treatment on the brightness and the degradation of the cellulose was investigated. The results are presented in Fig. 6. It can also be seen that the brightness of the pulp increases linearly with the pH of the peroxide stage, whereas the diminution of the DP is the highest at a low pH. Increasing the pH-values above 7 the diminution in DP slows permanently down (2). This means it is not possible to degrade the cellulose chains under alkaline conditions up to the required level.

Therefore, several possibilities for degrading cellulose such as a treatment by acid peroxide or ozone and a degradation by the help of energy-rich electrons or a steam-explosion process, respectively, have been investigated.

sequence	ΔDP (P_1, P_2) (P_1, P_A)	B %
EOP $P_1 P_2$	50	86.0
EOP $P_1 P_A$	210	82.7

Tab. 4 Influence of alkaline and peroxide steps on brightness and on the change in DP (P_A - acid peroxide stage)

Firstly two peroxide stages have been combined. One of them was carried out with a high alkalinity and one at a low pH. The results of the investigations did not reflect the expected ones as can be seen from Table 4.

For this reason other ways must be chosen for getting a chlorine-free bleached pulp with a good brightness and the required viscosity.

Nowadays one possibility for influencing the pulp during the bleaching process is given

by using ozone. The first trial using ozone for bleaching showed that the degree of polymerization may be influenced both by the ozone charge and the bleaching step which follows the ozone stage and the increase in brightness was promising, too. The influence of the charged ozone amount on the degradation of cellulose and the pulp brightness was further investigated.

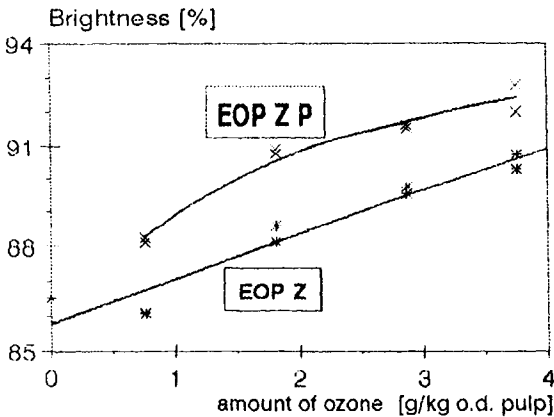


Fig. 7 Influence of the amount of ozone on the brightness

The results showed that the DP diminished in dependence on the ozone charge (0.15-0.3% on pulp o. d.) up to about 250 units. In the enclosed alkaline peroxide stage the DP decreases by another 150 units. The diminution in DP is also influenced by the charged amount of peroxide. The brightness increases with the charged amount of ozone nearly linearly (Fig. 7). During the peroxide stage the brightness of the pulp increases also but only by a few points.

The results show that in consideration of certain points a way is given for bleaching a pulp with a

high brightness and an adjustable viscosity. The reactivity of ozone bleached pulps tested at its viscoses was very good.

THE REACTIVITY OF POST-TREATED PULPS

Other possibilities such as a steam-explosion treatment or a treatment with energy-rich electrons have been tested in order to degrade the cellulose of a fully bleached pulp. The post-treated pulps were investigated in respect to the changes of the DP, their molecular weight distributions, the filterability of the viscoses produced from these pulps, and partly by MAS ¹³C-NMR spectroscopy and crystallinity values in comparison to its parent pulps.

A pulp produced in a chlorine reduced way and a chlorine-free bleached one were intensively investigated. In respect to the degradation of the cellulose the decrease of

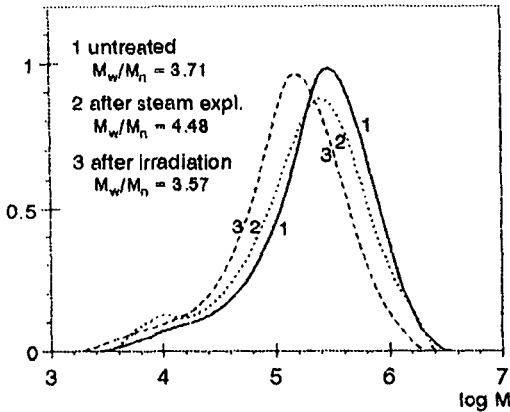


Fig. 8 Molecular weight distribution of a DEHH bleached pulp, after irradiation, and steam explosion

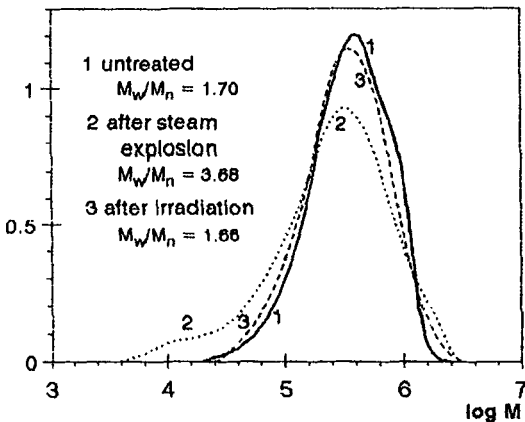


Fig. 9 Molecular weight distribution of an EOP PEP bleached pulp, after irradiation, and steam explosion

the DP (Tab. 6) and a shifting of the molecular weight distributions towards the lower molecular range can be observed on both pulps as well as after a treatment with energy-rich electrons and a steam-explosion treatment (Fig. 8, 9).

It is further recognized that by the steam-explosion treatment the amount of low molecular cellulose is increased on both pulps. By treatment of the pulps with energy-rich electrons the effect on the low molecular cellulose is not so pronounced. A special effect is to recognize the molecular weight distribution of the pulp which was bleached by help of oxygen and peroxide only after a steam-explosion treatment (Fig. 9). The post-treatment influences as well as the low molecular part of the cellulose and the high molecular one. The picture of this distribution seems to indicate a recrystallization of the cellulose. In order to check this assumption X-ray wide-angle investigations have been carried out. In Table 5 the results of the investigations for a chlorine-free bleached pulp are given. In comparison to the original pulp the crystallinity and the area of the crystal lattice is increased by the steam-explosion treatment.

Similar results were obtained for the chlorine reduced bleached pulp after an steam-explosion treatment although the broadening of the high molecular part in the molecular weight distribution curve is not so visible.

From the measured MAS ^{13}C -NMR-spectra no differences caused by the steam-explosion process could be recognized.

Also the clogging values from the viscoses of such post-treated pulps have been determined. The results are summarized in Table 6.

From the results can be seen that the reactivity of the pulp in respect to the viscose process may be increased as well as by a treatment with energy-rich electrons or a

steam explosion treatment when the origin pulp shows a bad filterability of the viscoses produced from it.

Processing a pulp which shows a high reactivity by itself so it is possible to retain the viscose quality by using a post-treatment of the pulp with energy-rich electrons eliminating the aging step. A post-treatment of such a pulp by steam-explosion shows a slight slow down of the clogging value. The aging step was also eliminated.

	X_C %	crystal lattice area nm ²
EOP PEP	50	16.7
EOP PEP steam-exploded	55	22.4

Tab. 5 X-ray wide-angle investigations
(X_C - degree of crystallinity)

sequence	treatment	DP	R_V
D/C EHH	-	714	466
	irradiation	381	431
	steam expl.	437	335
EOP PEP	-	954	223
	irradiation	346	279
	steam expl.	447	333

Tab. 6 Influence of a post-treatment of fully bleached pulps by help of energy-rich electrons or steam-explosion

ACKNOWLEDGEMENTS

This work was supported by the Federal Ministry of Science and Technology of Germany.

The authors wish to thank Dr. Fink from the *Fraunhofer Gesellschaft, Institut für Angewandte Forschung, Teltow* for carrying out the X-ray investigations and Prof. Keßler from the *Institut für Angewandte Forschung of the FH Reutlingen* for supporting the steam-explosion treatments.

REFERENCES

1. Fischer, K. et.al.; *Das Papier* 46 (1992), Nr. 12 S. 703-709
2. Fischer, K.; Schmidt, I.; Lindig, H.
VII. ISWPC 1993 Beijing, Proceedings Vol. 1, S. 406-409

71 The effect of plasma-chemical treatment on the properties of cellulosic materials

T Mironova and R Belodubrovskiy – 194021, St Petersburg, Shvernik av. 49, VNIIB; S Krapivina and G Paskalov – St Petersburg, Zagorodniy pr. 68, NPP 'Plasma', Russia

ABSTRACT

The modification of the submolecular structure of different fiber types may be carried out by physical methods. The effect of plasma-chemical treatment (PCT) on the change of pulp reactivity, hydrophilic and absorption properties were studied. The subjects of study for PCT were the following: the hardwood viscose and softwood cord pulps as well as the paper base for sausage casing. After PCT the capillary absorption of the paper base increases by 1.5-2.5, the time of water rise to 25 mm height decreases by 6.0-17.0 times and the paper base absorption capacity at full impregnation with viscose solution increases by 1.7-10 times. The outflow rate of viscose solution after xathation of viscose at CS₂/NaOH ratio (%) 90/11 and 110/12 increases by 2.0-3.0 times, respectively.

MATERIALS AND METHODS

For our experiments we used a low temperature plasma (LTP) of glow discharge under lowered pressure. This plasma is non-equilibrium and non-isothermic i.e. the electronic temperature is much higher (30000⁰K) than the gas one (375⁰K). The treatment of cellulosic materials was performed on the pilot HF glow discharge unit with external circular electrodes. In the case of hydrophilic treatment of cellulosic materials oxygen was used as a plasma-producing gas. The samples of paper base for sausage casing containing flax pulp as

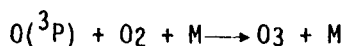
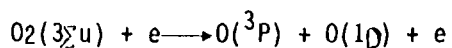
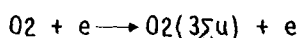
the main component were treated by LTP. The X-ray analysis of paper base for sausage casing before and after LTP treatment was made by means of an X-ray diffractometer DPOH-3 with CuK α radiation monochromated by a graphite monochromator. The operating parameters of the diffractometer were the following: 36kV, 20 mA, the rate of detector movement - 2°/min.

RESULTS AND DISCUSSIONS

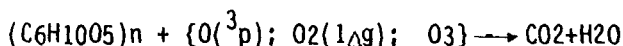
The use of some cellulose fibers in the production of speciality papers is limited by its specific structural properties. The low hydrophilicity of flax pulp connected primarily with the submolecular structure features is well-known. The high degree of its crystallinity (0,75-0,8) close to that for synthetic fiber is the reason for the smaller submicroscopic pore size than for cotton or Manila hemp fibers (Mel'nikov et al., 1983). It was established earlier that the commercial use of paper base for viscose reinforced sausage casing as the main composition component for flax long-fibered pulp does not provide paper with the necessary absorptivity. The structural modification of flax fibers produced by toughening the technological cooking parameters (raising of the temperature, active alkali consumption etc.) increased hydrophilicity but resulted in a loss of mechanical strength.

The structural modification of various fiber types (synthetic and natural) can be implemented by means of physical methods such as HF and EHF (extra high frequency) current treatment, low frequency infra-red and ultraviolet irradiation, etc (Mel'nikov et al., 1983; Gordberg et al., 1983; Krichevskiy et al., 1989). Probably the most interesting result can be obtained after ionizing irradiation which causes the looseness of polymeric submolecular structure and formation of additional active centers.

In O₂ atmosphere activating processes have the following form (Maximov, 1984; Krapivina, 1989):



The active components O(³P), O₂(1g), O₃ are characterized by a long lifetime and high chemical activity at the low temperatures. The concentration of active components may reach 10 %. During plasma-chemical treatment (PCT) of cellulosic materials at the gas-solid interface chemical reactions resulted in surface modification:



X-ray diffractograms of paper base before and after treatment do not have the pronounced differences. The degree of order (DO), according to Ant-Vuorinnen's method (Ant-Vuorinnen, 1965), was used for comparison of X-ray diffractograms. The decrease of DO during PCT of paper base from 0.727 ± 0.006 to 0.709 ± 0.011 defines cellulose crystallinity reduction. It should be noted that structural ununiformity of cellulose resulted from LTP increases.

The PCT process is ecologically more superior than for example corona discharge

Table 1. The changes in hydrophilic properties of paper base for sausage casing during plasma-chemical treatment (PCT)

Paper base characteristics	Method of physical action								
	Corona discharge treatment				Plasma-chemical treatment				
	Condi- tions N1		Condi- tions N2		Condi- tions N3		Condi- tions N4		
	MD	CD	MD	CD	MD	CD	MD	CD	
Capillary absorption, mm (per 10 min)									
before treatment	--	47	48	47	48	47	48	44	44
after treatment	--	86	80	88	84	85	70	109	94
% increment	--	83	66.7	97.2	75	80.8	45.8	147.7	113.6
		MD	CD	MD	CD	MD	CD	MD	CD
Time of water rise to 25 mm height (sec)									
before treatment	5.3	161	178	161	178	161	178	245	245
after treatment	4.4	16	26	16	26	20	35	12	17
Time reduction, %	17.0	90.1	85.4	90.1	85.4	87.6	80.3	95.1	93.1
Time of complete impregnation with viscose, sec									
before treatment	46.3		360		360		360		249
after treatment	32.3		30		90		90		143
Time reduction, %	30.2		91.7		75.0		75.0		42.6

treatment where air is used instead of O₂. This results in formation of nitrogen oxides and makes the ecological characteristics of our process worse. Moreover, in the case of corona discharge treatment one often cannot avoid the local thermal effect on treated material. Our investigations showed that PCT increases the hydrophilicity of

different cellulosic materials. Thus, modification of flax fibers by PCT provides an increase of delignification selectivity.

LTP treatment of viscose and cord cellulose causes an increase of efflux rate of viscose solution after xanthation at CS₂/NaOH ratio (%) 90/11 and 110/12, respectively, by 2.0-3.0 times.

Further research showed the possibility of considerable increase of hydrophilicity and absorption properties of paper base for sausage casing (it contains the flax fibers as a main component) by LTP. Strength properties are almost unchanged. Absorption properties were estimated by time of complete impregnation of paper base with 7% viscose solution. In Table 1 all results are compared to that for Manila hemp paper base treated by corona discharge according to the French patent N 2333084. It can be seen from the table data that the hydrophilic properties of paper base for sausage casing produced from Russian long-fibered cellulose characterized by the index of capillary absorption and the time of water rise to the 25 mm height increase approximately (in 2 directions) by 1.5 - 2.5 and 6.0 - 17.5 times, respectively (much more than corona discharge treatment gives for Manila hemp fibers).

Considerable increase by 1.7 - 12.0 times of flax paper absorption properties by PCT leads to uniformity and complete penetration of viscose solution during sausage casing production and finally to increase of strength characteristics.

The increased hydrophilic properties obtained at the PCT of flax pulp conserve well for a long time during air storage. After 2 months it decreases slightly, still being much more (1.5 - 1.8 times) for capillary absorption index than for untreated paper. As a result of the presented research the necessary parameters of LTP produced by HF glow discharge in O₂ atmosphere and under lowered pressure were defined.

CONCLUSIONS

Plasma-chemical treatment (PCT) of paper base for viscose reinforced sausage casing containing flax pulp as the main component is, as we think, the only ecologically sound technology for production of paper with the high absorptivity.

ACKNOWLEDGEMENT

The authors wish to express their gratitude to Dr. A. Shashilov for his invaluable assistance in X-ray analysis of paper base for sausage casing.

REFERENCES

1. Ant-Vuorinnen. Evaluation method of degree of order. Paperi ja Puu, v.27, N 5, 1965, p.311-322.

2. B.L.Gordberg, A.I.Maximov, B.N.Mel'nikov. Izv.Vuz ov. Himija i himicheskaia tehnologija. 1983. v.26, N 11, pp.1362-1876.
3. S.A.Krapivina. Non-isothermal gaseous discharge plasma and its application in technological processes. Leningrad,LIT "Lensoveta", 1989,p.80.
4. G.E.Krichevski, V.A.Nikitkov. Theory and practise of textile material preparation. Moscow, Legprombytizdat, 1989,p.208.
5. A.N.Maximov. Theory of non-equilibrium processes in electronic devices technology. ICTI. Ivanovo, 1984, p.306.
6. B.N.Mel'nikov, M.N.Kirillova, A.P.Moryganov. Modern state and development of dyeing technology of textile materials. Moscow,1983.

72 Spinning of fibres through the N-methylmorpholine-N-oxide process

S A Mortimer* and A Péguy** – * Courtaulds Fibres, PO Box 111, Lockhurst Lane, Coventry, CV6 5RS, England; ** Centre de Recherches sur les Macromolécules Végétales, affiliated with the Joseph Fourier University of Grenoble, BP 53X, 38041 Grenoble, France

ABSTRACT

The formation of the structure during the spinning process of a fibre spun from a solution of cellulose in N-methylmorpholine-N-oxide (NMMO) has been studied. The diameter and birefringence of a spinning monofilament were traced through the air gap that is used in the process. The effects of the spinneret diameter and the draw ratio on the structure evolution have been studied. The influence of the draw ratio on the fibrillation tendency of the fibre has also been evaluated. It is shown that the NMMO process is rather robust with respect to the tensile properties of the resulting fibres, but it is still possible to vary the amount of fibrillation.

INTRODUCTION

The fundamentals of the NMMO/water/cellulose solution system have been widely studied over the past fifteen years [1-6]. The process can be used to make a wide range of products, but most development effort has concentrated on the spinning of fibres. Some workers have studied this subject [7,8] and others the influence of spinning process parameters on the structure of the fibre [9]. A detailed study tracing the growth of the structure through the spinning process and relating this to the final fibre structure, however, has not been attempted before.

The objective of this work was to understand the formation of the structure of the fibre during the spinning process. As it moves down the spinning line, the fibre is never in a state of equilibrium, but is always undergoing some change, such as drawing, cooling, relaxation, coagulation and drying. These changes have been monitored in the initial part of the spinning process by studying the diameter and the birefringence (which is related

to orientation) of a spinning monofilament. The effect of the fibre diameter and the draw ratio has also been studied.

EXPERIMENTAL

A solution of dissolving pulp in a mixture of NMMO and water was spun from a Davenport Melt Indexer at 115°C into a 250mm air gap and subsequently into a water bath (dry-jet wet spinning). The apparatus was set up at CERMAV[10] and specially modified for this work. Spinneret sizes of 100µm, 150µm, 200µm and 300µm were used with drawratios (D_R) varying from 1 to 40.

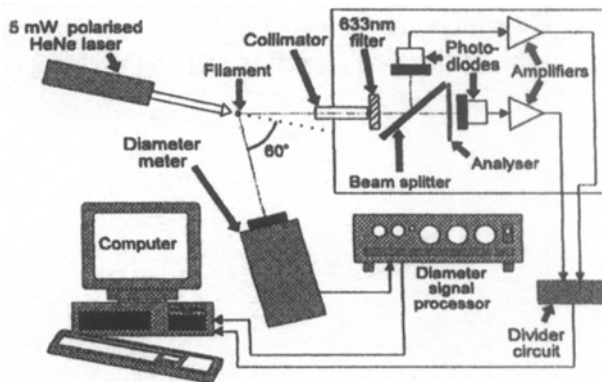


Figure 1: Apparatus for measuring the birefringence and diameter of the filament

The birefringence and diameter of the filament were studied in the air gap, using the apparatus shown in Figure 1. The intensity of light I transmitted by the analyser is related to the birefringence Δn by the formula:

$$\frac{I}{I_0} = \sin^2\left(\frac{\pi}{\lambda} \Delta n \phi\right) \quad (1)$$

where I_0 = intensity of reference beam that has not passed through the analyser, λ = wavelength of light used and ϕ = diameter of the filament, which is measured by a device developed at the Laboratoire de Rhéologie (Grenoble) by A. Magnin and J. M. Piau.

The birefringence of finished dry fibres was measured on an Olympus optical microscope, using a Berek Compensator. Fibre tenacity, extension at break and initial modulus were measured on an Instron 4301 tester, on 20 fibres from each sample. The crystallinity of the fibres was measured using Wide-Angle X-ray Diffraction (WAXD). The equipment used was a Siemens Krystalloflex generator (CuK α radiation) with a Warhus flat film vacuum camera. The sample was rotated during exposure to smear the diffraction peaks. The resulting film was scanned and digitised using a Joyce-Loebl 3CS Microdensitometer. The crystallinity of the sample was calculated using a correlative technique developed by Statton[11] and Wakelin et al[12], in which the unknown spectrum is compared with crystalline and amorphous standards. In our case, the crystalline standard was mercerised and hydrolysed ramie and the amorphous standard was amorphous cellotetraose. It should be noted that this is a relative, rather than an absolute technique, since the standards are neither wholly crystalline nor wholly amorphous.

Fibrillation was measured by an ultrasound technique. 10 filaments of 20mm length were immersed in 10ml of distilled water in a 30ml phial. These were then treated for 15 minutes on a Branson Sonifier B12 ultrasonic probe, whilst cooling the outside of the phial. The probe was fitted with a 13mm flat tip. The fibrillation index (F_f) was calculated from optical micrographs of the fibrillated fibres. The lengths of the fibrils, l , over a length of fibre, L were measured. The fibrillation index is given by:

$$F_f = \frac{\sum l}{L} \quad (2)$$

RESULTS AND DISCUSSION

The shape of the filament in the air gap with 200 μ m and 300 μ m spinnerets and a draw ratio of 10.4 is shown in Figure 2. It appears that, with the narrower spinneret, the filament reaches its final diameter at a distance closer to the spinneret, that is, the "draw length" is shorter. The curves appear to begin at a value higher than one, owing to die swell at the exit of the spinneret. The die swell is greater with the larger spinneret, due, to a difference in cooling. Finally, the curves appear to have an inverse exponential shape.

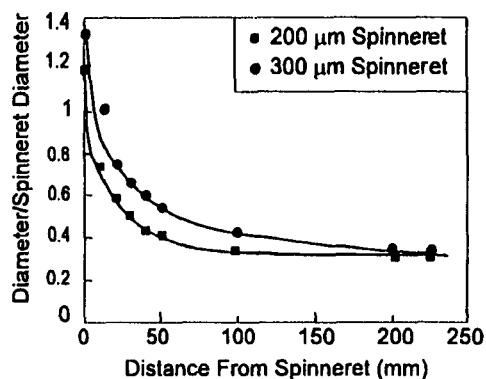


Figure 2: Diameter of the filament as a function of distance from the spinneret

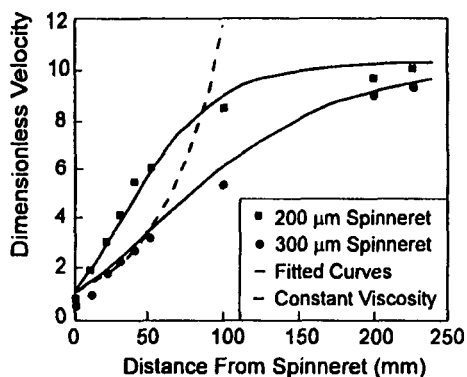


Figure 3: Dimensionless velocity of the filament as a function of distance from the spinneret

We have shown elsewhere [13], that the velocity profile $V(x)$ approximates to the following formula:

$$\frac{d \ln V}{dx} = \frac{1}{\eta_e} \frac{F}{Q} \quad (3)$$

where F = force on the filament, Q = throughput and η_e = extensional viscosity. Therefore V depends essentially on how the extensional viscosity varies with distance from the spinneret. We have also shown that the shear viscosity of our solutions varies approximately exponentially with distance from the spinneret as the filament cools. It is reasonable to assume that the extensional viscosity will display the same behaviour. According to this

hypothesis, and setting the boundary conditions $V/V_0 = 1$ at the spinneret and $V/V_0 = D_R$ for $x \rightarrow \infty$, the general formula for the velocity profile is given by:

$$\frac{V}{V_0} = D_R \exp[-\ln D_R \exp(-ax)] \tag{4}$$

Where a is a constant which takes into account different effects such as mass transfer, viscous flow etc.

Figure 3 shows the diameter data recalculated as a dimensionless velocity and fitted to curves from equation 4, with an arbitrary value for a . The overall fit to the shape is very good. In contrast, a constant viscosity (isothermal) case is also shown as a dashed line. The velocity in this case increases rapidly and does not stabilize, so the fibre “necks down” and breaks.

Figure 4 shows how the material orients in the air gap. With the draw ratio used, the birefringence is proportional to the velocity. This means that it is inversely proportional to the cross-sectional area and proportional to the stress. Similar results have been obtained for non-crystalline melt-spun polymers[14]. The birefringence with the 200µm spinneret reaches a higher value than with the 300µm spinneret.

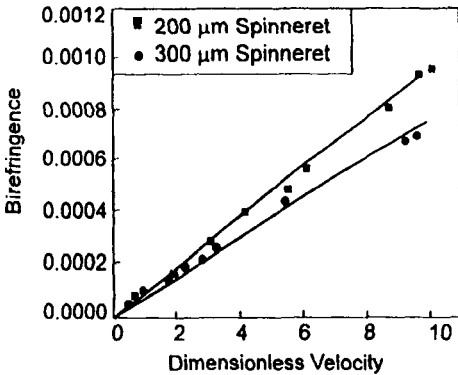


Figure 4: Birefringence of the filament as a function of dimensionless velocity

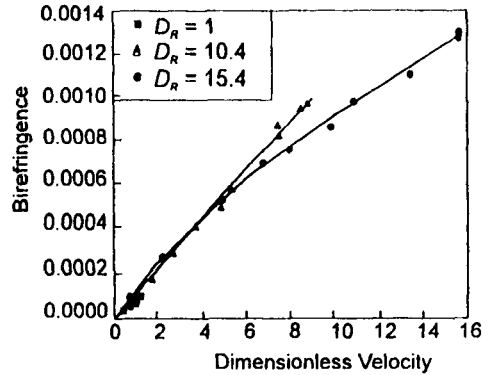


Figure 5: Birefringence of the filament as a function of dimensionless velocity, with different draw ratios

The effect of the draw ratio on birefringence growth is shown in Figure 5. Initially, the relationship of the birefringence to the velocity is similar in the three cases. As would be expected, the final birefringence reached increases with increasing draw ratio. Note that with a draw ratio of about 15, the relationship deviates significantly from linearity. This phenomenon has been observed in other systems[15] and is evidence for slippage of the chains as they approach full extension.

The effect is more clearly seen in Figure 6, which shows the relationship between the birefringence of the drawn filament (at the end of the air gap, just above the spin bath) and the draw ratio, using different sizes of spinneret. At low draw ratios, the birefringence appears to increase rapidly as the draw ratio is increased, before tending towards an asymptote at a birefringence of 0.0013. This maximum appears to be independent of the spinneret hole size used. A qualitative explanation for this is that the polymer chains are approaching their finite maximum orientation, when they are close to being fully extended and aligned.

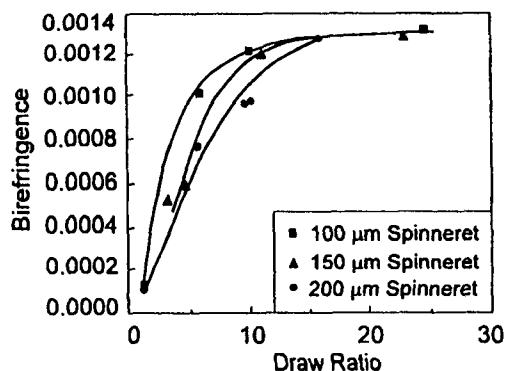


Figure 6: Birefringence of the filament at the end of the air gap as a function of draw ratio

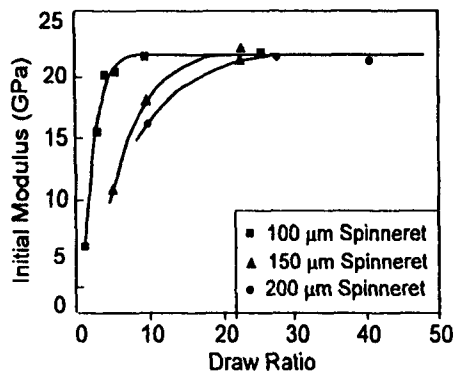


Figure 7: Initial modulus as a function of draw ratio

The relationship between the birefringence and the draw ratio does depend on the spinneret hole size in that, with a smaller spinneret, a smaller draw ratio is required to give a high birefringence.

Table 1: Physical properties of fibres spun with different draw ratios.

Draw Ratio	Birefringence	Initial Modulus GPa	Tenacity GPa	Extension at Break %	Crystallinity %
1.0	0.023±0.001	6.2±0.5	0.25±0.02	80.0±8.0	43±2
2.9	0.032±0.001	15.5±1	0.37±0.03	17.5±2.0	45±2
4.0	0.038±0.001	20.0±1	0.41±0.04	13.0±1.0	46±2
6.5	0.040±0.001	20.4±1	0.41±0.04	10.9±1.0	43±2
10	0.041±0.001	21.7±1	0.50±0.05	10.0±1.0	46±2

The effect of draw ratio on the physical properties of the fibres is shown in Table 1. At low draw ratios, the birefringence, modulus and tenacity increase with increasing draw, but they reach a plateau. This plateau is little above a draw ratio of four for the birefringence and modulus, but is somewhat higher for the tenacity. The extension at break is extremely

high (80%) with a low draw ratio, but this levels out to around 10% above a draw ratio of about 6. The really remarkable point about this set of data is the crystallinity, which appears completely independent of draw! This suggests that the crystallisation of the cellulose is energetic enough to overcome a high degree of disorientation.

A plot of the effect of draw ratio on initial modulus with different spinnerets is shown in Figure 7. The maximum modulus reached is 22 GPa, independent of the spinneret size used, but, similarly to the birefringence at the end of the air gap, the smaller the spinneret used, the lower the draw needed to reach this maximum. The existence of the plateau suggests that high performance cellulose fibres cannot be made from this system simply by increasing the amount of draw. It does indicate, however, that, above a certain threshold, the process is very robust, the final properties of the fibres being largely independent of the spinning conditions used.

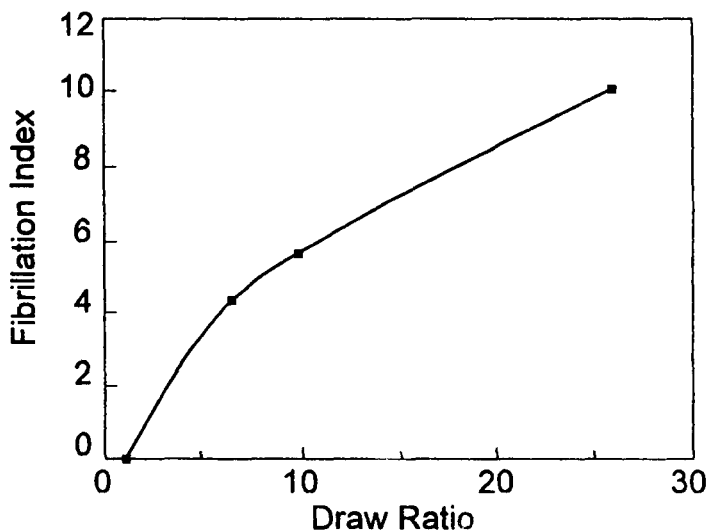


Figure 8: Fibrillation index as a function of draw ratio

The effect of the draw ratio on the fibrillation characteristics can be seen in Figure 8. As might be expected, fibrillation increases with increasing draw ratio. It does not, however, follow the bulk orientation of the polymer as measured by the birefringence: No asymptote is reached. This means that, by selecting the draw ratio, it is possible to make a fibre with either a high or a low fibrillation index without significantly affecting the tensile properties. The diameter of the fibres was not found to influence the fibrillation tendency.

CONCLUSIONS

We have shown how a fibre spun from a solution of cellulose in NMMO draws and orients in the air gap. The velocity profile fits a shape predicted by exponential viscosity growth.

Orientation of the polymer increases with increasing stress, but chain slippage occurs at high draw ratios. Overall, the system appears very robust, since the orientation and modulus are independent of the draw ratio above a certain limit. Nevertheless, the fibrillability of the fibre can be varied, without significantly affecting its tensile properties.

REFERENCES

1. Chanzy, H., Dubé, M. and Marchessault, R.H., *J. Polym. Sci., Polym. Lett. Ed.*, **17**, 219-226 (1979)
2. Gagnaire, D., Mancier, D. and Vincendon, M., *J. Polym. Sci., Polym. Chem. Ed.*, **18**, 13-25 (1980)
3. Chanzy, H., Nawrot, S., Peguy, A. and Smith P., *J. Polym. Sci., Polym. Phys. Ed.*, **20**, 1909-1924 (1982)
4. Maia, E.R. and Pérez, S., *Nouv. J. de Chim.*, **7**, 89-100 (1983)
5. Lang, H., Laskowski, I., Lukanoff, B., Schleicher, H., Mertel, H., Franz, H. and Taeger, E., *Cell. Chem. Technol.*, **20**, 289-301 (1986)
6. Belousova, T.A., Shablygin, M.V., Belousov, Yu. Ya., Golova, L.K. and Papkov, S.P., *Polym. Sci. U.S.S.R.*, **28**, 1115-1122 (1986)
7. Navard, P. and Haudin, J.M., *Polym. Proc. Engng.*, **3**, 291-301 (1985)
8. Loubinoux, D. and Chaunis, S., *Textile Res. J.*, **57**, 61-65 (1987)
9. Dubé, M. and Blackwell, R.H., *Tappi Proceedings, Boston, USA*, 111-119 (1983)
10. Quenin, I., *Doctoral Thesis, UJF Grenoble* (1985)
11. Statton, W.O., *J. Appl. Polym. Sci.*, **7**, 803-815 (1963)
12. Wakelin, J.H., Virgin, H.S. and Crystal, E., *J. Appl. Phys.*, **30**, 1654-1662 (1959)
13. Mortimer, S.A. and Péguy, A.A., *Textile Res. J.* submitted
14. Ziabicki, A., *Fundamentals of Fibre Formation, John Wiley & Sons, London* (1976)
15. Muller, R. and Froelich, D., *Polymer*, **26**, 1477-1482 (1985)

Index

- 2, 3-di-O-carboxymethyl cellulose 167
Absorbent 141–150
Acetic acid 219–226
Acetic anhydride 219–226
Acetobacter xylinum 3–7, 9, 10, 15–27
Acetylation 219–226, 514
Acetylenedicarboxylic acid methyl ester 173
Acid anhydride 141–146
Acid chlorine 141–146
Acid hydrolysis 374
Acrylamide, graft copolymers 191–198
Activation 141–146
Activity 4–7
Acyl chloride formation 215
Adsorbed layer, structure of 425
Adsorption, temperature dependence of 363, 425
Alginate 270
Alkali-cellulose 523–526
Alkalinization 523–527
Alkylpyridinium 298–303
Amidation of carboxycellulose 216
Amine oxides 131–136
Amphiphile 295
Amphiphile electrode 296
Amphiphilic derivatives 339–344
Amylose 174, 175
Amylose esters 170
1, 6-Anhydrides 128, 129
Amylose ethers 171
Anionic surfactant 287
Anthraquinone 517–521
Antiparallel structure 57
Arabinogalactan 471
Arrangement of chains 386, 390
Artefacts 245–248
Associative polymers 323
Associative thickener 287
Atomic force microscopy 69
Average fibre length 531
Avicel 447
B-Parameter 269
Bacterial cellulose 9, 13, 15–27
Bacterial cellulose composite 9–14
Bacterial cellulosic film 18–26
Bacterial type cellulose 78
Ball milling 81
Banana tree 535
Beating 98
Bentonite 466
Binding isotherm 298–303
Biocompatibility 151, 152
Biodegradable material 10, 14
Biodegradation, of bacterial cellulose 18–26
Biopolymers 463
Biosynthesis 15–26
Biotransformation, of cellulose 29–34
Bleached pulp 486
Bleaching 547
Blend 407
Blends, of cellulose derivatives 393–400
Bound water 249–253
Bromodeoxycellulose 233
¹³C-CP/MAS-NMR 93, 523–526
¹³C NMR 153, 163, 167
¹³C-NMR spectrum of carboxycellulose 218
¹³C NMR of cellulase 185–190
Cadoxen 177, 272
Cahn's linear theory 316
Calorimetric cell 101–106
Calorimetry 271
Carbamate 141–152

- C-6-carboxycellulose (COC) 213
Carboxymethyl cellulose 161, 177,
199–206, 249–253, 266, 316
Carboxymethyl cellulose, in tunnelling
463
Carboxymethyl cellulose-maleates 172
Carboxymethylation of 6-O-
triphenylmethyl 165
Carsson sinking 467
Casein 409
Catalysts 125–130, 141–145
Cationic hydrophobically modified
hydroxyethylcellulose (Quatrisoft)
—adsorption at solid-liquid interfaces
—forces between layers of
—interaction with SDS, C₁₂E₅ 355
Cationic polyelectrolyte 287
Cationically modified hydroxyethyl
cellulose 332, 333
(cat HEC)
Cellobiohydrolase II (*Trichoderma
reesei*) 37
Cellooligosaccharide hydrolysis 39
Cellulase 3–7, 276
Cellulose 85, 107–114, 125–130,
131–137, 517–521, 541–545
Cellulose, derivatisation 141–152
Cellulose, matrices 445–452
Cellulose, metallic derivatives of
185–190
Cellulose, miscibility 499–504
Cellulose, native 51, 53
Cellulose, production 3–7
Cellulose, structure 51
Cellulose 2-methylstilbene-5-carboxylate
227–232
Cellulose acetate 158
Cellulose amylose esters 170
Cellulose carbamate, fibres 207–211
Cellulose crystal structure 57
Cellulose crystallinity 63–66
Cellulose crystallites 373
Cellulose degradation kinetics 118,
119
Cellulose derivatives 257–262, 544,
545
Cellulose derivatives, blends of
393–400
Cellulose derivatives, water sorption
249–253
Cellulose esterification 154
Cellulose ethers 174, 307–311,
345–353, 453–462
Cellulose hydrolysis 39
Cellulose I 93
Cellulose I α 93
Cellulose II 93
Cellulose II β 93
Cellulose nitrate 245–248
Cellulose phosphate 159
Cellulose—polyacrylamide graft
copolymers 191–198
Cellulose polymorphs 85
Cellulose starting materials 435
Cellulose stilbene-4-carboxylate
227–230
Cellulose sulphate 156, 249–253
Cellulose triacetate 219–226
Cellulose tribenzoate (CTB) 382
Cellulose triphenylcarbamate/methyl
391
Cellulose viscose 475–482
Cellulose, water sorption 101–106
Cellulosic fibres, from cellulose
carbamate 210, 211
Cellulosic fibres, manufacture of
29–31
Celsol 29–34
Cement extrusion 453–462
Chain stiffness 269, 270
Chemometrics 93
Chiral nematic phase 373
Chlorine-free bleaching 486–488
Chlorodeoxycellulose 148
Cleavage pattern 39
Co³⁺ initiated polymerisation
coefficient 191–198
Compatibility 412, 499–504
Complex 541–543
Concentration dependency of
sedimentation 239–244
Concentration effects 178

- Conformational transition 270–274
 Controlled drug delivery 451, 452
 Convolution 72
 Cooking 517–521
 Cord pulp 487, 488
 Cotton-ramie type cellulose 78
 Counterions 249–253
 Cross-linking 199–206
 Crosslinking of cellulose 175
 Crosslinking reactions 169
 Crystal plane 73
 Crystal structure of CTB 382
 Crystalline cellulose 69
 Crystalline domains of CTB 386
 Crystalline structure 51
 Crystallinity 63–66
 Cure experiments 279–286
 Cysteine 234
- Deconvolution 76
 Degradation 265–275
 Degradation, of cellulose nitrate
 245–248
 Degree of order 557
 Degree of polymerization 81
 Degree of substitution, deterioration
 of 153
 Dehydration 125–130
 Delignification 517–521, 535
 Deoxycellulose 141–149
 Depolymerization 265, 274
 Derivatisation, of cellulose 141
 Derivatives, of cellulose 185–190
 Diazotization 234
 Dibucaine 300
 Differential scanning calorimetry 271,
 404, 406
 Diffusion spreading 179
 Dimethylacetamide (DMAc) 142–151
 Direct soluble cellulose 29–34
 Dissolution of cellulose 153
 Dissolving pulp 219–226, 547
 D₂O exchange 81
 Double-stranded 265–276
 Draw ratio 559
 DRIFT spectrometry 63–66
- Dynamic rheological measurements
 279–286
- Effect of pulp drying 531, 533
 Electric birefringence 333
 Electron microscopy 268–273
 Ellipsometry 356, 363
 Enhancement 3–7
 Enthalpy of sorption 417–422
 Enzymes as bleaching aids 43–48
 Esterification, of cellulose 154
 Esters, cellulose 141–152
 Ether, cellulose 141–152
 Ethyl(hydroxyethyl)cellulose 298,
 307–311, 363, 425
 Eucalypt pulp 530
 Extra high frequency current (EHF)
 556
 Extrusion 453–462
- Fibre diffraction 266
 Fibre length distribution 531, 532
 Fibre spinning 559
 Fibre structure 559
 Fibres 559
 Fibres, carboxymethylcellulose
 249–253
 Fibres, cellulosic 107–114
 Fibres, polyethylene terephthalate
 491–497
 Fibres, properties of 210, 211
 Fibrillation 559
 Filterability 547
 Flow-induced structures 393–400
 Fluorescence 341–344
 Freeze-fracture scanning electron 336,
 337
 Freezing water 249–253
 FTIR spectrum of cellulose 185–190
 Furfural analysis in oil 121
- Gas sorption calorimeter 417–422
 Gel 315
 Gel filtration 275
 Gel time 279–286
 Gelation 267, 276

- Gelation rate 279–286
- Gellan gum 301
- Gels, ageing temperature of 279–286
- Gels, high-methoxyl pectin 279–286
- Glucomannan triacetate 219–226
- Glucose inhibition 41
- β -D-Glucosidase 3–7
- Graft copolymers, of cellulose 191–198
- Graphite suspension 472
- Grinding of pulp and linters 507–516

- Helix 268, 271
- Hemicellulose, miscibility 499–504
- Hemicelluloses 517–521
- Hemodialysis 151, 152
- Heterogeneous carboxymethylation 163
- Heterogeneous sulphate 435
- High-methoxyl pectin, gelation 279–286
- High-performance chromatography 162, 166
- High frequency current (HF) 556
- Homogeneous carboxymethylation 164
- Homogeneous conditions 234
- HPLC 39
- Humidification 75
- Humidity 249–253
- Hydrogels 199–207
- Hydrogen bonds 527
- Hydrolytical degradation 435
- Hydrophobic associations 339–344
- Hydrophobically associating polymers 339–344
- Hydrophobically modified hydroxyethyl 332, 333
- Hydrophobically modified polymer 287, 323
- Hydrothermal treatment 78, 79
- Hydroxyethyl cellulose (HEC) 274, 331
- Hydroxypropyl cellulose 346
- Hydroxypropyl cellulose/acetic acid/polyester resin blends 401, 403

- Hydroxypropyl cellulose 180
- Hydroxypropylcellulose, in blends 393–400

- Inhomogeneity 177
- Insoluble residue 219–226
- Insulation life prediction 120
- Interaction 4, 7
- Interconnecting lacy structure 315
- Interfacial behaviour 363
- Interfacial tension 395
- Intermolecular H-bonds 77, 78
- Ion exchange 249–253
- IR-characterisation, of carboxycellulose 217
- Irradiation 547
- Irreversible change 85, 87
- Isocyanate, 142, 149
- Isomerization 227–231

- Ketoester 141–146
- Kinetic rates 39
- Kraft paper insulation 116
- Kraft pulping 98

- Level-off DP 511
- LiBr/*N,N*-dimethylacetamide 234
- Lignin 517–521, 544–546
- Lignin, miscibility 499–504
- Lignin based additives 491–497
- Lignin bleaching 43–48
- Lignin modification 491–497
- Lignin modifying enzymes 43–48
- Lignocellulose 535
- Lignocellulosics 93
- Lignosulfonates 491–497
- Linters 523
- Liquid crystal 373
- Liquid crystalline polymers 393–400
- Liquid crystalline state 391
- Lithium chloride 141–151
- Low-grade dissolving pulp 219–226
- Low-temperature plasma (LTR) 555–558
- Lytotropic HPC 401–403
- Lysozyme action 18–26

- Maleic acid half esters, 170
Mark-Houwink-Sakurada 269, 272
Mechanical property 409
Membrane 141, 151, 152
Metallic derivatives 185–190
Methyl orange structure 238
Methylcellulose 239–244
Mica 356
Microbial delignification 535
Microcalorimetry 101–106
Microcrystalline cellulose 185–190
Microencapsulation 435
Microscopic observations 533, 534
Milling 85–91
Miscibility, of lignin 499–504
Modulated structure 315
Molecular characteristics 239–244
Molecular hydrodynamic 542–545
Molecular modelling 57, 58, 73
Molecular weight distribution 31–33,
182, 547
Monte Carlo 274, 275
Morphology 393–400, 403, 404
- N-methylglycolchitosan 298
N-methylmorpholine-N-oxide 559
N-methylpyrrolidone (NMP) 142–152
Nitrocellulose 239–244
Nonionic cellulose ether 323
Nucleophilic substitution 233
- OH/CH₂ valency vibrations 75
Oil, furfural analysis in 121
Optical rotation 271, 275
- Packing, parallel-antiparallel 390
Packing energy calculation 51, 52,
57–60
Parallel structure 57
Partial least squares 94
Pattern recognition 94
Permeability 414
Persistence length 257–262, 269, 270
PFI refining 530, 531
Phanerochaete chrysosporium 535
Pharmaceutical formulation 445–452
- Phase behaviour 325
Phase separation 287, 315, 375
Photofunctional material 227
Photosurfactant 302
Physical properties 533
Plasma-chemical treatment (PCT)
555–558
Plasticizer 471–473
Plastified cement 453–462
Poly(diallyldimethyl ammonium
chloride) 435
Poly(*N*-vinylpyrrolidone) 316
Poly(acrylamide) 315
Poly(ethylene oxide) 316
Poly(methacrylic acid) 315
Polydimethylinoxanes 393–400
Polyelectrolyte 435
Polyelectrolyte complex formation 435
Polyethylene oxide—EHEC interaction
307–311
Polyethylene terephtholite fibres
491–497
Polymer-solvent interaction 391
Polymer-surfactant interactions 355
Polymer complex 316
Polymer consolute interaction 325, 327
Polymer surfactant interaction 287
Polymolecularity 182
Polysaccharide derivatives unsaturated
169
Polysaccharides 257–262
Porous ceramics 471–473
Porous matrices 445–452
Potassium cellulose 185–190
Power law 321
Power transformers 115
Principal component analysis 94
Procaine 300
Propionic 146
Propylene glycol alginate 339–344
Proton NMR spectroscopy 38
PTIR spectre 78, 82
Pulp 486, 488, 517–521
Pulp, eucalypt 530
Pulp, grinding 507–516
Pulp, spuce 526

- Pulping 517–521
Pyrene 342, 343
Pyrene-labelled 347–353
Pyrolysis 125–130
Pyruvate 266–271
- Quantum chemical calculation 133, 134
- Reactivity 547
Reactivity of cellulose 514
Recrystallization 517–521
Regenerated cellulose membrane 407
Regioselectivity 154
Renaturation 274
Replica cellulose 245–248
Rheology 393–395
Rheology, yield stress value 334–336
Rheology of viscose 475–482
Rigid-ring method 52, 53
Ripening of xanthogenate 478
- Scaled structure factor 319
Scanning electron micrographs of cellulose 185–190
Sedimentation analysis 177
Sedimentation parameter 239–244
Self-diffusion 307–311
Silica 356
Silyl cellulose 156
Single-stranded 268–276
Slurry tunnelling 466
Sodium cellulose sulphate 435
Sodium dextran sulphate 298
Sodium dodecyl sulphate 287, 298
Solid state ¹³C-nmr spectroscopy 508–510, 515
Solka-flow 447
Solubility 265–267
Solubility parameter 132, 133, 219–226
Solvents 131–136
Sorption 417–422
Sorption, water vapour 101–106
Space-filling atomic-molecular models 58
Spinning 559
Spinodal decomposition 315
Spinoral ring 317
Spruce dissolving pulp 523
Stabiliser 471, 472
Stability 265–273
Steam-explosion 547
Steam explosion lignin 491–497
Stearic 146, 151
Steeping of cellulose 477
Steric stabilisation 425
Strand separation 268–272
Structural change 85
Structure, of cellulose 18–26
Substituent pattern of CMC 162
Sulfonic 147
Sulfuric acid 219–226
Surface force apparatus 356
Surface interaction, temperature 425
Surface tension 107–114
Surfactant-polymer interaction 307–311
Surfactant interactions 287
Surfactants, interaction with hydrophobically modified hydroxyethylcellulose 355
Suspensions 373
Swelling ability 227–232
Swelling systems 172
Swelling values 512, 513
- Tabletting 451
Tetracaine 300
Thermal treatment 79, 80
Thermooptical analysis 404, 406
Thiols 234
Thrombogenic 151, 152
Time-resolved light scattering 316
Tosyl chloride esterification 172
Transformer insulation failure 117
Transformer monitoring 121
Tunnelling 463
- Unbleached pulp 485, 486
- Velocity sedimentation (ultracentrifugation) 239–244

- Viscose pulp 486–488
Viscosity 257–262, 327, 476, 477,
547
- Water-soluble polymer 9–14
Water adsorption 78
Water cadoxen 177
Water retention 453–462
Water sorption 101–106, 249–253
WAXS 63–66
Wetting 107–114
- Wood 517–521
Wood matrix 499–504
Wormlike chain 257–262
- X-ray analysis 517–521
X-ray diffractograms, of cellulae
185–190
X-ray scattering 523–526
Xanthan 265–276, 463
Xanthogenation of cellulose 477
Xanthomonas 265

